25 March 2005

Science

Vol. 307 No. 5717
Pages 1821–2016 $10

The Gut
INNER TUBE OF LIFE

Science

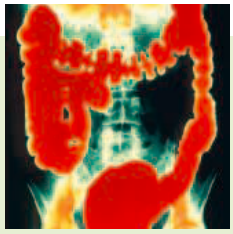

Special Issue

The Gut: Inner Tube of Life

A colored barium x-ray image of the colon of a patient in the early stages of Crohn's disease. A special section explores the diverse biology of our gut, including the abundant yet largely unknown microorganisms it harbors, its normal functions of digestion and delivery of nutrients, and diseases to which it is prone. [Image: Gjlp/Photo Researchers Inc.]

Volume 307
25 March 2005
Number 5717

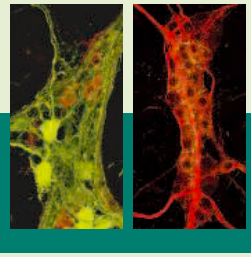

For related online content in SAGE and STKE, see page 1833 or go to www.sciencemag.org/sciext/gut/

Departments

News of the Week

News Focus

Letters

Contents continued

Books *et al.*

Policy Forum

Perspectives

Science Express www.sciencexpress.org

Brevia

Research Articles

Reports

1890 & 1928

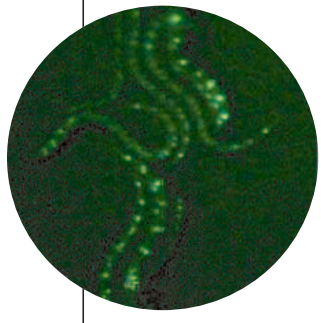

1938

Contents continued

REPORTS CONTINUED

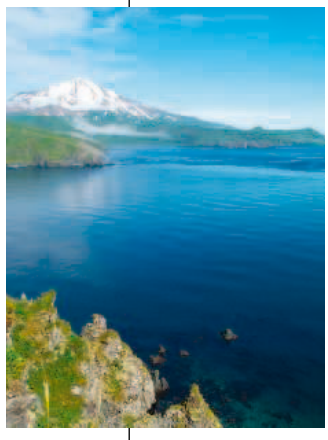

1959

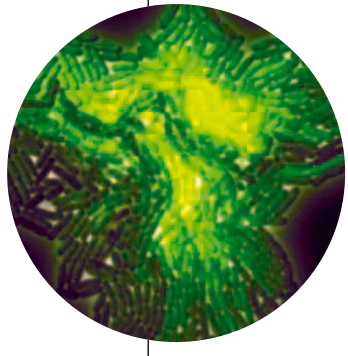

1886, 1962, & 1965

AAAS
ADVANCING SCIENCE, SERVING SOCIETY

SCIENCE (ISSN 0036-8075) is published weekly on Friday, except the last week in December, by the American Association for the Advancement of Science, 1200 New York Avenue, NW, Washington, DC 20005. Periodicals Mail postage (publication No. 484460) paid at Washington, DC, and additional mailing offices.

Domestic individual membership and subscription (51 issues): $135 ($74 allocated to subscription). Domestic institutional subscription (51 issues): $550; Foreign postage extra: Mexico, Caribbean (surface mail) $55; other countries (air assist delivery) $85. First class, airmail, student, and emeritus rates on request. Canadian rates with GST available upon request, GST #1254 88122. Publications Mail Agreement Number 1069624. **Printed in the U.S.A.**

Change of address: allow 4 weeks, giving old and new addresses and 8-digit account number. **Postmaster:** Send change of address to *Science*, P.O. Box 1811, Danbury, CT 06813–1811. **Single copy sales:** $10.00 per issue prepaid includes surface postage; bulk rates on request. The identification code for *Science* is 0036-8075/83 $15.00. *Science* is indexed in the *Reader's Guide to Periodical Literature* and in several specialized indexes.

Contents continued ▶

sciencenow www.sciencenow.org Daily News Coverage

Broad-Minded Babies
Visual training prolongs mental flexibility in infants.

Saving the Scavengers
Indian government will phase out drug linked to vulture deaths.

Bacteria's Sweet Deception
Microbes survive in the gut by giving themselves a sugar coating.

What's next after your postdoc contract?

science's next wave www.nextwave.org Career Resources for Young Scientists

UK: Facing the Great Unknown *P. Dee*
What do you do at the end of your postdoc contract when your next grant is not funded?

US: Educated Woman, Chapter 37—Cold Sweat, Anyone? *M. P. DeWhyse*
Keep your thesis proposal simple and tell a good story.

Canada: Taking a Gamble—A Wildlife Biologist's Journey to Vegas *A. Fazekas*
Canadian turtle researcher Raymond Saumure explains how his career led him to Las Vegas.

MiSciNet: Creating a Positive Graduate Experience (No Matter What) *E. Francisco*
A postdoctoral fellow talks about the additional challenges she had to face as a disabled graduate student.

GrantsNet: International Grants and Fellowships Index *Next Wave Staff*
Get the latest listing of funding opportunities and competitions happening outside the United States.

science's sage ke www.sageke.org Science of Aging Knowledge Environment

Related Inner Tube of Life section page 1895

Perspective: Age-Related Neurodegenerative Changes and How They Affect the Gut *P. R. Wade and P. J. Hornby*
Although the gut "loses its mind" with age, it remains relatively functional.

News Focus: β Blocker *R. J. Davenport*
Diabetes-linked mutations cripple gene-control protein in pancreas cells.

News Focus: Hormone Give-and-Take *M. Leslie*
Paucity of growth hormone doesn't buy extra time for rats.

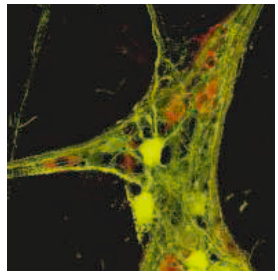

Ganglion from an aging gut.

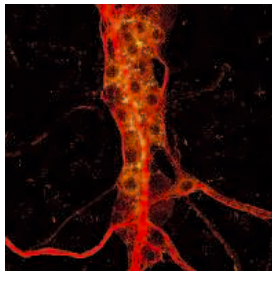

Cannabinoid receptors in the gut.

science's stke www.stke.org Signal Transduction Knowledge Environment

Related Inner Tube of Life section page 1895

Editorial Guide: Focus Issue—Going for the Gut *E. M. Adler*
Signaling processes from the nervous system to the gut as well as signaling in gut epithelia are featured.

Perspective: Food Fight—The NPY-Serotonin Link Between Aggression and Feeding Behavior *R. B. Emeson and M. V. Morabito*
The synaptic circuits connecting aggression and eating are revealed in NPY receptor knockout mice.

Perspective: Signaling the Junctions in Gut Epithelium *F. Hollande, A. Shulkes, G. S. Baldwin*
The cell-to-cell junctions that seal the gut epithelium are also centers for cell signaling.

Perspective: Orchestration of Aberrant Epithelial Signaling by *Helicobacter pylori* CagA *R. M. Peek Jr.*
CagA-dependent SHP-2 activation is involved in the morphogenetic effects of *H. pylori*.

Perspective: Central and Peripheral Signaling Mechanisms Involved in Endocannabinoid Regulation of Feeding—A Perspective on the Munchies *K. A. Sharkey and Q. J. Pittman*
Endocannabinoids coordinate food intake, metabolism, and energy expenditure.

Separate individual or institutional subscriptions to these products may be required for full-text access.

edited by Stella Hurtley and Phil Szuromi

Epigenetics, Differentiation, and Cancer

Loss of imprinting (LOI, a change in DNA methylation) of the gene encoding insulin-like growth factor–2 (IGF-2) correlates with the development of human colorectal cancer and may serve as a possible marker for cancer screening. To determine if this epigenetic change, which modestly increases IGF-2 expression, has a causal role in tumorigenesis, **Sakatani *et al.*** (p. 1976, published online 24 February 2004) created a mouse model of LOI. The LOI mice developed twice as many intestinal tumors as did controls, and their normal intestinal epithelium was shifted toward a less differentiated state, a pathological change also detected in humans with LOI. Thus, epigenetic changes may affect cancer risk by altering the maturational state of the normal tissue from which tumors arise.

T. rex Gets Soft

The fossil record contains some spectacular examples of the fossilization of soft tissues of animals and plants. Usually, and particularly in fossils more than a few million years old, however, these are preserved as impressions or by mineralization, for example, in petrified wood. **Schweitzer *et al.*** (p. 1952; see the news story by **Stokstad**) now report the remarkable preservation of soft cellular tissues in the interior of several *T. rex* and other dinosaur bones. These include soft, pliable, and translucent blood vessels and osteocytes associated with collagen in the bones.

CREDIT: SCHWEITZER *ET AL.*

Arming Sticklebacks

Parallel evolution is seen in sticklebacks that colonized freshwater streams and lakes around the world at the end of the last ice age 10,000 to 20,000 years ago. A common change in freshwater variants is loss of the extensive body armor of marine species. A single major locus controls the armor phenotype. **Colosimo *et al.*** (p. 1928; see the Perspective by **Gibson**) now show that the gene primarily responsible for these changes is *ectodysplasin*, and that almost all low-armor populations share a common ancestry for this gene. However, this is not because a single low-armor population migrated around the globe. Instead, the low armor allele of *ectodysplasin*, which originated well before the last ice age, is present cryptically and at a low frequency in armored sticklebacks. Thus, the parallel evolution for low armor seen worldwide has been due to repeated local selection for the low-armor allele brought into freshwater environments by marine founders.

Leading and Lagging

A vigorous debate has been waged about whether rapid climate changes were triggered by shifts between distinct ocean circulation states, or whether changes in the location and strength of deepwater formation were driven by climate. **Piotrowski *et al.*** (p. 1933; see the news story by **Kerr**) analyzed the Nd-isotopic compositions of the iron and manganese oxides (a proxy for deep ocean circulation) of two cores from Cape Basin in the southeast Atlantic Ocean, and compared them to the carbon isotopic composition of benthic foraminfers (a proxy for climate and the global carbon cycle) from the same cores. They found that, during both the last glaciation and the last deglaciation, the global carbon budget changed before ocean circulation strengthened. This lead-lag relationship is not observed during the abrupt millennial warming events during the last ice age, indicating that ocean circulation could have been be a trigger for them.

High-Energy Milky Way

The Milky Way Galaxy is full of high-energy emissions, produced by pulsars, supernovae, and unknown sources. **Aharonian *et al.*** (p. 1938) used the High Energy Stereoscopic System (HESS) of four telescopes arrayed in Namibia to search for the highest energy gamma-ray emissions (energies greater than 10^{12} electron volts) in the central part of the Galaxy. They found eight new high-energy emitters, some of which are associated with pulsar wind nebulae or supernova remnants. Determining the source of these emissions and understanding the mechanisms that lead to these highest energy particles will eventually help to resolve the mystery of the source of the Galactic cosmic rays that bombard Earth.

A Capacity for Sensing

Electrical detection can greatly simplify gas sensing. For low-power applications, chemicapacitors, which detect gases through changes in dielectric constant, can offer higher stability than sensors based on chemiresistive polymers. However, the response times of chemicapacitors can be slow (on the order of minutes to respond and recover). **Snow *et al.*** (p. 1942) show that response times can be reduced to the order of a few seconds for common organic vapors by using single-walled carbon nanotubes as one of the electrodes. Fringing fields that radiate from the nanotube's surface polarize adsorbed molecules and enhance the capacitive response. The coatings used to make the device chemically selective can thus be made thinner, which decreases diffusion limitations and improves the response times.

Remote Interference

Atoms in a Bose-Einstein condensate (BEC) have the property of all being in the same phase. The phase difference of two separate BECs can be measured by allowing the clouds of atoms to collide, thereby producing an interference pattern in the atom density. Using the associated wavelength of such atomic ensembles has already been demonstrated in sensitive interferometric measurements and metrology. However, colliding the separate BECs has so far been a destructive process. **Saba *et al.*** (p. 1945; see the Perspective by Javanainen) use light scattering to couple a small portion of the atoms from each BEC and show that an interference pattern can be produced. The almost nondestructive technique should provide a method to continuously probe the phase difference between two spatially separate BECs without the need to destructively split and collide the atomic clouds.

Feeding the Five Trillion

More prokaryotic cells are present in the gut microflora than there are eukaryotic cells in the human body, but almost nothing is

CONTINUED ON PAGE 1837

known about their contribution to their host. **Sonnenburg *et al.*** (p. 1955) reveal that a prominent gut occupant *Bacteroides thetaiotaomicron* harvests otherwise indigestible nutrients from our diet contents such as plant polysaccharides until that supply is exhausted. Then the bacteria can turn to the host's mucopolysaccharide secretions to supplement their energy supply. Thus, although the floral composition tends to stay constant, its metabolic activities shift according to energy supply.

Conformational Signaling

In bacteria, sigma σ^{54} factors that bind to core RNA polymerase (RNAP) are required for specific promoter recognition and initiation of transcription. Unlike holoenzymes containing other σ^{54} factors, σ^{54}-RNAP is transcriptionally silent until it binds to an ATP-dependent activator protein. Now **Rappas *et al.*** (p. 1972) have determined a 20 Å resolution cryo-electron microscopy structure of σ^{54} in complex with the binding domain of its activating protein [$PspF_{(1-275)}$] containing an ATP transition-state analog. Combining this with a 1.8 Å crystal structure of apo PspF, comparison to an alternative conformation of a homologous activator (NtrC1) and mutational analysis, they suggest that nucleotide hydrolysis transmits a conformational signal that frees two loops to interact with σ^{54}.

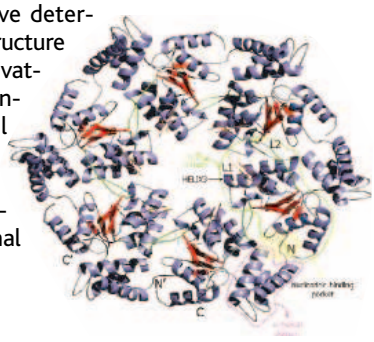

CREDIT: RAPPAS *ET AL.*

Top Dog?

The role of apex predators in ecological communities and the potential ubiquity of resulting "trophic cascades," have led to the idea that the world is green because predators limit herbivores, protecting plant communities from restriction by herbivory. **Croll *et al.*** (p. 1959) studied seven Aleutian Islands on which Arctic foxes were introduced long ago for the fur trade, and seven that remained fox-free. Foxes preyed on the native seabirds, thereby reducing the import of guano, changing soil fertility, and inducing major changes in the plant community. Fertilization of plots on an island with foxes allowed the vegetation to change to resemble that of fox-free islands. Thus trophic cascades have the capacity for effects beyond the immediate food web, and connectivity exists between marine and terrestrial ecosystems.

Modeling Gene Regulation

Modeling gene regulation is a fundamental goal in systems biology (see the Perspective by **Isaacs *et al.***). **Rosenfeld *et al.*** (p. 1962) combine modeling with experiments in their analysis of gene networks. The quantitative function relating transcription factor concentration and gene factor production is termed Gene Regulation Function (GRF). Biochemical parameters, noise, and cellular states affect the GRF. Noise in gene expression results from fluctuations in factors such as mRNA and protein abundance and environmental conditions. **Pedraza and van Oudenaarden** (p. 1965) now model and test networks in which gene interactions are controlled and quantified in single cells. Quantitation of noise propagation will assist in understanding the complex dynamics of gene networks in prokaryotic and eukaryotic systems and will assist in designing synthetic networks.

Biochemical Prehistory

The transition from an early RNA-based biochemistry to one that was (and is) based on proteins required a set of components that could convert the nucleic acid code for amino acids into the actual amino acid. The set of aminoacyl–transfer RNA (aa-tRNA) synthetases does just that, attaching the amino acid to its cognate tRNA, which is then used by the ribosome to translate the genetic code into proteins. There is, however, evidence that some of the 20 canonical amino acids are relative latecomers, and **Sauerwald *et al.*** (p. 1969) show that cysteine may be one of these add-ons. Archaea that lack the aa-tRNA synthetase for cysteine rely on an alternative pathway (likely a relic) in which phosphoserine is attached to tRNA and then enzymatically converted in an anaerobic, pyridoxal phosphate–dependent reaction to cysteinyl-tRNA.

Cancers of the Gut and Western Ills

In their well-known 1981 review on the causes of cancer in the United States, Doll and Peto* estimated that around one-third of deaths from cancer could be attributed to diet and were therefore, in principle, preventable. Epidemiological evidence continues to support this general conclusion, but in contrast to cardiovascular disease, for which the link to nutrition is now generally recognized, the relationship between diet and cancer has made much less impact on both policy-makers and the general public. One reason for this is the absence of any single hypothesis on which to build a dietary strategy for cancer prevention; this itself is a reflection of the complexity of human diets and the obvious fact that cancer is not a single disease. Although there has been huge progress in our understanding of the molecular basis of many cancers in recent years, most of the new knowledge has been deployed in the search for new therapies rather than to understand the role of nutrition in their causation. Nevertheless, the mechanisms linking diet to cancer can be understood and exploited for prevention as much as for treatment, and there are sound scientific and strategic reasons to focus such research on carcinomas of the alimentary tract.

The hypothesis that "overnutrition" increases the risk of bowel cancer is supported by studies within the populations of the developed world, where overconsumption of energy, low levels of physical activity, high body mass index, and abdominal obesity are strong independent risk factors for colorectal carcinoma, much as they are for insulin resistance and cardiovascular disease. A similar link to obesity has been established for esophageal adenocarcinoma, once the rarest form of cancer of the esophagus but now advancing rapidly throughout North America and Western Europe.

What do we know about the links between gut-related cancer progression and diet? Although mutagens are present in foods and feces at low concentrations, there is little evidence that the adverse effects of diet on alimentary cancers in the West are caused by food-borne carcinogens that can be identified and eliminated from the food chain. It seems more plausible that the Western gut becomes vulnerable to neoplasia because of adverse metabolic factors, such as pro-inflammatory agents produced by adipose tissue, and because of low intakes of anticarcinogens from plant foods. The chronic use of aspirin and other nonsteroidal anti-inflammatory drugs significantly reduces the risk of colorectal and esophageal cancers, perhaps by inhibiting the expression of the pro-inflammatory enzymes in precancerous tissues. Both diseases are also less common among consumers of diets rich in fruits and vegetables, which harbor a huge variety of biologically active secondary metabolites such as glucosinolates and flavonoids, which may act synergistically in the human diet.

There are profound and fascinating biological problems to be solved in the search for the links between nutrition and cancer, and the human digestive tract is likely to prove an immensely rewarding focus for future research. Meanwhile, carcinomas of the gut are among the most common causes of morbidity and death from cancer in the developed world. The role of weight, lack of exercise, and inadequate consumption of plant foods in their etiology needs to be more widely acknowledged and publicized.

Ian T. Johnson

Ian T. Johnson is head of the Gastrointestinal Biology and Health Programme at the Biotechnology and Biological Sciences Research Council's Institute of Food Research, Norwich, UK.

*R. Doll, R. Peto, *J. Natl. Cancer Inst.* **66**, 1191 (1981).

10.1126/science.1111871

EDITORS' CHOICE

edited by Gilbert Chin

APPLIED PHYSICS

Imaging Surface Plasmons

The drive to integrate optics with nanoelectronics presents a number of problems, one of which is the several orders of magnitude mismatch in the size of the respective components. For example, optical waveguides are typically of micrometer size, whereas active structures such as quantum dots tend to measure only several nanometers. Surface plasmons, which are coupled excitations of light and electrons that propagate on metallic surfaces and that are much smaller than the photon wavelength, are one route being pursued to bridge this gap in scale. Tetz *et al*. present an imaging technique for studying the excitation and propagation of surface plasmons. The ability to observe directly how these excitations propagate should provide an important step forward in coupling them to nanoscale structures. — ISO

Appl. Phys. Lett. **86**, 111110 (2005).

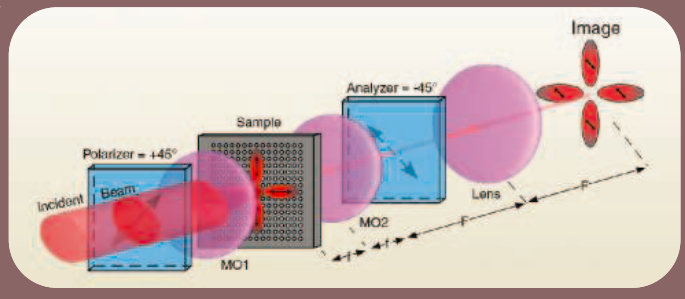

Imaging surface plasmon propagation.

GEOCHEMISTRY

Dating Service

Radiocarbon dating is the preeminent method for determining the age of carbonaceous materials younger than about 50,000 years. The determination of accurate calendar ages from radiocarbon ages requires a calibration curve, though, because the production of ^{14}C and its distribution between atmospheric, oceanic, and terrestrial carbon reservoirs both vary with time.

Charged with the task of producing the official calibration curve for terrestrial radiocarbon dating, the IntCal working group has just released the latest version, IntCal04. Reimer *et al*. present this new curve, which replaces the previous version that has been in effect since 1998. IntCal04 extends the calibration backward by 2000 years, to 26,000 calendar years before the present (cal yr B.P., where the present is defined as 1950), increases the resolution of the period earlier than 11,400 cal yr B.P., and considers the uncertainty in both the calendar age and the ^{14}C age in the calibration. Tree ring data contribute the bulk of the ages in the interval between today and 12,400 cal yr B.P., and marine data from corals and foraminifera provide the calibration for samples older than 12,400 years. Associated papers in the same issue describe the details of this impressive and valuable achievement. — HJS

Radiocarbon **46**, 1029 (2005).

MICROBIOLOGY

Taking the Low Road

Listeria monocytogenes bacteria are well known among cell biologists for their spectacular hijacking of the actin cytoskeleton early after infection, which enables them to zoom around inside target cells, propelled by actin comet tails. At later stages of infection, *Listeria* use another clever strategy to spread between host cells without risking exposure to the host immune system: They invade neighboring cells by inducing bacteria-containing cellular protrusions that somehow transfer the bacteria to the neighboring cell without it ever being exposed to the extracellular milieu.

Pust *et al*. examined the process of cell-cell transfer of *Listeria* and found that in addition to the actin cytoskeleton, the bacteria exploit the cellular protein ezrin, which functions as a plasma membrane–cytoskeleton linker. Interfering with the phosphorylation of ezrin leads to short collapsed protrusions that fail to deliver bacteria efficiently between cells. — SMH

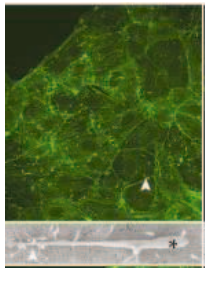

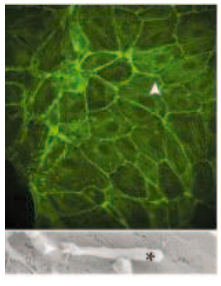

***Listeria* (small green rods) spread into the middle of a cell monolayer (left) via extended protrusions (lower left) unless (right) ezrin cannot be phosphorylated and the protrusions are attenuated (lower right).**

EMBO J. 10.1038/sj.emboj.7600595 (2005).

IMMUNOLOGY

A Signal for Suppression

T cells with a dedicated regulatory function (T-reg) maintain a crucial balance in immune responses and prevent autoimmune responses by effector T cells. Although the cytokine transforming growth factor–β (TGF-β) is central to T-reg cell activity, key questions remain about how T-reg cells use this mediator.

Fahlén *et al*. explored the role of TGF-β using a model of colitis, in which pathogenic T cells induce severe intestinal inflammation after transfer to healthy lymphocyte-deficient mice; the inflammatory response can be suppressed if T-reg cells are cotransferred. In animals that received pathogenic T cells expressing a nonfunctional TGF-β receptor, T-reg cells were unable to prevent colitis, demonstrating that pathogenic effector T cells must receive TGF-β signals directly. However, the critical source of TGF-β appeared not to be the T-reg cells themselves, indicating that TGF-β is furnished by a distinct population of cells and that the role of T-reg cells is to provide an unidentified signal that acts in conjunction with TGF-β. Furthermore, in the absence of TGF-β, T-reg cells developed normally and retained the ability to suppress effector T cells. These results address the function and source of TGF-β in T-reg cell activity and point to unexplored pathways involved in mediating regulatory events. — SJS

J. Exp. Med. **201**, 737 (2005).

CONTINUED ON PAGE 1843

CHEMISTRY

A Boron Bridge

Boron compounds have been of continued fundamental interest because of their tendency to adopt unusual electron-deficient bonding. Unlike carbon, boron can form so-called 3-center, 2-electron bonds with two other atoms. Braunschweig *et al.* have now coaxed boron into a different arrangement, which resembles that of the central carbon in allene. They prepared two compounds in which a lone B atom bridges two transition metal centers: a pentamethylcyclopentadienyl iron dicarbonyl on one side, and either iron tetracarbonyl or chromium pentacarbonyl on the other. X-ray crystallography confirmed an essentially linear bridge structure in both compounds. Density functional theory suggests that the boron forms a traditional 2-electron σ bond with each metal, as well as a partial π bond. Similar compounds have been prepared with the heavier group 13 elements (gallium and thallium), but in those cases π bonding is absent. — JSY

Angew. Chem. Int. Ed. **44**, 1658 (2005).

ECOLOGY/EVOLUTION

The Difference a Week Makes

Migration is well established as a mechanism by which animals cope with seasonal variations in food supply. It is has also been suggested as a possible way of reducing the burden of parasitism in a range of hosts, either by weeding out infected individuals or by allowing them to escape from environments in which parasites have accumulated. Bradley and Altizer provide evidence that one of the more spectacular examples of migration—that of the monarch butterfly in the North America—may have evolved at least in part as such a mechanism.

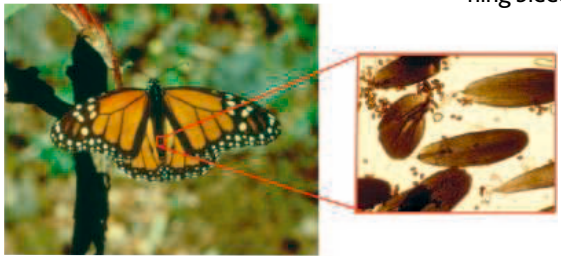

Parasite spores (right, small ovoids) among abdominal scales (right, large ovals) of the monarch (left).

CREDITS: BRADLEY AND ALTIZER, *ECOL. LETT.* **8**, 290 (2005)

Not all monarch populations migrate, and parasite prevalence is known to be lower in the migratory monarch populations. Butterflies from migratory populations inoculated with a protozoan parasite showed reductions in flight performance and endurance in experimental cages, probably because the parasite influenced metabolic processes associated with flight (there were no changes in wing morphology associated with the presence of the parasite). The authors estimate that the impairment would lengthen the migratory journey from 9 to 10 weeks. Under these conditions, parasitized butterflies would likely suffer a reduced chance of reaching their destination, thus accounting for the differences in parasite burden between migrant and nonmigrant monarchs. Because habitat loss and climate change are expected to affect migrant populations more severely, the prevalence of parasites is likely to increase. — AMS

Ecol. Lett. **8**, 290 (2005).

BEHAVIORAL SCIENCE

First In, Last Out

In a first-price auction, players submit sealed bids for a known item, which is then sold to the highest bidder at the price of that bid. In a seller's English clock auction, the initial price is high and decreases at a steady rate; players choose not to buy by exiting, and the auction ends when the item is sold to the last player at the price at which the penultimate player exited.

Berg *et al.* have modified these two types of auction protocols to explore risk-phobic and risk-philic behavior of subjects. In their version of the first-price auction, the winning bidder is then awarded a monetary sum equal to the difference between the resale price of the item and their bid (generally less than the resale price); for the English clock auction, the last player receives a sum equal to the sale price, whereas the other players receive the same sum but only with a known, non-zero probability (i.e., in some cases they would receive nothing). The authors find that subjects in the first-price auction do not risk making low bids in the hope of gaining a larger payoff and do, in fact, place their bids somewhere between the risk-neutral threshold and the actual resale price. However, in the English clock auction, subjects are more apt to play the gamble, so that they exit the auction earlier than expected value would predict. — GJC

Proc. Natl. Acad. Sci. U.S.A. **102**, 4209 (2005).

www.sciencemag.org

Science

1200 New York Avenue, NW
Washington, DC 20005
Editorial: 202-326-6550, FAX 202-289-7562
News: 202-326-6500, FAX 202-371-9227

Bateman House, 82-88 Hills Road
Cambridge, UK CB2 1LQ
+44 (0) 1223 326500, FAX +44 (0) 1223 326501

Subscription Services For change of address, missing issues, new orders and renewals, and payment questions: 800-731-4939 or 202-326-6417, FAX 202-842-1065. Mailing addresses: AAAS, P.O. Box 1811, Danbury, CT 06813 or AAAS Member Services, 1200 New York Avenue, NW, Washington, DC 20005

Institutional Site Licences please call 202-326-6755 for any questions or information

Reprints Ordering/Billing/Status 800-635-7171; Corrections 202-326-6501

Permissions 202-326-7074, FAX 202-682-0816

Member Benefits Bookstore: AAAS/BarnesandNoble.com bookstore www.aaas.org/bn; Car purchase discount: Subaru VIP Program 202-326-6417; Credit Card: MBNA 800-847-7378; Car Rentals: Hertz 800-654-2200 CDP#343457, Dollar 800-800-4000 #AA1115; AAAS Travels: Betchart Expeditions 800-252-4910; Life Insurance: Seabury & Smith 800-424-9883; Other Benefits: AAAS Member Services 202-326-6417 or www.aaasmember.org.

science_editors@aaas.org (for general editorial queries)
science_letters@aaas.org (for queries about letters)
science_reviews@aaas.org (for returning manuscript reviews)
science_bookrevs@aaas.org (for book review queries)

Published by the American Association for the Advancement of Science (AAAS), *Science* serves its readers as a forum for the presentation and discussion of important issues related to the advancement of science, including the presentation of minority or conflicting points of view, rather than by publishing only material on which a consensus has been reached. Accordingly, all articles published in *Science*—including editorials, news and comment, and book reviews—are signed and reflect the individual views of the authors and not official points of view adopted by the AAAS or the institutions with which the authors are affiliated.

AAAS was founded in 1848 and incorporated in 1874. Its mission is to advance science and innovation throughout the world for the benefit of all people. The goals of the association are to: foster communication among scientists, engineers and the public; enhance international cooperation in science and its applications; promote the responsible conduct and use of science and technology; foster education in science and technology for everyone; enhance the science and technology workforce and infrastructure; increase public understanding and appreciation of science and technology; and strengthen support for the science and technology enterprise.

Information for Contributors

See pages 135 and 136 of the 7 January 2005 issue or access www.sciencemag.org/feature/contribinfo/home.shtml

Every day, 1,600 children die of HIV/AIDS… their lives cut short.

12 million children have been **orphaned by HIV/AIDS** in sub-Saharan Africa alone—who will raise them?

Last year, 1 million African schoolchildren **lost their teachers** to HIV/AIDS[1]—who is going to teach these children?

Up to 20% of the nurses in South Africa are HIV positive[2]—**who will care for the children?**

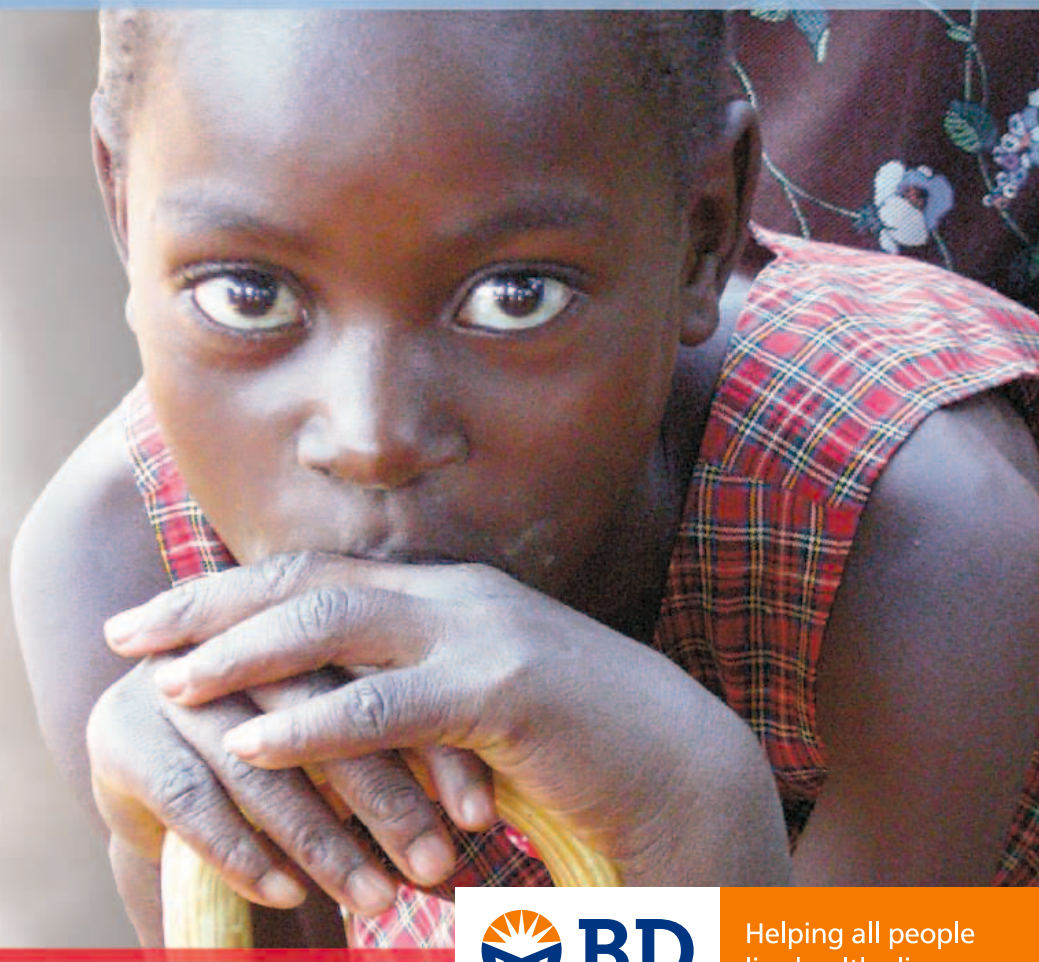

Save the Children®

GBC
GLOBAL BUSINESS COALITION ON HIV/AIDS

CLINTON HIV/AIDS INITIATIVE

iavi
International AIDS Vaccine Initiative

BD

Helping all people live healthy lives

Partners in the battle against HIV/AIDS

The impact of HIV/AIDS on children is nearly incomprehensible. A crisis of this magnitude requires an assault on many fronts.

BD, a medical technology company, is privileged to fight for future generations with partner organizations across the healthcare and policy spectrum.

Working to discover vaccines to prevent infection, the International AIDS Vaccine Initiative is using a $1 million BD gift, as well as the BD FACSCalibur™ flow cytometry system.

For those infected with HIV, the William J. Clinton Presidential Foundation is enabling providers to access affordable CD4 immunocytometry tests from BD.

With Save the Children, BD donates medical supplies and money to establish clinics in Eurasia, where infection rates are rising faster than anywhere else in the world.

Because in developing countries the reuse of injection devices is a significant cause of disease transmission, BD is working with the United Nations and nongovernmental organizations to help ensure that childhood immunizations and other injections are administered safely.

In addition, through its active association with the Global Business Coalition on HIV/AIDS, BD is helping to mobilize businesses in the fight against AIDS.

BD—selected as one of America's Most Admired Companies by *FORTUNE* magazine[3]—is proud to partner with these and other organizations to protect life by addressing fundamental healthcare issues in every corner of the world.

BD—Helping all people live healthy lives.

Please visit www.bd.com.

[1] UNAIDS statistics, 2000, 2003.

[2] *Nursing World*.

[3] "America's Most Admired Companies" annual survey, 2005; *FORTUNE* magazine, March 7, 2005.

Photo ©Gary Cohen

NetWatch

edited by Mitch Leslie

IMAGES

Neurons on Display

The Cell Centered Database from the University of California, San Diego, is a destination for everyone from anatomists charting the nuances of neuron branching to modelers hoping to devise more realistic cell simulations. Launched in 2002, the archive houses images, reconstructions, and models of nerve cells of brain neurons based on microscopy data, including confocal and electron. The site helps fill the gap between gene and protein databases and those holding images of larger brain structures, says project leader Maryann Martone. Visitors can access images and raw data on more than 30 nervous system cells. The colors in this image (above), for instance, indicate the different dendrite segments in a Purkinje neuron from a rat's cerebellum. The listings also include measurements such as the cell's surface area and the lengths of major branches. So far the archive only encompasses nerve cells, but Martone and colleagues will soon add mitochondrial data.

ccdb.ucsd.edu/CCDB/index.shtml

EXHIBITS

Lakota Timekeeping

Today, photos, videos, history books, and newspaper archives help us hold on to the past. The Lakota people of the U.S. Great Plains relied on their memories and on winter counts, illustrated calendars that feature an evocative drawing for each year. Visitors can peruse a collection of winter counts and anthropologists can analyze their iconography at this new exhibit from the Smithsonian Institution. The records served as mnemonics, helping Lakota oral historians keep events in the right order. The symbol the count keeper chose to represent a particular year depicted an occurrence that everyone would recall. The site lets users scroll through 10 counts covering mainly the 18th and 19th centuries, such as the one kept by Battiste Good, a Lakota in South Dakota. Click on the drawings to read a description of what happened during those years. The 1849 symbol (above) in Good's count records an attack on a Crow man disguised as a woman, and the 1850 illustration shows Crow warriors taking refuge on a butte after a reprisal raid.

www.wintercounts.si.edu

DATABASE

Foundations of Fertility

A female mouse can ovulate a fresh batch of eggs about every 4 to 6 days. To learn more about the genes that sustain egg production and orchestrate other ovarian functions, click on this collection from researchers at Stanford University. The Ovarian Kaleidoscope Database describes more than 1800 genes that work in the ovaries of humans, mice, rats, and other animals. Entries indicate the gene's function, where it's active in the ovary, what controls its expression, the effects of particular mutations, and more. Links lead to additional information about the gene's structure and its roles in biochemistry and diseases.

ovary.stanford.edu

LINKS

Stuck on Sugars

Like many unsuccessful dieters, the proteins called lectins are drawn to carbohydrates. The molecules, which range from the poison ricin to infection-squelching compounds in the blood, glom onto sugars and kindred substances. Delve into the world of lectins with this sprawling collection of some 2000 links from Thorkild Bøg-Hansen of the University of Copenhagen in Denmark. A primer on lectins introduces groups such as the collectins, which recognize carbohydrates in bacterial cell walls and rouse the body's defensive proteins. Visitors can also scan a database with 3D lectin structures or read up on the lectin in kidney beans that occasionally causes food poisoning.

plab.ku.dk/tcbh/lectin-links.htm

COMMUNITY SITE

Herp Haven

How many species of corn snakes are slithering around the United States? Were any new kinds of salamanders discovered last year? Catch up on the latest developments in reptile and amphibian taxonomy at the Center for North American Herpetology, headed by Joseph Collins of the University of Kansas, Lawrence. There you can check the standard scientific and common names for 596 species of reptiles and amphibians—including the two species of corn snakes, one of which scientists recognized only in 2002. The site announces newly described species and records classification and nomenclature updates for existing ones. Above, the striking gray-banded king snake (*Lampropeltis alterna*) of Texas and Mexico.

www.cnah.org/index.asp

Send site suggestions to netwatch@aaas.org. Archive: www.sciencemag.org/netwatch

CREDITS (TOP TO BOTTOM): MARYANN MARTONE/UC SAN DIEGO; SUZANNE L. COLLINS/THE CENTER FOR NORTH AMERICAN HERPETOLOGY; NATIONAL ANTHROPOLOGICAL ARCHIVES/SMITHSONIAN INSTITUTION

This Week

PAGE 1852
T. rex's inner plumbing

1855
A cheap, portable MRI?

PALEOANTHROPOLOGY

Discoverers Charge Damage to 'Hobbit' Specimens

Yet another skirmish has erupted in the battle over the bones of the "hobbit," the diminutive hominid found in the Indonesian island of Flores and last year announced as a new species of human, *Homo floresiensis*. Late last month the 18,000-year-old bones were returned to their official home, the Center for Archaeology in Jakarta, after being borrowed by Indonesia's most prominent paleoanthropologist Teuku Jacob of Gadjah Mada University in Yogyakarta (*Science*, 4 March, p. 1386). Now archaeologist Michael Morwood of the University of New England (UNE) in Armidale, Australia, leader of the team that discovered the bones, charges that the specimens were seriously damaged in transit or while in the Yogyakarta lab. Jacob insists that the bones were intact when they left his lab, and that any damage must have occurred when they were no longer under his care.

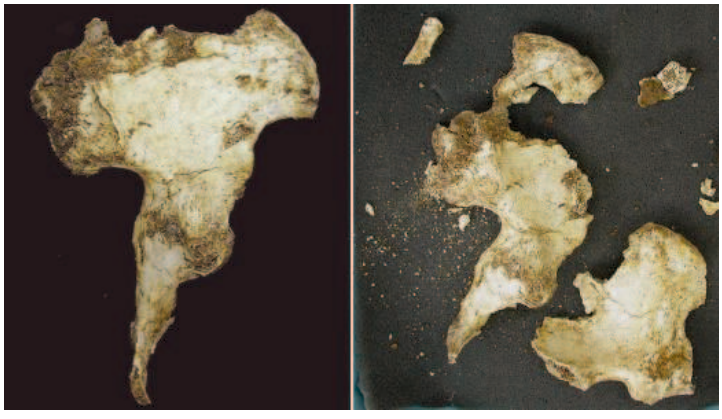

Broken bones. The Flores hominid pelvis before transport, and after.

Morwood says the left side of the pelvis—which he calls one of the hominid's most distinctive features—was "smashed," perhaps during transport. He and his UNE colleague, paleoanthropologist Peter Brown, also say that at least one Silastic mold was apparently taken of some of the delicate bones, which were described as the consistency of "wet blotting paper" when found. The molding process caused breakage and loss of anatomic detail in the cranial base of the skull and jawbone, they say. Morwood adds in an e-mail that a second, still-unpublished jawbone "broke in half during the molding process and was badly glued back together, misaligned, and with significant loss of bone."

Jacob strongly denies that the bones suffered any damage—"at least not in our lab. We have photographs, taken on the last day, and [the bones are] not damaged," he told *Science*. "They used a suitcase [to carry the bones back to Jakarta]," he adds. "I do not use this to transport fossils; we use special bags to carry bones."

Jacob, who says his lab is the only one in Indonesia set up for paleoanthropological analysis, says researchers made a mold and one cast of the skeleton, but that it was "impossible" for the procedure to have damaged the bones. He adds that his team reconstructed some of the remains, putting pieces together in order to study them, because this had not yet been done.

Paleopathologist Maciej Henneberg of the University of Adelaide in Australia says the bones, including the left side of the pelvis, were intact when he viewed them in Yogyakarta on 17 February. He adds that "Professor Jacob's laboratory has decades of experience caring for fossils, and I would be surprised to learn that if they made a mold it would damage the bones," an opinion echoed by paleoanthropologist Jean-Jacques Hublin of the Max Planck Institute for Evolutionary Anthropology in Leipzig, Germany, who visited Jacob in January.

Wherever the damage to the pelvis occurred, says Brown, "the most important point is that it was too fragile to move in the first place. [It] should never have left Jakarta."

–ELIZABETH CULOTTA

ETHICS

Doctors Pay a High Price for Priority

AMSTERDAM—The drive for priority may have gotten doctors at an academic hospital in the Netherlands in trouble with the law. Several were so intent on publishing the first report on the re-emergence of a rare sexually transmitted disease in 2003, a government agency says, that they did not convey their findings to health authorities while an article was in press, squandering a chance to limit the international spread of the disease. According to a report from the Dutch Health Care Inspectorate last week, the authors violated a law requiring hospitals to report unusual outbreaks immediately.

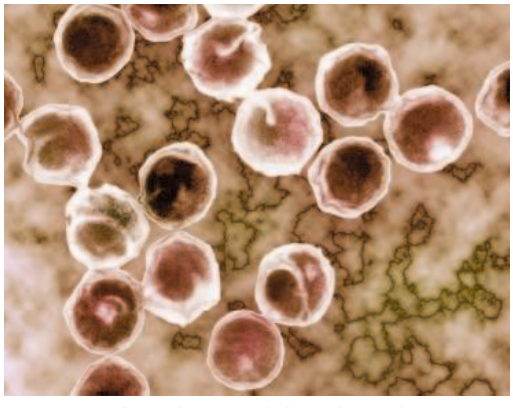

Unreported. Authorities did not hear about a rare *Chlamydia trachomatis* outbreak.

The report describes the 2003 discovery of an outbreak of *Lymphogranuloma venereum* (LGV) in gay and bisexual men in the Netherlands, many of them infected with HIV. LGV, which can produce painful ulcers and swelling of the lymph nodes, is caused by certain types of the microbe *Chlamydia trachomatis*. When treated with the right antibiotics, LGV can be cured completely; it is prevalent in the tropics but almost never seen in the Western world.

That changed in December 2003, however, when a group led by Martino Neumann at Erasmus Medical ▶

CREDITS (TOP TO BOTTOM): PETER BROWN/UNIVERSITY OF NEW ENGLAND; DAVID PHILLIPS/VISUALS UNLIMITED

Center in Rotterdam published a case study about a single patient with LGV in *Sexually Transmitted Infections*. Shortly afterward, Dutch public health authorities, who had not heard about the case, issued an international alert. Since then, more than 200 cases of LGV have been found in the Netherlands, Germany, France, the United Kingdom, and the United States.

The warning could have come 6 to 8 months earlier, according to the Dutch health inspectors. The Erasmus group saw its first patient in January 2003 and the second in April, and then traced more than a dozen others during the course of 2003. Although some members repeatedly proposed reporting the cluster to the Municipal Health Service, the report says, the group failed to do so—out of "fear that others would run with the data and publish about the matter first." The result, it says, "in all likelihood [was] a much wider spread of the infection" than necessary.

LGV is not a notifiable disease in the Netherlands, but the inspectors say that the group broke article 7 of the Dutch Infectious Diseases Law, which obliges the heads of certain institutions to report any unusual clusters of possibly infectious diseases. The report puts most of the responsibility on two doctors, identified only as the "department head of the department of dermatology and venereology" and the "medical head of the STD clinic," although the latter was not a co-author on the paper. A spokesperson says the inspectorate will file a complaint with the Dutch Medical Disciplinary Board citing these two, as well as a former head of the clinic who acted as a consultant.

In a statement, Erasmus Medical Center said it believes the delay did not endanger public health. The statement welcomed the disciplinary procedure—"even if it is aggravating to the staff members concerned"—because it could bring clarity about reporting requirements under Dutch law.

Sexually Transmitted Infections, which accepted the LGV manuscript on 21 July 2003, didn't instruct the team not to report the findings to health authorities, says that journal's editor, Helen Ward of Imperial College in London. Indeed, no medical journal would do that, says former *New England Journal of Medicine* editor Arnold Relman: "Clearly, public health should always come first."

–MARTIN ENSERINK

CAREER TRANSITIONS

Panel Throws Lifeline to Bio Postdocs

For years, postdoctoral scholars have complained that they receive too little help in making the crucial transition from trainee to independent investigator. Last week a new report by the National Academies suggested shoring up that support in ways that might benefit the entire biomedical community.

The report, from a panel chaired by Howard Hughes Medical Institute president Thomas Cech, asks the National Institutes of Health (NIH) to create individual awards and training grants for postdocs that would make them less dependent on their principal investigators. It recommends allowing foreign postdocs to apply for training awards that are currently open only to U.S. citizens and permanent residents. And it suggests limiting the length of postdoctoral training to 5 years, regardless of a postdoc's source of funding.

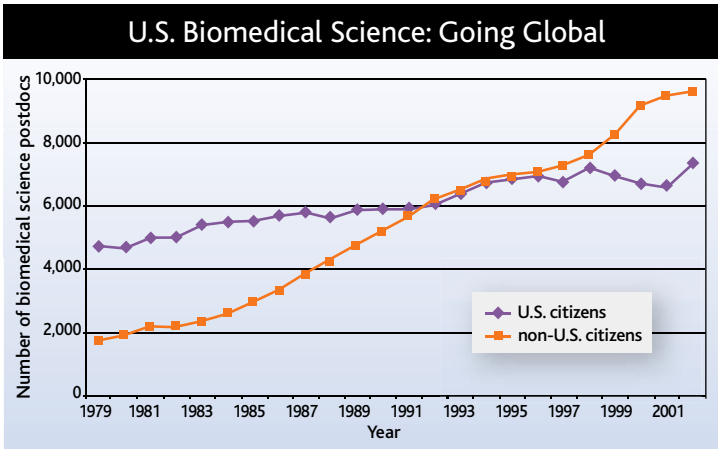

Melting pot. A new report says foreign-born postdocs, a rising share of the pool, should also be eligible for the NRSA program.

The cost of implementing these recommendations could strain an NIH budget that is no longer growing rapidly. But NIH Director Elias Zerhouni seems willing to give them a try. "There's no wrong time to do the right thing," he says.

One recommendation that's already under consideration is to create starter grants for investigators who have a research idea but no preliminary findings to include in their proposal (*Science*, 25 June 2004, p. 1891). Such applications would be reviewed separately from those proposals, called R01s, submitted by established investigators. Another recommendation, without a price tag, would require senior grant applicants to provide a detailed plan for mentoring their postdocs. That change would force "investigators to think about the careers of young researchers in their laboratory instead of just using them as scientific labor," says Cech.

Two of the panel's recommendations—waiving the citizenship requirement for the National Research Service Awards (NRSA) and other postdoctoral training awards, and shifting money from R01s into career development awards—could well face significant opposition. "Making federal support available to those who are not U.S. citizens or permanent residents can be controversial," the report says about the NRSA program. "But … those who would receive such training awards are likely already supported on research grants and are critical to advances in U.S. biomedical research." One panelist who requested anonymity noted that a 1998 academies report also called for tapping the R01 pot to fund early-career grants. "It didn't go anywhere," she says.

Zerhouni praised other recommendations in the report as being consistent with his belief that NIH should be doing more to nurture the creativity of young scientists. One would expand a small program at several institutes by setting up 200 agencywide career transition awards each worth $500,000. Another would award renewable R01-like grants, with a cap of $100,000 in indirect costs, to university researchers not on the tenure track.

Offering independent awards to investigators early in their careers, he says, sends the message that NIH wants them to "show us what you can do." The goal, he adds, is to avoid a situation in which a young scientist regrets not having the chance to demonstrate that "I coulda been a contender."

–YUDHIJIT BHATTACHARJEE

SOURCE: THE NATIONAL ACADEMIES AND BLS

SCIENTIFIC MISCONDUCT

Researcher Faces Prison for Fraud in NIH Grant Applications and Papers

In the most extensive scientific misconduct case the National Institutes of Health (NIH) has seen in decades, a researcher formerly at the University of Vermont College of Medicine in Burlington has admitted in court documents to falsifying data in 15 federal grant applications and numerous published articles. Eric Poehlman, an expert on menopause, aging, and metabolism, faces up to 5 years in jail and a $250,000 fine and has been barred for life from receiving any U.S. research funding.

Scientists say the falsified data—including work in

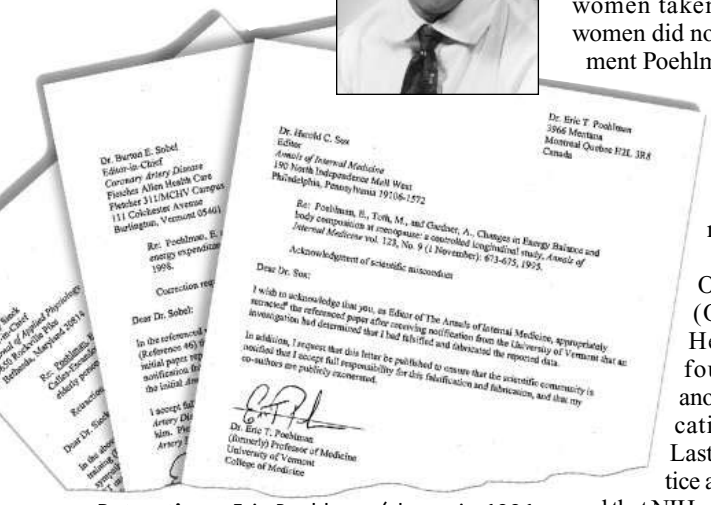

Retractions. Eric Poehlman (shown in 1991 photo) has notified journals about 10 papers that required retractions.

10 papers for which Poehlman has requested retractions or corrections—have had relatively little impact on core assumptions or research directions. But experts say the number and scope of falsifications discovered, along with the stature of the investigator, are quite remarkable. "This is probably one of the biggest misconduct cases ever," says Fredrick Grinnell, former director of the Program in Ethics in Science at the University of Texas Southwestern Medical Center in Dallas. "Very often [in misconduct cases], it's a young investigator, under pressure, who needs funding. This guy was a very successful scientist." Neither Poehlman nor his attorney returned calls from *Science*.

Poehlman, 49, first came under suspicion in 2000 when Walter DeNino, then a 24-year-old research assistant, found inconsistencies in spreadsheets used in a longitudinal study on aging. The data included energy expenditures and lipid levels for elderly patients. "[V]alues for total cholesterol, insulin, resting metabolic rate, and glucose" were falsified or fabricated, said a statement Poehlman signed last week. In an effort to portray worsening health in the subjects, DeNino tells *Science*, "Dr. Poehlman would just switch the data points."

After DeNino filed a formal complaint, a university investigative panel looked into Poehlman's research and uncovered falsified data in three papers. These included a much-cited 1995 *Annals of Internal Medicine* study that suggested hormone replacement therapy could prevent declines in energy expenditure and increases in body fat during menopause. In that paper Poehlman presented metabolic data on 35 women taken 6 years apart. Most of the women did not exist, according to the statement Poehlman signed. (In 2003 the paper was retracted.) Poehlman left Vermont in 2001, before the investigation ended, for the University of Montreal. He left there in January and now lives in Montreal.

A 2-year review by the Office of Research Integrity (ORI) at the Department of Health and Human Services found more falsified data in another dozen federal grant applications, ORI investigators said. Last week the Department of Justice announced that the total was 17, and that NIH and the U.S. Department of Agriculture had given Poehlman $2.9 million in grants based on fraudulent applications. In addition to pleading guilty to making a false statement on a federal grant application, Poehlman agreed to pay $180,000 to settle a civil suit with the government. A plea hearing and sentencing are pending.

Colleagues say Poehlman's work was extensive but did not affect underlying assumptions about how the body changes during aging. Richard Atkinson, editor of the *International Journal of Obesity*, said in an e-mail that removing Poehlman's work may reduce the evidence that energy expenditure decreases across time with menopause, but "it does not invalidate the concept." Judy Salerno, deputy director of the National Institute on Aging in Bethesda, Maryland, says his work "wasn't the final answer."

Journal editors say it's hard to guard against such misconduct. A rigorous review process can do only so much, says Harold Sox, who became *Annals*'s editor in 2001: "You just have to trust the authors." —ELI KINTISCH

CREDITS (TOP TO BOTTOM): UNIVERSITY OF VERMONT PHOTO; P. BAGLA

ScienceScope

A Numbers Game at NSF

Those upset that President George W. Bush proposed only a 2.4% increase in the 2006 budget for the National Science Foundation now have reason to believe NSF's new director, Arden Bement, is on their side. But don't ask him to talk about it.

Appearing 11 March before a House spending panel that handles NSF's budget, Bement was asked how much the agency requested last fall in its 2006 budget submission to the White House. Most officials duck the commonly asked question, but Bement, known for his straight talk, decided to answer. "To my best recollection it was 15%," he replied, a figure in keeping with an NSF authorization passed 3 years ago that would have doubled NSF's budget over 5 years. The agency actually submits "several scenarios," he told the panel, and this year the final request wound up "somewhere between the median and the low end."

Asked later for details, however, Bement told *Science* that the number "was based on a fuzzy memory." He declined to give the actual figure, citing "predecisional" negotiations with the Administration.

—JEFFREY MERVIS

India to Outlaw Animal Drug

NEW DELHI—The Indian government has decided to phase out veterinary use of a painkiller implicated in the catastrophic decline of vultures on the subcontinent. Officials are now asking farmers to replace diclofenac with alternatives, like ketoprofen and meloxicam, believed to be less toxic to the birds.

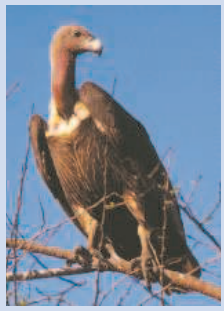

Vultures carry out an important function in the food chain. But their once-abundant numbers have dropped precipitously in the past decade, and studies in India, Pakistan, and Nepal have found the drug in dead vultures. "The only way of saving the vultures was to ban the use of the drug in animals," says Asad Rahmani, director of the Bombay Natural History Society. The decision, announced last week by Prime Minister Manmohan Singh, embraces a recommendation from the government's National Board for Wildlife, which proposed a 6-month phaseout. —PALLAVA BAGLA

GENETICS

Talking About a Revolution: Hidden RNA May Fix Mutant Genes

When it comes to plants and animals, biologists think of DNA as the sole storehouse of genetic information. But a surprising new study of the mustard plant *Arabidopsis thaliana* challenges that notion. In the 24 March issue of *Nature*, Susan Lolle and Robert Pruitt of Purdue University in West Lafayette, Indiana, and their colleagues report that in this weed, gene inheritance can somehow skip generations: Plants sometimes end up with their grandparents' good copy of a gene instead of the mutant ones belonging to their parents. The researchers put forth the radical proposal that plants contain an inheritable cache of RNA that can briefly reverse evolution, undoing mutations and restoring a gene to its former glory.

"[The paper] suggests the existence of a unique genetic memory system that can be invoked at will," says Vincent Colot of the Plant Genomics Research Unit at Genopole in Evry, France. If confirmed and extended to animals, the new findings could profoundly affect biomedicine as well as population genetics. For example, geneticists trying to assess disease risk would have to take into consideration the makeup of this RNA memory, notes Emma Whitelaw of the University of Sydney, Australia.

Mutation in reverse. RNA may undo a mutation that causes *A. thaliana* flower parts to fuse (*left*) such that offspring flowers just fine (*right*).

Pruitt and Lolle first discovered that genes could go back in time about 3 years ago while studying one in *A. thaliana* called *HOTHEAD*. In plants with both copies of *HOTHEAD* mutated, the floral parts are all stuck together into a little ball.

Typically, when such a mutant plant self-fertilizes, its progeny inherit two copies of the gene responsible for the abnormal trait. Thus, when this *Arabidopsis* strain reproduced that way, there should have been two mutant *HOTHEAD* genes passed on, and all the progeny should have had balls instead of flowers. Instead, Lolle and Pruit found that 1% to 10% of the offspring produced normal flowers, indicating that at least one copy of the mutant gene had reverted to its nonmutated form in those plants. "It's something that Mendelian genetics has not prepared us for," says Pruitt.

They tested whether the progenies' wild-type version of *HOTHEAD* had been derived from mutated ones by fertilizing a wild-type *Arabidopsis* strain with pollen from the original mutant strain. Most of the time, the offspring had the expected genetic makeup—one mutated *HOTHEAD* and one wild-type allele—and normal flowering. But 8 out of 164 embryos examined had two wild-type alleles, says Pruitt.

To ensure that wild-type seeds hadn't inadvertently gotten mixed up in their experiments, they checked the DNA of plant embryos removed directly from the *HOTHEAD* ▶

PALEONTOLOGY

Tyrannosaurus rex Soft Tissue Raises Tantalizing Prospects

It's not *Jurassic Park*–style cloning, but a remarkable find has given paleontologists their most lifelike look yet inside *Tyrannosaurus rex*—and, just possibly, a pinch of the long-gone beast itself.

On page 1952, a team led by Mary Schweitzer of North Carolina State University in Raleigh describes dinosaur blood vessels—still flexible and elastic after 68 million years—and apparently intact cells. "If we have tissues that are not fossilized, then we can potentially extract DNA," says Lawrence Witmer, a paleontologist at Ohio University College of Osteopathic Medicine in Athens. "It's very exciting." But don't fire up the sequencing machines just yet. Experts, and the team itself, say they won't be convinced that the original material has survived unaltered until further test results come in.

The skeleton was excavated in 2003 from the Hell Creek Formation of Montana by co-author Jack Horner's crew at the Museum of the Rockies in Bozeman, Montana. Back in the lab, Schweitzer and her technician demineralized the fragments by soaking them in a weak acid. As the fossil dissolved, transparent vessels were left behind. "It was totally shocking," Schweitzer says. "I didn't believe it until we'd done it 17 times." Branching vessels also appeared in fragments from a hadrosaur and another *Tyrannosaurus* skeleton. Many of the vessels contain red and brown structures that resemble cells. And inside these are smaller objects similar in size to the nuclei of the blood cells in modern birds. The team also found osteocytes, cells that deposit bone minerals, preserved with slender filipodia still intact.

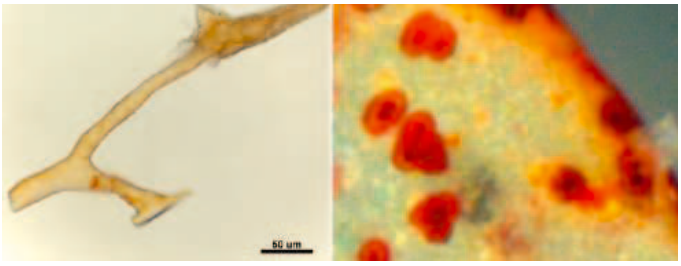

A stretch? Dissolved *T. rex* bone yielded flexible, branching vessels (*left*), some of which contain cell-like structures (*right*).

If the cells consist of original material, paleontologists might be able to extract new information about dinosaurs. For instance, they could use the same sort of protein antibody testing that helps biologists determine evolutionary relationships of living organisms. "There's a reasonable chance that there may be intact proteins," says David Martill of the University of Portsmouth, United Kingdom. Perhaps, he says, even DNA might be extracted.

Hendrik Poinar of McMaster University in Hamilton, Ontario, cautions that looks can deceive: Nucleated protozoan cells have been found in 225-million-year-old amber, but geochemical tests revealed that the nuclei had been replaced with resin compounds. Even the resilience of the vessels may be deceptive. Flexible fossils of colonial marine organisms called graptolites have been recovered from 440-million-year-old rocks, but the original material—likely collagen—had not survived.

Schweitzer is seeking funding for sophisticated tests that would use techniques such as mass spectroscopy and high performance liquid chromatography to check for dino tissue. As for DNA, which is less abundant and more fragile than proteins, Poinar says it's theoretically possible that some may have survived, if conditions stayed just right (preferably dry and subzero) for 68 million years. "Wouldn't it be cool?" he muses, but adds "the likelihood is probably next to none."

—ERIK STOKSTAD

CREDITS (TOP TO BOTTOM): S. J. LOLLE *ET AL.*, *NATURE* **434**, 505 (2005); M. H. SCHWEITZER

mutant plant, before any exposure to other plants or seeds. Most of the embryos had two mutant genes, but a few showed signs of a reverted version. They also closely examined the *HOTHEAD* gene sequence and ruled out that the reversions were the result of random mutations or extra copies of the good genes stowed away in the genome.

"This is the first time that it is shown that an organism can harbor, in a hidden form, additional sets of genetic information from previous generations and that this information can be copied back onto the DNA at the next generation," say Colot. RNA "templates" derived from the original gene and stored in the gametes are the best candidates for reverting the mutant gene to its original state, says Pruitt.

Other labs will undoubtedly rush to test that remarkable suggestion. If true, it would join several other recently discovered functions for RNA that biologists are just now beginning to appreciate. "I am not sure the mechanism will turn out to be the right one," notes Elliot Meyerowitz, a plant developmental geneticist at the California Institute of Technology in Pasadena, California. "But I can't think of any [explanation] that's much brighter than what they have." –ELIZABETH PENNISI

ASTRONOMY

Alien Planets Glimmer in the Heat

Exoplanets have finally become real. After a decade of inferring the presence of nearly 150 other worlds from oscillating patterns in starlight, astronomers announced this week that they have measured light from two of them for the first time. "We are moving out of the realm of merely counting planets and knowing their orbital paths," says planetary scientist Heidi Hammel of the Space Science Institute in Boulder, Colorado. "It's a new ball game now."

The research, described 22 March at a NASA briefing in Washington, D.C., concerns two "hot Jupiters" eclipsed by their host stars every few days as seen from Earth. In visible light, the stars blaze 10,000 times brighter than the planetary pinpricks. But in infrared light, that factor dwindles to 400 because the planets reradiate torrents of heat from their scalding orbits—just a 10th of Mercury's distance from our sun. Although that is too close for telescopes to make an image, NASA's Spitzer Space Telescope can pick up those faint extra dollops of warmth.

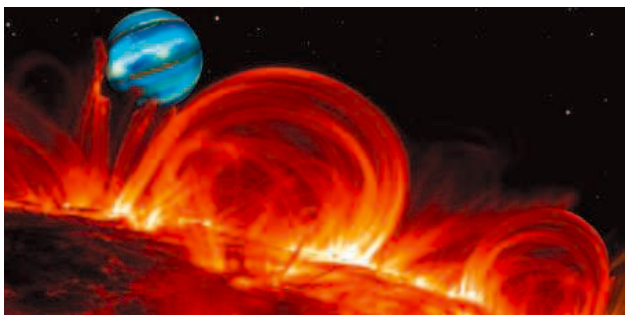

Extra warmth. The Spitzer Space Telescope saw tiny heat signatures from two exoplanets as they emerged from behind their parent stars.

CREDIT: DAVID A. AGUILAR/CFA

Two independent teams used Spitzer in late 2004 to stare at the stars for several hours each, spanning the times when each planet was predicted to pass directly behind its sun. Like clockwork, the total infrared light from the stars dimmed by about 0.25% when the planets disappeared and then edged back up again when they emerged. "It was bang-on what we expected from a hot planet going behind its star," says astronomer David Charbonneau of the Harvard-Smithsonian Center for Astrophysics in Cambridge, Massachusetts, whose team will report on the planet TrES-1 in the 20 June *Astrophysical Journal*.

Spitzer detected each planet at just one or two wavelengths. Proposed studies of the subtle signatures with all of the satellite's instruments will produce a full infrared spectrum of the planets' gaseous atmospheres, revealing their temperatures and ingredients such as carbon monoxide, water vapor, and sodium, forecasts astronomer Drake Deming of NASA's Goddard Space Flight Center in Greenbelt, Maryland. "Spitzer will pin this down beautifully," says Deming, lead author of a paper on the planet HD 209458b in this week's online edition of *Nature*.

The early results deepen one mystery about HD 209458b, Deming says. Studies had shown that the planet is unusually "puffy," with a radius 35% larger than Jupiter's. Theorists predicted that an unseen sister planet must be forcing HD 209458b into an oval orbit, raising tides in the planet's interior and making it expand. However, Spitzer's timing of the eclipse shows a perfectly circular orbit, says Deming—as do new studies of the star's back-and-forth wobbles by a team led by astronomer Gregory Laughlin of the University of California, Santa Cruz. "I'm sure there will be another flurry of theoretical explanations" for the planet's hefty size, Deming says.

Ongoing searches for other eclipsing planets will lead to a new cottage industry of measuring light from exoworlds, Hammel believes. "These hot Jupiters are just the starting point," she says. "These are the biggest, brightest, and easiest." –ROBERT IRION

ScienceScope

NIH Fellows Avoid Stock Ban

The National Institutes of Health has exempted research and clinical fellows from its tough new ethics rules, easing fears that the rules would scare away talented young scientists. People on staff for less than 4 years won't be required to limit or sell their family's medically related stock, NIH announced last week, although they are still barred from consulting for industry.

Cynthia Dunbar of the National Heart, Lung, and Blood Institute, who chairs a committee overseeing fellows, says she's "pleased" about the exemption but that NIH scientists still object to the "unfairness and illogical nature of the regulations in general." In addition, employees now have 90 more days, or until October, to divest. –JOCELYN KAISER

Keep Your Eye on Your iPod

The prospect of humanlike computers became a partisan issue for federal legislators last week. Republicans on the House Science Committee rejected an amendment from a California Democrat to have the National Science Foundation study the societal implications of "the creation of a sentient, cognitive intelligence on this planet." The amendment, for which committee Republicans had voted last year, was part of a bill to promote supercomputing.

"All the experts tell us we are nowhere near the dystopia that Mr. [Brad] Sherman fears," said committee chair Sherwood Boehlert (R–NY), explaining why he and his fellow Republicans had changed their minds. The amendment lost by a party-line vote of 19 to 17; the bill was approved and sent to the floor. –ELI KINTISCH

Bioboard Not on Board

Work on U.S. guidelines for "dual use" biological experiments has not begun because the members of a new federal board created 1 year ago have yet to be appointed.

The National Science Advisory Board for Biosecurity was a key recommendation from a National Academy of Sciences report that looked for ways to prevent the misuse of genetic engineering by terrorists without stifling legitimate experiments (*Science*, 17 October 2003, p. 368). The Department of Health and Human Services (HHS) announced on 4 March 2004 that the 25-member board would take on the job, which researchers hope will offer concrete advice for scientists and biosafety boards without censoring scientific efforts. HHS spokesperson Bill Hall says a final slate of members is now being cleared and that the first meeting should be held "later this year." –JOCELYN KAISER

PALEOCLIMATE

Ocean Flow Amplified, Not Triggered, Climate Change

Figuring out what's going on with this year's weather is hard enough, so pity the poor paleoclimatologists trying to understand how the world drifted into the last ice age 70,000 years ago. For half a century, paleoceanographers have been studying elements or isotopes preserved in deep-sea sediments as markers of the workings of past climate. This "proxy" approach has worked, but only up to a point. Both the climate system and paleoclimate proxies can be unexpectedly subtle and complex.

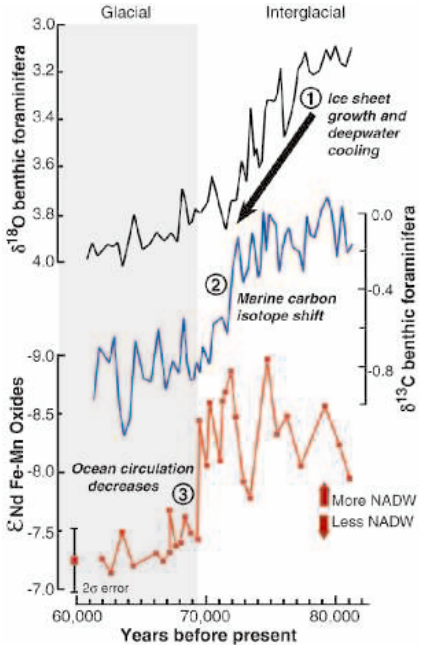

Lagged. Glacial cold and ice grew (1, top) thousands of years before ocean circulation flowed (3, bottom).

On page 1933, a group of geochemists and paleoceanographers advances another proxy: isotopes of the rare-earth element neodymium, which they believe faithfully trace the ups and downs of the heat-carrying Gulf Stream flow. By their reading of neodymium, changes in the speed of the Gulf Stream—a much-discussed mechanism for altering climate—came too late in major climate transitions to have set the climate change in motion. "It's groundbreaking work," says paleoceanographer Christopher Charles of the Scripps Institution of Oceanography at the University of California, San Diego. "It's going to stimulate quite a bit of work either to try to extend the analysis or shoot it down."

Researchers at Columbia University's Lamont-Doherty Earth Observatory in Palisades, New York, began pursuing neodymium as a circulation tracer because it seemed to offer a prized trait: immutability. The ratio of neodymium-143 to neodymium-144 in North Atlantic and Pacific waters differs enough, thanks to the range of ratios of surrounding continental rocks, that it can be used to follow the mixing of waters as currents flow from basin to basin.

Ocean circulation changes should dominate the changes in the neodymium ratio, say Lamont group members Alexander Piotrowski (now a postdoc at the University of Cambridge, U.K.,), geochemists Steven Goldstein and Sidney Hemming, and paleoceanographer Richard Fairbanks. For example, plankton can't change the ratio—as it does the isotopic composition of carbon—because neodymium is too massive an element for biology to separate its isotopes. And in fact, the isotope ratio preserved in the microscopic bits of iron-manganese in a classic sediment core from the southeastern South Atlantic matches the story told by previous tracers. During each of four temporary warmings during the last ice age, the ratio swung down and then back up—just as it should have done if the warm, north-flowing Gulf Stream had temporarily sped up, as more North Atlantic water flowed south in the deep arm of the "conveyor belt" flow.

In the run-up to the ice age, by contrast, the core told a more complicated tale. Starting about 70,000 years ago, bottom waters cooled as glacial ice grew on the polar continents, as indicated by oxygen isotopes of microscopic skeletons of bottom-living organisms. Then, a couple of thousand years later, carbon isotopes shifted as the growing ice and climatic deterioration shrank the mass of plants on land, sending their isotopically light carbon into the sea. Only after another couple of thousand years did the conveyor belt flow slow down, according to neodymium.

Given that millennia-long lag behind the growing cold and ice, "ocean circulation responded to climate change," says Goldstein. At least at glacial transitions, the slowing of warm currents could have put the final chill on the ice age, but "it's not the trigger of climate change." Presumably, the initial cooling was an indirect response to the decline of solar heating over high northern latitudes brought on by the so-called Milankovitch orbital variations: the ever-changing orientation of Earth's orbit and rotation axis. However, changes in ocean circulation may have triggered abrupt climate shifts once the ice age was under way, Goldstein notes.

Although many paleoceanographers like the idea of ocean circulation as a follower rather than a leader, a single core is not likely to win the day. Neodymium "seems to be working remarkably well," says paleoceanographer Jerry F. McManus of Woods Hole Oceanographic Institution in Massachusetts. But the history of climate proxies and a few hints in the South Atlantic record tell him that neodymium may not be the perfect ocean circulation proxy. He and others will be looking for weaknesses.

–RICHARD A. KERR

PROTEOMICS

Protein Chips Map Yeast Kinase Network

Score another victory for high-throughput biology. In one fell swoop, researchers at Yale University in New Haven, Connecticut, have vastly extended decades' worth of research into the molecular communications between proteins that govern the lives of yeast cells. The Yale team, led by molecular biologist Michael Snyder, used glass chips arrayed with thousands of yeast proteins to track down the molecular targets of the organism's protein kinases, enzymes that modify the function of other proteins by tagging them with a phosphate group. About 160 interactions between specific yeast kinases and their targets had previously been identified; the chip study added more than 4000, allowing the Yale researchers to map out a complex signaling network within yeast cells. Snyder presented this large-scale survey of yeast protein phosphorylation last week in Arlington, Virginia, at the first annual symposium of the U.S. Human Proteome Organization.

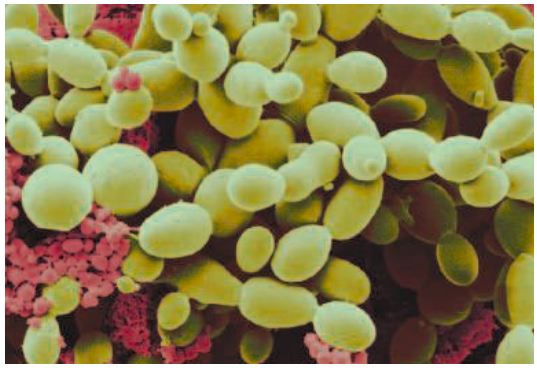

En masse. Biochips reveal thousands of new interactions between kinases and their molecular targets in yeast cells like these.

"This is extremely important for the signal transduction community," says Charles Boone, a yeast geneticist at the University of Toronto in Canada. Drugmakers, Boone adds, are likely to pore over the new bounty of yeast results to find ▶

CREDITS (TOP TO BOTTOM): ADAPTED FROM A. M. PIOTROWSKI; SCIMAT/PHOTO RESEARCHERS INC.

similar kinase interactions in human cells that they can affect.

Setting the stage for the new work, Snyder and his colleagues initially developed protein chips displaying the majority of yeast proteins (*Science*, 14 September 2001, p. 2101). A company called Invitrogen in Carlsbad, California, now makes these chips commercially, and for the current study it provided ones that harbor 4088 of yeast's 6000 or so proteins.

Snyder's team expressed and purified 87 of yeast's 122 protein kinases. (The remainder are difficult to express.) They then washed each kinase over a different chip along with radiolabeled ATP, the molecule that provides the phosphate group that kinases attach to a targeted protein. An autoradiography machine then imaged sites on the chips where a radiolabeled phosphate group had modified a protein.

The results revealed 4192 interactions between the yeast kinases and some 1300 different protein targets. Among the surprises, Snyder says, were the targets of a well-studied family of three protein kinases. Biochemists had previously concluded that these three were redundant, meaning that if one or two were absent, the third would take their place and allow the yeast cells to survive. That suggested they phosphorylate the same proteins. But Snyder reported that each kinase had a very different profile of targets.

In addition to teasing out individual kinase-protein interactions, the Yale researchers also integrated their results with other yeast protein data sets, including one for the transcription factors that turn genes on and off. That allowed them to build a complex map of protein encounters that regulate life inside yeast cells. Among the lessons from the map, Snyder reported, was that eight particular patterns of protein interactions show up over and over. For example, so-called adaptor proteins commonly interact with both a kinase and a protein it modifies. These adaptor proteins, Snyder says, likely help control the rate at which other proteins are activated.

The research by Snyder's team is "very exciting and enabling work," says Harvard University yeast geneticist Steve Elledge.

Researchers at pharmaceutical companies are likely to be among the scientists most interested in following up on this work. Protein kinases already constitute one of the most important classes of drug targets, with kinase inhibitors such as the cancer drugs Herceptin and Gleevec accounting for billions of dollars a year in sales. The Yale group's yeast research doesn't reveal the critical kinases at work in humans, but it gives drug companies a leg up on identifying equivalent kinase interactions in humans and possibly clues about how to block them.

–ROBERT F. SERVICE

MAGNETIC IMAGING

Atom-Based Detector Puts New Twist On Nuclear Magnetic Resonance

Cheap, portable magnetic resonance imaging (MRI) machines could be on the horizon thanks to an exquisitely sensitive magnetic field detector. In their lab at Princeton University in New Jersey, physicists Igor Savukov and Michael Romalis have used an "atomic magnetometer"—essentially, a vial of gas and a pair of lasers—to detect the wobble of atomic nuclei in a magnetic field. That motion, known as nuclear magnetic resonance, provides the signal tracked in MRI scans.

The approach might open the way for one-shot MRIs for patients instead of tedious scans, the researchers say. But others say such applications are far from a sure thing.

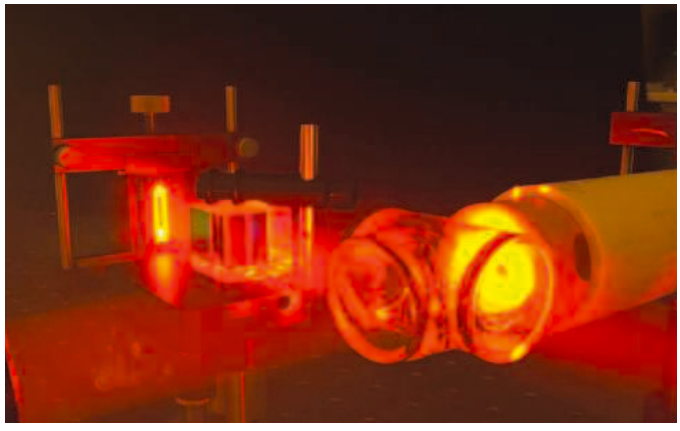

See them spin. A gas-filled cell and laser beams can track the twirl of atomic nuclei and could eventually lead to cheap, portable MRIs.

An atomic magnetometer–based system "is really very simple and cheap in principle," says Dmitry Budker, a physicist at the University of California, Berkeley, who is also developing the devices. In contrast to competing techniques, such a system requires neither a powerful, pricey magnet nor cryogenic equipment, Budker says. That means an entire system could conceivably cost "a few thousand dollars compared to a few million" for a conventional scanner, he says. But John Wikswo, a physicist at Vanderbilt University in Nashville, Tennessee, says the idea is still a long way from a practical technology. "I would not get carried away with anything that's not proved in the paper," Wikswo says.

An MRI machine senses the gyration of atomic nuclei, which can wobble, or precess, in a magnetic field much as spinning tops do under the pull of gravity. By prodding hydrogen nuclei with radio waves, a medical MRI scanner twirls the nuclei and maps the abundance of water molecules in living tissue. Wobbling in concert, the nuclei produce their own oscillating magnetic field, which a conventional MRI machine senses with a coil of wire.

To produce detectable signals, however, a system with a pickup coil requires powerful, expensive magnets. Nuclei precessing in far weaker fields can be tracked with a loop of superconductor known as a SQUID. But SQUIDs must be kept at temperatures near absolute zero, which requires expensive and bulky cryogenic equipment.

To detect the wobbling nuclei with similar sensitivity, Savukov and Romalis employed a glass chamber filled with helium and potassium vapor. Because of the arrangement of its electrons, each potassium atom acts like a magnet, and the researchers line the atoms up by shining a strong "pump" laser beam on them. The atoms then wobble when exposed to even a tiny magnetic field, and the researchers detect their precession by shining a second "probe" laser through them.

The magnetometer recorded the oscillating magnetic field produced by protons precessing in water, the researchers report in a paper to be published in *Physical Review Letters*. It also measured the wobble of nuclei of xenon atoms mixed with the potassium, a technique that might be used to image the lungs by studying traces of exhaled gas. Potentially, the vapor in the cell can encode a three-dimensional image of an object that can be read out like a snapshot, Romalis says.

But atomic magnetometers present technological challenges of their own, including susceptibility to extraneous magnetic fields. The gas chamber must be heated to 180°C, and shielding it so that it can be placed next to living tissue may not be easy, Wikswo says. Ronald Walsworth, a physicist at the Harvard-Smithsonian Center for Astrophysics in Cambridge, Massachusetts, agrees that several "big engineering challenges" remain, but he credits Romalis "for doing some of that hard engineering work." Whether those efforts will pay off remains, quite literally, to be seen.

–ADRIAN CHO

CREDIT: TOM KORNACK/PRINCETON UNIVERSITY

ECOLOGY

Savannah River Lab Faces Budget Ax

A 54-year-old University of Georgia ecology lab funded primarily by the Department of Energy (DOE) is fighting for its life.

Located on a 780-square-kilometer nuclear industrial site in southwest South Carolina that is off-limits to development, the Savannah River Ecology Laboratory (SREL) is well respected for its expertise in subjects including the movement of pollutants in streams and the effect of radiation on reptiles. Two years ago, however, DOE moved the lab from its office for cleanup projects to one that focuses on the science of remediation and asked it to focus on issues such as the migration of radionuclides to deep aquifers. Now President George W. Bush has proposed eliminating the lab's budget in 2006.

Last fall an outside review said that SREL was making progress toward its new subterranean emphasis, although it urged DOE to make use of the lab's "unique" capabilities. Independent science advisers to DOE have also repeatedly urged the agency to nurture its ground-level ecology science. Yet despite that advice and the lab's efforts at refocusing its work, the president's budget request put a priority on subsurface science and high-level radioactive waste. Research on radioecology and surface science was to be wound down this year, the budget stipulated, and terminated in the fiscal year that begins 1 October. "We had to get out of one area of research, [and we picked] surficial science," says DOE's Ari Patrinos, whose office oversees the lab.

SREL Director Paul Bertsch thinks that decision is shortsighted. He argues that other DOE cleanup sites in Tennessee and Colorado will require an understanding of the movement of radioisotopes on the surface that SREL scientists already possess. Indeed, a 1994 decision by DOE not to drain a lake at the Savannah site and remove contaminated sediment, he says, was based on SREL research that suggested the habitat could survive with the sediment intact. Experts believe the decision has saved billions of dollars in cleanup costs (*Science*, 12 March 2004, p. 1615). "For an $8 million organization, we've had a huge impact," says Bertsch.

Not a snap. SREL is shifting its focus from aboveground ecology, including herpetology, to subsurface science.

Patrinos says that SREL scientists are being encouraged to seek support from other federal agencies. But he concedes that the lab "will most likely have to shut down" at some point if Congress accepts the 2006 budget proposal. The University of Georgia, Athens, which provides about $1 million a year, will be hard pressed to make up the difference. "We have our own budget problems," says Gordhan Patel, the university's vice president for research.

Ecologists say that much will be lost if the lab is closed. "SREL has been without a doubt the most productive and significant organization in herpetological ecology for the last 25 years," says ecologist David Wake of the University of California, Berkeley, who notes that the lab has taken advantage of the size and undisturbed nature of the site. That advantage could disappear unless lab officials can escape the president's budget ax. —ELI KINTISCH

PROPOSITION 71

Proposed Legislation Threatens to Slow California Stem Cell Rush

Although California voters last November approved a proposition that promises to push the state to the forefront of embryonic stem (ES) cell research, legislation introduced in the state senate last week may significantly constrain the way that the new California Institute for Regenerative Medicine (CIRM) conducts business.

Proposition 71 created CIRM to award up to $3 billion over the next decade to academic and industry researchers working in the state on stem cell projects that are ineligible for federal funds because of restrictions on human embryonic research. One far-reaching new measure introduced on 17 March aims to amend the state constitution to redefine CIRM. It would increase scrutiny of potential conflicts of interest, require more open meetings, and guarantee that products or treatments derived from this research are both affordable to low-income residents and pay increased royalty or licensing fees to the state.

Zach Hall, CIRM's interim president, takes issue with several concerns raised by the legislators. "It really does seem to be a gap between two cultures," says Hall, a neuroscientist who once headed the National Institute of Neurological Disorders and Stroke in Bethesda, Maryland. One point of contention: whether the working groups that evaluate grants can hold closed-door meetings. "This is the gold standard of peer review, and scientists in public won't speak openly and frankly," says Hall. He similarly wonders how the state will determine what is "affordable" and cautions that industry will shy away from collaborations that have such limits.

California state senators Deborah Ortiz (D) and George Runner (R), who introduced the measure, also co-authored a separate bill that calls for a 3-year moratorium on using state funds to pay for hyperovulation of women and retrieval of multiple eggs, which they contend may cause harm. Many researchers hope to create ES cells through somatic cell nuclear transfer (SCNT), which requires human eggs. SCNT uses a hollowed-out egg to "reprogram" cells to their embryonic state. ES cell lines derived from SCNT may enable scientists to study pathogenesis, test drugs, and even treat people directly.

Nobel laureate Paul Berg of Stanford University, an influential backer of Proposition 71, is surprised that Ortiz, who pioneered legislation encouraging ES cell research, is pushing for these changes. "Ortiz supported the thing all the way through," he says. R. Alta Charo, a lawyer and bioethicist at the University of Wisconsin, Madison, says she is "dismayed" by the idea of an egg-donation moratorium, which she asserts violates a woman's right to choose and could effectively halt SCNT research.

Ortiz insists she is merely fine-tuning Proposition 71. She adds that the egg-donation moratorium does not prevent researchers from using private funds to obtain eggs.

The egg-donation moratorium requires a majority vote in the legislature. The proposed constitutional amendment, however, would need the support of two-thirds of the legislature, which would then place the issue before the voters in November.

—JON COHEN

CREDIT: SREL PHOTO

Particle air pollution clearly causes substantial deaths and illness, but what makes fine particles so toxic—the size, the chemical compound, or both?

Mounting Evidence Indicts Fine-Particle Pollution

Talk about heart-stopping news: Spending time in traffic may triple some people's risk of having a heart attack an hour later. That's what German researchers reported last October in the *New England Journal of Medicine* (*NEJM*), based on responses from 691 heart attack survivors about their activities in the days before they fell ill. The study seemed to support the notion that tiny air pollution particles from tailpipes, along with stress, could help trigger a heart attack. Yet in another recent study in which volunteers in upstate New York breathed in lungfuls of these so-called ultrafines, particles less than 0.1 micrometer (μm) in diameter, the effects were minimal. If ultrafines were the main culprit, "you would have expected to see something more," says Daniel Greenbaum, president of the Health Effects Institute (HEI) in Cambridge, Massachusetts.

The discordant studies illustrate the dilemma posed by fine particle air pollution. The term refers to particles of dust, soot, and smoke consisting of hundreds of chemicals that are defined by their mass and size—2.5 μm in diameter or less, or about one-30th the width of a human hair. They are known collectively as $PM_{2.5}$. Hundreds of studies have suggested that breathing fine particles spewed by vehicles, factories, and power plants can trigger heart attacks and worsen respiratory disease in vulnerable people, leading to perhaps 60,000 premature deaths a year in the United States. In response, the U.S. Environmental Protection Agency (EPA) in 1997 added new regulations to existing rules for coarser particles (PM_{10}), issuing the first-ever standards for $PM_{2.5}$. But the move came only after a bitter fight over whether the science supported the rules and a mandate from Congress for EPA to expand its particle research program.

At risk. Studies with elderly volunteers have shown that slight changes in outdoor particle levels can change heart rate variability.

Now the issue is getting another look as EPA faces a December 2005 deadline for revisiting its $PM_{2.5}$ standard. EPA scientists, after reviewing piles of new data implicating $PM_{2.5}$ in health effects, have proposed tightening the 1997 standard to further reduce ambient concentrations of fine particles. Some scientists and industry groups remain skeptical, noting that researchers still haven't pinned down what makes particles dangerous—whether it's mainly size, and that the tiniest particles are most potent; or chemistry, such as metal content; or some combination of the two. Despite 8 years and some $400 million in research, finding out exactly how fine particles do their dirty work has proved frustratingly elusive, researchers say. "We've gotten glimpses, but we don't yet have enough systematic coverage of the problem," says epidemiologist Jon Samet of Johns Hopkins University in Baltimore, Maryland.

Unmasking a killer

Although the evidence against fine particles, initially circumstantial, has grown stronger, gaps still remain. It began with epidemiologic studies finding that when levels of particulate matter (PM) edged up in various cities, hospital visits and deaths from heart and lung disease rose slightly, too. Two landmark studies

How Dirty Air Hurts the Heart

A decade ago, most cardiologists never suspected that breathing tiny particles of soot and dust could damage their patients' hearts, let alone trigger a heart attack. Today "there's no doubt that air pollution plays a role in cardiovascular disease," says cardiovascular researcher Robert Brook of the University of Michigan, Ann Arbor.

Fine particles seems to affect the heart in two ways: by changing the heart's rhythm and by causing systemic inflammation. Many studies—from animal experiments to tests in which retirement home residents wore heart monitors—have shown that breathing particle pollution can slightly quicken the pulse and make the heartbeat less variable. The mechanism isn't yet known, but one possibility is that airway receptors stimulate nerves in the heart. A less variable heart rate, in turn, makes the heart more prone to arrhythmia (irregular heartbeat), which can presage cardiac arrest.

People don't usually die from arrhythmias unless they are very ill already, Brook notes. But particles also penetrate the lung's alveoli and cause inflammation and oxidative stress. The lung cells then pump proteins called cytokines into the bloodstream. This apparently sparks other immune responses that promote blood clot formation and the constriction of blood vessels. These effects, in turn, may cause deposits of lipids known as plaques to rupture and block blood flow to the heart. "If these things all come together, somebody who's vulnerable might be pushed over the edge" and have a heart attack, says epidemiologist Annette Peters of the National Research Center for Environment and Health in Neuherberg, Germany.

Over the long term, inflammation from breathing particles may also contribute to atherosclerosis, or hardening of the arteries, in the same way that secondhand tobacco smoke is thought to inflict

in the early 1990s that tracked more than half a million individuals in cleaner and dirtier cities for many years suggested that PM was shortening the lives of 60,000 people each year. EPA generally regulates air pollutants by chemistry—ozone, sulfates, and mercury, for example—but the 1970 Clean Air Act also regulates total particles. In 1987, EPA switched from controlling total particles to coarse particles 10 μm or less in diameter. These new observations suggested, however, that the rules, which are based on the total mass of particles (liquid or solid) with a diameter of 10 μm or less, weren't enough. The PM_{10} rule was not catching fine particles that aren't readily expelled by the lungs and can penetrate deep into airways.

But when EPA proposed the $PM_{2.5}$ standards in 1996 (along with tighter ozone standards), industry groups and some scientists cried foul, arguing there was no direct evidence that these fine particles were killing people. Congress agreed to the regulations only on the condition that EPA would re-review the science before implementing the rule. Lawmakers also mandated that the National Research Council (NRC) oversee a long-term EPA particle research program funding both in-house scientists and extramural researchers.

Those and other new studies have firmed up the fine particle–death link. Larger studies and new analyses verified the key epidemiological studies, which held up despite a statistics software problem that lowered the short-term risks slightly. Deaths per day are now estimated to tick upward 0.21% for each 10 micrograms/meter^3 increase in PM_{10} exposure, and long-term risks of dying rise 4% for each 10 μg/m^3 rise in annual $PM_{2.5}$. Similar patterns were reported in Europe: After Dublin banned soft coal in 1990 and levels of black smoke and sulfur dioxide (both contributors to PM) dropped, death rates from heart and lung disease declined as well. Another study found that people living near busy, polluted roads in the Netherlands had twice the risk of dying from a heart attack over an 8-year period than people living in cleaner areas. Although the epidemiologic studies cannot completely disentangle $PM_{2.5}$ effects from those of other pollutants, such as carbon monoxide, most researchers say the link with $PM_{2.5}$ is robust. "There's an association with particles that doesn't go away," says Greenbaum.

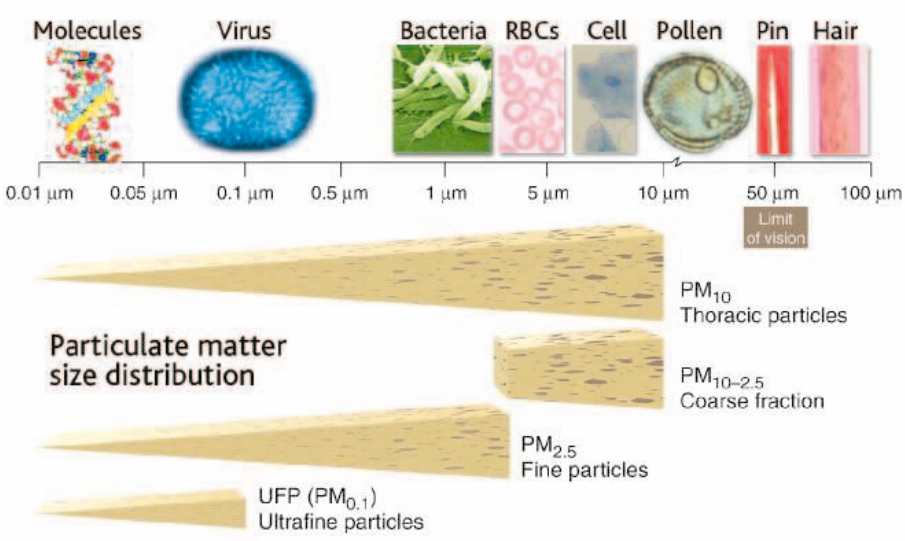

Meanwhile, the list of health effects linked to fine particles keeps growing. An American Cancer Society study found that chronic exposure to $PM_{2.5}$ is on par with secondhand smoke as a cause of lung cancer (*Science*, 15 March 2002, p. 1994). Particles of various sizes have been tentatively linked to low birth weight, preterm birth, and sudden infant death syndrome. A study last year in *NEJM* found that children who grow up in parts of southern California with higher $PM_{2.5}$, nitrogen dioxide, and acid vapor pollution levels have less developed lungs. Earlier this year came a report that the newborn babies of New York City mothers exposed to $PM_{2.5}$ containing higher levels of polycyclic aromatic hydrocarbons (PAH), a carcinogenic chemical, had more chromosomal damage that can later lead to cancer than did the babies of mothers with lower PAH exposures. Another report, published in *Science*, found that fine particles from traffic can cause DNA mutations in male mice that are passed on to their offspring (*Science*, 14 May 2004, p. 1008).

Others studies have tightened the link by showing that $PM_{2.5}$ can cause heart and lung health effects in lab animals with conditions such as heart disease that make them susceptible, as well as subtle effects in human volunteers. Studies in which heart monitors were attached to elderly people, for example, have found that their heart rhythm becomes less variable when outdoor particle levels rise—which makes the heart more vulnerable to cardiac arrhythmia. Researchers are now searching for the mechanisms behind this phenomenon (see sidebar, p. 1858).

Mass confusion

But researchers are still grappling with what makes fine particles toxic. $PM_{2.5}$ consists of hundreds of liquid and solid chemicals, including carbon, nitrates, sulfates, metals, and organic compounds, produced by sources ranging from diesel

Hardhearted. The aortas of mice prone to atherosclerosis developed more lipid plaques (red) when they breathed concentrated particles for 5 months than did the same strain of mouse breathing clean air.

damage. For instance, a report in the 15 April 2005 issue of *Inhalation Toxicology* found that mice engineered to be prone to atherosclerosis develop lipid plaques over 57% more area in the aorta if they breathe concentrated ambient particles instead of filtered air for up to 5 months. "This is the first animal study mimicking" long-term exposures of people, says lead author Lung-Chi Chen of New York University.

Although particle pollution is a minor risk factor for heart disease compared to, say, high cholesterol, the impact is large because so many people are exposed. A recent examination of cause-of-death data from a long-term study tying particle pollution to mortality revealed that few extra deaths are from pulmonary disease; the majority are from cardiovascular disease. Citing the body of evidence, an American Heart Association scientific panel in last June labeled fine particles a "serious public health problem" and urged the Environmental Protection Agency to consider "even more stringent standards."

—JOCELYN KAISER

CREDITS (TOP): P. HUEY/*SCIENCE*; ADAPTED FROM BROOK *ET AL.*/ AHA SCIENTIFIC STATEMENT NO. 71-0289; IMAGES: EOL BERKELEY NATIONAL LABORATORY, CDC, JUPITER IMAGES; (BOTTOM): L. C. CHEN AND C. NADZEJKO/NYU SCHOOL OF MEDICINE

Regulations Spark Technology Competition

The clampdown on particle air pollution in the United States (see main text) and similar regulations expected in Europe are forcing diesel vehicle manufacturers and industries to update technologies and look for new ones. "In the next 5 years, the diesel industry will clean itself up as much as the car industry has done in 30 years," predicts Richard Kassel, director of clean vehicle projects at the Natural Resources Defense Council (NRDC) in New York.

In the United States, efforts are mainly focused on trucks, buses, and larger diesel engines, which produce a major fraction of fine-particle emissions known as $PM_{2.5}$. Several Environmental Protection Agency (EPA) diesel regulations issued since 2000 will steeply reduce emissions by 2015. Besides requiring low-sulfur fuels, which reduce sulfates (a $PM_{2.5}$ component), the rules mandate that the heavy diesel fleet (including buses) be retrofitted with particle filters; EPA estimates costs at $400 to $1000 per vehicle. EPA expects that the majority of new diesel vehicles in 2007 will have particle filters. The devices generally work with a combination of a metal catalyst and a very hot multichannel trap in which soot particles burn off.

During the past 5 years, the U.S. diesel industry has put almost $5 billion into the development of better technologies. For example, researchers are working to find materials that are more resistant to the high temperatures needed to burn off the particles so the filters will last longer.

Car manufacturers are further ahead in Europe, where diesel cars are more common. The French company Peugeot launched its first diesel car with a catalyst particle filter 5 years ago; over 1 million Peugeots are now equipped with these filters, which burn off 99.9% of the particles. Mercedes-Benz also offers an optional filter in new diesel cars for 580 euros ($800). Some U.S. car manufacturers, such as Ford, are about to follow suit in anticipation of future regulatory requirements.

Industries that produce $PM_{2.5}$, such as coal-burning power plants, have the option of using off-the-shelf technologies—usually a combination of electrostatic filters and bag filters to catch the finest particles. These filters are quite expensive—in the range of $1 million to $2 million for a small power plant using low-sulfur fuel. Some U.S. plants are also adopting a newer device called an agglomerator, developed in Australia, that reduces emissions of both $PM_{2.5}$ particles and mercury, enabling them to satisfy two regulations. The agglomerator uses a so-called bipolar charger to separate the dust and give half of it a positive charge and the other half a negative charge. It then switches the charges and mixes the particles, which causes even the smallest particles to form agglomerates that are then easily captured by an electrostatic filter.

Utilities and other industries will need to install such technologies to comply with a March 2005 regulation to control nitrogen oxides, sulfur dioxide, and particles by 2010. As these and other new regulations controlling $PM_{2.5}$ emissions kick in, EPA predicts that $PM_{2.5}$ levels will fall 10% to 20% over the next decade. **–MARIE GRANMAR**

Marie Granmar is an innovation journalism fellow.

Culprit. The heavy diesel fleet in the U.S. is a major source of fine particles.

engines to soil blown from farmers' fields. But efforts to sort out which are the most potent components—or whether it's some combination of size and chemistry—have fallen short.

One reason is that in their animal studies, EPA and academic scientists have often used high doses of particle mixtures such as metal-laden exhaust from oil-burning power plants. These are convenient, but they differ from what people are exposed to. Researchers have also typically inserted the particles directly into the animals' tracheas, which isn't the same as inhaling them. And academic researchers who got grants from EPA have used different protocols or animal models, which makes it difficult to compare experiments to each other and to EPA's. "Lots of the research was relevant, but it wasn't systematic because of the nature of how we do research," says Samet, who chaired a final NRC review that last year pointed out this problem.

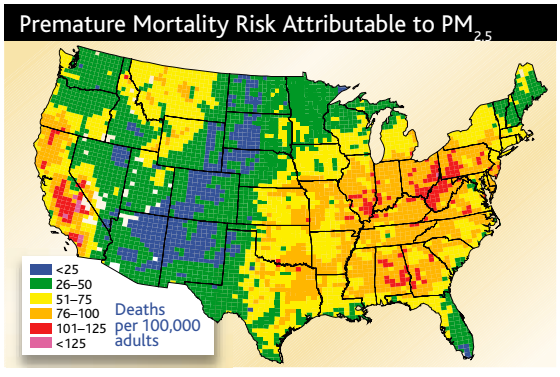

Danger zones. Risks of premature death from $PM_{2.5}$ pollution are highest on the West Coast and in the Midwest.

So far, the evidence on which components are the most dangerous remains confusing. Researchers have, at least, decided that crustal dust, particles on the large end of $PM_{2.5}$, seem fairly harmless. Particles of various sizes containing metals such as zinc and copper, on the other hand, can cause lung inflammation and heart damage in lab animals. The metals theory got a boost in 2001 from an unusual study. Researchers dug up stored air filters from the Utah Valley during the mid-1980s, when epidemiologists had observed a drop in hospital admissions for respiratory problems that coincided with a 1-year closure of a steel mill. The filters from when the mill was open were richer in metals, and these extracts caused more health effects in lab animals and human volunteers—suggesting that the metals explained the jump in hospital admissions. Still, in general, the amount of metals needed to see toxic effects in lab animals is much higher than the levels in the air people breathe, says EPA toxicologist Daniel Costa.

Other suspects seem relatively harmless when examined in isolation. Sulfates cause only minimal health effects in animals, and these acids don't seem linked to health effects in short-term epidemiologic studies. The power plant industry—which produces most of the sulfates—has cited these studies as evidence that they're not the problem. Yet sulfates are clearly associated with health effects in some studies following people over many years.

Others suspect that it's size that determines toxicity, and that ultrafine particles smaller than 0.1 μm in diameter are the culprits. Toxicologists have found that if coarser particles are ground up into ultrafines, they are much more toxic, most likely because the smaller particles have a greater surface area to react with tissues. And ultrafine particles can get into lung tissue and possibly the blood and even the brain. A few epidemiologic studies, such as the one last fall in *NEJM* on heart attack survivors from epidemiologist Annette Peters's group at the National Research Center for Environment and Health in Neuherberg, Germany, have pointed toward ultrafines, whatever their chemical composition, as the most toxic $PM_{2.5}$ component. Peters's study didn't find an association with ambient air pollution, only with time spent in cars, buses, trams, or on bicycles or motorcycles; traffic pollution contains more ultrafines than air in general. Yet when Mark Utell and Mark Frampton's team at the University of Rochester in New York had 28 resting or exercising volunteers breathe small amounts of carbon ultrafines, they saw only very slight

CREDITS (TOP TO BOTTOM): JUPITER IMAGES; DONALD MCCUBBIN/ABT ASSOCIATES USING 2002 $PM_{2.5}$ MONITORING DATA ADJUSTED FOR BACKGROUND LEVELS; RISK CALCULATION BASED ON POPE *ET AL.*, *JAMA* **287**, 1132 (2002)

changes in measures such as heart rhythm and white blood cells—even in asthmatics, whose damaged lungs contained up to six times as many particles as healthy people.

The explanation may be that it's not size or chemistry alone. The ultrafines used in the Rochester study were pure carbon black, but ultrafines in the real world are likely coated with metals and organic compounds, Frampton says. (Also, the researchers may need to test people with cardiovascular disease.) Likewise, sulfates may form the core of a particle that also contains nastier compounds such as metals, or they could change the chemistry of metals so they're more soluble in blood. Larger particles may irritate and inflame airways, exacerbating the toxicity of PM constituents such as organics and metals, says Costa. And particles may have different effects in the short term and after years of exposure. "It's far more complex than trying to decide which chemicals are toxic," says toxicologist Joseph Mauderly of Lovelace Respiratory Research Institute in Albuquerque, New Mexico.

Newer experiments are seeking to use more realistic mixtures. That became possible only a few years ago when researchers invented devices that can collect ambient air from outside a lab and concentrate the particles for use in experiments. Others are looking at pollutants from a range of sources. For example, Mauderly's group at Lovelace is conducting animal studies comparing particles from diesel engines, gas engines, wood smoke, cooking, road dust, and coal to pin down which type is most toxic. HEI, meanwhile, is sponsoring epidemiologic and toxicology studies that will take advantage of a new monitoring network at 54 sites that measures a finer breakdown of the chemicals in particles, such as sulfates, elemental carbon, and trace elements, than has been gathered previously. And EPA recently launched a $30 million, 10-year study led by University of Washington researchers that tracks correlations between these finer air pollution measurements and the health of 8700 people over age 50.

Down the road, this new information should help guide regulations—for instance, if carbon particles from wood burning were the main problem, or diesel engines, EPA could specifically target those sources. Controlling only mass, as EPA does now, might actually be counterproductive. For example, if larger $PM_{2.5}$ particle levels go down but levels of ultrafines do not, "that could make things even worse," Frampton says. That's because ultrafines tend to glom onto larger $PM_{2.5}$ particles, so they don't stay in the air as long when the larger particles are around.

Time to act

Those results won't be available for years, however, and EPA is under a court order to decide whether to tighten the current $PM_{2.5}$ standard by the end of 2005. EPA scientists in January recommended that the agency consider tightening the standards from the current annual average of 15 $\mu g/m^3$ to 12 to 14 $\mu g/m^3$, and the daily average from 65 $\mu g/m^3$ to as low as 25 $\mu g/m^3$. They also suggested replacing the PM_{10} standard with a new one for particles between PM_{10} and $PM_{2.5}$ to better target coarser particles between those sizes. In April, EPA's clean air advisory board will weigh in.

$PM_{2.5}$ levels have already dropped at least 10% since 1999 due to acid rain regulations and new diesel engine standards (see sidebar, p. 1860). They will fall further thanks to additional cuts in sulfates and nitrates from coal-burning power plants through new regulations issued this month and possibly the Administration's proposed Clear Skies program. But a tighter standard could trigger additional controls in areas with the highest particle levels, such as Los Angeles and the Northeast. Environmental and health groups as well as many scientists say that, as with tobacco smoke and lung cancer, policymakers can't wait for all the scientific answers before taking action to prevent deaths from dirty air.

—JOCELYN KAISER

CREDIT: U.S. DEPARTMENT OF EDUCATION

U.S. Education Research

Can Randomized Trials Answer The Question of What Works?

A $120 million federal initiative to improve secondary math education hopes to draw on an approach some researchers say may not be ready for the classroom

When Susan Sclafani and her colleagues in Houston, Texas, received a $1.35 million grant from the National Science Foundation (NSF) to work with secondary math and science teachers, nobody asked them to demonstrate whether the training improved student performance. "All we had to do was produce qualitative annual reports documenting what we had done," she says. Sclafani thought that wasn't nearly enough and that NSF should be more concerned about whether the project helped students learn. Now, a decade later, she's in a position to do a lot more. And that's exactly what worries many education researchers.

As assistant secretary for vocational and adult education at the Department of Education (ED), Sclafani is championing a $120 million initiative in secondary school mathematics that is built in part on money shifted from the same NSF directorate that funded the Houston grant. The initiative, included in President George W. Bush's 2006 budget request for ED now pending in Congress, will give preference to studies that test the effectiveness of educational interventions in the same way that medical researchers prove the efficacy of a drug. Randomized controlled trials (RCTs) of new approaches to teaching math, Sclafani says, will help school officials know what works, and they can then scale up the most promising new curricula and teaching methods. "Randomized studies are the only way to establish a causal link between educational practice and student performance," she says.

Prove it. The Department of Education's Susan Sclafani wants to see more experimental evaluations in math and science education.

But some researchers say that such trials won't tell educators what they need to know. And they believe their discipline is too young to warrant a large investment in experimental studies. "Rushing to do RCTs is wrongheaded and bad science," says Alan Schoenfeld, a University of California, Berkeley, professor of math education and adviser to both NSF and ED. "There's a whole body of research that must be done before that."

The proposed math initiative at ED would be a competitive grants program to prepare students to take Algebra I, a gateway course for the study of higher mathematics and the sciences. Applicants will be encouraged to use RCTs and quasi-experimental designs to measure whether the reform works, Sclafani

says. The initiative comes at the same time the Administration has requested a $107 million cut in NSF's $840 million Education and Human Resources (EHR) directorate. The cuts include a phasing out of NSF's portion of the $240 million Math/Science Partnership program—a joint effort with ED to improve K–12 math and science education by teaming universities with local school districts—and a 43% decrease for the foundation's division that assesses the impact of education reform efforts (*Science*, 11 February, p. 832). Sclafani says this "reallocation of education dollars" reflects the Administration's eagerness for clear answers on how to improve math and science learning across the country. That's OK with NSF Director Arden Bement, who says ED is in a better position than NSF to implement reforms nationwide.

Although NSF watchers are unhappy with the proposed cuts to the foundation's education budget, a bigger concern for some education researchers is that ED may be overselling RCTs. It's unrealistic to think that RCTs and other quasi-experimental studies will magically produce answers about what works, they say. Before comparing the performance of students in the experimental and control groups (one receives the intervention, the other doesn't), researchers must study the factors affecting any change in curriculum or teaching methods, such as group vs. individualized instruction, or working with students whose native language is not English. Answering such contextual questions, the critics say, is similar to finding out whether a medicine needs to be taken before or after meals.

"You can design an RCT only after you've done all this work up front and learned what variables really count," Schoenfeld says. ED's approach, he argues, is likely to drive researchers to skip those necessary steps and plan randomized studies without knowing why an intervention seems to work.

Department officials insist that the time is ripe and have begun funding a handful of projects drawn from 15 years of work in curriculum development and teacher training, including efforts funded by NSF. One is a study of Cognitive Tutor, a computer-based algebra course for middle school students. Another looks at a new approach to training 6th grade science teachers in Philadelphia. Diana Cordova of the department's Institute of Education Sciences predicts that within 3 years, "they will tell us with reasonable certainty if an intervention can improve student learning."

Some of the researchers conducting these studies aren't so sure, however. One hurdle is convincing a large enough sample of schools to agree to randomization. "Everybody wants to have the treatment, nobody wants to have the placebo," says Kenneth Koedinger, a psychologist at Carnegie Mellon University in Pittsburgh, Pennsylvania, who's leading the Cognitive Tutor study. Another problem is inconsistent implementation across the experimental group. Allen Ruby, a researcher at Johns Hopkins University in Baltimore, Maryland, who is conducting the Philadelphia study, says that problems at two of the three schools involved could end up masking evidence of whether the training is working.

CREDIT: COURTESY OF ELK RIDGE SCHOOL

Luck of the draw. Elk Ridge School is one of three Philadelphia, Pennsylvania, schools implementing a grade 6 reform curriculum as part of a randomized controlled trial.

Schoenfeld predicts that these and other problems will confound any analysis. "The likely findings from this study would be something like this: Sometimes it works; sometimes it doesn't; and on average, the net impact is pretty slight compared to a control group," he says. "What do you learn from such findings? Nothing." On the other hand, Schoenfeld says, a detailed analysis of how the implementation was done at each school and how teachers and students reacted to it could tell educators the conditions under which it would be most likely to work.

The still-emerging field of evaluation research needs investments in both qualitative and experimental studies, says Jere Confrey, a professor of mathematics education at Washington University in St. Louis, Missouri, who last year chaired a National Research Council report on the need to strengthen evaluations (*Science*, 11 June 2004, p. 1583). "You need content analysis to determine if a curriculum is comprehensive. You need a case study, because a randomized trial makes sense only if you know exactly what a program is and are certain that it can be implemented over the duration of the experiment," she says. Analyses are lacking on hundreds of interventions now in use, she adds.

Sclafani says she doesn't disagree with the value of contextual studies. But she says that taxpayers deserve more from their considerable investment in school reform. "NSF has supported exploratory work for a long time. There was an opportunity to collect evidence about their effectiveness, but that opportunity has been lost [because NSF didn't insist on experimental evaluations]."

Judith Ramaley, who recently stepped down as head of NSF's EHR directorate, says she's glad that ED wants to build on NSF's work in fostering innovations in math and science education by testing their performance in the classroom. "The medical model makes sense for them," says Barbara Olds, who directs NSF's evaluation division within EHR. "We think there are many fundamental questions in education that have not been answered."

ED officials are working with states to spread the gospel of experimental evaluations. Under the department's $178 million Math/Science Partnership program—the money from which has flowed directly to the states for the past 2 years—state governments have funded more than three dozen projects with a randomized or quasi-experimental study component. (None has yet yielded results.) And the department plans to do the same thing with the new math initiative.

"Teachers are telling us: 'We know what works in reading; tell us what works in math and science,' " says Sclafani. "We hope to be able to tell them that, if you do a, b, and c, you'll be sure to see results."

–YUDHIJIT BHATTACHARJEE

American Astronomers Lobby For the Next Big Thing

With a successor to the Hubble Space Telescope seemingly assured, U.S. researchers state their case for a complementary mammoth telescope on the ground

Astronomers like to view the heavens through as many eyes as possible: some on Earth, some in orbit, some tuned to every reach of the electromagnetic spectrum. Soaring costs for next-generation telescopes, however, are forcing researchers in the United States to make hard choices—or vigorous arguments. The top item on their wish list—the $1.6 billion James Webb Space Telescope (JWST), successor to the Hubble Space Telescope—enjoys steady support from NASA and seems on track for launch in late 2011. Less certain are the prospects for priority number two: a multi-mirrored behemoth on the ground spanning 20 to 30 meters, aimed at surpassing Hawaii's Keck Telescopes. Astronomers want it up and running by 2015 to make simultaneous observations they consider crucial during JWST's projected 10-year lifetime.

Fearful that funding shortfalls might narrow that window, U.S. astronomers have sharpened their case for the giant ground-based telescope. On 15 March, the Astronomy and Astrophysics Advisory Committee (AAAC)—established in 2002 at the request of the National Academy of Sciences—issued a report* to Congress urging the National Science Foundation (NSF) to boost its early funding of technology research for the telescope, which to date has relied almost entirely on private grants. What's more, the next-generation ground and space science working groups—usually isolated—are finishing a novel white paper titled, in part, *The Power of Two*. The document claims that the field's central questions are within reach of JWST and an earthbound partner.

Both reports raise the specter of foreign competition. "We felt that if we did not have a large enough telescope in place during the JWST era and our European colleagues did, then our competitiveness at the frontier would be diminished significantly," says *Power of Two* co-author Stephen Strom of the National Optical Astronomy Observatory (NOAO) in Tucson, Arizona.

To set the scene, the reports cite major advances from the pairing of Hubble and the 10-meter Keck Telescopes, such as the discovery of "dark energy" by observing distant supernovas from space and their dim host galaxies from the ground. A partnership in the next decade promises more deep insights, says Strom, thanks to facilities that will be an order of magnitude more powerful.

With its 6.5-meter mirror and a cold orbit 1.5 million kilometers from Earth, JWST will peer to the dawn of galaxies and into the hearts of star-forming clouds and planetary nurseries in infrared light. A ground telescope will examine the same objects in near-infrared and optical light, but five times more crisply than JWST because the vast mirror will collect so much light. Spectrographic analysis of that light should yield exquisite details about motions and compositions of gas that will elude JWST, says astronomer Alan Dressler of the Carnegie Observatories in Pasadena, California. "JWST's sensitivity will be fantastic, and its images will be untouchable," he says. But the ground spectra will show how the first galaxies actually assembled their gas. The spectra also may shed light on worlds like our own in the innermost zones of planetary systems around nearby stars, which JWST won't see, Dressler says.

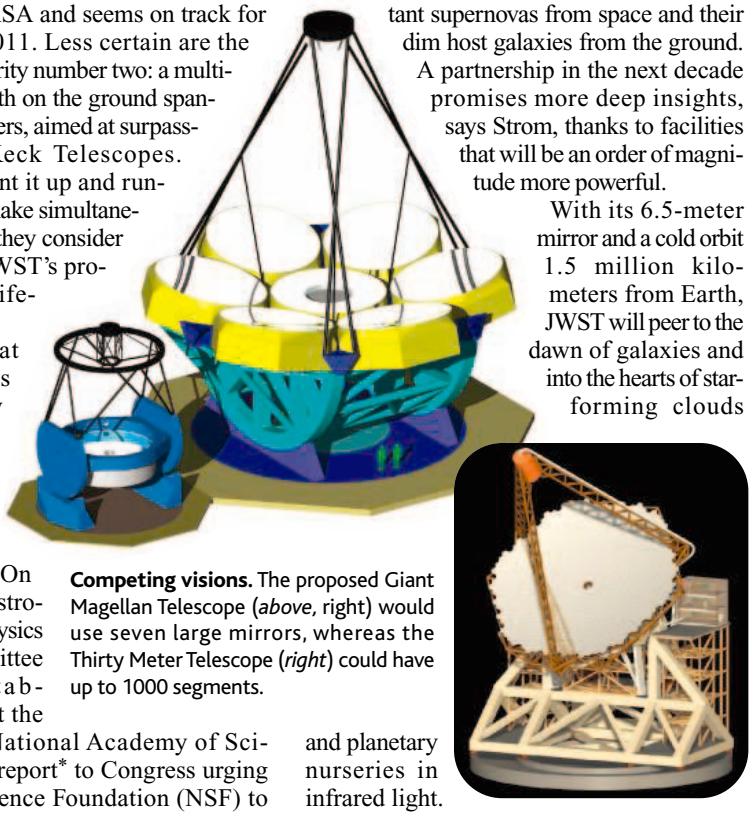

Competing visions. The proposed Giant Magellan Telescope (*above*, right) would use seven large mirrors, whereas the Thirty Meter Telescope (*right*) could have up to 1000 segments.

The space telescope's designers won't duplicate those strengths. "We're very strict about that," says JWST senior project scientist John Mather of NASA's Goddard Space Flight Center in Greenbelt, Maryland. "If anybody's ever going to do it on the ground, we don't do it."

How the terrestrial telescope will work its magic is hotly debated. Two teams have devised distinct ideas for a Giant Segmented Mirror Telescope (GSMT), and each is convinced its approach is superior. One consortium of more than a half-dozen institutions, led by the Carnegie Observatories, proposes seven 8.4-meter mirrors in a tight floral pattern. The other group—the California Institute of Technology, the University of California, NOAO, and Canada—wants to scale up the 36-mirror honeycomb of the twin Keck Telescopes to a huge surface made of 800 to 1000 segments. Both designs require rapidly flexible optics and a daunting array of laser beams pointed at the sky to detect and erase the blurring of Earth's atmosphere.

The technology challenges are steep, with price tags to match: $500 million and $800 million for the respective designs. Both teams expect more than half of the money to come from universities and private U.S. donors, but even that may not be enough. "For the next-generation facilities … it would be very advantageous to have international partnerships," says astronomer Rolf-Peter Kudritzki of the University of Hawaii, Manoa, chair of the GSMT science working group.

Ideally, those ties should include European astronomers, the AAAC report urges. Current plans in Europe call for a 60-meter to 100-meter "Overwhelmingly Large Telescope," which many researchers view as overly ambitious. If U.S. agencies keep channels open with European colleagues, the world community might sustain two 30-meter-class telescopes—one in the north and one in the south—the report states.

Meanwhile, AAAC urges NSF to up the ante for the technology development needed to explore both U.S.-led designs. A $35 million proposal is pending at NSF, but this year's bleak budget outlook means the two teams probably will get some small fraction of that, according to an astronomer familiar with the deliberations. Even so, NSF is likely to support as much as 50% of one project when resources permit, says Wayne Van Citters, director of the agency's division of astronomical sciences.

But further slippage of up-front funding might push the completion date for a huge ground telescope uncomfortably deep into JWST's limited life span. It's time to make progress toward the best design, says NASA's Mather: "We just want somebody to build one."

–ROBERT IRION

CREDITS (TOP TO BOTTOM): GMT/CARNEGIE OBSERVATORIES; AURA (INSET)

* www.aas.org/aaac/2005AR.pdf

CREDIT: ASSOCIATED PRESS

Food for thought. Contact with ducks—which can carry H5N1 without symptoms—is a risk factor for human infection.

True Numbers Remain Elusive in Bird Flu Outbreak

Confounding reports about human cases of bird flu have fueled concerns about a pandemic. But the true spread of H5N1 remains unknown

When 5-year-old Hoang Trong Duong from Vietnam's Quang Binh province was diagnosed with avian influenza last week—about 10 days after his 13-year-old sister died, presumably from the same disease—he became the 70th victim since the H5N1 bird flu strain started its march across Asia.

That's the official number. But most flu experts believe that H5N1 has infected many more people, and some are increasingly worried that, 17 months into the current outbreak, there still hasn't been a concerted effort to establish the true extent of the spread of the virus—which could spawn a pandemic—among humans. "I'm very worried that information has been slow to emerge," says flu scientist Nancy Cox of the U.S. Centers for Disease Control and Prevention (CDC) in Atlanta, Georgia.

There are many reasons for the information gap—from quirky test results to a lack of lab capacity in the affected countries to political sensitivities. A broad testing program, combined with carefully collected epidemiological information, is "absolutely crucial" to answer some basic questions, says virologist Albert Osterhaus of the University of Rotterdam, the Netherlands. Among them: How many people have become infected? What are the ways in which the virus spreads? And is the virus getting better at human-to-human transmission—the first step on the road to a pandemic?

There's good reason to assume that there are more cases than those found so far, researchers say. Mostly seriously ill patients get tested for H5N1, says Cox; milder cases are likely to slip through the cracks. (That may also be why the official death rate stands at a staggering 67%.) Moreover, during H5N1's first outbreak, in 1997 in Hong Kong, several infected children had mild or no illnesses. Two weeks ago, Vietnam also reported two asymptomatic infections.

As an example of what needs to be done, Osterhaus points to a study done after the 1997 outbreak by a team from the Hong Kong Department of Health and CDC, which included Cox. They screened 51 household contacts of H5N1 patients, as well as 26 people who went on a 4-day plane and bus trip with one of the patients and 47 co-workers of a bank employee who became ill; they also collected detailed information about each subject's contacts with the patients. (The results were somewhat reassuring: Only one member of the tour group and six household contacts had antibodies to H5N1.)

Cox says several recent developments reinforce the need for broader testing. A paper published online by the *New England Journal of Medicine* on 17 February reports that H5N1 can cause diarrhea and brain inflammation, suggesting that cases may be missed because doctors simply don't think of bird flu. The increasing number of reported family clusters of H5N1 in Vietnam might also signal human-to-human transmission, she says.

But broad efforts have been stymied. One problem is the technical difficulty of testing for antibodies. Flu researchers traditionally rely on hemagglutinin inhibition tests to detect antibodies in serum samples. But those have proven "simply not sensitive enough" in the case of avian influenza, says Klaus Stöhr, who coordinates WHO's global influenza program. The alternative—a so-called microneutralization assay—is more reliable but also more time-consuming and expensive. And because it uses live H5N1 virus that infects cells, it should only be carried out in a biosafety level 3 laboratory, of which the region has very few.

Amassing samples and epidemiological questionnaires is labor-intensive. "The Vietnamese are too busy just trying to keep track of the cases of serious illness," says Peter Cordingly, spokesperson for WHO in Manila. Nonetheless, the Hospital for Tropical Diseases in Ho Chi Minh City now has several hundred samples—from cullers, contacts of patients, health care workers, and controls—that may be shipped to the WHO collaborating center in Hong Kong, says Peter Horby, a WHO official in Hanoi.

In Thailand, meanwhile, two groups have tested hundreds of samples collected during the outbreak last year. Unfortunately, some of the corresponding epidemiological data weren't properly recorded. The results are still being reviewed, but Scott Dowell of the International Emerging Infections Program in Bangkok, a collaboration of the Thai Ministry of Health and CDC, says that so far, the data don't suggest large numbers of subclinical cases—a result virologist Malik Peiris of the University of Hong Kong characterizes as "surprising."

The lack of information has been frustrating for labs with the expertise but no samples to test. CDC, for instance, has trained Vietnamese researchers and has tested some samples from Thai health care workers, but would like to do more, says Cox. Getting renowned international labs involved should also help avoid mistrust and confusion about the results, says Osterhaus. But such collaborations require diplomacy, says Stöhr: "You can't just march into Vietnam with an army of researchers."

Meanwhile, fresh bird outbreaks of H5N1 were reported in Indonesia last week, and South Korean newspapers reported that North Korea culled thousands of chickens last month to curb an outbreak near Pyongyang. As a member of the World Organization for Animal Health, North Korea must report outbreaks of avian influenza, which so far it hasn't done. Stöhr notes that an outbreak in the secretive nation would be hard to investigate or bring under control.

–Martin Enserink and Dennis Normile

RANDOM SAMPLES

Edited by Jennifer Couzin

A Cure for the Common Mold

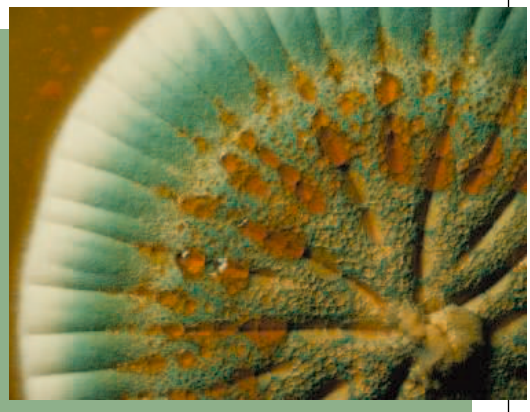

After Alexander Fleming stumbled upon penicillin in 1928, a problem with his find surfaced: The mold that made the drug, *Penicillium notatum*, only did so in small quantities. In 1943, scientists turned to another species of mold: one discovered on cantaloupe that today churns out 1000 times more penicillin. A single genetic mutation, it now turns out, explains the cantaloupe strain's superlative production.

To make penicillin, mold first produces a precursor acid. The acid can be converted into either penicillin or another chemical, 2-hydroxy-PA, but José Luis Barredo and colleagues at Antibióticos, a pharmaceutical company in Leon, Spain, found that *P. chrysogenum*, the high-producing species, has a gene defect that prevents it from producing much of the latter. So it's stuck with making penicillin instead, the researchers report online this month in *Fungal Genetics and Biology*.

Upright Ancestors From Ethiopia

Ever since the 3.1-million-year-old skeleton of Lucy was unearthed in Ethiopia 30 years ago, paleoanthropologists have wondered when and how her ancestors began walking upright. New clues may come from two recent discoveries: a well-preserved partial skeleton, dug up in February in the badlands of Ethiopia by Ethiopian paleoanthropologist Yohannes Haile-Selassie of the Cleveland Museum of Natural History in Ohio (*Science*, 11 March, p. 1545), and a thighbone just announced. Both help fill a gap in the fossil record when bipedalism was evolving.

The second find, by a team led by Horst Seidler of the University of Vienna, was discovered at an Ethiopian site called Galili. The thighbone (photo, left) reveals an individual who walked upright, but perhaps differently than did Lucy (photo, right) and the original owner of a 6-million-year-old thighbone from Kenya, whose discoverers say it walked with a modern gait.

Muscles and ligaments appear to have attached differently to the thighbone than in Lucy's species, *Australopithecus afarensis*, suggesting a different walk, says anthropologist Gerhard Weber of the University of Vienna. That could mean early hominids didn't all evolve to walk upright in the same way. But the thighbone is rebuilt from 26 fragments, so its gait may be tough to discern.

Big Brains Rule the Roost

When it comes to brains, people naturally assume bigger is better. But why should size matter? Now an international team of researchers has shown that a popular hypothesis may be right: In birds, at least, a bigger brain makes it easier to adapt to a new environment.

The team, which included biologists Daniel Sol of the Center for Ecological Research and Applied Forestry in Barcelona, Spain, and Louis Lefebvre of McGill University in Montreal, Canada, analyzed an existing database of the results of 645 attempts by humans to introduce 195 bird species to new places, such as an island or a different continent. In 243 of the attempts, the birds established a self-sustaining population. The bigger the species' brain relative to its body size, the better it was at overcoming challenges of a new environment such as finding food or avoiding predators, the team reports this week in the online early edition of the *Proceedings of the National Academy of Sciences*. Members of the parrot family, which have a very large relative brain size, had a particularly easy time of it, succeeding on average 200% more often than members of the partridge and pheasant families, with their small relative brain sizes.

The new study is an "exciting marriage between ecology and psychology," says behavioral biologist Simon Reader of the University of Utrecht in the Netherlands.

Smart Robot

Rolling over Chile's Atacama Desert, the robotic rover Zoë (below) snapped dozens of fluorescent photographs that helped document the presence of life—microorganisms—in this forbidding environment, a team at Carnegie Mellon University and NASA's Ames Research Center reported last week at the Lunar and Planetary Science Conference in Houston, Texas. To map the distribution of microbes, Zoë spent 2 months in the Chilean desert last fall. Scientists accompanied her in part so that she didn't "drive off a cliff," says David Wettergreen, a Carnegie Mellon roboticist and the project leader. The robot's pictures, which can detect chlorophyll and DNA, correlated with soil samples the scientists took to confirm that Zoë's results were accurate. Next field season, the team hopes Zoë will chug over 200 km of desert—up from 30 km last year—and shed light on the extreme environmental conditions in which life can still flourish. They're also working with NASA to apply Zoë's technology to extraterrestrial robots.

CREDITS (TOP TO BOTTOM): ANDREW MCCLENAGHAN/PHOTO RESEARCHERS INC.; INST. FOR ANTHROPOLOGY, UNIVERSITY OF VIENNA, WITH PERMISSION OF THE NATL. MUSEUM OF ETHIOPIA; CARNEGIE MELLON

PEOPLE

Edited by Yudhijit Bhattacharjee

POLITICS

Law-abiding. A controversy over a German scientific prize awarded to the creator of Dolly has been defused after Ian Wilmut promised not to use the money for cloning.

Wilmut, a researcher for more than 30 years at the Roslin Institute in Edinburgh, U.K., received the $134,000 Paul Ehrlich and Ludwig Darmstaedter prize last week at a ceremony that was picketed by sheep-costumed protesters. They noted that his work on creating human cell lines using nuclear transfer would be illegal in Germany, which forbids all forms of human cloning.

Wilmut says the prize money—half of which comes from the German government—will only support attempts to piece together the molecular processes behind nuclear reprogramming in mice. And the work may not be done at Roslin: Wilmut told reporters before the event that he was leaving the institute this summer. He declined to name his new employer.

AWARDS

New heights. The two researchers who share this year's $200,000 Tyler Prize for Environmental Achievement reached for the sky to take the pulse of the climate system and, ultimately, raise awareness of the global warming threat.

In 1958, atmospheric chemist Charles Keeling (above) of the Scripps Institution of Oceanography in La Jolla, California, went to the top of Hawaii's 4170-meter Mauna Loa to see what the burning of fossil fuels was doing to the atmosphere. Within a few years Keeling's lengthening record of precisely measured carbon dioxide, now known as the "Keeling curve," had revealed the seemingly inexorable accumulation of the greenhouse gas in the atmosphere. By committing to meticulous analysis of a neglected trace gas, says atmospheric scientist Stephen Schwartz of Brookhaven National Laboratory in Upton, New York, the now-retired Keeling "has changed the world."

Paleoclimatologist Lonnie Thompson (right) of Ohio State University in Columbus has trudged up to glaciers as high as 7200 meters to drill out millennia-long climate records from tropical ice (*Science*, 18 October 2002, p. 518). They have helped him show that the tropics suffer far larger climatic swings than scientists had suspected. His next goal: Bring back ice from more tropical mountain glaciers before global warming melts them.

RISING STARS

Helping others. The 2001 attack on the World Trade Center gave 17-year-old David Bauer of New York City's Hunter College High School the idea for his prizewinning Intel Science Talent Search project. With help from Valeria Balogh-Nair, a biochemist at the City College of New York, Bauer designed a toxic sensor based on fluorescent nanocrystals that dim in the presence of neurotoxins. Bauer hopes that paramedics and other first responders might someday have the sensor coated on their badges to detect toxic agents such as nerve gas.

Last week, Intel awarded Bauer first place and a $100,000 scholarship. Timothy Frank Credo, 17, of the Illinois Mathematics and Science Academy in Highland Park placed second—and won $75,000—for a more precise method of clocking photons across a plate in a particle detector. Kelley Harris, 17, of C. K. McClatchy High School in Sacramento, California, came in third—and received $50,000—for her work on viral proteins that bind to Z-DNA.

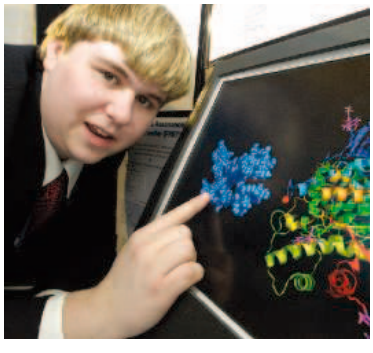

JOBS

In-house star. The chief scientist of Argonne National Laboratory in Illinois has been promoted to director. Robert Rosner, an astrophysicist who has studied plasmas and fluid dynamics within stars, will take over the $475 million Department of Energy (DOE) facility next month. He takes the reins from Hermann Grunder, who is retiring in April after a 37-year career at DOE labs including the last four at Argonne.

The 57-year-old Rosner, who penned the facility's 20-year plan in 2003, says he wants "stronger ties between basic science and applications," citing work in transportation and a new center focusing on infrastructure vulnerabilities. The lab is run by the University of Chicago.

NONPROFIT WORLD

New HHMI researchers. After a 5-year hiatus, the Howard Hughes Medical Institute (HHMI) in Chevy Chase, Maryland, has selected a new crop of 43 biomedical investigators (www.hhmi.org). A fifth of the winners earned their Ph.D.s in the physical sciences, a ratio that reflects not a deliberate target but rather "a sign of the times," says HHMI president Thomas Cech.

Like the 298 current HHMI investigators, the new class will become institute employees (funded at $1 million a year per person, on average) but remain on their campuses. Cech says the new awards reflect a rebound for the $13 billion HHMI endowment, which dropped by one-quarter in the early 2000s, and a sustained commitment to investigators despite the massive Janelia Farm project (*Science*, 8 October 2004, p. 210).

Got any tips for this page? E-mail people@aaas.org

CREDITS (TOP TO BOTTOM): AP PHOTO/MICHAEL PROBST; (INSET): RICK KOZAK; SCRIPPS INST. OF OCEANOGRAPHY; SOURCE: THE OHIO STATE UNIVERSITY; BOB GOLDBERG

Congratulations

to the AAAS Student Poster Winners!

AAAS recognizes the winners of the 2005 Student Poster Competition at the AAAS Annual Meeting in Washington, D.C., this past February. Their work in a variety of fields displayed originality and understanding that set them apart from their colleagues. This year, first-place winners also will receive cash prizes thanks to the generous support of Subaru and the Canadian Embassy. Congratulations!

Brain and Behavior

Sarita Shaevitz, University of California, Berkeley

Honorable Mention: Elaine M. Tan, Salk Institute for Biological Studies

Environment and Ecology

Lara Dehn, Cheryl Rosa, University of Alaska, Fairbanks

Honorable Mention: Mona Rezapour, China Lunde, University of California-Berkeley; Lysa M. Styfurak, Katie D. Hogan, Melissa Pope, Adam C. Miller, Lorain County Community College; James M. Wittler, Colorado State University

Information, Math, and the Internet

Kelly VanOchten, Jessica Muntz, Central Michigan University with Noah Streib, Oberlin College

Medicine and Public Health

Beri Massa, University of North Carolina, Chapel Hill

Honorable Mention: Vicki D. Johnson, University of North Carolina, Chapel Hill; Christopher L. Price, University of California, Irvine; John Yi, Beth Holbrook, Wake Forest University Baptist Medical Center

Molecular and Cellular

Jessica M. Blanton, Amherst College

Kalpalatha Melmaiee, Kathryn Lee, Sathya Elavarthi, Oklahoma State University

Benjamin Savitch, Arizona State University

Edna C. Suárez-Castillo, University of Puerto Rico

Honorable Mention: Albert E. Almada, University of California, Irvine; Melissa Hernandez, University of California, Irvine; Vikash Kumar, University of Leeds and University of York; Joshua J. Plant, University of Utah; Roberto Tinoco, University of California, Irvine

Organismic

Steve Hicks, Marist College

Kathryn A. Matthias, Angela Interrante, Ursinus College

Physical Sciences

Kendra A. Denson, Monroe Community College

Rupa Hiremath, Georgetown University

Kevin W. Reynolds, Norfolk State University

Honorable Mention: Guido Cervone, George Mason University; Erik Garnett, University of California, Berkeley

Social Sciences

Andrew P. Martin, Rodrick Megraw, University of Washington

Jennifer M. Lancaster, University of Central Oklahoma

Honorable Mention: Amanda G. Berry, Stevenson School; Pamela K. Harjo, University of Central Oklahoma; Erin E. Peters, George Mason University; Leslie Snyder, Tanya O'Boyle, DeSales University

Technology and Engineering

Daniel L. Rokusek, University of Illinois at Urbana-Champaign

Honorable Mention: Melisa M. Carpio, University of California, Berkeley

For more information, please visit:

www.aaasmeeting.org

AAAS

ADVANCING SCIENCE, SERVING SOCIETY

Letters to the Editor

Letters (~300 words) discuss material published in *Science* in the previous 6 months or issues of general interest. They can be submitted through the Web (www.submit2science.org) or by regular mail (1200 New York Ave., NW, Washington, DC 20005, USA). Letters are not acknowledged upon receipt, nor are authors generally consulted before publication. Whether published in full or in part, letters are subject to editing for clarity and space.

Abuse of Prisoners at Abu Ghraib

IN THEIR POLICY FORUM "WHY ORDINARY people torture enemy prisoners" (26 Nov. 2004, p. 1482), S. T. Fiske and colleagues suggest that almost anyone could have committed the Abu Ghraib atrocities (*1*). They go on to say, "lay-observers may believe that explaining evil amounts to excusing it and absolving people of responsibility for their actions…" Any humane person should react to their "explanation" in exactly this way. I think they make the mistake of trying to divorce "science" from politics in an area where the two are inextricably mixed. There is no mention in their Policy Forum of the fact that the U.S. Department of Justice advised the White House that torture "may be justified" (*2*–*4*); that the "war on terrorism" renders obsolete Geneva's strict limitations on questioning of enemy prisoners and renders quaint some of its provisions (*2*–*4*); or that torture was endorsed at the very highest levels of the government and military (*5*). Is it really irrelevant that General Miller is quoted (*6*) as saying that prisoners are "like dogs and if you allow them to believe at any point that they are more than a dog then you've lost control of them"? Why was none of this mentioned?

Studying the effect of "one dissenting peer" may be relatively harmless academic amusement, but if you really want to stop this sort of thing what you need are leaders, both political and military, who have the moral fiber to make it absolutely clear that abuse and torture are intolerable in a civilized society. Sadly, the political and military leadership did exactly the opposite in this case. Fiske *et al.* should have said so.

DAVID COLQUHOUN

Department of Pharmacology, University College London, Gower Street, London WC1E 6BT, UK. E-mail: d.colquhoun@ucl.ac.uk

References and Notes

1. The conclusion is pretty dubious, as it appears to be heavily dependent on meta-analysis, the poor man's substitute for doing proper research.
2. D. Priest, R. J. Smith, *Washington Post*, 8 June 2004, p. A1 (www.washingtonpost.com/wp-dyn/articles/A23373-2004Jun7.html).
3. Full text of the Gonzales memo is available at http://msnbc.msn.com/id/4999148/site/newsweek/.
4. A compendium of relevant government documents: K. J. Greenberg, J. L. Dratel, *The Torture Papers: The Road to Abu Ghraib* (Cambridge Univ. Press, Cambridge, 2005).
5. R. J. Smith, J. White, *Washington Post*, 12 June 2004, p. A1 (www.washingtonpost.com/wp-dyn/articles/A35612-2004Jun11.html).
6. Brigadier General Janis Karpinski said that current Iraqi prisons chief Major General Geoffrey Miller—who was in charge at Guantanamo Bay—visited her in Baghdad and said, "At Guantanamo Bay we learned that the prisoners have to earn every single thing that they have." She said, "He said they are like dogs and if you allow them to believe at any point that they are more than a dog then you've lost control of them." "Iraq abused 'ordered from the top,'" *BBC News*, http://news.bbc.co.uk/1/hi/world/americas/3806713.stm.

THE ATTEMPT BY SCIENTIFIC PSYCHOLOGY TO explain mayhem like Abu Ghraib ("Why ordinary people torture prisoners," S. T. Fiske *et al.*, Policy Forum, 26 Nov. 2004, p. 1482) emphasizes findings from academic studies on the power of social context. Just one example of where Fiske *et al.*'s account misunderstands what social psychology really has to say about Abu Ghraib comes from the authors' citation of Stanley Milgram's classic *Obedience to Authority* experiments (*1*).

Actually, Milgram was cautious about the possibility of extrapolating the "obedience paradigm" to real-life atrocities (*2*). He once wrote back to an enthusiastic young replicator of his results, "it is quite a jump… from an experiment of this sort to general conclusions about the Nazi epoch, and I, myself, feel that I have sometimes gone too far in generalising. Be cautious about generalising." (*3*).

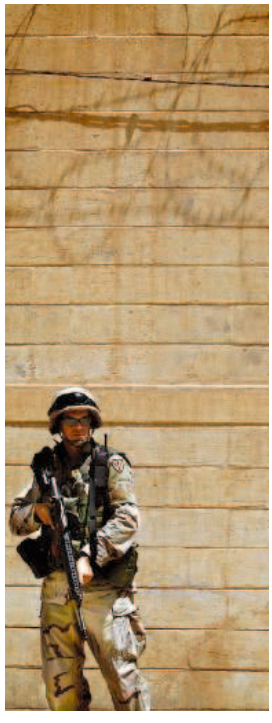

Instead, Milgram suggested that the true explanation of evil like the Holocaust was linked to his experiments by their demonstration of "a propensity for people to accept definitions of action provided by legitimate authority. That is, although the subject performs the action, he allows authority to define its meaning." [(*1*), p. 145].

Authority figures of governments headed by George Bush and Tony Blair define what is happening, in Iraq and across the world, as a "war on terror" involving certain nations and peoples who pose an immediate threat to us because they are mad and/or evil and bent on our total annihilation. The public and the army may accept the official definition of our predicament unquestioningly, which in turn naturally legitimizes extreme force to be used against our "enemy."

If U.S. psychologists and scientists are going to stray outside of the narrow confines of the laboratory and attempt to explain the appalling behavior of its citizens abroad, science is ill-served by accepting unflinchingly the definitions of "situation" and "enemy" provided by politicians.

RAJ PERSAUD

The Maudsley Hospital and Institute of Psychiatry, Westways Clinic, 49 St James Road, West Croydon, London CR0 2UR, UK.

References

1. S. Milgram, *Obedience to Authority: An Experimental View* (Harper & Row, New York, 1974).
2. Letter to Miss Harriet Tobin, 9 April 1964, Stanley Milgram Papers, Yale University Library, Manuscripts and Archives.
3. T. Blass, *The Man Who Shocked the World: The Life and Legacy of Stanley Milgram* (Basic Books, New York, 2004).

THE POLICY FORUM "WHY ORDINARY PEOPLE torture prisoners" by S. T. Fiske *et al.* (26 Nov. 2004, p. 1482) has provoked a great deal of discussion among social psychologists. Much of it has been concerned with the seemingly excessive number of half-baked social-psychological ideas that can be invoked, post hoc, to "explain" Abu Ghraib—or any other social phenomenon.

However, the skeptical reactions to the Policy Forum mirror it in failing to ask a more fundamental question, which concerns the politics of science: Why is it that American social scientists become galvanized to explain evil as something that can be committed by "anyone," given a particular "context," only when Americans commit the atrocities?

The point here is that the might (or spin) of American social science has seldom been invoked to semi-excuse (in the popular mind) others' atrocities. "They," these others, are simply genetically and historically assumed to be evil or savage.

There is a shadow over Fiske *et al.*'s paper: The rest of the world may well think that American social science works for the U.S. State Department.

VLADIMIR J. KONEČNI

Department of Psychology, University of California, San Diego, La Jolla, CA 92093–0109, USA.

CREDIT: REUTERS/DAMIR SAGOLJ

IN THEIR POLICY FORUM "WHY ORDINARY people torture enemy prisoners" (26 Nov. 2004, p. 1482), S. T. Fiske *et al.* point out that abhorrent actions such as those that occurred at Abu Ghraib can be prevented by "even one dissenting peer." This brings to mind a statement made by Elie Wiesel in his 1986 Nobel Peace Prize acceptance speech: "I swore never to be silent whenever and wherever human beings endure suffering and humiliation. We must take sides. Neutrality helps the oppressor, never the victim. Silence encourages the tormentor, never the tormented. Sometimes we must interfere. When human lives are in danger, when human dignity is in jeopardy, national borders and sensitivities become irrelevant." Would that we all could remember this and act accordingly, when under the prevalent influence of conforming pressures.

DAVID C. MUSCH

Departments of Ophthalmology and Visual Sciences, and Epidemiology, University of Michigan, Kellogg Eye Center, 1000 Wall Street, Ann Arbor, MI 48105, USA.

Response

OUR CRITICS RAISE TWO PRIMARY OBJECTIONS to our Policy Forum: the nature of the evidence and the scope of the conclusions.

Konečni expresses skepticism for which he presents no evidence: He implies that our summary of peer-reviewed, published meta-analyses by respected scholars represents a fringe perspective, claiming that our article "provoked a great deal of discussion among social psychologists"; in fact, there has been little discussion on any social psychology list-serve, e-mail, or newsletter to that effect as far as we know. Konečni suggests that the principles invoked in our article (aggression under stress, prejudice against outgroups, conformity to peers, obedience to authorities, and step-by-step social influence) are "half-baked": These principles are supported not only by the meta-analyses across dozens of studies, but each also is widely accepted as a fundamental scientific principle.

Colquhoun objects that meta-analytic evidence is the "poor man's substitute for doing proper research." I would challenge him to do that research, because social scientists have not been permitted to examine the evidence and interview the perpetrators and victims. In the absence of new data, the cumulative evidence of research indeed helps to account for the events. Our purpose was not to conduct fresh research but to publicize a reliable database that might have averted these events, had the right people cared to look. It might still help to avert future such actions by Americans and by others.

Persaud protests extrapolation from laboratory studies to real-life atrocities. But would he have us ignore the decades of replications across cultures and settings—both laboratory and field—that indicate the power of stress, prejudice, peers, authorities, and commitment?

Konečni demonizes our inferred politics and urges us to identify other torturers around the world. Colquhoun urges us to take stronger, more explicit political stands. In contrast, Persaud chastises us for "stray[ing] outside the narrow confines of the laboratory."

We think that the implications of the evidence are self-evident, but our brief as scientists is to report the evidence. We believe that the evidence speaks for itself, and we think that science is more credible when it acts as an honest broker, presenting the available, reliable data but refraining from arguing for a particular political solution. We reiterate our already published stand: The evidence indicates that the individuals are responsible, yes, because sometimes (rarely) they can and do resist social

pressures. But also responsible are their peers and superiors up the chain of command, who determine the powerful social context that encourages atrocities.

These principles help explain an event of special significance to Americans because the perpetrators are Americans. Clearly, it applies beyond the American context, as recent events distressingly indicate. Indeed, we concur with Musch.

SUSAN T. FISKE, LASANA T. HARRIS, AMY J. C. CUDDY
Department of Psychology, Princeton University, Princeton, NJ 08544–1010, USA.

Reinventing the Wheel in Ecology Research?

WE ARE PLEASED WITH M. SOLAN *ET AL.*'S findings that "species extinction is generally expected to reduce the depth of bioturbated sediments" ("Extinction and ecosystem function in the marine benthos," Reports, 12 Nov. 2004, p. 1177) and support their conclusion that "Such changes might be expected to alter the fluxes of energy and matter that are vital to the global persistence of marine communities," significantly altering ecosystem function.

At the University of Texas Marine Science Institute, we conducted a 5-year study of benthic community structure and function in South Texas Gulf of Mexico coastal waters. Our findings documented the effects of larger fauna (e.g., enteropneusts and ophiuroids) on benthic community structure, sediment metabolism, and nutrient regeneration (*1*). Changes in biodiversity, depth of the oxygenated sediments, and sediment nutrient release rates were influenced by the presence or absence of a "key" benthic macroinfaunal species (i.e., *Schizocardium* sp.). Our studies of two decades ago, from natural field observations aided by the extinction of a "key" bioturbator, support the conclusions of the Solan modeling strategy (*2*–*6*).

In his related Perspective "How extinction patterns affect ecosystems" (12 Nov. 2004, p. 1141), D. Raffaelli surmises that ecologists are challenged in advising policymakers about the effects of benthic changes on ecosystems throughout a food web. Solan *et al.*'s statement of the need to "protect coastal environments from human activities that disrupt the ecological functions species perform" echoes what we (as well as many others) stated 20 years ago. Why do we keep repeating aspects of ecological research instead of building on historical accounts? If we were better at telling the evolving story instead of simply repeating pronouncements over decades, we would not face such a "challenge" in convincing policy-makers to develop a more comprehensive, adaptive approach to marine ecosystem management.

R. WARREN FLINT[1] AND RICHARD D. KALKE[2]
[1]Five E's Unlimited (http://www.eeeee.net), 28 Randolph Place, NW, Washington, DC 20001, USA. E-mail: rwflint@eeeee.net. [2]University of Texas, Marine Science Institute, Port Aransas, TX 78373, USA.

References
1. R. W. Flint, R. D. Kalke, *Mar. Ecol. Prog. Ser.* **31**, 23 (1986).
2. R. W. Flint, D. Kamykowski, *Estuar. Coastal Shelf Sci.* **18**, 221 (1984).
3. R. W. Flint, *Mar. Chem.* **16**, 351 (1985).
4. R. W. Flint *et al.*, *Estuaries* **9** (no. 4A), 284 (1986).
5. R. W. Flint, R. D. Kalke, *Contrib. Mar. Sci.* **28**, 33 (1985).
6. R. W. Flint, R. D. Kalke, *Estuar. Coastal Shelf Sci.* **22**, 657 (1986).

Response

FLINT AND KALKE SUGGEST THAT THE ISSUES that Solan *et al.* and Raffaelli discuss have been addressed before. Ecologists have historically focused on biodiversity as a response variable driven by, or correlated with, ecological processes. When studies have explored the effect of organisms on

LETTERS

these processes, the focus has been on the roles played by individual species or, sometimes, the impact of whole species assemblages. The papers to which Flint and Kalke refer us can be firmly placed within this earlier tradition.

In the past decade, a new paradigm has become prominent—one that considers how biological diversity per se regulates, rather than responds to, ecosystem-level processes (*1*). The Solan *et al.* paper is set squarely within this new tradition (*2*), which represents a shift away from the concepts surrounding earlier biodiversity research of benthic and other ecosystems. We therefore disagree with the Flint and Kalke assertion that ecology just keeps spinning its wheels.

Flint and Kalke ask, "Why do we keep repeating aspects of ecological research instead of building on historical accounts?" The perception that historical accounts are not being built on is misplaced. For instance, Emmerson and Huxham (*3*) demonstrate how published data similar to those of Flint and Kalke can be synthesized to provide valuable insights into the linkages between biodiversity and ecosystem functioning. Similarly, the BioMERGE initiative (*4*), which gave rise to the work of Solan *et al.*, uses preexisting data and concepts from multiple ecological disciplines to parameterize models of global change. Only by integrating invaluable historical accounts with novel data and synthesizing our knowledge into new frameworks can our research stimulate the natural sciences and provide compelling evidence-based arguments for policy-makers.

DAVID RAFFAELLI,[1] BRADLEY J. CARDINALE,[2] AMY L. DOWNING,[3] KATHARINA A. M. ENGELHARDT,[4] JENNIFER L. RUESINK,[5] MARTIN SOLAN,[6] DIANE S. SRIVASTAVA[7]

[1]Environment Department, University of York, York YO10 5DD, UK. [2]Department of Ecology, Evolution and Marine Biology, University of California, Santa Barbara, Santa Barbara, CA 93106, USA. [3]Department of Zoology, Ohio Wesleyan University, Delaware, OH 43015, USA. [4]University of Maryland Center for Environmental Science, Appalachian Laboratory, 301 Braddock Road, Frostburg, MD 21532–2307, USA. [5]Department of Biology, University of Washington, Box 351800, Seattle, WA 98195, USA. [6]Oceanlab, University of Aberdeen, Main Street, Newburgh, Aberdeenshire, AB41 6AA, Scotland. [7]Department of Zoology, University of British Columbia, 6270 University Boulevard, Vancouver, BC V6T 1Z4, Canada.

References

1. M. Loreau *et al.*, *Science* **294**, 804 (2001).
2. S. Naeem, *Ecology*, **83**, 1537 (2002).
3 M. Emmerson, M. Huxham, in *Biodiversity and Ecosystem Functioning. Synthesis and Perspectives*, M. Loreau, S. Naeem, P. Inchausti, Eds. (Oxford Univ. Press, Oxford, 2002), pp. 139–146.
4. S. Naeem, J. P. Wright, *Ecol. Lett.* **6**, 567 (2003).

A Central Repository for Published Plasmids

TO STUDY THE FUNCTION OF A SEGMENT OF DNA, researchers typically insert it into a DNA-based vector called a plasmid. Plasmids can then be used in a variety of experimental systems. Circulation of plasmids among the academic community is essential for scientific progress but is hindered because of inefficiencies in the current distribution process.

When a plasmid appears in an academic publication, it is considered to be public domain and should be made available to the scientific community upon request. Each laboratory presently stores its own published plasmids and is responsible for answering requests in a timely fashion. However, turnover of students and post-doctoral fellows and busy research schedules contribute to variable plasmid quality and delays in shipment.

Addgene, a nonprofit organization, is creating a central plasmid repository where scientists can search for and request plasmids online. A plasmid repository will provide standardized quality control and reliable deliveries and will serve as an archive to prevent plasmid and information loss over time.

Addgene accepts plasmids in either DNA or bacterial form and stores them as bacterial glycerol stocks both on-site and at a backup facility off-site. Vector maps and information regarding plasmid construction will be submitted by the originating laboratory and will be available on Addgene's Web site.

Addgene will distribute plasmids through direct online ordering. Addgene's Web site will also contain a searchable database of its stored plasmids, making it convenient to locate all available plasmids containing different versions of a particular gene, such as tagged versions, dominant active or negative mutants, or those expressed in unique vectors.

Addgene will not only collect plasmids from newly published papers, but will also retroactively collect plasmids from those investigators who would like to submit frequently requested plasmids. By doing so, Addgene will relieve investigators of the time and effort needed to answer requests, as well as provide a reliable archival service for plasmids and maps. All scientists who submit plasmids to Addgene will have access to the list of researchers who have requested their reagents.

Addgene is currently working with high-impact journals to collect plasmids at the time of publication. Addgene invites the scientific community to participate in this endeavor. Investigators and journals that would like to partner with Addgene to build this resource are welcome to submit plasmids or learn more about the initiative by visiting www.addgene.org.

MELINA FAN,[1] JUDY TSAI,[1] BENJIE CHEN,[1] KENNETH FAN,[1] JOSHUA LABAER[2]

[1]Addgene, One Kendall Square, Building 600, 3rd Floor, Cambridge, MA 02139, USA. [2]Departments of Biological Chemistry and Molecular Pharmacology, Harvard Medical School, 320 Charles Street, Cambridge, MA 02141, USA.

CORRECTIONS AND CLARIFICATIONS

Perspectives: "Malaria vaccines: back to the future?" by A. P. Waters *et al.* (28 Jan., p. 528). On page 529, in the seventh line of the second paragraph, the sentence should read "In previous work (*10*), Matuschewski *et al.* had used suppression subtractive cDNA hybridization to identify 29 genes."

Reports: "Spindle multipolarity is prevented by centrosomal clustering" by N. J. Quintyne *et al.* (7 Jan., p. 127). There was an error in Fig. 3. Panel B, a was mistakenly printed twice, with the second printing slightly overlapping panel B, a′. The corrected figure is shown here.

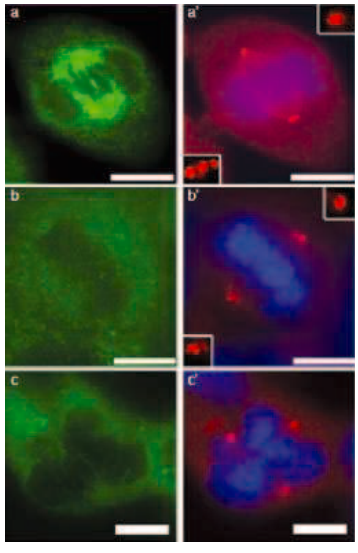

Research Articles: "Dissection of the mammalian midbody proteome reveals conserved cytokinesis mechanisms" by A. R. Skop *et al.* (2 July 2004, p. 61). This paper reported the identification of glucose transporters GLUT1 and GLUT4 in the midbody. The correct protein names should be GLUT1 CBP and GLUT4 vesicle protein, respectively, as indicated in Table S1 (see Supporting Online Material available at www.sciencemag.org/cgi/data/1097931/DC1/2). Nevertheless, the suggestion that glucose transporters function during cytokinesis is supported by the presence of GLUT1 CBP and GLUT4 vesicle protein; the cytokinesis defects observed in *C. elegans* after RNAi of both homologs of these genes; and the localization of GLUT1, a glucose transporter that binds to GLUT1 CBP [R. C. Bunn, M. A. Jensen, B. C. Reed, *Mol. Biol. Cell* **10**, 819 (1999)], to mammalian midbodies using a GLUT1-specific antibody (Fig. 3). The authors thank N. Manel for pointing out the error in the original paper and apologize for any confusion that this mistake has caused.

Ready for Their Close-Up

Hans Sues

In the theater of Mesozoic terrestrial life, mammals have long been cast as bit players—mouse-sized, furry creatures leading furtive existences in the wings while dinosaurs chewed up the scenery. This traditional view may be questioned because mammals and dinosaurs were very different in terms of size and biology, and, aside from one occasionally feeding on the other, the two groups probably had relatively little direct interaction.

The Mesozoic fossil record of mammals represents more than two-thirds of the group's entire evolutionary history and shows that they, like their dinosaurian contemporaries, rapidly diversified soon after their first appearance in the Late Triassic. The first announcement, in 1824, of the presence of mammals in Mesozoic strata (Middle Jurassic Stonesfield slates in England) shocked most scientists because it challenged then-prevailing notions concerning the succession of life through geological time. Additional discoveries through the 1860s, most also in England, quickly established the existence of a diversity of Mesozoic mammals, and in 1871 Richard Owen provided the first detailed study of these finds (*1*). In the second half of the 19th century, collectors working for Othniel Charles Marsh at Yale recovered a wealth of Jurassic and Cretaceous mammalian fossils in the American West. In the 1920s, George Gaylord Simpson reviewed all known Mesozoic mammals and published two major monographs on the European and American specimens (*2*, *3*).

Research in the field was rekindled in the 1940s, with discoveries of early Mesozoic mammals in Britain. The pace of exploration accelerated in the 1960s. Unlike in earlier years, when finds of mammalian remains were usually an accidental by-product of the quest for dinosaurs, paleontologists now systematically searched for mammalian fossils, especially the durable and diagnostic teeth. New techniques for breaking down and screening sedimentary rocks made this effort more productive. At the same time, discoveries of scores of well-preserved skulls and postcranial remains in Late Cretaceous strata in the Gobi Desert of Mongolia by Polish-Mongolian expeditions led by Zofia Kielan-Jaworowska initiated major advances in our understanding of the skeletal morphology of several major clades of Mesozoic mammals. In 1979, Jason Lillegraven, Kielan-Jaworowska, and William Clemens edited a comprehensive survey of the structure and diversity of Mesozoic mammals (*4*), but such was the pace of research that much of the volume quickly became outdated. The most significant development in recent years has been the discovery of exquisitely preserved skeletons of various Early Cretaceous mammals in the Yixian Formation of Liaoning Province (northeast China), which have had a profound impact on our understanding of the origin and early evolution of marsupials and placentals.

Clearly mammals were a significant component of many Mesozoic terrestrial ecosystems. Yet their fossil record still remains sparse for much of the Mesozoic, and many issues remain unresolved. For example, the record is still too incomplete to test divergence dates for most of the principal lineages of placental mammals proposed by molecular evolutionary studies. Today the search for Mesozoic mammals continues worldwide, with almost every year bringing exciting new discoveries.

Mammals from the Age of Dinosaurs, written by Kielan-Jaworowska, Richard Cifelli, and Zhe-Xi Luo, represents a much needed, authoritative survey of Mesozoic mammalian diversity and evolution. The authors, leading investigators in the field, have produced a landmark study that provides a phylogenetic framework for future work on mammalian history. (Kudos to the publisher for including the character-taxon matrix used for the parsimony analysis as an appendix to the text, rather than relegating it to an ephemeral Web site.)

They view the phylogenetic tree of Mesozoic mammals as a "bush" of lineages, with successive radiations throughout the era. This picture differs from the fundamental dichotomy between nontherian and therian mammals favored by many authors since the 1970s as well as from Simpson's earlier concept of Mammalia as a grade comprising several lineages with separate origins among nonmammalian cynodonts. The most radical aspect of the authors' phylogenetic hypothesis is the dual origin of tribosphenic ("reverse triangle") molars, with a Southern Hemisphere clade (Australosphenida) that includes monotremes developing this type of cheek teeth independently from a Northern Hemisphere clade (Boreosphenida) that includes marsupials and placentals. Recently discovered Early Cretaceous fossils in Australia indicate that monotremes also developed the characteristic mammalian three-bone middle ear independently from therians.

The authors devote the bulk of the volume to a comprehensive survey of Mesozoic mammalian diversity, one

CREDIT: MARK A. KLINGLER/CARNEGIE MUSEUM OF NATURAL HISTORY

Not just a dental record. The single specimen of *Jeholodens jenkinsi* is a nearly complete articulated skeleton and skull (from the Early Cretaceous of Liaoning Province, China). This eutriconodont probably weighed less than 30 g and fed mainly on insects and other invertebrates.

Mammals from the Age of Dinosaurs
Origins, Evolution, and Structure
by Zofia Kielan-Jaworowska, Richard L. Cifelli, and Zhe-Xi Luo
Columbia University Press, New York, 2004. 648 pp. $195, £126. ISBN 0-231-11918-6.

The reviewer is at the National Museum of Natural History, Smithsonian Institution, MRC 106, Post Office Box 37012, Washington, DC 20013-7012, USA. E-mail: suesh@si.edu

grounded in the wealth of their own primary studies. For each major group of Mesozoic mammals, they offer a concise review of the group's anatomy and paleobiology, followed by a synopsis of all known genera (each of which is diagnosed and illustrated). This makes the book a particularly useful resource for specialist and novice alike because the primary literature on the subject (covered in a 52-page bibliography) is vast, multilingual, and widely scattered.

Like Simpson's classic studies, *Mammals from the Age of Dinosaurs* provides a solid foundation for the continuing quest to shed light on the extensive Mesozoic history of mammals, including the most distant roots of our own species.

References

1. R. Owen, *Monograph of the Fossil Mammalia of the Mesozoic Formations* (Palaeontographical Society, London, 1871).
2. G. G. Simpson, *A Catalogue of the Mesozoic Mammalia in the Geological Department of the British Museum* [British Museum (Natural History), London, 1928].
3. G. G. Simpson, *American Mesozoic Mammalia* (Yale Univ. Press, New Haven, CT, 1929).
4. J. A. Lillegraven, Z. Kielan-Jaworowska, W. A. Clemens, Eds., *Mesozoic Mammals: The First Two-Thirds of Mammalian History* (Univ. California Press, Berkeley, CA, 1979).

10.1126/science.1109678

ECOLOGY

Place Matters

Sahotra Sarkar

Biogeography has come a long way since the journeys of Humboldt and Wallace in the 19th century. Over the last three decades, the field has been revolutionized by the spread of geographic information systems (GIS) technology and the increasing power of desktop computers. Indeed, according to James Brown's contribution to *Frontiers of Biogeography*, the field only emerged as a recognizable subdiscipline during this period. It has become an international enterprise drawing on interactions not only with various biological and geographical subdisciplines but also with climatology, economics, geology, and sociology. Biogeography has also become central to the new discipline of conservation biology: without accurate relevant knowledge of biota localized to individual places, any conservation strategy is a shot in the dark. However, biogeographers and their collaborators, especially in academia, tend to be segregated into different departments and institutes. This volume is intended by its editors, Mark Lomolino and Lawrence Heaney, to play an integrative role by both summarizing the present state of the field and encouraging interdisciplinary interaction.

Frontiers of Biogeography
New Directions in the Geography of Nature
Mark V. Lomolino and Lawrence R. Heaney, Eds.
Sinauer Associates, Sunderland, MA, 2004. 448 pp. $79.95, £51.99. ISBN 0-87893-479-0. Paper, $49.95, £31.99. ISBN 0-87893-478-2.

The volume's 18 chapters were developed from plenary papers presented at the inaugural meeting of the International Biogeography Society (January 2003 at Mesquite, Nevada). The authors include most of the major researchers in the field from North America and the United Kingdom, but the only other countries represented by contributors are Mexico and Chile. The new society's quest for international participation obviously has a way to go. The editors have divided the material among five sections that correspond to the field's major divisions: paleobiogeography, phylogeography and diversification, diversity gradients, marine biogeography, and conservation biogeography. Nearly all the papers focus on general principles rather than case studies (the chief exception being Heaney's chapter, which mainly concerns the Philippines). In addition, the contributors generally emphasize conceptual issues rather than technical detail. Both of these factors make the volume useful for introductory students.

The sections on paleogeography and phylogeography (the geographic distributions of genealogical lineages) complement each other well enough that they easily could have been merged. Using plate tectonics reconstructions based on 25 years of data synthesis and modeling in the PALEOMAP project, Christopher Scotese illustrates the changing global geography from the Early Triassic through to the current world. Bruce Lieberman also illustrates the importance of a deep-time perspective in his consideration of range expansion, extinction, and biogeographic congruence. Brett Riddle and David Hafner explore the relevance of phylogeography to historical biogeography. These two sections also include contributions by Julio Betancourt on arid lands biogeography, Stephen Jackson on quaternary biogeography, and Christopher Humphries and Malte Ebach on cladistic biogeography as well as Daniel Brooks's comparison of what he distinguishes as cladistic versus phylogenetic biogeography.

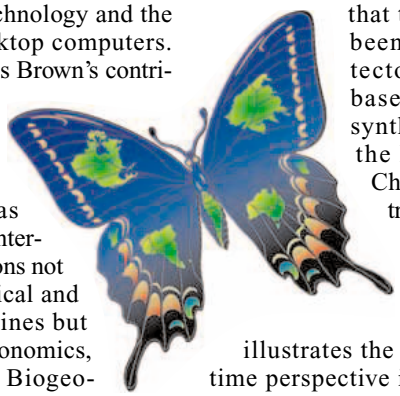

CREDIT: AFTER BERNARD CAHILL'S 1909 BUTTERFLY MAP OF THE WORLD/COURTESY SINAUER ASSOCIATES

Although the remaining sections are not quite as well integrated, they are more cohesive than those in a typical conference product. Several individual papers stand out: Kaustuv Roy and collaborators attempt to quantify spatial patterns of biogeographic diversity using information on the function and morphology of organisms. This effort is intriguing because, while different measures of diversity are routinely used in biodiversity conservation planning, functional and morphological data are usually ignored in spite of their obvious relevance to the viability of the biota in any particular area. Robert Whittaker explores the importance of spatial scale in processes that influence species richness from local sites to global patterns. Geerat Vermeij's interesting essay offers a marine perspective on island life. Despite its presence in the marine biogeography section, John Briggs's paper focuses on conservation, particularly of the East Indies Triangle—a major center of evolutionary radiation in the Indo-West Pacific. Julie Lockwood provides a useful summary of the effects of biological invasions on diversity patterns. Víctor Sánchez-Cordero and collaborators demonstrate how GIS-based modeling of niches can be integrated into conservation planning. Michael Rosenzweig's paper underscores the inability of island biogeography theory to guide conservation area network design while exploring the future use of general species-area relationships.

The book ends with a concise overview by Brown of biogeography's current state and future promise. He notes how recent developments have unexpectedly challenged many standard views of the 1980s, including the applicability of the equilibrium theory to islands, the preponderance of allopatric speciation, and high integration within communities. By and large, the papers are well written and endorse his conclusion that biogeography is presently in a state of flux, with few of the traditional certainties holding up under the scrutiny of new data and techniques. It is clear, however, that biogeography's crucial importance in efforts to conserve biodiversity makes it a subject of considerable contemporary significance. *Frontiers of Biogeography* successfully conveys some of the field's excitement.

10.1126/science.1109954

The reviewer is in the Section of Integrative Biology and the Department of Philosophy, University of Texas at Austin, Austin, TX 78712-1180, USA. E-mail: sarkar@mail.utexas.edu

ETHICS

Ethics: A Weapon to Counter Bioterrorism

Margaret A. Somerville and Ronald M. Atlas*

Advances in the life sciences, especially in molecular biology and informatics, and the potential for misuse of scientific research (the "dual-use" dilemma) raise the possibility that an act of terrorism could involve biological agents. International consensus is crucial on the steps needed to reduce this grave threat to humanity. One such step is to ensure that all people and institutions involved in science are aware of their ethical obligations.

An important way to promote the necessary international consensus and to raise the necessary awareness is through adoption of a code of ethics to govern research in the life sciences. It is with this thought that we set out to capture the critical elements that a code of ethics for the life sciences should include—one that we believe can help prevent the life sciences from becoming the death sciences (see the table on page 1882).

The code we propose is built on ethically relevant facts and the substantive and procedural principles of ethics that must govern its interpretation and application (*1*). They include nonmaleficence; beneficence; respect for life, especially human life; maintaining trust; embedding ethics in science; establishing a high ethical tone in institutions; acknowledging individual and collective responsibilities; and recognizing and fulfilling needs for ethics review and monitoring, notification of breaches of ethics, ethics education, and the transmission of ethical values to colleagues and those we mentor.

Yet, although many agree with such an approach, many strongly oppose it for reasons ranging from cognitive (it won't work) to emotional (fear that it will shut down science); philosophical (science is value free, it's only its applications that need ethical guidance); misguided (scientists are ethical people, and all that ethics requires is that they act in good conscience); monetary (it will bankrupt our company); and personal (it will ruin my career). But even those who question the value of a code agree that research in the life sciences, including biodefense research, must be conducted in a safe and ethical manner. Bodies speaking out publicly about this need for ethics include the General Assembly of the World Medical Association (*2*), the British Medical Association, (*3*) the U.S. National Research Council, (*4*) the British Parliament (*5*), and the Asia-Pacific Economic Cooperation (APEC) Leaders (*6*), among others (*7*).

There have been recurring debates since the tragic events of September 11, 2001, concerning what research should and should not be conducted and what information should and should not be disseminated in the open literature (*4*, *5*, *8*). That dialogue has generated calls for a code or codes of conduct to provide guidance for scientists, publishers, and others facing extremely difficult decisions in the context of the dual-use dilemma. The National Science Advisory Board for Biosecurity (NSABB) of the National Institutes of Health has been charged with developing such a code for professional organizations and institutions (*9*). In 2005, the Expert and State Parties Meeting of the Biological Weapons Convention (BWC) will consider how to promote a common understanding of needed actions toward this end as well.

We know that a code will not be sufficient to ensure that science is not misused—we have already heard the laments "pious words will not solve the problem,"… "they are not worth the paper they are written on," … " they have no teeth" (*10*, *11*). Codes of ethics did not prevent scientists and physicians from leading the efforts of Aum Shinrikyo to develop biological weapons (*12*). Even the Hippocratic Oath has been violated by physicians' participating in biological weapons programs (*13*–*17*). Ken Alibek, for example, led the bioweapons program of the former Soviet Union even after the signing of the Biological Weapons Convention banned such programs (*18*); and Shiro Ishii directed the secret Japanese unit that engaged in human experimentation for biological weapons development during World War II (*19*, *20*).

Recognizing that past breaches of ethics have occurred, despite the existence of a code, presents a challenge, namely, guarding against the cynicism or despair that may evoke. Research in the philosophy of science shows that as long as a small clustered nucleus of ethical voices remains, ethics has a high probability of reasserting itself (*21*, *22*). We must continue to try to be ethical and to encourage and to help others to do likewise. A code of ethics will help in both respects.

Ethics brings deep values and beliefs into play, which means we may not always agree with each other. But we need to establish a code and then use it as a basis for engaging in an ongoing debate, because ethics is an ongoing process not an isolated event (*23*). A code not only raises awareness of the need for ethics and provides guidelines against which to judge the ethical acceptability of any given conduct, but also functions as a teaching tool and provides less senior people, including students, with a means of raising ethical concerns, especially with respect to the conduct of those in authority. We should continue to foster "ethics talk"—because that is an important way in which ethics can move forward in conjunction with science as it advances (*23*).

To reiterate the ancient Hippocratic Oath, physicians and scientists must today, even more crucially than in the past, first do no harm. To paraphrase a provision in the modern Hippocratic Oath: Physicians and scientists shall remember that they have a pact with society to advance knowledge and to apply that knowledge for the good of humanity. Scientists and scientific institutions must act responsibly to limit potential misuse of scientific materials and information by bioweaponeers.

A code is a living instrument that will need to be supplemented, on a continuing basis, by interpretations, applications, and analysis of new case examples. Below, we consider how it would apply in one recent situation. In this analysis, the applicable articles of the proposed code are referenced.

Thomas Butler, a researcher at Texas Tech and former director of their medical center's Division of Infectious Diseases, had reported to the responsible university official in 2003 that he could not account for 30 vials of cultures of *Yersinia pestis*; later, he claimed that he had inadvertently

M. A. Somerville is at the McGill Centre for Medicine, Ethics, and Law, McGill University, Montreal, Canada, H3A 1W9. R. M. Atlas is at the Center for the Deterrence of Biowarfare and Bioterrorism at the University of Louisville, KY 40205, USA. E-mail:

*Author for correspondence. E-mail: r.atlas@louisville.edu

CODE OF ETHICS FOR THE LIFE SCIENCES

All persons and institutions engaged in any aspect of the life sciences must

1. Work to ensure that their discoveries and knowledge do no harm
   (i) by refusing to engage in any research that is intended to facilitate or that has a high probability of being used to facilitate bioterrorism or biowarfare; and
   (ii) by never knowingly or recklessly contributing to development, production, or acquisition of microbial or other biological agents or toxins, whatever their origin or method of production, of types or in quantities that cannot be justified on the basis that they are necessary for prophylactic, protective, therapeutic, or other peaceful purposes.

2. Work for ethical and beneficent advancement, development, and use of scientific knowledge.

3. Call to the attention of the public, or appropriate authorities, activities (including unethical research) that there are reasonable grounds to believe are likely to contribute to bioterrorism or biowarfare.

4. Seek to allow access to biological agents that could be used as biological weapons only to individuals for whom there are reasonable grounds to believe that they will not misuse them.

5. Seek to restrict dissemination of dual-use information and knowledge to those who need to know in cases where there are reasonable grounds to believe that the information or knowledge could be readily misused through bioterrorism or biowarfare.

6. Subject research activities to ethics and safety reviews and monitoring to ensure that
   (i) legitimate benefits are being sought and that they outweigh the risks and harms; and
   (ii) involvement of human or animal subjects is ethical and essential for carrying out highly important research.

7. Abide by laws and regulations that apply to the conduct of science unless to do so would be unethical and recognize a responsibility to work through societal institutions to change laws and regulations that conflict with ethics.

8. Recognize, without penalty, all persons' rights of conscientious objection to participation in research that they consider ethically or morally objectionable.

9. Faithfully transmit this code and the ethical principles upon which it is based to all who are or may become engaged in the conduct of science.

destroyed the cultures. The initial report submitted by the university official (article 3) sent Federal Bureau of Investigation agents racing to the campus and set off panic that terrorists might have acquired the cultures. Butler was a leading researcher who had pioneered therapy for treating plague victims that has saved innumerable lives. Butler, apparently, had carried the plague-containing material on a commercial airliner from Tanzania to the United States, had sent cultures back to Africa by air transport, and had transported cultures to laboratories within the United States—including government laboratories of the U.S. military and the Centers for Disease Control and Prevention—all without obtaining the necessary authorizations [articles 1(i) and 6]. He was criminally charged with illegally transporting Tanzanian plague samples and with defrauding the university in research contracts (article 7). Several Nobel laureates and others came to the defense of Thomas Butler, protesting his prosecution (*24*, *25*). Although their loyalty and concern for him are to be admired, the same is not true of their implied acceptance of his breach of laws and regulations. Our code calls for compliance with the law unless it would be unethical to do so, and working to change laws and regulations with which one does not agree (article 7).

The Butler case sent a clear signal to the research community, especially scientists and university researchers, that all ethical and legal requirements must be respected when undertaking research [articles 1(i), 4, 6, and 7]. Biosafety regulations are not merely legal technicalities. They constitute some of the terms of the pact between science and the public that establishes public trust. That trust is the basis upon which research is conducted.

Certainly, the code we put forward is not the total solution, but it can contribute, in conjunction with other measures, to the deterrence of bioterrorism and biowarfare. Past experience tells us that violations of a code can result in loss of respect by peers; loss of public trust and thereby public support; loss of research funding; and censures for breaches of ethics and legal penalties, including loss of professional licenses to practice (*26*). But more important than the consequences for breaches, a code of ethics can serve as a guide for all persons engaged in science, articulating the values to which we all must aspire and the standards to which we all must adhere to ensure our conduct is ethical and fulfills our fiduciary responsibilities to society.

References and Notes

1. See supporting material on *Science* Online.
2. World Medical Association, "Policy: Declaration of Washington on Biological Weapons" (Document 17.400, World Medical Association, Ferney-Voltaire, France, 2002); available at www.wma.net/e/policy/b1.htm.
3. British Medical Association, *Biotechnology, Weapons and Humanity* (Harwood Academic Publishers, London, 1999).
4. Committee on Research Standards and Practice to Prevent the Destructive Application of Biotechnology, National Research Council, *Biotechnology Research in an Age of Terrorism* (National Academies Press, Washington, DC, 2004).
5. House of Commons, "Security of Research" (Select Committee on Science and Technology Eighth Report, 2003); available at www.publications.parliament.uk/pa/cm200203/cmselect/cmsctech/415/41515.htm.
6. Asia-Pacific Economic Cooperation (APEC) Leaders' Statement on Health Security (2003); available at www.apecsec.org.sg/apec/leaders__declarations/2003/2003_StmtHealthSecurity.html.
7. University of Exeter, "Biological weapons and codes of conduct," available at www.ex.ac.uk/codesofconduct/Chronology/.
8. Editorial, *Proc. Natl. Acad. Sci. U.S.A.* **100**, 1464 (2003).
9. National Science Advisory Board for Biosecurity, www4.od.nih.gov/nsabb/ (last updated 3/4/2004).
10. B. Rappert, "Toward a life sciences code: Countering the threats from biological weapons" (Briefing Paper No. 13, Department of Peace Studies, Univ. of Bradford, Bradford, UK, 2004); available at www.brad.ac.uk/acad/sbtwc/briefing/BP_13_2ndseries.pdf.
11. B. Rappert, *Biosecur. Bioterror.* **2**, 164 (2004); available at www.biosecurityjournal.com/PDFs/v2n304/p164.pdf.
12. R. Lifton, *Destroying the World to Save It: Aum Shinrikyo, Apocalyptic Violence and the New Global Terrorism* (Holt, New York, 2000).
13. R. Kadlec, A. Zelicoff, *JAMA* **279**, 273 (1998).
14. M. Leitenberg, *Crit. Rev. Microbiol.* **27**, 257 (2001).
15. B. Balmer, Britain and Biological Warfare: Expert Advice and Science Policy 1935–65 (Macmillan, London, 2001).
16. D. Avery, *The Science of War: Canadian Scientists and Allied Military Technology During the Second World War* (Univ. of Toronto Press, Toronto, 1998).
17. S. Burgess, H. Purkitt, "The rollback of South Africa's biological warfare program" (INSS Occasional Pap. 37, U.S. Air Force Institute for National Security Studies, 2001); available at www.usafa.af.mil/inss/OCP/ocp37.pdf.
18. K. Alibek, S. Halderman, *Biohazard: The Chilling True Story of the Largest Covert Biological Weapons Program in the World—Told from Inside by the Man Who Ran It* (Random House, New York, 1999).
19. P. Williams, D. Wallace, *Unit 731: Japan's Secret Biological Warfare in World War II* (Hodder & Stoughton, London, 1989).
20. S. Harris, *Factories of Death: Japanese Biological Warfare, 1932–1945, and the American Cover-up* (Routledge, London, 2002).
21. G. Malinas, J. Bigelow, in *The Stanford Encyclopedia of Philosophy*, E. N. Zalta, Ed. (The Metaphysics Research Lab, Stanford, CA, 2004); available at http://plato.stanford.edu/archives/spr2004/entries/paradox-simpson/.
22. M. Nowak, R. M. May, K. Sigmund, *Sci. Am.* **272**, 50 (June 1995).
23. M. Somerville, *The Ethical Canary: Science, Society and the Human Spirit* (Viking, Toronto, 2000),
24. M. Enserink, D. Malakoff, *Science* **302**, 2054 (2003).
25. P. Agre, S. Altman, R. Curl, T. Wiesel, "Statement regarding the case of Thomas Butler, Lubbock, Texas" (Federation of American Scientists, Washington, DC, 2003); available at www.fas.org/butler/nobellet.html.
26. American Medical Association Council on Ethical and Judicial Affairs, *Code of Medical Ethics: Current Opinions with Annotations, 2004–05 Edition* (AMA Press, Chicago, 2004).

Supporting Online Material

www.sciencemag.org/cgi/content/full/307/5717/1881/DC1

10.116/science.1109279

PHYSICS

Bose-Einstein Condensates Interfere and Survive

Juha Javanainen

At very low temperatures, certain atomic gases undergo a phase transition to a Bose-Einstein condensate. In such a condensate, the atoms lose their individuality, and the entire condensate behaves as if it were a quantum mechanical wave with a phase. On page 1945, Saba *et al.* (*1*) show how the phase difference between two condensates can be measured without destroying the condensates. In a major step toward applications in both science and engineering, it is now possible to follow the evolution of the phase difference in time, and maybe even to use repeated measurements of the phase to control the state of the system.

As is the case with all waves, the quantum wave associated with a Bose-Einstein condensate has the potential for interference. In the first experiments on the phase difference between condensates (*2*), two condensates were overlaid (see the figure). This produces an interference pattern; areas with a high gas density alternate with low-density areas. The locations of the peaks and valleys of the interference pattern depend on the phase difference between the condensates. If the condensates are prepared independently, their phases have random values, and the interference pattern changes unpredictably from one experiment to another.

The intriguing question is how the condensates acquire their phases. In other words, how does nature decide where two seemingly unstructured gases combine to make, say, a region of higher density?

Similar situations are actually not rare in physics. For example, a small grain of iron cooled below 770°C picks up a magnetization pointing in some direction. There need not be an observable reason for any particular direction. However, in the case of a magnet, an environmental magnetic field—no matter how small—is always present and may force its direction upon the magnetization. Not so with a Bose-Einstein condensate: No known physical interaction can fix its phase. Besides, if a Bose-Einstein condensate has a definite number of atoms (even if that number is not known), theory does not allow for a phase. The solution to the dilemma is that, even if the individual condensates do not carry phases, a measurement of the phase difference creates a phase difference (*3*).

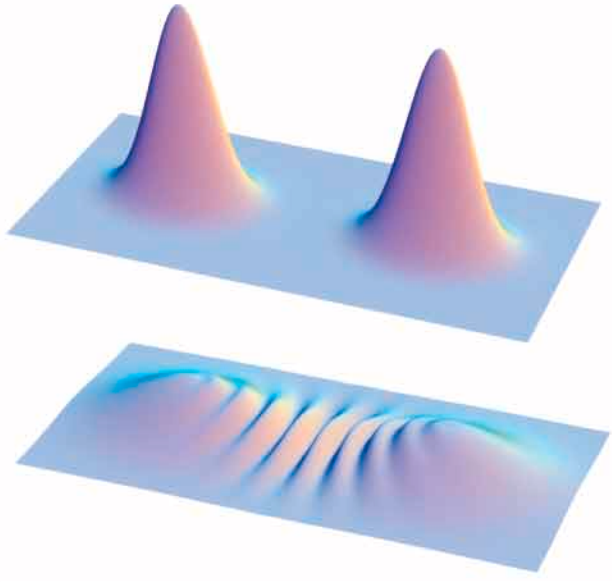

Interfere and vanish. In the first demonstration (*2*) of the phase difference, two condensates were confined to adjacent atom traps (**top**). When the condensates were released, they expanded, overlapped, and developed an interference pattern (**bottom**). The position of the interference pattern depends on the phase difference between the condensates. In this experiment, the condensates were destroyed. The strategy of Saba *et al.* (*1*) avoids their destruction.

Before the work of Saba *et al.*, all experiments required the two condensates to be destroyed before the phase difference became known. The authors (*1*) overcome this problem by using light beams to extract small samples from two condensates and then allowing the samples to interfere. Because the samples carry with them the phases of the mother condensates, this scheme allows a nondestructive measurement of the phase difference. Furthermore, the same light beams that extract the atoms get attenuated or amplified depending on the atom interference. To detect the phase difference, one therefore only need measure light intensities; atom detection is not required.

Once in existence, the phase difference evolves in time depending on the forces acting on the atoms. Repeated or continuous measurements of the phase difference probe the evolution, and therefore constitute an interferometric measurement of the forces. Proof-of-principle experiments of this kind are reported in (*1*).

Precise measurements of force and acceleration have many uses. Laser gyroscopes carried on aircraft are used both to determine the orientation of the plane and as navigational tools, and mechanical gravimeters are used in ore and oil exploration. These are mature, entrenched technologies, but schemes based on atom interferometry possess fundamental scientific advantages.

First, according to quantum mechanics, an atom is associated with a wave. An atomic wave could replace the light wave in a laser gyroscope. A gyroscope measures the rate of rotation. A device based on interferometry, such as a laser gyroscope, must use a physical mechanism that converts rotation rate into a phase. Here, atoms enjoy an intrinsic advantage over light: The intrinsic sensitivity of an atom gyroscope is higher by a factor of around 10^{10} (the rest energy of the atom divided by the photon energy) than that of a laser gyroscope. In a laboratory setting, short-term sensitivities of gyroscopes based on matter waves and light waves are comparable (*4*).

Signal-to-noise ratio is the second essential ingredient to the sensitivity of an interferometer: The less noise, the more precisely one can determine a phase. In this context, two (or more) Bose-Einstein condensates could help. The idea is based on the fact that a Bose-Einstein condensate can act as a quantum system, and that a measurement alters the state of a quantum system. Indeed, the very phase difference between interfering condensates may originate from a measurement. In a form of "quantum engineering," one could therefore design strate-

The author is in the Department of Physics, University of Connecticut, Storrs, CT 06269, USA. E-mail: jj@phys.uconn.edu

gies that steer the system toward a state with an improved signal-to-noise ratio (*5*). The experiments of Saba *et al.* (*1*) should inspire a new generation of work on the quantum mechanics of phase and atom number (*6*, *7*).

Since their discovery in 1995, gas-phase Bose-Einstein condensates have offered fascinating insights into basic physics, but in the words of a quip about lasers from the 1960s, they are a solution looking for a problem. Some of the first applications are likely to be in interferometric measurement devices. The advance reported by Saba *et al.* (*1*) is an important step in this direction.

References and Notes

1. M. Saba *et al.*, *Science* **307**, 1945 (2005).
2. M. R. Andrews *et al.*, *Science* **275**, 637 (1997).
3. J. Javanainen, S. M. Yoo, *Phys. Rev. Lett.* **76**, 161 (1996).
4. T. L. Gustavson *et al.*, *Class. Quantum Grav.* **17**, 2385 (2000).
5. JM Geremia, J. K. Stockton, H. Mabuchi, *Science* **304**, 270 (2004).
6. C. Orzel *et al.*, *Science* **291**, 2386 (2001).
7. M. Greiner *et al.*, *Nature* **415**, 39 (2002).
8. Supported by NSF grant PHY-0354599 and NASA grant NAG3-2880.

10.1126/science.1110247

CELL BIOLOGY

Whither Model Organism Research?

Stanley Fields and Mark Johnston

Almost everything we know about the fundamental properties of living cells—how they grow and divide, how they express their genetic information, and how they use and store energy—has come from the study of model organisms. These simple creatures traditionally include the bacterium *Escherichia coli* and its bacteriophage viruses, bakers' yeast *Saccharomyces cerevisiae*, the nematode worm *Caenorhabditis elegans*, the fruit fly *Drosophila melanogaster*, and the mouse *Mus musculus*, each a representative of the diversity of life. Our colleague Gerry Fink has likened this handful of organisms to the Security Council of the United Nations because, among the world's multitude of organisms, they garner most of the attention of researchers and dictate the distribution of most of the biomedical research funds that are not targeted to specific diseases. A few other organisms—the fission yeast *Schizosaccharomyces pombe*, the mustard plant *Arabidopsis thaliana*, the zebrafish *Danio rerio*, and the frog *Xenopus laevis*—may qualify for seats on the council, but membership is limited. But has the very success of experimental approaches using model organisms made them (and the scientists who study them) endangered? Now may be an opportune time to ask: What more can model organisms tell us about fundamental biological processes?

Three daunting issues confront biologists who devote their careers to studying model organisms. First, some of the most crucial questions have been answered, at least in part. Thus, we know a lot about the mechanisms that underlie the cell cycle; the cellular components that synthesize, modify, repair, and degrade nucleic acids and proteins; the signaling pathways that allow cells to communicate; and the mechanisms that lead to the selective expression of subsets of genes. Remarkably, the operating principles of these cellular processes have been conserved throughout the tree of life. Second, problems of human biology and human disease are becoming increasingly seductive. Given that the flow of information and molecules around individual cells is established, at least in outline, many biologists find more excitement in, for example, discovering how organ systems develop and function, how learning and memory operate, and how innate and adaptive immunity coordinate their responses. We want to understand how people get old, why they get sick, and what we can do about it. The intrinsic appeal of these topics is bolstered by encouragement from the National Institutes of Health and other funding agencies to conduct "translational research," studies that directly address the prevention or treatment of disease. Third, the tools and resources that made uncomplicated model organisms so attractive to begin with can be applied increasingly well to much more complex creatures including mice and humans. Thus, we now have essentially complete mammalian genome sequences, an expanding resource of purified genes and proteins, DNA chips to measure gene expression, and vast numbers of DNA sequence polymorphisms to map traits such as susceptibility to disease. Perhaps most disquieting for the model organism researcher is the recent acquisition by mammalian biologists of a method that was once the sole province of those working on simpler creatures: facile elimination of gene function. The new method of RNA interference has leveled this playing field.

S. Fields is in the Howard Hughes Medical Institute, Departments of Genome Sciences and Medicine, University of Washington, Seattle, WA 98195, USA. M. Johnston is in the Department of Genetics, Washington University Medical School, St. Louis, MO 63110, USA. E-mail: fields@u.washington.edu, mj@genetics.wustl.edu

So what does the future hold for model organism research? In the case of *S. cerevisiae*, the eukaryotic model organism with the smallest number of genes, we contend that it will be "solved" within the next 20 to 30 years. Of course, not every facet of yeast biology will be known: Precise biochemical functions will not be available for every gene product, the level of every metabolite will not have been measured under all possible environmental stresses, and the subtle effects of mutations on protein folding, stability, or modification will not be wholly predictable. But no basic molecular process in yeast will remain obscure. This is a remarkable accomplishment that should be celebrated. And if we expect to essentially "solve" over the next few decades a cell constructed from 6000 genes, how much longer can it be before we "solve" the fruit fly with only twice as many genes, or the roundworm with only about three times as many genes?

The benefits that we will realize from these successes include a working blueprint first of a cell, then of multicellular organisms, that will enable researchers to decipher ever more complex biological processes such as tissue development, the immune response, and neurobiology. Because of the spectacular progress of model organism research, we can expect to reach a thorough understanding of the molecular basis of life. This Security Council, unlike its political counterpart, is proving to be a resounding success.

That said, are we playing a dirge to model organism research or singing a paean to its reinvention? We are singing, because we believe that the hegemony of model organisms in biological research will persist. We see at least five reasons why.

1) Over the coming few decades, model organisms will continue to provide insights into replication, transcription, translation, protein secretion, metabolism, and many other aspects of cell biology, biochemistry, and physiology, because they offer the keenest methods of analysis. In fact, the value of model organisms will only increase, because the human geneticist who identifies a disease gene implicated in a conserved cellular process will turn to these models to provide deeper insights into the function of that gene. And that researcher will discover a rich

encyclopedia of knowledge that can be drawn upon for formulating incisive experiments to illuminate the disease process.

2) Model organisms will increasingly be used for the direct investigation of medical problems that seemingly have little to do with them. For example, the misfolding or aggregation of proteins implicated in the process of neurodegeneration in disorders like Alzheimer's disease, Parkinson's disease, and Huntington's disease, can be recapitulated in yeast, worms, and flies. In addition, other components discovered in these organisms may be important in the disease process. Analysis of aging in simple models is turning up genes that play analogous roles in more complex organisms. Model organisms will provide further insights into the cell cycle and cancer, glucose metabolism and diabetes, chromosome segregation and mental retardation, protein glycosylation and lysosomal storage diseases, mechanisms of drug action and resistance, and much more. Studies of *S. cerevisiae* will help us to unravel the workings of its pathogenic cousins such as *Candida albicans*; studies of *D. melanogaster* will reveal secrets of the *Anopheles* mosquito.

3) Model organisms will remain at the forefront for the foreseeable future in efforts to sort out biological complexity and achieve a more quantitative understanding of life processes, which is needed to unravel the network of molecular interactions that constitute an organism as complicated as a human. For example, it is with yeast that biologists first will elucidate how DNA binding proteins, DNA sequence elements, components of the transcriptional machinery, chromatin structure, and signaling pathways combine in the circuitry of gene regulation. The resulting comprehension of biological networks that will result will bestow upon biologists the predictive powers and design capabilities long held by physicists and engineers. Such insights will require the application of multiple technologies, the confluence of individual investigator's experiments and genomewide data sets, and the intense collaboration of experimentalists and computational biologists. Learning how to carry off this ambitious project is itself a lofty goal of model organism research.

4) Model organisms offer the best hope for coming to grips with the breadth of genetic diversity and the depth of its consequences. Most of the variance among individuals of a species is due to small differences in multiple genes, and it is with model organisms that we will first learn how to analyze and understand complex quantitative traits. Such an understanding will provide the principles and procedures for predicting disease susceptibilities in humans and tailoring optimal methods for prevention and treatment. Genetic diversity is the grist for the mill of natural selection that produced the remarkable diversity of life on Earth, and model organisms should continue to teach us about the origin of the species.

5) Model organisms will remain the proving ground for developing new technologies, which typically spread quickly throughout the research community. For example, our skills in isolating and manipulating genes were won while studying bacteria and bacteriophages. Many other technologies got their start or achieved their apogee in yeast, including two-hybrid analysis, high-throughput protein purification and localization, genomewide epistasis analysis (synthetic lethality), gene expression profiling, protein arrays, and genomewide chromatin immunoprecipitation (ChIP). Worms and flies have been the test beds for large-scale RNA interference screens. We don't see these developments abating. Indeed, the more the fund of knowledge of simple organisms grows, the more useful they become for subsequent technological innovation.

But will an organism like yeast be able to maintain its seat on the Security Council? Not indefinitely. And just as yeast has led the way in many areas of research, we expect that its fate as an experimental organism will foreshadow that of the rest of the council. Does this mean that the end of biology is near? Hardly. We will still be a long way from a comparably deep-seated understanding of humans and our afflictions. How do cells and organs regenerate after damage? How do eukaryotic parasites, which are so different from model organisms, wreak havoc with fatal diseases like malaria, African sleeping sickness, and Chagas' disease? How do strange bacteria and viruses elude our immune systems and stymie our best efforts at drug therapy? How do genes and the environment interact in behavioral diseases like schizophrenia or autism? What is the basis of memory and consciousness?

The reductionist approach of biologists has enabled remarkable achievements by causing us to focus on just a few experimentally tractable organisms, but it also has tended to restrict our vision. There is much to learn about the many organisms that populate our planet, most in ways we can't yet begin to fathom. How do creatures survive in extreme environments? How do some manage to metabolize bizarre substrates? How do individuals organize themselves into incredibly complex communities? This list of questions seems endless (as seemed the list of genes in model organisms not so long ago). Providing adequate answers to these and many other questions is certain to occupy us for a long time. And the knowledge and sophisticated analytical tools that model organism research has laid at our feet bring the entire General Assembly of organisms within our reach, enabling us eventually to answer a question that has framed our enterprise from its beginning: What is life?

References and Notes

1. We are grateful to C. Berg, G. Fink, E. Grayhack, M. Olson, E. Phizicky, J. Thomas, and R. Waterston for their thoughtful comments.

10.1126/science.1108872

MOLECULAR BIOLOGY

Signal Processing in Single Cells

Farren J. Isaacs, William J. Blake, James J. Collins

Consider a high-tech version of the "telephone game" in which you and a group of your friends attempt to transmit a message via your cell phones. One person in the chain has a phone from the 1990s, which is very noisy. Another person is standing in the middle of Times Square in New York City. It would not be surprising if the message received by the person at the end of the chain, or cascade, were corrupted as a result of noise intrinsic to the old phone and the noise arising from the Times Square environment. In this issue, Rosenfeld *et al.* on page 1962 (*1*) and Pedraza and van Oudenaarden on page 1965 (*2*) investigate a living-cell version of this game by exploring how signals are transmitted through gene cascades in noisy cellular environments.

Cell phones consist of multiple, interacting components. Engineers characterize the performance of such devices by determining quantitatively the input-output relationships, or transfer functions, of the respective components. Rosenfeld *et al.* present a new method for calculating the transfer function for the expression of a single gene. Specifically, they investigate the relationship between the concentration of active transcription factor (input) and the rate at which target protein is produced (output) in

F. J. Isaacs is at the Lipper Center for Computational Genetics and Department of Genetics, Harvard Medical School, Boston, MA 02115, USA. W. J. Blake and J. J. Collins are at the Center for BioDynamics and Department of Biomedical Engineering, Boston University, Boston, MA 02215, USA. E-mail: jcollins@bu.edu

single cells. They define this relationship as the gene regulation function. To experimentally measure the gene regulation function, they constructed a synthetic "λ-cascade" system (see the figure) in *Escherichia coli*, in which the expression of a target, or output, gene (CFP, cyan fluorescent protein) is modulated by the activity of an input transcription factor (CI-YFP, λ repressor fused to yellow fluorescent protein). This scheme allows simultaneous measurement of both input and output protein levels in vivo, and is well suited to quantitatively derive the gene regulation function.

To vary the concentration of the CI-YFP input protein, the authors used a "regulator dilution method" in which a given amount of regulator is systematically decreased through successive cell divisions. As the level of CI-YFP decreases, the production of the CFP target increases. By analyzing binomial errors in protein partitioning, the authors obtain the relative fluorescence intensity of individual protein molecules, which allows them to determine the apparent number of molecules per cell. This information was used to determine the gene regulation functions for individual cells, from which a mean gene regulation function was calculated for a select population.

The gene regulation function was subsequently used to extract a number of system-specific properties. For example, the mean gene regulation function was fit to a Hill function to calculate in vivo values of several biochemical parameters. These values were used to provide a molecular-level representation of a transcriptional input-output relationship in individual cells. Interestingly, these values were comparable to previously calculated in vitro estimates.

Rosenfeld and colleagues noted significant deviations of single-cell gene regulation functions from the calculated mean gene regulation function. The authors detected and quantified the effects of factors such as cell cycle phase and gene copy number on these deviations. After compensating for these sources of noise in the analysis, the authors examined whether the variability of the gene regulation functions arises from random fluctuations in other cellular factors that globally affect gene expression (extrinsic noise), or from fluctuations in the biochemical processes involved in the expression of an individual gene (intrinsic noise). Consistent with their previous work (*3*), they detected only a minor noise contribution from intrinsic factors, implicating extrinsic factors as the prominent noise culprits.

In contrast to previous experiments that collected steady-state snapshots of gene expression (*3*–*6*), Rosenfeld *et al*. measured temporal changes in the rates of input (CI-YFP) and output (CFP) production levels. The authors noted that fluctuations occurring on different time scales can lead to identical steady-state distributions (see the figure). They also found that intrinsic noise decays rapidly, whereas single-cell responses depart from the mean gene regulation function over long time periods (about one cell cycle), indicating that extrinsic noise can occur on slow time scales. The authors suggest that cells would have to integrate signals over long time periods to account for such noise, which means that there may be a trade-off between accuracy and response time of a transcriptional network. Feedback, as noted by the authors, can be used to affect this trade-off, as has been demonstrated experimentally in studies involving both positive (*7*, *8*) and negative (*9*, *10*) feedback loops.

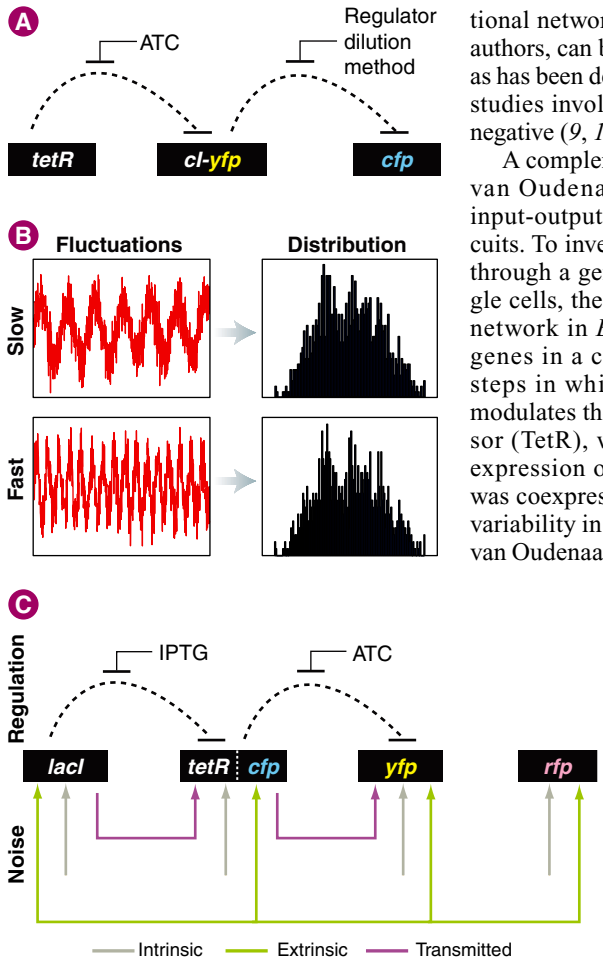

Synthetic gene network cascades. (**A**) Gene network used to determine gene regulation function (*1*). TetR represses the expression of a CI-YFP fusion protein, which, in turn, represses the expression of CFP. The chemical anhydrotetracycline (ATC) modulates repression by TetR, and the "regulator dilution" method was used to control the concentration of CI-YFP. (**B**) Time course of slow (top) and fast (bottom) fluctuations can both result in similar population distributions (right). (**C**) Regulatory connections and noise sources for a synthetic gene cascade used to study noise propagation in gene networks (*2*). LacI represses the expression of TetR, which, in turn, represses the expression of YFP. CFP and YFP fluorescent reporters were used to measure noise properties of the network. Unregulated expression of red fluorescent protein (RFP) was used to measure variability due to global sources of noise not influenced by the properties of the network.

A complementary study by Pedraza and van Oudenaarden (*2*) investigated the input-output relationships of genetic circuits. To investigate how noise propagates through a gene regulatory cascade in single cells, the authors designed a synthetic network in *E. coli*. They arranged three genes in a cascade with two regulation steps in which the lac repressor (LacI) modulates the expression of the tet repressor (TetR), which, in turn, regulates the expression of YFP (see the figure). CFP was coexpressed with TetR to measure the variability in TetR expression. Pedraza and van Oudenaarden systematically perturbed the effective regulation along this cascade by using the chemical inducers IPTG (isopropyl-β-D-thiogalactopyranoside) and ATC (anhydrotetracycline). This method allowed them to investigate how interactions among network components affect the transmission of noise along the cascade (see the figure).

As the repressive effect of LacI was decreased by the addition of IPTG, its target, CFP, responded with an increase in expression. Expression of the downstream YFP target in the next regulatory step was inversely correlated to the CFP signal, but it exhibited a much steeper response. These results illustrate that genetic cascades can display sharp, switchlike responses to input signals, a recognized property of analogous protein kinase systems (*11*).

The experiments also showed that the two fluorescent reporters in the cascade, both regulated by single repressors, display strikingly different levels of noise in their response to varying strengths of regulation. To interpret these results, Pedraza and van Oudenaarden developed a stochastic model of their cascade that distinguished between various sources of noise influencing the expression of each gene (see the figure). Importantly, the authors included in the model contributions from transmitted noise, that is, intrinsic and extrinsic noise influences transmitted from a regulator gene to its target.

The model demonstrated that expression variability of a target gene in the cascade was most influenced by noise transmitted from the upstream regulator. This interesting finding suggests that network connectivity can have a greater effect on the variability of expression than noise intrinsic to the expression of a gene itself. Remarkably, the authors' model was able to accurately predict the noise properties of single genes within the cascade, as well as correlations between each of their fluorescent reporters, demonstrating that such behavior can be described in a quantitative manner.

In similar recent work, Hooshangi *et al.* (*12*) constructed gene regulatory cascades of varying lengths in *E. coli* to explore the effects of cascade length on the timing, variability, and sensitivity of the network's response. They found that the sensitivity of the network's response to changes in an input signal increased with cascade length, similar to the results discussed above (*2*, *11*). Moreover, they showed that longer cascades, which are more sensitive, amplify cell-cell variability, especially at intermediate signal levels. Noise due to high levels of expression in genetic cascades can also have dynamic effects, with phenotypic consequences. For example, an earlier study involving a synthetic gene regulatory cascade in yeast (*5*) showed that increased variability in an upstream regulator can cause a cell population to display prolonged bistable states of gene expression.

To date, studies of synthetic gene regulatory networks have relied primarily on qualitative models that describe general system behavior (*13*). The work by Rosenfeld *et al.* (*1*) and Pedraza and van Oudenaarden (*2*) represents an important advance toward a more quantitative synthetic biology. These studies offer insights into gene regulation, and, together, provide a framework for the further characterization of input/output relationships among regulators and their targets. These quantitative approaches can be applied to natural gene networks and used to generate a more comprehensive understanding of cellular regulation. This will enable a better characterization of individual genetic components and modules, opening up the possibility of designing more complex synthetic gene networks. Such networks could be engineered with specific properties that filter unwanted noise from signaling networks or exploit noise-induced switching to sample more diverse phenotypes.

References

1. N. Rosenfeld, J. W. Young, U. Alon, P. S. Swain, M. B. Elowitz *Science* **307**, 1962 (2005).
2. J. M. Pedraza, A. van Oudenaarden, *Science* **307**, 1965 (2005).
3. M. B. Elowitz, A. J. Levine, E. D. Siggia, P. S. Swain, *Science* **297**, 1183 (2002).
4. E. M. Ozbudak, M. Thattai, I. Kurtser, A. D. Grossman, A. van Oudenaarden, *Nature Genet.* **31**, 69 (2002).
5. W. J. Blake, M. Kaern, C. R. Cantor, J. J. Collins, *Nature* **422**, 633 (2003).
6. J. M. Raser, E. K. O'Shea, *Science* **304**, 1811 (2004).
7. A. Becskei, B. Seraphin, L. Serrano, *EMBO J.* **20**, 2528 (2001).
8. F. J. Isaacs, J. Hasty, C. R. Cantor, J. J. Collins, *Proc. Natl. Acad. Sci. U.S.A.* **100**, 7714 (2003).
9. A. Becskei, L. Serrano, *Nature* **405**, 590 (2000).
10. N. Rosenfeld, M. B. Elowitz, U. Alon, *J. Mol. Biol.* **323**, 785 (2002).
11. J. E. Ferrell, E. M. Machleder, *Science* **280**, 895 (1998).
12. S. Hooshangi, S. Thiberge, R. Weiss, *Proc. Natl. Acad. Sci. U.S.A.* **102**, 3581 (2005).
13. J. Hasty, D. McMillen, J. J. Collins, *Nature* **420**, 224 (2002).

10.1126/science.1110797

ATMOSPHERIC SCIENCE

Something in the Air

Daniel M. Murphy

Aerosol particles in the atmosphere play important roles in climate change and human health. Some of the largest uncertainties in how human activities affect climate come from the effects of aerosols (*1*). Epidemiological studies have shown significant excess mortality from particle pollution (*2*). In both cases, particles less than 1 or 2 μm in diameter are particularly influential, because they efficiently scatter light, influence cloud formation, and can penetrate into human lungs. In recent years, new instrumentation has led to important advances in the detection and characterization of these particles.

Enhanced online at www.sciencemag.org/cgi/content/full/307/5717/1888

The measurement of aerosol composition poses substantial analytical challenges. Sample sizes are small: A particle with a diameter of 200 nm weighs about 6 fg (6×10^{-15} g), and outside of polluted regions, a liter of air may contain just 1 ng (10^{-9} g) of particles. This material is typically a complex mixture of inorganic and organic compounds. Some compounds are so volatile that pressure and temperature changes during sampling cause evaporation, biasing the results. Others are so sticky that it is nearly impossible to recover them from a filter or other substrate without changing their composition.

The evaporation and recovery issues have pushed new instrumentation toward techniques that analyze particles directly from the air. Such "on-line" techniques are also attractive because measurements need to be made every few minutes to track changing wind conditions or sample from mobile platforms such as aircraft. The cost of handling filters or other off-line samples acquired at these short time intervals quickly becomes prohibitive (*3*). Furthermore, on-line samples can be more easily compared to gas-phase measurements, as shown in the figure, where the combined analysis of gas-phase and particle chemistry provides important insights into the sources of different substances.

Because of its sensitivity and fast response time, mass spectrometry is an important technique for the on-line analysis of aerosols (*4*, *5*). At least 20 mass spectrometers have been developed for this purpose. In many of these instruments, a nozzle brings nearly all particles into a vacuum chamber in a highly collimated beam while reducing the gas pressure by seven orders of magnitude (*4*, *6*). Some instruments examine one particle at a time, whereas others analyze an ensemble. Most single-particle instruments ionize material with a pulsed laser, and then use a time-of-flight mass spectrometer to obtain a complete mass spectrum of the abated material. The most common ensemble configuration evaporates particles with a hot filament, then ionizes the gas-phase material with electron impact or chemical ionization. There are trade-offs between the detailed information from single-particle instruments and the better quantitation of organics, sulfate, and nitrate achieved by ensemble instruments.

Other techniques for on-line aerosol composition analysis include automated samplers that feed directly into ion chromatographs, and instrumentation for detecting specific chemical groups such as nitrate (*7*). Off-line analyses use increasingly advanced versions of electron microscopy, atomic force microscopy, and accelerator-based nuclear techniques.

The analytical techniques discussed above have contributed to a paradigm shift in atmospheric science: the recognition of the global role of organic compounds. Before 1995, global models of aerosols generally did not include organics (*1*). Since then, traditional and on-line techniques have found that organics are of com-

The author is at the National Oceanic and Atmospheric Association (NOAA) Aeronomy Laboratory, Boulder, CO 80305, USA. E-mail: daniel.m.murphy@noaa.gov

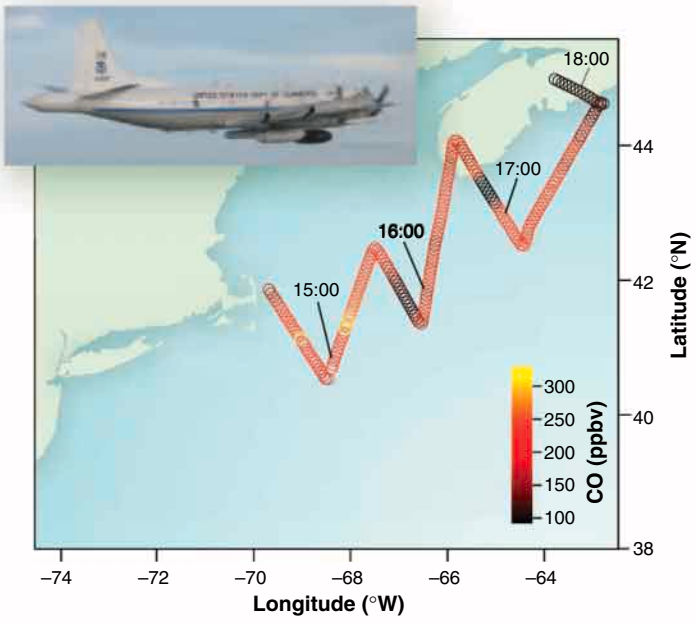

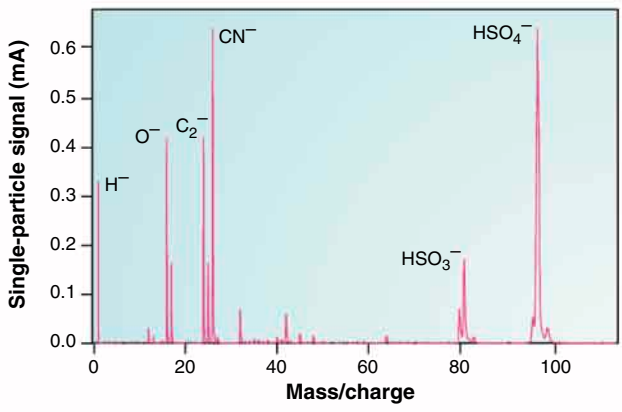

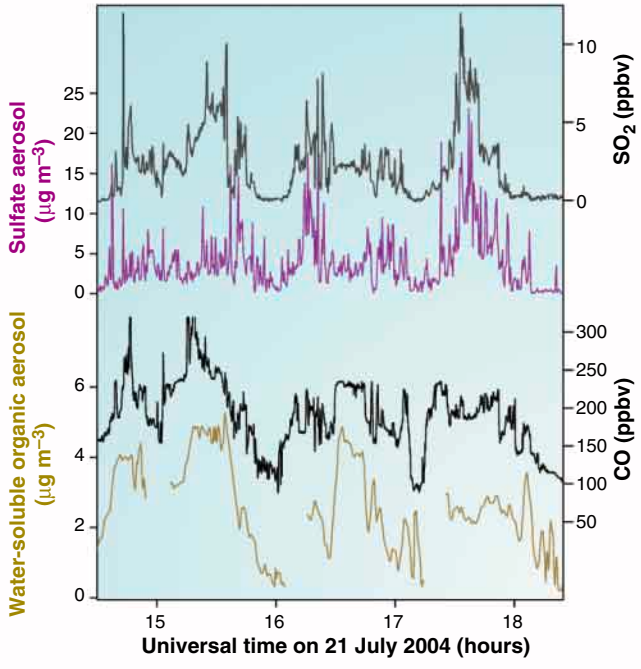

The strength of combined analysis. The data were collected by the NOAA P-3 research airplane on 21 July 2004, downwind of New York and nearby regions (**top left**). The plume from New York causes the high-CO regions shown in yellow on the southwestern part of the flight track. Sulfate and organic concentrations in aerosol particles peak at different times because they have different sources (**bottom right**). Water-soluble organics in the particles correlate with gas-phase CO, whereas sulfate is better correlated with SO_2. Nevertheless, organics and sulfate are often found in the same particle (**top right**). Single-particle composition was measured with pulsed laser mass spectrometry and sulfate with an Aerodyne aerosol mass spectrometer, both operated by the NOAA Aeronomy Laboratory. Water-soluble aerosol organics are from a particle-into-liquid sampler operated by the Georgia Institute of Technology.

parable importance to sulfates (*8*, *9*). Besides their contribution to the overall mass budgets of aerosols, organics have specific implications for both climate and health. In contrast to the common inorganic constituents of atmospheric aerosols (such as ammonium sulfate), the organic constituents range from hydrophilic to hydrophobic, and some act as surfactants. The resulting changes in water uptake near 100% relative humidity could affect the properties of clouds. Furthermore, the toxicity of many organic compounds in atmospheric particles is unknown.

The organic compounds present in atmospheric particles are a highly complex mixture. An orthogonal gas chromatography/mass spectrometry analysis of a single sample yielded more than 10,000 peaks (*10*). It is likely that many more compounds did not even make it through the chromatographic column. Yet the thermal and mass spectrometric techniques used for on-line measurements separate the mixture into just a few components. An intense effort is under way to develop techniques that obtain more information, especially on the sources of the polyfunctional and polymeric substances found in atmospheric particles (*11*, *12*).

The presence of so many organic compounds poses conceptual difficulties beyond the analytical challenge of dealing with a complex mixture. Even if it could be done, it may not be useful to obtain a list of the concentrations of thousands of compounds, most of which have never been studied in the laboratory. A shorter list ordered by functional group and/or physical properties may be more useful, but it is not yet clear what groupings are relevant to the climate and health policy questions that drive this research. Also, the physical chemistry of complex mixtures can differ considerably from that of the pure substances or binary mixtures often used in laboratory experiments (*13*).

This Perspective has focused on organics, but new instrumentation has also contributed to our understanding of inorganic species. Nevertheless, key challenges remain to be addressed. There is a pressing need for better instrumentation to measure light-absorbing particles, which can strongly affect climate even when they constitute only a few percent of the particle mass. Much rainfall originates in clouds that contain ice, yet it is not known what fraction of ice-nucleating particles is anthropogenic (*1*). Dust, one of the most important aerosol components by mass, has a complicated and variable composition. Furthermore, many dust particles are nonspherical, making it difficult to relate the measured concentration of an element such as silicon to how the particles might penetrate into a lung or reduce visibility.

The recent advances in aerosol detection are promising, but the new techniques must also be applied wisely. Large portions of the atmosphere, including most of the Southern Hemisphere, are poorly sampled. Gas-phase and particle measurements are increasingly performed together, but these detailed local measurements must be put in the context of regional and global measurements from satellites and other remote sensors. Last but not least, additional study is needed on the chemical compounds and mechanisms responsible for the human-health effects of particles.

The aerosol-detection instruments discussed in this article have yielded many insights beyond the policy issues they were

designed to address. Examples are a new estimate of the flux of meteors entering the atmosphere (*9*), the idea that mixed organic/salt particles could have had a role in the origin of life (*14*), and the tracking of smoke from fireworks (*15*). Yet public policy questions continue to provide a focus to the researchers involved in developing instrumentation to measure the composition of particles in the atmosphere.

References

1. International Panel on Climate Change, *Climate Change 2001, The Scientific Basis* (Cambridge Univ. Press, Cambridge, UK, 2001).
2. D. W. Dockery *et al.*, *N. Engl. J. Med.* **329**, 1753 (1993).
3. P. H. McMurry, *Atmos. Environ.* **34**, 1959 (2000).
4. J. T. Jayne *et al.*, *Aerosol Sci. Technol.* **33**, 49 (2000).
5. C. A. Noble, K. A. Prather, *Mass Spectrom. Rev.* **19**, 248 (2000).
6. P. Liu *et al.*, *Aerosol Sci. Technol.* **22**, 314 (1995).
7. R. Weber *et al.*, *J. Geophys. Res.* **108**, 8421 (2003).
8. T. Novakov, D. A. Hegg, P. V. Hobbs, *J. Geophys. Res.* **102**, 30023 (1997).
9. D. M. Murphy, D. S. Thomson, M. J. Maloney, *Science* **282**, 1664 (1998).
10. J. F. Hamilton *et al.*, *Atmos. Chem. Phys.* **4**, 1279 (2004).
11. M. P. Tolocka *et al.*, *Environ. Sci. Technol.* **38**, 1428 (2004).
12. M. Kalberer *et al.*, *Science* **303**, 1659 (2004).
13. C. Marcolli, B. Luo, T. Peter, *J. Phys. Chem. A.* **108**, 2216 (2004).
14. C. M. Dobson, G. B. Ellison, A. F. Tuck, V. Vaida, *Proc. Natl. Acad. Sci. U.S.A.* **97**, 11864 (2000).
15. D.Y. Liu, D. Rutherford, M. Kinsey, K. A. Prather, *Anal. Chem.* **69**, 1808 (1997).

10.1126/science.1108160

EVOLUTION

The Synthesis and Evolution of a Supermodel

Greg Gibson

Synthesis is the merging of disparate sources of knowledge to create a stronger, more compelling whole. In the biological sciences, barriers to synthesis—including the specialization of subdisciplines and their fractionation into departments and curricula—have increased over the past few decades. Developmentalists dissect their favorite ecologically irrelevant models with exquisite detail, while evolutionists tap away at hundreds of fascinating species with genetically toothless tools. Organismal biologists can take great solace in a report on page 1928 of this issue by Colosimo and colleagues (*1*) that shows how genomics can be used to buck this trend and lead us to new insights into fundamental evolutionary problems.

The threespine stickleback (*Gasterosteus aculeatus*) is a finger-sized species of fish that exhibits multiple examples of parallel evolution. The threespine stickleback populations that inhabit the streams and lakes of the northern Pacific and Atlantic rims show intriguing variations in morphology and behavior compared to marine populations (*2*). A particularly striking instance is the reduction in body armor exhibited by freshwater populations. Whereas marine sticklebacks carry a row of up to 36 armor plates extending from head to tail (complete morph), freshwater sticklebacks either carry a gap in the row of plates (partial morph) or retain only a few plates at their anterior end (low morph). Sticklebacks reside in diverse freshwater habitats that include numerous glacial lakes in western Canada that were formed as the last ice age retreated 10,000 or so years ago (*3*). Lindsey hypothesized in 1962 (*4*) that rather than a single stickleback population with reduced body armor founding the populations in all of these lakes, parallel evolution must have occurred. He attributed parallel evolution to selection either on independent mutations or on a rare allele whose phenotypic effect is cryptic, that is, remains hidden in the marine population. The new study (*1*) combines quantitative genetics, genomics, population genetics, molecular evolution, field studies, and molecular developmental biology to demonstrate that both new mutations and cryptic variation have contributed to body armor reduction. In so doing, this study provides one of the first dissections of a skeletal polymorphism to the gene level, and thereby elevates the stickleback to the status of supermodel for the study of developmental evolution.

The story begins with high-resolution linkage mapping of a major effect locus for armor reduction in a cross between "complete" and "low" body plate morphs of the threespine stickleback. This locus was mapped to an approximately 0.7-cM interval of the genome. Although expression of the phenotype varies in different crosses because of the segregation of modifier loci, loss of body plates is largely dependent on a generally recessive allele that accounts for as much as 75% of the difference between morphs (*5*). To positionally clone the gene responsible for this effect, Colosimo *et al.* (*1*) performed a chromosome walk across the region of interest, tiling six bacterial artificial chromosome clones covering more than a megabase. Half of this walk was completely sequenced, and microsatellites at 12-kb intervals were typed in a set of 46 of the complete-armor morphs and 45 of the low-plate-number morphs from an interbreeding stream population in California. This so-called linkage disequi-

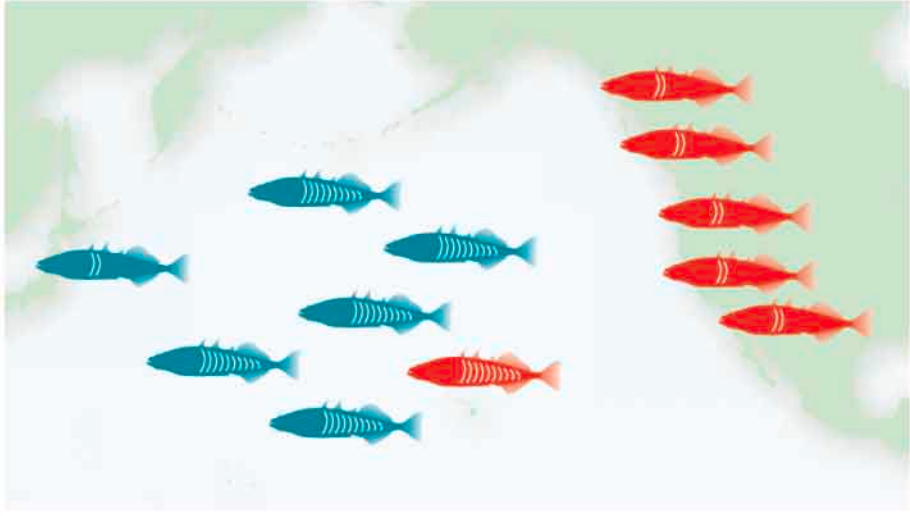

Lightening the load. Marine threespine sticklebacks (blue) have a robust set of body armor (indicated as multiple rays in each body), whereas multiple freshwater populations on either side of the north Pacific rim have independently lost their body armor during the course of evolution. Each low-morph stickleback population in lakes and streams of western North America carries an *Eda* allele (red coloration) that resembles the rare allele found in marine populations. This finding suggests that the *Eda* allele has increased in frequency under adaptive selection. By contrast, a Japanese marine population has a different *Eda* allele on the common background, implying that this case of armor reduction evolved through an independent mutation.

CREDIT: PRESTON HUEY/*SCIENCE*

The author is in the Department of Genetics, North Carolina State University, Raleigh, NC 27695, USA. E-mail: ggibson@ncsu.edu

librium approach—now the standard in mapping human disease genes—reduced the peak of the candidate interval to just 16 kb, centered on a marker in the second intron of a gene called *Ectodysplasin* (*Eda*).

Eda encodes a member of the tumor necrosis factor (TNF) family of secreted signaling proteins (*6*). The gene has a history of involvement in abnormal development of skin. Mutations in this gene cause a variety of human syndromes (*7*) and the Tabby phenotype in mice (*8*); meanwhile, absence of the EDA receptor results in loss of scales in medaka fish (*9*). Similarly severe mutations in these genes in natural populations would be likely to have such deleterious pleiotropic effects that selection would preclude their reaching high frequencies. Sequencing of a low-morph *Eda* allele detected multiple nucleotide differences with respect to the complete-morph allele, but only four of these led to an amino acid change in the EDA protein, and none of these changes obviously affected EDA's function (*1*). Thus, the precise polymorphism that leads to the quantitative skeletal phenotype is still unknown. Reverse transcription polymerase chain reaction methods detected the expected alternative splice products in both morphs of stickleback, but because the transcript abundance in developing epidermis was too low to detect by whole-mount in situ hybridization, it is not yet clear whether there is a quantitative or spatial difference in expression that might explain the phenotypic effect of the low-morph allele.

It remains possible that *Eda* is not the causative gene, particularly because the refined interval includes another TNF ligand and two other genes of interest (these may also, or alternatively, influence a couple of correlated physiological traits). Kingsley's group (*1*) has established more direct evidence for the involvement of EDA in plate development by generating transgenic sticklebacks that transiently overexpress a murine version of the gene. A handful of these fish exhibit partial rescue of plate development in a homozygous low-morph background. Thus, there is little doubt that Colosimo and co-workers have nailed the source of parallel morphological evolution in the threespine stickleback to a single gene.

The authors next performed a population survey of *Eda* genotypes to address the question of whether adaptive evolution has favored multiple independent mutations or repeated selection of an allele that is rare in marine populations (see the figure). All of the North American and European low-morph populations share a haplotype consisting of a set of single-nucleotide polymorphisms covering the interval centered on *Eda*, whereas the Japanese low-morph allele is clearly distinct. Because the Japanese allele fails to complement the North American one, this implies that at least two independent mutations have led to a reduction in body armor on either side of the Pacific. By contrast, detection of at least 14 instances of a similar haplotype in North America—one that is rare in the marine population from which the stream and lake populations of Canada and California were founded—strongly implies a single genetic basis for these instances of parallel evolution.

Counting up the number of nucleotide substitutions between the two sequenced high- and low-morph alleles suggests a date of 2 million years for their separation, which is two orders of magnitude longer than the inferred age of the postglacial populations. This method does not actually date the causative mutation, which could have arisen on the low-morph haplotype at any time before the founding of the freshwater populations in which it has risen to a high frequency. The haplotype has an estimated allele frequency of 0.6 to 3.8% in populations of marine fish sampled from coastal British Columbia and California. This is too low to produce an appreciable number of homozygotes, but large enough to create a pool of alleles that would be available for selection upon introgression into freshwater environments. Preliminary sequence comparisons suggest that the causal site itself is quite ancient, as there is considerable diversity even within the low-morph haplotype. Had the mutation appeared relatively recently in an isolated stream, then found its way back into the marine pool from whence the other populations were founded, sequence diversity in the haplotype would be much lower than that observed in the prevalent marine haplotype.

Ancient or recent, the more important point is that for the first time we have a clear demonstration that after alteration of environmental circumstances, adaptive evolution can act independently on an allele that is present in but has little effect on the morphology of the ancestral species. Colosimo *et al*. (*1*) refer to this phenomenon as selection on cryptic variation. A more technical definition of cryptic variation allows us to expand the scope of the potential impact of standing variation on rapid morphological evolution (*10*). In marine sticklebacks, the low-morph effect is hidden by the fact that only rare fish carry the relevant allele, and these fish are heterozygous rather than homozygous for the low-morph variant. Strictly speaking, though, cryptic variation refers to the situation where the phenotype of individuals is modified by the genetic background or environment such that a previously neutral variant becomes functional and adaptive. Because plate reduction is modified by other loci (*5*) and may be influenced by environmental factors such as calcium concentration in the water, it is likely that more than just selection on *Eda* is contributing to the uncovering of this hidden variation.

These results should provide fuel for those who wish to emphasize the distinction between soft and hard selection. Hard selection—positive selection on new mutations—is known to lead to a substantial reduction in nucleotide diversity around the focal site, which can be used as the basis for detection of selective sweeps (*11*). By contrast, soft selection acts on standing variation that has been in the population for some time, as a result of a change in the environment or genetic background (both of which should occur when marine sticklebacks admix with those inhabiting streams). It is expected to leave a very different genetic footprint (*12*, *13*), and this system provides a superb opportunity to contrast these scenarios. There is also a lovely symmetry in the fact that the mouse Tabby mutation, now known to be due to a mutation in the *Eda* gene (*8*), provides a classic example of canalization (*14*). Canalization refers to the buffering of genetic variation and promotes the maintenance of cryptic variation.

Studies such as that by Colosimo and colleagues highlight how the disparate branches of biology can be synthesized to provide fresh perspectives on fundamental evolutionary phenomena. The National Evolutionary Synthesis Center (*15*) in Durham, North Carolina, has just received NSF funding to promote synthetic research. Few groups have the capacity to pull off such an integrative accomplishment, but there is little reason why interactive teams cannot contribute to the emergence of numerous other supermodel organisms.

References

1. P. F. Colosimo *et al.*, *Science* **307**, 1928 (2005).
2. M. A. Bell, S. A. Foster, Eds., *The Evolutionary Biology of the Threespine Stickleback* (Oxford Univ. Press, Oxford, 1994).
3. G. Orti, M. A. Bell, T. E. Reimchen, A. Meyer, *Evolution* **48**, 608 (1994).
4. C. C. Lindsey, *Can. J. Zool.* **40**, 271 (1962).
5. P. F. Colosimo *et al.*, *PLoS Biol.* **2**, E109 (2004).
6. A. T. Kangas, A. R. Evans, I. Thesleff, J. Jernvall, *Nature* **432**, 211 (2004).
7. K. Paakkonen *et al.*, *Hum. Mutat.* **17**, 349 (2001).
8. A. K. Srivastava *et al.*, *Proc. Natl. Acad. Sci. U.S.A.* **94**, 13069 (1997).
9. S. Kondo *et al.*, *Curr. Biol.* **11**, 1202 (2001).
10. G. Gibson, I. M. Dworkin, *Nature Rev. Genet.* **5**, 681 (2004).
11. N. L. Kaplan, R. R. Hudson, C. H. Langley, *Genetics* **123**, 887 (1989).
12. H. Innan, Y. Kim, *Proc. Natl. Acad. Sci. U.S.A.* **101**, 10667 (2004).
13. J. Hermisson, P. S. Plennings, *Genetics*, in press.
14. R. B. Dun, A. S. Fraser, *Nature* **181**, 1018 (1958).
15. National Evolutionary Synthesis Center (www.nescent.org).

10.1126/science.1109835

edited by Edward W. Lempinen

ANNUAL MEETING

Jackson: Scientists Should Work to Solve Problems and Build Trust

Public mistrust and diminishing government support have put American science and engineering at a "critical juncture," despite myriad life-enhancing achievements that have emerged from the recent era of discovery, Shirley Ann Jackson said in her AAAS Presidential Address.

In a speech that formally opened the 2005 AAAS Annual Meeting in Washington, D.C., Jackson urged scientists and engineers to renew their commitment to public engagement and serving humanity, saying that they needed to be a voice of reason in a time of conflict and confusion.

"On issues ranging from genetic engineering and stem cell research to the search for weapons of mass destruction, our public discourse abounds with controversy—and the volume and passion of the rhetoric sometimes drowns the voice of science," Jackson said. "The war on terror, the uneven economic expansion of the recent past, and the U.S. federal budget deficit have weakened U.S. government resolve to invest in basic research and the development of scientific talent. This is happening just when we should be investing more—not less."

Jackson, a physicist, is president of Rensselaer Polytechnic Institute in Troy, New York. At the close of the annual meeting last month, she became chair of the AAAS Board of Directors, having served as President since February 2004. Her interests include science and technology policy and nuclear energy and regulation. She has built a record of accomplishment and service that today makes her one of the most influential figures in global science.

During her 17 February address, Jackson described four trends that are shaping the landscape for science and engineering early in the 21st century. A more multidisciplinary approach to science has yielded new insights and new solutions, she said. But in the concern over national security that has followed the terror attacks of September 11, 2001, policy has too often overlooked how issues of food, health, infrastructure, and environment in developing countries can influence security in developed nations.

Further, Jackson said, the United States is at risk of losing its capacity to innovate because the science and engineering workforce is rapidly aging, and there are not enough students—U.S. or international—in the pipeline to replace them. These trends are compounded by a communications environment that features more sources of information and more opposing perspectives from a host of "new experts," making it more difficult for the public to decipher what is "fact."

"The result is the devaluing of information, and even the devaluing of science," Jackson told the audience. "This trend threatens the concept of the scientist as the dispassionate, objective voice of reason—and, also, the authoritative role of science in helping to shape sound public policy."

Jackson urged the science and engineering communities to engage more in key public policy debates. She also called for "a full-fledged national commitment to invest in basic research in science and engineering across a broad disciplinary front," and for a "national focus and commitment to develop the complete talent pool," recruiting young scientists and engineers from every cultural group and class. And she urged discipline-specific scientific and engineering societies to follow AAAS's lead in engaging with the public.

Shirley Ann Jackson

By following this broad course of education, capacity-building, and "respectful" engagement, Jackson said, "we can heal rifts, address rising expectations worldwide, ensure our security by helping others to feel secure, and usher in a new "golden age of scientific discovery."

(The full text of the AAAS Presidential Address is at www.aaas.org/news/releases/2005/0217jacksontext.shtml).

EDUCATION

Awards Issued for Excellence in Science Books

Four children's book authors, a general-interest science writer, and an illustrator won the first-ever AAAS/Subaru *SB&F* Prize for Excellence in Science Books.

The prizes, awarded for the first time this year, were given to winners who had compiled a superior body of work over the course of their careers. In future years, the prize will be awarded for recently published individual titles.

"Many scientists credit books as being responsible for turning them on to science," said Shirley Malcom, AAAS head of Education and Human Resources. "We're grateful to be able to honor those authors whose books have been essential in fostering a better understanding and appreciation of science in children and youth."

Winners in the Children's Science Book category were Patricia Lauber, author of more than 125 books, including *Journey to the Planets*; Laurence Pringle, author of over 100 books, including *Sharks! Strange and Wonderful*; and Seymour Simon, author of 200 books, many of which have won awards from the National Science Teachers Association.

Bernie Zubrowski, author of 16 books, won in the Hands-on Science Book category. Jim Arnosky, author/illustrator of *Drawing From Nature*, won in the Children's Science Book Illustrator category. And physicist James Trefil, known for work that teaches science to nonscientists, won in the Popular Science Book category.

SB&F (Science, Books & Film) is a journal published by AAAS that evaluates books, videos, and software (see www.sbfonline.com).

INTRODUCTION

The Gut: Inside Out

The average adult human is, in essence, a 10-meter-long tube. The inner lining of this tube—the gut—absorbs nutrients and defends against would-be pathogens, yet the number of microorganisms it accepts and even embraces is higher than the number of cells making up our entire body. Its tissues are wreathed in sensory cells and awash in hormones relaying information back and forth. What goes on within the gut is still largely mysterious, and in this issue we explore some of its most interesting secrets.

The development and evolution of the gut, as Stainier (p. 1902) points out, is one of the earliest consequences of multicellularity. As a tube, the gut is not straight, nor is it smooth: Radtke and Clevers (p. 1904) reveal how the gut's topology of villi and crypts, combined with its amazing rate of self-renewal, make it particularly vulnerable to malignancy but also valuable for studying stem cell biology. A Report by Sakatani *et al*. (p. 1976) describes how epigenetic changes in the intestinal epithelium may also affect the risk of cancer. On *Science*'s Signal Transduction Knowledge Environment (STKE), Hollande *et al*. (www.sciencemag.org/sciext/gut) throw light on the role of local signaling in maintaining the integrity of this thin lining of cells, even as they face high rates of renewal and the shear forces of the flow of the gut's liquid contents. A News story by Pennisi (p. 1896) explores how such features facilitate adaptive changes in gut size as an energy-saving device for fasting animals.

Colonization of the gut by bacterial cells starts at birth, and they develop into an unusually diverse adult microbial community. One such niche is the mouth, and in a second News piece, Pennisi describes how both beneficial and harmful oral microorganisms jockey for supremacy (p. 1899). Bäckhed and colleagues (p. 1915) review strategies for investigating the interaction between the gut flora and human biology, and in an example of such a study, Sonnenburg *et al*. (p. 1955) describe new results on bacterial polysaccharide foraging within the gut. The gut epithelium and the associated mucosal immune system act as the mediators between the host and its symbiotic flora, and as MacDonald and Monteleone (p. 1920) discuss, different factors that interrupt this interplay can lead to inflammatory disorders of the gut. Despite the gut's extensive surveillance system, intestinal pathogens can wreak havoc, and on STKE, Peek explains how the notorious bacterium *Helicobacter pylori* disrupts stomach function to cause gastritis and possible cancer.

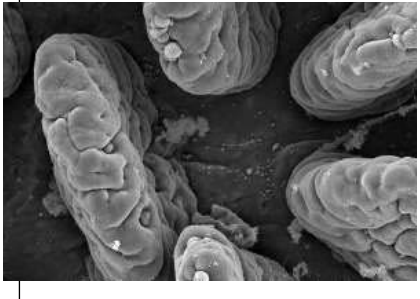

Information flow is as vital as transit times for proper gut function. Badman and Flier (p. 1909) review humoral and neural signals that regulate energy balance and food intake, as well as their potential for therapies in treating obesity. On STKE, Sharkey and Pittman explain how part of the pleasure of eating relates to cannabinoid receptors in the brain, whereas Emeson and Morabito reveal how "food fights" arise through the hormonal link between aggression circuits and the feeding pathway. Finally, Wade and Hornby describe how age-related neurodegenerative changes affect gastrointestinal function.

There are enormous amounts of information about the gut still to digest, but it is hoped that this journey through our inner tube will leave readers with an appetite to learn more.

–STEPHEN SIMPSON, CAROLINE ASH, ELIZABETH PENNISI, JOHN TRAVIS

CONTENTS

See also Editorial on p. 1839; Reports on p. 1955 and p. 1976; SAGE KE material on p. 1833; and STKE material on p. 1833.

Science

CREDIT: JUSTIN SONNENBURG, JAIME DANT, AND JEFFREY GORDON

NEWS

The Dynamic Gut

As snakes, frogs, birds, and other wild creatures attest, digestive systems need flexibility to meet energy demands as well as the challenges of environment, diet, and predators

You haven't had a meal for so long that your stomach and intestines have atrophied. And when you finally do get something to eat, it's almost as big as you are. Yet you cram it into your mouth and hope that your gut can somehow cope with it. That's what life's like for many snakes: feast or famine.

Other animals ride similar nutritional roller coasters. Birds travel thousands of kilometers without eating, then gorge themselves when they stop to refuel—often on a completely different type of food than they are accustomed to. Not a morsel of food or liquid passes the lips of a hibernating animal for months, yet their digestive systems kick in as soon as they greet the world again.

How does the gut accommodate such extremes without shriveling up and dying or being completely overwhelmed by a sudden flood of nutrients? Those are questions that have given biologists a lot of food for thought.

"Most of us learned in our textbooks about a rather static digestive system," says William Karasov, a physiological ecologist at the University of Wisconsin, Madison. But "the gut is a very dynamic organ." It can "adjust to changing demands and energy supply," adds Matthias Starck, a functional morphologist at the University of Munich, Germany. And those adjustments can be radical in the extreme.

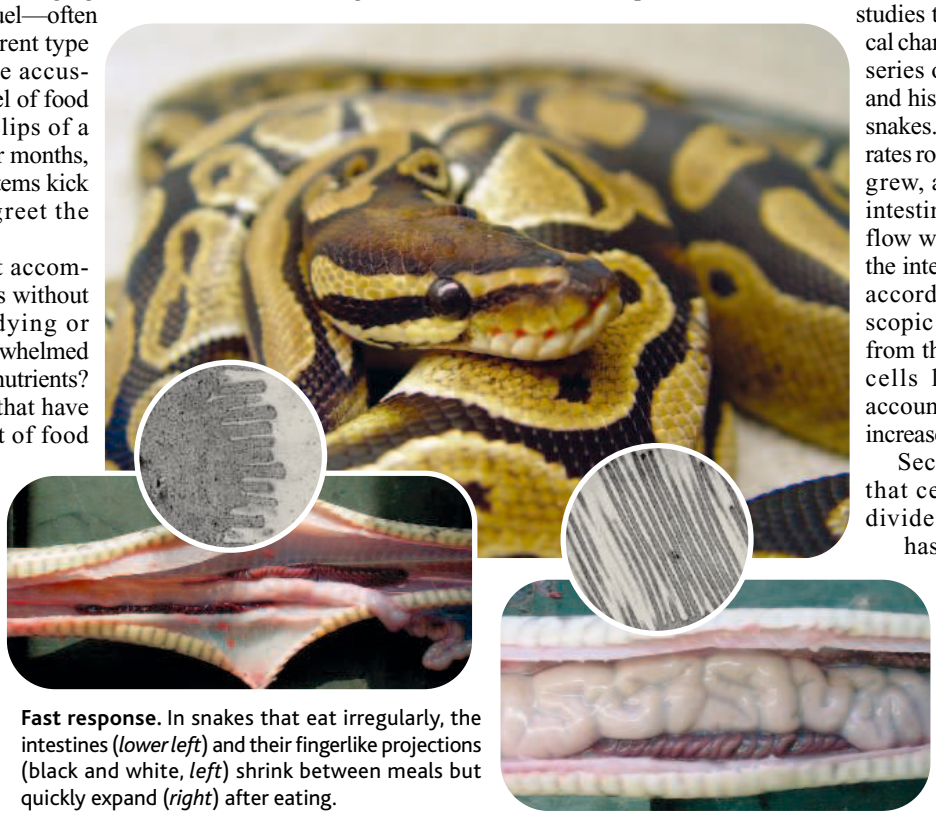

Fast response. In snakes that eat irregularly, the intestines (*lower left*) and their fingerlike projections (black and white, *left*) shrink between meals but quickly expand (*right*) after eating.

CREDITS (TOP AND MIDDLE RIGHT): MATTHIAS STARCK; (MIDDLE LEFT AND BOTTOM LEFT AND RIGHT) STEPHEN SECOR

The guts of a python's survival

Among those intrigued by the gustatory habits of snakes are Jared Diamond, a physiologist at the University of California, Los Angeles, and Stephen Secor, a physiologist now at the University of Alabama, Tuscaloosa. In 1995, they reported that during the months between meals, the python's stomach and intestine atrophy. Yet once the snake begins to eat, it quickly revs up its digestive function. Secor and Diamond's work suggested that the first food to reach the gut—particularly proteins or their amino acids—stimulates a dramatic expansion of the gut lining. The intestine doubles in size, significantly increasing its absorptive surface area.

Over the past decade, Secor, Starck, and, more recently, Jean Hervé Lignot of the Louis Pasteur University/CEPE-CNRS in Strasbourg, France, have worked independently and collaboratively to sort out how this gastrointestinal rebirth occurs with every meal. The gut lining consists of "fingers" of cells called villi, and the cells themselves sport projections called microvilli. Secor's initial research indicated that new cells are added to the gut lining when the intestine shifts into high gear. That shift, especially the rapid reactivation of the stomach and the production of stomach acids, is quite energy-intensive, taxing the body's reserves, he says.

Over the past 5 years, Starck has developed an alternative explanation, one he will detail in an upcoming issue of the *Journal of Experimental Biology*. He finds that the gut lining grows not because the number of cells increases but because blood pours into shrunken villi once a snake eats, expanding the surface area of the villi and flooding them with materials needed to digest the incoming meal. According to Starck, this proposed mechanism requires less energy than Secor's original explanation; digestion can begin even when fat reserves are relatively low, he notes. And once digestion starts, the ingested food provides the energy needed to complete it.

Starck's new proposal draws on ultrasound measurements of blood flow to and within the gut lining, as well as histological studies that characterize physical changes in the lining. In one series of experiments, Starck and his colleagues fed mice to snakes. The snakes' metabolic rates rose, their small intestines grew, and blood flow to the intestines tripled. This blood flow was responsible for half the intestine's increase in size, according to Starck. Microscopic globs of fat absorbed from the gut further bloat the cells lining the intestine, accounting for the rest of the increase, he says.

Secor too has now found that cells swell rather than divide, but he thinks blood has little to do with their expansion. Instead, his work indicates that the lining's villi absorb the digestive fluids from the gut itself. Working with Secor, Lignot has used electron microscopy to show that each cell's microvilli also swell significantly, quadrupling in size within 24 hours.

Even though Secor maintains that increased blood flow is not the secret to the rapid growth of a snake gut, he has shown that it is important to digestion. Animals typically divert blood to the gut during digestion, just as exercise results in increased circulation to muscles. Last year, Secor and his colleagues reported that snakes go to extremes, increasing blood flow to the gut by about 10-fold compared to the 50% increase humans experience during digestion. "[It's] really going through the roof," Secor notes. "The cardiac output is comparable to somebody going full-

What's Eating You?

Sometimes, it's who's digesting you that determines how you digest. In general, long guts absorb more food and make digestion more efficient. But having a big belly, so to speak, can slow an organism down—and that's bad news in a world of predators.

Demonstrating a link between a creature's gut size and its enemies, Rick Relyea of the University of Pittsburgh in Pennsylvania and his graduate student Josh Auld have raised wood frog tadpoles under different conditions. They've set up tanks with all the ingredients of the tadpole's natural pond environment. In some, they put just tadpoles, anywhere from 20 to 160 per tank. In others, the researchers added a predator: immature dragonflies. These insects were kept in underwater cages, so the tadpoles were safe, but the dragonfly smell signaled danger. In the first experiment, which lasted a month, Auld removed 10 tadpoles from each tank several times, measured their sizes, and preserved the specimens. He later dissected the preserved specimens and measured gut lengths.

Big tail. When these tadpoles live among predators, they sacrifice gut size for larger tails (*right*) and faster escapes.

Au naturel. Tanks that simulate the wood frog tadpole's natural environment enable University of Pittsburgh graduate student Nancy Schoeppner to study how predation and competition affect its gut size.

In the September 2004 *Ecology Letters*, Relyea and Auld reported that the greater the competition for food—such as in tanks with 160 tadpoles—the longer the tadpoles' guts grew. In crowded conditions, if a tadpole is lucky enough to find food, it needs to extract as much energy as possible, notes Relyea. "A great way to increase [digestive] efficiency is to have longer intestines because it forces the food to spend more time traveling through [them]," he explains—the slow journey provides more opportunities for the gut lining to absorb nutrients.

In the tanks with the caged dragonflies, however, the fear-provoking chemical cues emitted by the insect stunted gut growth. This makes sense, says Relyea. In the wild, tadpoles use their tails to dart away from dragonfly larvae, and the longer the tail, the better. But growing a long tail puts demands on the tadpole's resources, and gut length is sacrificed.

The shorter gut may be poorer at processing food, but in dragonfly-infested waters, the tradeoff for a swifter escape is likely worth it. "Animals can be amazingly sophisticated at fine-tuning their gut length to strike an effective balance between the two opposing forces of predation and competition," Relyea concludes.

–E.P.

out in exercise." And the python can sustain this additional blood flow for days—plenty of time for its intestinal muscles to work without fatigue at breaking down the skin, bones, and underlying tissue of its prey.

It takes a lot of heart to pump all that blood. Indeed, the snake's heart actually grows once it eats, increasing 40% in mass in just 2 days, James Hicks, a comparative physiologist at the University of California, Irvine, and his colleagues reported in the 3 March issue of *Nature*. Athletes' hearts can also expand—but that growth happens over years, says Secor.

Ready reserves

Even as they digest their food, snakes stockpile resources for their next great feast, says Lignot. In pythons, the stomach operates for 4 to 6 days, then begins to wind down, while the intestines keep going for at least another week to finish the job. Lignot's latest experiments show that as the intestine takes these extra days to process nutrients, it generates and banks cells for a subsequent supper. "This is the key adaptive factor: a dormant gut with unused cells that can quickly restart functioning when food is available again," says Lignot.

A similar phenomenon occurs in fasting rats. Even as they are reduced to breaking down their body's proteins—a desperate measure that can cause organs to waste away—their intestine begins to produce new cells, and programmed cell death in the lining stops, Lignot and his colleagues reported last year. "After a prolonged fast, the intestinal lining prepares itself for eventual refeeding," says Lignot.

Other animals faced with widely spaced meals have also adapted their guts to keep some cells in their digestive system up and running during the lean times. Perhaps the most extreme examples are creatures that hibernate during the cold winter or their summer counterparts that burrow and become dormant to escape life-threatening heat or dryness, a strategy called estivation. For example, Rebecca Cramp and Craig Franklin of the University of Queensland in Brisbane, Australia, have investigated the guts of green-striped burrowing frogs, an Australian species whose estivation can last more than 10 months. Once it rains hard, the frogs surface—sometimes for just a week—and they must quickly stock up on food to help find mates and build up fat reserves. Cramp and Franklin collected frogs in the wild, then allowed them to estivate in mud trays for up to 9 months. Within 3 months, the animals lost as much as 70% of their gut mass, the researchers found, and an additional 10% had disappeared by

On duty. While hibernating (bottom), 13-lined ground squirrels maintain minimal function in their guts but efficient digestive capacity.

CREDITS (TOP): RICK RELYEA; (BOTTOM) HANNAH CAREY/UNIVERSITY OF WISCONSIN SCHOOL OF VETERINARY MEDICINE

9 months. The microvilli on cells of the frogs' intestinal lining also shrank.

Overall, this gastrointestinal atrophy saves energy for the frogs, explains Cramp. Nonetheless the gut of an estivating creature can still absorb nutrients, even though maintaining that readiness entails "a significant energetic cost" at a time when the frog has little energy to spare, says Cramp. But the cost is a worthwhile investment, she has discovered. Her tests have shown that frogs surfacing from estivation absorb nutrients 40% more efficiently than frogs that hadn't burrowed. Newly aroused frogs "can maximize their digestive capability from the outset," says Cramp.

Hibernating mammals called 13-lined ground squirrels also keep digestive capacity in reserve. To save energy as they hibernate, the animals' gut lining atrophies, and their intestines thin. Some cells undergo programmed cell death in response to fasting. But tissue damage is minimal as genes that promote survival and curtail cell death become active at the same time, says Hannah Carey, a physiologist at the University of Wisconsin School of Veterinary Medicine in Madison. She has taken a close look at the remaining cells and found that microvilli remain intact on the surviving cells, and their density on each cell sometimes increases. In these microvilli, transporter proteins and digestive enzymes continue to be plentiful. Thus, during brief moments when the animals come out of their stupor during those quiet months, they can absorb nutrients still left in the gut.

Indeed, when Carey warmed intestinal tissue from hibernating animals so that it could function normally, she observed that, gram for gram, the tissue worked more efficiently than did the intestines of the nonhibernating squirrels. "This is likely a beneficial adaptation," she suggests: Squirrels emerging from hibernation could make the most of spring's low food supply and still have enough energy for breeding.

Always on standby. Australia's green-striped burrowing frog keeps a few gut cells up and running in preparation for a feeding frenzy when it surfaces.

Food-flight dilemma. Because they have different refueling strategies, red knots (*above*) have shrunken guts when they migrate, but western sandpipers (*inset*) do not.

Meals on the fly

Like hibernation, migration places unusual demands on the gut. Migrating birds, for example, devote extraordinary amounts of energy to flying, and they must be able to digest the different foods they encounter along the way. For many migrating birds, "the way to cope with season-to-season differences in food quality and energy expenditure is to change gut size," says Theunis Piersma, an evolutionary biologist with the Royal Netherlands Institute for Sea Research on the island of Texel and the University of Groningen.

Piersma studies the red knot, a bird species that migrates between Antarctica and Northeastern Canada and Greenland. He recently showed that its gut can adjust to different diets. Red knots typically eat two types of food: relatively soft stuff such as shrimp, crabs, or spiders, and hard stuff—cockles, mussels, and other bivalves. The red knot's gizzard, the muscular extra stomach used to crunch shells, grows quickly when the bird switches from soft food to hard food, Piersma reported last year.

He and his colleagues first measured the gizzards of red knots fed trout chow for several years. They then began serving small mussels to the birds. Over the next 3 weeks, the gizzards grew by 4.9 grams; the red knots only weighed about 130 grams total. Overall, the birds gained 7.3 grams. The dietary changes experienced by migrating birds "have apparently favored the evolution of intestinal plasticity," says Rick Relyea of the University of Pittsburgh, Pennsylvania.

Piersma and his colleagues then used ultrasound to see what happens to a red knot's gut during migration. They found that when the birds arrive at a stopover, their guts are much reduced. Less intestinal baggage apparently gives the birds a better shot at making it to their destination. Yet Piersma's group has documented that when red knots make a pit stop along the Wadden Sea, their digestive systems quickly regain their ability to process food and absorb nutrients, albeit temporarily.

His team's observations show that the speed at which the gut comes back online is critical to the birds' ability to replenish the fat reserves they need to complete their journey. According to some physiologists, that ability should be limited by how fast the birds can catch their prey. But Piersma's studies show that the gut's ability to process food is the limiting step, and that their food choice—and therefore their rate of consumption—is in large part dictated by the size of their gizzards. The faster gizzards can bulk up, the greater the birds' range of food choices. "There are incredibly strong interactions between the type of food and type of digestive machinery," Piersma points out.

He and his colleagues have looked at food choices of red knots at the Wadden Sea stopover. The researchers set up patches of food along the mudflats that differed in food quality. One had many good-sized mollusks, which are relatively tough to digest. The other had a sparse smattering of crabs, which are easier for the gizzard to process but gram for gram pack less nutritional value than the mollusks. They watched as radio-tagged birds foraged in these patches and used ultrasound to measure their gizzards.

CREDITS: (TOP) CHRIS KELLY; (INSET) TOM MIDDLETON/PACIFIC WILDLIFE FOUNDATION; (BOTTOM) ED MEYER

Red knots with large gizzards, which could digest the shelled food faster, favored the larger bivalves. Those with small gizzards—the majority of the migrating birds when they first arrived—had to forage almost exclusively in the other patch. As a result, they needed to spend more time—and wasted precious energy—looking for meals. Thus, the gizzard's size seems to drive the food choice and foraging strategy of the migrating red knot, Piersma and his colleagues reported in the January *Journal of Animal Ecology*, and only if the gizzard grows fast enough will the migrants be able to lay in the stores they need for the final leg of their trip. Says Starck: "[Red knots] that optimize gut size and function arrive with more energy reserves in their breeding grounds and thus [have an] advantage over others."

In contrast to red knots, having a big gut seems to be the secret to success for some migrating birds. Consider Western Sandpipers, which migrate from Central America to Alaska. These birds actually increase the size of digestive organs for migration, according to research by Tony Williams of Simon Fraser University in Burnaby, British Columbia, his graduate student R. Will Stein, and Christopher Guglielmo, now at the University of Western Ontario, Canada.

The researchers attribute the difference between red knots and sandpipers to the species' contrasting migration habits. Red knots travel very long distances, fueling up just once during a monthlong stopover. Sandpipers hop from food stop to food stop, so they don't need to be as trim as red knots to get to their destinations.

These gastrointestinal tales of famished snakes and ravenous frogs may have implications beyond explaining how animals adjust to the nutritional ups and downs of life in the wild. Maybe, researchers speculate, a key to understanding some of the digestive diseases that affect millions of people lies in the intestines of a hibernating squirrel or the stomach of a migrating bird. "Wild animals provide model systems to study regulatory physiology [of the gut] that may be of biomedical importance," says the University of Wisconsin's Karasov.

–ELIZABETH PENNISI

NEWS

A Mouthful of Microbes

Oral biologists are devouring new data on the composition, activity, and pathogenic potential of microbes in the mouth, the gateway to the gut

Thanks to dentists, "open wide" has become a command to fear. A century ago, dental practitioners depended on a shot of whiskey and pliers to treat toothaches and sore gums. Today's dentists have laser drills and Novocain, but they haven't completely shed the aura of pain. In the near future, however, the tools of choice may be less scary: a DNA test followed by a chaser of "good" bacteria, for example.

Over the past 40 years, oral biologists have been taking stock of the vast microbial communities thriving on and around teeth, gums, and the tongue. It's been known for quite some time that bacteria that normally reside in the mouth can escape to other parts of the body and cause problems. There's a well-substantiated link between one oral pathogen and heart problems, for example. And last year, tests in mice lent support to the theory that a common mouth bacterium can slip into the bloodstream of pregnant women and infect their uterus and placenta, eventually causing premature births.

Father of oral biology. Using the recent invention of microscopes to explore the human body, Antony van Leeuwenhoek discovered the first microbes in the mouth and recorded the diversity of these organisms.

CREDIT: CORBIS

But poor oral health also causes harm directly. Three out of 10 people over 65 have lost all their teeth. In the United States, half of all adults have either gum disease or tooth decay; Americans spend more than $60 billion a year to treat tooth decay alone. Indeed, cavities are the single most common chronic disease of childhood, with a rate five times greater than that seen for the next most prevalent disease, asthma. Adding insult to injury, about one-third of the general population also suffers from halitosis, better known as bad breath.

A lot of those problems can be traced to the mouth's microbes, say oral biologists. In healthy mouths, "good" bacteria and other microbes compete with nefarious cousins and keep them in check. But if conditions change, pathogenic microbes can gang up against the beneficial species and gain control of the mouth's surfaces. Bleeding gums, cavities, and bad breath can result.

By comparing healthy mouths to unhealthy ones, researchers are now rooting out the problematic microorganisms, which include bacteria, viruses, fungi, and even archaea. In addition, efforts to sequence the genes, if not the whole genomes, of oral microbes are helping identify the villains in the mouth and how they trigger disease. "We've been able to get a better understanding of the variety and scale of the microorganisms that are present," says Richard Lamont, a microbiologist at the University of Florida, Gainesville.

The new research clearly shows that the mouth is a complex eco-system. Some microbial species are pioneers, producing proteins that serve as welcome mats to later colonizers. It's also become evident that in the mouth, microbes gang up to cause troubles. Unlike other infectious diseases, "we are looking at infections that are caused by more than one organism," says Howard Jenkinson, a molecular microbiologist at the University of Bristol in the United Kingdom.

No microbe is an island

The study of oral bacteria goes back almost 400 years. When Dutch glassmaker Antony van Leeuwenhoek began using microscopes to study the human body, the microbial world of the mouth opened up to him. He examined samples of plaque from his own teeth and made some of the first drawings of what we now call bacteria. His notes set the stage for oral microbiology. "He pointed out the nature of the diversity [in the mouth]," says David Relman, a microbiologist at Stanford University in California. Since then, "there's always been a sense that the community is what matters; the community is capable of doing things that individual [species] cannot."

Still, it didn't hit home that many oral problems came from microbes until the 1960s, when Sigmund Socransky of the Forsyth Institute in Boston, Massachusetts, discovered bacteria buried in the gums of people with trench mouth. Soon afterward he and Forsyth's Anne Haffajee found that the population of microbes associated with plaque-encrusted teeth changes with the severity of the disease, indicating that more than one microbe is involved.

It also became clear that bacteria grow in thin layers—called biofilms—on the mouth's surfaces. Studying these bio-films, however, was problematic. Researchers would try to use a cheek swab or tooth scraping to grow oral microorganisms in the lab, but only about half the microbial species took hold, leaving a knowledge gap.

In the early 1990s, Socransky and colleagues developed a method, called checkerboard DNA-DNA hybridization, that greatly sped up the characterization of the bacterial community in an individual's mouth. Instead of being limited to analyzing 100 samples per year, they could look for 40 bacteria in 28 samples simultaneously. "We can [now] do tens of thousands," says Haffajee. Since then, oral biologists have added another tool to their repertoire; they've been identifying oral bacteria that have yet to be cultured by differences in the gene for 16S, a ribosomal RNA subunit.

Using this latter approach, Bruce Paster, a molecular microbiologist at the Forsyth Institute, and others have built extensive databases of 16S gene sequences collected from different parts of the mouth. Each sequence represents a different microorganism. "Collectively speaking, there are over 700 species in the human oral cavity, of which over half cannot yet be grown," says Paster. He's now putting together a microarray with all the 16S genetic sequences on it. Researchers could then use it to check DNA from clinical samples: "You can quickly assess the microbial profiles of [each] mouth," says Paster.

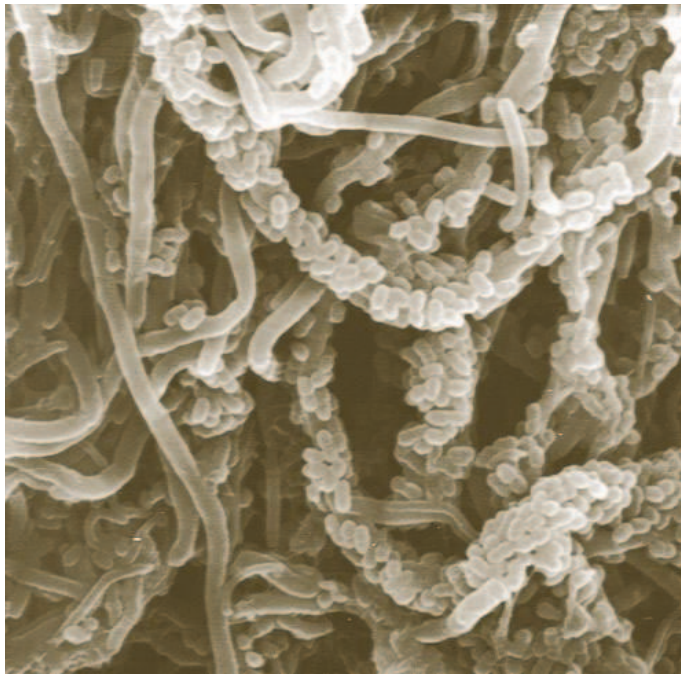

Mixed communities. The mouth contains a vast number of microbial inhabitants of all different shapes and sizes.

Microorganism	Disease	Site
Actinobacillus actinomycetemcomitans	Severe gum disease in young adults	University of Oklahoma
Porphyromonas gingivalis	Adult gum disease	TIGR*; Forsyth Institute
Streptococcus mutans	Tooth decay	University of Oklahoma
Tannerella forsythensis	Gum disease, implant failure/infection	TIGR
Prevotella intermedia	Gum disease	TIGR
Treponema denticola	Gum disease	TIGR; Baylor College of Medicine
Streptococcus gordonii	Plaque development	TIGR

* The Institute for Genomic Research

Genes, genes, genes. Seven sequenced genomes, with more on the way, are revealing the secrets of the mouth's microbes.

Microbial whodunit

To a microbe, the mouth is a planet full of different surfaces and environmental conditions. Not surprisingly then, oral microbes have their favorite homes—teeth or the tongue, for example. In each case, says Paul Lepp, a microbiologist at Minot State University in North Dakota, "if you can figure out which organisms should be present during health, that may lead us down the road to find some way of trying to encourage those to survive."

Like the microbes they study, oral biologists tend to specialize in particular areas of the mouth and the diseases arising there. Some researchers analyze microbial invasions of teeth. That's the site of perhaps the most studied mouth microbe, *Streptococcus mutans*. This bacterium colonizes the teeth of almost every child and feeds off sugar in the mouth, generating lactic acid that destroys tooth enamel and leads to lesions known as caries or cavities.

As for Relman and Lepp, it's the microbes that reside in the deepest part of the narrow crevice between the gums and the base of the tooth that are of great interest. In a healthy mouth, there's a tight fit between the tooth and the gum collar. But if disease sets in, the crevice widens and deepens, gums swell and bleed, and teeth loosen.

In 2004, as part of their surveys of this crevice, Relman, Lepp, and their colleagues discovered that some of these more troublesome microbes weren't even bacteria. They were archaea, members of a group of microbes best known for thriving in extreme conditions. The researchers initially found these archaea in a third of 58 people with diseased crevices but not in individuals with healthy mouths. The more severe the disease, the larger the archaea population—and that population shrank with treatments that lessened gum disease. Oral "disease involves all sorts of organisms that we've never [thought of]," says Lepp.

Paster's chosen territory is the tongue. He's pinpointed 92 groups of microorganisms living there and is homing in on species that may create bad breath. In early 2003, Paster and his colleagues compared data from six people with bad breath to five without it. There were key differences in the microbial milieu of the two groups' mouths. Three bacterial species thrived in the healthy mouths but not in the six

CREDITS (TOP): ZIE SKOBE FORSYTH INSTITUTE; (BOTTOM) ADAPTED FROM NATIONAL INSTITUTE OF DENTAL AND CRANIOFACIAL RESEARCH

mouths with bad breath. Paster's team also identified a half-dozen microorganisms on foul-smelling tongues that were not found on the sweet-smelling ones. In an experiment whose data have yet to be published, they have confirmed that the tongue's microbial makeup is important in halitosis. The investigators tracked the microbial communities on the tongues of 33 people with halitosis before and after their bad breath was eliminated through daily scraping of the tongue and use of mouthwash and toothpaste containing zinc. As halitosis lessened, the tongue's microbial communities changed, says Paster.

Sometimes a microbe in one oral setting helps other microbes establish themselves elsewhere. Take the gram-positive bacterium called *S. gordonii*. These microbes settle on the saliva film coating teeth early in life by recognizing certain saliva proteins, which they proceed to break down and use as nutrients. In turn, surface proteins of the streptococci attract other bacteria, such as the pathogen *Porphyromonas gingivalis*. It attaches to the streptococci to get a toehold at the tooth-gum interface. But in a matter of minutes, it moves on to invade the gum's epithelial cells.

To help understand how *P. gingivalis* colonizes the gums, Lamont has recently chronicled the pathogen's changing repertoire of proteins. Using a series of analytical techniques, including tandem mass spectrometry, capillary high performance liquid chromatography, and two-dimensional gel electrophoresis, he and his colleagues documented that the bacterium made about 220 new proteins when it encountered gum epithelial cells. Many of them are surface proteins that likely establish a nutrient pipeline from the host or protect the bacteria from immune responses, Lamont and his colleagues reported in the January issue of *Proteomics*.

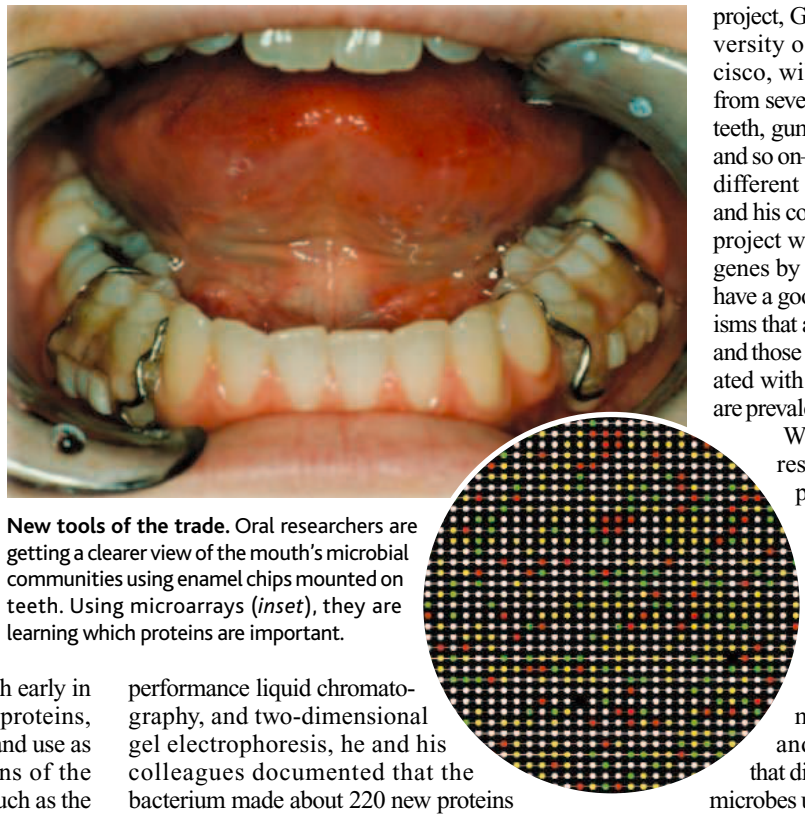

New tools of the trade. Oral researchers are getting a clearer view of the mouth's microbial communities using enamel chips mounted on teeth. Using microarrays (*inset*), they are learning which proteins are important.

Wash that mouth out

Although the genomes of dozens of microbes are now in the public databases, the sequencing of oral bacteria is just ramping up. Thus far, researchers have sequenced seven species that settle in the mouth, and a half-dozen more are in the pipeline, says Dennis Mangan, a microbiologist at the National Institute of Dental and Craniofacial Research (NIDCR) in Bethesda, Maryland, which supports the sequencing projects. And in late December 2004, NIDCR started a 3-year study with Relman and The Institute for Genomic Research in Rockville, Maryland, to catalog all the microbial genes in the mouth. For this project, Gary Armitage of the University of California, San Francisco, will collect DNA samples from seven sites in the mouth—the teeth, gums, tongue, palate, cheek, and so on—from a mix of people in different states of oral health. He and his colleagues estimate that the project will identify about 40,000 genes by its conclusion. "We will have a good handle on those organisms that are associated with health and those organisms that are associated with disease, and what genes are prevalent in disease," says Lepp. With that knowledge, researchers may be able to pinpoint weaknesses in pathogenic oral microbes or learn how to boost the mouth's response to microbial attacks. That might ultimately lead to mouthwashes that inhibit just bad mouth microbes instead of good and bad alike, or to drugs that disable the surface proteins microbes use to infect the mouth.

Armed with the growing understanding of the mouth microbial ecosystem, one company, Oragenics Inc. in Alachua, Florida, has already taken steps to pit bacteria against bacteria in the battle for healthy teeth. The approach, called replacement therapy, would use genetically modified *S. mutans* bacteria to supplant normal cavity-causing ones; the altered germs don't make lactic acid. The company's microbe-laden mouthwash has been controversial, however, and the Food and Drug Administration put the first clinical trials of it on hold because of concerns that the researchers couldn't guarantee that, should something go wrong, they could get rid of the microbes once in the mouth. But in December 2004, Oragenics got approval to continue the trial with denture wearers whose dentures—and bacteria—could be removed if a problem occurs.

It may be years before Oragenics's cavity-fighting bacterium makes it into dental practice. And it's not clear how popular this particular approach will be. But Mangan is convinced that all the work characterizing the mouth's microbial communities will eventually have a big payoff. "[It's] going to point to ways to control the numbers and the species of bacteria there, particularly the dangerous ones," he says. That could make cavities, gum disease, and bad breath a thing of the past—and bring a healthy smile to the mouths of many people.

—ELIZABETH PENNISI

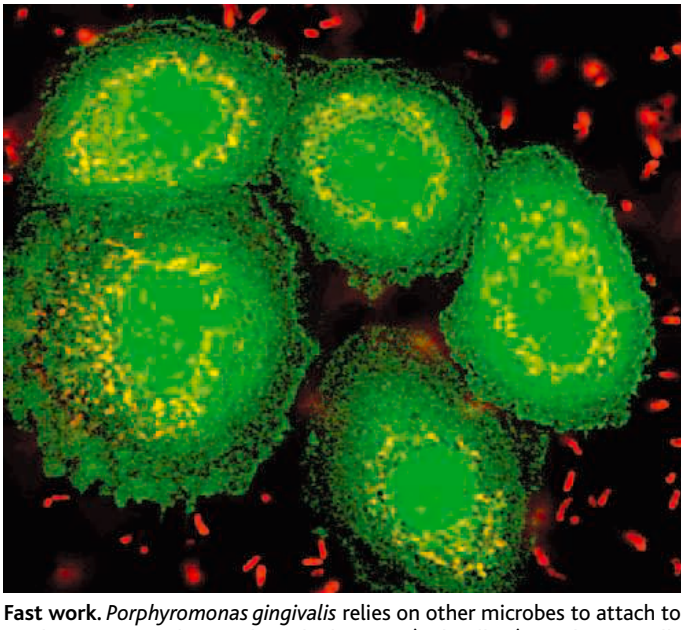

Fast work. *Porphyromonas gingivalis* relies on other microbes to attach to teeth. In minutes, thousands of the bacteria (red, yellow) invade gum cells (green) and head to each cell's nucleus.

CREDITS (TOP): P. KOLENBRANDER/NIDCR; (INSET) Y. ZHANG, T. WANG, W. CHEN, O. YILMAZ, Y. PARK, I. Y. JUNG, M. HACKETT, R. J. LAMONT, *PROTEOMICS* 5, 198 (2005); (BOTTOM) C. M. BELTON, K. T. IZUTSU, P. C. GOODWIN, Y. PARK, R. J. LAMONT, *CELL MICROBIOL.* 1, 215 (1999)

VIEWPOINT

No Organ Left Behind: Tales of Gut Development and Evolution

Didier Y. R. Stainier

The function of an organ is dependent on its cellular constituents as well as on their assembly into a cohesive unit. The developing gut faces unique challenges as one of the longest and largest organs in the body and also because it is constantly interfacing with external factors through the diet. Its location deep within the body has until recently hampered investigation into its formation. The patterning of the gut along its longitudinal, dorsoventral, left-right, and radial axes is one of the fascinating issues that pertain to the development, function, and homeostasis of this understudied organ.

At first glance, the gut looks deceptively simple: an epithelial tube composed of a few cell types and surrounded by an innervated muscle layer (Fig. 1). Yet in evolutionary terms, the gut, as an endodermal organ, predates any mesodermal organ, and it has reached a level of complexity and sophistication that is only starting to be appreciated.

Gut formation is one of the first outcomes of multicellularity. Bringing cells together allowed the organism the opportunity to make specialized cell types, with selective pressure leading to the emergence of an outer protective coat (the ectoderm) and an inner layer (the endoderm) involved in food absorption. The mesoderm, or middle layer, arose approximately 40 million years after the emergence of the ectoderm and endoderm and was most probably a derivative of the latter.

The originally simple aggregate of cells involved in food absorption has thus evolved into a very large and complex structure that is highly patterned in its longitudinal, dorsoventral (DV), left-right (LR), and radial axes. Starting with the formation of the endodermal germ layer, I will highlight some of the fascinating issues that pertain to the development and function of the gut, many of which remain largely unexplored.

Formation of the Endodermal Germ Layer

Over the past decade or so, studies in a number of invertebrate and vertebrate model systems, including *Caenorhabditis elegans*, *Drosophila*, sea urchins, ascidians, *Xenopus*, zebrafish, the chick, and the mouse, have provided insights into the genes and cellular mechanisms regulating endoderm formation (*1*, *2*). These studies have revealed a high degree of conservation in some of the transcriptional regulators of endoderm formation; for example, members of the Gata and Forkhead transcription factor families have been implicated in this process across the phyla, although the intercellular events regulating endoderm formation appear to be more divergent. The Wnt signaling pathway has been implicated in the formation of the endoderm in *C. elegans*, sea urchins, and ascidians, whereas transforming growth factor–β (more specifically Nodal) signaling has been implicated in the formation of the endoderm in vertebrate embryos. However, this apparent lack of conservation of the signaling pathways regulating endoderm formation probably reflects our incomplete understanding of the process. Indeed, we have not yet gained sufficient knowledge to control the efficient differentiation of mammalian stem cells into endoderm, meaning that the investigation of endoderm formation must proceed using multiple approaches in multiple model systems.

As mentioned above, the mesoderm can be thought of, at some level, as a derivative of the endoderm and indeed, the endoderm and mesoderm often originate from the same or adjacent regions of the embryo. Although the mechanisms leading to the segregation of these two lineages are fairly well understood in *C. elegans* and sea urchins, for example, much remains to be learned about this process in vertebrates. Again, this knowledge will be necessary to enhance our ability to coax stem cells into various endodermal or mesodermal lineages.

Patterning of the Gut Along the Anteroposterior Axis

After segregating from the mesoderm during late blastula stages, the endoderm undergoes complex morphogenetic processes, first during gastrulation and then as it converges toward the midline and extends to cover the entire anteroposterior (AP) extent of the embryo. These movements lead to the formation of a hollow tube either from the cavitation of a solid rod, as in zebrafish and *Xenopus*, or the folding of a sheet, as in birds and mammals. Thus, what started out in the most primitive multicellular organisms as a small aggregate of cells involved in food absorption has evolved into a tube several times the length of the organism, so long in fact that it has to fold extensively to fit into the body cavity. The primitive gut is divided, somewhat arbitrarily, into foregut, midgut, and hindgut, each of which will give rise to specialized regions of the differentiated gut tube, as well as, in the case of the foregut, accessory organs such as the thyroid, lungs, liver, and pancreas. The precise location of these accessory organs as well as the demarcation of the various territories along the gut tube has been attributed to a set of complex yet mostly uncharacterized interactions between the gut and the surrounding mesoderm, both of which appear to be patterned along the AP axis. For example, in *Drosophila*, specific *Hox* genes are expressed in localized regions of the midgut endoderm and the visceral mesoderm surrounding it. One of the best-studied examples is the regulation of *labial* expression in the endoderm by *Ubx*, which itself is expressed in the adjacent mesoderm (*3*). By regulating Bmp and Wnt signals, Ubx controls the segmental expression of *labial*, which in turn regulates the differentiation of a specialized set of endodermal cells. *Hox* genes have also been implicated in endoderm patterning in chordates. They are expressed in specific AP domains in both the endodermal and mesodermal germ layers, and loss- and gain-of-function experiments have illustrated a few of their roles in patterning the gut along the AP axis (*4*–*6*). For example, *Hoxd-13* is expressed in the hindgut region of mouse and chick embryos (*7*–*9*), and mice that are homozygous mutant for this gene have a hindgut defect (*10*). In addition, misexpression of *Hoxd-13* in the embryonic chick midgut mesoderm results in the induction of aspects of hindgut morphology in the midgut epithelium (*11*). Therefore, mesodermal expression of *Hox* genes can function in the mesoderm-endoderm interactions to pattern the endodermal epithelium, although the downstream targets of the *Hox* genes that induce this patterning remain unknown. Similarly, how the pattern of *Hox* gene expression is determined is unclear, although it lies

Department of Biochemistry and Biophysics, Programs in Developmental Biology, Genetics and Human Genetics, University of California, San Francisco, San Francisco, CA 94143–2711, USA. E-mail: didier_stainier@biochem.ucsf.edu

downstream of the events that pattern the early embryo. There is also strong evidence that retinoic acid signaling is involved in patterning the endoderm along the AP axis (*12*), probably acting directly on *Hox* gene expression (*13*, *14*). In addition to *Hox* genes, at least two *ParaHox* transcription factor genes, *Cdx2* and *Pdx1,* are critical for gut tube development. Cdx2 is specifically important for hindgut development in humans, mice, and *Drosophila,* and Pdx1 is critical for pancreas formation in humans and mice (*15*). Cdx2 likely patterns the vertebrate gut by regulating *Hox* gene expression in the endoderm, as it appears to do so in *Drosophila*, *C. elegans*, and the mouse spinal cord (*5*). In summary, the early patterning of the embryo determines the expression pattern of *ParaHox*, *Hox*, and other transcription factor genes in the endoderm and adjacent mesoderm. Thereafter, a complex dialogue between these two tissues leads to the final pattern of the gut tube along the AP axis.

In addition to its elaborate patterning along the AP axis, the gut also undergoes some fascinating morphogenetic processes, including extensive and, at least initially, highly stereotyped looping movements. Again, as is the case with AP patterning, the adjacent mesoderm appears to play a critical role in this process. For example, the initial looping of the zebrafish foregut appears to result from the asymmetric displacement of the neighboring lateral plate mesoderm (*16*). Whether the subsequent and extensive looping movements of midgut derivatives seen in higher vertebrates are also driven by the surrounding tissues remains to be investigated.

Radial Patterning of the Gut

Although the mammalian gut tube forms through a folding process, rearrangement of the endodermal epithelium leads to the complete occlusion of the lumen (*17*). Defects in the subsequent recanalization, or reluminization, of the gut tube can lead to partial stenosis or duplication of the digestive tract. As the lumen expands and epithelial cells proliferate, the gut epithelium, possibly because it is constrained in its outer diameter by the surrounding muscle layer, starts undergoing folding morphogenesis. This process leads to the formation of characteristic fingerlike intestinal villi, which greatly increase the absorptive surface of the digestive tract (*18*–*22*). Pitlike intestinal crypts also form at the base of the villi, and they contain the stem cells that serve as the source of epithelial cells for the entire intestinal surface. The life-span of differentiated intestinal epithelial cells in humans is estimated to be approximately 4 days, with as many as 1400 cells per villus shed into the lumen on a daily basis. There are four cell types currently recognized in the intestinal epithelium. Enterocytes secrete enzymes that help digest sugars and proteins and absorb nutrients. Goblet cells, most abundant in the posterior gut, secrete mucus, which protects against shear stress and chemical damage (among other functions). The rare enteroendocrine cells secrete hormones such as serotonin, substance P, cholecystokinin, gastrin, and secretin. Paneth cells secrete antimicrobial peptides such as defensins (cryptdins), as well as enzymes such as lysozyme and phospholipase A2 (and they live for about 20 days). The signaling pathways and transcriptional effectors regulating the differentiation of these cells are only starting to be investigated and, not surprisingly, a role for Notch signaling in this process has been reported (*22*, *23*). Another interesting question concerns the migration of these different cell types in the radial axis, because Paneth cells remain at the bottom of the crypts while the other cell types migrate upward toward the tip of the villi. Ephrin signaling has been implicated in this fascinating process, which begs for further investigation (*19*).

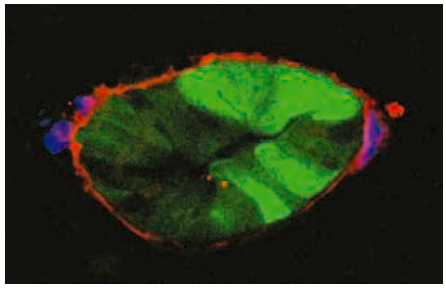

Fig. 1. Transverse section through the gut of a zebrafish embryo 120 hours after fertilization, showing the endodermal epithelial cells in green (*31*), the visceral smooth muscle cells in red, and the enteric neurons in purple.

Intestinal stem cells have been studied for many years because of their well-defined position, extreme sensitivity to chemo- and radiotherapy, and likely association with the development of cancer (*18*–*22*). Each crypt is estimated to contain between one and six stem cells and, in the mouse intestine, each of these cells appears to divide about once a day. Interestingly, despite the roughly equivalent number of stem cells in the large and small intestine in humans, the incidence of cancer in the former is about 70 times greater than in the latter, for reasons that remain largely unknown. Recent work has started to shed light on the genes that regulate the behavior of the intestinal stem cells in vivo. For example, Wnt signaling has been implicated in many aspects of intestinal stem cell biology, including stem cell maintenance and the proliferation/differentiation switch in intestinal crypts and subsequent positioning of the differentiated cells (*18*, *19*, *22*). However, many interesting issues remain unresolved, including how Wnt signaling regulates so many different aspects of stem cell biology, as well as the identity and location of the putative Wnt source close to the crypt bottom (*19*, *22*).

As the gut tube forms, cells from the lateral plate mesoderm begin to encircle it. These cells proliferate and differentiate into connective tissue as well as the characteristic circular and longitudinal muscle layers. At the same time, cranial neural crest cells migrate ventrally, and once in contact with the developing gut, they migrate posteriorly to colonize its entire AP extent. Defects in this process lead to the common intestinal motility disorder Hirschsprung disease (*24*). Again, the tissue interactions leading to the differentiation of both mesodermal and ectodermal cells in the vicinity of the gut endoderm are only starting to be investigated at the molecular level.

Patterning of the Gut in the DV and LR Axes

The most visible manifestation of DV and LR patterning of the gut is in the stereotyped emergence of gut-associated organs such as the thyroid, lungs, liver, and pancreas. For example, the thyroid and lungs bud from a ventral region of the foregut, and the homeobox gene *Nkx2.1*, whose expression is restricted ventrally, is required for this process (*15*). Concomitant with the looping movement mentioned above, the gut is also thought to rotate slightly, thereby blurring the lines between DV and LR patterning. However, as with the other patterning events (AP and radial), the surrounding mesodermal tissues are thought to play critical roles in patterning the gut along the DV and LR axes and in the resulting emergence of the various organ buds.

Signaling Pathways in Gut Development

Hedgehog, Bmp, Fgf, and Wnt signaling have all been implicated in various aspects of gut development (*15*, *19*, *22*, *25*). Such studies have revealed that these signaling pathways are used at multiple steps of the process, as the endoderm and mesoderm become involved in an increasingly complex set of interactions. As a consequence, understanding the role of these signaling pathways in gut development will require sophisticated genetic studies in which one modulates them with precise spatiotemporal control. For example, expressing the pan-Hedgehog (Hh) inhibitor Hhip (Hedgehog-interacting protein) in the intestinal epithelium (using the mouse *Villin1* promoter) has shed some light on the complex role of Hh signaling in patterning the intestinal crypt-villus axis (*26*). Further insights into the signaling pathways regulating gut development are likely to come from such intricate loss- and gain-of-function approaches.

Epigenetic Control of Gut Development

In addition to the hardwired program of gut development discussed above, it is clear that environmental influences, such as diet (*27*) and the microbial community of the gut (*28*), play important roles in the differentiation and function of the gut. For example, in mammals, the changing dietary input in the pre- and postnatal periods imposes different demands on the intestine and influences its morphology, enzymatic diversity, and transport. In addition, the diet contains substances such as polyamines and epidermal growth factor that do not play a nutritional role but appear to directly stimulate the growth of the intestinal epithelium (*27*). Similarly, *C. elegans* worms adjust the size of their pharynx, intestine, and intestinal microvilli depending on their nutritional state (*29*), and such plasticity is also seen in the willow ptarmigan, in which the winter consumption of fibrous food is associated with relatively long caecae. Investigations into the cellular and molecular underpinnings of such phenomena are just beginning.

Molecular Basis of Human Gut Malformations

In addition to the few disorders mentioned earlier in this article, naturally occurring human gut malformations are not rare; in fact, they are a major cause of perinatal morbidity and mortality. Also, because the endoderm extends along most of the AP axis of the embryo, it plays critical roles in many developmental events. For example, the anterior or pharyngeal endoderm contributes substantially to craniofacial structures and lies in close proximity to the developing heart, and thus defects in this tissue are likely to play a major role in the formation of these organs. It is clear, however, that although we can make educated guesses about which signaling pathway is likely to be defective in a select subset of gut malformations (*30*), much work remains to be done to establish molecular causality. In this regard, human genetic studies of gut malformations have certainly lagged behind those of the cardiovascular system, for instance. And as has already been illustrated regarding other organ systems such as the cardiovascular system, more subtle mutations in key developmental genes are likely to predispose one to gut disease and/or functional defects. Closer interactions between clinical and basic scientists interested in the gastrointestinal tract will greatly accelerate the pace of discovery in these areas.

Summary

Compared to readily accessible organs such as the limb, or to organs such as the heart and pancreas that are the focus of resourceful charities, the gut has been left behind. However, it is clear from the few vignettes presented here that the many fascinating developmental, evolutionary, and medical aspects of the gut will continue to attract much attention and generate pertinent information.

References and Notes

1. D. Y. Stainier, *Genes Dev.* **16**, 893 (2002).
2. D. Clements, M. Rex, H. R. Woodland, *Int. Rev. Cytol.* **203**, 383 (2001).
3. M. Bienz, *Trends Genet.* **10**, 22 (1994).
4. F. Beck, F. Tata, K. Chawengsaksophak, *Bioessays* **22**, 431 (2000).
5. A. Grapin-Botton, D. A. Melton, *Trends Genet.* **16**, 124 (2000).
6. J. C. Kiefer, *Dev. Dyn.* **228**, 287 (2003).
7. Y. Yokouchi, J. I. Sakiyama, A. Kuroiwa, *Dev. Biol.* **169**, 76 (1995).
8. D. J. Roberts *et al.*, *Development* **121**, 3163 (1995).
9. P. Dollé *et al.*, *Mech. Dev.* **36**, 3 (1991).
10. T. Kondo, P. Dollé, J. Zakani, D. Duboule, *Development* **122**, 2651 (1996).
11. D. J. Roberts, D. M. Smith, D. J. Goff, C. J. Tabin, *Development* **125**, 2791 (1998).
12. D. Yelon, D. Y. Stainier, *Curr. Biol.* **12**, 707 (2002).
13. D. Huang, S. W. Chen, A. W. Langston, L. J. Gudas, *Development* **125**, 3235 (1998).
14. M. Schubert *et al.*, *Development* **132**, 61 (2005).
15. J. M. Wells, D. A. Melton, *Annu. Rev. Cell Dev. Biol.* **15**, 393 (1999).
16. S. Horne-Badovinac, M. Rebagliati, D. Y. Stainier, *Science* **302**, 662 (2003).
17. A. Matsumoto, K. Hashimoto, T. Yoshioka, H. Otani, *Anat. Embryol. (Berlin)* **205**, 53 (2002).
18. F. Radkte, H. Clevers, *Science* **307**, 1904 (2005).
19. E. Sancho, E. Battle, H. Clevers, *Curr. Opin. Cell Biol.* **15**, 763 (2003).
20. E. Marshman, C. Booth, C. S. Potten, *Bioessays* **24**, 91 (2000).
21. M. Brittan, N. A. Wright, *Cell Prolif.* **37**, 35 (2004).
22. E. Sancho, E. Battle, H. Clevers, *Annu. Rev. Cell Dev. Biol.* **20**, 695 (2004).
23. J. Jensen *et al.*, *Nature Genet.* **24**, 36 (2000).
24. M. A. Parisi, R. P. Kapur, *Curr. Opin. Pediatr.* **12**, 610 (2000).
25. K. Fukuda, S. Yasugi, *J. Gastroenterol.* **37**, 239 (2002).
26. B. B. Madison *et al.*, *Development* **132**, 279 (2005).
27. J. Pacha, *Physiol. Rev.* **80**, 1633 (2000).
28. F. Bäckhed, R. E. Ley, J. L. Sonnenburg, D. A. Peterson, J. I. Gordon, *Science* **307**, 1915 (2005).
29. W. Ao *et al.*, *Science* **305**, 1743 (2004).
30. P. De Santa Barbara, G. R. Van Den Brink, D. J. Roberts, *Am. J. Med. Genet.* **115**, 221 (2002).
31. H. Field, E. A. Ober, T. Roeser, D. Y. Stainier, *Dev. Biol.* **253**, 279 (2003).
32. I would like to apologize to the many authors whose research papers relevant to this review I was not able to reference because of space constraints. Gastrointestinal tract work in my lab is funded by NIH (National Institute of Diabetes and Digestive and Kidney Diseases), the Juvenile Diabetes Research Foundation, and the Packard Foundation. Thanks to M. Santoro (University of California, San Franscisco) for contributing the figure.

10.1126/science.1108709

REVIEW

Self-Renewal and Cancer of the Gut: Two Sides of a Coin

Freddy Radtke[1] and Hans Clevers[2]*

The intestinal epithelium follows the paradigms of stem cell biology established for other self-renewing tissues. With a unique topology, it constitutes a two-dimensional structure folded into valleys and hills: the proliferative crypts and the differentiated villi. Its unprecedented self-renewal rate appears reflected in a high susceptibility to malignant transformation. The molecular mechanisms that control homeostatic self-renewal and those that underlie colorectal cancer are remarkably symmetrical. Here, we discuss the biology of the intestinal epithelium, emphasizing the roles played by Wnt, bone morphogenic protein, and Notch signaling cascades in epithelial self-renewal and cancer.

The intestinal epithelium represents an exquisite model for the study of stem cell biology and lineage specification. It is likely the simplest mammalian study model for tissue self-renewal, yet it features multipotent stem cells, transit-amplifying compartments, several binary lineage decisions, as well as programmed cell death. The function of the mammalian intestinal epithelium poses formidable challenges that evolution has met, often very elegantly. Like the epidermis of the skin, the intestinal epithelium constitutes a barrier between the body and the outside world (of which the intestinal lumen may be considered a particularly threatening version). Whereas the epi-

[1]Ludwig Institute for Cancer Research, Lausanne Branch, University of Lausanne, Chemin de Boveresses 155, CH-1066 Epalinges, Switzerland. [2]Hubrecht Institute, Netherlands Institute for Developmental Biology, Uppsalalaan 8, 3584CT Utrecht, Netherlands.

*To whom correspondence should be addressed. E-mail: clevers@niob.knaw.nl

dermis consists of multiple layers of cells and cell remnants that are harnessed by robust internal meshes of keratins, the intestinal epithelium consists of a single layer of fragile epithelial cells. These cells digest food and absorb the resulting mix of biological building blocks while keeping indigestible bulk and associated microflora inside the lumen. For this, the intestinal epithelium has distributed divergent biological tasks over only four differentiated cell types.

The basic tissue architecture of the mouse intestine is established during mid- to late gestation (*1*). At first, a pseudostratified intestinal epithelium of endodermal origin proliferates vigorously. In mice, conversion of this pseudostratified epithelium into a single-layered epithelium occurs around embryonic day 14.5 (E14.5) in a wave that progresses from stomach to colon. The epithelium of the small intestine forms protrusions, the prospective villi, and cell cycling becomes restricted to shallow pockets positioned between these villi. Simultaneously, the surrounding splanchnic mesoderm differentiates into smooth muscle and connective tissue. These processes are completed at E18.5. Around the third week of life, the proliferative pockets invade into the submucosa to form mature crypts of Lieberkühn (*2*).

The epithelium of the adult small intestine forms a contiguous two-dimensional sheet (Fig. 1). New cells are added in the crypts and removed by apoptosis upon reaching the villus tips a few days later (*3*). Stem cells and Paneth cells at the crypt bottom escape this flow (*4*). Although intestinal stem cells cannot currently be studied ex vivo and no unique in vivo markers are available, they can be labeled with ^{3}H-thymidine or bromodeoxyuridine during early postnatal life or after irradiation (*5*). Long-term label retention and the study of mouse chimeras (*6*, *7*) and postinjury regeneration have allowed an operational definition of stem cell characteristics. Stem cells of the small intestine occupy position +4, the fourth cell position counting from the crypt bottom [positions 1 to 3 being taken by the Paneth cells (Fig. 1)]. In the colon, Paneth cells are absent, and the stem cells reside directly at the crypt bottom (*8*). The epithelial stem cells self-renew throughout life, cycling infrequently to produce vigorously proliferating transit-amplifying cells that fill the remainder of the crypts. Transit-amplifying cells have a very limited self-renewal capacity; after three to four cell divisions, their offspring inevitably differentiates into one of the mature cell lineages. Whereas the shallow neonatal intervillus pockets are polyclonal, all cells in an adult crypt derive from one stem cell (*7*). Committed progenitors differentiate upon reaching the crypt-villus junction and migrate in colinear bands toward the tips of the villi. Thus, each villus receives inputs from several crypts and is essentially polyclonal (*7*, *9*). The surface epithelium of the colon lacks villi: Proliferative cells occupy the bottom two-thirds of colonic crypts, whereas differentiated cells constitute the top third and the surface epithelium. The crypt architecture of the small intestine is compared to that of the colon in Fig. 2.

A sheath of specialized fibroblasts is directly apposed to the epithelial crypt cells, separated only by the basal lamina (*10*). These so-called myo-epithelial fibroblasts form a syncytium that extends along the intestinal tract. It is believed that these cells are critical to the establishment of the crypt niche, which as discussed above harbors a few stem cells as well as a much larger number of transit-amplifying cells and Paneth cells. The crypt epithelium shapes the underlying myo-epithelial meshwork through secreted Hedgehog signals (*11*). Very little is known about putative reverse signals emanating from the myo-epithelial fibroblasts. Moreover, although a specialized stem cell niche is likely to exist within crypts, such a niche has not been identified yet by either morphological or molecular criteria.

Two main lineages of differentiated cell types are discerned within the intestinal epithelium: the enterocyte or absorbtive lineage and the secretory lineage. The latter lineage encompasses goblet cells, the enteroendocrine lineage, and Paneth cells (Fig. 1). Enterocytes are abundant in the small intestine, secreting hydrolases and absorbing nutrients. Goblet cells, secreting protective mucins, increase in numbers from duodenum to the colon. Enteroendocrine lineage cells can be further subdivided on the basis of the hormones they secrete, e.g., serotonine, substance P, or secretin (*12*, *13*), and these represent a small proportion (less than 1%) of all cells. Paneth cells occur only in the small intestine and reside at the crypt bottom. Paneth cells secrete antimicrobial agents such as cryptdins and defensins and lysozyme to control the microbial content of the intestine (*14*, *15*).

Colorectal Cancer (CRC)

About 50% of the Western population develops an adenomatous polyp by the age of 70. Some of these will progress to cancer, and the lifetime cancer risk is estimated to be 5% (*16*). From a molecular-genetic perspective, CRC is likely the best-understood solid malignancy, which relates to the accessibility of the tumors and the fact that different stages of the same malignancy can coexist within one patient. Histopathological and molecular analyses have led to the definition of the seminal adenoma-carcinoma sequence of tumor progression (*17*). The model integrates the notions that (i) colorectal tumors result from mutational activation of oncogenes combined with the inactivation of tumor-suppressor genes, (ii) multiple gene mutations

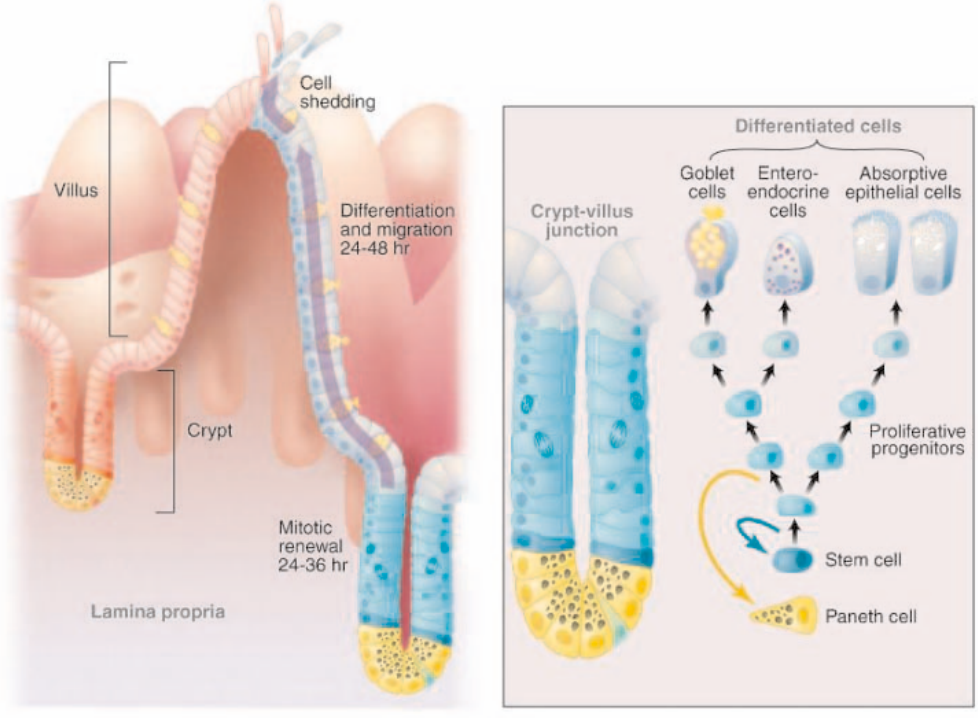

Fig. 1. The anatomy of the small intestinal epithelium. The epithelium is shaped into crypts and villi (**left**). The lineage scheme (**right**) depicts the stem cell, the transit-amplifying cells, and the two differentiated branches. The right branch constitutes the enterocyte lineage; the left is the secretory lineage. Relative positions along the crypt-villus axis correspond to the schematic graph of the crypt in the center.

are required to produce malignancies, and (iii) genetic alterations may occur in a preferred sequence, yet the accumulation of changes rather than their chronologic order determines histopathological and clinical characteristics of the colorectal tumor.

In the adenoma-carcinoma sequence, the earliest identifiable lesion is an aberrant crypt focus, a small dysplastic lesion in the colonic epithelium. Two different models propose the origin and growth of dysplastic aberrant crypt foci. Vogelstein and colleagues suggested a top-down morphogenesis model in which mutant cells at the surface epithelium of the colon spread laterally and downward to form new crypts (*18*). This view was challenged with an alternative model proposing that adenomas grow initially in a bottom-up pattern (*19*). Aberrant crypt foci expand over time to form macroscopically visible adenomatous polyps. The transition from benign (adenoma) to malignant growth (carcinoma) is believed to be progressive. Adenomas first advance to the carcinoma in situ stage. Overtly invasive carcinomas often represent the first clinical presentation of colorectal tumors. Little is known about the genetic alterations and precise mechanisms driving progression from early stage in situ carcinomas through the successive clinically defined stages of regional invasion and distant metastasis.

Our current molecular insights into CRC rely heavily on studies on hereditary forms of this disease. Five to 10% of CRC cases are inherited in an autosomal-dominant fashion (*20*). Hereditary cancer syndromes are often divided into two categories on the basis of absence or presence of polyposis, best exemplified by the two major forms of hereditary colorectal cancer: hereditary nonpolyposis CRC and familial adenomatous polyposis (FAP). The hallmark of tumors in hereditary nonpolyposis CRC is instability of microsatellites (repeats of short DNA sequences) (*21*, *22*). Indeed, hereditary nonpolyposis CRC can be caused by mutations in mismatch repair genes, such as *MSH2* and *MLH1* (*23*, *24*), collectively termed the caretakers of genome integrity (*25*). It is believed that these DNA repair defects lead to mutations in cancer-causing genes such as adenomatous polyposis coli (APC) (*26*), which in turn transform cells. For further reading on the subject of microsatellite instability, we refer the reader to the above references; the polyposis syndrome FAP is more extensively discussed below.

Wnt signaling maintains crypt progenitor compartments. A crypt and its associated villus can be viewed as the smallest self-renewing unit from which the epithelium is built. Position along the crypt-villus axis defines the various stages in the life of an epithelial cell (Fig. 1). Current evidence indicates that the Wnt cascade is the dominant force in controlling cell fate along the crypt-villus axis. Wnt genes encode secreted signaling proteins and are found in the genomes of all animals. Signaling is initiated when Wnt ligands engage a complex consisting of a serpentine receptor of the frizzled family and a member of the low-density lipid receptor family, Lrp5 or Lrp6 (*27*) (Fig. 3A). The key molecule in the cascade is a cytoplasmic protein termed β-catenin, whose stability is regulated by the so-called destruction complex. When Wnt receptors are not engaged, two scaffolding proteins in the destruction complex, the tumor suppressors adenomatous polyposis coli (APC) and axin, bind newly synthesized β-catenin. CKI and GSK3, two kinases residing in the destruction complex, then sequentially phosphorylate a set of conserved Ser and Thr residues in the N terminus of β-catenin. The resulting phosphorylated footprint recruits a β-TrCP–containing E3 ubiquitin ligase, which targets β-catenin for proteasomal degradation. When Wnts bind the receptor complex, the activity of the destruction complex is inhibited. As a consequence, β-catenin accumulates and binds to nuclear DNA binding proteins of the Tcf/Lef family (*27*). In the absence of a Wnt signal, Tcf/Lef proteins repress target genes through association with corepressors such as groucho. The interaction with β-catenin transiently converts Tcf/Lef factors into transcriptional activators, a process that also involves legless/Bcl9 and pygopus, two additional partner proteins of β-catenin. In sum, the canonical pathway translates a Wnt signal into transient transcription of a Tcf/Lef target gene program (*27*).

Wnt signaling is intimately linked with the biology of the intestinal epithelium. This first became clear when APC, originally identified as an intestinal tumor suppressor gene, was recognized as a key negative regulator of the cascade (see below). Later evidence implied a role for the Wnt cascade in controlling epithelial physiology. Nuclear β-catenin, the indicator of active Wnt signaling, was observed in crypts (*28*). In Tcf4$^{-/-}$ neonatal mice, the proliferative compartment was entirely absent, indicating that Wnt is required for maintenance of progenitors (*29*). Concordantly, inhibition of Wnt receptors by transgenic dickkopf-1 leads to loss of proliferative crypts in adult mice (*30*). Expression analysis of all mouse Wnt genes has revealed that at least four are expressed by the crypt cells proper, whereas no Wnt expression was detected in the directly

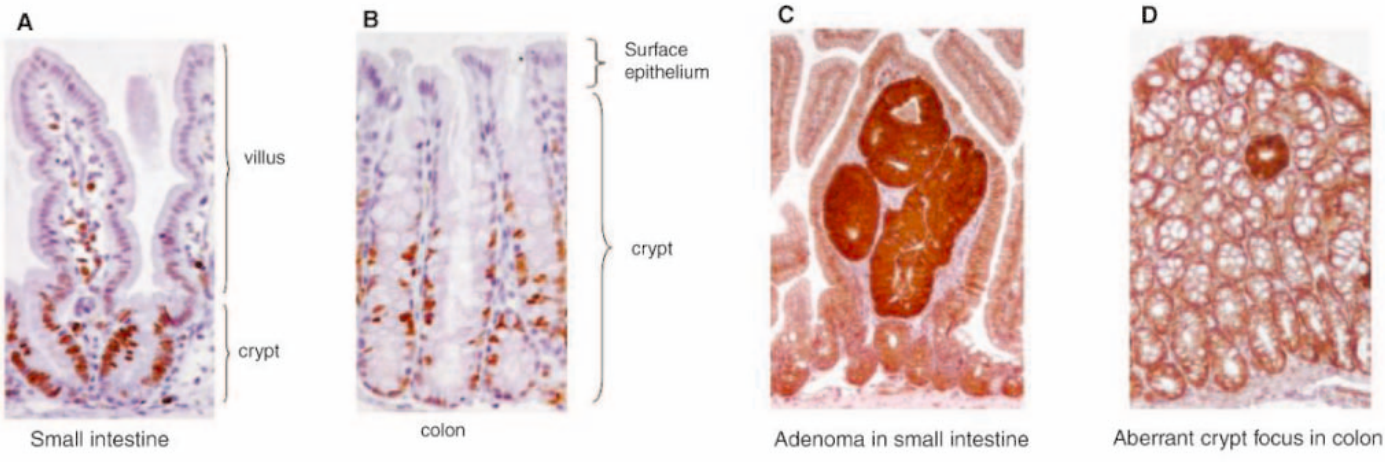

Fig. 2. Comparison of normal epithelium and adenomas in murine small intestine and colon. (**A**) Small intestinal crypt and villus. (**B**) Colonic crypt and surface epithelium. Proliferative cells are stained for the cell cycle marker Ki67 (brown nuclei) in (A) and (B). (**C**) An adenoma residing inside a villus of the small intestine of a *min* mouse. (**D**) A small aberrant crypt focus in the colon of a *min* mouse. (C) and (D) are stained for β-catenin. Note the presence of β-catenin (in brown) in the cell boundaries of all nondiseased epithelial cells and the accumulation of β-catenin throughout the cells in the adenoma and aberrant crypt focus.

apposed mesenchyme, implying the existence of an autocrine mechanism (*31*).

Wnt Signaling, FAP, and CRC

FAP patients carry in their colon numerous florid adenomatous polyps, which are defined as benign epithelial neoplasia (polyps) built from glandular elements (adenomatous) (*32*). Because of the polyp burden, FAP patients invariably develop colorectal cancer around the age of 40. FAP patients carry one mutant copy of the tumor suppressor gene *adenomatous polyposis coli* (*APC*) in their genome (*33*, *34*). *APC* is not only mutated in the hereditary FAP syndrome, but somatic *APC* mutations also occur in the vast majority of sporadic adenomas and adenocarcinomas (*35*–*37*). The earliest identifiable lesion in the adenoma-carcinoma sequence (*17*), the aberrant crypt focus, already bears detectable *APC* mutations (*38*), implying that loss of APC function represents the initiating event in sporadic CRC. Taking these observations together, *APC* appears to be the key gene, the gatekeeper, in the molecular pathogenesis of most sporadic and hereditary forms of CRC.

The *APC* mutations in intestinal polyps and adenocarcinomas typically truncate the protein, suggesting a critical tumor-suppressive role for the C-terminal domain. This domain binds to and causes the degradation of cytoplasmic β-catenin (*39*–*42*). Indeed, stable β-catenin accumulates to high concentrations in the cytoplasm and nucleus of epithelial cells transformed upon loss of APC function. The discovery of the partnership of β-catenin and Tcf proteins as the ultimate effectors of Wnt signaling (*43*, *44*) led to the realization that the increased amounts of β-catenin in *APC* mutant cancer cells inappropriately activate transcriptional activity of the intestinal Tcf family member TCF4 (*45*). The recognition of nuclear β-catenin/Tcf4 complexes as the key effectors in cancer initiation was confirmed by rare mutations in other WNT pathway components, i.e., in β-catenin (*46*, *47*) and in axin2/conductin (*48*). Ultimately, malignant transformation of intestinal epithelial cells is thus caused by the inappropriate, constitutive transcription of Tcf target genes.

On the basis of the determination of the Tcf4 target gene program in human CRC cell lines, we have proposed the following scenario (*49*). In crypts, Wnt signaling drives the formation of β-catenin/Tcf4 complexes, thus imposing a proliferative phenotype onto crypt epithelial cells. The strict compartmentalization along the crypt-villus axis itself is controlled at least in part by the Wnt source at the crypt bottom and translated through Wnt-controlled expression of the EphB sorting receptors (*28*). The absence of Wnt signaling in the villus compartment results in rapid cell cycle arrest and differentiation. Thus, Tcf4 constitutes the dominant switch between the proliferative progenitor and the differentiated epithelial cell. At all stages of CRC this switch is permanently on, because Tcf4 is constitutively activated by mutations in the Wnt cascade. This overrides the physiological signals leading to cell cycle arrest and induces the slow formation of long-lived adenomatous polyps.

Several *Apc*-mutant mouse models have been generated (*37*). *Min* (*multiple intestinal neoplasia*) mice carry a nonsense mutation at codon 850 of *Apc* (*50*). Heterozygous Apc^{min} mice develop as many as 100 intestinal tumors, which have typically inactivated the second *Apc* allele. Although most *Min* tumors develop in the small intestine rather than the colon, these mice are used extensively as animal models for FAP and CRC. Because homozygosity for *Apc* mutations invariably results in embryonic lethality (*37*), conditional *Apc* mutant mice have also been generated. In these mice, focal deletion of both alleles of *Apc* rapidly induced colorectal adenomas, proving that loss of APC is the only requirement for adenoma formation (*51*). When deletion of the *Apc* gene was induced throughout the adult intestine, all epithelial cells displayed a proliferative crypt progenitor phenotype within days (*52*). DNA array analysis revealed upregulation of a Tcf4-driven crypt progenitor program, resembling that of human CRC cell lines (*49*). The induced transgenic expression of an activated β-catenin gene has independently confirmed that persistent Wnt signaling is sufficient to induce adenomas (*53*). Taken together, mutational activation of the Wnt signaling pathway now appears strongly to represent the key initiating event of intestinal tumorigenesis in human and mouse.

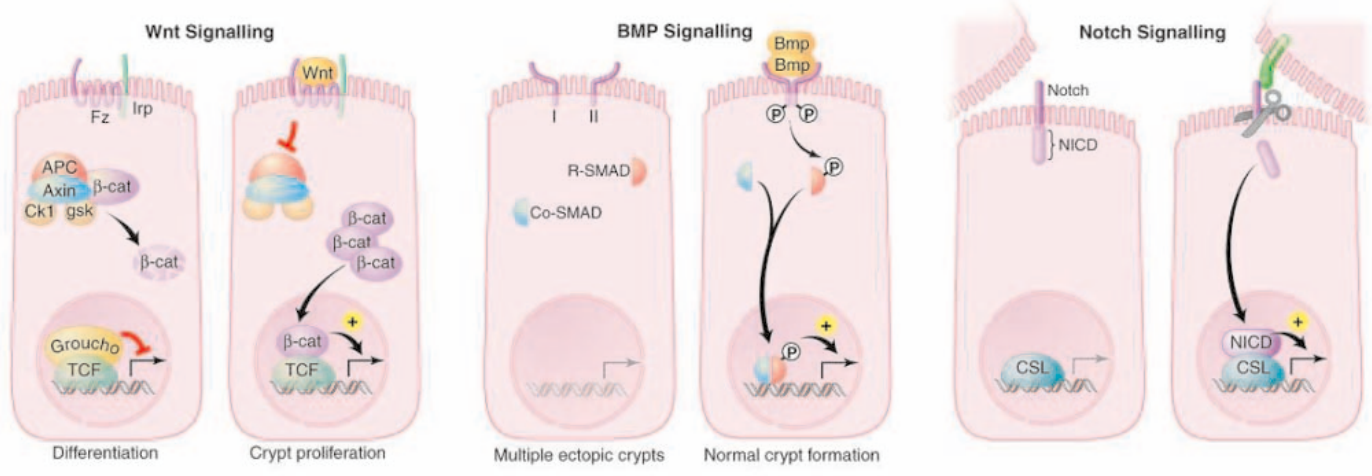

Fig. 3. Wnt, BMP, and Notch pathways control target gene transcription. **(Left)** Wnt-responsive cells carry a receptor complex consiting of a frizzled seven-transmembrane receptor (Fz) and Lrp5 or Lrp6. In the absence of secreted Wnt factor (left), the destruction complex (APC, axin, and the kinases CK1 and GSK3 β) induces degradation of cytoplasmic β-catenin. Tcf complexed to corepressors such as groucho represses specific Wnt target genes. Receptor engagement (right) blocks the destruction complex; β-catenin accumulates and binds to Tcf in the nucleus to activate transcription of Wnt target genes. **(Center)** Type I and type II BMP receptors are not complexed in the absence of signal. Secreted BMP factors bring the two receptors together, ultimately leading to the phosphorylation of R-SMADs, their association with co-SMAD, translocation to the nucleus, and subsequent activation of BMP target genes in the nucleus. **(Right)** When Notch receptor meets its cell-bound ligand (jagged or delta), sequential proteolytic steps lead to the release of its intracellular domain (NICD), which travels to the nucleus, where it complexes with the transcription factor CSL to activate Notch target gene transcription.

Bone Marrow Protein Signaling, Juvenile Polyposis Syndrome, and the Induction of Crypt Formation

Not all polyposis syndromes are manifested as adenomatous lesions. Hamartomatous polyposis syndromes are characterized by an overgrowth of tissues native to the organ area, which are usually of mesenchymal origin (*54*). The juvenile polyposis syndrome (JPS) is one

such autosomal hamartoma syndrome, and in this condition patients bear between 50 and 200 polyps, usually in the rectosigmoid region of the gut. Polyps display gross chronic inflammation and contain cystic spaces lined by a columnar epithelium and surrounded by abundant stroma (*55*). JPS patients have an increased risk of developing gastrointestinal polyps and colorectal cancer. Inactivating mutations in *Smad4* (*56*) and *bone morphogenic protein* (*BMP*) *receptor type 1A* (*57*, *58*) account for up to 50% of JPS cases, implying that loss of intestinal BMP signaling is the primary cause of JPS. This in turn suggests a role for the BMP pathway in epithelial homeostasis.

BMP Signaling and JPS

BMPs form a large subgroup of signaling cytokines within the TGF-β superfamily. Originally identified as molecules inducing cartilage and bone formation, they now rival the Wnts as general regulators of development (*59*). TGF-β superfamily ligands signal through a common mechanism by bringing together type I and type II serine–threonine kinase receptors. This results in the phosphorylation of the type I receptor by the type II receptor and activation of the intracellular SMAD transcriptional regulators (*59*). These fall into three classes: receptor-regulated SMADs (R-SMADs), common SMAD (co-SMADs), and inhibitory SMADs (I-SMADs). Upon receptor activation, R-SMADs become phosphorylated by type I receptors, resulting in association with the co-SMAD SMAD4 and in translocation of the complex to the nucleus (Fig. 3B). Once in the nucleus, the SMAD complex can interact with either co-activators or co-repressors of transcription to control target gene expression. BMP signaling is mediated through SMAD1, 5, and 8 (*59*).

BMPs are expressed in the stroma of villi, whereas phosphorylated SMAD1, 5, and 8, indicative of active BMP signaling, are observed in the nuclei of the differentiated villus epithelial cells. This implies that constitutive BMP signaling occurs from the villus mesenchyme to the epithelium (*60*). Most mutations in BMP pathway components are embryonic-lethal in mice, precluding a genetic assessment of a role for the BMP pathway in the gut (*2*). However, inhibition of BMP signaling in the villus through the transgenic expression of the secreted BMP inhibitor noggin resulted in a JPS-like phenotype, including the late development of adenomatous polyps (*60*). The stromal BMP signal apparently confines the postnatal formation of crypts to regions directly opposed to the intestinal wall. When BMP signaling is blocked, crypts appear de novo anywhere in the epithelium, leading to the characteristic JPS histology and ultimately to adenomas. A similar phenotype was observed in mice mutant for the *Bmpr1a* gene (*61*). Vogelstein has coined the term ''landscaper'' for the molecular defect in JPS (*25*), and although much remains to be learned about crypt initiation, it appears appropriate that the JPS-landscaper genes control spatial positioning of crypts in the intestinal epithelium.

Notch/bHLH Signaling

The Notch cascade represents a third developmental signaling pathway that plays a controlling role in intestinal homeostasis. *Notch* genes encode evolutionarily conserved single-transmembrane receptors, which regulate many cell fate decisions and differentiation processes. Mice and humans possess four Notch receptors, and these can be activated by transmembrane ligands of the delta and jagged families expressed on neighboring cells (*62*). This initiates a cascade of proteolytic cleavages of the receptor close to and within the transmembrane domain. Ultimately, the intramembrane γ-secretase protease liberates NICD (Notch intracellular domain), which translocates to the nucleus and engages the transcription factor CSL {CBF1/RBPjk in vertebrates, suppressor of hairless [Su(H)] in *Drosophila*, and Lag-1 in *C. elegans*}, thereby activating transcription (*62*). Some of the best-characterized Notch target genes encode members of the hairy-enhancer of split (Hes) family of transcriptional repressors, which are nuclear basic helix-loop-helix (bHLH) proteins. These HES family members regulate downstream genes, involved (at least in *Drosophila*) in the segregation of neuronal and epidermal lineages (*63*, *64*).

Notch/bHLH Signaling in the Intestinal Epithelium

Genetic evidence implies a role for several putative Notch target genes in the control of intestinal homeostasis. For example, *Hes1* mutant mice die perinatally because of severe neurological defects, whereas the intestines of $Hes1^{-/-}$ fetuses contain increased numbers of secretory cells at the expense of adsorptive enterocytes (*65*). The transcription factor gene *Math1* is repressed by Hes1 in multiple organs, including the intestine (*65*, *66*). The intestines of *Math1*-deficient mice show a relatively normal crypt-villus architecture that is populated entirely by enterocytes, indicating that Math1 is required for all secretory cell lineages (*66*). This phenotype is somewhat reciprocal to the phenotype observed in $Hes1^{-/-}$ mice. Taken together, these results suggest that Notch-mediated *Hes1* expression regulates a binary decision between adsorptive and secretory cell fates whereas other bHLH proteins may refine these fate decisions. For example, mice deficient in the bHLH factor neurogenin-3 specifically lack enteroendocrine precursors (*67*). BETA2/neuroD, a bHLH protein best known for its role in pancreatic differentiation, appears to further refine the enteroendocrine fate by controlling terminal differentiation of the enteroendocrine secretin- and cholecystokinin (CKK)-producing cells (*68*). Additional indirect support for the control of intestinal cell fate by Notch stems from the use of γ-secretase inhibitors developed for the treatment of Alzheimer's disease (*69*). The generation of NICD from Notch requires γ-secretase (*70*). Rodents treated with γ-secretase inhibitors display increases in goblet cell numbers in the gut (viewed as an undesirable side effect), most probably through the inhibition of Notch signaling (*69*, *71*).

Concluding Remarks

The crypt-villus unit represents one of the simplest self-renewing entities in mammalian biology. Although a molecular understanding is still in its infancy, several principles are taking shape: First, regulatory signaling pathways that have emerged from the study of embryonic development of model organisms play key roles in this adult mammalian structure. Second, the malignant transformation of the intestinal epithelial cells does not rely on mutational changes in generic oncogenes or tumor suppressors. Rather, the transformation process appears to specifically subvert the physiological regulators of the epithelium. Third, structure and function of the crypt-villus unit are intricately linked. The epithelium is therefore preferably studied in its histological context, allowing marker analysis while preserving the positional information of individual cells. By contrast, the best-understood self-renewing tissue, the bone marrow, is usually treated as an unordered suspension of cells studied by flow cytometry outside the natural context. Nevertheless, this reductionist approach has yielded spectacular results. Elaborate cell culture systems have been established to study the hemopoietic system, often at the level of single primary cells (*72*). Unfortunately, no such culture system exists yet for primary epithelial cells of the intestine.

The insights that are emerging from the studies discussed in this review are painting a growing picture of the factors that control intestinal cell behavior in physiology as well as in cancer. Apparently, the transformation process uses crucial physiological regulators of normal intestinal epithelium as a strategy to open the most efficient road to cancer. Malignancies that arise in other self-renewing tissues may exploit similar strategies. In-depth insights into the molecular physiology of the self-renewal process of gut epithelium should ultimately allow the design of sophisticated modes of therapeutic interference in the diseased intestine.

References

1. D. Y. R. Stanier, *Science* **307**, 1902 (2005).
2. E. Sancho, E. Batlle, H. Clevers, *Annu. Rev. Cell Dev. Biol.* **20**, 695 (2004).
3. J. P. Heath, *Cell Biol. Int.* **20**, 139 (1996).

4. C. S. Potten, *Philos. Trans. R. Soc. Lond. B Biol. Sci.* **353**, 821 (1998).
5. C. S. Potten, G. Owen, D. Booth, *J. Cell Sci.* **115**, 2381 (2002).
6. M. Bjerknes, H. Cheng, *Gastroenterology* **116**, 7 (1999).
7. G. H. Schmidt, D. J. Winton, B. A. Ponder, *Development* **103**, 785 (1988).
8. C. Booth, C. S. Potten, *J. Clin. Invest.* **105**, 1493 (2000).
9. K. A. Roth, M. L. Hermiston, J. I. Gordon, *Proc. Natl. Acad. Sci. U.S.A.* **88**, 9407 (1991).
10. D. W. Powell *et al.*, *Am. J. Physiol.* **277**, C183 (1999).
11. B. B. Madison *et al.*, *Development* **132**, 279 (2005).
12. G. S. Evans, C. S. Potten, *Virchows Arch. B Cell Pathol. Incl. Mol. Pathol.* **56**, 191 (1988).
13. M. Hocker, B. Wiedenmann, *Ann. N. Y. Acad. Sci.* **859**, 160 (1998).
14. E. M. Porter, C. L. Bevins, D. Ghosh, T. Ganz, *Cell. Mol. Life Sci.* **59**, 156 (2002).
15. T. Ayabe *et al.*, *Nat. Immunol.* **1**, 113 (2000).
16. A. Jemal, A. Thomas, T. Murray, M. Thun, *CA A Cancer J. Clin.* **52**, 23 (2002).
17. E. R. Fearon, B. Vogelstein, *Cell* **61**, 759 (1990).
18. I. M. Shih *et al.*, *Proc. Natl. Acad. Sci. U.S.A.* **98**, 2640 (2001).
19. S. L. Preston *et al.*, *Cancer Res.* **63**, 3819 (2003).
20. H. T. Lynch, A. de la Chapelle, *N. Engl. J. Med.* **348**, 919 (2003).
21. P. Peltomaki *et al.*, *Cancer Res.* **53**, 5853 (1993).
22. S. N. Thibodeau, G. Bren, D. Schaid, *Science* **260**, 816 (1993).
23. C. E. Bronner *et al.*, *Nature* **368**, 258 (1994).
24. F. S. Leach *et al.*, *Cell* **75**, 1215 (1993).
25. K. W. Kinzler, B. Vogelstein, *Science* **280**, 1036 (1998).
26. J. Huang *et al.*, *Proc. Natl. Acad. Sci. U.S.A.* **93**, 9049 (1996).
27. R. H. Giles, J. H. van Es, H. Clevers, *Biochim. Biophys. Acta* **1653**, 1 (2003).
28. E. Batlle *et al.*, *Cell* **111**, 251 (2002).
29. V. Korinek *et al.*, *Nat. Genet.* **19**, 379 (1998).
30. D. Pinto, A. Gregorieff, H. Begthel, H. Clevers, *Genes Dev.* **17**, 1709 (2003).
31. A Gregorieff, H. Clevers, unpublished data.
32. R. C. Haggitt, B. J. Reid, *Am. J. Surg. Pathol.* **10**, 871 (1986).
33. J. Groden *et al.*, *Cell* **66**, 589 (1991).
34. K. W. Kinzler *et al.*, *Science* **253**, 661 (1991).
35. H. Nagase, Y. Nakamura, *Hum. Mutat.* **2**, 425 (1993).
36. S. M. Powell *et al.*, *Nature* **359**, 235 (1992).
37. R. Fodde, R. Smits, H. Clevers, *Nat. Rev. Cancer* **1**, 55 (2001).
38. M. R. Nucci *et al.*, *Hum. Pathol.* **28**, 1396 (1997).
39. B. Rubinfeld *et al.*, *Science* **262**, 1731 (1993).
40. L.-K. Su, B. Vogelstein, K. W. Kinzler, *Science* **262**, 1734 (1993).
41. S. Munemitsu *et al.*, *Proc. Natl. Acad. Sci. U.S.A.* **92**, 3046 (1995).
42. B. Rubinfeld *et al.*, *Science* **272**, 1023 (1996).
43. M. Molenaar *et al.*, *Cell* **86**, 391 (1996).
44. J. Behrens *et al.*, *Nature* **382**, 638 (1996).
45. V. Korinek *et al.*, *Science* **275**, 1784 (1997).
46. P. J. Morin *et al.*, *Science* **275**, 1787 (1997).
47. B. Rubinfeld *et al.*, *Science* **275**, 1790 (1997).
48. W. Liu *et al.*, *Nat. Genet.* **26**, 146 (2000).
49. M. van de Wetering *et al.*, *Cell* **111**, 241 (2002).
50. L.-K. Su *et al.*, *Science* **256**, 668 (1992).
51. H. Shibata *et al.*, *Science* **278**, 120 (1997).
52. O. J. Sansom *et al.*, *Genes Dev.* **18**, 1385 (2004).
53. N. Harada *et al.*, *EMBO J.* **18**, 5931 (1999).
54. R. C. Haggitt, B. J. Reid, *Am. J. Surg. Pathol.* **10**, 871 (1986).
55. A. Rashid *et al.*, *Gastroenterology* **119**, 323 (2000).
56. J. R. Howe *et al.*, *Science* **280**, 1086 (1998).
57. J. R. Howe *et al.*, *Nat. Genet.* **28**, 184 (2001).
58. X. P. Zhou *et al.*, *Am. J. Hum. Genet.* **69**, 704 (2001).
59. Y. Shi, J. Massague, *Cell* **113**, 685 (2003).
60. A.-P. G. Haramis *et al.*, *Science* **303**, 1684 (2004).
61. X. C. He *et al.*, *Nat. Genet.* **36**, 1117 (2004).
62. S. Artavanis-Tsakonas, M. D. Rand, R. J. Lake, *Science* **284**, 770 (1999).
63. P. Heitzler *et al.*, *Development* **122**, 161 (1996).
64. N. Oellers, M. Dehio, E. Knust, *Mol. Gen. Genet.* **244**, 465 (1994).
65. J. Jensen *et al.*, *Nat. Genet.* **24**, 36 (2000).
66. Q. Yang, N. A. Bermingham, M. J. Finegold, H. Y. Zoghbi, *Science* **294**, 2155 (2001).
67. M. Jenny *et al.*, *EMBO J.* **21**, 6338 (2002).
68. F. J. Naya *et al.*, *Genes Dev.* **11**, 2323 (1997).
69. G. T. Wong *et al.*, *J. Biol. Chem.* **279**, 12876 (2004).
70. B. De Strooper *et al.*, *Nature* **398**, 518 (1999).
71. J. Milano *et al.*, *Toxicol. Sci.* **82**, 341 (2004).
72. M. Kondo *et al.*, *Annu. Rev. Immunol.* **21**, 759 (2003).

10.1126/science.1104815

REVIEW

The Gut and Energy Balance: Visceral Allies in the Obesity Wars

Michael K. Badman and Jeffrey S. Flier*

In addition to digesting and assimilating nutrients, the intestine and associated visceral organs play a key sensing and signaling role in the physiology of energy homeostasis. The gut, the pancreatic islets of Langerhans, elements in the portal vasculature, and even visceral adipose tissue communicate with the controllers of energy balance in the brain by means of neural and endocrine pathways. Signals reflecting energy stores, recent nutritional state, and other parameters are integrated in the central nervous system, particularly in the hypothalamus, to coordinate energy intake and expenditure. Our understanding of regulatory neural circuits and the signaling molecules that influence them has progressed rapidly, particularly after the discovery of the adipocyte hormone leptin. These discoveries have led to exploration of novel routes for obesity control, some of which involve gut-derived pathways.

In addition to the obvious role of the gut in the digestion and absorption of nutrients, the intestine and associated visceral organs, including the pancreas, liver, and visceral adipose depots, have important sensing and signaling roles in the regulation of energy homeostasis. To accomplish this role, the gut uses neural and endocrine pathways to communicate with controllers of energy balance in the hypothalamus and hindbrain. In this Review, we examine the role of the gut in energy balance and assess the possibility that insights into gut-derived signals will stimulate previously unexplored therapeutics for obesity and other disorders of energy balance.

Division of Endocrinology, Diabetes, and Metabolism, Beth Israel Deaconess Medical Center, Finard 202, 330 Brookline Avenue, Boston, MA 02215, USA.

*To whom correspondence should be addressed. E-mail: JFlier@bidmc.harvard.edu

Integration of Peripheral Signals of Energy Balance

There is no doubt that food intake in humans is influenced by emotional factors, social cues, and learned behavior. These influences overlay highly conserved systems within the brain that sense and integrate signals reflecting overall energy stores, recent energy intake, and presence of specific classes of nutrients (Fig. 1). The hypothalamus, especially the arcuate nucleus, is relatively accessible to circulating factors and also receives inputs from other areas of the brain. Here, signals are received that relate to total energy stores in fat and to immediate changes in energy availability, including nutrients within the gut. These two categories of signals are not exclusive, because signals relating to long-term energy stores, including insulin and leptin, can modulate responses to short-term nutritional inputs. The hypothalamus integrates these peripheral and central signals and exerts homeostatic control over food intake, levels of physical activity, basal energy expenditure, and endocrine systems, including those that determine reproductive competence (Fig. 2).

Short-term eating behavior is also controlled by the hindbrain. The nucleus of the tractus solitarius (NTS) receives input from vagus nerve afferents, whereas the area postrema is a target for circulating factors such as amylin and glucagon-like peptide 1 (GLP-1) (*1*). Classical studies show that when higher inputs are surgically interrupted, the hindbrain can regulate food intake in response to peripheral signals (*2*).

Signals of Long-Term Energy Balance

Insulin, produced by pancreatic β cells, is vital for regulating the storage of absorbed nutrients and also acts as an adiposity signal to the

brain for the regulation of energy balance (*3*). Mechanisms exist for transporting insulin across the blood-brain barrier and insulin receptors are expressed in appetite-controlling areas of the brain. Administration of insulin to the brain not only reduces appetite in rodents and subhuman primates but also potentiates satiety factors such as cholecystokinin (CCK). Clinically, insulin deficiency is associated with hyperphagia in uncontrolled type 1 diabetes, and intrahypothalamic administration of antibodies to insulin or neuronal disruption of insulin receptors modestly increases food intake and body weight in rodents (*4*).

Leptin is an adipocyte-derived factor, or adipokine, that is the dominant long-term signal informing the brain of adipose energy reserves (*5*). Similar to insulin, leptin is transported across the blood-brain barrier, where it binds to specific receptors on appetite-modulating neurons, most notably but not exclusively in the arcuate nucleus (*6*). The long form of the leptin receptor activates Janus kinase–signal transducer and activator of transcription (JAK-STAT) signaling among several other signal transduction pathways.

Leptin-deficient *ob*/*ob* mice and both *db*/*db* mice and Zucker *fa*/*fa* rats that lack functional leptin receptors are hyperphagic and obese. Apart from promoting hunger, leptin deficiency reduces energy expenditure and fecundity (*7*). Exogenous leptin reverses obesity caused by its absence in mice and humans (*8*, *9*); however, absolute leptin deficiency is an uncommon cause of human obesity. Instead, leptin resistance results from defects in transport across the blood-brain barrier or impaired intracellular signaling. Suppressor of cytokine signaling 3 (SOCS3) is an intracellular protein that acts to limit leptin signaling and is an important mediator of leptin resistance. Although lack of SOCS3 is embryonically lethal, mice with haploinsufficiency of SOCS3 have enhanced leptin sensitivity and are protected against diet-induced obesity and its metabolic consequences (*10*). Because SOCS3 also limits insulin signaling, its expression provides a potentially important point of interaction between insulin and leptin pathways that may be important in the pathogenesis of the metabolic syndrome (*11*). Protein tyrosine phosphatase-1b is another factor implicated through both gain- and loss-of-function experiments as a key regulator of insulin and leptin signaling (*12*).

Leptin is also produced in the stomach, where it may have local paracrine functions. Its synthesis in the stomach is regulated by nutritional state and other gut hormones (*13*), but no physiological role of gut-derived leptin in appetite regulation has been established.

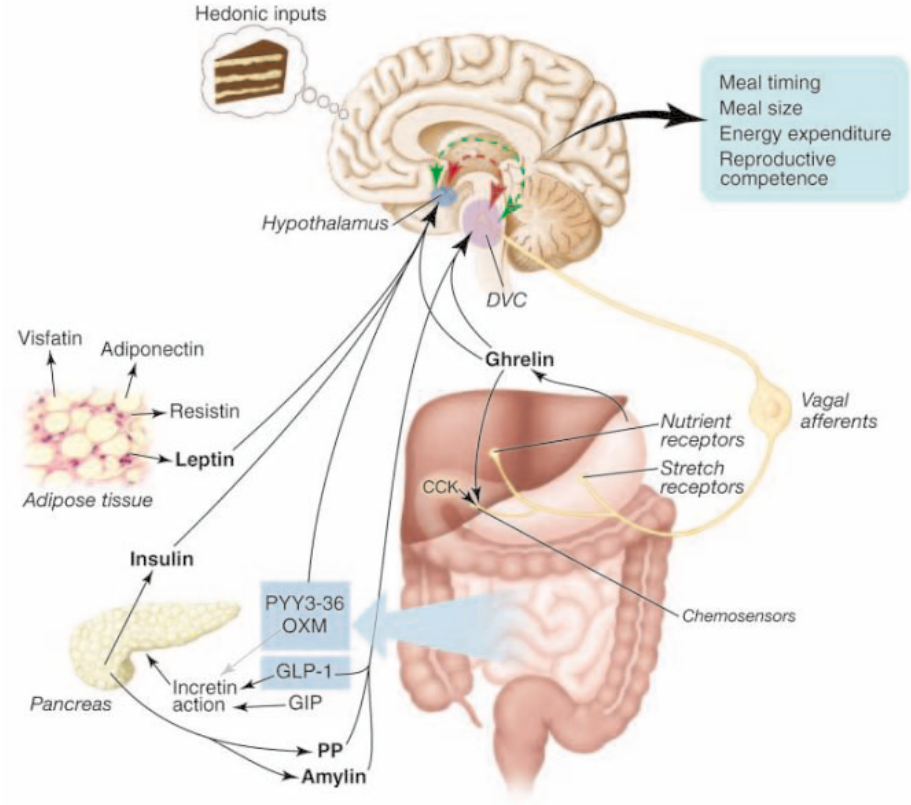

Fig. 1. The brain integrates long-term energy balance. Peripheral signals relating to long-term energy stores are produced by adipose tissue (leptin) and the pancreas (insulin). Feedback relating to recent nutritional state takes the form of absorbed nutrients, neuronal signals, and gut peptides. Neuronal pathways, primarily by way of the vagus nerve, relate information about stomach distention and chemical and hormonal milieu in the upper small bowel to the NTS within the dorsal vagal complex (DVC). Hormones released by the gut have incretin-, hunger-, and satiety-stimulating actions. The incretin hormones GLP-1, GIP, and potentially OXM improve the response of the endocrine pancreas to absorbed nutrients. GLP-1 and OXM also reduce food intake. Ghrelin is released by the stomach and stimulates appetite. Gut hormones stimulating satiety include CCK released from the gut to feedback by way of vagus nerves. OXM and PYY are released from the lower gastrointestinal tract and PP is released from the islets of Langerhans.

The Enteric Nervous System and Energy Balance

The enteric nervous system is implicated in every aspect of gut function. Mastication and defecation are under higher control, but the nervous system also exerts influence on gastric and pancreatic exocrine secretion, motility, blood supply, and secretion of gut hormones. Local signaling occurs within and between submucosal and myenteric plexuses, whereas afferent signals from the gut to the brain are carried in vagal and splanchnic nerve pathways. Vagal afferents respond to specific luminal chemical stimuli, physiological levels of distention or nutrients in the portal circulation, whereas splanchnic afferents convey information regarding noxious stimuli.

Vagal afferents originate from numerous areas within the abdominal viscera (Fig. 1) and different stimuli may be associated with different patterns of nerve firing. Responses to physical and chemical stimuli may be modulated by CCK, suggesting a degree of peripheral signal integration (*14*). In the brain, *c-fos*–like immunoreactivity (CFLI), a marker of neuronal activation, increases in the area postrema and the NTS after feeding but not sham feeding. Specific patterns of CFLI in the NTS can be induced by balloon mimicry of gastric distention (*15*) or duodenal infusions of nutrients. The importance of vagal afferents for meal termination is demonstrated by surgical or chemical interruptions that prevent suppression of meal size by gastric load, suppression of sham feeding by infusion of nutrients into the gut lumen, and satiety effects of exogenous CCK during real and sham feeding.

Humoral Messengers of Gut Function

The gut is a source of numerous peptides, many of which can alter appetite. These peptides have numerous targets, including gastrointestinal exocrine glands, smooth muscle, afferent nerve terminals, and the brain. Single enteroendocrine cells appear set adrift in the gut, in contrast to the archipelago of islets within the pancreas. Yet this belies the true integration of these cells into both humoral and neural systems. These highly specialized cells within the stomach, proximal small intestine, distal ileum, and colon are polar-

ized with their apical poles at the gut lumen "tasting" the nutritional milieu within the gut.

Secretion of gut hormones is regulated by receptors that sense specific chemical signals. The previously orphan G protein–coupled receptor (GPCR) GPR 120 is stimulated by free fatty acids (FFA) in vitro and is expressed abundantly in GLP-1–containing cells of the distal gastrointestinal tract, which release their contents in response to luminal FFA (*16*). Sensing of circulating FFA by β cells may occur by a similar mechanism involving the family of GPR 40 to GPR 43 to directly stimulate insulin release, complementing the incretin effect of GLP-1. GPCRs of the T2 receptor family, which sense bitter taste on the tongue, are also expressed in the stomach and duodenum and have been postulated to play a role in sensing luminal contents (*17*). There is also evidence that the extracellular calcium-sensing receptor is located within the gut, where it acts as a sensor for aromatic amino acids in foodstuffs (*18*). The fatty acid oleylethanolamide (OEA) is a ligand for peroxisome proliferator-activated receptor α (PPARα), which specifically reduces food intake by means of a vagal mechanism (*19*).

Metabolic signals also play a role in stimulus-secretion coupling of enteroendocrine cells. For example, glucose stimulates secretion of GLP-1 in vitro by a mechanism involving adenosine 5′-triphosphate (ATP)–sensitive potassium channels, closure of which depolarizes the cell in a mechanism analogous to the β cell (*20*). It also appears that carbohydrate-sensing mechanisms exist that act independently of intracellular glucose metabolism (*21*).

Multiple peptides may be produced and packaged in secretory granules within single cell types, whereas single peptides may have numerous effects (Fig. 1). Differential processing by prohormone convertases and other posttranslational modifications, such as acylation or sulfation, further increase the repertoire of possible signaling molecules. Likewise, multiple receptor types direct distinct physiological effects that depend on the availability of the cognate receptor in a particular cell type. In addition, many gut peptides are expressed in the brain, where they function distinctly as neuromodulators. There is a complex interplay between hypothalamic and brainstem systems; hypothalamic areas such as the paraventricular nucleus have reciprocal projections with the NTS. Hence, the anorectic effects of central leptin and peripheral CCK potentiate each other. This apparent redundancy of enteroendocrine function safeguards energy intake and allows integrated responses to signals from a variety of nutrient sources.

Satiety Peptides from the Gut

CCK is the prototypical satiety hormone, produced by mucosal enteroendocrine cells of the duodenum and jejunum and secreted in response to the presence of food within the gut lumen. Multiple biologically active forms of CCK coordinate postprandial gall bladder contraction and pancreatic secretion with gastric emptying and gut motility. Reduction in meal size is mediated by CCK_1 receptors, which preferentially bind sulfated CCK on vagal afferent neurons; hence, vagotomy reduces the effect of CCK on satiety (*22*). Gastric emptying is also inhibited by CCK_1 receptors on the pyloric sphincter, which may contribute to satiety. Infusion of CCK in human subjects suppresses food intake and causes earlier meal termination (*23*), and by contrast, infusion of a CCK_1 antagonist increases caloric intake (*24*).

Preproglucagon gene product yields two important satiety peptides, GLP-1 and oxyntomodulin (OXM). Both are released from L cells in response to nutrients in the form of FFA or carbohydrate. GLP-1(7–36) amide inhibits gastric acid secretion and emptying and stimulates the endocrine pancreas with postprandial insulin release, inhibition of glucagon secretion, and, in some species, β-cell neogenesis (*25*, *26*). Circulating GLP-1 is rapidly inactivated by the enzyme dipeptidyl peptidase IV (DPP-IV), leading to a circulating half-life of only 2 min (*27*). Long-acting DPP-IV–resistant GLP-1 agonists reduce food intake and induce weight loss when given peripherally to rats (*28*). GLP-1 receptors are present in the brain, and in rats, the blockade of endogenous GLP-1 by intracerebroventricular infusion of the specific GLP-1 antagonist exendin(9–39) increases food intake and causes obesity (*29*), although knockout of the GLP-1 receptor does not in mice (*30*). The effect of GLP-1 on human weight is inconsistent, but a meta-analysis of studies reveals that GLP-1 treatment brings about a small reduction in food intake (*31*).

OXM potently inhibits food intake when administered to rodents (*32*) and suppresses appetite in humans (*33*) by means of GLP-1–like receptors. Surprisingly, the areas of the brain stimulated by OXM and GLP-1 differ:

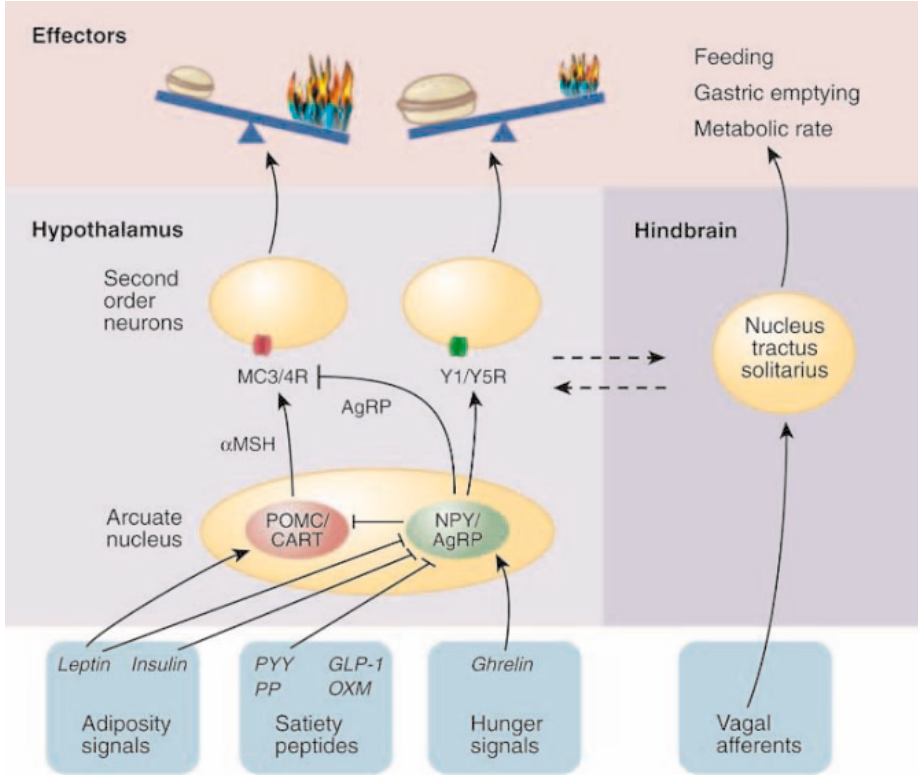

Fig. 2. Simplified representation of potential action of gut peptides on the hypothalamus. Access circulating agents into the arcuate nucleus of the hypothalamus is facilitated by a relaxed blood-brain barrier. Primary neurons in the arcuate nucleus contain multiple peptide neuromodulators. Appetite-inhibiting neurons (red) contain pro-opiomelanocortin (POMC) peptides such as α melanocyte-stimulating hormone (αMSH), which acts on melanocortin receptors (MC3 and MC4) and cocaine- and amphetamine-stimulated transcript peptide (CART), whose receptor is unknown. Appetite-stimulating neurons in the arcuate nucleus (green) contain neuropeptide Y (NPY), which acts on Y receptors (Y1 and Y5), and agouti-related peptide (AgRP), which is an antagonist of MC3/4 receptor activity. Integration of peripheral signals within the brain involves interplay between the hypothalamus and hindbrain structures including the NTS, which receives vagal afferent inputs. Inputs from the cortex, amygdala, and brainstem nuclei are integrated as well, with resultant effects on meal size and frequency, gut handling of ingested food, and energy expenditure. ⟶, direct stimulatory; ⟞, direct inhibitory; ⇢, indirect pathways.

GLP-1 activates cells in the brainstem (*34*) and other central autonomic control sites (*35*), whereas OXM-mediated increase in CFLI is limited to the arcuate nucleus (*36*). Moreover, injection of exendin(9–39) into the arcuate nucleus inhibits the effect of peripherally administered OXM but not GLP-1 (*36*), and studies examining mice deficient in the GLP-1 receptor suggest that these two peptides differentially regulate food intake and energy expenditure (*37*). Preproglucagon also yields GLP-2 and glucagon. Although a role of GLP-2 in appetite regulation has yet to be established, administration into the brain reduces feeding in rats, possibly by means of GLP-1 receptors. GLP-2 has not been discovered to have any effect on appetite or food intake in humans (*38*).

Glucose-dependent insulinotropic polypeptide (GIP) is an important incretin hormone. Similar to GLP-1, GIP is rapidly inactivated by DPP-IV. Whereas the insulinotropic effect of GIP is diminished with diabetes, GLP-1 continues to stimulate insulin secretion even in advanced stages of the disease. Release of GIP from the duodenal K cells is stimulated primarily by ingested fat such that mice fed a high-fat diet have elevated GIP levels. Notably, food intake is not affected by centrally administered GIP (*39*) and knockout of the receptor protects against obesity in diet-induced and *ob*/*ob* mice in the absence of changes in food intake by increasing energy expenditure (*40*). This peptide has multiple effects on adipocytes, including enhancement of insulin-stimulated glucose transport and stimulation of fatty acid synthesis and incorporation into triglycerides. Further work is needed to clarify the mechanism by which GIP promotes efficient storage of ingested energy as fat. Inhibition of this system may provide a useful anti-obesity therapeutic strategy.

The PP-fold peptide family includes neuropeptide Y (NPY), peptide YY (PYY), and pancreatic polypeptide (PP). All are produced as 36–amino acid, tyrosine-containing peptides and are recognized by a family of receptors. NPY, produced in the arcuate nucleus, is the most potent short-term stimulus for appetite. PYY is produced in enteroendocrine cells in the ileum and colon and is secreted after a meal, acting as an ''ileal brake'' to delay gastric emptying. In the brain, PYY(3–36) preferentially binds to presynaptic Y2 receptors within the hypothalamus to inhibit NPY neurons, release inhibition of proopiomelanocortin neurons, and depress feeding. The anorectic effect of PYY in rodents is controversial, but recent findings in nonhuman primates suggest that intramuscular administration of PYY(3–36) is associated with modestly reduced food intake (*41*). In humans, intravenous infusion of physiological levels of PYY(3–36) does reduce caloric intake in normal weight (*42*) and obese subjects (*43*). Malabsorptive states and diarrhea substantially increase circulating PYY.

Pancreatic polypeptide is released from specific pancreatic islet cells, primarily under nutrient control (*44*), to act on Y4 and Y5 receptors in the brain and peripherally to alter exocrine pancreatic and biliary function, gastric acid secretion, and gut motility. Chronic peripheral administration of PP reduces food intake in lean and obese mice (*45*), but central administration increases food intake. This disparity, also seen with PYY, may be caused by differential stimulation of Y4 receptors in the area postrema (which reduce food intake) and Y5 receptors expressed elsewhere in the brain (which increase food intake). In humans, PP reduces appetite and food intake without affecting gastric emptying (*46*).

It is clear that the field has a robust capacity to identify gut-derived factors that acutely suppress food intake in one or more experimental paradigms. Although interest in this area continues to grow, the true challenge will be to integrate the action of these multiple gut hormones. Both genetic and pharmacological approaches will be necessary to elucidate the relative importance of these numerous satiety factors to physiology, pathology, and potential therapeutics.

A Gut Peptide That Stimulates Hunger

Ghrelin is a 28–amino acid acylated hormone with appetite-stimulating and growth hormone–releasing activities mediated by the growth hormone secretagogue receptor (*47*). Cells that synthesize ghrelin are located throughout the gastrointestinal tract, at highest density in the fundus of the stomach. Plasma levels of ghrelin rise during fasting and immediately before meals and fall within an hour of food intake, suggesting a role in meal initiation (*48*).

In the arcuate nucleus of the hypothalamus, ghrelin activates neurons expressing NPY (*49*). Stimulation of gastric vagal afferents (*50*) and direct ghrelin action on the dorsal vagal complex (*51*) also appear to mediate ghrelin signaling. However, the role of ghrelin in obesity is open to question, as ghrelin levels tend to be low in obese humans, only increasing after dietary weight loss (*52*), and initial reports suggest that deletion of ghrelin (*53*) or its receptor (*54*) does not impair food intake or substantially alter body weight. Given that intravenous administration of ghrelin increases appetite and food intake in volunteers of normal weight and increases food intake of patients with cancer-related anorexia by over 30% (*55*), ghrelin or the activation of its receptor may find a use in the treatment of anorexia.

Loss of appetite and cachexia may occur in many gastrointestinal disorders, including hepatopancreaticobiliary disorders, celiac disease, gastrointestinal infections and infestations, radiation enteritis, and intestinal resection. Changes in the endocrine milieu have been reported in malabsorptive states (*56*). The future availability of peptide and small molecule antagonists of gut-peptide receptors will permit testing the hypothesis that such appetite loss may be due to altered secretion of gut-derived satiety factors.

Other Peptides of Visceral Origin Potentially Linked to Energy Balance

Amylin (islet amyloid polypeptide) is a 37–amino acid peptide cosecreted with insulin by pancreatic β cells (*57*). In animal studies, synthetic amylin analogs delay gastric emptying and decrease food intake (*58*), an effect mediated by the area postrema in rats. Studies in humans involving an amylin analog, pramlintide, have produced weight loss in diabetic populations (*59*). The bombesin homologs, gastrin-releasing peptide and neuromedin B, reduce meal size in several species, including humans (*60*).

Enterostatin is a pentapeptide cleaved from procolipase released by the exocrine pancreas. Peripheral and central administration reduce food intake in rats and alter food preference away from fatty foodstuffs, but in humans, recent metabolic studies have failed to show an effect of oral enterostatin on food intake, appetite, energy expenditure, or body weight (*61*).

A Special Role for Visceral Fat in Obesity and Energy Balance?

Deposition of fat within the abdomen, so-called visceral adiposity, confers greater risk of metabolic and cardiovascular complications than does adipose accumulation elsewhere. The mechanistic basis for this association has stimulated much interest. Whereas adipose tissue was viewed as a means of storage and release of energy in response to shifts between fed and starved states, the adipocyte is now recognized as a bona fide endocrine cell. Adipocyte hormones influence appetite, glucose homeostasis, vascular function, and even reproductive competence, among other functions (*62*). It is likely that adiposity within the abdomen is metabolically harmful both because of its unique anatomical relation to the hepatic portal circulation and because of the specific endocrine features of this adipose depot. Adiponectin is an adipokine with insulin-sensitizing and anti-inflammatory actions that is suppressed in obesity in parallel to reduced insulin sensitivity (*63*). By contrast, resistin, a 108–amino acid peptide hormone that is expressed in adipocytes in rodents and in macrophages in humans is induced in obesity and leads to insulin resistance (*64*). The induction of resistin by cytokines may be a link between obesity and inflammatory states resulting in insulin resistance (*65*). Visfatin is a newly discovered adipokine expressed at high levels in visceral fat that has the notable property of activating the insulin receptor by bind-

ing at a site distinct from that recognizing insulin. Visfatin stimulates glucose uptake by adipocyte and muscle cells in vitro and decreases blood glucose levels in mice (*66*). It is a paradox that an insulinomimetic factor is produced by visceral fat in a state of insulin resistance. Further studies will be required to elucidate a physiologic role for visfatin and whether resistance to its action is seen in insulin-resistant states.

Obese Zucker rats overexpress the glucocorticoid reactivating enzyme 11β-hydroxysteroid dehydrogenase 1 (11β-HSD1) in adipose depots, presenting the possibility of "Cushing's disease of the omentum" resulting from local overproduction of cortisol in humans. Mice overexpressing 11β-HSD1 in fat are hyperphagic, have visceral obesity, and develop insulin-resistant diabetes and hypertension (*67*). Conversely, mice with global deletion of 11β-HSD1 are protected from diet-induced obesity and related hyperglycemia. In humans, increased 11β-HSD1 expression and activity has been reported in adipose tissue in some but not all studies.

Potential Gut Mechanisms in Obesity Therapeutics

The expanding understanding of gut endocrinology has produced a number of potentially fruitful avenues for the development of obesity therapies. The traditional approaches of caloric restriction, exercise, and behavioral therapies can each produce substantial weight loss, but in the majority of people this is not sustained. Two pharmacological agents are currently licensed for weight loss. Orlistat interferes with fatty acid hydrolysis and uptake by the gut through inhibition of pancreatic lipases. Sibutramine, a centrally acting norepinephrine and serotonin reuptake inhibitor, reduces appetite and may increase energy expenditure. Both produce only modest weight loss and may have unwelcome side effects.

Regulation of energy balance presents numerous potential targets for intervention in both the periphery and the central nervous system. Leptin replacement is effective in the rare cases of human leptin deficiency (*9*), but leptin resistance limits its utility in ordinary obesity. Increasing leptin action by promoting its transport into the brain or by antagonizing inhibitors of leptin signaling pathways might be effective, but the relevant pharmaceutical targets have proven challenging. Axokine, a reengineered recombinant human ciliary neurotrophic factor, acts through leptin-like pathways in the hypothalamus. Although effective in animal models, human obesity trials were limited by neutralizing antibodies (*68*).

Rimonabant is a compound that acts both centrally and peripherally to antagonize the cannabinoid-1 (CB1) receptors that play a role in energy balance. Recently reported phase III clinical trails show that 2-year treatment with rimonabant reduced weight, reduced abdominal fat, and improved cardiovascular risk factors (*69*). The first in a new class of pharmaceutical agents, rimonabant is promising as an antiobesity therapy, but its clinical value compared with that of existing therapies must await results of future investigations. Antagonists of the receptor for melanin-concentrating hormone and agonists for the melanocortin 4 receptor might be efficacious and are being pursued.

The favorable action of GLP-1 on both insulin secretion and energy balance makes it an attractive candidate for drug development. Exendin-4 is a 39–amino acid peptide originally isolated from the saliva of the Gila Monster that resists degradation by DPP-IV while retaining GLP-1–like effects on glucose metabolism and food intake (*70*). Activity of GLP-1 is prolonged by conjugation to albumin (liraglutide) or inhibition of DPP-IV. An amylin analog (pramlintide) causes weight loss in diabetic cohorts, but its efficacy in the general population is uncertain. A number of formulations of PYY(3–36) are currently under development as obesity therapeutics, although effective small-molecule mimics are lacking. Stimulation of endogenous GLP-1 and PYY(3–36) secretion by specific L cell secretagogues is a promising avenue that remains to be exploited. Ghrelin may ameliorate anorexia (*55*), but the efficacy of ghrelin antagonists for treatment of obesity remains unproven. Whether energy balance will be improved in humans by inhibition of 11β-HSD1 or alternatively activation of PPARα, as suggested by studies of OEA action, will await the results of clinical trials.

Obesity Surgery

It has been estimated that 15,000,000 adults in the United States meet current guidelines for surgical intervention to treat obesity (*71*). Once a last resort, surgery is increasing rap-

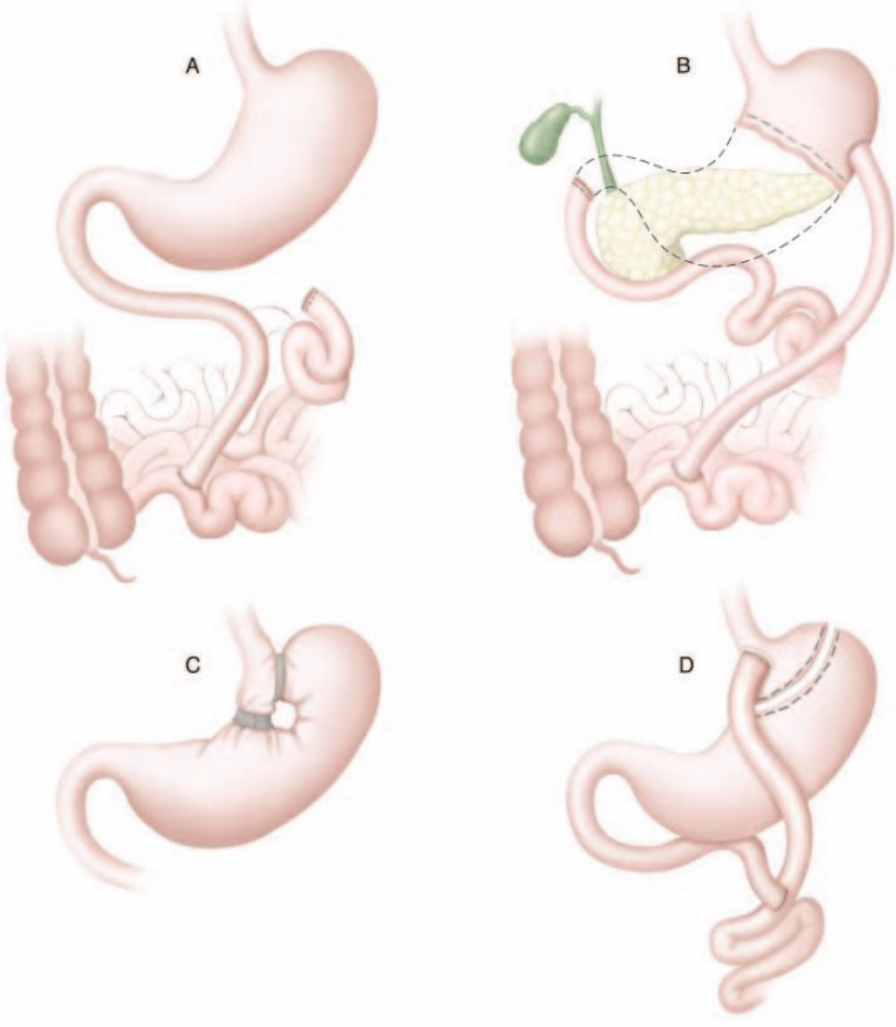

Fig. 3. Surgical procedures have developed from interventions causing gross malabsorption, such as jejunoileal bypass (**A**), and restriction and malabsorption, including biliopancreatic diversion (**B**). Currently, popular procedures include restriction of gastric volume with vertical banded gastroplasty (**C**) and the RYGB (**D**). The latter is free of malabsorption after an initial phase of adjustment and subsequently produces an advantageous gut hormonal milieu.

idly as a means of weight control, from approximately 15,000 annual procedures in the early 1990s to over 100,000 operations in the United States in 2003 (*72*). Bariatric surgery can achieve substantial and long-term weight loss and can improve or in some cases cure diabetes, hyperlipidemia, hypertension, and obstructive sleep apnea. Jejunoileal bypass was the original widely accepted bariatric procedure (Fig. 3) but can cause malabsorption, hepatic failure, and nephrolithiasis. Biliopancreatic diversion and duodenal switch restrict gastric volume and avoid bacterial overgrowth in the bypassed small bowel, but Roux-en-Y gastric bypass (RYGB) is the most commonly performed procedure in the United States. Its success stems from limiting the size of the gastric pouch, a small amount of malabsorption, and effects on hormonal signals from the gut, which may be critical to the efficacy of this procedure. Diabetes is rapidly ameliorated after RYGB and glycemic improvements often precede weight loss, supporting the view that changes in the gut hormonal milieu may be involved. An effect of surgery to increase PYY and GLP-1 levels has been reported (*73*). A postoperative fall or a failure of ghrelin levels to rise after surgery, as it does after weight loss due to food restriction, has been observed (*52*, *73*), but proof that ghrelin suppression accounts for reduced appetite after RYGB awaits experiments in which ghrelin is replaced in such patients. A second procedure gaining wide application is adjustable gastric banding. While this surgery is less complex, the results are somewhat less impressive than RYGB, and the effect of this procedure on gut endocrine factors is less explored. Removal of omental fat during gastric surgery for obesity may improve glucose homeostasis (*74*), and future studies of this approach are warranted.

In gastric pacing, electrical stimulation of the antrum of the stomach causes reverse peristalsis and delayed gastric emptying. A U.S. trial of this procedure revealed that up to 40% of excess weight could be lost 2 years after treatment without complications (*75*). Similarly, direct pyloric stimulation reduces gastric emptying and food intake in an animal model (*76*). However, it is not yet known how these interventions work. A limited study showed that gastric pacing was associated with a decrease in CCK, somatostatin, and GLP-1 levels (*77*) and a mechanistic role for stimulation of vagal afferents has also been propounded. There is some support for this idea in that direct vagal stimulation is known to lead to weight loss in animal models (*78*).

Conclusion and Perspective

A new understanding of the role of the gut in obesity and energy balance has recently developed. The list of peptide hormones emanating from the gastrointestinal system and influencing energy balance continues to grow, and it seems likely that additional gut hormones will be identified. Although loss-of-function studies indicate a high degree of redundancy, this does not preclude the potential efficacy of obesity-regulating drugs acting on these targets. Indeed, the likely introduction of GLP-1 agonists as diabetes treatments with weight loss potential heralds a new era of anti-obesity therapy. Moreover, the apparent importance of alterations in the gut hormonal milieu caused by surgical intervention on the gastrointestinal tract could lead to new approaches to surgery or devices. Of course, many unanswered questions remain. Among these are the possible roles of gut pathways in the genetic etiology of obesity and diabetes, a better understanding of the receptors and signals that sense specific nutrients in the gut, and a better understanding of the hierarchy and interactions between different gut signals and between gut signals and those related to long-term energy stores, such as leptin.

Perhaps it is fortuitous that the obesity epidemic has been paralleled by a rapid advance in understanding of mechanisms that control energy balance. Interventions that modulate gut-related satiety signals either pharmacologically, surgically, or electrically may offer a new armamentarium in our efforts to curb this threat to human health.

References and Notes

1. H. Yamamoto *et al.*, *J. Neurosci.* **23**, 2939 (2003).
2. H. J. Grill, G. P. Smith, *Am. J. Physiol.* **254**, R853 (1988).
3. S. C. Benoit, D. J. Clegg, R. J. Seeley, S. C. Woods, *Recent Prog. Horm. Res.* **59**, 267 (2004).
4. J. C. Bruning *et al.*, *Science* **289**, 2122 (2000).
5. J. S. Flier, *Cell* **116**, 337 (2004).
6. Y. Zhang *et al.*, *Nature* **372**, 425 (1994).
7. R. S. Ahima *et al.*, *Nature* **382**, 250 (1996).
8. J. L. Halaas *et al.*, *Science* **269**, 543 (1995).
9. I. S. Farooqi *et al.*, *N. Engl. J. Med.* **341**, 879 (1999).
10. J. K. Howard *et al.*, *Nature Med.* **10**, 734 (2004).
11. H. Shi, I. Tzameli, C. Bjorbaek, J. S. Flier, *J. Biol. Chem.* **279**, 34733 (2004).
12. J. M. Zabolotny *et al.*, *Dev. Cell* **2**, 489 (2002).
13. A. Bado *et al.*, *Nature* **394**, 790 (1998).
14. G. J. Schwartz, *Nutrition* **16**, 866 (2000).
15. N. Vrang, C. B. Phifer, M. M. Corkern, H. R. Berthoud, *Am. J. Physiol. Regul. Integr. Comp. Physiol.* **285**, R470 (2003).
16. A. Hirasawa *et al.*, *Nature Med.* **11**, 90 (2005).
17. S. V. Wu *et al.*, *Proc. Natl. Acad. Sci. U.S.A.* **99**, 2392 (2002).
18. A. D. Conigrave, S. J. Quinn, E. M. Brown, *Proc. Natl. Acad. Sci. U.S.A.* **97**, 4814 (2000).
19. J. Fu *et al.*, *Nature* **425**, 90 (2003).
20. F. Reimann, F. M. Gribble, *Diabetes* **51**, 2757 (2002).
21. F. M. Gribble, L. Williams, A. K. Simpson, F. Reimann, *Diabetes* **52**, 1147 (2003).
22. G. P. Smith, C. Jerome, B. J. Cushin, R. Eterno, K. J. Simansky, *Science* **213**, 1036 (1981).
23. N. Muurahainen, H. R. Kissileff, A. J. Derogatis, F. X. Pi-Sunyer, *Physiol. Behav.* **44**, 645 (1988).
24. C. Beglinger, L. Degen, D. Matzinger, M. D'Amato, J. Drewe, *Am. J. Physiol. Regul. Integr. Comp. Physiol.* **280**, R1149 (2001).
25. B. Kreymann, G. Williams, M. A. Ghatei, S. R. Bloom, *Lancet* **2**, 1300 (1987).
26. C. Tourrel, D. Bailbe, M. J. Meile, M. Kergoat, B. Portha, *Diabetes* **50**, 1562 (2001).
27. T. J. Kieffer, C. H. McIntosh, R. A. Pederson, *Endocrinology* **136**, 3585 (1995).
28. P. J. Larsen, C. Fledelius, L. B. Knudsen, M. Tang-Christensen, *Diabetes* **50**, 2530 (2001).
29. K. Meeran *et al.*, *Endocrinology* **140**, 244 (1999).
30. L. A. Scrocchi *et al.*, *Nature Med.* **2**, 1254 (1996).
31. C. Verdich *et al.*, *J. Clin. Endocrinol. Metab.* **86**, 4382 (2001).
32. C. L. Dakin *et al.*, *Endocrinology* **142**, 4244 (2001).
33. M. A. Cohen *et al.*, *J. Clin. Endocrinol. Metab.* **88**, 4696 (2003).
34. M. Tang-Christensen, N. Vrang, P. J. Larsen, *Int. J. Obes. Relat. Metab. Disord.* **25** (suppl. 5), S42 (2001).
35. H. Yamamoto *et al.*, *J. Clin. Invest.* **110**, 43 (2002).
36. C. L. Dakin *et al.*, *Endocrinology* **145**, 2687 (2004).
37. L. L. Baggio, Q. Huang, T. J. Brown, D. J. Drucker, *Gastroenterology* **127**, 546 (2004).
38. P. T. Schmidt *et al.*, *Regul. Pept.* **116**, 21 (2003).
39. S. C. Woods *et al.*, *Diabetologia* **20** (suppl.), 305 (1981).
40. K. Miyawaki *et al.*, *Nature Med.* **8**, 738 (2002).
41. T. H. Moran *et al.*, *Am. J. Physiol. Regul. Integr. Comp. Physiol.* **288**, R384 (2005).
42. R. L. Batterham *et al.*, *Nature* **418**, 650 (2002).
43. R. L. Batterham *et al.*, *N. Engl. J. Med.* **349**, 941 (2003).
44. G. Katsuura, A. Asakawa, A. Inui, *Peptides* **23**, 323 (2002).
45. C. L. McLaughlin, C. A. Baile, *Physiol. Behav.* **26**, 433 (1981).
46. R. L. Batterham *et al.*, *J. Clin. Endocrinol. Metab.* **88**, 3989 (2003).
47. M. Kojima *et al.*, *Nature* **402**, 656 (1999).
48. D. E. Cummings *et al.*, *Diabetes* **50**, 1714 (2001).
49. M. Nakazato *et al.*, *Nature* **409**, 194 (2001).
50. Y. Date *et al.*, *Gastroenterology* **123**, 1120 (2002).
51. L. F. Faulconbridge, D. E. Cummings, J. M. Kaplan, H. J. Grill, *Diabetes* **52**, 2260 (2003).
52. D. E. Cummings *et al.*, *N. Engl. J. Med.* **346**, 1623 (2002).
53. Y. Sun, S. Ahmed, R. G. Smith, *Mol. Cell. Biol.* **23**, 7973 (2003).
54. Y. Sun, P. Wang, H. Zheng, R. G. Smith, *Proc. Natl. Acad. Sci. U.S.A.* **101**, 4679 (2004).
55. N. M. Neary *et al.*, *J. Clin. Endocrinol. Metab.* **89**, 2832 (2004).
56. T. E. Adrian *et al.*, *Gastroenterology* **90**, 379 (1986).
57. A. Clark, M. R. Nilsson, *Diabetologia* **47**, 157 (2004).
58. R. D. Reidelberger, L. Kelsey, D. Heimann, *Am. J. Physiol. Regul. Integr. Comp. Physiol.* **282**, R1395 (2002).
59. O. Schmitz, B. Brock, J. Rungby, *Diabetes* **53** (suppl. 3), S233 (2004).
60. R. J. Lieverse *et al.*, *J. Clin. Endocrinol. Metab.* **76**, 1495 (1993).
61. E. M. Kovacs, M. P. Lejeune, M. S. Westerterp-Plantenga, *Br. J. Nutr.* **90**, 207 (2003).
62. E. E. Kershaw, J. S. Flier, *J. Clin. Endocrinol. Metab.* **89**, 2548 (2004).
63. C. Weyer *et al.*, *J. Clin. Endocrinol. Metab.* **86**, 1930 (2001).
64. C. M. Steppan *et al.*, *Nature* **409**, 307 (2001).
65. M. Lehrke *et al.*, *PLoS Med.* **1**, e45 (2004).
66. A. Fukuhara *et al.*, *Science* **307**, 426 (2005); published online 16 December 2004 (10.1126/science.1097243).
67. H. Masuzaki *et al.*, *Science* **294**, 2166 (2001).
68. M. P. Ettinger *et al.*, *JAMA* **289**, 1826 (2003).
69. H. E. Bays, *Obes. Res.* **12**, 1197 (2004).
70. C. M. Edwards *et al.*, *Am. J. Physiol. Endocrinol. Metab.* **281**, E155 (2001).
71. B. M. Wolfe, I. T. Austrheim-Smith, N. Ghaderi, *Gastroenterology* **128**, 225 (2005).
72. R. Steinbrook, *N. Engl. J. Med.* **350**, 1075 (2004).
73. J. Korner *et al.*, *J. Clin. Endocrinol. Metab.* **90**, 359 (2005).
74. A. Thorne, F. Lonnqvist, J. Apelman, G. Hellers, P. Arner, *Int. J. Obes. Relat. Metab. Disord.* **26**, 193 (2002).
75. S. A. Shikora, *Obes. Surg.* **14** (suppl. 1), S40 (2004).
76. X. Xu, H. Zhu, J. D. Chen, *Gastroenterology* **128**, 43 (2005).
77. V. Cigaina, A. L. Hirschberg, *Obes. Res.* **11**, 1456 (2003).
78. M. Roslin, M. Kurian, *Epilepsy Behav.* **2**, S11 (2001).
79. Funded by grants from the NIH and Takeda Pharmaceutical Company Limited. We thank J. Elmquist and S. Freedman for their helpful comments during preparation of this manuscript. J.F. is on the Scientific Advisory Board of and a paid consultant for Novartis, Beyond Genomics, and Elixer.

10.1126/science.1109951

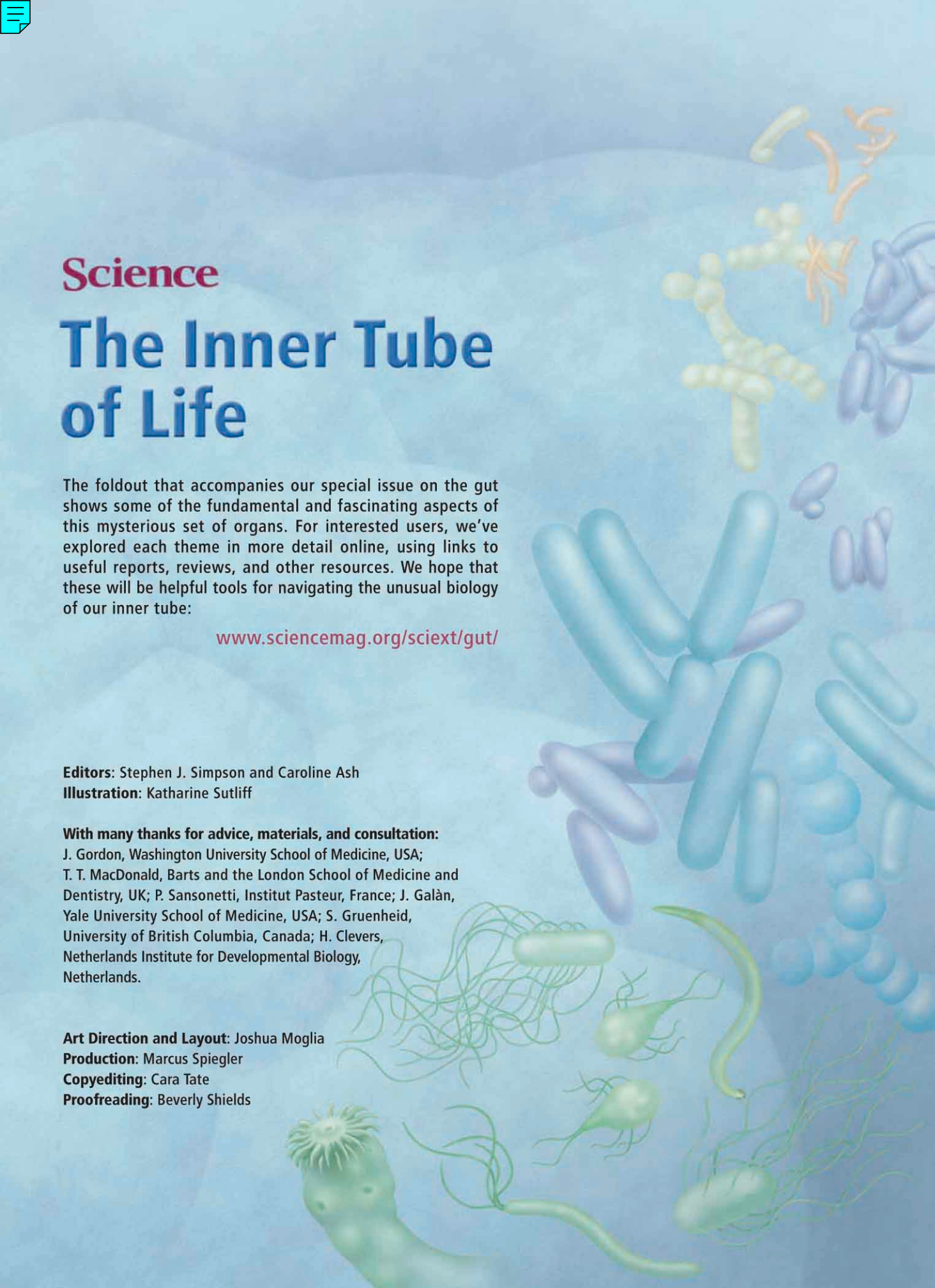

Science

The Inner Tube of Life

The foldout that accompanies our special issue on the gut shows some of the fundamental and fascinating aspects of this mysterious set of organs. For interested users, we've explored each theme in more detail online, using links to useful reports, reviews, and other resources. We hope that these will be helpful tools for navigating the unusual biology of our inner tube:

www.sciencemag.org/sciext/gut/

Editors: Stephen J. Simpson and Caroline Ash
Illustration: Katharine Sutliff

With many thanks for advice, materials, and consultation:
J. Gordon, Washington University School of Medicine, USA; T. T. MacDonald, Barts and the London School of Medicine and Dentistry, UK; P. Sansonetti, Institut Pasteur, France; J. Galàn, Yale University School of Medicine, USA; S. Gruenheid, University of British Columbia, Canada; H. Clevers, Netherlands Institute for Developmental Biology, Netherlands.

Art Direction and Layout: Joshua Moglia
Production: Marcus Spiegler
Copyediting: Cara Tate
Proofreading: Beverly Shields

The Inner Tube of Life

Our gut is huge—as long as a bus and if flattened out, sufficient to cover a football field. It is home to 100 trillion microorganisms; 10 times more microbial cells than all of the human cells in our adult body. It is continuously assaulted by extraordinary volumes of foodstuffs, noxious chemicals, and potentially harmful bacteria. It oversees a remarkably efficient salvage operation, extracting essential nutrients from an intermittently flowing river of food and water. Energy homeostasis, immune integrity, and the movement of its contents mean that the gut has to be in continuous dialogue with the rest of the body: It is our powerhouse and has even been called our second brain.

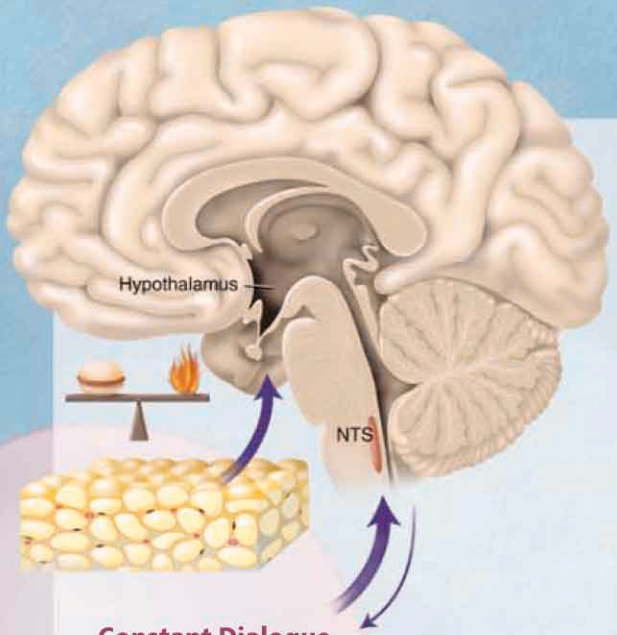

Constant Dialogue
The gut maintains a complex interchange of information with the brain and other visceral organs through nervous, metabolic, and endocrine signals. Vast amounts of neural information flow from the enteric nervous system to the brain, while a series of peptide hormones are the gut's ultimate gatekeepers, telling us what to eat and drink and when to stop. Once excess fat is deposited, excess peptides produced by fat cells may overwhelm eating controls. One key in the obesity war may be the removal of hormone-producing fat cells and the restoration of a semblance of hormonal control. *See Badman and Flier, page 1909*

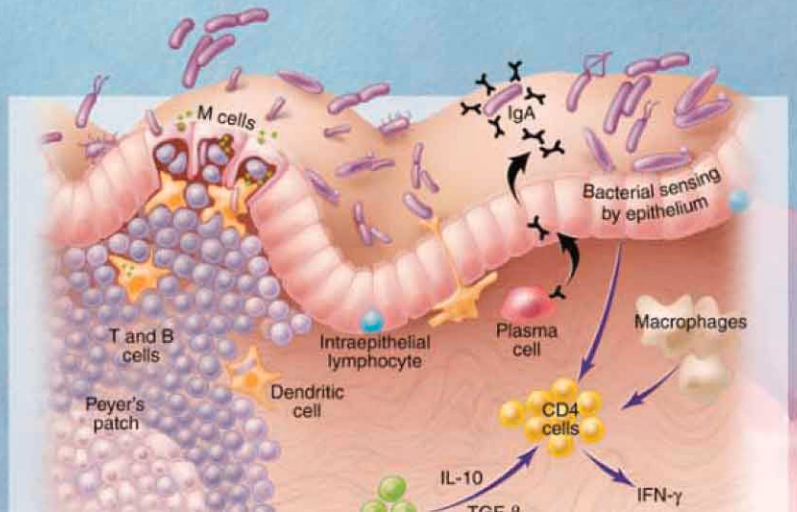

Under Surveillance

The gut's immune system dwarfs that needed for the rest of the body: It constantly has to sample and monitor the gut environment for pathogens, yet simultaneously dampen responses to benign organisms or antigens that we ingest. When the huge machinery of the gut's immune surveillance is perturbed, the consequences are severe and life-threatening. *See MacDonald and Monteleone, page 1920*

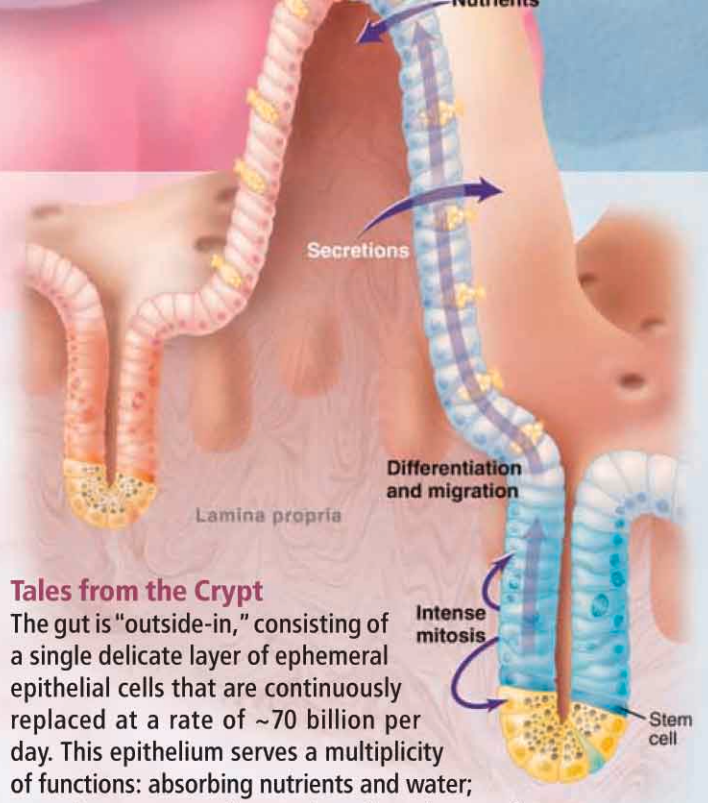

Tales from the Crypt

The gut is "outside-in," consisting of a single delicate layer of ephemeral epithelial cells that are continuously replaced at a rate of ~70 billion per day. This epithelium serves a multiplicity of functions: absorbing nutrients and water; secreting mucus; and exporting a broad array of enzymes, hormones, and antimicrobial compounds. Although the great proliferative activity of crypt stem cells helps ensure that our gut lining is always refreshed, it brings with it the risk of malignancy. *See Radtke and Clevers, page 1904*

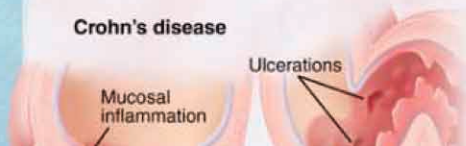

Bad Reaction

The developed world is experiencing an increase in the incidence of inflammatory diseases of the gut, such as Crohn's

disease. Complex genetic predisposing influences are at play, which lead to a breakdown of the strict regulation of the mucosal immune system's response to our bacterial microbiota. In celiac disease, the culprit is gluten, a common protein in cereals such as wheat, which triggers immune-mediated changes in the normal villous architecture, hindering the absorption of nutrients.

See MacDonald and Monteleone, page 1920

Micobial Melting Pot

Our gut flora is as individual as our personalities and contains a diverse ensemble of representatives from all three branches of life on Earth. There are at least 800 species of bacteria, most of which are completely mysterious. This means that the genome buried inside of our gut—the "microbiome"—may harbor 100 times more genes than our own genome, and it endows us with traits that, thankfully, we have not had to evolve on our own.

Our colon represents a feat of environmental engineering; an anoxic bioreactor in which our symbionts release nutrients from inaccessible foodstuffs for energy homeostasis. They also deal with toxins, keep pathogens at bay, contribute to epithelial homeostasis, and help to protect against injury. *See Bäckhed et al., page 1915*

Stealth Invaders

Any surveillance system can be undermined, and the gut is a cozy, nutrient-rich environment for some giant invaders. The menagerie is manifold, and playing host to a diverse array of flukes, cestodes, nematodes, and protozoa is an evolutionary normal state of affairs for human beings. These animals can take their toll; they may not kill immediately, but they cause immeasurable morbidity and misery for humankind across the globe. Nevertheless, it seems that we can also suffer from their absence, paying with immune dysfunction.

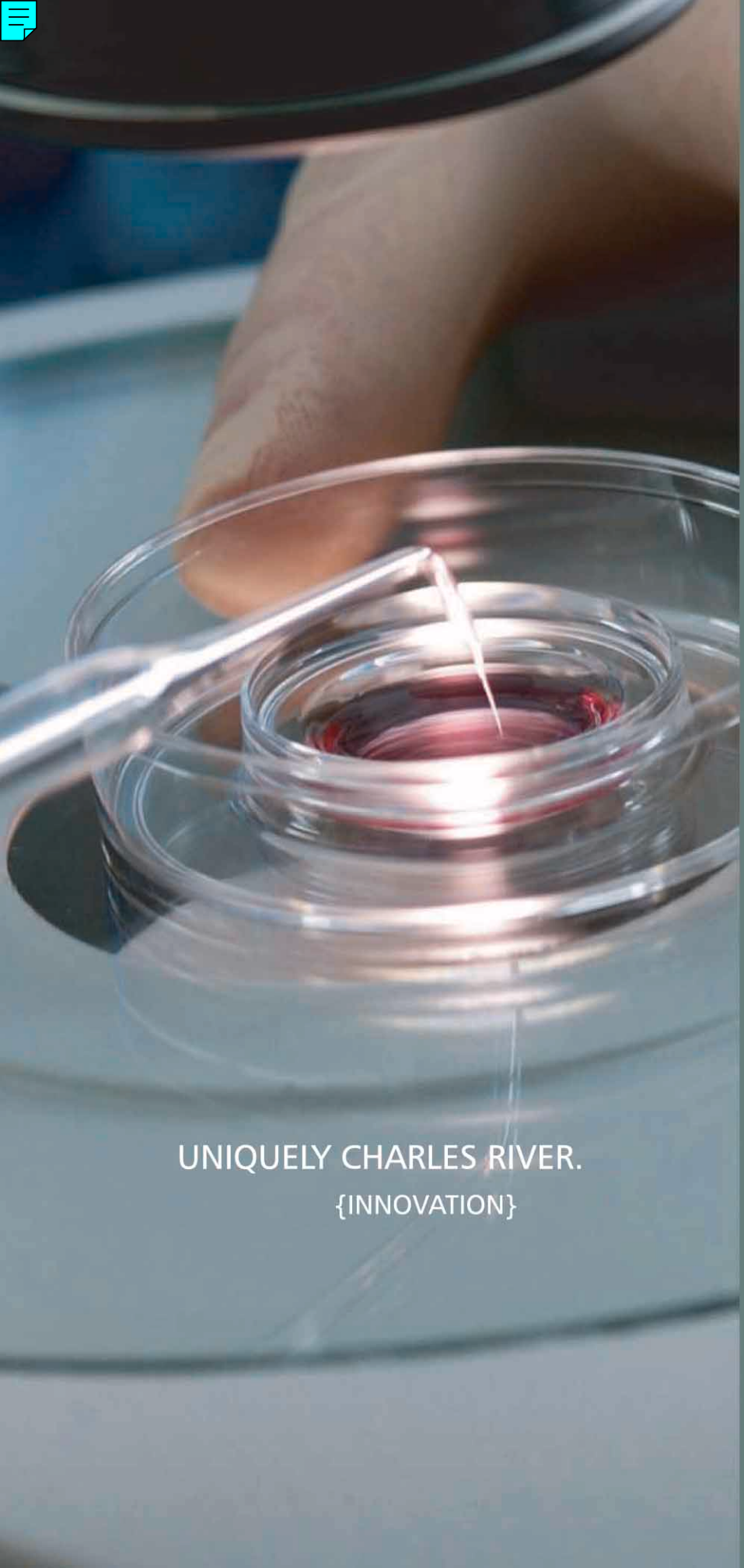

UNIQUELY CHARLES RIVER.
{INNOVATION}

Charles River Laboratories continually updates its portfolio with products and technologies that support your research.

Offerings include:

- Models of cardiovascular, metabolic, renal, and oncogenic disease
- Assisted Reproductive Technologies including ICSI
- Molecular Phenotyping

For more information, please call us at 1-877-CRIVER-1.

CHARLES RIVER
LABORATORIES
Research Models and Services
1.877.CRIVER.1 • www.criver.com/innovate

Host-Bacterial Mutualism in the Human Intestine

Fredrik Bäckhed,* Ruth E. Ley,* Justin L. Sonnenburg, Daniel A. Peterson, Jeffrey I. Gordon†

The distal human intestine represents an anaerobic bioreactor programmed with an enormous population of bacteria, dominated by relatively few divisions that are highly diverse at the strain/subspecies level. This microbiota and its collective genomes (microbiome) provide us with genetic and metabolic attributes we have not been required to evolve on our own, including the ability to harvest otherwise inaccessible nutrients. New studies are revealing how the gut microbiota has coevolved with us and how it manipulates and complements our biology in ways that are mutually beneficial. We are also starting to understand how certain keystone members of the microbiota operate to maintain the stability and functional adaptability of this microbial organ.

The adult human intestine is home to an almost inconceivable number of microorganisms. The size of the population—up to 100 trillion—far exceeds that of all other microbial communities associated with the body's surfaces and is ~10 times greater than the total number of our somatic and germ cells (*1*). Thus, it seems appropriate to view ourselves as a composite of many species and our genetic landscape as an amalgam of genes embedded in our *Homo sapiens* genome and in the genomes of our affiliated microbial partners (the microbiome).

Our gut microbiota can be pictured as a microbial organ placed within a host organ: It is composed of different cell lineages with a capacity to communicate with one another and the host; it consumes, stores, and redistributes energy; it mediates physiologically important chemical transformations; and it can maintain and repair itself through self-replication. The gut microbiome, which may contain ≥100 times the number of genes in our genome, endows us with functional features that we have not had to evolve ourselves.

Our relationship with components of this microbiota is often described as commensal (one partner benefits and the other is apparently unaffected) as opposed to mutualistic (both partners experience increased fitness). However, use of the term commensal generally reflects our lack of knowledge, or at least an agnostic (noncommittal) attitude about the contributions of most citizens of this microbial society to our own fitness or the fitness of other community members.

The guts of ruminants and termites are well-studied examples of bioreactors "programmed" with anaerobic bacteria charged with the task of breaking down ingested polysaccharides, the most abundant biological polymer on our planet, and fermenting the resulting monosaccharide soup to short-chain fatty acids. In these mutualistic relationships, the hosts gain carbon and energy, and their microbes are provided with a rich buffet of glycans and a protected anoxic environment (*2*). Our distal intestine is also an anaerobic bioreactor that harbors the majority of our gut microorganisms; they degrade a varied menu of otherwise indigestible polysaccharides, including plant-derived pectin, cellulose, hemicellulose, and resistant starches.

Microbiologists from Louis Pasteur and Ilya Mechnikov to present-day scientists have emphasized the importance of understanding the contributions of this microbiota to human health (and disease). Experimental and computational tools are now in hand to comprehensively characterize the nature of microbial diversity in the gut, the genomic features of its keystone members, the operating principles that underlie the nutrient foraging and sharing behaviors of these organisms, the mechanisms that ensure the adaptability and robustness of this system, and the physiological benefits we accrue from this mutualistic relationship. This Review aims to illustrate these points and highlight some future challenges for the field.

Microbial Diversity in the Human Gut Bioreactor

The adult human gastrointestinal (GI) tract contains all three domains of life—bacteria, archaea, and eukarya. Bacteria living in the human gut achieve the highest cell densities recorded for any ecosystem (*3*). Nonetheless, diversity at the division level (superkingdom or deep evolutionary lineage) is among the lowest (*4*); only 8 of the 55 known bacterial divisions have been identified to date (Fig. 1A), and of these, 5 are rare. The divisions that dominate—the Cytophaga-Flavobacterium-Bacteroides (CFB) (e.g., the genus *Bacteroides*) and the Firmicutes (e.g., the genera *Clostridium* and *Eubacterium*)—each comprise ~30% of bacteria in feces and the mucus overlying the intestinal epithelium. Proteobacteria are common but usually not dominant (*5*). In comparison, soil (the terrestrial biosphere's GI tract, where degradation of organic matter occurs) can contain 20 or more bacterial divisions (*6*).

Our knowledge of the composition of the adult gut microbiota stems from culture-based studies (*7*), and more recently from culture-independent molecular phylogenetic approaches based on sequencing bacterial ribosomal RNA (16*S* rRNA) genes. Of the >200,000 rRNA gene sequences currently in GenBank, only 1822 are annotated as being derived from the human gut; 1689 represent uncultured bacteria. rRNA sequences can be clustered into relatedness groups based on their percent sequence identity. Cutoffs of 95 and 98% identity are used commonly to delimit genera and species, respectively. Although these values are somewhat arbitrary and the terms "genus" and "species" are not precisely defined for microbes, we use them here to frame a view of human gut microbial ecology. When the sequences (n = 495 greater than 900 base pairs) are clustered into species, and a diversity estimate model is applied, a value of ~800 species is obtained (Fig. 2). If the analysis is adjusted to estimate strain number (unique sequence types), a value of >7000 is obtained (Fig. 2). Thus, the gut microbiota, which appears to be tremendously diverse at the strain and subspecies level, can be visualized as a grove of eight palm trees (divisions) with deeply divergent lineages represented by the fan(s) of closely related bacteria at the very top of each tree trunk.

Diversity present in the GI tract appears to be the result of strong host selection and coevolution. For example, members of the CFB division that are predominantly associated with mammals appear to be the most derived (i.e., farthest away from the common ancestor of the division), indicating that they underwent accelerated evolution once they adopted a mutualistic lifestyle. Moreover, a survey of GenBank reveals that several subgroups in CFB are distributed among different mammalian species (Fig. 1B), suggesting that the CFB-mammal symbiosis is ancient and that distinct subgroups coevolved with their hosts.

Center for Genome Sciences, Washington University School of Medicine, St. Louis, MO 63108, USA.

*These authors contributed equally to this work.
†To whom correspondence should be addressed. E-mail: jgordon@molecool.wustl.edu

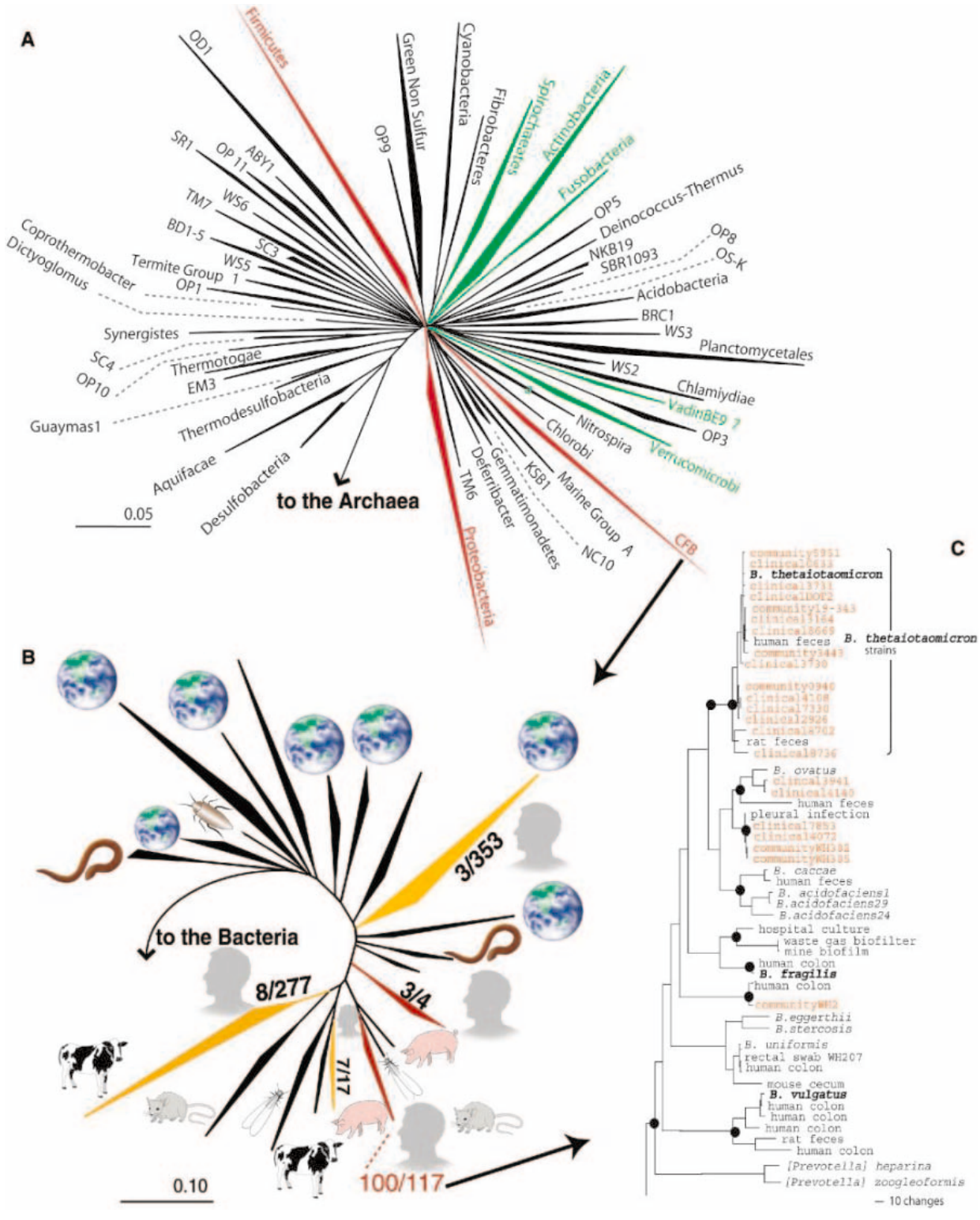

Fig. 1. Representation of the diversity of bacteria in the human intestine. (**A**) Phylogenetic tree of the domain bacteria based on 8903 representative 16*S* rRNA gene sequences. Wedges represent divisions (superkingdoms): Those numerically abundant in the human gut are red, rare divisions are green, and undetected are black. Wedge length is a measure of evolutionary distance from the common ancestor. (**B**) Phylogenetic tree of the CFB division based on 1561 sequences from GenBank (>900 nucleotides) and their ecological context. Wedges, major subgroups of CFB; symbols, source of the sequences [Earth, environmental; cow, ruminants; rodent, rat and/or mouse; person, human GI tract; others are termite, cockroach, worm (including hydrothermal), and pig]. Ratios are the number of sequences represented in the human gut relative to the total number in the subgroup; red, yellow, and black indicate majority, minority, and absence of sequences represented in human GI tract, respectively. (**C**) Phylogenetic (parsimony) tree of *Bacteroides*. Strains classified as *B. thetaiotaomicron* based on phenotype are in red; 16*S* rRNA analysis did not confirm this classification for all strains. *Bacteroides* spp. with sequenced genomes are in bold. Black circles indicate nodes with high (>70%) bootstrap support (*41*). Scale bars indicate the degree of diversity (evolutionary distance) within a division or subgroup [(A) and (B), respectively] in terms of the fraction of the 16*S* rRNA nucleotides that differ between member sequences; in (C), the evolutionary distance between organisms is read along branch lengths, where scale indicates number of changes in 16*S* rRNA nucleotide composition.

The structure and composition of the gut microbiota reflect natural selection at two levels: at the microbial level, where lifestyle strategies (e.g., growth rate and substrate utilization patterns) affect the fitness of individual bacteria in a competitive ensemble; and at the host level, where suboptimal functionality of the microbial ensemble can reduce host fitness. Microbial consortia whose integrated activities result in a cost to the host will result in fewer hosts, thereby causing loss of their own habitat. Conversely, microbial consortia that promote host fitness will create more habitats. Thus, the diversity found within the human GI tract, namely, a few divisions represented by very tight clusters of related bacteria, may reflect strong host selection for specific bacteria whose emergent collective behavior is beneficial to the host. This hypothesis has two important implications: (i) A mechanism exists to promote cooperation, and (ii) the structure promotes functional stability of the gut ecosystem.

To benefit the host, bacteria must be organized in a trophic structure (food web) that aids in breaking down nutrients and provides the host with energetic substrates. Cooperative behavior that imposes a cost to the individual while benefiting the community can emerge within groups of bacteria (*8*) and can be maintained by group selection as long as consortia are isolated and new consortia form periodically (e.g., new GI tracts). Furthermore, selection must act simultaneously at multiple levels of biological organization (*9*). These criteria are met in the human GI tract where new acts of colonization occur at birth, with a small founding population of noncheaters from the mother, and selection occurs both at the microbial and host level.

Diversity is generally thought to be desirable for ecosystem stability (*10*). One important way diversity can confer resilience is through a wide repertoire of responses to stress [referred to as the insurance hypothesis (*11*)]. In man-made anaerobic bioreactors used to treat wastewater (a system analogous to the gut but where no host selection occurs), rates of substrate degradation can remain constant, whereas bacterial populations fluctuate chaotically as a result of blooms of subpopulations (*12*). Functional redundancy in the microbial community ensures that key processes are unaffected by such changes in diversity (*13*). By contrast, in the human gut, populations are remarkably stable within individuals (*14*), implying that mechanisms exist to suppress blooms of subpopulations and/or to promote the abundance of desirable bacteria. A study of adult monozygotic twins living apart and their marital partners has emphasized the potential dominance of host genotype over diet in determining microbial composition of the gut bioreactor (*15*). The role of the immune system in defining diversity and suppressing subpopulation blooms remains to be defined. One likely mediator of bacterial selection is secretory immunoglobulin A (*16*).

The human gut is faced with a paradox: How can functional redundancy be maintained in a system with low diversity (few divisions of bacteria), and how can such a system withstand selective sweeps in the form of, for example, phage attacks? [The estimated 1200 viral genotypes in human feces (*17*) suggest that phage attack is a powerful shaper of the gut's microbial genetic landscape (*18*, *19*)]. Enough diversity of genome and transcriptome must be represented at the subspecies level to lend resilience to the gut ecosystem. Ecological studies of macroecosystems have shown that less diversity is required to maintain stability if individual species themselves have a wide repertoire of responses (*11*). In the following section we discuss recent genome-based studies exploring how a presumed keystone bacterial species in our gut is able to adapt to (i) changing dietary conditions in ways that should stabilize the microbiota's food web and (ii) changing immune and phage selective pressures in ways that should stabilize the ecosystem.

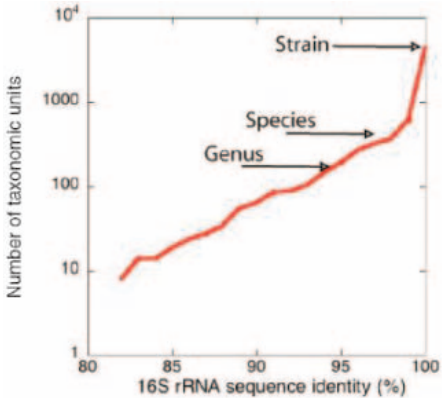

Fig. 2. Taxon richness estimates for bacteria in the human GI tract. Taxon richness estimates (*41*) for varying levels of 16*S* rRNA sequence identity, ranging from below the "genus" level (95% identity), to the "species" level (98% identity), to the strain level (unique sequences). Estimates are based on sequences available in GenBank, annotated as derived from the human GI tract, after alignment and clustering into taxonomic units ranging from 80 to 100% identity (*41*).

Bacteroides thetaiotaomicron—A Highly Adaptive Glycophile

Bacteroides thetaiotaomicron is a prominent mutualist in the distal intestinal habitat of adult humans. It is a very successful glycophile whose prodigious capacity for digesting otherwise indigestible dietary polysaccharides is reflected in the fully sequenced 6.3-Mb genome of the type strain (ATCC 29148; originally isolated from the feces of a healthy adult human) (*20*). Its "glycobiome" contains the largest ensemble of genes involved in acquiring and metabolizing carbohydrates yet reported for a sequenced bacterium, including 163 paralogs of two outer membrane proteins (SusC and SusD) that bind and import starch (*21*), 226 predicted glycoside hydrolases, and 15 polysaccharide lyases (*22*). By contrast, our 2.85-Gb genome only contains 98 known or putative glycoside hydrolases and is deficient in the enzyme activities required for degradation of xylan-, pectin-, and arabinose-containing polysaccharides that are common components of dietary fiber [we have one predicted enzyme versus 64 in *B. thetaiotaomicron* (table S1)].

The carbohydrate foraging behavior of *B. thetaiotaomicron* has been characterized during its residency in the distal intestines (ceca) of gnotobiotic mice colonized exclusively with this anaerobe (*23*). Scanning electron microscopy studies of the intestines of mice maintained on a standard high-polysaccharide chow diet, containing xylose, galactose, arabinose, and glucose as its principal monosaccharide components, revealed communities of bacteria assembled on small undigested or partially digested food particles, shed elements of the mucus gel layer, and exfoliated epithelial lining cells (*23*). Whole-genome transcriptional profiling of *B. thetaiotaomicron* (*23*) disclosed that this diet was associated with selective up-regulation of a subset of SusC and SusD paralogs, a subset of glycoside hydrolases (e.g., xylanases, arabinosidases, and pectate lyase), as well as genes encoding enzymes involved in delivering the products of mannose, galactose, and glucose to the glycolytic pathway and arabinose and xylose to the pentose phosphate pathway. In contrast, a simple sugar (glucose and sucrose) diet devoid of polysaccharides led to increased expression of a different subset of SusC and SusD paralogs, glycoside hydrolases involved in retrieving carbohydrates from mucus glycans, as well as enzymes that remove modifications that make these host glycans otherwise resistant to degradation (O-acetylation of sialic acids and sulfation of glycosoaminoglycans) (*23*).

These findings provide insights about how functional diversity and adaptability are achieved by a prominent member of the human colonic microbiota (Fig. 3). Dining occurs on particulate nutrient scaffolds (food particles, shed mucus, and/or exfoliated epithelial cells). For a bacterium such as *B. thetaiotaomicron*, which lacks adhesive organelles, seating at the "dining table" is determined in part by the repertoire of glycan-specific outer membrane–binding proteins it produces, and this repertoire is itself shaped by the menu of available glycans (*23*). Attachment to nutrient platforms helps avoid washout from the intestinal bioreactor, in much the same way as dense, well-settling, granular biofilms help oppose elimination from engineered (man-made) an-

aerobic upflow bioreactors (*24*). Attachment also presumably increases the efficiency of oligo- and monosaccharide harvest by adaptively expressed bacterial glycoside hydrolases and their subsequent distribution to other members of the microbiota whose niche overlaps that of *B. thetaiotaomicron*. In this conceptualization, microbial nutrient metabolism along the length of the intestine is a summation of myriad selfish and syntrophic relationships expressed by inhabitants of these nutrient platforms. Diversity in these microhabitats and mutualistic cooperation among their component species (including the degree to which sanctions must be applied against cheats) are reflections of a dynamic interplay between the available nutrient foundation and the degree of flexible foraging (niche breadth) expressed by microhabitat residents. *Bacteroides* spp., such as *B. thetaiotaomicron*, impart stability to the gut ecosystem by having the capacity to turn to host polysaccharides when dietary polysaccharides become scarce. The highly variable outer chain structures of mucus and epithelial cell surface glycans are influenced by host genotype and by microbial regulation of host glycosyltransferase gene expression. Coevolution of host glycan diversity and a large collection of microbial glycoside hydrolases that are regulated by nutrient availability provides insurance that the "system" (microbiota and host) can rapidly and efficiently respond to changes in the diet, and maximize energy harvest, without having to undergo substantial changes in species composition. Rather than minimizing genome size, a keystone species such as *B. thetaiotaomicron* has evolved an elaborate and sizable genome that can mobilize functionally diverse adaptive responses.

Diet-associated changes in the glycan foraging behavior of *B. thetaiotaomicron* are also accompanied by changes in expression of its capsular polysaccharide synthesis loci (*CPS*), indicating that *B. thetaiotaomicron* is able to change its carbohydrate surface depending upon the nutrient (glycan) environment. This could be part of a strategy for evading an adaptive immune response. Whole-genome genotyping studies of *B. thetaiotaomicron* isolates, with the use of GeneChips designed from the sequenced genome of the type strain, disclose that their *CPS* loci differ, whereas their housekeeping genes are conserved (*25*). Because selective sweeps are most likely to come from the immune system and phages, both of which respond to surface structures, the associated genes are likely to be the most diverse in the genome. Accordingly, *B. thetaiotaomicron* has a remarkable apparatus for altering its genome content. The sequenced type strain contains a plasmid, 63 transposases, 43 integrases, and four homologs of a conjugative transposon (*20*). Gene transfer and mutation mechanisms endow strains of bacterial species with the (genetic) versatility necessary to withstand selective sweeps that would eradicate more clonal populations (*26*).

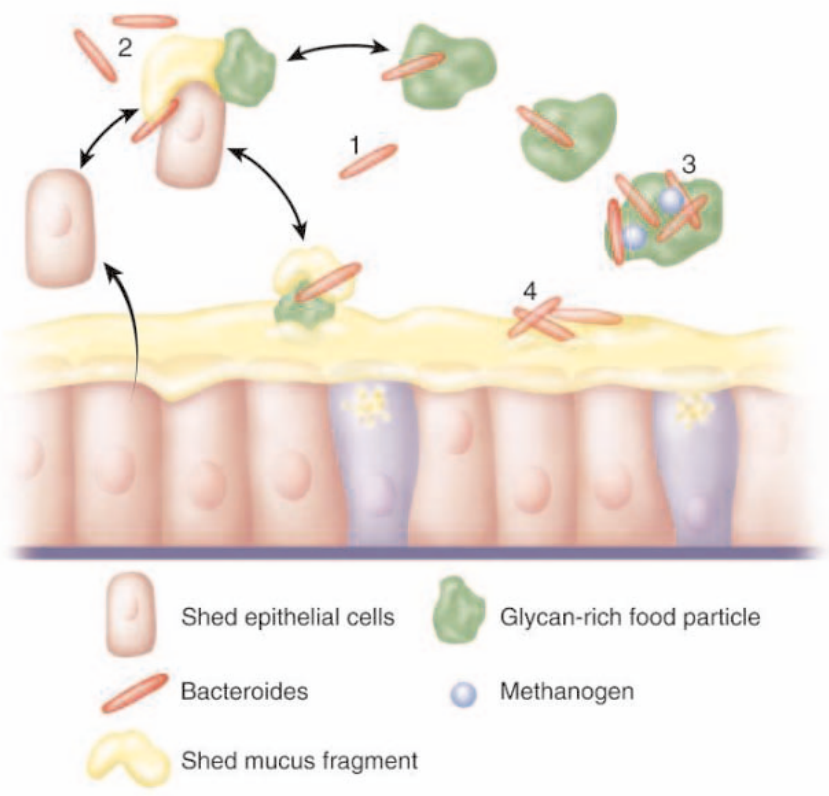

Fig. 3. Lessons about adapative foraging for glycans obtained from *B. thetaiotaomicron*. (1) *B. thetaiotaomicron* does not have adhesive organelles. Without outer membrane polysaccharide-binding protein-mediated attachment to glycan-rich nutrient platforms, it is at risk for being washed out from the intestinal bioreactor. Substrate access is limited under these conditions. (2) Small nutrient platforms are composed of undigested or partially digested food particles (e.g., dietary fiber), shed host epithelial cells, and/or mucus fragments. These platform elements may be in dynamic equilibrium with one another and with the mucus layer overlying the intestinal epithelium. Microbial fermentation of otherwise indigestible polysaccharides in these platforms is made possible by induced expression of substrate-appropriate sets of bacterial polysaccharide-binding proteins and glycoside hydrolases. (3) Mesophilic methanogens drive carbohydrate utilization by removing products of fermentation (H_2 and CO_2 are converted to methane), thereby improving the overall efficiency of energy extraction from polysaccharides. (4) When dietary polysaccharides are scarce, *B. thetaiotaomicron* turns to host mucus by deploying a different set of polysaccharide binding proteins and glycoside hydrolases. This adaptive foraging reflects the coevolved functional versatility of *B. thetaiotaomicron*'s glycobiome and the structural diversity of the host's mucus glycans.

The Gut Microbiota as a "Host" Factor That Influences Energy Storage

Comparisons of mice raised without exposure to any microorganisms [Germ-Free (GF)] with those that have acquired a microbiota since birth [Conventionally Raised (CONV-R)] have led to the identification of numerous effects of indigenous microbes on host biology (table S2), including energy balance. Young adult CONV-R animals have 40% more total body fat than their GF counterparts fed the same polysaccharide-rich diet, even though CONV-R animals consume less chow per day (*27*). This observation might seem paradoxical at first but can be explained by the fact that the gut microbiota allows energy to be salvaged from otherwise indigestible dietary polysaccharides (*28*). "Conventionalization" of adult GF mice with cecal contents harvested from CONV-R donors increases body fat content to levels equivalent to those of CONV-R animals (*27*). The increase reflects adipocyte hypertrophy rather than hyperplasia and is notable for its rapidity and sustainability (*27*).

The mutualistic nature of the host-bacterial relationship is underscored by mechanisms that underlie this fat-storage phenotype. Colonization increases glucose uptake in the host intestine and produces substantial elevations in serum glucose and insulin (*27*), both of which stimulate hepatic lipogenesis through their effects on two basic helix-loop-helix/leucine zipper transcription factors—ChREBP and SREBP-1c (*27*, *29*). Short-chain fatty acids, generated by microbial fermentation, also induce lipogenesis (*30*). Triglycerides exported by the liver into the circulation are taken up by adipocytes through a lipoprotein lipase (LPL)–mediated process. The microbiota suppresses intestinal epithelial expression of a

circulating LPL inhibitor, fasting-induced adipose factor (Fiaf, also known as angiopoietin-like protein-4) (*27*). Comparisons of GF and conventionalized wild-type and *Fiaf*$^{-/-}$ mice established Fiaf as a physiologically important regulator of LPL activity in vivo and a key modulator of the microbiota-induced increase in fat storage (*27*).

The caloric density of food items is portrayed as a fixed value on package labels. However, it seems reasonable to postulate that caloric value varies between individual ''consumers'' according to the composition and operation (e.g., transit time) of their intestinal bioreactors, and that the microbiota influences their energy balance. Relatively high-efficiency bioreactors would promote energy storage (obesity), whereas lower efficiency reactors would promote leanness (efficiency is defined in this case as the energy-harvesting and storage-promoting potential of an individual's microbiota relative to the ingested diet).

The idea that individual variations in bioreactor efficiencies may be a significant variable in the energy balance equation is supported by several observations. First, individual variations in the composition of the microbiota occur and are influenced by host genotype (*15*). Second, small but chronic differences between energy intake and expenditure can, in principle, produce major changes in body composition [e.g., if energy balance is +12 kcal/day, >0.45 kg of fat could be gained per year if there are no compensatory responses by the host; this is the average weight increase experienced by Americans from age 25 to 55 (*31*)]. Third, the microbiota is a substantial consumer of energy. One group estimated that individuals on a ''British Diet'' must ferment 50 to 65 g of hexose sugars daily to obtain the energy required to replace the 15 to 20 g (dry weight) of bacteria they excrete per day (*32*).

These considerations emphasize the need to assess the representation of species with large capacities for processing dietary polysaccharides, such as *Bacteroides*, in lean versus morbidly obese individuals, and in cohorts of obese individuals before, during, and after weight reduction achieved by high-polysaccharide/low-fat versus high-fat/low-polysaccharide diets [or by bariatric (gastric bypass) surgery]. The results, coupled with coincident assessments of energy extraction from the diet, should provide a proof-of-concept test of whether differences in the composition of the microbiota are associated with differences in gut bioreactor efficiency (and predisposition to obesity).

Lessons that have been learned by environmental engineers who study how to optimize the efficiency of man-made anaerobic bioreactors (table S3) suggest that these enumeration studies should also include members of archaea. Thermodynamics dictates that the energy obtained from substrate conversions will be higher if low concentrations of products are maintained (*33*, *34*). In the human gut, methanogenic archaea provide the last microbial link in the metabolic chain of polysaccharide processing. Bacteria degrade polysaccharides to short-chain fatty acids, CO_2, and hydrogen gas. Methanogens lower the partial pressure of hydrogen by generating methane, and thereby may increase microbial fermentation rates. Defining the representation of mesophilic methanogens in the colonic microbiota of individuals, sequencing their genomes [as we are currently doing with *Methanobrevibacter smithii*, a prevalent isolate from the human colon (*35*)], and characterizing archaeal-bacterial syntrophy in simplified gnotobiotic mouse models consuming different diets should provide a starting point for defining the role of archaea in shaping the functional diversity, stability, and beneficial contributions of our distal gut microbiota. Devising ways for manipulating archaeal populations may provide a novel way for intentionally altering our energy balance.

Looking to the Future

A comprehensive 16*S* rRNA sequence–based (bacterial and archaeal) enumeration of the microbiotas of selected humans, representing different ethnic groups, living in similar or distinct milieus, would provide an invaluable database for studying normal and diseased populations (*36*). The concept of using the microbiota as a biomarker of impending or fully manifest diseases within or outside of the GI tract and for monitoring responses to therapeutic interventions needs to be explored.

Several groups are embarking on metagenome sequencing projects to define gene content in the human gut microbiome. If we view ourselves as being a composite of many species, this represents a logical continuation of the Human Genome Project. A complementary approach to metagenomic analysis is to determine genome-level diversity among bacterial populations belonging to a specific genus or species residing within a defined gut habitat of a single individual or a few individuals. Members of *Bacteroides* provide a natural experiment for examining the impact of habitat on genome content since they have yet to be encountered in any environment other than animal GI tracts. Figure 1C illustrates how a collection of just 29 isolates phenotyped as *B. thetaiotaomicron* provided a broad range of 16*S* rRNA sequences, including several new species. We are close to producing finished genome sequences for two prominent members of the colonic microbiota, *B. vulgatus* and *B. distasonis* (*37*). *B. fragilis*, a less prominent member, has recently been sequenced (*38*, *39*). The results will allow us to ask how evolutionary history relates to genome content and what constitutes a minimal *Bacteroides* genome.

We also need to obtain a direct view of how the metabolites originating from the microbiome influence host physiology. This will be a formidable task, requiring new techniques for measuring metabolites generated by single and defined collections of symbionts during growth under defined nutrient conditions in single-vessel chemostats, in more elaborate mechanical models of the human gut, and in vivo after colonization of specified habitats of the intestines of gnotobiotic mice. The results should help formulate and direct hypothesis-based investigations of the microbiota's ''metabolome'' in humans.

Databases that connect molecular data with ecosystem parameters are still rare (*40*). A human intestinal microbiome database is needed to organize genomic, transcriptomic, and metabolomic data obtained from this complex natural microbial community, and would provide a substrate for generating testable hypotheses.

Finally, just as microbiotas have coevolved with their animal hosts, this field must coevolve with its academic hosts and their ability to devise innovative ways of assembling interactive interdisciplinary research groups necessary to advance our understanding.

References and Notes

1. D. C. Savage, *Annu. Rev. Microbiol.* **31**, 107 (1977).
2. A. Brune, M. Friedrich, *Curr. Opin. Microbiol.* **3**, 263 (2000).
3. W. B. Whitman, D. C. Coleman, W. J. Wiebe, *Proc. Natl. Acad. Sci. U.S.A.* **95**, 6578 (1998).
4. P. Hugenholtz, B. M. Goebel, N. R. Pace, *J. Bacteriol.* **180**, 4765 (1998).
5. P. Seksik *et al.*, *Gut* **52**, 237 (2003).
6. J. Dunbar, S. M. Barns, L. O. Ticknor, C. R. Kuske, *Appl. Environ. Microbiol.* **68**, 3035 (2002).
7. W. E. Moore, L. V. Holdeman, *Appl. Microbiol.* **27**, 961 (1974).
8. P. B. Rainey, K. Rainey, *Nature* **425**, 72 (2003).
9. M. Travisano, G. J. Velicer, *Trends Microbiol.* **12**, 72 (2004).
10. K. S. McCann, *Nature* **405**, 228 (2000).
11. S. Yachi, M. Loreau, *Proc. Natl. Acad. Sci. U.S.A.* **96**, 1463 (1999).
12. A. S. Fernandez *et al.*, *Appl. Environ. Microbiol.* **66**, 4058 (2000).
13. B. M. Goebel, E. Stackebrandt, *Appl. Environ. Microbiol.* **60**, 1614 (1994).
14. E. G. Zoetendal, A. D. Akkermans, W. M. De Vos, *Appl. Environ. Microbiol.* **64**, 3854 (1998).
15. E. G. Zoetendal *et al.*, *Microb. Ecol. Health Dis.* **13**, 129 (2001).
16. K. Suzuki *et al.*, *Proc. Natl. Acad. Sci. U.S.A.* **101**, 1981 (2004).
17. M. Breitbart *et al.*, *J. Bacteriol.* **185**, 6220 (2003).
18. J. A. Fuhrman, *Nature* **399**, 541 (1999).
19. C. Winter, A. Smit, G. J. Herndl, M. G. Weinbauer, *Appl. Environ. Microbiol.* **70**, 804 (2004).
20. J. Xu *et al.*, *Science* **299**, 2074 (2003).
21. J. A. Shipman, J. E. Berleman, A. A. Salyers, *J. Bacteriol.* **182**, 5365 (2000).
22. More information about these enzymes is available at http://afmb.cnrs-mrs.fr/CAZY.
23. J. L. Sonnenburg *et al.*, *Science* **307**, 1955 (2005).
24. J. L. Sonnenburg, L. T. Angenent, J. I. Gordon, *Nature Immunol.* **5**, 569 (2004).
25. R. E. Ley, J. I. Gordon, unpublished data.
26. F. Taddei, I. Matic, B. Godelle, M. Radman, *Trends Microbiol.* **5**, 427 (1997).

27. F. Bäckhed *et al.*, *Proc. Natl. Acad. Sci. U.S.A.* **101**, 15718 (2004).
28. M. Yamanaka, T. Nomura, M. Kametaka, *J. Nutr. Sci. Vitaminol. (Tokyo)* **23**, 221 (1977).
29. H. C. Towle, *Proc. Natl. Acad. Sci. U.S.A.* **98**, 13476 (2001).
30. R. H. Rolandelli *et al.*, *J. Nutr.* **119**, 89 (1989).
31. K. M. Flegal, R. P. Troiano, *Int. J. Obes. Relat. Metab. Disord.* **24**, 807 (2000).
32. N. I. McNeil, *Am. J. Clin. Nutr.* **39**, 338 (1984).
33. R. K. Thauer, K. Jungermann, K. Decker, *Bacteriol. Rev.* **41**, 100 (1977).
34. A. J. Stams, *Antonie Van Leeuwenhoek* **66**, 271 (1994).
35. T. L. Miller, M. J. Wolin, *Arch. Microbiol.* **131**, 14 (1982).
36. O. Chacon, L. E. Bermudez, R. G. Barletta, *Annu. Rev. Microbiol.* **58**, 329 (2004).
37. More information about these genomes is available at http://genome.wustl.edu/projects/bacterial/cmpr_microbial/index.php?cmpr _microbial=1.
38. T. Kuwahara *et al.*, *Proc. Natl. Acad. Sci. U.S.A.* **101**, 14919 (2004).
39. A. M. Cerdeño-Tárraga *et al.*, *Science* **307**, 1463 (2005).
40. M. Y. Galperin, *Nucleic Acids Res.* **32**, D3 (2004).
41. Materials and methods are available as supporting material on *Science* Online.

42. We thank L. Angenent for many helpful discussions. Work cited from the authors' lab is supported by the NIH and NSF. F.B. and J.L.S. are supported by postdoctoral fellowships from the Wenner-Gren and W. M. Keck Foundations, respectively.

Supporting Online Material
www.sciencemag.org/cgi/content/full/307/5717/1915/DC1
Materials and Methods
Tables S1 to S3
References

10.1126/science.1104816

REVIEW

Immunity, Inflammation, and Allergy in the Gut

Thomas T. MacDonald[1]*† and Giovanni Monteleone[2]

The gut immune system has the challenge of responding to pathogens while remaining relatively unresponsive to food antigens and the commensal microflora. In the developed world, this ability appears to be breaking down, with chronic inflammatory diseases of the gut commonplace in the apparent absence of overt infections. In both mouse and man, mutations in genes that control innate immune recognition, adaptive immunity, and epithelial permeability are all associated with gut inflammation. This suggests that perturbing homeostasis between gut antigens and host immunity represents a critical determinant in the development of gut inflammation and allergy.

The gastrointestinal tract is the site where the divergent needs of nutrient absorption and host defense collide: The former requires a large surface area and a thin epithelium that has the potential to compromise host defense. Many infectious diseases involve the gut, and the investment by the gut in protecting itself is evident in the abundant lymphoid tissue and immune cells it harbors. In westernized countries, most infectious diseases of the gut are largely under control, yet gastrointestinal food allergies and idiopathic inflammatory conditions have dramatically increased; in other words, we now have inflammation without infection. Although the reason for this remains unknown, a prevailing notion is that the absence of overt gut infection has upset the balance between the normal bacteria that colonize the healthy gut and the mucosal immune system.

The Gut Epithelial Barrier

The primary cellular barrier of the gut in preventing antigens encountering the immune system is the single layer of gut epithelium, the surface area of which is expanded to the order of 400 m^2, largely because it is formed into millions of fingerlike villi in the small bowel. Each epithelial cell maintains intimate association with its neighbors and seals the surface of the gut with tight junctions. In the upper bowel, the bulk of the antigen exposure comes from diet, whereas in the ileum and colon, the additional antigenic load of an abundant and highly complex commensal microflora exists.

Nevertheless, the gut epithelial barrier does not completely prevent lumenal antigens from entering the tissues. Thus, intact food proteins can be detected in plasma (*1*), and a few gut bacteria can be detected in the mesenteric lymph nodes draining the gut of healthy animals (*2*). Antigens can cross the epithelial surface through breaks in tight junctions, perhaps at villus tips where epithelial cells are shed, or through the follicle-associated epithelium (FAE) that overlies the organized lymphoid tissues of the intestinal wall (*3*). Peyer's patches (PP) in the small bowel are aggregates of lymphoid tissue numbering ~200 in the average adult, although tens of thousands of much smaller individual follicles also line the small bowel and colon. FAE contains specialized epithelial cells termed M cells whose function is to transport lumenal antigens into the dome area of the follicle (*3*) (Fig. 1). Antigen-presenting dendritic cells (DC) also send processes between gut epithelial cells without disturbing tight junction integrity and sample commensal and pathogenic gut bacteria (*4*, *5*). The gut epithelial barrier therefore represents a highly dynamic structure that limits, but does not exclude, antigens from entering the tissues, whereas the immune system constantly samples gut antigens through the FAE and DC processes.

Commensal Bacteria in Epithelial/Immune Cell Function in the Gut

Interaction of commensals with gut epithelium. The gut epithelium itself can also directly sense commensal bacteria and pathogens; integral to this are the mammalian pattern recognition receptors (PRRs), which recognize conserved structures of bacteria and viruses and generally activate pro-inflammatory pathways alerting the host to infection (*6*). Two different classes of PRRs are involved. The Toll-like receptors (TLRs) are usually associated with cell membranes and have an external leucine-rich repeat (LRR) recognition domain and an intracellular interleukin-1 receptor (IL-1R)–like signaling domain (*7*). The nucleotide-binding oligomerization domain (Nod) molecules, Nod1 and Nod2 [also known as CARD4 and CARD15 (caspase activation and recruitment domain)], are present in the cytosol of epithelial cells and immune cells. These proteins also have LRRs at the C terminus, a Nod domain, and CARD domains at the N terminus (*8*). There is abundant evidence that signaling through Nod or TLR activates transcription factor NF-κB, leading to pro-inflammatory gene expression (*7*, *8*)

TLR1 to TLR9 and Nod1 and Nod2 are each expressed by gut epithelial cells (*6*, *9*). Nod1 and Nod2 recognize slightly different muropeptide motifs derived from bacterial peptidoglycans (*6*), which suggests that they sense intracellular infection or attempted bacterial subversion of epithelial cells (*10*). TLRs recognize many different components of bacteria and viruses. For example, TLR4 recognizes

[1]Division of Infection, Inflammation, and Repair, University of Southampton School of Medicine, Southampton General Hospital, Southampton, SO16 6YD, UK. [2]Dipartimento di Medicina Interna e Centro di Eccellenza per lo Studio delle Malattie Complesse e Multifattoriali, Università Tor Vergata, Rome, Italy.

*Present address: Barts and the London School of Medicine and Dentistry, Turner Street, London E1 2AD, UK.
†To whom correspondence should be addressed. E-mail: t.t.macdonald@qmul.ac.uk

lipopolysaccharide from the Gram-negative bacterial cell wall, and TLR5 recognizes bacterial flagellin (*6*, *7*). An unresolved question is how the gut distinguishes between pathogens and commensal bacteria. One means by which inappropriate responses to innate signals from commensals may be achieved is through the compartmentalization of TLRs to the basolateral aspects of epithelial cells or inside epithelial cells (*11*, *12*).

Mutualism also appears to exist between the commensal flora and the gut epithelium to maintain epithelial integrity. For example, recognition of TLR2 or TLR9 ligands by epithelial cells increases gut barrier function (*13*, *14*). The normal flora also induces cytoprotective proteins hsp25 and hsp72 in colonic epithelial cells (*15*). Mice deficient in MyD88, the adapter molecule essential for TLR signaling, fail to express epithelial hsp25 and hsp72 (*16*) and are highly susceptible to experimental inflammatory bowel disease (IBD) initiated by dextran sodium sulfate, which suggests that through TLR signaling, the bacterial flora may help protect the gut epithelium from nonspecific damage. Nonpathogenic microorganisms in the gut have also been shown to regulate inflammation negatively in other ways (*17*, *18*). For example, avirulent Salmonella inhibits activation of NF-κB in epithelial cells by blocking polyubiquitination of phosphorylated IκBα (*17*).

Overall, there is good evidence that the normal commensal flora exerts an anti-inflammatory influence and protects epithelial cells from toxic insult. Epithelial pro-inflammatory responses to the commensal flora exist in vitro (*19*, *20*), but most individuals maintain an abundant intestinal flora without incurring disease.

Interactions of commensals with the mucosal immune system. Healthy individuals possess an abundant and highly active gut immune system that is tightly regulated to prevent excessive immune responses to foods and gut bacteria (Fig. 1) (*21*, *22*). A major difference between the systemic and mucosal immune system is the anatomical separation of the inductive sites of mucosal immunity in the organized lymphoid tissue, such as PP, from the effector sites in the lamina propria (LP) and epithelium (Fig. 1) (*22*).

When T and B cells are activated in PP, they express the α4β7 integrin and migrate to the blood (*23*). Gut-specific homing is achieved by expression of the ligand for α4β7, MADCAM-1, on gut endothelial cells, which allows PP-derived cells to migrate through blood vessels into the LP (*23*). Chemokines produced by either colon or small bowel epithelial cells fine-tune the localization of lymphocytes to these tissues (*23*).

The LP is filled with antibody-producing plasma cells that secrete between 3 and 5 g of the IgA immunoglobulin isotype into the gut lumen each day (*22*). Numerous other immune cells also reside in the gut LP, including large numbers of CD4$^+$ T cells (*24*), macrophages, DC, mast cells, and eosinophils (*21*). The gut epithelium also contains abundant intraepithelial lymphocytes (IEL) (*25*), an intriguing population made up mostly of CD8$^+$ T cells. Compared with other tissues, IEL are enriched in T cells expressing the γδ T cell receptor and often express the homodimeric form of the CD8α coreceptor (*26*). The exact function of IEL is not known, although it has been suggested that they may play a role in epithelial tumor surveillance, protection against epithelial pathogens, or promotion of healing of the gut after injury (*25*, *26*).

The presence of an extensive and activated intestinal immune system depends on the commensal flora. Thus, mice bred under germ-free conditions possess small, underdeveloped PP lacking germinal centers, few IgA plasma cells and CD4 cells in the LP, and reduced numbers of IEL. Furthermore, reconstitution of germ-free mice with a microbial flora is sufficient to restore the mucosal immune system (*27*, *28*).

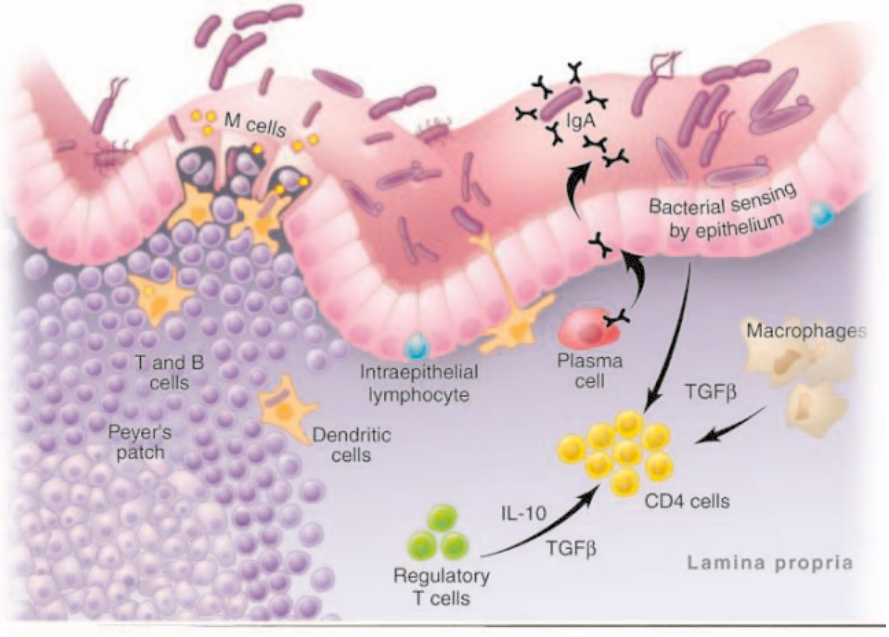

Fig. 1. The gut makes a huge investment in maintaining an extensive and highly active immune system. The epithelium overlying organized gut-associated lymphoid tissue (GALT) contains specialized M cells that constantly transport gut bacteria and antigens from the gut lumen into the lymphoid tissue. DC in the LP reach through epithelial cells and also sample gut bacteria. The epithelium is filled with CD8$^+$ T cells, and the LP contains many CD4 T cells, macrophages, and IgA antibody–producing plasma cells. Potentially tissue-damaging T cell responses may be inhibited by immunosuppressive cytokines and regulatory T cells.

The Commensal Flora as the Antigenic Stimulus for Gut Inflammation

The relationship between the immune system and the commensal flora is a precarious one, and perturbations in immune or epithelial homeostasis can lead to gut inflammation. In this situation, the commensal flora appears to act as a surrogate bacterial pathogen, and it is thought that lifelong inflammation ensues because the host response is incapable of eliminating the flora.

Chronic inflammatory bowel disease in humans. Two main types of IBD exist: Crohn's disease and ulcerative colitis (UC) (*29*) (Table 1). Patients suffer from chronic diarrhea and weight loss, abdominal pain, fever, and fatigue. Extra-intestinal manifestations can also occur, including skin ulcers, arthritis, and bile-duct inflammation, the last especially in UC. Both UC and Crohn's disease are characterized by mucosal ulceration, which is patchy in Crohn's disease but continuous in UC (Fig. 2). In Crohn's disease, ulcers penetrate into the gut wall, and fistulous tracts may develop between loops of bowel or to the skin. The downstream effector pathways that drive tissue injury are similar to those in immune-mediated diseases in other organs. Thus, excess immune activation leads to an influx of inflammatory cells from the blood and to increased concentrations of cytokines, free radicals, and lipid mediators (*30*). There is also massive overexpression of matrix-degrading enzymes, the matrix metalloproteinases, by fibroblasts, which are ultimately responsible for ulceration and fistulae (*30*).

Crohn's disease bears the immunological stigmata of an exaggerated CD4 T helper cell type I response. Thus, intestinal CD4 T

cells isolated from Crohn's patients produce large amounts of the Th1 signature cytokine interferon-γ (*31*) and display marked overexpression of the Th1 cell–specific transcription factor, T-bet (*32*). Mucosal macrophages from Crohn's patients also produce large amounts of the Th1-inducing cytokines IL-12 (*33*) and IL-18 (*34*). Th1 cell resistance to apoptosis and increased cell cycling in Crohn's disease inflammation appear to be sustained by cytokines (*35*, *36*). Blocking the pathways that confer resistance of Th1 cells to apoptotic stimuli and the use of drugs that enhance mucosal T cell death, such as the immunosuppressive agent azathioprine or the antibody to TNFα, Infliximab, are effective in down-modulating intestinal inflammation (*37*–*39*).

Identifying the particular antigen(s) that drive the Th1 inflammatory response in the face of the myriad of potential antigens in the gut has proven difficult. Nevertheless, the likelihood is that bacterial antigens are involved, because stimulation of mucosal CD4 cells from Crohn's disease patients with extracts of their own commensal flora can induce interferon-γ production (*40*), and in murine colitis, flagellin from commensal bacteria also activates mesenteric lymph node CD4 cells (*41*). Clinical observations also support a role for antigens derived from the commensal flora. Thus, for example, the antibiotic metronidazole is of therapeutic benefit in Crohn's disease of the distal colon (*42*).

Gut inflammation induced by the commensal flora: Evidence from animal models. The more than 30 models of IBD in rodents fall into four major groups: colitis that develops spontaneously, chemically induced colitis, colitis that develops from defects in epithelial barrier function, and colitis in mice in which the immune system has been genetically manipulated or regulatory cell function has been disrupted (*43*).

In a number of these models, the absence of commensal bacteria under germ-free conditions leads to an absence of or reduction in disease (*44*). Consistent with evidence from human IBD, there is evidence in some models that CD4 T cell lines reactive to enteric bacterial antigens can cause colitis (*45*), although no individual component of the flora has been yet identified as being specifically important. Nevertheless, in some models, particular bacteria species have been shown to cause disease (*45*). For example, in human leukocyte antigen–B27 (HLA-B27) transgenic rats, monoassociation with *Bacteroides vulgatus* induces colitis, while *Escherichia coli* elicit no lesions. In IL-10–deficient mice, although *B. vulgatus* does not induce colitis, commensal *E. coli* can induce disease (*45*). These models have been enormously important in demonstrating that immune responses to the flora can cause IBD, as well as the numerous pathways that can lead to chronic gut inflammation (*43*).

Crohn's disease susceptibility genes and their relation to innate immunity and intestinal permeability. Crohn's disease and UC represent complex genetic diseases but also tend to run in families. Genome-wide mapping has identified Crohn's disease susceptibility loci on chromosomes 1, 5, 6, 12, 14, 16, and 19 (*46*). In 2001, two groups mapped the locus on chromosome 16 to Nod2 (*47*, *48*). Three major polymorphisms have been specifically associated with ~15% of Crohn's disease cases (Arg702Trp, Gly908Arg, and Leu1007fsinsC), and all are in, or around, the LRR region of the protein required for recognition of bacterial muramyl dipeptide (MDP). Individuals who carry two copies of the risk alleles have a 20- to 40-fold increase in their risk of developing Crohn's disease. About 8 to 17% of Crohn's patients carry two copies of the major risk-associated alleles, compared with 1% of the general population. Interestingly, Nod2 has not been found to be associated with Crohn's disease in Japan (*49*), again highlighting the complex nature of this disease

Nod2 is expressed in the cytosol of gut epithelial cells, macrophages, and DC (*8*). After ligand binding, Nod2 oligomerizes and recruits RICK/RIP, which leads to phosphorylation and degradation of IκB and activation of NF-κB (*50*). A consequence of mutations in Nod2 may therefore be a decreased ability to kill gut bacteria (*51*). Consistent with this, monocytes from patients with common Crohn's disease mutations show defective activation of NF-κB and IL-8 secretion when stimulated with MDP (*52*).

Interestingly, Nod2-deficient mice do not develop spontaneous gut inflammation (*53*, *54*), and their macrophages show normal NF-κB activation and pro-inflammatory cytokine production to ligands for TLR3, 4, and 9. However, they secrete large amounts of IL-12 in response to TLR2 ligands (*55*). Concomitant activation through Nod2 inhibits TLR2 induction of IL-12 in cells from wild-type mice but has no effect in Nod2-deficient mice, suggesting that enhanced IL-12 production in Crohn's disease may be due to a failure of Nod2 to negatively regulate TLR2 signaling, which then facilitates a Th1 response through IL-12. It is not known whether Nod2-mediated negative regulation of TLR2 signaling occurs in Crohn's patients bearing the common mutations. In other studies, macrophages from mice engineered to express the *3020insC* Nod2 mutation show increased activation of NF-κB and increased IL-1β and IL-6 production when activated with MDP, which suggests that Nod2 mutations may, in some situations, lead to a gain of function and increased pro-inflammatory cytokine production (*56*).

Nod2-deficient mice are also unusually susceptible to intestinal infection with the pathogen *Listeria monocytogenes* (*54*) and have been found to be deficient in cryptdin 4 and 10, bacteriacidal defensins produced by Paneth cells found in small intestinal crypts (*57*). In the human gut, Nod2 is highly expressed in Paneth cells (*58*), and reduced defensin expression has been reported in Crohn's patients with Nod2 mutations (*59*). Nod2 mutations may thus also predispose to Crohn's disease indirectly by reducing defensin-mediated innate antimicrobial immunity.

Two other genes associated with Crohn's disease have been identified. The first of these, located on 5q31, encodes the organic cation transporter (OCTN) genes, and mutations at these loci affect the ability of the transporters to pump xenobotics and amino acids across cell membranes (*60*). In the gut, these genes are expressed in epithelial cells, macrophages, and T cells, correlating closely with their potential function in IBD. The second gene is located on 10q23 and encodes the guanylate kinase DLG5 (*61*). The mutation in this gene involves a single amino acid substitution that is thought to impair the ability of DLG5 to maintain epithelial polarity. Both genes may be important in epithelial permeability, and disruption of this function could

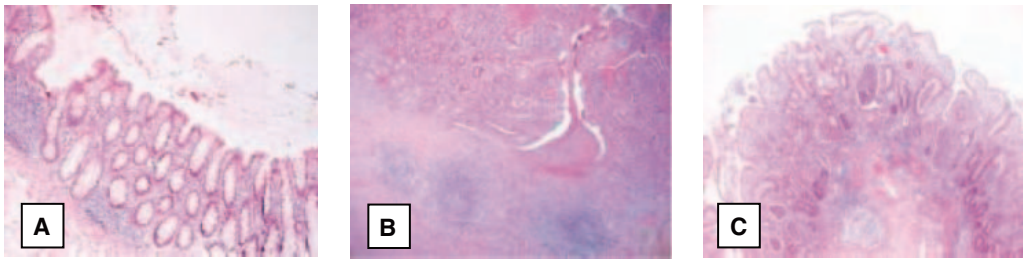

Fig. 2. Histological appearance of (**A**) normal colon, (**B**) Crohn's disease, and (**C**) ulcerative colitis. The normal colon contains glands filled with mucus-producing goblet cells. The image contains a small lymphoid follicle with FAE on the left. In the low-power image of Crohn's disease, the massive mucosal thickening and distortion of the glands is evident, there is a massive lymphoid infiltrate, and an ulcer penetrates through the mucosa from the lumen into the submucosa. In ulcerative colitis, the mucosa is also massively thickened and filled with inflammatory cells. Numerous neutrophil-filled crypt abscesses are present.

Table 1. Inflammatory diseases of the intestine.

	Crohn's disease	Ulcerative colitis	Celiac disease
Incidence	Presently 10–200/100,000 per year. Increased 8 to 10-fold since 1960s.	10–20/100,000 per year. Incidence stable since 1960s.	Around 0.5% of the European and North American population.
Distribution	A disease of westernized societies, with the highest incidence in northern Europe. Excess of cases in urban compared with rural environments.	UC is seen world-wide and appears to show no relation with westernization or affluence.	Restricted to regions of the world where wheat, barley, and rye are a major part of the diet.
Cause	Probably an excessive cell-mediated immune response to antigens of the normal bacterial flora.	Unknown, but perhaps an organ-specific autoimmune disease.	An excessive cell-mediated immune response to the storage proteins of wheat, barley, and rye (gluten) in individuals with HLA-DQ2 or HLA-DQ8 haplotypes.
Site of disease	Can affect any part of the gut from mouth to anus, but most commonly occurs in the ileum and colon. The lesions are characteristically patchy, with areas of normal mucosa between ulcers (skip lesions). Some extra-intestinal involvement.	UC first occurs in the rectum and, as disease progresses, lesions become more proximal. Inflammation is continuous and is restricted to colon.	Upper small intestine—the duodenum and jejunum.
Inflammatory response	Inflammation consists mainly of T cells and macrophages. Granulomas are seen in just over half the cases. Inflammatory cells are present throughout the gut wall, and deep fissuring ulcers can lead to fistulae. Fibrosis of the external muscle layers frequently occurs.	Inflammation is restricted to the mucosa. Neutrophils are the major infiltrating inflammatory cells. These form crypt abscesses and damage the epithelium. There is loss of mucus-secreting goblet cells.	Inflammation restricted to the mucosa. There is a marked mononuclear infiltrate into the lamina propria and an increase in the density of intraepithelial lymphocytes, which results in a transformation of mucosal structure from a situation of long villi and short crypts to the flat mucosa, with short or absent villi.
Other features	Smoking is a risk factor for Crohn's disease.	Smoking appears to protect against the development of UC, as does appendectomy.	Celiac patients show an increased prevalence of autoimmune diseases.
Treatment	Corticosteroids, azathioprine, antibody to TNFα.	Corticosteroids, azathioprine, aminosalicylates.	Gluten-free diet.

lead to inappropriate exposure of the mucosal immune system to bacterial products.

Inflammatory Immune Responses to Food Antigens

The other major antigenic challenge facing the gut derives from ingested food antigens. Under normal circumstances, oral administration of protein antigens induces systemic unresponsiveness when the same antigen is given parenterally (a phenomenon known as oral tolerance). In animal models, oral tolerance appears to be a specific consequence of the immune environment in the gut, which favors the generation of T regulatory cells (*62*). In recent years, food allergy has become increasingly common, and although there has been little progress in understanding host mechanisms involved at the molecular level, there has been great progress in clinical management (*63*).

Celiac disease. In contrast to the lack of progress in understanding food allergy, huge progress has been made in understanding celiac disease. This condition occurs in some genetically susceptible individuals after the ingestion of cereal products, including those from wheat, barley, or rye, and the disease is treated by adherence to a gluten-free diet (Table 1). Many celiacs are undiagnosed (silent celiacs); the disease may affect as many as 0.5 to 1% of the European and North American population. Celiac disease shows classical morphological changes to the mucosa of the upper bowel, with long crypts and partial or complete atrophy of villi.

Celiac disease involves four components: gluten; T cells; the major histocompatability complex locus HLA-DQ; and the endogenous enzyme, tissue transglutaminase (tTG). The past 10 years have seen a huge increase in our understanding of the immunology of celiac disease and how the interplay among these four components produces enteropathy. The original gluten-specific T cell clones isolated from intestinal biopsies of celiac patients were found to respond to a peptic/tryptic digest of gluten restricted by HLA-DQ2 (*64*). The peptide anchor positions of HLA-DQ2 preferentially bind negatively charged amino acids (*65*), yet gluten, which is very proline and glutamine rich, has very few such residues. A key observation in helping resolve this was that tTG, which is expressed ubiquitously in the gut, can deamidate glutamine to glutamic acid, producing the negatively charged residues necessary for efficient binding to DQ2 and for T cell activation (*66*).

In theory, the identification of the immunogenic peptides in gluten would allow the derivation of genetically modified cultivars of wheat that would not cause disease. A polypeptide of α2 gliadin (residues 57 to 89) appears to survive digestion in the gut (*67*). Interestingly, this polypeptide contains three concatemerized epitopes that are recognized by T cells from celiac patients and can be deamidated by tTG; removing this polypeptide could, theoretically, make gluten much less able to activate T cells. However, the in vivo situation is complex because T cell clones have been identified, especially from celiac children, which recognize epitopes of high molecular weight glutenins and diverse gliadin epitopes (*68*, *69*). It may therefore not be possible to remove all disease-inducing T cell epitopes from wheat. An alternative approach may be to modify gluten epitopes so that they tolerize T cells (*70*).

A polypeptide of A-gliadin (residues 31 to 49) produces rapid villus atrophy when infused into the gut of celiac patients (*71*), but of the many T cell lines and clones made against gluten peptides, only a single T cell line clone has been identified that recognizes peptide 31-49 (*72*). However, if a similar peptide, 31-43, is added to ex vivo cultured biopsies

from celiac patients, within hours there is a rapid increase in HLA-DR mRNA, an increase in the number of macrophages making IL-15, and phosphorylation of p38 MAP kinase (*73*), which suggests T cell–independent innate immune activation by gluten.

A number of potential pathways exist to explain the effector mechanisms that cause the pathology in celiac disease (*74*). One of the primary pathways is thought to involve the major histocompatibility complex class I chain–related gene (MICA), which is a dominant ligand for the NKG2D-activating receptor on human NK cells and CD8 T cells. The addition of peptide 31-49 to biopsies of treated celiac disease patients increases MICA on epithelial cells, which can be blocked by antibody to IL-15 and recapitulated by recombinant IL-15 (*75*). NKG2D is expressed on the majority of IEL, and MICA+ epithelial cells have been shown to be killed by NKG2D + IEL (*75*, *76*). It is possible therefore that some peptides of gliadin may activate gut macrophages to produce IL-15, which then increases MICA on epithelial cells and arms IEL to kill MICA+ epithelial cells. Celiac disease is also marked by a significant increase in the numbers of γδ cells, yet their possible role in this condition is not established.

Control of Inflammation in the Gut

Recent years have seen the identification and characterization of dedicated regulatory T cells, in both mice and humans, that have the ability to profoundly suppress a variety of immune responses (*77*, *78*). These regulatory T cells have been shown to be able to significantly control gut inflammation in mouse models of IBD (*79*) and appear to mediate their effects through the cytokines IL-10 and transforming growth factor–β1 (TGFβ1) (*79*). Other work has shown that such cells with specificity for gut bacteria can also inhibit colitis (*80*). It is still not clear whether there is active suppression of T cell responses to the flora in normal mice, because systemic injection of antigens cloned from commensal flora results in a vigorous T cell response, suggesting ignorance rather than specific immune tolerance (*81*).

Compared with their characterization in the mouse, relatively little is known about regulatory T cells in the human gut (*82*). However, the potential for regulatory T cells to suppress IBD in humans through the production of immunosuppressive TGFβ is theoretically limited, because inflammatory cells in IBD lesions express high levels of Smad7, which prevents TGFβ signaling and immune down-regulation (*83*). Nevertheless, the possible role of T regulatory cells in controlling immune responses to bacterial flora in both mice and humans is a question that needs further investigation.

An understanding of how the gut remains disease free in the face of constant immune challenge may involve the separation of the inductive sites in the PP from the effector sites in the rest of the mucosa (Fig. 3) (*22*). Because T cells in the PP may potentially respond to all gut antigens, the problem of activated cells accumulating in the PP is solved by T cells leaving and migrating to the LP. If the T cell has specificity for a pathogen invading the mucosal tissues, antigen-driven cell-mediated immunity in the LP would ensue. However, if the T cell had responded to an antigen from a commensal or a food antigen, in a healthy individual, the epithelial barrier would help prevent the antigen from entering the LP. The few commensal organisms that do cross the barrier will be phagocytosed and killed by macrophages without provoking pro-inflammatory cytokine production (*84*), and in the absence of reactivation the T cells would die by apoptosis.

If this notion is correct, then situations in which the normal flora either enters in increased numbers or persists in the LP should lead to T cell activation and Crohn's-like disease. To support this notion, children with genetic defects that lead to impaired killing of commensal bacteria by phagocytes can develop a condition virtually indistinguishable from Crohn's disease (*85*, *86*). Furthermore, some healthy relatives of Crohn's patients have increased intestinal permeability (*87*), which suggests that genetically determined epithelial permeability is an important contributing factor in the development of disease. Chimeric mice with patchy increases in small intestinal epithelial permeability also develop spontaneous transmural Crohn's-like inflammation (*88*). Considered together, such data suggest that a major determinant in the initiation of mucosal inflammation is the ability of antigen to enter into the LP and trigger T cell activation.

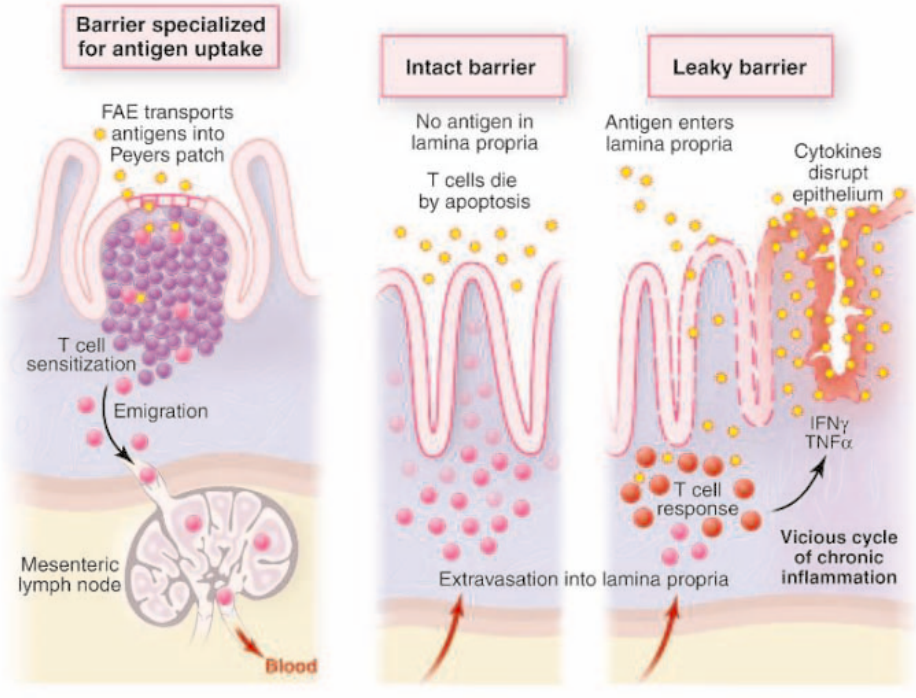

Fig. 3. Increased epithelial permeability may be important in the development of chronic gut T cell–mediated inflammation. CD4 T cells activated by gut antigens in Peyer's patches migrate to the LP. In healthy individuals, these cells die by apoptosis. Increased epithelial permeability may allow sufficient antigen to enter the LP to trigger T cell activation, breaking tolerance mediated by immunosuppressive cytokines and perhaps T regulatory cells. Pro-inflammatory cytokines then further increase epithelial permeability, setting up a vicious cycle of chronic inflammation.

Conclusions

In the evolutionary battle against infectious disease, the immune system cannot afford to err on the side of caution, because failure to mount effective and vigorous immune responses will be exploited by pathogens. This is best exemplified by celiac disease, in which the high prevalence of HLA-DQ2 in the general population suggests an evolutionary advantage of this allele against infection, even in the face of the negative effects of the coincidental affinity of gluten peptides for HLA-DQ2 to cause celiac disease.

With this in mind, it is probably unrealistic to prevent chronic inflammatory diseases, especially in the gut, so attention has to be paid to new treatments based on understanding disease at the molecular level. Great advances have already been made, with the best to date being the therapeutic antibody to TNFα, Infliximab, in Crohn's disease. At the same time, in the gut there is a silent partner

whose influence on the host immune response is only beginning to be appreciated, namely the commensal flora. There are clear indications that the flora is beneficial but also has the potential to be harmful, and increasing knowledge of how the flora interacts with the immune system should allow exploitation of the former and minimization of the latter.

References and Notes

1. S. Husby, J. C. Jensenius, S. E. Svehag, *Scand. J. Immunol.* **22**, 83 (1985).
2. R. D. Berg, *Trends Microbiol.* **3**, 149 (1995).
3. M. R. Neutra, N. J. Mantis, J. P. Kraehenbuhl, *Nature Immunol.* **2**, 1004 (2001).
4. M. Rescigno *et al.*, *Nature Immunol.* **2**, 361 (2001).
5. J. H. Niess *et al.*, *Science* **307**, 254 (2005).
6. D. J. Philpott, S. E. Girardin, *Mol. Immunol.* **41**, 1099 (2004).
7. K. Takeda, S. Akira, *Semin. Immunol.* **16**, 3 (2004).
8. N. Inohara, G. Nunez, *Nature Rev. Immunol.* **3**, 371 (2003).
9. J. M. Otte, E. Cario, D. K. Podolsky, *Gastroenterology* **126**, 1054 (2004).
10. J. Viala *et al.*, *Nature Immunol.* **5**, 1166 (2004).
11. A. T. Gewirtz, T. A. Navas, S. Lyons, P. J. Godowski, J. L. Madara, *J. Immunol.* **167**, 1882 (2001).
12. M. W. Hornef, B. H. Normark, A. Vandewalle, S. Normark, *J. Exp. Med.* **198**, 1225 (2003).
13. K. Madsen *et al.*, *Gastroenterology* **121**, 580 (2001).
14. E. Cario, G. Gerken, D. K. Podolsky, *Gastroenterology* **127**, 224 (2004).
15. K. Kojima *et al.*, *Gastroenterology* **124**, 1395 (2003).
16. S. Rakoff-Nahoum, J. Paglino, F. Eslami-Varzaneh, S. Edberg, R. Medzhitov, *Cell* **118**, 229 (2004).
17. A. S. Neish *et al.*, *Science* **289**, 1560 (2000).
18. D. Kelly *et al.*, *Nature Immunol.* **5**, 104 (2004).
19. D. Haller *et al.*, *J. Biol. Chem.* **278**, 23851 (2003).
20. M. Akhtar, J. L. Watson, A. Nazli, D. M. McKay, *FASEB J.* **17**, 1319 (2003).
21. T. T. MacDonald, *Parasite Immunol.* **25**, 235 (2003).
22. P. Brandtzaeg, R. Pabst, *Trends Immunol.* **25**, 570 (2004).
23. D. J. Campbell, C. H. Kim, E. C. Butcher, *Immunol. Rev.* **195**, 58 (2003).
24. T. T. MacDonald, G. Monteleone, in *Mucosal Immunology*, J. Mestecky, J. Bienenstock, M. Lamm, W. Strober, J. McGhee, L. Mayer, Eds. (Elsevier, San Diego, CA, ed. 3, 2005), pp. 407–413.
25. A. Hayday, E. Theodoridis, E. Ramsburg, J. Shires, *Nature Immunol.* **2**, 997 (2001).
26. H. Cheroutre, *Annu. Rev. Immunol.* **22**, 217 (2004).
27. H. L. Klaasen *et al.*, *Infect. Immun.* **61**, 303 (1993).
28. Y. Umesaki, Y. Okada, S. Matsumoto, A. Imaoka, H. Setoyama, *Microbiol. Immunol.* **39**, 555 (1995).
29. D. Podolsky, *N. Engl. J. Med.* **347**, 417 (2002).
30. T. T. MacDonald, S. L. Pender, in *Kirsner's Inflammatory Bowel Disease*, R. B. Sartor, W. J. Sandborn, Eds. (Saunders, London, 2004), pp. 163–178.
31. T. T. MacDonald, G. Monteleone, *Trends Immunol.* **22**, 244 (2001).
32. M. F. Neurath *et al.*, *J. Exp. Med.* **195**, 1129 (2002).
33. G. Monteleone *et al.*, *Gastroenterology* **112**, 1169 (1997).
34. G. Monteleone *et al.*, *J. Immunol.* **163**, 143 (1999).
35. M. Boirivant *et al.*, *Gastroenterology* **116**, 557 (1999).
36. A. Sturm *et al.*, *Gut* **53**, 1624 (2004).
37. R. Atreya *et al.*, *Nature Med.* **6**, 583 (2000).
38. I. Tiede *et al.*, *J. Clin. Invest.* **111**, 1133 (2003).
39. J. M. Van den Brande *et al.*, *Gastroenterology* **124**, 1774 (2003).
40. R. Duchmann *et al.*, *Clin. Exp. Immunol.* **102**, 448 (1995).
41. M. J. Lodes *et al.*, *J. Clin. Invest.* **113**, 1296 (2004).
42. P. Rutgeerts *et al.*, *Gastroenterology* **108**, 1617 (1995).
43. G. Bouma, W. Strober, *Nature Rev. Immunol.* **3**, 521 (2003).
44. R. B. Sartor, in *Kirsner's Inflammatory Bowel Disease*, R. B. Sartor, W. J. Sandborn, Eds. (Saunders, London, 2004), pp. 138–162.
45. Y. Cong *et al.*, *J. Exp. Med.* **187**, 855 (1998).
46. G. E. Wild, J. D. Rioux, *Best Pract. Res. Clin. Gastroenterol.* **18**, 541 (2004).
47. Y. Ogura *et al.*, *Nature* **411**, 603 (2001).
48. J. P. Hugot *et al.*, *Nature* **411**, 599 (2001).
49. N. Inoue *et al.*, *Gastroenterology* **123**, 86 (2002).
50. Y. Ogura *et al.*, *J. Biol. Chem.* **276**, 4812 (2001).
51. T. Hisamatsu *et al.*, *Gastroenterology* **124**, 993 (2003).
52. J. Li *et al.*, *Hum. Mol. Genet.* **13**, 1715 (2004).
53. A. L. Pauleau, P. J. Murray, *Mol. Cell. Biol.* **23**, 7531 (2003).
54. K. S. Kobayashi *et al.*, *Science* **307**, 731 (2005).
55. T. Watanabe, A. Kitani, P. J. Murray, W. Strober, *Nature Immunol.* **5**, 800 (2004).
56. S. Maeda *et al.*, *Science* **307**, 734 (2005).
57. A. J. Ouellette, *Best Pract. Res. Clin. Gastroenterol.* **18**, 405 (2004).
58. Y. Ogura *et al.*, *Gut* **52**, 1591 (2003).
59. J. Wehkamp *et al.*, *Gut* **53**, 1658 (2004).
60. V. D. Peltekova *et al.*, *Nature Genet.* **36**, 471 (2004).
61. M. Stoll *et al.*, *Nature Genet.* **36**, 476 (2004).
62. A. M. Mowat, *Nature Rev. Immunol.* **3**, 331 (2003).
63. H. A. Sampson, *J. Allergy Clin. Immunol.* **113**, 805 (2004).
64. K. E. Lundin *et al.*, *J. Exp. Med.* **178**, 187 (1993).
65. Y. van de Wal, Y. M. Kooy, J. W. Drijfhout, R. Amons, F. Koning, *Immunogenetics* **44**, 246 (1996).
66. O. Molberg *et al.*, *Nature Med.* **4**, 713 (1998).
67. L. Shan *et al.*, *Science* **297**, 2275 (2002).
68. W. Vader *et al.*, *Gastroenterology* **122**, 1729 (2002).
69. O. Molberg *et al.*, *Gastroenterology* **125**, 337 (2003).
70. C. Y. Kim, H. Quarsten, E. Bergseng, C. Khosla, L. M. Sollid, *Proc. Natl. Acad. Sci. U.S.A.* **101**, 4175 (2004).
71. R. Sturgess *et al.*, *Lancet* **343**, 758 (1994).
72. H. A. Gjertsen, K. E. Lundin, L. M. Sollid, J. A. Eriksen, E. Thorsby, *Hum. Immunol.* **39**, 243 (1994).
73. T. T. MacDonald, M. Bajaj-Elliott, S. L. Pender, *Immunol. Today* **20**, 505 (1999).
74. L. Maiuri *et al.*, *Lancet* **362**, 30 (2003).
75. S. Hue *et al.*, *Immunity* **21**, 367 (2004).
76. B. Meresse *et al.*, *Immunity* **21**, 357 (2004).
77. C. A. Piccirillo, E. M. Shevach, *Semin. Immunol.* **16**, 81 (2004).
78. A. O'Garra, P. Vieira, *Nature Med.* **10**, 801 (2004).
79. K. J. Maloy, F. Powrie, *Nature Immunol.* **2**, 816 (2001).
80. Y. Cong, C. T. Weaver, A. Lazenby, C. O. Elson, *J. Immunol.* **169**, 6112 (2002).
81. C. O. Elson, personal communication.
82. S. Makita *et al.*, *J. Immunol.* **173**, 3119 (2004).
83. G. Monteleone, F. Pallone, T. T. MacDonald, *Trends Immunol.* **25**, 513 (2004).
84. L. E. Smythies *et al.*, *J. Clin. Invest.* **115**, 66 (2005).
85. J. A. Winkelstein *et al.*, *Medicine* (*Baltimore*) **79**, 155 (2000).
86. D. Melis *et al.*, *Acta Paediatr.* **92**, 1415 (2003).
87. R. J. Hilsden, J. B. Meddings, L. R. Sutherland, *Gastroenterology* **110**, 1395 (1996).
88. M. L. Hermiston, J. I. Gordon, *Science* **270**, 1203 (1995).

89. The authors wish to thank L. Sollid for advice and A. Bateman for assistance with the illustrations. T.T.M. receives payment for consultancy to Danone UK Ltd. and Oxagen Ltd.

10.1126/science.1106442

Underwater Bipedal Locomotion by Octopuses in Disguise

Christine L. Huffard,[1]* Farnis Boneka,[2] Robert J. Full[1]

As described in Steinbeck's *Cannery Row* (*1*), "the creeping murderer, the octopus… pretending now to be a bit of weed, now a rock… runs lightly on the tips of its arms." Far from the California tide pools in this book, we have observed octopuses that do indeed walk. Individuals of *Octopus marginatus* (from Indonesia) and *Octopus* (*Abdopus*) *aculeatus* (from Australia) move bipedally along sand using a rolling gait. This locomotion differs from their normal crawling, which usually involves several arms sprawling around the body, using the suckers to push and pull the animal along (*2*).

Underwater video allowed kinematic analyses of the strides (*3*). (A stride is defined as two steps or a complete cycle of leg movements in which a leg returns to its initial relative position.) While crawling quickly, *O. marginatus* draws six arms around its body and moves backward on the backmost (ventral) arm pair (Fig. 1A and movie S1). The animal is pushed back as each arm tip alternates rolling along the oral face (sucker edge) of approximately its distal half. The phase is variable (Fig. 1B), sometimes with short periods during which no arm is on the bottom. On average, each arm is on the sand for more than half the stride, which kinematically qualifies these strides as walking (duty factor 0.56, SD 0.08, $n = 4$ strides, two each from two animals). Two individual *O. marginatus*, both ~55 mm in mantle (or body sac) length (ML), moved bipedally at 1.2 and 2.6 ML per s, corresponding to ~0.06 and ~0.14 m/s, respectively. These speeds are slightly faster than the average speed calculated for the same octopuses crawling with several arms (1.1 ML per s, SD 0.36, or 0.06 m/s, SD 0.02; $n = 4$ strides, two each from two animals).

O. aculeatus moves bipedally in a slightly different manner. Walking is preceded by a cryptic display in which the octopus coils and raises the two front (dorsal) arms above its head and generally sits on the other six (this is named the "flamboyant display") (*4*). *O. aculeatus* may then raise the four lateral arms and walk backward using the ventral arms (Fig. 1D and movie S2). Relative to mantle length, *O. aculeatus* has longer arms than *O. marginatus*, and this is evident in their stride. The distal ~75% of the walking arm rolls under the body, sometimes completing more than a full wheel (Fig. 1D, frame 4). The octopus rolls along the sand as if on alternating conveyer belts. The phase of this stride is also variable, but at least one of the two arms is always on the bottom (duty factor: right arm, 0.69; left arm, 0.91) (Fig. 1C), kinematically qualifying this movement as walking.

Bipedal locomotion has been thought to require the opposition of muscle against a rigid skeleton (*5*). Instead, transverse, longitudinal, and oblique bands of muscle in the arms allow octopuses exceptional flexibility, while their internal volume remains constant and provides support (*6*). Bends propagate down single arms from base to tip in a relatively stereotyped wavelike fashion (*7*) that appears to underlie bipedal locomotion in these animals. This motion has been elicited in severed arms, without direct control from the brain (*7*, *8*), and we hypothesize that it allows the octopuses described here to move bipedally with minimal neural feedback.

Crypsis is the primary defense of most octopuses, yet camouflage requires cephalopods to remain still or move only very slowly (*9*). When an octopus moves quickly, it becomes visually conspicuous and must employ unique behaviors to evade its predator's search image (*9*). By walking, both *O. marginatus* and *O. aculeatus* are able to move quickly while using six of their arms to remain disguised: *O. marginatus* perhaps as a rolling coconut and *O. aculeatus* as a clump of algae tiptoeing away.

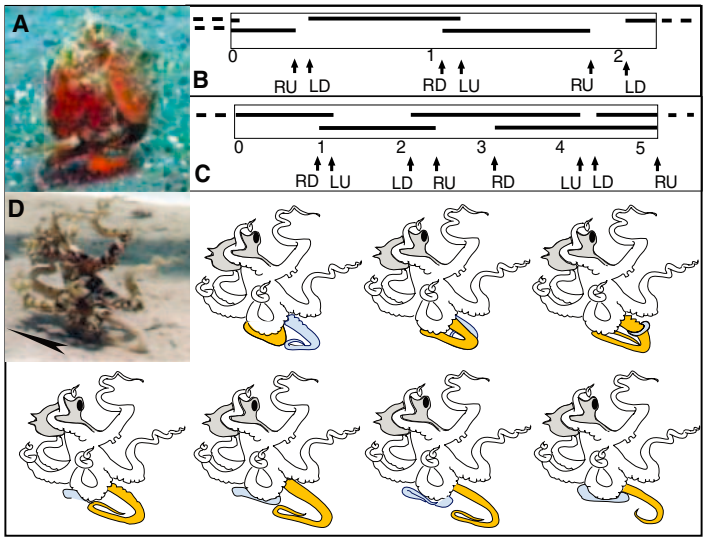

Fig. 1. Kinematics of bipedal movements in octopuses. (**A**) Video frame of *O. marginatus* walking bipedally. (**B**) Phase diagram of *O. marginatus*. L, left arm; R, right arm; U, arm lifted from the bottom; D, arm placed on the bottom. (**C**) Phase diagram of *O. aculeatus*. (**D**) Gait diagram of *O. aculeatus* drawn from video (7/60-s lapse between each panel). The arrowhead in the first frame indicates the direction of walking. Six arms (white) coil, raise off the bottom, and obscure the head and mantle (gray). The right arm (orange) pushes the animal backward throughout the sequence. The left arm (blue) is lifted from the bottom in frame 4 and replaced on the bottom in frame 5. At least one arm is in contact with the bottom at all times. (Video courtesy of Sea Studios, Inc.)

References and Notes

1. J. Steinbeck, *Cannery Row* (Viking, New York, 1945).
2. J. A. Mather, *J. Comp. Psychol.* **112**, 306 (1998).
3. Materials and methods are available as supporting material on *Science* Online.
4. A. Packard, G. D. Sanders, *Anim. Behav.* **19**, 780 (1971).
5. C. L. Vaughan, *J. Biomech.* **36**, 513 (2003).
6. W. M. Kier, K. K. Smith, *Zool. J. Linn. Soc.* **83**, 307 (1985).
7. Y. Gutfreund, T. Flash, G. Fiorito, B. Hochner, *J. Neurosci.* **18**, 5976 (1998).
8. G. Sumbre, Y. Gutfreund, G. Fiorito, T. Flash, B. Hochner, *Science* **293**, 1845 (2001).
9. R. T. Hanlon, J. W. Forsythe, D. E. Joneschild, *Biol. J. Linn. Soc.* **66**, 1 (1999).
10. Supported by an American Malacological Society Student Research Grant to C.L.H. and by NSF Frontiers in Integrative Biological Research grant no. 0425878 to R.J.F. Video of *O. marginatus* is provided by Sea Studios, Inc., Monterey, CA, USA (cameraman, Bob Cranston).

Supporting Online Material
www.sciencemag.org/cgi/content/full/307/5717/1927/DC1
Materials and Methods
Movies S1 and S2

11 January 2005; accepted 14 February 2005
10.1126/science.1109616

[1]Department of Integrative Biology, University of California, Berkeley, CA 94720–3140, USA. [2]Department of Fisheries and Marine Science, Universitas Sam Ratulangi, Manado, North Sulawesi, Indonesia.

*To whom correspondence should be addressed. E-mail: chuffard@berkeley.edu

Widespread Parallel Evolution in Sticklebacks by Repeated Fixation of Ectodysplasin Alleles

Pamela F. Colosimo,[1] Kim E. Hosemann,[1] Sarita Balabhadra,[1] Guadalupe Villarreal Jr.,[1] Mark Dickson,[3] Jane Grimwood,[3] Jeremy Schmutz,[3] Richard M. Myers,[3] Dolph Schluter,[4] David M. Kingsley[1,2]

Major phenotypic changes evolve in parallel in nature by molecular mechanisms that are largely unknown. Here, we use positional cloning methods to identify the major chromosome locus controlling armor plate patterning in wild threespine sticklebacks. Mapping, sequencing, and transgenic studies show that the Ectodysplasin (EDA) signaling pathway plays a key role in evolutionary change in natural populations and that parallel evolution of stickleback low-plated phenotypes at most freshwater locations around the world has occurred by repeated selection of *Eda* alleles derived from an ancestral low-plated haplotype that first appeared more than two million years ago. Members of this clade of low-plated alleles are present at low frequencies in marine fish, which suggests that standing genetic variation can provide a molecular basis for rapid, parallel evolution of dramatic phenotypic change in nature.

Particular phenotypic traits often evolve repeatedly when independent populations are exposed to similar ecological conditions (*1*, *2*). The threespine stickleback species complex (*Gasterosteus aculeatus*) provides an ideal system for further studying the molecular mechanisms that underlie widespread parallel evolution of phenotypic traits in nature. Parallel evolution within this species complex has occurred in countless freshwater lake and stream environments colonized by marine sticklebacks after widespread melting of glaciers 10,000 to 20,000 years ago. The young age of the freshwater populations, the ability to generate fertile hybrids between divergent populations, and the recent development of stickleback genomic resources make it possible to map the genes that control evolutionary change and to compare the genetic basis of similar traits that have evolved in different locations (*3*–*7*).

Several marine phenotypes have changed repeatedly in new freshwater environments, which includes reduction of the extensive bony armor found in ocean fish (*8*, *9*). Marine sticklebacks typically have a continuous row of 32 to 36 armor plates extending from head to tail ("complete" morph, Fig. 1A). In contrast, innumerable freshwater populations have a gap in the middle of the row of plates ("partial" morph), or retain only zero to nine plates at the anterior end ("low" morph, Fig. 1A) (*10*, *11*). Several factors have been proposed that could contribute to the selective advantage of armor plate reduction after colonization of new lakes and streams by completely plated marine ancestors, including low calcium levels, increased body flexibility and maneuverability, changes in swimming performance, and changes in predation regimes in freshwater environments (*12*–*17*).

Positional cloning of the plate morph region. Further understanding of the molecular basis of parallel evolution requires the identification of the genes and mutations that underlie major phenotypic change. We previously used genome-wide linkage mapping in a marine by freshwater F_2 cross to show that armor plate patterns are controlled primarily by a single major QTL that maps to linkage group IV and by four minor modifier QTL that cause smaller quantitative variation in the size and number of plates (*4*). To refine the position of the major locus, we screened for new amplified fragment-length polymorphism markers (*18*) that differed in allele size or frequency in pools of low and completely plated progeny from a marine by freshwater cross. Newly isolated markers *Stn345* and *Stn346* were much more closely linked than previous markers, defining a new interval of 0.68 cM for the plate morph locus (Fig. 1B).

Stn345 and *Stn346* were used to screen a bacterial artificial chromosome (BAC) library derived from completely plated marine fish from Salmon River, Canada (SRMA) (*7*). Three rounds of chromosome walking led to the isolation of six overlapping BAC clones spanning the interval of interest (Fig. 1B). In a total of 1166 chromosomes, *Stn345* and BAC end marker *Stn347* mapped two recombination events proximal and one recombination event distal of the plate morph locus, respectively. These recombination events define a physical region of about 539 kb that must contain the plate morph locus. BAC clones A and B (Fig. 1B) were completely sequenced during the chromosome walk, generating a contiguous sequence assembly of 407,051 base pairs (bp) derived from the plate morph region.

Linkage disequilibrium screening. Meioses and interbreeding in natural populations tend to homogenize allele frequencies at most loci. However, particular alleles that are very closely linked to a mutation of interest may remain in linkage disequilibrium with that mutation for many generations (*19*). To test for possible linkage disequilibrium in the region controlling plate morph phenotypes, we designed microsatellite markers at intervals of ~12 kb throughout the BAC sequence assembly and examined the distribution of alleles at each marker in a sample of 46 completely and 45 low-plated fish from a single interbreeding wild population from Friant, CA (FRI) (*4*, *20*). The difference in allele distribution at *Stn365* in completely and low-plated fish was 10^7 times more significant than the differences at flanking markers *Stn364* and *Stn366*, which define a region of peak linkage disequilibrium of ~16 kb (Fig. 1C).

Gene predictions show that the marker at the peak of linkage disequilibrium is located within intron 2 of the stickleback *Ectodysplasin* (*Eda*) gene. EDA is a member of the tumor necrosis family of secreted signaling molecules and, in mammals, is required for proper development of a number of ectodermal derivatives (e.g., teeth, hair, and sweat glands) and dermal bones (*21*, *22*). Previous studies have shown that a mutation in the *Ectodysplasin receptor* (*Edar*) gene in medaka (*Oryzias latipes*) causes loss of most scales (*23*), which are elements of the dermal skeleton (*24*). Many elements of the dermal skeleton in fishes, including scales and the dermal lateral plates of sticklebacks, have likely evolved from a common ancestral element (*24*). The position of *Eda* at the peak of linkage disequilibrium in the stickleback candidate interval and the known role of EDA signaling in scale formation suggested that changes in the *Eda* locus may underlie the molecular basis of plate morph evolution in sticklebacks.

[1]Department of Developmental Biology and [2]Howard Hughes Medical Institute, Stanford University School of Medicine, Stanford, CA 94305–5329, USA. [3]Department of Genetics and Stanford Human Genome Center, Stanford University, Stanford, CA 94305–5120, USA. [4]Zoology Department and Biodiversity Research Centre, University of British Columbia, Vancouver, British Columbia, Canada, V6T 1Z4.

***Eda* structure in low and complete morphs.** To compare the structure of *Eda* and linked genes in marine and freshwater sticklebacks, we isolated two overlapping BAC clones from a library derived from the low-plated benthic Paxton Lake, Canada population (PAXB) (*7*), and completely sequenced the *Eda* region. Comparison to the sequence of the completely plated SRMA marine population identified numerous non-coding changes (table S2), and four mutations that lead to amino acid changes in EDA protein (Fig. 2). None of the amino acid changes occur at sites that are highly conserved between mammals and fish or in residues that have previously been associated with defects in humans (*25*, *26*). Three of the four sites also vary among other fish species.

Previous studies in mammals have shown that *Eda* undergoes alternative splicing to produce two protein isoforms that differ in length by two amino acids and bind different receptors (*27*, *28*). Both splicing isoforms were recovered from developing low- and completely plated fish (10- to 20-mm standard length) with the use of reverse transcription polymerase chain reaction (RT-PCR), and no other splicing changes were seen in the low-plated fish.

We also generated probes to examine the spatial pattern of expression of *Eda* in sticklebacks, but we were unable to detect significant *Eda* expression in any samples using whole-mount in situ hybridization, even at stages where we could recover spliced *Eda* mRNA using RT-PCR. Difficulties in detecting *Eda* expression by in situ hybridization have also been reported in several other organisms, presumably because of low levels of expression during normal development (*29*, *30*).

Molecular basis of parallel evolution. Because previous complementation and genetic mapping results suggest that the same major locus controls lateral plate patterning in multiple freshwater populations around the world (*2*, *4*, *6*), we expanded the survey of *Eda* sequence to 10 completely plated marine populations and 15 low-plated populations collected from sites throughout the Northern Hemisphere (Fig. 3A, table S1). It was interesting that most of the low-plated populations, although from diverse regions, shared many of the base-pair changes previously seen in the PAXB population. One clear exception was a low-morph population from Nakagawa Creek, Japan (NAKA), which had no mutations that would alter the EDA amino acid sequence found in marine sticklebacks (SRMA) (Fig. 2). Previous genetic crosses show that low-plated fish from the NAKA population fail to complement the low-plated phenotype of fish from Salmon River, British Columbia (SRST) (*2*), a population that does share the characteristic *Eda* sequence changes seen in PAXB and most other low-plated populations. These data suggest that the low-plated phenotype in NAKA is due to an independently derived allele of *Eda*.

To further analyze the history of sequence changes in the plate morph region, we built phylogenetic trees using 1328 bp of exon and intron sequence from the *Eda* locus (Fig. 3B). Bayesian, maximum parsimony, and maximum likelihood trees all showed that *Eda* sequences from every low-plated population except NAKA belonged to a distinct clade (posterior probability of 1.00 in MrBayes trees and bootstrap support of 99.7 and 100% in parsimony and maximum likelihood trees, respectively). These results show that *Eda* alleles of most low-plated populations share a common ancestry. The exception is the low-plated allele within the NAKA population, which clearly has a separate origin.

Despite the shared ancestry of *Eda* alleles, it is highly unlikely that an ancestral population of low-plated fish migrated through the ocean to found most other low-plated populations in freshwater lakes and streams around the world. Ocean sticklebacks are virtually always completely plated. In addition, previous phylogenetic analysis of mitochondrial sequences reject the possibility that low-plated fish have a single origin (*9*, *31*, *32*). To further test whether low-plated populations have multiple origins, we amplified sequences from 25 random nuclear genes and scored single-nucleotide polymorphisms (SNPs) at 193 sites from 20 different completely and low-plated populations. Trees built from the nuclear sequences showed no evidence for a single origin of low-plated populations (Fig. 3C). The

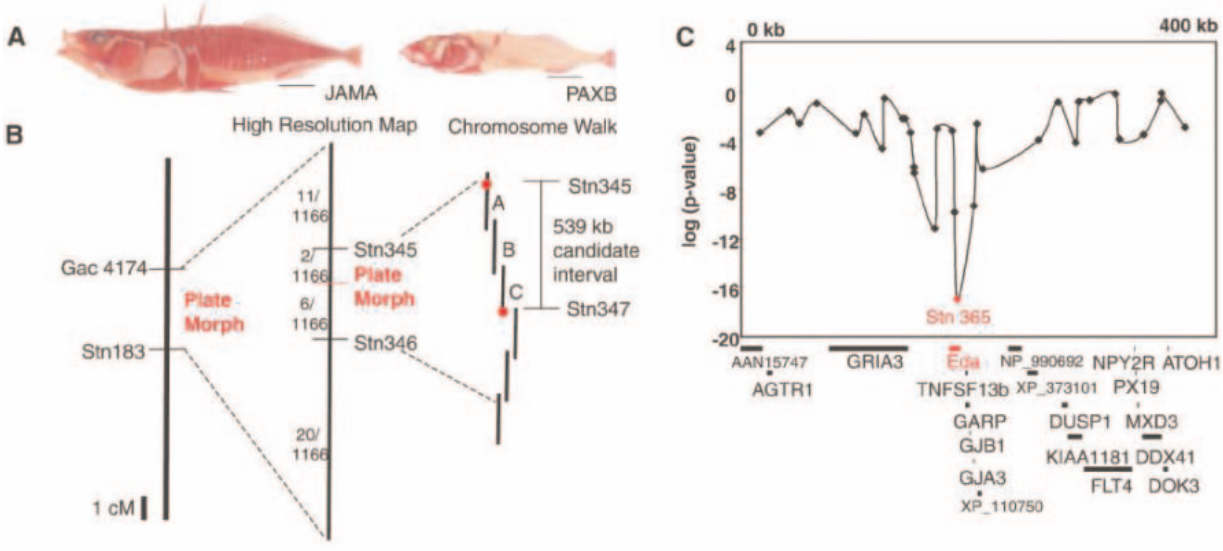

Fig. 1. Genetic, physical, and linkage disequilibrium map of the plate morph interval. (**A**) Complete and low-morph phenotypes in alizarin red–stained specimens (*4*) of Japanese Marine (JAMA, left) and benthic Paxton Lake (PAXB, right) sticklebacks, the parent populations of a large F_2 mapping cross. Other skeletal changes evident in PAXB fish, such as reduction of pelvis and spines, map to different chromosomes (*5*). Scale bars, 1 cm. (**B**) High-resolution genetic and physical mapping. Newly isolated markers *Stn345* and *Stn346* rarely recombine with the plate morph locus (numbers of recombinants in 1166 chromosomes shown). Six overlapping BAC clones span the genetic interval, and markers *Stn345* and *Stn347* (red dots) map to opposite sides of the plate morph locus. (**C**) Linkage disequilibrium screening. Two sequenced BAC clones were used to develop new microsatellite markers (*Stn348*–*Stn379*) located 15, 39, 48, 63, 96, 103, 118, 120, 135, 137, 142, 145, 145, 163, 165, 177, 179, 182, 195, 198, 203, 250, 267, 282, 284, 293, 315, 319, 339, 353, 354, and 374 kilobases from *Stn345* (black dots). *Stn365*, located in the stickleback *Eda* locus, showed large differences in allele frequency in completely and low-plated fish from Friant, CA. Positions of other genes in the sequenced interval are shown, with human genome nomenclature committee (HGNC) designations, or accession numbers of the best matches in National Center for Biotechnology Information (NCBI) BLAST searches.

best-supported branches were related by geography rather than plate phenotype. For example, a clade from the Atlantic ocean contained both completely and low-plated populations (posterior probability of 1.00 in MrBayes trees and bootstrap support of 68 and 54% in maximum likelihood and parsimony trees, respectively). The topologies of EDA and nuclear sequence trees for identical populations were significantly different, whether trees were constructed using Bayesian and maximum likelihood methods (Kishino-Hasegawa tests: $P < 0.0005$), or maximum parsimony approaches (Wilcoxon signed rank test: $P < 0.0001$). Most important, the nuclear data firmly reject the specific hypothesis of monophyly for all low-plated populations except NAKA (Kishino-Hasegawa test on maximum likelihood trees: $P < 0.0005$, Wilcoxon test on parsimony trees: $P < 0.0015$). On the basis of these and the previous mitochondrial studies, current low-plated populations are clearly not derived from a single low-plated population that has colonized different environments.

The most likely interpretation to account for the global sharing of closely related low-plated alleles at the *Eda* locus is that the alleles controlling the low-plated phenotype are present at some frequency in marine populations. To test this, we collected large samples of completely plated fish at the ocean outlets of the Navarro River in California (NAV) and the Little Campbell River in British Columbia (LITC). We typed DNA samples from all individuals with two markers that are located within introns 2 and 6 of *Eda* and that distinguish complete and low-morph alleles found in most populations (*Stn380* and *Stn381*). Eight of 109 completely plated fish from NAV were heterozygous for complete and low-morph alleles at both markers, which gave an estimated frequency of low-morph alleles of 3.8% (8/218 chromosomes). One of 302 completely plated marine sticklebacks collected from LITC was also heterozygous at both markers and gave an estimated allele frequency of 0.2% (1/604 chromosomes). These experiments confirm that the alleles shared by low-plated fish are also present at modest levels in completely plated migratory marine fish and suggest that worldwide evolution of the low-plated phenotype has occurred mainly by recurrent local selection for a family of alleles repeatedly brought into freshwater populations by marine founders.

Size and age of the shared genomic region in low-morph populations. To define the boundaries of the region of shared ancestry in different low-plated fish, we compared the sequence of *Eda* exons and selected flanking regions in different populations. Haplotype analysis showed that most low-plated populations shared characteristic sequences at positions extending from exon 1 of *Eda* through the flanking genes *Tumor necrosis factor (ligand) superfamily member 13b* (*Tnfsf13b*), *Glycoprotein A rich protein* (*Garp*), and *Gap junction protein beta 1* (*Gjb1*) (Table 1). However, low morphs from some populations resembled marine animals at either exon 1 of *Eda*, near the final exon of *Garp*, or at the sole exon of *Gjb1* (Table 1). These recombinant haplotypes show that the minimal interval conserved in low-plated fish is 16 kb, which spans intron 1 of *Eda* through the end of the coding region of *Garp*. Information from the entire conserved low haplotype is present in heterozygous form within the migratory marine individual from the Little Campbell River (LITC58) (Table 1).

To estimate the age of the shared haplotype, we examined the rate of neutral sequence evolution at third–base pair positions from all genes (*EDA* to *Garp*) in the shared region. The number of synonymous base pair substitutions per synonymous site (K_s) in the complete (SRMA) and low-morph (PAXB) haplotypes was larger than the number observed between Japan Marine (Pacific Ocean) (JAMA) and Japan Sea (JASE) [thought to have diverged ~2 million years ago on the

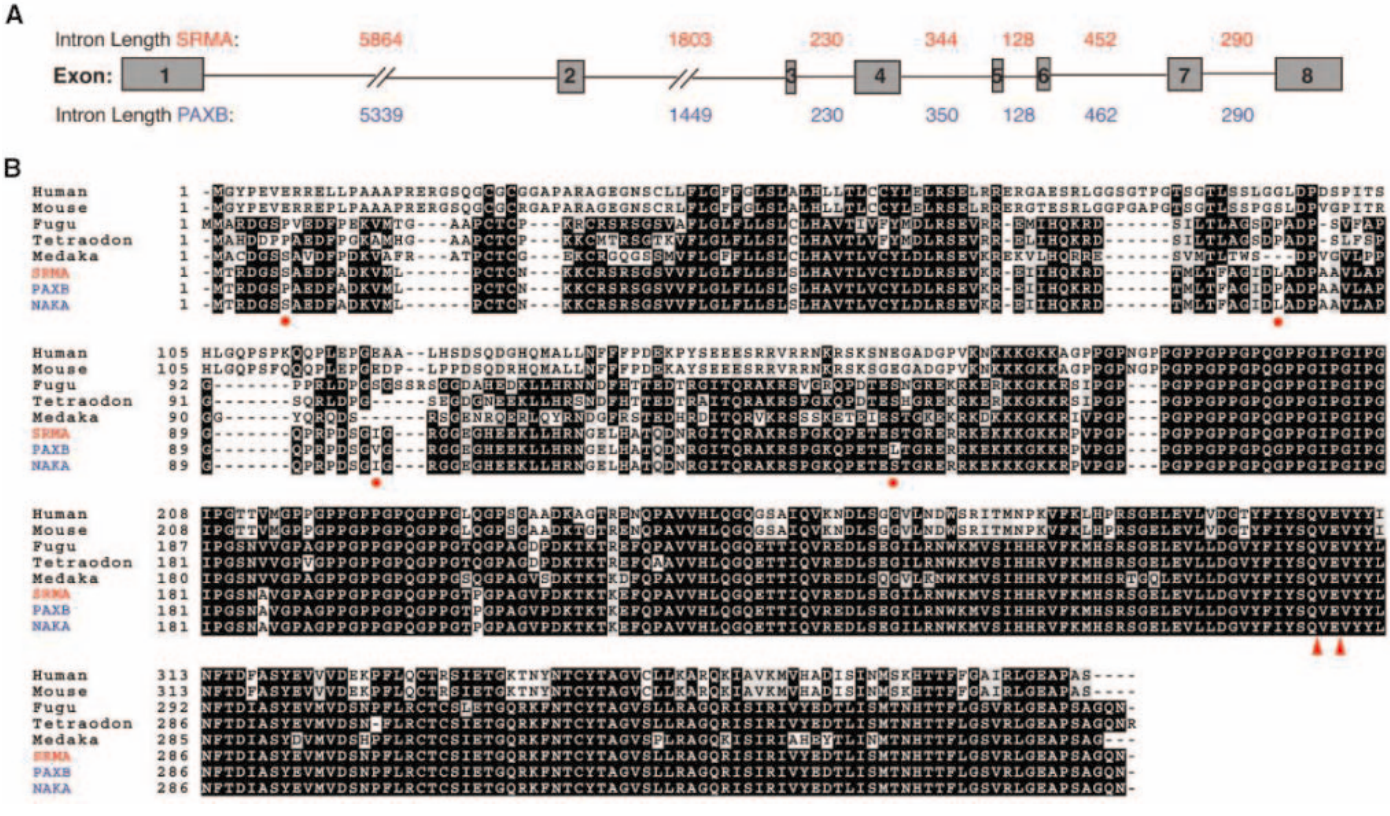

Fig. 2. Structure and sequence of stickleback Ectodysplasin. (**A**) The stickleback *Eda* locus is shown with exons shaded. Intron lengths differ in the marine (SRMA) and freshwater (PAXB) fish. (**B**) Alignment of EDA protein sequences from human, mouse, *Fugu*, *Tetraodon*, *Medaka*, SRMA (complete morph), PAXB (low morph), and NAKA (low morph) sticklebacks. Red arrowheads mark the two amino acids that differ in EDA-A1 and EDA-A2 splice forms. Red dots indicate amino acids different between PAXB and SRMA. Identical amino acids are shaded black, and conservative substitutions are shaded grey.

basis of genetic and geological estimates (*33*)], but smaller than the number between *G. aculeatus* (SRMA) and the sister species *G. wheatlandi* [thought to have diverged ~ten million years on the basis of the split between Pacific and Atlantic populations (*8*)] (K_s values of 0.01938, 0.01384, and 0.05875, respectively). The common clade of low-plated alleles thus probably arose between 2 and 10 million years ago. This date is at least 100 to 1000 times older than the recent divergence of modern stickleback populations in postglacial lakes and streams that formed at the end of the last Ice Age.

EDA-A1 transgenic sticklebacks develop extra lateral plates. Although the previously established role of EDA signaling in dermal bone and scale development (*23*) makes *Eda* a compelling candidate for the locus controlling lateral plate phenotypes, several other genes are present in the shared haplotype found in most low-plated populations. To test directly whether changing levels of EDA signaling could alter plate development in sticklebacks, we injected one-cell embryos from low-plated parents with a full-length mouse EDA-A1 cDNA under the control of the broadly expressed human cytomegalovirus (CMV) promoter. This construct has previously been shown to restore development of teeth, hair, and sweat glands when introduced into *Tabby* mutant mice carrying a null mutation at the *Eda* locus (*34*). Because of the mosaic inheritance of injected DNA constructs in transgenic sticklebacks (*35*), we scored injected and control siblings for mosaic patches of ectopic lateral plate formation after raising animals to 33- to 40-mm standard length. PCR genotyping confirmed that all fish from the cross were homozygous for an indel marker in intron 1 of *Eda* that is characteristic of the low-morph allele. Of 23 injected animals, 14 were also positive for the transgene (Fig. 4B). All 33 control siblings displayed the expected low-morph phenotype, having eight or fewer anterior plates per side (Fig. 4A). However, 3 out of 14 transgene-positive animals developed extra plates on their sides and caudal peduncles. The animal shown in Fig. 4, C and D, had six extra plates on its left side and one keel plate on its right peduncle. The other transgenic fish with additional plates also displayed them in a mosaic fashion, with one fish having one extra plate on the right side and two keel plates on the left peduncle and the other animal having one extra plate on the right side and two extra plates on the left side. No extra plates developed after injection of low-plated embryos with constructs containing the same vector backbone and a GFP insert instead of the EDA cDNA (*35*). These results confirm that EDA signaling is sufficient to trigger lateral plate formation on both the flank and tail regions of the body and that introduction of *Eda* transgenes can partially rescue the low-plated phenotype of freshwater sticklebacks.

Mutational spectrum in mammals and sticklebacks. In both humans and mice, a diverse set of mutations in three different genes of the EDA signaling pathway cause nearly indistinguishable defects in hair, teeth, sweat glands, and bone (*21*, *22*). In contrast, our studies show that widespread evolution of low-plated phenotypes in sticklebacks has occurred by repeated selection of a small number of related alleles at *Eda*. Several factors may account for this narrow spectrum of alleles that produce the low-plated phenotype. The diverse human *Eda* mutations (*25*, *26*), originally identified in rare patients with a medical disorder, have pleiotropic effects that would decrease fitness in the wild. By contrast, the low-plated phenotype in sticklebacks represents the first known example whereby specific *Eda* alleles have been repeatedly fixed by natural selection in the wild. The limited amino acid changes seen in most low-plated fish and the absence of any amino acid changes in the NAKA population suggest that natural variation in lateral plates is likely caused by coding or regulatory alleles of *Eda* that are not null mutations. Such limited changes may avoid the pleiotropic effects of a complete loss-of-function of *Eda* and thereby produce a spectrum of mutations very different from those found in human patients.

In addition, the repeated fixation of a particular haplotype at the *Eda* locus could be due to coselection for additional phenotypes produced by genes closely linked to *Eda*. Low-plated populations show correlated changes in salt tolerance (*36*), parasite susceptibility (*37*), and behavior (*38*, *39*). Although our transgenic results show that changes in lateral plate patterning are controlled by *Eda* itself, the multiple linked coding and noncoding changes in the common haplotype could also influence the structure or regulation of *Tnfsf13b*, *Garp*, or *Gjb1*. *Tnfsf13b* has previously been implicated in B cell development (*40*) and parasitic worm load in humans (*41*). The functions of *GARP* are unknown, but *Gjb1* belongs to a family of connexins that can produce changes in myelination and conduction velocity of neurons, hearing, skin thickness, and salt secretion (*42*). Related nonplate phenotypes caused by closely linked genes may contribute to the overall selective advantage of the ancient low-morph haplotype in freshwater (*36*).

Table 1. Distinctive haplotypes surrounding *Eda* in completely and low-plated sticklebacks. Genotypes are shown at 22 selected SNP positions throughout the plate morph region. Ten different completely plated (red) populations (AKMA, GJOG, JAMA, JASE, LITC, LLOY, NEU, NHR, SRMA, NAV) and four low-plated (blue) populations (BLAU, PAXB, WMSO, SFC) differ at all 22 positions, defining a shared haplotype characteristic of most complete and low populations. Recombinant haplotypes in SCX, FADA, PAXL, NOST, WALL, AKST, COND, SRST, and FRIL populations define a minimum shared haplotype, including SNPs 5-15. SNP genotypes in the completely plated LITC58 animal confirm that low-plated alleles are present in migratory marine populations. SNPs are either intergenic (I), synonymous (S), or nonsynonymous (N) changes and are located at the following nucleotide positions in the CHORI213-2D11 BAC sequence: 195422 (EDA Ser7Pro), 195496 (EDA Ser31Ser), 195649 (EDA Leu79Pro), 195692 (EDA Ile97Val), 203488 (EDA Ser140Leu), 203815 (EDA Pro172Pro), 207116 (TNFSF13B Leu69Phe), 208941 (TNFSF13B Gly197Gly), 208557 (TNFSF13B Ile219Ile), 210237 (GARP Met197Leu), 210240 (GARP Leu198Leu), 211414 (GARP Ser589Ile), 211415 (GARP Ser589Ile), 211573 (GARP Phe642Cys), 211615, 211677, 221853, 221944 (GJB1 His16His), 222209 (GJB1 Val105Ile), 222692 (GJB1 Thr266Ala), 222758, and 222759.

	EDA						TNFSF13B			GARP					Intergenic			GJB1			Intergenic	
Exon:	1	1	1	1	3	4	2	6	6	2	2	2	2	2	-	-	-	1	1	1	-	-
Type of Change:	N	S	N	N	N	S	N	S	S	N	S	N	S	N				S	N	N		
SNP:	1	2	3	4	5	6	7	8	9	10	11	12	13	14	15	16	17	18	19	20	21	22
10 COMPLETE POPULATIONS	T	T	T	A	C	G	G	C	C	A	T	G	C	T	T	C	T	C	G	A	G	T
4 LOW POPULATIONS	C	C	C	G	T	A	C	T	T	C	C	T	T	G	A	G	A	T	A	G	A	G
SCX (26)	T	T	T	G	T	A	C	T	T	C	C	T	T	G	A	G	A	T	A	G	A	G
FADA (23)	T	T	T	A	T	A	C	T	T	C	C	T	T	G	A	G	A	T	A	G	A	G
PAXL (8)	T	T	T	A	T	A	C	T	T	C	C	T	T	G	A	G	A	T	G	A	G	T
NOST (24)	C	C	C	G	T	A	C	T	T	C	C	T	T	G	A	C	T	C	G	A	G	T
WALL (4), AKST (5), & COND (12)	C	C	C	G	T	A	C	T	T	C	C	T	T	G	A	G	A	T	G	A	G	T
SRST (9)	C	C	C	G	T	A	C	T	T	C	C	T	T	G	A	G	A	T	A	A/G	G/A	T/G
FRIL (15)	C	C	C	G	T	A	C	T	T	C	C	T	T	G	A	G	A	T	A	G	G/A	T/G
OMPL(19)	C	C	T	G	T	A	C	T	T	C	C	T	T	G	A	G	A	T	A	G	A	G
LITC58 (10)	T/C	T/C	T/C	A/G	C/T	G/A	G/C	C/T	C/T	A/C	T/C	G/T	C/T	T/G	T/A	C/G	T/A	C/T	G/A	A/G	G/A	T/G
NAKA (1)	T	T	T	A	C	G	G	C	C	A	T	G	C	T	T	C	T	C	G	A	G	T

Mechanism for rapid parallel evolution. Forty years ago, Lindsey proposed that parallel evolution of stickleback lateral plate patterns could occur either by independent mutations in different populations or by repeated selection on the standing genetic variation already present in marine ancestors (*43*). Our studies show that both mechanisms have contributed. The EDA sequences in low-plated NAKA fish are distinct from those in other low populations (Fig. 3B). However, the presence of a shared haplotype in most low-plated populations suggests that selection on standing variation is the predominant mechanism underlying the recent rapid evolution of changes in lateral plate patterns in wild sticklebacks.

One surprising finding of this study is the enormous geographical distance over which related low-plated alleles are shared. Both nuclear and mitochondrial data (*9*, *31*, *32*) rule out the possibility that these alleles have spread by migration of a single low-plated population of fish throughout the world. In contrast, our surveys of large numbers of marine fish show that low-plated alleles are present at detectable frequencies in completely plated sticklebacks. This low frequency is likely maintained by the occasional hybridization that occurs when marine sticklebacks come into contact with low-plated freshwater populations in coastal streams during the breeding season (*38*) or perhaps by fitness effects in heterozygotes. The annual migration of marine sticklebacks from ocean to freshwater could provide a mechanism for repeated flow of the ancient low-morph alleles back into marine populations and, from there, into new freshwater environments. Fish heterozygous for completely and low-plated alleles at *Eda* typically have either complete or partial lateral plates (*4*, *6*), facilitating the persistence of a cryptic genetic variant within marine populations, and providing a genetic mechanism that could lead to rapid emergence of the low-plated phenotype after colonization of new environments.

The differences in armor plate patterns of sticklebacks are so large that Cuvier originally classified plate morphs as distinct species (*10*).

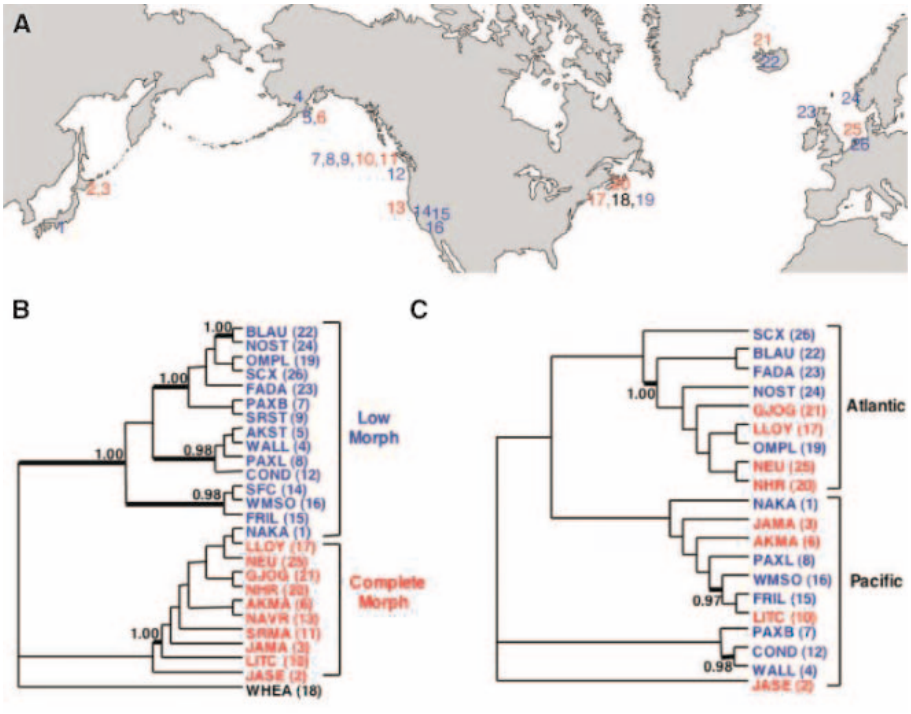

Fig. 3. Most low-plated populations have a shared history at the *Eda* locus, but not at other nuclear genes. (**A**) Geographic origin of 25 low-plated (blue numbers) and completely plated (red numbers) stickleback populations used for sequencing. (**B**) MrBayes tree of *Eda* sequences. *G. wheatlandi*, a sister species of *G. aculeatus*, was used as an outgroup (black, number 18). *Eda* alleles in most low populations share a common origin. Posterior probabilities greater than 95% are shown (branches in bold). (**C**) MrBayes phylogeny based on genetic differences in 193 SNPs from 25 random nuclear loci. Tree topology is significantly different from the EDA tree, ruling out the possibility that all present-day low-plated populations are derived from a single population sharing alleles at most genes.

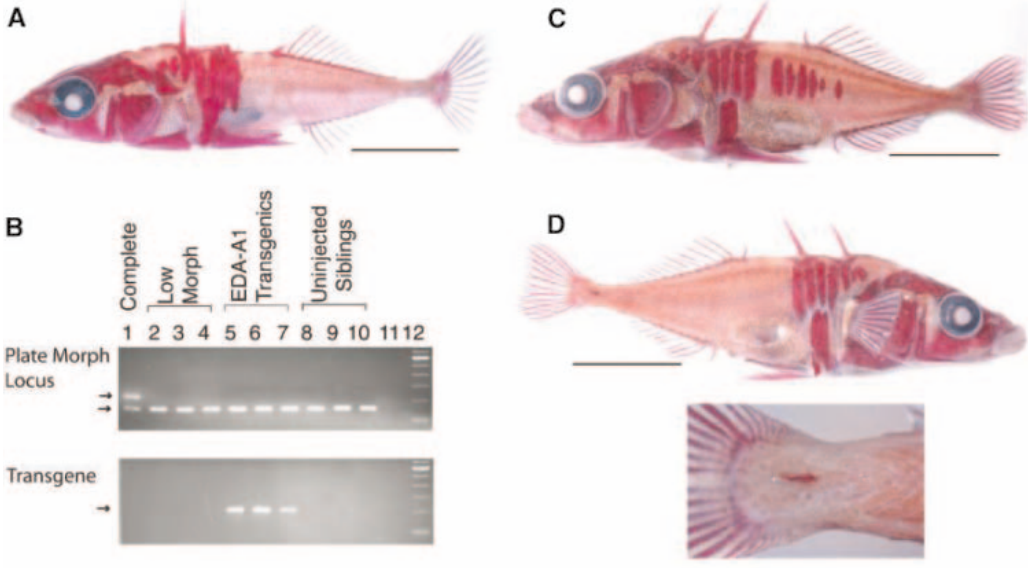

Fig. 4. EDA-A1 stimulates lateral plate formation in transgenic sticklebacks. (**A**) Typical low-plated pattern in control fish stained with alizarin red. (**C** and **D**) A sibling from the same clutch after introduction of a transgene containing a full-length mouse EDA-A1 cDNA driven by a CMV promoter (*34*). Note six extra lateral plates that have formed in the flank region on the left side (C), and the new keel plate on the right tail (D). Differences in spine number are due to clipping for DNA recovery. Scale bars, 1 cm. (**B**) (top) PCR genotyping confirms that transgenic animals are homozygous for a 150-bp allele characteristic of the ancestral low-plated allele at the endogenous *Eda* locus, just like wild-caught low-plated fish from FRI, San Francisquito Creek (SFC) and uninjected siblings. In contrast, completely plated fish from FRI are either heterozygous for the 218-bp allele and the 150-bp allele (lane 1) or homozygous for the 218-bp allele (not shown). (B) (bottom) Primers specific for mouse EDA-A1 amplify a 211-bp fragment from transgenic fish, but not from uninjected control animals. Genomic DNA samples: Lane 1, FRI Complete; 2, FRI Low; lanes 3 to 4, SFC Low; lanes 5to 7, EDA-A1 transgenic animals with additional lateral plates; lanes 8 to 10, uninjected siblings of EDA-A1 transgenic animals; lane 11, water control; lane 12, 100-bp DNA size ladder (Invitrogen).

In the past, it has been difficult to trace such large-scale changes in body form to the action of particular genes and mutations. Our results show that large changes in vertebrate skeletal morphology in the wild can be created by relatively simple genetic mechanisms. Natural populations have variants of the same major signaling genes already known to play a crucial role in normal development and human disease. The variant alleles preexist at low frequency in ancestral marine populations and can be repeatedly fixed in new environments to produce a rapid shift to an alternative body form. Many other dramatic morphological, physiological, and behavioral changes are known in sticklebacks. With the recent advent of forward genetic approaches in this system, it should now be possible to identify the genes that underlie many ecologically important traits, which will bring a new molecular dimension to the study of how phenotypic changes arise during vertebrate evolution.

References and Notes

1. D. J. Futuyma, *Evolutionary biology* (Sinauer Associates, Sunderland, MA, ed. 3, 1998).
2. D. Schluter, E. A. Clifford, M. Nemethy, J. S. McKinnon, *Am. Nat.* **163**, 809 (2004).
3. C. L. Peichel *et al.*, *Nature* **414**, 901 (2001).
4. P. F. Colosimo *et al.*, *PLoS Biol.* **2**, 635 (2004).
5. M. D. Shapiro *et al.*, *Nature* **428**, 717 (2004).
6. W. A. Cresko *et al.*, *Proc. Natl. Acad. Sci. U.S.A.* **101**, 6050 (2004).
7. D. M. Kingsley *et al.*, *Behavior* **141**, 1331 (2004).
8. M. A. Bell, S. A. Foster, Eds., *The Evolutionary Biology of the Threespine Stickleback* (Oxford Univ. Press, Oxford, 1994).
9. B. E. Deagle, T. E. Reimchen, D. B. Levin, *Can. J. Zool.* **74**, 1045 (1996).
10. G. L. Cuvier, M. A. Valenciennes, *Histoire naturelle des poissons: Tome quatrieme* (Chez F. G. Levrault, Paris, 1829).
11. D. W. Hagen, L. G. Gilbertson, *Evolution Int. J. Org. Evolution* **26**, 32 (1972).
12. N. Giles, *J. Zool.* **199**, 535 (1983).
13. E. B. Taylor, J. D. McPhail, *Can. J. Zool.* **64**, 416 (1986).
14. C. A. Bergstrom, *Can. J. Zool.* **80**, 207 (2002).
15. D. W. Hagen, L. G. Gilbertson, *Heredity* **30**, 273 (1973).
16. T. E. Reimchen, *Evol. Int. J. Org. Evol.* **46**, 1224 (1992).
17. T. E. Reimchen, *Behaviour* **137**, 1081 (2000).
18. D. G. Ransom, L. I. Zon, *Methods Cell Biol.* **60**, 195 (1999).
19. E. S. Lander, D. Botstein, *Cold Spring Harb. Symp. Quant. Biol.* **51**, 49 (1986).
20. J. C. Avise, *Genet. Res.* **27**, 33 (1976).
21. I. Thesleff, M. L. Mikkola, *Sci. STKE* **2002**, pe22 (2002).
22. A. T. Kangas, A. R. Evans, I. Thesleff, J. Jernvall, *Nature* **432**, 211 (2004).
23. S. Kondo *et al.*, *Curr. Biol.* **11**, 1202 (2001).
24. J. Y. Sire, A. Huysseune, *Biol. Rev. Camb. Philos. Soc.* **78**, 219 (2003).
25. K. Paakkonen *et al.*, *Hum. Mutat.* **17**, 349 (2001).
26. M. C. Vincent, V. Biancalana, D. Ginisty, J. L. Mandel, P. Calvas, *Eur. J. Hum. Genet.* **9**, 355 (2001).
27. M. Bayes *et al.*, *Hum. Mol. Genet.* **7**, 1661 (1998).
28. M. Yan *et al.*, *Science* **290**, 523 (2000).
29. J. Kere *et al.*, *Nature Genet.* **13**, 409 (1996).
30. M. L. Mikkola *et al.*, *Mech. Dev.* **88**, 133 (1999).
31. G. Orti, M. A. Bell, T. E. Reimchen, A. Meyer, *Evol. Int. J. Org. Evol.* **48**, 608 (1994).
32. E. B. Taylor, J. D. McPhail, *Biol. J. Linn. Soc.* **66**, 271 (1999).
33. M. Higuchi, A. Goto, *Environ. Biol. Fishes* **47**, 1 (1996).
34. A. K. Srivastava *et al.*, *Hum. Mol. Genet.* **10**, 2973 (2001).
35. K. E. Hosemann, P. F. Colosimo, B. R. Summers, D. M. Kingsley, *Behavior* **141**, 1345 (2004).
36. M. J. Heuts, *Evol. Int. J. Org. Evol.* **1**, 89 (1947).
37. J. MacLean, *Can. J. Zool.* **58**, 2026 (1980).
38. D. W. Hagen, *J. Fish. Res. Board Can.* **24**, 1637 (1967).
39. G. E. E. Moodie, J. D. McPhail, D. W. Hagen, *Behaviour* **47**, 95 (1973).
40. B. Schiemann *et al.*, *Science* **293**, 2111 (2001).
41. S. Williams-Blangero *et al.*, *Proc. Natl. Acad. Sci. U.S.A.* **99**, 5533 (2002).
42. C. J. Wei, X. Xu, C. W. Lo, *Annu. Rev. Cell Dev. Biol.* **20**, 811 (2004).
43. C. C. Lindsey, *Can. J. Zool.* **40**, 271 (1962).

44. We thank K. Peichel, J. McKinnon, B. Jónsson, F. von Hippel, M. Kalbe, S. Mori, K. Olivera, and members of the Kingsley laboratory for generous help with fish collecting and population samples; D. Schlessinger and V. Thermes for the pCI neo-Eda A1 and pISceI-pBSIISK+ plasmids; J. Weir for help with phylogenetic analysis; M. McLaughlin for fish care; and W. Talbot, K. Peichel, and lab members for useful comments on the manuscript. This work was supported in part by a Center of Excellence in Genomic Science grant from the National Institutes of Health (1P50HG02568; D.M.K., R.M.M.); the Ludwig Foundation (D.M.K.); and the Natural Sciences and Engineering Research Council and the Canada Foundation for Innovation (D.S.). D.S. is a Canada Research Chair, and D.M.K. is an Investigator of the Howard Hughes Medical Institute. This work is dedicated in fond memory of Kim Hosemann, a passionate and talented scientist who died a few months after completing the key transgenic experiments.

Supporting Online Material

www.sciencemag.org/cgi/content/full/307/5717/1928/DC1
Materials and Methods
Fig. S1
Tables S1 and S2
References and Notes

8 November 2004; accepted 12 January 2005
10.1126/science.1107239

Temporal Relationships of Carbon Cycling and Ocean Circulation at Glacial Boundaries

Alexander M. Piotrowski,*† Steven L. Goldstein, Sidney R. Hemming, Richard G. Fairbanks

Evidence from high-sedimentation-rate South Atlantic deep-sea cores indicates that global and Southern Ocean carbon budget shifts preceded thermohaline circulation changes during the last ice age initiation and termination and that these were preceded by ice-sheet growth and retreat, respectively. No consistent lead-lag relationships are observed during abrupt millennial warming events during the last ice age, allowing for the possibility that ocean circulation triggered some millenial climate changes. At the major glacial-interglacial transitions, the global carbon budget and thermohaline ocean circulation responded sequentially to the climate changes that forced the growth and decline of continental ice sheets.

Records of past global climate preserve evidence of large-scale changes in temperature and ice volume at glacial-interglacial boundaries. Although the timing of ice ages is broadly driven by Milankovich orbital cycles, the small insolation changes require amplifying mechanisms to produce the large glacial-interglacial climate changes. Fluctuation in North Atlantic Deep Water (NADW) production is a potential amplifier and has been suggested as a trigger for rapid global climate shifts (*1*). Carbon dioxide (CO_2) is another possible amplifier on glacial-interglacial time scales, because its atmospheric concentration is predominantly controlled by changes in deep-ocean storage (*2*) and the terrestrial carbon reservoir (e.g., *3*–*5*). Carbon isotope ratios are distinct in different reservoirs, making it a powerful tool to constrain the timing of global carbon budget reorganizations relative to other changes in the climate system. In the oceans, carbon isotope ratios of benthic foraminifera (benthic $\delta^{13}C$) are commonly used as a proxy for ocean circulation because they vary systematically in water masses [e.g., (*6*–*8*)]. However, temporal benthic $\delta^{13}C$ changes at any location reflect a combination of the global carbon mass balance, ocean-circulation changes, air-sea equilibration, and productivity changes. If carbon budget and ocean-circulation signals can be deconvolved, the temporal sequence of major shifts in global ice volume, carbon mass balance, and ocean circulation can help to clarify the ocean's role as a trigger of, or a response to, major climate changes. In this study, we compare the temporal sequence of these changes since the last interglacial period. Chronological ambiguities are obviated through study of different proxy signals in the same core, and thus the sequence of events associated with climate change and ocean circulation can be extracted.

Nd isotopic systematics. We use Nd isotopes as a proxy of the balance between NADW and southern-sourced waters in the South Atlantic. $^{143}Nd/^{144}Nd$ ratios vary in the

Lamont-Doherty Earth Observatory and Department of Earth and Environmental Sciences, Columbia University, Palisades, NY 10964, USA.

*Present address: Department of Earth Sciences, Cambridge University, Downing Street, Cambridge, CB2 3EQ, UK.
†To whom correspondence should be addressed. E-mail: apio04@esc.cam.ac.uk

Earth as a result of the α decay of ^{147}Sm ($t_{1/2} \sim 106 \times 10^9$ years), and in the oceans, the values reflect the age of the continental sources of dissolved Nd (*9*). The utility of Nd isotopes as a paleocirculation proxy stems from its variability in the oceans. In seawater and Fe-Mn nodule and crust surfaces, Nd isotope ratios geographically vary over a large range from $\varepsilon_{Nd} < -20$ in the Labrador Sea to values as high as $\varepsilon_{Nd} \sim 0$ in the northwest Pacific (*10*). Unlike low-mass stable isotope and element ratios, Nd isotope ratios do not show measurable mass-dependent fractionation by biological and low-temperature processes (*11*). Nd isotopes are conservative in seawater unless new Nd is added along the transport path. Water-column profiles show that water masses conserve the Nd isotopic fingerprint of the dissolved Nd source regions over long transport paths. For example, the NADW Nd isotope signature ($\varepsilon_{Nd} \sim -14$) can be traced into the South Atlantic, and the Antarctic Bottom Water (AABW) signature ($\varepsilon_{Nd} \sim -7$ to -9) can be traced northward in the Atlantic (*9*, *12*, *13*).

The Nd isotopic signal of deep-water masses can be preserved at submillennial time resolution in the Fe-Mn oxide fraction of deep-sea cores, and recent studies found Nd isotopic variability in the oceans on glacial-interglacial and millennial time scales (*14*–*18*). This study focuses on cores RC11-83 (40°36′S, 9°48′E, 4718 m) and TNO57-21 (41°08′S, 7°49′E, 4981 m) from the Cape Basin, southeast Atlantic (tables S1 and S2), whose chronology is based on radiocarbon ages and spliced stable isotope stratigraphy (*8*, *18*–*20*). High sedimentation rates (~20 and ~15 cm/1000 years, respectively) allow subcentury-scale temporal resolution. An initial application of Nd isotope ratios of Fe-Mn leachates in RC11-83 at orbital time resolution (*15*) showed that the NADW signals were stronger during warmer climate intervals and weaker during cold intervals through the last ice age. These variations were subsequently confirmed in a Holocene to Last Glacial Maximum (LGM) profile of core MD96-2086 from the northern Cape Basin (*16*, *21*). Our more detailed studies of RC11-83 and TNO57-21 show fine-scale variability that parallels other climate proxies (*18*) (Fig. 1). The previous studies include extensive discussions of evidence that Nd isotope ratios in the Fe-Mn oxide leachates of these cores reflect deep seawater (*15*, *16*, *18*, *22*). In RC11-83/TNO57-21, Sr isotope ratios are indistinguishable from Quaternary seawater ($^{87}Sr/^{86}Sr \sim 0.7092$) and much lower than associated terrigenous detritus (0.717 to 0.723) (*23*). This precludes detrital contamination of the leached Sr. Nd is less likely to be contaminated by the detritus, because it is much less soluble than Sr. Moreover, bottom-water SiO_2 concentrations (*24*) and core top leachate Nd isotope ratios are consistent with ε_{Nd}-SiO_2 covariations of present-day Atlantic seawater (*15*).

Climate transitions. During Marine Isotope Stages (MIS) 1 and 5, Nd isotopes are the most NADW-like (Fig. 1), whereas during MIS 2 and 4 (full glacial stages), values shift beyond modern Southern Ocean values of $\varepsilon_{Nd} \sim -7$ to -9 (*9*), indicating that the Southern Ocean was more Pacific-like than today. Major Nd isotope shifts occurred at the MIS 5a/4 and 2/1 boundaries. Millennial excursions occur between MIS4/5 and the LGM, corresponding in timing and form to Greenland interstadials 3, 4, 8, 12, 14, and 17 on the basis of comparison to Greenland ice cores $\delta^{18}O$ records (*25*–*27*). Piotrowski *et al.* (*18*) discuss the detailed temporal relationships between changes in Nd isotope ratios and Greenland ice $\delta^{18}O$ during the most recent deglaciation. For example, there is increased NADW during the Bølling warming, a decline during the Allerød cooling, and an increase from the Younger Dryas minimum (labeled YD; see Fig. 1B) to the early Holocene. In contrast, there is no corresponding effect during the Antarctic Cold Reversal (ACR). These associations demonstrate a strong linkage between Northern Hemisphere climate variability and the Nd isotope ratios of South Atlantic deep waters.

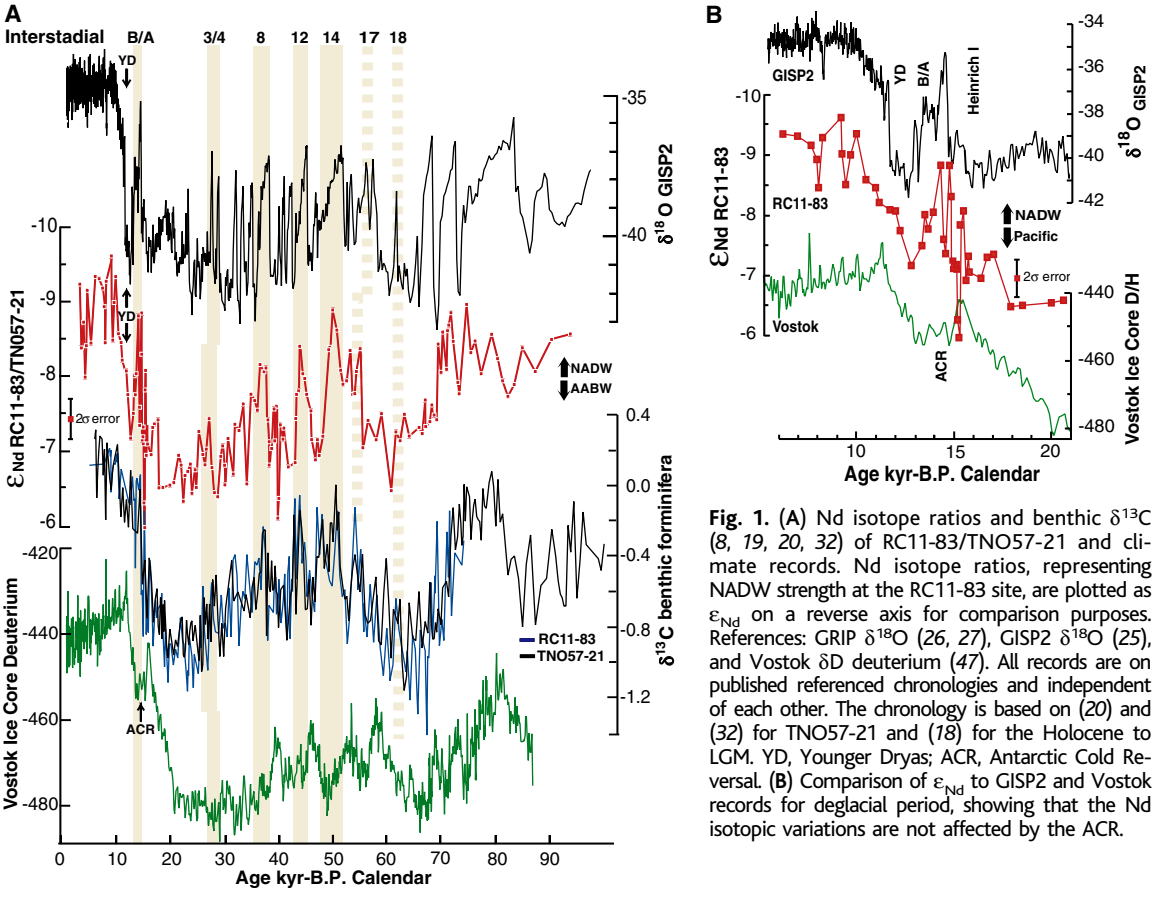

Fig. 1. (**A**) Nd isotope ratios and benthic $\delta^{13}C$ (*8*, *19*, *20*, *32*) of RC11-83/TNO57-21 and climate records. Nd isotope ratios, representing NADW strength at the RC11-83 site, are plotted as ε_{Nd} on a reverse axis for comparison purposes. References: GRIP $\delta^{18}O$ (*26*, *27*), GISP2 $\delta^{18}O$ (*25*), and Vostok δD deuterium (*47*). All records are on published referenced chronologies and independent of each other. The chronology is based on (*20*) and (*32*) for TNO57-21 and (*18*) for the Holocene to LGM. YD, Younger Dryas; ACR, Antarctic Cold Reversal. (**B**) Comparison of ε_{Nd} to GISP2 and Vostok records for deglacial period, showing that the Nd isotopic variations are not affected by the ACR.

The covariation of the temporal patterns of benthic $\delta^{13}C$ and Nd isotopes on long-term and millennial time scales (Fig. 1) confirms earlier conclusions that the benthic $\delta^{13}C$ pattern mimics ocean-circulation changes (*8*, *19*, *20*). However, the magnitude of the benthic $\delta^{13}C$ changes over glacial-interglacial cycles are too large to have been caused entirely by water-mass mixing. The mean $\delta^{13}C$ of the deep ocean reflects the climate-forced partition of carbon between terrestrial and ocean carbon reservoirs. The deep ocean $\delta^{13}C$ was 0.46‰ to 0.32‰ lower during ice ages than today (*28*–*30*), likely caused by increased storage of ~500 gigatons of terrestrial organic carbon ($\delta^{13}C$ ~ –25‰) in the ocean (*31*). The interglacial to glacial benthic $\delta^{13}C$ shift of ~–0.8‰ in RC11-83/TNO57-21 overshoots the glacial Pacific end member by ~–0.4‰ (*32*–*34*), which reflects additional productivity and perhaps air-sea exchange and local pore-water effects in the Southern Ocean (*35*).

To isolate the noncirculation effects on the benthic $\delta^{13}C$ signal, we use Nd isotopes to monitor thermohaline circulation and interpret the $\delta^{13}C$ shifts that are unsupported by the Nd isotope record as caused by non-circulatory effects. A cross-plot of the entire data set is compared to Holocene and glacial binary mixing curves for global end-member water masses (Fig. 2A). The Nd isotope ratios fall between the NADW and Pacific end members throughout, whereas the $\delta^{13}C$ data lie below the mixing lines and shift beyond the glacial Pacific value during glacial climate. The NADW-Pacific mixing lines are an oversimplification of the ocean-circulation system (Fig. 2), which we regard as reference lines allowing a first-order evaluation of large non-circulation effects on Southern Ocean $\delta^{13}C$. They assume that the temporal variability of the Nd isotope ratios is not controlled by shifts in the end-member water masses. Our previous studies extensively discuss the current constraints on the Pacific and North Atlantic end members (*15*, *18*) and are only summarized here. There is strong evidence for stability of Nd isotope ratios of deep Pacific seawater (*36*). Constraining the Nd isotope ratio of NADW through time is more problematic because of encroachment of AABW into the North Atlantic during cold climate and shallowing of northern-sourced deep waters and the failure of Fe-Mn oxides leached from many North Atlantic cores to yield marine Sr isotope ratios (*37*). Rutberg *et al.* [figure 2a in (*15*)] addressed the issue indirectly by comparing bottom-water SiO_2 concentrations (*24*) and Nd isotope ratios in global Fe-Mn nodules and crusts with the modern seawater-dissolved SiO_2-ε_{Nd} trend. Samples from Fe-Mn nodules and crusts represent average ambient water values over 10^5 to 10^6 years, encompassing several glacial cycles. Most of the North Atlantic data lie on the modern SiO_2-ε_{Nd} trend, indicating a roughly constant NADW Nd isotope signature. Recent suggestions that the Nd isotope signature of glacial NADW may have been lower (e.g., *38*–*40*) than the present day would not affect our primary conclusions (*41*).

Further insights into the Nd isotope-benthic $\delta^{13}C$ relationships are gained by separating the data into discrete time slices. Although all the data (Fig. 2A) show a negative correlation, the glacial-interglacial transitions (MIS 5a/4 and LGM-Holocene) data outline a "parallelogram" (Fig. 2B), and those from the MIS 4/3 through the LGM fill its gap (Fig. 2C). Further examination shows that the parallelogram reflects the temporal relationships between Nd and carbon isotope shifts. For example, the data associated with the last deglaciation (Fig. 3A) exhibit a two-stage change. The LGM to Bølling warming data lie on a steep trend, because the $\delta^{13}C$ undergoes a major change toward its Holocene range, whereas the Nd isotopes show a small shift. The benthic $\delta^{13}C$ increases by 0.8‰, representing 90% of the total LGM to Holocene shift, whereas the Nd isotopes decrease by ~–0.6 ε_{Nd} units, representing only ~15% of its total shift. The shallow trend of the post-Bølling data reflects the major glacial-interglacial Nd isotope shift occurring after the benthic $\delta^{13}C$ had already shifted to the interglacial mode. These observations indicate that the ε_{Nd}-$\delta^{13}C$ coupling before the Bølling warming was distinct from that afterward. The pre-Bølling interval was associated with substantial climate amelioration and glacial retreat in Europe (*42*). The data indicate that for ~1500 years before the Bølling warming (*43*), initial melting of the continental ice sheets was associated with large changes in the deep-water $\delta^{13}C$ and small variations in deep-water circulation.

Deep-water $\delta^{13}C$ shifted before the Bølling warming, at which time it had already attained its Holocene composition. After the Bølling warming, benthic $\delta^{13}C$ was primarily affected by changes in the balance of the water masses. The shallow slope of the mixing curves (Fig. 2) illustrates that Nd isotopes are a more sensitive proxy for water-mass mixing than benthic

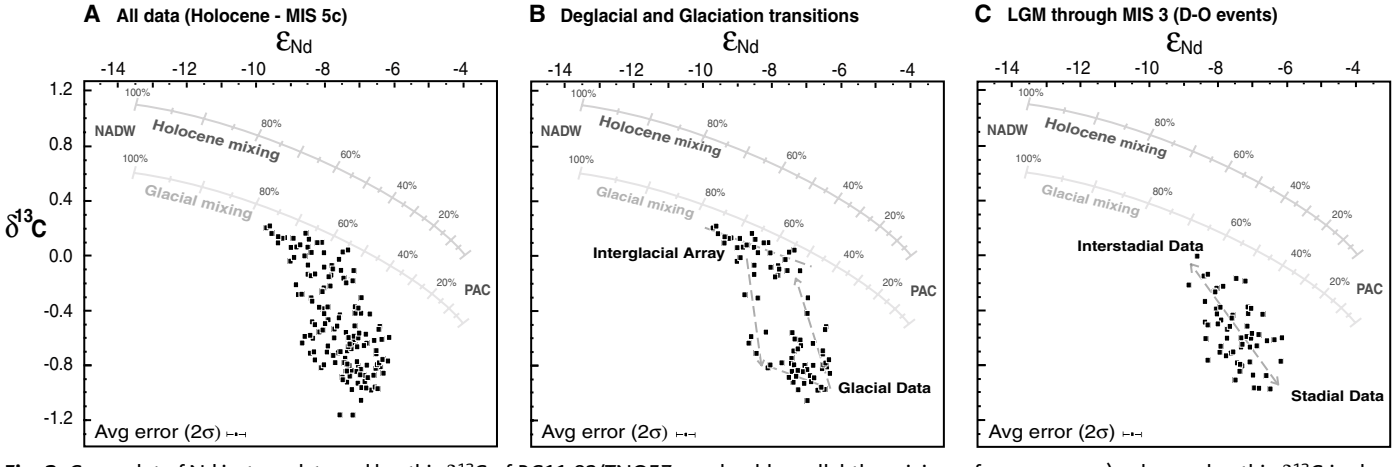

Fig. 2. Cross-plot of Nd isotope data and benthic $\delta^{13}C$ of RC11-83/TNO57-21. (**A**) The entire 100,000-year record. (**B**) Only the glaciation (MIS 5a-4) and deglacial (LGM-Holocene) transitions. (**C**) Only glacial interstadial events (within MIS 3 and early MIS 2). Simple binary mixing curves are shown between NADW and Pacific (PAC) isotopic end members for the Holocene and the LGM; the $\delta^{13}C$ difference between them is the 0.4‰ mean ocean $\delta^{13}C$ difference (*28*–*30*) due to ocean-biosphere carbon budget change (*31*). The Nd isotopes and benthic $\delta^{13}C$ recorded by RC11-83/TNO57-21 are monitoring the relative mixing proportion of NADW and Pacific-sourced waters in the Southern Ocean (changes in which should parallel the mixing reference curves), whereas benthic $\delta^{13}C$ is also affected by noncirculatory carbon budget changes. Dashed arrows show sequential Nd isotope-benthic $\delta^{13}C$ changes relative to general ocean mixing (Fig. 3). NADW-Pacific mixing curves are based on the following parameters. For the Holocene end members, –NADW: ε_{Nd} = –13.5, Nd = 21 pmol/kg, $\delta^{13}C$ = 1.1, dissolved CO_2 = 2175 umol/kg; Pacific: ε_{Nd} = –4, Nd = 40 pmol/kg, $\delta^{13}C$ = 0.0, dissolved CO_2 = 2350 umol/kg. For the Glacial end members, NADW: $\delta^{13}C$ = 0.6; Pacific: $\delta^{13}C$ = –0.5; all other parameters are the same. Mixing curves are based on (*32*–*34*, *48*–*51*). Benthic $\delta^{13}C$ are from (*8*, *19*, *20*, *32*).

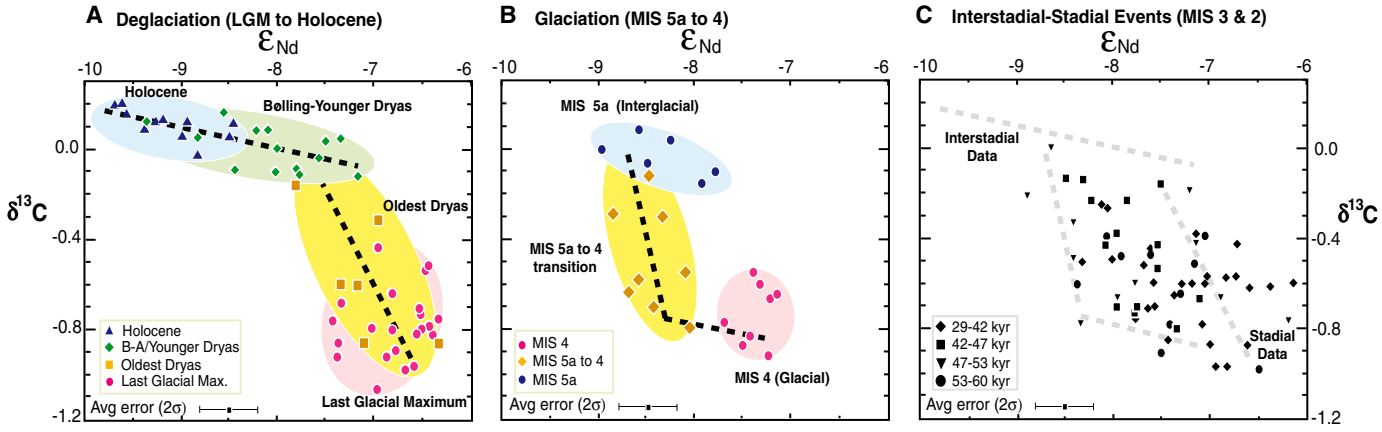

Fig. 3. Nd isotope ratios versus benthic $\delta^{13}C$ further separated into distinct time slices. (**A**) Deglaciation interval (LGM-Holocene). (**B**) The last glaciation (MIS 5a-4). (**C**) Major MIS 3 and early MIS 2 interstadial-stadial events. Scales differ from Fig. 2. Dashed lines in (A) and (B) indicate sequential changes during glacial-interglacial transitions and are reproduced in (C) to illustrate that during major interstadial-stadial events, bottom-water carbon and Nd isotopes shifted from glacial compositions toward interglacial compositions and back again, without the same lead-lag relationship as glacial-interglacial transitions.

$\delta^{13}C$. The Bølling warming to Holocene trend nearly parallels the NADW-Pacific mixing lines, whereas LGM to Bølling warming data comprise a steeper slope (Fig. 3A). This is why Nd isotopes record a large Younger Dryas change, whereas Charles *et al.* (*8*) found only a hint of a benthic $\delta^{13}C$ change. During the Younger Dryas, the range of ε_{Nd} values approaches that of the entire shift from the LGM to the Holocene without a comparable benthic $\delta^{13}C$ shift (Fig. 3A). A 20% reduction of NADW after the Bølling warming produces an increase in the Nd isotope ratio of ~2 ε_{Nd} units, with only a ~0.2‰ change in $\delta^{13}C$.

The sequence of events during the last interglacial-glacial transition (MIS 5a to 4) is identical to the deglacial sequence, with benthic $\delta^{13}C$ shifting toward glacial values before Nd isotopes (Fig. 3B), manifested by a steep trend followed by a shallow one, a mirror image of the deglacial transition. In the initial steep trend, the decrease in benthic $\delta^{13}C$ values is equal in magnitude to the deglaciation shift, without a significant change in Nd isotope ratios. Subsequently, a rapid ε_{Nd} shift occurred, resulting in the shallow trend, consistent with a reduction in NADW intensity. The MIS 5a/4 NADW shift lags the benthic $\delta^{13}C$ shift by ~2,500 years (corresponding to 27 cm in TNO57-21). As discussed above for the Younger Dryas, water-mass mixing dynamics is also responsible for the small $\delta^{13}C$ change compared with the natural scatter that accompanies the abrupt Nd isotope shift during the MIS 5a-4 transition (Fig. 4).

The comparisons of Nd and benthic carbon isotopes have important implications for the sequence of events at major climate transitions. The data indicate that during the last glaciation and deglaciation, major changes in South Atlantic deep-water $\delta^{13}C$ occurred prior to major changes in the global overturning circulation.

Significant variability in Nd and benthic $\delta^{13}C$ also occurred during the millennial Dansgaard-Oeschger (D-O) interstadial warmings of MIS 3 and early MIS 2 (Fig. 1), which fill the parallelogram formed by the glacial-interglacial transition data (Fig. 2 and Fig. 3C). During interstadials, the data shifts directly from full glacial values (higher ε_{Nd} and lower $\delta^{13}C$) toward the NADW end member, although there is some scatter. Here, the carbon and ocean-circulation changes do not display a consistent two-stage lead-lag relationship as during the main glacial-interglacial transitions (Fig. 3C). This simple relationship shows that benthic $\delta^{13}C$ and Nd isotopes were responding synchronously to circulation changes during MIS 3 and early MIS 2, which (unlike the glacial-interglacial transitions) may allow for a causal role for ocean circulation to trigger the interstadial warmings.

It is unlikely that the consistent benthic $\delta^{13}C$ lead over ε_{Nd} at the glacial-interglacial boundaries was produced by bioturbation or diagenesis. The benthic $\delta^{13}C$ record was generated on *Cibicidoides wüllerstorfi*, which live at or above the sediment-water interface. Processes that might affect the relative position of benthic $\delta^{13}C$ and ε_{Nd} changes include seawater intrusion into sediment porewaters, bioturbation, and postdepositional smearing of the Fe-Mn oxides. Precipitation of Fe-Mn oxides from bottom-water–derived porewaters at depth within the sediment column would cause the Nd isotope record to lead, rather than lag, the benthic $\delta^{13}C$ record, opposite to what we observe. Bioturbation could cause downward mixing of foraminifera relative to other substrates containing Fe-Mn oxide coatings. If this occurred, the depth difference would have to be >20 cm (the lead-lag depth difference of glacial-interglacial Nd and benthic $\delta^{13}C$ changes), which is highly unlikely. The overall RC11-83/TNO57-21 ε_{Nd} and benthic $\delta^{13}C$ profiles (Fig. 1) give strong evidence against smearing of Fe-Mn oxides generating the lag in Nd isotope changes during the transitions. First, the glacial-interglacial changes are abrupt. Second, there is no lead-lag relationship during millennial fluctuations throughout the record. During most millennial events, benthic $\delta^{13}C$-ε_{Nd} covary on centimeter scales [e.g., the "false start" at 15.5 thousand years before the present (ky cal. B.P.), 277 cm (*8*)]. We conclude that the carbon and Nd isotope data and their lead-lag relationship at major stage boundaries reflect bottom-water chemistry changes at this site.

Temporal relationships. The temporal relationship between the benthic $\delta^{13}C$ and Nd isotopes indicates that the $\delta^{13}C$ of the deep South Atlantic shifted by 0.8‰ during glacial-interglacial transitions at ~1000 to 3000 years before changes in the balance between northern- and southern-sourced waters. The abruptness of the early benthic $\delta^{13}C$ shifts strongly indicates that they include both the glacial-interglacial mean ocean carbon isotope change of ~0.4‰ (*28*–*30*) and an additional ~0.4‰ reflecting processes related to Southern Ocean productivity or air-sea equilibration of carbon isotopes. If the mean ocean and Southern Ocean $\delta^{13}C$ shifts occurred separately, the record would show two steps rather than the single abrupt shift seen clearly during the last interglacial-glacial transition (Fig. 4). Moreover, all other ~0.4‰ $\delta^{13}C$ shifts are supported by Nd isotopes changes and, therefore, are attributable to circulation change. Although we are currently unable to quantitatively separate the different noncirculatory effects on the $\delta^{13}C$ record, the data strongly indicate that the Southern Ocean and mean ocean $\delta^{13}C$ changed simultaneously and before ocean circulation.

As the mean ocean $\delta^{13}C$ change was caused by redistribution of terrestrial biosphere and deep-ocean carbon, the relationship between $\delta^{13}C$ and Nd isotopes during the MIS 2/1 and 5/4 transitions implies that the transfer of isotopically light terrestrial

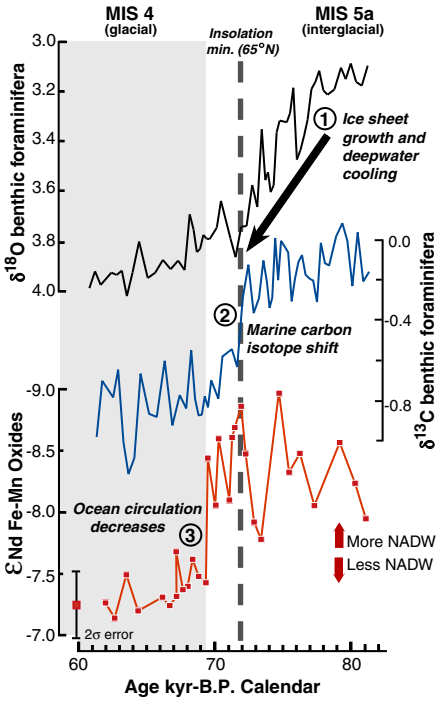

Fig. 4. Detail of MIS 5a/4 transition of benthic $\delta^{18}O$, benthic $\delta^{13}C$ (*20*, *32*), and Nd isotope records in core TNO57-21. Sequential events include the benthic $\delta^{18}O$ change signifying nucleation and growth of continental ice sheets and cooler bottom waters; the major shift in benthic $\delta^{13}C$, unsupported by Nd isotopes and attributed to a noncirculatory signal from carbon budget reorganization; and the ε_{Nd} shift reflecting reduction of the NADW signal to glacial levels. The dashed line at 72 ky B.P. corresponds to the $\delta^{13}C$ shift as well as a minimum in Northern Hemisphere insolation. Ages were assigned by matching the benthic $\delta^{18}O$ to SPECMAP (*52*) by (*20*, *32*). However, since all three records are from the same core, the sequences of events are directly comparable.

carbon between these reservoirs occurred prior to the shift between glacial-interglacial modes of ocean circulation. Because the terrestrial biosphere primarily responds to climate change, this strongly indicates that glacial-interglacial climate change occurred before changes in thermohaline circulation. The sequence of events during the MIS 5/4 transition can be shown by using benthic $\delta^{18}O$, benthic $\delta^{13}C$, and Nd isotopes to constrain the timing of ice-sheet growth and deep-water temperature, budget changes, and thermohaline circulation, respectively (Fig. 4). The growth of continental ice sheets is the primary cause of the benthic $\delta^{18}O$ change (*32*), which occurs first and is followed by a large benthic $\delta^{13}C$ shift (*32*) a few thousand years later, which is then followed by the Nd isotope shift. Colder deep-water temperatures causing a large portion of the glacial-interglacial $\delta^{18}O$ shift is also consistent with the establishment of glacial conditions concurrent with still-strong Atlantic overturning, followed by a reduction of thermohaline circulation (*44*). The sequence of events for the last deglaciation is not as easily seen because of complex millennial-scale variations, although the early deglacial carbon shift compared with the Nd isotope shift shows up well in the benthic $\delta^{13}C$–ε_{Nd} cross-plots (*45*). The glaciation sequence shows that only after the growth of large continental ice sheets and a reorganization of both the global and Southern Ocean carbon budget was a weaker ocean-circulation regime established.

Conclusions. Comparison of proxies from a single core thus yields a temporal sequence of major climate events for the last glacial initiation and termination. During the last glaciation, climate and ice volume changed first, followed by the global carbon budget, which was in turn followed by ocean circulation. During deglaciation, the global carbon budget changed before ocean circulation strengthened. These temporal sequences show that thermohaline circulation changes did not trigger ice-sheet changes and global carbon budget reorganization. During the glaciation, strong ocean circulation and maritime conditions in the North Atlantic likely provided an important source of moisture for continental ice-sheet growth during the sustained cold conditions associated with the Northern Hemisphere insolation minimum at ~72 ky B.P. During interstadials through the last ice age, on the other hand, simultaneous changes in benthic $\delta^{13}C$ and Nd isotope ratios allow for the possibility of an ocean-circulation trigger for these millennial interstadial warmings. The observation that ice-sheet growth and global carbon cycle shifts precede ocean circulation changes at major glacial-interglacial boundaries shows that thermohaline circulation was a later amplifier but not the primary instigator of glacial-interglacial climate change.

References and Notes

1. W. S. Broecker, *Prog. Oceanogr.* **2**, 151 (1982).
2. W. S. Broecker, *The Glacial World According to Wally* (Eldigio Press, Palisades, NY, ed. 3, 2002).
3. J. M. Adams, H. Faure, L. Fauredenard, J. M. McGlade, F. I. Woodward, *Nature* **348**, 711 (1990).
4. J. M. Adams, W. M. Post, *Global Planet. Change* **20**, 243 (1999).
5. T. J. Crowley, *Global Biogeochem. Cycle* **9**, 377 (1995).
6. W. B. Curry, G. P. Lohmann, *Quat. Res.* **18**, 218 (1982).
7. D. W. Oppo, R. G. Fairbanks, *Earth Planet. Sci. Lett.* **86**, 1 (1987).
8. C. D. Charles, R. G. Fairbanks, *Nature* **355**, 416 (1992).
9. S. L. Goldstein, S. R. Hemming, in *Treatise on Geochemistry*, H. Elderfield, Ed. (Elsevier, Oxford, 2003), vol. 6, pp. 453–489.
10. F. Albarède, S. L. Goldstein, *Geology* **20**, 761 (1992).
11. The ε_{Nd} is the deviation of the $^{143}Nd/^{144}Nd$ of a sample from the bulk Earth value of 0.512638 (*46*) in parts per 10,000. The high-atomic-masses Nd isotopes (142 to 150 atomic mass units) and their single oxidation state (+3) inhibit significant mass-dependent fractionation. Moreover, corrections applied during mass-spectrometry measurement eliminate effects of any natural mass-dependent fractionation.
12. F. von Blanckenburg, *Science* **286**, 1862 (1999).
13. M. Frank, *Rev. Geophys.* **40**, 1001 (2002); 10.1029/2000RG000094.
14. K. W. Burton, D. Vance, *Earth Planet. Sci. Lett.* **176**, 425 (2000).
15. R. L. Rutberg, S. R. Hemming, S. L. Goldstein, *Nature* **405**, 935 (2000).
16. G. Bayon *et al.*, *Chem. Geol.* **187**, 179 (2002).
17. D. Vance *et al.*, *Paleoceanography* **19**, PA2009 (2004).
18. A. M. Piotrowski, S. L. Goldstein, S. R. Hemming, R. G. Fairbanks, *Earth Planet. Sci. Lett.* **225**, 205 (2004).
19. C. D. Charles, J. Lynch-Stieglitz, U. S. Ninnemann, R. G. Fairbanks, *Earth Planet. Sci. Lett.* **142**, 19 (1996).
20. U. S. Ninnemann, C. D. Charles, D. A. Hodell, in *Mechanisms of Global Climate Change at Millennial Time Scales* (American Geophysical Union, Washington, DC, 1999), vol. Geophysical Monograph 112, pp. 99–112.
21. The Sr isotopes and rare-earth-element patterns of leaches from this core match that of seawater, which is evidence for a marine rather than detrital origin for the Nd isotopes.
22. G. Bayon, C. German, K. Burton, R. Nesbitt, N. Rogers, *Earth Planet. Sci. Lett.* **224**, 447 (2004).
23. R. L. Rutberg, S. L. Goldstein, S. R. Hemming, R. Anderson, L. Burckle, *Paleoceanography*, in press.
24. S. Levitus, R. Burgett, T. Boyer, in *NOAA Atlas NESDros. Inf. Serv.* (U.S. Department of Commerce, Washington, DC, 1994), vol. 3.
25. P. M. Grootes, M. Stuiver, *J. Geophys. Res.* **102**, 26455 (1997).
26. G. R. I. P. Members, *Nature* **364**, 203 (1993).
27. S. J. Johnsen *et al.*, *J. Geophys. Res.* **102**, 26397 (1997).
28. W. B. Curry, J. C. Duplessy, L. D. Labeyrie, N. J. Shackleton, *Paleoceanography* **3**, 317 (1988).
29. E. A. Boyle, *Annu. Rev. Earth Planet. Sci.* **20**, 245 (1992).
30. J. C. Duplessy *et al.*, *Paleoceanography* **3**, 343 (1988).
31. U. Siegenthaler, in *Global Changes of the Past*, R. S. Bradley, Ed. (Univ. Corporation for Atmospheric Research, Boulder, CO, 1991), pp. 245–260.
32. U. S. Ninnemann, C. D. Charles, *Earth Planet. Sci. Lett.* **201**, 383 (2002).
33. K. Matsumoto, T. Oba, J. Lynch-Stieglitz, H. Yamamoto, *Quat. Sci. Rev.* **21**, 1693 (2002).
34. K. Matsumoto, J. Lynch-Stieglitz, *Paleoceanography* **14**, 149 (1999).
35. A. Mackensen, H. W. Hubberten, T. Bickert, G. Fischer, D. K. Futterer, *Paleoceanography* **8**, 587 (1993).
36. W. Abouchami, S. L. Goldstein, S. J. G. Galer, A. Eisenhauer, A. Mangini, *Geochim. Cosmochim. Acta* **61**, 3957 (1997).
37. A. M. Piotrowski, thesis, Columbia Univ. (2004).
38. C. Innocent, N. Fagel, R. K. Stevenson, C. Hillaire-Marcel, *Earth Planet. Sci. Lett.* **146**, 607 (1997).
39. N. Fagel, C. Innocent, R. K. Stevenson, C. Hillaire-Marcel, *Paleoceanography* **14**, 777 (1999).
40. F. von Blanckenburg, T. F. Nagler, *Paleoceanography* **16**, 424 (2001).
41. If the Nd isotope ratio of the North Atlantic end member decreased and the Pacific end member remained constant at the time of the major $\delta^{13}C$ change during the glaciation, it would be possible to buffer the Nd isotope ratio of South Atlantic deep water despite a weakening of thermohaline circulation. For example, the ε_{Nd} of NADW would have to shift from $\varepsilon_{Nd} = -14$ to -18 in concert with the MIS 5a/4 $\delta^{13}C$ change (Fig. 1) and then rapidly shift back to -14 when we observe the change in the Nd isotope ratios. A complementary abrupt shift to -10 and then another shift back to -14 could explain the apparent $\delta^{13}C$ lead during the deglaciation. Although such scenarios, and variations thereof, cannot be completely ruled out, they require coincidental end-member ε_{Nd} and $\delta^{13}C$ shifts in both magnitude and timing, such that the ε_{Nd} at the core sites remain roughly constant. Thus, they would require evidence before they can be considered seriously. On the longer term, as explained in the text, there is good evidence that the Pacific end member remained nearly constant on glacial-interglacial time scales, whereas the North Atlantic end member is less well constrained, but current evidence indicates near constancy (*15*, *18*).

42. G. H. Denton *et al.*, *Geogr. Ann. Ser. A Phys. Geogr.* **81A**, 107 (1999).
43. A 35-cm interval in RC11-83, which has an average sedimentation rate through this section of 24 cm/1000 years [a 29-cm interval in RC11-83 (*19*, *20*)], would correspond to a time period of 1450 years.
44. W. F. Ruddiman, *Quat. Sci. Rev.* **22**, 1597 (2003).
45. Most Nd and carbon isotope measurements in the deglacial and Bølling warming portion of the record were not made on the same sample depths or splits. We therefore conservatively confine our interpretations to lead-lag relationships >150 years or >3 cm of core length.
46. S. B. Jacobsen, G. J. Wasserburg, *Earth Planet. Sci. Lett.* **50**, 139 (1980).
47. J. Jouzel *et al.*, *Nature* **329**, 403 (1987).
48. D. J. Piepgras, S. B. Jacobsen, *Geochim. Cosmochim. Acta* **52**, 1373 (1988).
49. D. J. Piepgras, G. J. Wasserburg, *Geochim. Cosmochim. Acta* **51**, 1257 (1987).
50. C. Jeandel, *Earth Planet. Sci. Lett.* **117**, 581 (1993).
51. D. Hodell, K. A. Venz, C. D. Charles, U. S. Ninnemann, *Geochem. Geophys. Geosyst.* **4**, 1 (2003).
52. D. G. Martinson *et al.*, *Quat. Res.* **27**, 1 (1987).
53. This manuscript benefited from discussions with R. Anderson, S. Barker, W. Broecker, H. Elderfield, E. Martin, J. McManus, U. Ninnemann, H. Scher, and A. Tripati; laboratory assistance from D. Zylberberg; and comments by anonymous reviewers. This study was supported by NSF grants OCE 98-09253 and OCE 00-96427 to S.L.G. and S.R.H. and ATM03-27722 and OCE99-11637 to R.G.F. Samples used in this project were provided by the Lamont-Doherty Earth Observatory Deep-Sea Sample Repository, supported by the NSF (grant OCE 00-02380) and the Office of Naval Research (grant N00014-02-1-0073). This is LDEO Contribution #6702.

Supporting Online Material
www.sciencemag.org/cgi/content/full/307/5717/1933/DC1
Tables S1 and S2

7 September 2004; accepted 31 January 2005
10.1126/science.1104883

REPORTS

A New Population of Very High Energy Gamma-Ray Sources in the Milky Way

F. Aharonian,[1] A. G. Akhperjanian,[2] K.-M. Aye,[3] A. R. Bazer-Bachi,[4] M. Beilicke,[5] W. Benbow,[1] D. Berge,[1] P. Berghaus,[6]* K. Bernlöhr,[1,7] C. Boisson,[8] O. Bolz,[1] C. Borgmeier,[7] I. Braun,[1] F. Breitling,[7] A. M. Brown,[3] J. Bussons Gordo,[9] P. M. Chadwick,[3] L.-M. Chounet,[10] R. Cornils,[5] L. Costamante,[1] B. Degrange,[10] A. Djannati-Ataï,[6] L. O'C. Drury,[11] G. Dubus,[10] T. Ergin,[7] P. Espigat,[6] F. Feinstein,[9] P. Fleury,[10] G. Fontaine,[10] S. Funk,[1]† Y. A. Gallant,[9] B. Giebels,[10] S. Gillessen,[1] P. Goret,[12] C. Hadjichristidis,[3] M. Hauser,[13] G. Heinzelmann,[5] G. Henri,[14] G. Hermann,[1] J. A. Hinton,[1] W. Hofmann,[1] M. Holleran,[15] D. Horns,[1] O. C. de Jager,[15] I. Jung,[1,13]‡ B. Khélifi,[1] Nu. Komin,[7] A. Konopelko,[1,7] I. J. Latham,[3] R. Le Gallou,[3] A. Lemière,[6] M. Lemoine,[10] N. Leroy,[10] T. Lohse,[7] A. Marcowith,[4] C. Masterson,[1] T. J. L. McComb,[3] M. de Naurois,[16] S. J. Nolan,[3] A. Noutsos,[3] K. J. Orford,[3] J. L. Osborne,[3] M. Ouchrif,[16] M. Panter,[1] G. Pelletier,[14] S. Pita,[6] G. Pühlhofer,[1,13] M. Punch,[6] B. C. Raubenheimer,[15] M. Raue,[5] J. Raux,[16] S. M. Rayner,[3] I. Redondo,[10]§ A. Reimer,[17] O. Reimer,[17] J. Ripken,[5] L. Rob,[18] L. Rolland,[16] G. Rowell,[1] V. Sahakian,[2] L. Saugé,[14] S. Schlenker,[7] R. Schlickeiser,[17] C. Schuster,[17] U. Schwanke,[7] M. Siewert,[17] H. Sol,[8] R. Steenkamp,[19] C. Stegmann,[7] J.-P. Tavernet,[16] R. Terrier,[6] C. G. Théoret,[6] M. Tluczykont,[10] D. J. van der Walt,[15] G. Vasileiadis,[9] C. Venter,[15] P. Vincent,[16] B. Visser,[15] H. J. Völk,[1] S. J. Wagner[13]

Very high energy γ-rays probe the long-standing mystery of the origin of cosmic rays. Produced in the interactions of accelerated particles in astrophysical objects, they can be used to image cosmic particle accelerators. A first sensitive survey of the inner part of the Milky Way with the High Energy Stereoscopic System (HESS) reveals a population of eight previously unknown firmly detected sources of very high energy γ-rays. At least two have no known radio or x-ray counterpart and may be representative of a new class of "dark" nucleonic cosmic ray sources.

Very high energy (VHE) γ-rays with energies $E > 10^{11}$ eV are probes of the nonthermal universe, providing access to energies far greater than those that can be produced in accelerators on Earth. The acceleration of electrons or nuclei in astrophysical sources leads inevitably to the production of γ-rays by the decay of π^0s produced in hadronic interactions, inverse Compton scattering of high-energy electrons on background radiation fields, or the nonthermal bremsstrahlung of energetic electrons. Several classes of objects in the Galaxy are suspected or known particle accelerators: pulsars and their pulsar wind

[1]Max-Planck-Institut für Kernphysik, Post Office Box 103980, D-69029 Heidelberg, Germany. [2]Yerevan Physics Institute, 2 Alikhanian Brothers Street, 375036 Yerevan, Armenia. [3]Department of Physics, University of Durham, South Road, Durham DH1 3LE, UK. [4]Centre d'Etude Spatiale des Rayonnements, CNRS/UPS, 9 av. du Colonel Roche, BP 4346, F-31029 Toulouse Cedex 4, France. [5]Institut für Experimentalphysik, Universität Hamburg, Luruper Chaussee 149, D-22761 Hamburg, Germany. [6]Physique Corpusculaire et Cosmologie, IN2P3/CNRS, Collège de France, 11 Place Marcelin Berthelot, F-75231 Paris Cedex 05, France. [7]Institut für Physik, Humboldt-Universität zu Berlin, Newtonstr. 15, D-12489 Berlin, Germany. [8]Laboratoire Univers et Théories (LUTH), UMR 8102 du CNRS, Observatoire de Paris, Section de Meudon, F-92195 Meudon Cedex, France. [9]Groupe d'Astroparticules de Montpellier, IN2P3/CNRS, Université Montpellier II, CC85, Place Eugène Bataillon, F-34095 Montpellier Cedex 5, France. [10]Laboratoire Leprince-Ringuet, IN2P3/CNRS, Ecole Polytechnique, F-91128 Palaiseau, France. [11]Dublin Institute for Advanced Studies, 5 Merrion Square, Dublin 2, Ireland. [12]Service d'Astrophysique, DAPNIA/DSM/CEA, CE Saclay, F-91191 Gif-sur-Yvette, France. [13]Landessternwarte, Königstuhl, D-69117 Heidelberg, Germany. [14]Laboratoire d'Astrophysique de Grenoble, INSU/CNRS, Université Joseph Fourier, BP 53, F-38041 Grenoble Cedex 9, France. [15]Unit for Space Physics, North-West University, Potchefstroom 2520, South Africa. [16]Laboratoire de Physique Nucléaire et de Hautes Energies, IN2P3/CNRS, Universités Paris VI and VII, 4 Place Jussieu, F-75231 Paris Cedex 05, France. [17]Institut für Theoretische Physik, Lehrstuhl IV: Weltraum und Astrophysik, Ruhr-Universität Bochum, D-44780 Bochum, Germany. [18]Institute of Particle and Nuclear Physics, Charles University, V Holesovickach 2, 180 00 Prague 8, Czech Republic. [19]University of Namibia, Private Bag 13301, Windhoek, Namibia.

*Present address: Université Libre de Bruxelles, Faculté des Sciences, Campus de la Plaine, CP230, Boulevard du Triomphe, 1050 Bruxelles, Belgium.
†To whom correspondence should be addressed. E-mail: stefan.funk@mpi-hd.mpg.de
‡Present address: Department of Physics, Washington University, 1 Brookings Drive, CB 1105, St. Louis, MO 63130, USA.
§Present address: Department of Physics and Astronomy, University of Sheffield, Hicks Building, Hounsfield Road, Sheffield S3 7RH, UK.

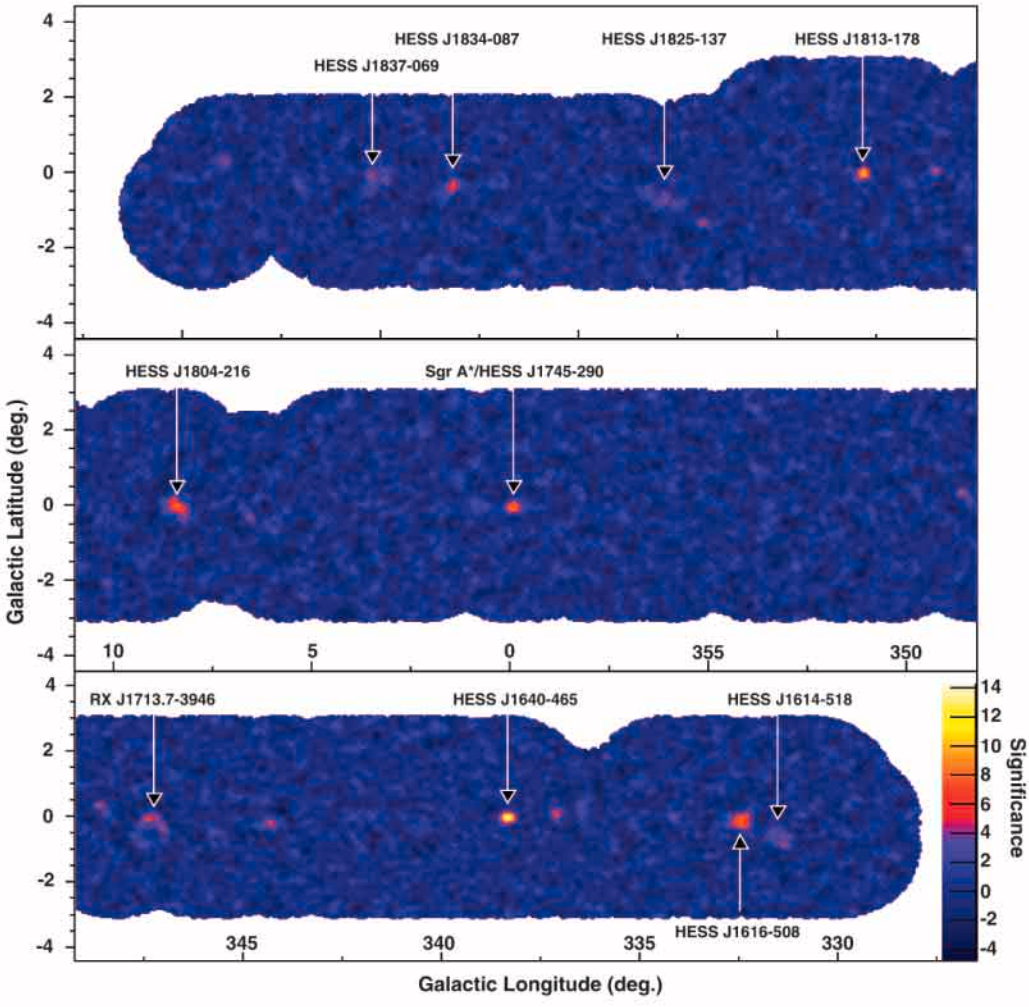

Fig. 1. Significance map of the HESS 2004 galactic plane scan. Reobservations of candidates from the initial scan are included here. The background level was estimated using a ring around the test source position (*12*). On-source counts are summed over a circle of radius θ, where θ = 0.14°, a cut appropriate for point-like sources. To calculate the significance, it is necessary to correct for the relative acceptance and area of the on and off regions. The correction is given by a runwise radially symmetric acceptance function, which describes the background at the 1% level. Events falling up to 2° from the pointing direction of the system are used. At this angle, the γ-ray acceptance efficiency has decreased to 20% of its peak value. After acceptance correction, the approach of Li and Ma (*30*) is used to calculate the significance at every point on the map. We note that consistent results are obtained for these eight sources with the use of a completely independent calibration and analysis chain (*31*).

nebulae (PWNs), supernova remnants (SNRs), microquasars, and massive star-forming regions. VHE γ-ray sources that have been detected in the Galaxy include PWNs, SNRs, and objects with no identified counterpart at other energies. Such sources without counterpart are particularly interesting, because a lack of x-ray emission could indicate that the primary accelerated particles are nucleons rather than high-energy electrons. Essentially all potential galactic sources cluster along the galactic plane. Thus, a systematic survey of the galactic plane is the best means to investigate the properties of these source classes and to search for currently unknown types of galactic VHE γ-ray emitters.

Large-scale γ-ray surveys in the TeV energy regime (1 TeV = 10^{12} eV) have been performed using the Milagro water-Cherenkov detector (*1*) and the Tibet air-shower array (*2*). These all-sky instruments have only modest sensitivity, reaching a flux limit comparable to the flux level of the Crab Nebula, $\sim 2 \times 10^{-11}$ cm^{-2} s^{-1} (for $E > 1$ TeV), in 1 year of observations. Both surveys covered $\sim 2\pi$ steradians of the northern sky and resulted only in flux upper limits. A survey of the part of the galactic plane accessible from the Northern Hemisphere ($-2° < l < 85°$, where l denotes galactic longitude) was performed by the stereoscopic High Energy Gamma Ray Astronomy (HEGRA) array of imaging Cherenkov telescopes (*3*). No sources of VHE γ-rays were found in this survey, but upper limits between 15% of the Crab flux for galactic longitudes $l > 30°$ and more than 30% of the Crab flux in the inner part of the Milky Way were derived (*4*). Until the completion of the High Energy Stereoscopic System (HESS) (*5*) in early 2004, no VHE γ-ray survey of the southern sky or of the central region of the Galaxy had been performed. The central part of the Galaxy contains the highest density of potential γ-ray sources. We conducted a survey of this region with HESS in 2004, at a flux sensitivity of 3% of the Crab flux.

HESS is an array of telescopes exploiting the imaging Cherenkov technique. The telescopes image the Cherenkov light emitted by atmospheric particle cascades initiated by γ-rays or cosmic rays in the upper atmosphere. Measurements of the same cascade by multiple telescopes allow improved rejection of the cosmic-ray background and better angular and energy resolution relative to single-dish telescopes. HESS consists of four atmospheric Cherenkov telescopes, each with 107 m^2 of mirror area (*6*) and equipped with a 960-pixel photomultiplier tube camera (*7*). The four telescopes are operated in a stereoscopic mode with a system trigger (*8*), requiring at least two telescopes to provide images of each cascade. HESS has the largest field of view (diameter 5°) of all imaging Cherenkov telescopes now in operation, which yields a considerable advantage for surveys (*9*).

HESS provides unprecedented sensitivity to γ-rays above 100 GeV, below 1% of the flux from the Crab Nebula, for long exposures. This sensitivity has already been demonstrated by high-significance detections of the galactic center (HESS J1745-290) (*10*) and the SNR RX J1713.7-3946 (*11*). The angular resolution for individual γ-rays is better than 0.1°, allowing a source position error of 30 arc sec to be achieved even for relatively faint sources.

We scanned the inner part of the galactic plane (galactic longitude $-30° < l < 30°$ and latitude $-3° < b < 3°$) with HESS from May to July 2004. Observations 28 min in duration

were made in steps of 0.7° in longitude and steps of 1° in latitude for a total observation time of 112 hours. An average 5-standard-deviation detection sensitivity of 3×10^{-11} photons cm^{-2} s^{-1} above 100 GeV (~3% of the Crab Flux) was reached for points on the galactic plane. Seven promising candidate sources from the survey were reobserved from July to September for typically 3.5 hours per source.

Eight unknown VHE sources were detected at the level of >6 standard deviations after accounting for all trial factors (Fig. 1 and Table 1). The known VHE sources HESS J1745-290 (at the galactic center) and RX J1713.7-3946 were also detected in the scan data. The analysis used the standard HESS analysis procedure, optimized for point-like sources (*12*).

The significance values shown in Fig. 1 (and S^3 in Table 1) do not directly reflect the probability that a given signal represents a γ-ray source, because the large number of search points in the sky map (250,000) enhances the chance for statistical fluctuations to mimic a signal. Probabilities must be scaled by a trial factor accounting for the number of attempts to find a source, here conservatively assumed to be equal to the number of points in the sky map. Simulations of randomly generated sky maps without γ-ray sources show that the effective number of trials is smaller than the number of points because of correlations between adjacent search points, which are more closely spaced than the instrumental width of the point spread function. Trial factors apply only for the initial search, where source candidates were identified (S^1, before trials), but not for follow-up observations, where the significance (S^2) of a signal was evaluated assuming the position derived from the initial search. The scaled-down significance from the initial search and the result of the follow-up observations were combined by summation in quadrature to give a final detection significance (S^4).

Because most sources appear moderately extended, S^5 in Table 1 lists the significance similar to S^4 but assuming extended sources. For each of these candidates, a spectral analysis was performed, and Table 1 also gives the best fit flux above 200 GeV.

For the purpose of source size and position fitting, an additional cut requiring an image size exceeding 200 photoelectrons in each camera was applied. This cut further suppresses the cosmic-ray background (by a factor of ~7) at the expense of reduced statistical significance and increased energy threshold (250 GeV). It also improves the angular resolution by 30%. After applying this cut, the spatial distribution of excess events for each candidate was fit to a model of a two-dimensional Gaussian γ-ray emission region (Table 1) convolved with the point spread function of the instrument (derived from Monte Carlo simulations and verified by observations of the Crab Nebula).

The new galactic VHE γ-ray emitters cluster close to the galactic plane, with a mean b of –0.25° and a root mean square (rms) of 0.25° (Fig. 2). This is a clear indication that we see a population of galactic (rather than extragalactic) sources. Furthermore, the observed distribution resembles that of galactic SNRs (*13*) and of energetic pulsars ($\dot{E} > 10^{34}$ erg/s) (*14*). However, because of the nonuniform exposure of the scan and the unknown luminosity distribution of the parent population, we cannot make a quantitative statement about the compatibility of these distributions.

All of the sources are significantly extended beyond the size of the HESS point spread function. Given that the search described here was optimized for point-like sources, it is likely that several more significant sources with an extended nature exist in this data set. We note that the new sources mostly have spectra with rather hard photon indices in the range between that expected for SNRs and that of the Crab Nebula.

We have searched for counterparts for the new γ-ray sources in other wavelength bands. Fig. 3 shows the γ-ray emission from the region around each source together with potential counterparts. Although the chance probability for spatial coincidences with SNRs in the region of the scan is not negligible (6%), plausible associations exist for three of the new sources—HESS J1640-465, HESS J1834-087, and HESS J1804-216—with an SNR.

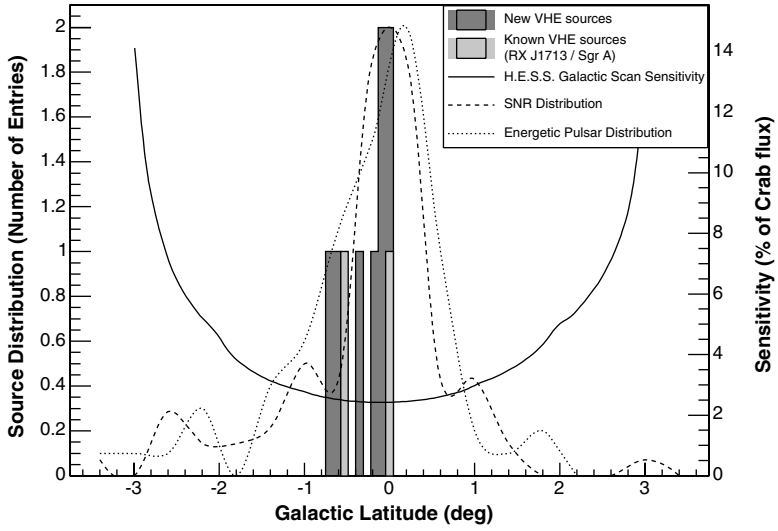

Fig. 2. Latitude distribution of the eight new VHE γ-ray sources (and two known sources in the scan region), along with the average sensitivity of the HESS galactic plane scan (for a 5σ detection, expressed as a percentage of the flux from the Crab Nebula). The distributions of galactic SNRs and of energetic pulsars (including only pulsars with spin-down luminosity $\dot{E}$ more than 10^{34} erg/s) are shown for comparison; for both distributions, only objects within the longitude range of the HESS survey ($-30° < l < 30°$) were selected.

Table 1. Characteristics of the new γ-ray sources. Position: galactic longitude (l) and latitude (b) with a statistical error in the range of 1 to 2 arc min. Size: estimated source extension σ for a brightness distribution of the form $\rho \propto \exp(-r^2/2\sigma^2)$ with a statistical error in the range of 10 to 30%. S_1: Significance for a point source cut of $\theta^2 = (0.14°)^2$, using scan data only, without correction for the number of trials. S_2: As for S_1 but only including follow-up observations of this source (no correction needed). S_3: Significance of combined scan and follow-up observations (as shown in Fig. 1). S_4: As for S_3 but including a correction for the number of trials (n = 250,000). S_5: As for S_4 but with an extended cut of $\theta^2 = (0.22°)^2$. Flux: Estimated flux above 200 GeV ($\times 10^{-12}$ cm^{-2} s^{-1}) with a statistical error of 10 to 35%.

Name	Position		Size σ (arc min)	Significance					Flux
	l	b		S_1	S_2	S_3	S_4	S_5	
HESS J1614-518*	331.54°	–0.59°	12	5.2	4.3	6.7	4.7	6.8	9
HESS J1616-508	332.40°	–0.15°	11	7.4	8.9	11.6	10.5	12.8	17
HESS J1640-465	338.32°	–0.02°	2	11.7	8.3	14.3	13.4	11.5	19
HESS J1804-216	8.44°	–0.05°	13	8.2	5.9	10.1	8.8	9.6	16
HESS J1813-178	12.81°	–0.03°	3	10.2	8.3	13.2	12.2	8.9	12
HESS J1825-137*	17.78°	–0.72°	10	4.4	3.7	5.8	3.7	6.5	9
HESS J1834-087	23.28°	–0.34°	12	6.7	5.6	8.7	7.2	7.8	13
HESS J1837-069	25.21°	–0.12°	4	6.0	6.0	8.4	6.9	6.4	9

*These sources were reobserved within the field of view of dedicated observations of another target.

HESS J1640-465 is spatially coincident with the SNR G338.3-0.0, which is a broken-shell SNR lying on the edge of a bright ultracompact H II region (*13*). This H II region could conceivably provide target material for nuclear particles accelerated in the SNR, generating VHE γ-rays by π^0 decay. The unidentified Energetic Gamma Ray Experiment Telescope (EGRET) source 3EG J1639-4702 (*15*) lies 35 arc min away and could also be connected to HESS J1640-465, given the position uncertainty of 34 arc min of the EGRET source. HESS J1834-087 is spatially coincident with the SNR G23.3-0.3 (W41), a shell-type SNR of diameter 27 arc min (*16*). HESS J1804-216 coincides with the southwestern rim of the shell-type SNR G8.7-0.1 (W30) of radius 26 arc min. From CO observations (*17*), the surrounding region is known to be associated with molecular gas where massive star formation is taking place. This SNR could be associated with the nearby (25 arc min) young pulsar PSR J1803-2137 (*18*).

HESS J1804-216 is one of three plausible associations with nebulae powered by sufficiently energetic young pulsars. The others are HESS J1825-137 and HESS J1616-508. HESS J1825-137 lies 13 arc min from the pulsar PSR J1826-1334, which has been associated with the nearby unidentified EGRET source 3EG J1826-1302 (*19*). A diffuse emission region, 5 arc min in diameter and extending asymmetrically to the south of the pulsar, was detected using the XMM (X-ray Multi-Mirror Mission) x-ray telescope (*20*). This diffuse emission is interpreted as synchrotron emission produced by a PWN. The VHE emission is similarly located south of PSR J1826-1334 and could be coincident with the PWN. The conversion efficiency implied from spin-down power to VHE γ-rays is less than 1%. HESS J1616-508 is located in the middle of a complicated region 9 arc min from the young hard x-ray pulsar PSR J1617-5055 (*21*). The VHE γ-ray flux is again less than 1% of the spin-down luminosity of the pulsar. The SNR G332.4-0.4 (RCW 103) (*13*), which harbors a compact x-ray source (1E 161348-5055) (*22*), lies 13 arc min away, as does the SNR G332.4+0.1 (Kes 32) (*23*), but neither of these SNRs is spatially coincident with the VHE emission. (Note that none of the discussed SNR or PWN associations currently meet the criteria necessary for promotion to counterparts. Counterpart identification requires positional agreement with an identified source, a plausible γ-ray emission mechanism, and consistent multifrequency behavior.)

For HESS J1837-069 a potential counterpart is the diffuse hard x-ray source G25.5+0.0, which is 12 arc min across and was detected in the Advanced Satellite for Cosmology and Astrophysics (ASCA) galactic plane survey (*24*). The nature of this bright x-ray source is unclear, but it may be an x-ray synchrotron emission–dominated SNR such as SN 1006 or a PWN. The brightest feature in the ASCA map (AX J1838.0-0655), located

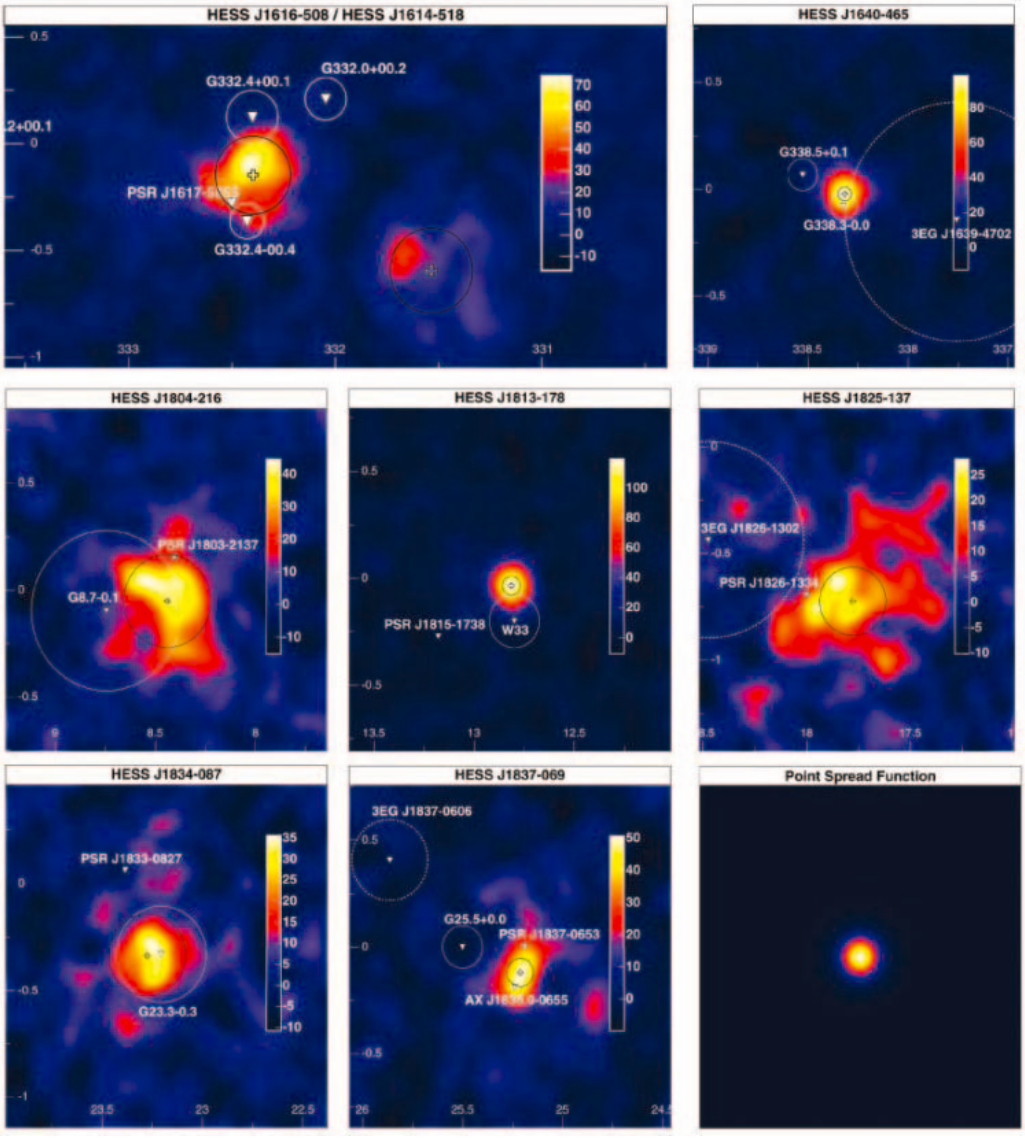

Fig. 3. Smoothed excess maps in units of counts of the regions around each of the eight new sources in galactic coordinates (in degrees). An image size cut (>200 photoelectrons) has been applied to reduce the background level and improve the angular resolution. A Gaussian of rms 0.05° is used for smoothing to reduce the impact of statistical fluctuations. The best fit centroids for the γ-ray emission are shown as crosses, and the best fit rms size as a black circle. Possible counterparts are marked by white triangles, with circles indicating the nominal source radius (or the position error in the case of EGRET sources). The lower right panel indicates the simulated point spread function of the instrument for these data, smoothed in the same way as the other panels.

south of G25.5+0.0, coincides with the center of gravity of the VHE emission and is therefore the most promising counterpart candidate. This still unidentified source was also serendipitously detected by the BeppoSAX x-ray satellite instrument and also in the hard x-ray (20 to 100 keV) band in the galactic plane survey performed with the Integral (International Gamma-Ray Astrophysics Laboratory) satellite (*25*).

For the two remaining sources, HESS J1813-178 and HESS J1614-518, no plausible counterparts have been found at other wavelengths. HESS J1813-178 is not spatially coincident with any counterparts in the region but lies 10 arc min from the center of the radio source W 33. W 33 extends over 15 arc min, with a compact radio core (G12.8-0.2) that is 1 arc min across (*26*). The region is highly obscured and has indications of recent star formation (*27*). In its extended emission and location close to an association of hot O and B stars, HESS J1813-178 resembles the unidentified TeV source discovered by HEGRA, TeV J2032+4130 (*28*), and the first HESS unidentified γ-ray source, HESS J1303-63 (*29*). HESS J1614-518 has no plausible SNR or pulsar counterpart. This source is in the field of view of HESS J1616-508, which is located nearby (~1° away). The lack of any counterparts for these two sources suggests the exciting possibility of a new class of "dark" particle accelerators in the Galaxy.

In conclusion, we have on the basis of the survey generated an unbiased catalog of VHE γ-ray sources in the central region of our Galaxy, extending our multiwavelength knowledge of the Milky Way into the VHE domain. Three of the eight newly discovered sources are potentially associated with SNRs, two with EGRET sources. In three cases an association with pulsar-powered nebulae is not excluded. At least two sources have no identified counterpart in radio or x-rays, which suggests the exciting possibility of a new class of "dark" nucleonic particle accelerators. This catalog provides insights into particle acceleration in our Galaxy and adds a piece to the long-standing puzzle of cosmic-ray origin.

References and Notes

1. R. Atkins *et al.*, *Astrophys. J.* **608**, 680 (2004).
2. M. Amenomori *et al.*, *Astrophys. J.* **580**, 887 (2002).
3. A. Daum *et al.*, *Astropart. Phys.* **8**, 1 (1997).
4. F. Aharonian *et al.*, *Astron. Astrophys.* **395**, 803 (2002).
5. W. Benbow *et al.*, in *International Symposium on High-Energy Gamma-Ray Astronomy*, F. A. Aharonian, H. J. Völk, D. Horns, Eds. (AIP Conference Proceedings 745, 2005), pp. 611–616.
6. K. Bernlöhr *et al.*, *Astropart. Phys.* **20**, 111 (2003).
7. P. Vincent *et al.*, in *Proceedings of the 28th International Cosmic Ray Conference*, T. Kajita *et al.*, Eds. (Universal Academy Press, Tokyo, 2003), pp. 2887–2890.
8. S. Funk *et al.*, *Astropart. Phys.* **22**, 285 (2004).
9. F. Aharonian *et al.*, *Astropart. Phys.* **6**, 369 (1997).
10. F. Aharonian *et al.*, *Astron. Astrophys.* **425**, L13 (2004).
11. F. Aharonian *et al.*, *Nature* **432**, 75 (2004).
12. F. Aharonian *et al.*, *Astron. Astrophys.* **430**, 865 (2005).
13. D. A. Green, *Bull. Astron. Soc. India* **32**, 335 (2004).
14. R. N. Manchester, G. B. Hobbs, A. Teoh, M. Hobbs, *Astron. J.*, in press (available at http://xxx.lanl.gov/abs/astro-ph/0412641).
15. R. C. Hartman *et al.*, *Astrophys. J. Suppl. Ser.* **123**, 79 (1999).
16. N. E. Kassim, *Astron. J.* **103**, 943 (1992).
17. L. Blitz, M. Fich, A. A. Stark, *Astrophys. J. Suppl. Ser.* **49**, 183 (1982).
18. N. E. Kassim, *Nature* **343**, 146 (1990).
19. P. L. Nolan, W. F. Tompkins, I. A. Grenier, P. F. Michelson, *Astrophys. J.* **597**, 615 (2003).
20. B. M. Gaensler, N. S. Schulz, V. M. Kaspi, M. J. Pivovaroff, W. E. Becker, *Astrophys. J.* **588**, 441 (2003).
21. K. Torii *et al.*, *Astrophys. J.* **494**, L207 (1998).
22. E. V. Gotthelf, R. Petre, U. Hwang, *Astrophys. J.* **487**, L175 (1997).
23. J. Vink, *Astrophys. J.* **604**, 693 (2004).
24. A. Bamba, M. Ueno, K. Koyama, S. Yamauchi, *Astrophys. J.* **589**, 253 (2003).
25. A. Malizia *et al.*, in *Proceedings of the V INTEGRAL Workshop*, Munich, 16 to 20 February 2004 (available at http://xxx.lanl.gov/abs/astro-ph/0404596).
26. A. Haschick, P. T. P. Ho, *Astrophys. J.* **267**, 638 (1983).
27. E. Churchwell, *Astron. Astrophys. Rev.* **2**, 79 (1990).
28. F. Aharonian *et al.*, *Astron. Astrophys.* **393**, L37 (2002).
29. M. Beilicke *et al.*, in *International Symposium on High-Energy Gamma-Ray Astronomy*, F. A. Aharonian, H. J. Völk, D. Horns, Eds. (AIP Conference Proceedings 745, 2005), pp. 347–352.
30. T. Li, Y. Ma, *Astrophys. J.* **272**, 317 (1983).
31. M. de Naurois *et al.*, in *Proceedings of the 28th International Cosmic Ray Conference*, T. Kajita *et al.*, Eds. (Universal Academy Press, Tokyo, 2003), pp. 2907–2910.

32. The support of the Namibian authorities and of the University of Namibia in facilitating the construction and operation of HESS is gratefully acknowledged, as is the support of the German Ministry for Education and Research (BMBF), the Max Planck Society, the French Ministry for Research, the CNRS-IN2P3 and the Astroparticle Interdisciplinary Programme of the CNRS, the UK Particle Physics and Astronomy Research Council (PPARC), the Institute of Particle and Nuclear Physics of the Charles University, the South African Department of Science and Technology and National Research Foundation, and the University of Namibia. We appreciate the excellent work of the technical support staff in Berlin, Durham, Hamburg, Heidelberg, Palaiseau, Paris, Saclay, and Namibia in the construction and operation of the equipment. L.C., C.M., M.O., I.R., and M.T. are also affiliated with the European Associated Laboratory for Gamma-Ray Astronomy, jointly supported by CNRS and the Max Planck Society.

13 December 2004; accepted 18 January 2005
10.1126/science.1108643

Chemical Detection with a Single-Walled Carbon Nanotube Capacitor

E. S. Snow,* F. K. Perkins, E. J. Houser, S. C. Badescu, T. L. Reinecke

We show that the capacitance of single-walled carbon nanotubes (SWNTs) is highly sensitive to a broad class of chemical vapors and that this transduction mechanism can form the basis for a fast, low-power sorption-based chemical sensor. In the presence of a dilute chemical vapor, molecular adsorbates are polarized by the fringing electric fields radiating from the surface of a SWNT electrode, which causes an increase in its capacitance. We use this effect to construct a high-performance chemical sensor by thinly coating the SWNTs with chemoselective materials that provide a large, class-specific gain to the capacitance response. Such SWNT chemicapacitors are fast, highly sensitive, and completely reversible.

Sorption-based microsensors are currently a leading candidate for low-power, compact chemical vapor detection for defense, homeland security, and environmental-monitoring applications (*1*–*9*). Such sensors combine a nonselective transducer with chemoselective materials that serve as a vapor concentrator, resulting in a highly sensitive detector that responds selectively to a particular class of chemical vapor. An array of such sensors, each coated with a different chemoselective material, produces a response fingerprint that can detect and identify an analyte (*1*–*3*). Sorption-based sensors provide sensitive detection for vapors ranging from volatile organic compounds to semivolatile chemical nerve agents, although low–vapor pressure materials such as explosives are challenging because they do not produce a sufficiently high concentration of vapor (*4*).

The transducer elements for such sensor arrays need to be small, low-power, and compatible with conventional microprocessing technology. Among the choice of transducers are mechanical oscillators that respond to changes in mass (*1*, *2*), chemicapacitors that detect changes in dielectric properties (*4*–*6*), and chemiresistors that monitor the resistance of a polymer laced with conductive particles (*7*–*9*). Of these transducers, chemicapacitors (*4*) and chemiresistors (*7*, *8*) are the best suited for low-power sensor arrays. Chemiresistors are simple to implement, but instability of the con-

Naval Research Laboratory, Washington, DC 20375, USA.

*To whom correspondence should be addressed. E-mail: snow@bloch.nrl.navy.mil

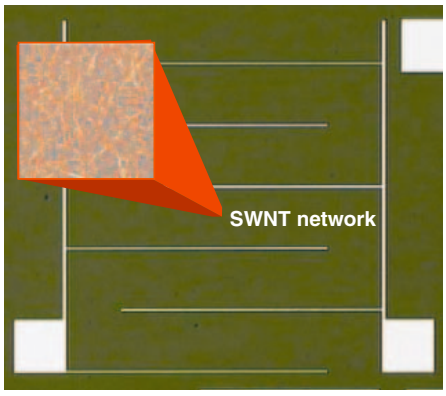

Fig. 1. Optical micrograph of a SWNT chemicapacitor. The region between the electrodes is covered with an optically transparent but electrically continuous network of SWNTs (shown in the inset atomic force microscope image). The capacitance was measured by applying an ac bias between this top surface and the underlying conducting Si substrate. The electrodes were interdigitated to allow simultaneous measurement of the network resistance, but were electrically shorted for data collected here.

Table 1. Capacitance response to various chemical vapors. Listed are the measured values of $\Delta C/C$ corresponding to P/P_0 = 1%. Also listed are the values of the dipole moment, μ, the equilibrium vapor pressure, P_0, at 25°C, and the vapor concentration, P, in parts per million.

Chemical vapor	P_0 (mbar) at 25°C	P (ppm) at 1% P/P_0	μ (D)	$\Delta C/C \times 10^{-3}$ at 1% P/P_0
Benzene	127	1290	0	0.3 ± 0.1
Hexane	200	2030	0	0.4
Heptane	61	618	0	0.2
Toluene	38	385	0.38	0.5
Trichloroethylene	91	922	0.8	0.6
Chloroform	257	2600	1.04	0.8
Trichloroethane	38	385	1.4	0.8
Isopropyl alcohol	108	1093	1.58	3.8
Ethanol	78	792	1.69	3.0
Chlorobenzene	16	162	1.69	0.4
Methyl alcohol	168	1702	1.7	2.7
Tetrahydrofuran	215	2180	1.75	5.9
Ethyl acetate	127	1290	1.78	3.1
Water	32	324	1.85	0.5
Dichlorobenzene	2	20.3	2.5	0.4
Acetone	304	3080	2.88	6.1
Dimethylmethylphosphonate	1.6	16.2	3.62	10.2
N,*N*-dimethylformamide	5	50.7	3.82	9.3
Dinitrotoluene	0.0028	0.028	4.39	0.5

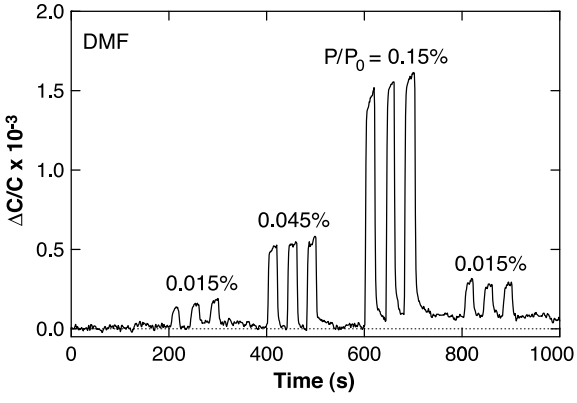

Fig. 2. Measured relative capacitance change, $\Delta C/C$, of a SWNT chemicapacitor in response to repeated 20-s doses of dimethyl formamide (DMF) at varying concentrations noted in the figure.

ductive particle/polymer interface can be a disadvantage. Chemicapacitors are more stable but can take minutes to respond and recover (*4*). This slow response is limited by the time necessary to load and then remove the analyte from the relatively thick layers of chemoselective dielectric (~1 μm) that are typically used.

We describe a chemicapacitor constructed from single-walled carbon nanotube (SWNT) electrodes that combines the features of stability, high sensitivity to a broad range of analytes, and fast response time. The capacitance response of the SWNT chemicapacitor is dominated by surface adsorbates, which allows us to use very thin layers of chemoselective material down to, and including, a single molecular monolayer. By achieving chemical selectivity with such a monolayer, we eliminate the time required to load and refresh a thick, chemoselective dielectric and can perform sensitive, real-time sensing.

The surface capacitance effect is caused by the large electric-field gradient radiating from the ~1-nm-diameter SWNT electrodes. This transduction mechanism is quite general and can be used to detect both volatile organics and low–vapor pressure explosives. We demonstrate the compatibility of this transducer with conventional chemoselective polymers by using a hydrogen-bonding polymer to achieve a minimum detectable level (MDL) of 0.5 parts per billion (ppb) for dimethylmethylphosphonate (DMMP), a simulant for the chemical nerve agent sarin.

To improve the response time, we replaced the polymer layer with a hydrogen-bonding molecular monolayer. In this case, we achieve a MDL of 50 ppb for DMMP with a 90% recovery time, t_{90}, < 4 s. By combining 1-nm-diameter electrodes with molecular-scale functionalization, we achieve a sorption-based chemicapacitor that offers stability, real-time sensing, and a high sensitivity to a wide spectrum of chemical vapors ranging from volatile organics to low–vapor pressure explosives.

We fabricated the SWNT chemicapacitors by using chemical vapor deposition to grow a SWNT network on a 250-nm-thick thermal oxide on a degeneratively doped silicon substrate (*10*). For each sensor, a 2 mm by 2 mm interdigitated array of Pd electrodes was deposited on top of the SWNT network by using photolithography and lift-off. The interdigitated electrodes provide contacts for the simultaneous measurement of both the capacitance and the resistance of the SWNT network. The region inside the array was protected by photoresist, and the unprotected SWNTs were removed from the substrate by a CO_2 snowjet. The photoresist was then removed, which left the SWNT network exposed to the ambient environment. We prepared the chemical vapors by mixing saturated vapors of the analyte with dry air at 25°C.

The SWNT network forms an array of nanoscale electrodes that serves as one plate of the capacitor, with the other electrode formed by the heavily doped Si substrate (Fig. 1). We measured the capacitance by applying a 30-kHz, 0.1-V ac voltage between the SWNTs and the substrate and detecting the out-of-phase ac current with a lock-in amplifier. The measured capacitance, ~ 10 nF/cm^2, is close to the parallel-plate value corresponding to a 250-nm-thick SiO_2 gate dielectric and is the expected value for an inter-SWNT spacing less than the SiO_2 thickness (*11*).

Under an applied bias, fringing electric fields (~10^5 to 10^6 V/cm, for a 0.1-V bias) radiate outward from the SWNTs. These fringing fields are strongest at the SWNT surface and produce a net polarization of the adsorbates that we detect as an increase in capacitance. The relative capacitance change, $\Delta C/C$, of one such device in response to repeated 20-s doses of *N*,*N*-dimethylformamide (DMF) at varying vapor concentrations (Fig. 2) shows that the observed response is rapid (limited by the 4-s response time of our vapor-delivery system), proportional

to the analyte concentration, and completely reversible. Of the chemical vapors that we have tested (Table 1), we observe a similar, rapid capacitance response that is completely reversible upon removal of the vapor. We also note that ΔC is independent of the applied voltage for $V_{ac} < 1$ V, which indicates that the polarization is a linear function of the electric field.

In Table 1, we list values of $\Delta C/C$ for a number of chemical vapors, each measured at a fixed fraction, $P/P_0 = 1\%$, of the equilibrium vapor pressure P_0. We also list literature values of P_0 (*12*), the vapor concentration, P, in parts per million (ppm) at $P/P_0 = 1\%$, and the molecular dipole moment, μ (*12*, *13*). In Fig. 3, we plot the values of $\Delta C/C$ reported in Table 1 for each of the analytes versus their respective dipole moments.

In Fig. 3, we observe that for several analytes, the magnitude of the capacitance response correlates with the value of its dipole moment. Nonpolar molecules such as hexane and benzene produce a small response, whereas relatively polar molecules like DMMP and DMF produce a large capacitance response. This correlation with dipole moment holds under the condition that the vapors are each delivered at a constant value of P/P_0, and not for a constant value of P. For example, acetone ($\mu = 2.88$ D) and DMMP ($\mu = 3.62$ D) produce a comparable capacitance response when both are delivered at $P/P_0 = 1\%$ even though this condition corresponds to vapor concentrations of 3080 ppm and 16 ppm, respectively. Several analytes such as chlorobenzene, 1,2-dichlorobenzene, 2,4-dinitrotoluene, and water (represented by squares in Fig. 3) produce a small capacitance response even though they have a relatively large dipole moment. These data indicate that the magnitude of the capacitance response is strongly modified by surface interactions.

The polarizability of a free vapor molecule is given by $\gamma = \gamma_{mol} + \frac{\mu^2}{3kT}$ (*14*), where the first term arises from the intrinsic molecular polarizability, γ_{mol}, and the second term arises from the field-induced alignment of the otherwise randomly oriented molecular dipole moment. From the Clausius-Mossotti equation, this polarizability is related to the dielectric constant, ε, by

$$\varepsilon = 1 + 4\pi\frac{N\gamma}{1 - \frac{4\pi}{3}N\gamma},$$

where N is the number of molecules, which is proportional to the vapor pressure, P. Thus, for a dilute vapor, the capacitance response should scale as $P\mu^2$. Instead, we observe that $\Delta C/C \propto \frac{P}{P_0}$ and that there are large deviations from simple μ^2 behavior.

For surface adsorbates, the polarization will be proportional to the number of the adsorbates, which is proportional to $\frac{P}{P_0}e^{(E_b - E_i)/kT}$ (*15*), where E_i is the analyte mutual interaction energy and E_b is the binding energy to the SWNT surface (approximately the thermal energy, kT, for physisorbed molecules). Thus, for adsorbates, we expect the capacitance to scale as P/P_0 with significant analyte-to-analyte variations caused by the differences in binding and interaction energies.

Additionally, surface interactions will preferentially orient the molecular dipole moment. For example, the low response of chlorobenzene, 1,2-dichlorobenzene, and 2,4-dinitrotoluene can be understood in the context of surface interactions. These analytes indicate that the capacitance response scales with the component of the dipole moment oriented perpendicular to the SWNT surface. Each of these molecules has a dipole moment that is oriented in the plane of an aromatic ring. Our density functional calculations (*16*) indicate that the lowest energy configuration corresponds to the ring lying flat on the SWNT surface. In this orientation, the dipole moment lies perpendicular to the radial electric field, which minimizes the polarization and results in a small capacitance effect. The cause of the small water response is not clear. However, it has been suggested that the dipole moment of water also aligns tangentially to the SWNT surface in its lowest energy configuration (*17*).

Our initial density functional calculations (*16*) indicate that for some analytes such as acetone the primary polarization effect derives from the field dependence of the binding energy, which causes a change in the number of adsorbates by a factor $\sim\Delta E_b/kT$. However, further study is needed to understand the precise polarization mechanism, which will differ for different analytes.

The rapid, completely reversible capacitance response that we observe contrasts with the behavior of SWNT chemiresistors (*18*–*25*). SWNT chemiresistors respond to a narrower range of analytes, and typically the resistance recovers very slowly after exposure. Part of the reason for this difference is that the SWNT chemiresistors detect charge transfer from analytes, whereas the SWNT chemicapacitors operate via a different transduction mechanism, the polarization of surface adsorbates (*26*). Our experience measuring both effects simultaneously on the same device indicates that, for most vapors, the capacitance response is more sensitive, recovers much faster, and applies to a broader range of analytes (*27*).

Because most chemical vapors, ranging from volatile organics such as acetone to low–vapor pressure solids such as 2,4-dinitrotoluene, produce an easily measured capacitance response, this transduction mechanism can be used to detect a broad spectrum of molecular analytes. To explore this possibility, we coated our sensors with a chemoselective polymer, HC,

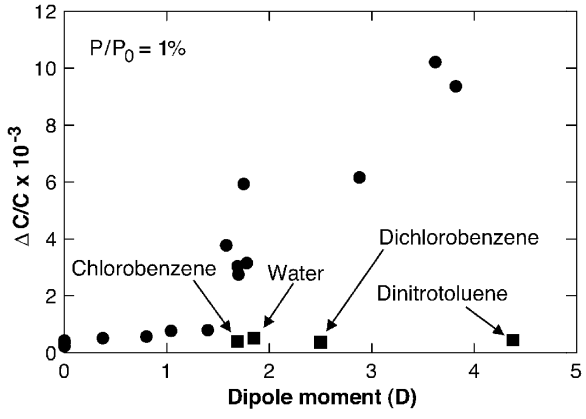

Fig. 3. Measured capacitance response to $P/P_0 = 1\%$ doses of various chemical vapors plotted as a function of their molecular dipole moment. The capacitance response generally increases with dipole moment; however, large deviations from this trend are observed.

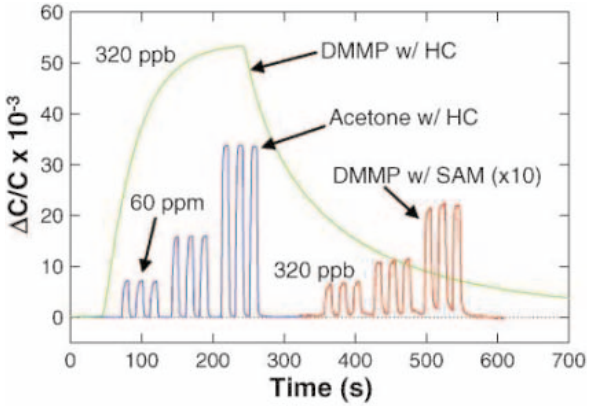

Fig. 4. Blue curve: Response to 10-s doses of acetone of a SWNT chemicapacitor coated with the polymer, HC. The concentration was set at 60, 180, and 540 ppm. Green curve: Response of the same HC-coated sensor to a single, 200-s dose of DMMP. Note the increased response time caused by the slower diffusion of the DMMP. Red curve: Response ($\times 10$) of a SAM-coated sensor to 10-s doses of DMMP. The concentration was set at 320 ppb, 960 ppb, and 2.9 ppm. Note the improvement in response time relative to the HC-coated sensor.

that we designed for preferential absorption of chemical nerve agents. HC is an acidic, strong–hydrogen-bonding polycarbosilane (*25*). We coated a sensor with a thin layer (~100 nm) of HC and tested the response to several analytes. The response of this polymer-coated sensor to repeated 10-s doses of acetone ranging from 60 to 540 ppm is shown in Fig. 4. The acetone produces a large, rapid response that is ~100 times larger than the response measured in the same sensor before the HC deposition. The HC concentrates the acetone vapor in the vicinity of the SWNTs, which increases the response while maintaining a rapid response time. The response to a single 200-s dose of DMMP delivered at 320 ppb shows that the measured gain for DMMP relative to the uncoated sensor is about 500 (Fig. 4). Note that the low diffusion rate of DMMP in the HC causes a slower recovery rate, t_{90} = 370 s. For water and chloroform, the polymer coating produces much lower response gains of 1 and 10, respectively. Thus, the HC provides a large chemically selective gain, demonstrating the feasibility of SWNT sorption-based chemical sensing.

These sensor characteristics compare favorably with those of commercial chemicapacitors. Using a signal-to-noise ratio of 3:1 as a detection criterion, we estimate that MDL = 0.5 ppm and t_{90} < 4 s for acetone and MDL = 0.5 ppb and t_{90} = 370 s for DMMP. For these same analytes, the commercial sensor achieves a MDL = 2 ppm and t_{90} = 228 s for acetone and MDL = 2 ppb and t_{90} = 3084 s for DMMP (*4*). We attribute our faster response and recovery times to the use of a much thinner layer of chemoselective material. For HC, the minimum layer thickness was limited by the tendency of the HC to form a discontinuous film below ~100 nm.

Our initial polymer-coated SWNT sensors achieve both higher sensitivity and faster response times than do current chemicapacitors. However, both of these properties can be substantially improved with a few design modifications. The sensitivity is currently limited by the small series capacitance of the thick SiO_2 layer. By thinning the SiO_2 layer or replacing it with a high–dielectric constant insulator (*28*), we estimate that we can increase the series capacitance by about a factor of 10, which should produce a comparable increase in response.

The response time for analytes such as DMMP is limited by diffusion through the layer of HC. Because the SWNT capacitor is based on a surface effect, we can improve the response time and still achieve chemical gain by using extremely thin layers of chemoselective material down to, and including, a single molecular monolayer.

To explore this limit of a chemoselective monolayer, we coated the SiO_2 surface with a self-assembled monolayer (SAM) of allyltrichlorosilane. We then reacted the terminal alkenes with hexafluoroacetone to produce a monolayer of hexafluoroisopropanol that partially covers the SWNTs with fluoroalchohol groups. The response of this SAM-coated sensor to repeated 10-s doses of DMMP ranging from 320 ppb to 2.9 ppm is shown in Fig. 4. For this sensor, the response tracks our vapor-delivery system, indicating that t_{90} < 4 s, and we measured a MDL = 50 ppb. Notably, with the SAM coating, the capacitance response of DMMP relative to that of water is increased by a factor of 40, indicating that we achieved substantial chemically selective gain. These initial promising results indicate that optimization of the chemoselective monolayers to better cover the SWNTs, combined with improved sensor design, can result in a new class of sorption-based sensors that combine the features of low power, high sensitivity, and fast response time.

References and Notes

1. R. A. McGill *et al.*, *Sens. Actuators B* **65**, 10 (2000).
2. J. W. Grate, B. M. Wise, M. H. Abraham, *Anal. Chem.* **71**, 4544 (1999).
3. H. T. Nagle, S. S. Schiffman, R. Gutierrez-Osuna, *IEEE Spectr.* **35**, 22 (1998).
4. S. V. Patel *et al.*, *Sens. Actuators B* **96**, 541 (2003).
5. G. Delapierre, H. Grange, B. Chambaz, L. Destannes, *Sens. Actuators* **4**, 97 (1983).
6. A. Hierlemann *et al.*, *Sens. Actuators B* **70**, 2 (2000).
7. M. P. Eastman *et al.*, *J. Electrochem. Soc.* **146**, 3907 (1999).
8. M. C. Lonergan *et al.*, *Chem. Mater.* **8**, 2298 (1996).
9. J. R. Li, J. R. Xu, M. Q. Zhang, M. Z. Rong, *Carbon* **41**, 2353 (2003).
10. E. S. Snow, J. P. Novak, P. M. Campbell, D. Park, *Appl. Phys. Lett.* **82**, 2145 (2003).
11. E. S. Snow, P. M. Campbell, J. P. Novak, *Appl. Phys. Lett.* **86**, 033105 (2005).
12. D. R. Lide, *CRC Handbook of Chemistry and Physics* (CRC Press, Boca Raton, FL, ed. 75, 1995), pp. 15-43–15-49.
13. G. M. Kosolapoff, *J. Chem. Soc.* 3222 (1954).
14. J. D. Jackson, *Classical Electrodynamics* (Wiley, New York, ed. 2, 1975), pp. 155–158.
15. S. Brunauer, P. H. Emmett, E. Teller, *J. Am. Chem. Soc.* **60**, 309 (1938).
16. Density functional calculations of adsorbates on graphene sheets in uniform electric fields were performed using the generalized-gradient approximation and the Perdue, Burke, Ernzerhof parameterization of exchange and correlation in the Gaussian 03 localized-basis package (Gaussian 03, Revision C.02; M. J. Frisch *et al.*, Gaussian, Inc., Pittsburgh PA, 2003).
17. J. H. Walther, R. Jaffe, T. Halicioglu, P. Koumoutsakos, *J. Phys. Chem. B* **105**, 9980 (2001).
18. J. Kong *et al.*, *Science* **87**, 622 (2000).
19. L. Valentini *et al.*, *Appl. Phys. Lett.* **82**, 961 (2003).
20. T. Someya, J. Small, P. Kim, C. Nuckolls, J. T. Yardley, *Nano Lett.* **3**, 877 (2003).
21. J. Li *et al.*, *Nano Lett.* **3**, 929 (2003).
22. A. Goldoni, R. Larciprete, L. Petaccia, S. Lizzit, *J. Am. Chem. Soc.* **125**, 11329 (2003).
23. P. Qi *et al.*, *Nano Lett.* **3**, 347 (2003).
24. L Valentini *et al.*, *Diamond Relat. Mater.* **13**, 1301 (2004).
25. J. P. Novak *et al.*, *Appl. Phys. Lett.* **83**, 4026 (2003).
26. Charge transfer from an analyte can potentially cause a capacitance response by changing the quantum capacitance of the nanotubes. We have simulated this chemical doping effect by applying to the substrate a small dc offset to the ac bias, which increases the charge in the SWNTs. By measuring the resulting capacitance and resistance responses, we calibrated the effect of a charge offset. For the vapors we have tested, most do not produce a measurable resistance response, and those that do, produce a resistance change that is much too small (based on this calibration) to account for the change in capacitance.
27. For an example, see the supplementary data available at *Science* Online.
28. B. M. Kim *et al.*, *Appl. Phys. Lett.* **84**, 1946 (2004).

29. We gratefully acknowledge financial support from the Homeland Security Advanced Research Projects Administration, the Office of Naval Research, and the Naval Research Laboratory Nanoscience Institute.

Supporting Online Material

www.sciencemag.org/cgi/content/full/307/5717/1942/DC1
SOM Text
Fig. S1

27 December 2004; accepted 1 February 2005
10.1126/science.1109128

Light Scattering to Determine the Relative Phase of Two Bose-Einstein Condensates

M. Saba,* T. A. Pasquini, C. Sanner, Y. Shin, W. Ketterle, D. E. Pritchard

We demonstrated an experimental technique based on stimulated light scattering to continuously sample the relative phase of two spatially separated Bose-Einstein condensates of atoms. The phase measurement process created a relative phase between two condensates with no initial phase relation, read out the phase, and monitored the phase evolution. This technique was used to realize interferometry between two trapped Bose-Einstein condensates without need for splitting or recombining the atom cloud.

The outstanding property of atoms in a Bose-Einstein condensate (BEC) is their coherence: They all have the same phase. This property became apparent when high-contrast interference between condensates was observed (*1–3*). Phase coherence between spatially separated condensates has led to the observation of a host of phenomena, including Josephson oscillations (*3*, *4*), number squeezing (*5*), and the transition from superfluid to Mott insulator (*6*).

The evolution of the phase is affected by external potentials acting on the atoms and has

been exploited for interferometric measures of gravity and other interactions (*3*, *7*–*9*). Ideally, one could reach extreme interferometric sensitivity by coherently extracting atoms from two distant condensates and letting them interfere (*10*). So far, however, the relative phase of condensates has been measured only destructively, by taking an absorption image of interfering atomic waves.

Several methods have been considered to determine the relative phase of two separated atomic wavepackets spectroscopically by the scattering of light. In the simple case of a single atom delocalized in two separate wells, spontaneous photon scattering leaves the atom localized in one well, destroying the spatial coherence without giving any interferometric information (*11*, *12*). On the other hand, selecting the frequency of the scattered photons makes it possible to retrieve interference from specially prepared wavepackets, like two spatially separated components moving on parallel trajectories (*13*). BECs offer the possibility of scattering many photons out of the same coherent ensemble, affecting only a small fraction of the atoms in the condensates and providing an almost nondestructive measurement of the relative phase between the two condensates (*14*–*16*). Thus, light scattering could be used to compare the phase of two separate condensates at multiple subsequent times, realizing an interferometer with neither coherent splitting nor recombination of the wavepacket.

Even if the condensates are in states with poorly defined relative phase (such as the so-called Fock states, in which the atom number is well defined), they still interfere with each other. In this case, the relative phase is "created" in the measurement process by projecting the system on a coherent state with a well-defined phase (*17*–*21*).

We show that stimulated light scattering can be used to continuously sample the relative phase between two spatially separate BECs. The basis of our measurement is that the structure factor of two neighboring BECs shows interference fringes in momentum space (*21*). This interference can be pictured in a very direct way: Let us continuously impart some momentum $\vec{q}$ to a fraction of the atoms in each condensate, so that they move parallel to the displacement of the two condensates. When the atoms from the first condensate reach the second one, the two streams of atoms moving with momentum $\vec{q}$ will overlap and interfere. The process can be rephrased as beating of two atom lasers originating from the two condensates. If the relative phase of the condensates is fixed, the total number of moving atoms depends on the value of the momentum q and oscillates sinusoidally with periodicity h/d as q is scanned (h is Planck's constant and d is the displacement of the condensates). If instead the phase evolves in time and the momentum $\vec{q}$ is fixed, the number of atoms in the moving stream will vary in time at the same rate as the relative phase.

The experimental tool used to impart a precise momentum to atoms in a BEC is Bragg scattering (*22*, *23*). Two counterpropagating laser beams with wavevectors $\vec{k}_{1,2}$ hit the atoms so that, by absorbing a photon from one beam and reemitting it into the other one, the atoms acquire recoil momentum $\hbar(\vec{k}_2-\vec{k}_1)$, provided that the energy difference between photons matches the atom recoil energy.

In our experiment (Fig. 1, A and B), two independent cigar-shaped BECs containing $\approx 10^6$ sodium atoms were prepared in a double-well optical dipole trap (*8*) and were

Department of Physics, MIT-Harvard Center for Ultracold Atoms, and Research Laboratory of Electronics, Massachusetts Institute of Technology, Cambridge, MA 02139, USA.

*To whom correspondence should be addressed. E-mail: msaba@mit.edu

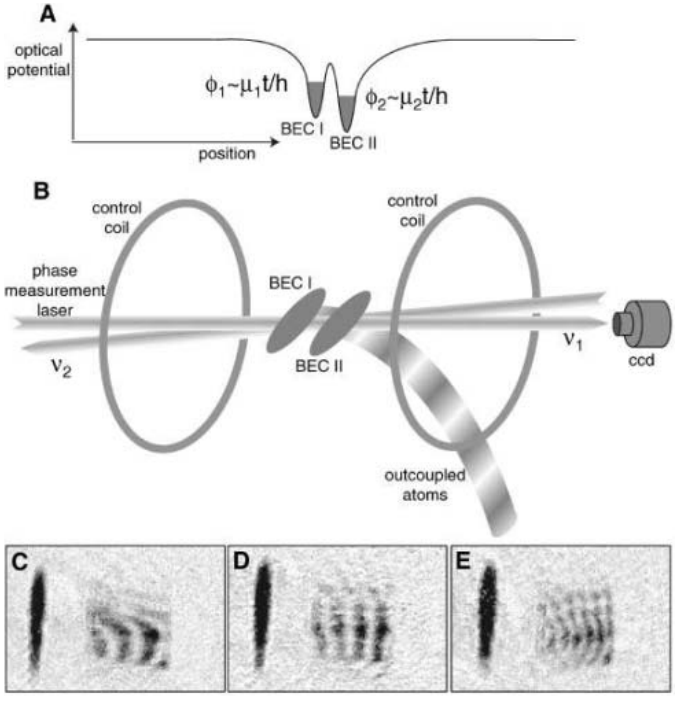

Fig. 1. Interference of two atom lasers coupled out from two independent condensates. (**A**) Energy diagram of the two BECs (BEC I and BEC II) confined in an optical double-well trap. (**B**) Experimental scheme for continuous phase measurement. Two laser beams were applied to the condensates to outcouple a few atoms from the trap. Detecting the rate of outcoupled atoms or the number of scattered photons gives a measurement of the relative phase between the condensates. The control coils generate magnetic field gradients that affect the frequency of interference oscillations. Gravity points down in this picture. (**C** to **E**) Absorption images showing the optical density of the atom clouds were taken from top after applying the Bragg beams (gravity points into the page). The thick shadows on the far left in each panel are the unresolved two condensates; to the right are the atoms that were continuously outcoupled and flew from left to right. High-contrast oscillations in the stream of outcoupled atoms are clearly visible. In the central picture (D), oscillations originated from the imbalance in the depth of the two wells. In (C), an additional magnetic field gradient of 1.15 G/cm was applied with the control coils; in (E), the gradient was −0.77 G/cm (with the positive direction pointing to the right). Images were taken after an additional 5 ms of time of flight, and the field of view in each picture is 1.35 mm × 0.90 mm.

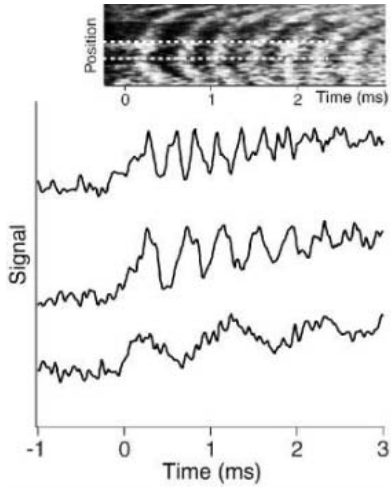

Fig. 2. Continuous optical readout of the relative phase of two condensates. In the upper panel is the optical signal image detected by streaking the CCD camera (*24*). The traces, offset vertically for clarity, are cross sections of the images (the central trace corresponds to the upper image integrated between the dashed lines). Bragg scattering starts at $t = 0$ when the second beam is turned on. The relative depth of the two wells was different for the three traces, generating a difference in the oscillation frequency. The overall slope on the traces was due to spontaneous Rayleigh scattering of the light from the atoms in the condensates. As the time went on, the condensates were depleted and the Rayleigh scattering was reduced. Excitations in the condensates appeared as tilted or curved fringes in the streak image; in such cases, we took cross sections from portions of the images where fringes were vertical and therefore the phase evolution was less perturbed.

illuminated with two counterpropagating Bragg beams to impart recoil momentum to a few atoms (*24*). The Bragg-scattered atoms flew away from the trap because the trap was shallower than the recoil energy. In the stream of outcoupled atoms (Fig. 1, C to E), the spatial modulations in the absorption images reflect temporal oscillations in the number of atoms outcoupled from the two condensates, implying a continuous evolution of the relative phase ϕ with time t at a rate $d\phi/dt = \Delta E/h$, caused by the energy offset ΔE between the condensates. The three images were taken with different magnetic field gradients applied with the control coils. The difference in magnetic field between the two wells modifed the energy offset ΔE and therefore affected the beat frequency $d\phi/dt$ of the two condensates. The fact that the fringes are not straight everywhere can be related to motional excitations in the condensates and the perturbing effect of the optical dipole potential on the time-of-flight trajectory of the atoms.

For each atom outcoupled from the condensate, a photon was transferred from one beam to the counterpropagating one. Therefore, all information contained in the stream of outcoupled atoms was also present in the scattered light and could be gathered in real time by monitoring the intensity of one of the Bragg laser beams, instead of interrupting the experiment to illuminate atoms with a resonant laser for absorption imaging. The dynamics of the optical signal was measured with a charge-coupled device (CCD) camera in streaking mode, generating images with time on one axis and spatial information on the other (Fig. 2) (*24*). The intensity of the Bragg beam oscillated in time at a frequency controlled by the relative energy between the two wells. The oscillating signal built up during the first $\approx$ 250 μs, this being the time required for the outcoupled atoms to travel from one condensate to the other one and start interference.

Interferometry between two trapped BECs was realized by continuous monitoring of their beat frequency. Figure 3 demonstrates the sensitivity of the interferometer to an applied external force (magnetic field gradient) and to the application of a potential difference between the two wells (dynamical Stark shift induced by increasing the laser power in one of the two wells).

We did not observe oscillation frequencies below 500 Hz. Short observation times and excitations could contribute to this, but there is a fundamental limitation to the minimum measurable frequency due to interactions between atoms. If the phase stays (almost) constant for a long time, one of the two condensates can end up continuously amplifying or deamplifying the atoms outcoupled from the other one, causing asymmetric depletion of the condensates and therefore a difference in chemical potential, as large as a few $h \times 100$ Hz in a few milliseconds under our experimental parameters. This is analogous to the inhibition of slow, large-amplitude Josephson oscillations in a nonlinear junction (*25*). If the relative phase is actively controlled, atoms can be coherently transferred from one well to the other, replenishing one of the two condensates without scrambling its phase; a method that could lead to a continuous atom laser (*26*).

The interferometric information contained in the beat frequency of two condensates is independent of the initial phase between the condensates and eliminates the need for coherent beam splitting (*10*). The present measurements already show a sensitivity below 100 Hz, limited by mechanical excitations that cause chirping of the frequency during the observation time and shot-to-shot variations. More fundamentally, the finite number of atoms in the condensates limits the number of Bragg-scattered photons and therefore the signal-to-noise ratio. No phase diffusion is expected during the measurement, the oscillations being continuously driven by the laser beams (*27*, *28*). This is a general manifestation of the influence of measurement on a quantum system (*29*), similar to the quantum Zeno effect, where the time evolution is suppressed by repeated or continuous measurements.

A more versatile interferometric scheme can be obtained by applying two successive Bragg pulses to the pair of condensates and exploiting the fact that the optical phase readout allows comparison of subsequent measurements on the same pair of condensates. A first Bragg pulse lasting 1 ms determined a randomly varying relative phase between the two condensates at each realization of the experiment (Fig. 4B). A second Bragg pulse followed after allowing the two condensates to evolve for some delay (0.5 ms) and measured a relative phase again random at each shot

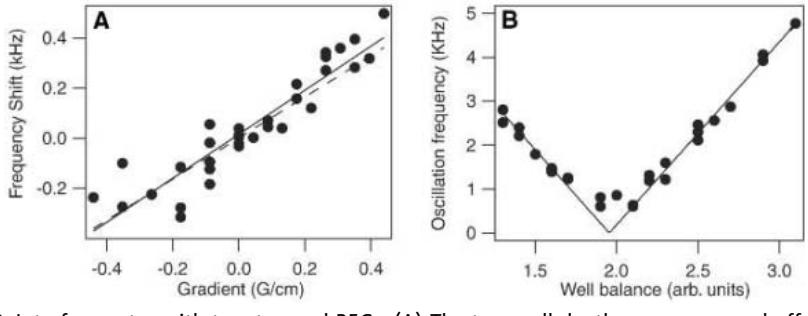

Fig. 3. Interferometry with two trapped BECs. (**A**) The two well depths were prepared offset by $\approx$ 0.53 kHz in the absence of magnetic field gradients, and the shift of the beat frequency with respect to this initial value is plotted versus the applied magnetic field gradient. The beat frequency is determined from pictures similar to those in Fig. 2. The solid line is a linear fit to the data; the dashed line represents the frequency $\mu_B B' d/2h$ expected for the evolution of the relative phase of the two condensates due to the difference in energy induced by the gradient (B' is the independently measured magnetic gradient, μ_B is half Bohr magneton corresponding to the magnetic moment of the atoms, and d is the displacement of the two condensates). (**B**) Beat frequency measured in the optical signal is shown as a function of the relative depth of the two potential wells. The well balance parameter is proportional to the difference in optical power used to create each of those wells and was controlled by the power in each of the two radio frequencies fed into the acousto-optical modulator. arb., arbitrary.

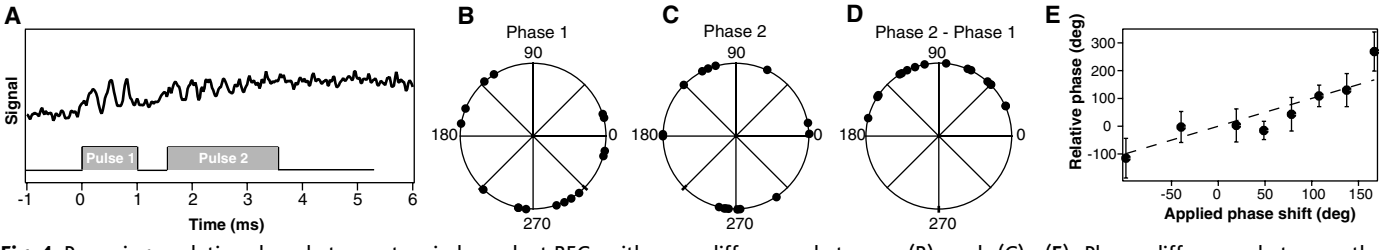

Fig. 4. Preparing a relative phase between two independent BECs with no initial phase relation. (**A**) The temporal trace of the Bragg beam intensity shown with the pulse sequence. (**B**) Phase of the oscillations recorded during the first pulse. (**C**) Phase during the second pulse. (**D**) Phase difference between (B) and (C). (**E**) Phase difference between the oscillations in two pulses as a function of the phase shift applied during the evolution time between pulses. Each point is the average of several shots (between 3 and 10).

(Fig. 4C). Comparison with the phase measured in the first pulse shows that the two measurements were correlated (Fig. 4D). In other words, the first measurement established a definite relative phase between the two condensates that may not have had a defined phase before, and the second measurement verified that the condensates evolved with that particular phase during the interval between pulses.

Interferometry was demonstrated by putting an interaction time between the two pulses and changing the outcome of the second measurement. We briefly modified the energy offset between the two wells during the interval between the pulses, when the phase was not being observed. Figure 4E compares the measured phase shift with the value $\Delta E \Delta t/h$ expected from an energy offset ΔE applied for a time Δt. The agreement between the prediction and the measurement demonstrates that the relative phase can be engineered by applying external forces to the atoms.

Active control of the phase opens interesting future perspectives: One could measure the light signal in real time and feed back the phase measurement into the control coils (or into the acousto-optical modulator that controls the two laser powers, creating the double-well potential), preparing the desired phase at the desired time. In principle, the uncertainty in the relative phase could even be squeezed by the feedback, allowing sub–shot noise interferometry (*5*, *10*, *30*).

Several physical interpretations of the experiment are possible besides the interference of two atom lasers. One is interference in momentum space (*21*): The zero-momentum component of the momentum distribution of the double condensate depends sinusoidally on the relative phase of the condensates and is probed with Doppler-sensitive spectroscopy (realized by Bragg scattering). Yet another point of view is that light scattering probes the excitation spectrum through the dynamical structure factor. The structure factor is phase-sensitive and shows interference fringes without requiring spatial overlap between the two condensates, as long as the excited states (after light scattering) have spatial overlap. This picture emphasizes that overlap between scattered atoms, as well as scattered photons, is crucial to our method: No phase information can be retrieved from two atomic wavepackets that scatter the same light but whose excited states are disconnected, like two condensates separated by a transparent glass wall.

The concept of beating atom lasers was previously exploited to measure spatial coherence in a single condensate (*31*) and for experiments done in optical lattices, where atoms outcoupled from a large vertical array of regularly spaced condensates interfered and their beating frequency measured gravity (*3*, *10*). In this case, condensates were split coherently by raising the optical lattice potential. Coupling was established by tunneling of atoms between adjacent lattice sites and depended exponentially on the barrier shape, whereas the laser beams in our scheme established a coupling through a state delocalized over the barrier. In principle, larger barriers could be overcome by imparting larger momenta in the Bragg process. From the standpoint of precision interferometry, optical lattices have the advantage of a very well-known and controlled displacement between condensates, whereas the optical detection that we introduce here measures the beat frequency continuously and in real time, with accuracy not depending on the calibration of image magnification (*3*) or other disturbances affecting atoms during time of flight.

Our scheme to nondestructively measure the beat frequency of two previously independent condensates, thus establishing phase coherence, could permit us to couple condensates displaced by tens of microns on atom chips or in other microtraps, to explore Josephson oscillations, phase diffusion, and self-trapping. We have already demonstrated its potential in exploiting the phase coherence of BECs to create a novel type of atom interferometer.

References and Notes

1. M. R. Andrews *et al.*, *Science* **275**, 637 (1997).
2. D. S. Hall, M. R. Matthews, C. E. Wieman, E. A. Cornell, *Phys. Rev. Lett.* **81**, 1543 (1998).
3. B. P. Anderson, M. A. Kasevich, *Science* **282**, 1686 (1998).
4. F. S. Cataliotti *et al.*, *Science* **293**, 843 (2001).
5. C. Orzel, A. K. Tuchman, M. L. Fenselau, M. Yasuda, M. A. Kasevich, *Science* **291**, 2386 (2001).
6. M. Greiner, O. Mandel, T. Esslinger, T. W. Hänsch, I. Bloch, *Nature* **415**, 39 (2002).
7. S. Gupta, K. Dieckmann, Z. Hadzibabic, D. E. Pritchard, *Phys. Rev. Lett.* **89**, 140401 (2002).
8. Y. Shin *et al.*, *Phys. Rev. Lett.* **92**, 050405 (2004).
9. Y. J. Wang *et al.*, preprint available at http://www.arxiv.org/abs/cond-mat/0407689 (2004).
10. M. A. Kasevich, *CR Acad. Sci. IV* **2**, 497 (2001).
11. C. CohenTannoudji, F. Bardou, A. Aspect, in *Laser Spectroscopy X*, M. Ducloy, E. Giacobino, Eds. (World Scientific, Singapore, 1992), p. 3.
12. K. Rzążewski, W. Żakovicz, *J. Phys. B* **25**, L319 (1992).
13. B. Dubetsky, P. R. Berman, *J. Mod. Opt.* **49**, 55 (2002).
14. J. Javanainen, *Phys. Rev. A* **54**, 4629(*R*) (1996).
15. A. Imamoglu, T. A. B. Kennedy, *Phys. Rev. A* **55**, 849(*R*) (1997).
16. J. Ruostekoski, D. F. Walls, *Phys. Rev. A* **56**, 2996 (1997).
17. J. Javanainen, S. M. Yoo, *Phys. Rev. Lett.* **76**, 161 (1996).
18. M. Naraschewski, H. Wallis, A. Schenzle, J. I. Cirac, P. Zoller, *Phys. Rev. A* **54**, 2185 (1996).
19. J. I. Cirac, C. W. Gardiner, M. Naraschewski, P. Zoller, *Phys. Rev. A* **54**, 3714(*R*) (1996).
20. Y. Castin, J. Dalibard, *Phys. Rev. A* **55**, 4330 (1997).
21. L. Pitaevskii, S. Stringari, *Phys. Rev. Lett.* **83**, 4237 (1999).
22. M. Kozuma *et al.*, *Phys. Rev. Lett.* **82**, 871 (1999).
23. J. Stenger *et al.*, *Phys. Rev. Lett.* **82**, 4569 (1999).
24. Information on materials and methods is available on *Science* Online.
25. A. Smerzi, S. Fantoni, S. Giovanazzi, S. R. Shenoy, *Phys. Rev. Lett.* **79**, 4950 (1997).
26. A. P. Chikkatur *et al.*, *Science* **296**, 2193 (2002).
27. M. Lewenstein, L. You, *Phys. Rev. Lett.* **77**, 3489 (1996).
28. J. Javanainen, M. Wilkens, *Phys. Rev. Lett.* **78**, 4675 (1997).
29. J. A. Wheeler, W. H. Zurek, *Quantum Theory and Measurement* (Princeton Univ. Press, Princeton, NJ, 1983).
30. J. M. Geremia, J. K. Stockton, H. Mabuchi, *Science* **304**, 270 (2004).
31. I. Bloch, T. W. Hansch, T. Esslinger, *Nature* **403**, 166 (2000).

32. This work was funded by the Army Research Office, the Defense Advanced Research Projects Agency, NSF, the Office of Naval Research, and NASA. M.S. acknowledges additional support from the Swiss National Science Foundation and C.S. from the Studienstiftung des deutschen Volkes. We thank G. Jo for experimental assistance, A. Schirotzek for contributions in the early stage of the work, and M. Zwierlein for a critical reading of the manuscript. We are indebted to A. Leanhardt for stimulating suggestions that initiated this research and insightful comments on the experiment and the manuscript.

Supporting Online Material

www.sciencemag.org/cgi/content/full/307/5717/1945/DC1

Materials and Methods

16 December 2004; accepted 3 February 2005

10.1126/science.1108801

Cool La Niña During the Warmth of the Pliocene?

R. E. M. Rickaby and P. Halloran

The role of El Niño–Southern Oscillation (ENSO) in greenhouse warming and climate change remains controversial. During the warmth of the early-mid Pliocene, we find evidence for enhanced thermocline tilt and cold upwelling in the equatorial Pacific, consistent with the prevalence of a La Niña–like state, rather than the proposed persistent warm El Niño–like conditions. Our Pliocene paleothermometer supports the idea of a dynamic "ocean thermostat" in which heating of the tropical Pacific leads to a cooling of the east equatorial Pacific and a La Niña–like state, analogous to observations of a transient increasing east-west sea surface temperature gradient in the 20th-century tropical Pacific.

In 1976, the equatorial Pacific, potentially driven by anthropogenic warming, switched from a weak La Niña state to one in which El Niño occurs with greater frequency and intensity (*1*). For the current climate system, El Niño years are warmer and La Niña years are cooler (*2*). In the future, more persistent El Niño could amplify global warming. Determining what drives ENSO and how

Department of Earth Sciences, University of Oxford, Parks Road, Oxford OX1 3PR, UK.

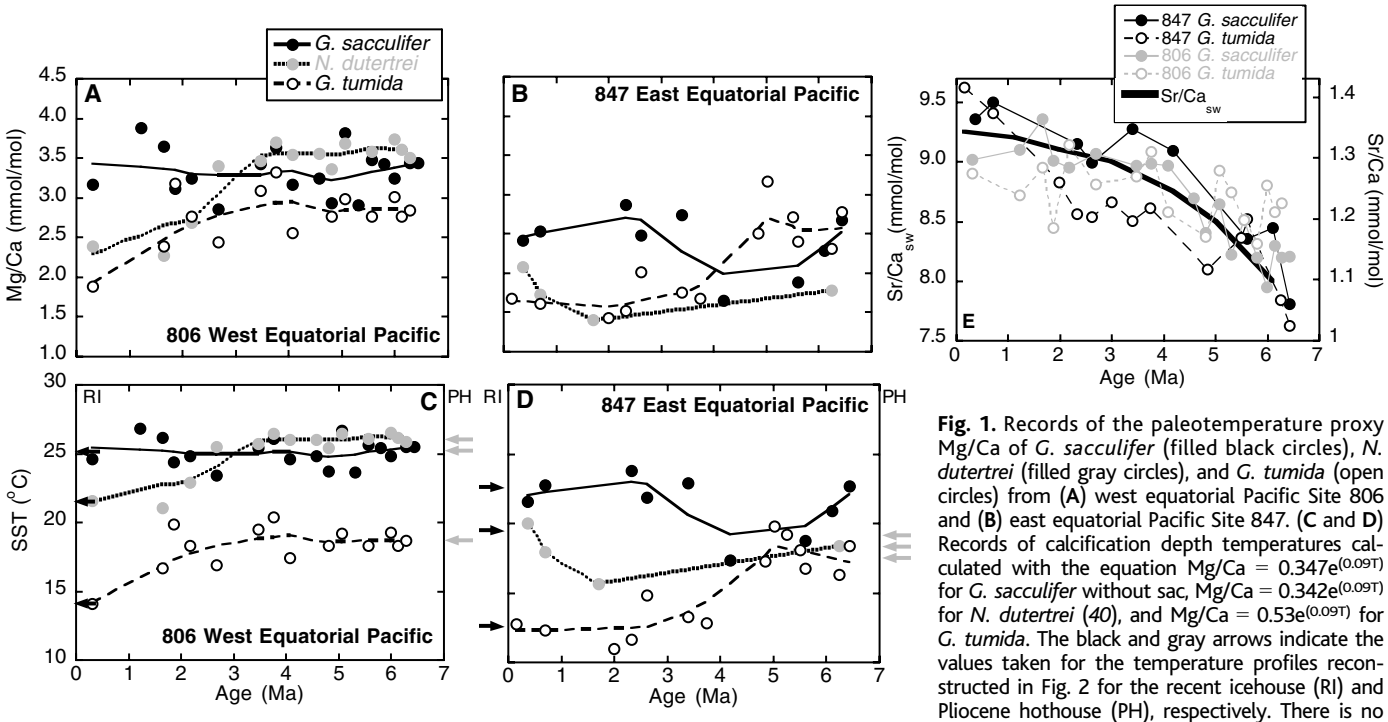

Fig. 1. Records of the paleotemperature proxy Mg/Ca of *G. sacculifer* (filled black circles), *N. dutertrei* (filled gray circles), and *G. tumida* (open circles) from (**A**) west equatorial Pacific Site 806 and (**B**) east equatorial Pacific Site 847. (**C** and **D**) Records of calcification depth temperatures calculated with the equation $Mg/Ca = 0.347e^{(0.09T)}$ for *G. sacculifer* without sac, $Mg/Ca = 0.342e^{(0.09T)}$ for *N. dutertrei* (*40*), and $Mg/Ca = 0.53e^{(0.09T)}$ for *G. tumida*. The black and gray arrows indicate the values taken for the temperature profiles reconstructed in Fig. 2 for the recent icehouse (RI) and Pliocene hothouse (PH), respectively. There is no published calibration for *G. tumida*, and we have assumed the sensitivity to be similar to all other species (*40*) with an exponent of 0.09 and calculated a pre-exponential constant of 0.53. This pre-exponential constant is similar to the calibrated pre-exponential constant for other deep dwellers such as *Globigerinella aequilateralis* and has been calculated with the consideration that most of the calcite is added as a keel at the base of the photic zone, i.e., ~ 200 m in the tropics (*38*). Our calibration for *G. tumida* is also constrained to provide a lower calcification temperature for *G. tumida* than for *G. sacculifer* (due to depth habit) at all times in all sites. The vital effects of deeper dwelling foraminifera can lead to increased incorporation of Mg at lower temperatures compared with shallower dwelling foraminifera (*40*). Our approach gives an accuracy of ±1.2°C in the estimation of calcification temperature but increases to ±3.0°C for *G. tumida*, given the uncertainty in the pre-exponential constant. The smoothed curve through each of the data sets represents a 50% weighted average. It seems reasonable to assume no change in seawater Mg/Ca during this period (*23*). (**E**) Records of Sr/Ca of *G. sacculifer* (filled circles), and *G. tumida* (open circles) from WEP Site 806 (gray) and EEP Site 847 (black) compared with whole-ocean change in Sr/Ca (*39*) to illustrate the minimal influence of dissolution.

the state of the Pacific thermocline has influenced past climates is critical to gain insight into Earth's response to future global warming.

The "hothouse" (*3*, *4*) climate of the early-mid Pliocene [~5 to ~2.7 million years ago (Ma), referred to as Pliocene] was the last extended period when global temperatures were warmer than present, peaking between 3 and 4 Ma, and provides an analog for a future global warming scenario. High-latitude air temperatures were ~10°C warmer (*4*), but tropical temperatures remained similar to today. Debate persists regarding the forcing of this warmth. Proxy-CO_2 reconstructions suggest that the perturbation was too small [~100 parts per million (ppm)] to effect such large changes in climate (*5*), and attention has focused on increased deep-ocean thermohaline circulation (*6*). Alternatively, teleconnections driven by the west equatorial Pacific warm pool (*7*) could propagate global warmth to induce a permanent El Niño–like state (*8*–*10*). The spatial climatic patterns of the "hothouse" largely resemble those of warm El Niño–like conditions (*10*), and there is $\delta^{18}O$ evidence for reduced thermocline tilt in the equatorial Pacific (*8*, *11*). However, the $\delta^{18}O$ of carbonate is controlled by the temperature and salinity of the water from which it precipitates. In the equatorial Pacific, zonal, depth, and seasonal variations in salinity have the potential to confound $\delta^{18}O$ temperature records. We use an independent record of surface and thermocline temperature, that is, Mg/Ca paleothermometry, to produce temperature records that, when used in conjunction with $\delta^{18}O$, yield a record of $\delta^{18}O_w$. We use these data to test the hypothesis that the Pacific collapsed onto a persistent El Niño–like state in the warm Pliocene.

Our records of Mg/Ca in three species of planktonic foraminifera from the east and west equatorial Pacific (EEP and WEP) (*12*) refute that El Niño–like conditions prevailed during the Pliocene hothouse (Fig. 1) (*8*, *11*). A feature of our temperature records is the divergence of surface and deeper water temperatures with time. *Globigerina sacculifer*, believed to calcify in the mixed layer, indicates that the sea surface temperature (SST) of the WEP warm pool remained relatively stable and consistently warmer than the EEP. The surface waters of the EEP warmed by ~5°C between 3 and 4 Ma. At each site, *Globorotalia tumida,* which adds calcite down to depths of 200 to 250 m, records a cooling of ~6°C. *Neogloboquadrina dutertrei*, with habitats ranging from 50 to 150 m, also shows a cooling trend similar to *G. tumida* in the WEP. The effects of dissolution are likely to be minimal (*13*).

We have reconstructed vertical profiles of contrasting cold Pleistocene and warm Pliocene surface hydrographies to show the evolution of the equatorial Pacific thermocline (Fig. 2). Between 3 and 4 Ma, the WEP thermocline shallowed. This cooling of subsurface waters could be related to the Cenozoic bottom-up cooling of the deep oceans and increased stratification in the Quaternary icehouse (*14*). By contrast, between 4 and 6 Ma in the EEP, the cold temperatures of the mixed layer and thermocline are identical, implying increased upwelling during the Pliocene. The EEP thermocline deepens to approach modern-day conditions.

Rather than indicating extreme El Niño–like conditions during hothouse climates evolving toward the modern east-west gradient in surface hydrography ~4 Ma (*8*, *10*), our data imply that the equatorial Pacific thermocline tilt was more extreme during the Pliocene, which indicates stronger trade winds, increased eastern upwelling, and La Niña–like conditions (*15*). Other evidence supports our notion. Aeolian sediments in the EEP sug-

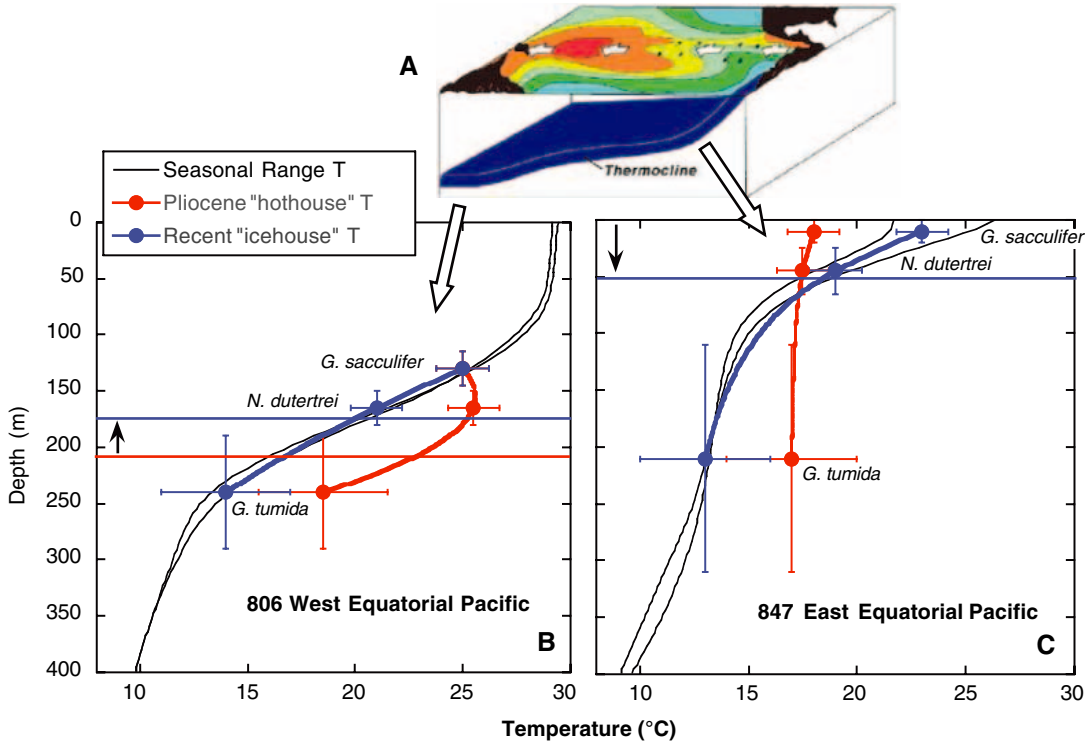

Fig. 2. (**A**) Schematic of the Pacific thermocline under normal conditions, illustrating the deepening beneath the west Pacific warm pool and shallowing to the east (adapted with permission from the Tropical Atmosphere Ocean Project, NOAA/Pacific Marine Environmental Laboratory). (**B** and **C**) Profiles of temperature derived from Mg/Ca for time-slice equivalents of the Pleistocene icehouse (0 to 1 My) in blue and the warm Pliocene (4 to 6 My) in red compared with the modern seasonal range in black taken from (*41*) for (B) WEP Site 806 and (C) EEP Site 847. The red and blue horizontal lines show the Pliocene and modern depths of the thermocline, and the black arrows indicate how this depth has changed since the Pliocene. We have used the modern seasonal temperature profile from (*41*) as a guide for habitat depth of each species. Error bars for *G. sacculifer* and *N. dutertrei* temperature reflect the quoted accuracy of ±1.2°C in the estimation of calcification temperature from published calibrations (*40*), which matches the scatter in our temperature records from the weighted average line from Fig. 1, C and D, and ±3.0°C for *G. tumida* to reflect the uncertainty in the pre-exponential constant. This envelope in temperature defines the depth error bar by comparison with the modern profiles, and we have assumed these errors to be the same for the Pliocene. The depth error bar encompasses the influence of a ~–2°C glacial cooling (*42*) on the modern temperature profile, which would result in an approximate 25 m shallowing of the thermocline (and our inferred depths) in both the EEP and the WEP. By comparison with (*41*), *G. sacculifer* consistently records colder temperatures than its mixed-layer habitat and appears to add calcite in the upper thermocline. *G. tumida* is described as a basal photic zone dweller. The tropical photic zone is deepest in the global ocean and is generally quoted at 200 m. *G. tumida* fits best with the modern-day temperature profile at a depth of 210 to 240 m, which is consistent with other observations that *G. tumida* can add calcite down to depths of 200 to 250 m (*43*). *N. dutertrei*, which is commonly described as a seasonal thermocline dweller associated with the deep chlorophyll maximum, calcifies at depths ranging from 60 to 150 m in the modern ocean. Compared with the modern profiles, the calcification temperature of *N. dutertrei* implies that it lives at 165 m in the WEP and at 45 m in the EEP. These depth habitats are also supported qualitatively by our reconstruction of $\delta^{18}O_w$ in Fig. 3.

gest very strong southeast trade winds 8 to 5 Ma, reducing in intensity until ~4 Ma (*16*). Higher rates of biogenic sedimentation occur along the equator during this interval (*17*) and reinforce our concept of increased divergent wind-driven upwelling enhancing productivity in the EEP prior to 4 Ma.

What could drive a La Niña–like state during Pliocene warmth? An "ocean thermostat" mechanism describes how greenhouse gas heating of the tropical Pacific leads to a cooling in the EEP (*18*, *19*), arising from the different SST response in the EEP and the WEP. In the west, where the thermocline is deep, the SST rises thermodynamically to attain a new equilibrium. In the east, where the thermocline is shallow, dynamic upwelling of cold waters counteracts the warming tendency. SST increases more in the west than in the east, enhancing the zonal temperature gradient. The atmosphere responds with increasing trade winds, which increase upwelling and thermocline tilt, cooling the surface waters in the east and further enhancing the temperature contrast. This "climatological" Bjerknes feedback reflects a shift in the mean state of the Pacific thermocline, which we invoke for our Pliocene La Niña–like state. External heating for a Pliocene feedback likely derives from a combination of greenhouse gases (~+100 ppm) and reduced planetary albedo due to enhanced oceanic heat transport to high latitudes (*5*, *6*). Alternative mechanisms to drive a persistent La Niña–like state or create a positive feedback to the Bjerknes mechanism are to enhance the thermocline tilt by increased flux of the Indonesian Throughflow (ITF) (*20*) or decrease the Pliocene temperature of the Equatorial Undercurrent (EUC), which ventilates the equatorial thermocline (*21*).

We reveal qualitative insight into the evolving character of the EUC by deconvolving the $\delta^{18}O_w$ ($\delta^{18}O_w$ of seawater) from existing $\delta^{18}O$ foraminifera data (*8*) using the Mg/Ca-derived temperature for each species (Fig. 3). The error in this $\delta^{18}O_w$ reconstruction from the combination of proxies is ~±0.6 (*22*), whereas whole-ocean $\delta^{18}O_w$ during this period is poorly constrained to be <0.5‰ (*23*), within the scatter of our data. At each Pacific site, the habitat of the deep dweller *G. tumida* stays at a relatively constant $\delta^{18}O_w$. In the WEP, *G. sacculifer* and *N. dutertrei* experience waters that are consistently isotopically heavier than *G. tumida*. This $\delta^{18}O_w$ signature implies that *G. sacculifer* captures the signature of the subsurface salinity maximum associated with the eastward thermocline flow of the EUC (Fig. 3C) by calcifying over a range in water depth, thus integrating the mixed layer and thermocline signatures (*24*, *25*). This is corroborated by the cooler-than-expected temperatures reconstructed from *G. sacculifer* Mg/Ca for the modern-day surface waters in the WEP (Fig. 2). There is a hint of an increase in $\delta^{18}O_w$ from *G. sacculifer* in the WEP over the past 2 million years (My), and from the *N. dutertrei* record in the EEP. The most striking feature, greater than the reconstruction error and modern seasonal variations, is the shift of $\delta^{18}O_w$ derived from *G. sacculifer* in the EEP from –0.6‰ in the Pliocene to 0.9‰ in the Pleistocene [equivalent to a Pliocene freshening of ~2.6 ± 1.8‰ (*26*)].

The surface waters of the EEP should experience a decrease in precipitation-evaporation (P-E) as the WEP "fresh pool" shifts westward in a La Niña–like Pliocene. Although Pliocene

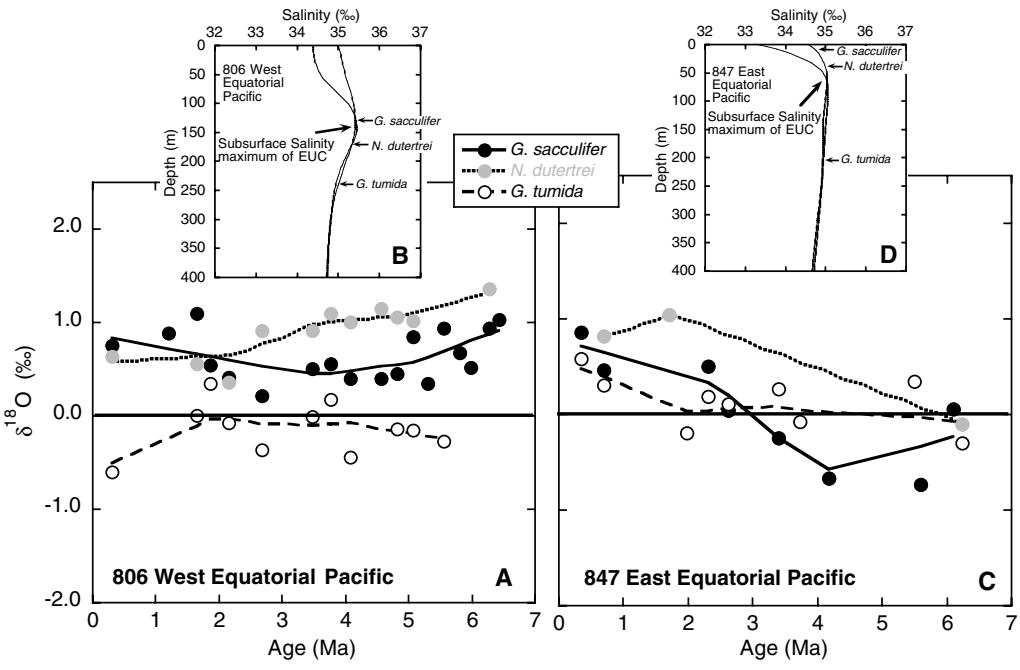

Fig. 3. The evolution of seawater $\delta^{18}O_w$ for *G. sacculifer* (black circles), *N. dutertrei* (gray circles), and *G. tumida* (open circles) from (**A**) Site 806 and (**C**) Site 847, calculated with the Mg/Ca calcification temperature and the paleotemperature equation T (°C) = 16.0 – 5.17 [$\delta^{18}O_c$ – ($\delta^{18}O_w$ – 0.27)] – 0.092[$\delta^{18}O_c$ – ($\delta^{18}O_w$ – 0.27)]^2, where the factor 0.27 was used to convert from water on the standard mean ocean water scale to calcite on the PeeDee Belemnite Scale. (**B** and **D**) Vertical profiles of the seasonal range in salinity (*41*) for (B) WEP Site 806 and (D) EEP Site 847. The likely depth habitats of the different species at each site are indicated. Although a quantitative reconstruction of paleosalinity from these combined proxy data is limited by likely error estimates between 0.6 and 1.8‰ (*26*), our reconstructed depth habits of *G. sacculifer* and *N. dutertrei* are strengthened by their reflection of more positive $\delta^{18}O_w$ values in the WEP, indicative of the subsurface salinity maximum.

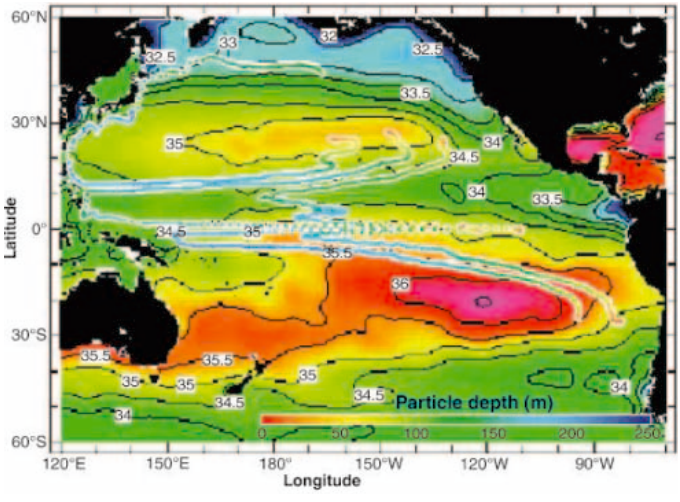

Fig. 4. A map of annual sea surface salinity (0-m depth) ranging from 32 to 37‰, showing contours every 0.5‰ or practical salinity unit (PSU) taken from (*41*) to illustrate the contrasting salinities in the northern and southern hemisphere source areas of water for the EUC. Also shown are selected paths of water parcels over a period of 16 years after subduction off the coasts of California and Peru, as simulated by means of a realistic general-circulation model forced with the observed climatological winds. From the colors, which indicate the depth of the parcels, it is evident that parcels move downward, westward, and equatorward unless they start too far west of California, in which case they join the Kuroshio Current. Along the equator, they rise to the surface while being carried eastward by the swift EUC, after (*21*).

precipitation is thought to have increased by ~5%, models suggest little change in P-E across the equatorial Pacific (*27*). The inference that *G. sacculifer* integrates a signature of the subsurface reconciles best our Mg/Ca-derived temperatures with existing studies of $\delta^{18}O$. *G. sacculifer* captures the nature of the EUC and records a change from cooler, fresher water during the Pliocene hothouse to warmer, saltier waters in the Quaternary icehouse. The increasing *G. sacculifer* $\delta^{18}O_w$ may be interpreted as a change in conditions of the source waters of the EUC from relatively cold and fresh during the Pliocene to warm and salty in the modern day. Today, the main subduction sites for surface waters entering the EUC are in the eastern and central South and North Pacific subtropical gyres and in the South and North Equatorial Currents (*20*, *28*); some typical pathways are shown in Fig. 4. Today, the contribution from warm and salty southern sources is more than double that of cool and fresh northern sources (*29*). To alter the character of the EUC to fresher and cooler during the Pliocene, either subtropical sources were fresher and cooler, or the dominant source of the EUC moved to higher latitudes, or the source changed from predominantly cold and fresh Northern hemisphere waters (NHW) during the Pliocene to warm and salty Southern hemisphere waters (SHW) today.

An interesting conjecture is that tectonic motions around the ITF switched the dominant source of the Pliocene EUC to be colder, fresher NHW (*9*, *29*). The emergence of Halmahera and the northward drift of New Guinea restricted the Indonesian seaway 3 to 4 Ma and diverted the ITF from 3°S to 2°N. The ITF plays an important role in determining the thermocline of the equatorial oceans. During the Pliocene, when the wider gateway caused a greater ITF flux, the contribution of cooler, fresher NHW dominated the Pacific EUC (*20*). Further, when the ITF opening is south of the equator, as in the Pliocene, warm and salty SHW tend to feed the ITF, and cold, fresh NHW supply the EUC. Conversely, when the opening is to the north, the ITF is primarily supplied by cold, fresh NHW, and there is a stronger southern component in the upwelling of the EEP.

We posit that the more southerly position of New Guinea ~5 Ma made cold, fresh NHW the dominant source of the EUC, which through upwelling in the EEP created an enhanced Bjerknes feedback, stronger southeasterly trade winds, Walker circulation, and a La Niña–like state. Can this La Niña–like state be reconciled with the warmer Pliocene climate?

The answer appears to be yes. Palaeoceanographic proxies suggest that deep thermohaline flow and heat transport to high latitudes was more vigorous during the Pliocene (*6*, *30*). Our proposed Pliocene La Niña–like state is consistent with elevated heat transport to high latitudes from two points of view. First, the reduced equator-pole temperature gradient of the Pliocene results in reduced intensity of Hadley cell circulation, a direct function of meridional pressure/temperature gradients (*31*).

Anomalies in the strength of the Hadley cells are inversely correlated with anomalies in the strength of the Walker oscillation (*18*, *31*): Weakened Hadley cells correlate with episodes of La Niña and strong Walker circulation. Second, the stronger oceanic heat flux to the high latitudes is consistent with enhanced Ekman flow of warm water poleward as a result of increased Walker circulation. The constraint of a balanced heat budget during the Pliocene implies that this increased heat loss at high latitudes through vigorous deep-ocean thermohaline circulation is accompanied by a shoaling of the tropical thermocline (*32*). Most oceanic heat gain occurs in low and mid-latitude upwelling zones and is large (small) when the thermocline is shallow (deep). During the Pliocene, the deeper thermocline in the WEP argues that thermocline tilt must be greater to allow shoaling of the EEP thermocline.

Our data rebut the hypothesis that "hothouse" climates collapse onto an El Niño–like state, in agreement with Eocene hothouse studies (*33*), and indicate that the tropical upper-ocean structure during the warm Pliocene was indicative of a La Niña–like state consistent with the dynamical "ocean thermostat." Twentieth-century global warming has also resulted in a stronger east-west SST gradient (*34*) on a contrastingly rapid time scale. Both of these scenarios, reflecting mean and transient Pacific states, respectively, support the role of the Bjerknes feedback inhibiting an El Niño positive feedback to global warming. Interestingly, during the Pliocene the increase in east-west SST gradient is due to eastern cooling, whereas during the 20th century it is due to WEP warming. In the near future, if the warming of the WEP warm pool reaches a limit without a compensating cooling in the east (afforded by the EUC during the Pliocene), could the Bjerknes feedback be reversed to incite accelerated warmth of an El Niño–like state?

References and Notes

1. W. J. Cai, P. H. Whetton, *Geophys. Res. Lett.* **27**, 2577 (2000).
2. K. E. Trenberth, D. P. Stepaniak, J. M. Caron, *J. Geophys. Res.* **107**, 4066 (2002); 10.1029/2000JD000297.
3. Here, we use "hothouse" to denote the warm early-mid Pliocene climate regime when the Northern Hemisphere lacked substantial ice sheets, and "icehouse" for the Middle to Late Pleistocene regime characterized by the waxing and waning of major Northern Hemisphere ice sheets.
4. M. Budyko, Y. A. Izrael, Eds., *Anthropogenic Climate Changes* (L. Gidrometeoizdat, Leningrad, 1987).
5. T. C. Crowley, *Quat. Sci. Rev.* **10**, 275 (1991).
6. M. E. Raymo, B. Grant, M. Horowitz, G. H. Rau, *Mar. Micropaleontol.* **27**, 313 (1996).
7. Global climate is influenced by the seesaw of the tropical Pacific thermocline tilt, or ENSO. This connection underpins the proposal of persistent El Niño conditions during geological "hothouse periods." The natural mode of oscillation is attributable to ocean-atmosphere interactions in which the trade winds create SST gradients that in turn reinforce the winds. In the Pacific, the prevailing easterly trade winds blow warm surface waters along the equator, creating a deep warm pool toward the western Pacific margin (*35*). This causes the tropical Pacific thermocline to become deeper in the west than in the east. Water is returned, along the thermocline, in the EUC, to the east, where it upwells. The zonal SST gradient between the west and east Pacific drives an east-west atmospheric circulation (the Walker Cell). This circulation further increases upwelling in the east Pacific, a process known as the Bjerknes feedback (*36*). Warm El Niño events occur when easterly trade winds decrease or reverse direction and warm water from the west Pacific spreads eastwards and, in doing so, reduces the Pacific thermocline tilt. This decreases the zonal temperature gradient, causing a breakdown of Walker Cell circulation. Cold La Niña events occur when trade winds are strong and induce a steep thermocline tilt. Changes in atmospheric circulation above the tropical Pacific cause changes in teleconnections to higher latitudes, with global climatic consequences on an interannual time scale. For this study, in which we investigate the average condition of the low-latitude ocean on million-year time scales, we refer to an El Niño (La Niña)–like state to reflect reduced (increased) east-west SST gradient, reduced (increased) thermocline tilt, and deeper (shallower) thermocline in the EEP. The detailed spatial patterns of atmosphere and ocean conditions associated with these two proposed states on geological time scales are currently unknown and may be very different from interannual configurations (*37*).
8. W. P. Chaisson, A. C. Ravelo, *Paleoceanography* **15**, 497 (2000).
9. M. A. Cane, P. Molnar, *Nature* **411**, 157 (2001).
10. P. Molnar, M. A. Cane, *Paleoceanography* **17**, 663 (2002); 10.1029/2001PA000663.
11. K. G. Cannariato, A. C. Ravelo, *Paleoceanography* **12**, 805 (1997).
12. Materials and methods are available as supporting material on *Science* Online.
13. At the critical site for our new interpretation, site 847, carbonate accumulation rates were higher prior to 4 Ma, which implies that preservation was improved during the Pliocene relative to today (*17*). The chemistry of *G. sacculifer* is insensitive to dissolution due to chemical homogeneity throughout the test (*38*). Planktonic Sr/Ca is a potential indicator of dissolution. Further evidence of the minimal influence of dissolution on these records is the covariation of Sr/Ca of *G. sacculifer* and *G. tumida* from both sites (Fig. 1E), which also parallels oceanic Sr/Ca evolution (*39*).
14. S. G. Philander, A. V. Federov, *Paleoceanography* **18**, 837 (2003); 10.1029/2002PA000837.
15. T. Izumo, J. Picaut, B. Blanke, *Geophys. Res. Lett.* **29**, 15073 (2002); 10.1029/2002GL015073.
16. S. A. Hovan, *Proc. ODP Sci. Results* **138**, 615 (1995).
17. T. King, *Mar. Micropaleontol.* **27**, 63 (1996).
18. A. C. Clement, R. Seager, M. A. Cane, S. E. Zebiak, *J. Clim.* **9**, 2190 (1996).
19. M. A. Cane *et al.*, *Science* **275**, 957 (1997).
20. K. B. Rodgers, M. A. Cane, N. H. Naik, D. P. Schrag, *J. Geophys. Res.* **104**, 20,551 (1999).
21. D. Gu, S. G. H. Philander, *Science* **275**, 805 (1997).
22. E. J. Rohling, *Mar. Geol.* **163**, 1 (2000).
23. C. H. Lear, Y. Rosenthal, J. D. Wright, *Earth Planet. Sci. Lett.* **210**, 425 (2003).
24. Y. Rosenthal, G. P. Lohmann, K. C. Lohmann, R. M. Sherrell, *Paleoceanography* **15**, 135 (2000).
25. H. J. Spero, K. M. Mielke, E. M. Kalve, D. W. Lea, D. K. Pak, *Paleoceanography* **18**, 1022 (2003); 10.1029/2002PA000814.
26. G. A. Schmidt, *Paleoceanography* **14**, 422 (1999).
27. L. C. Sloan, T. J. Crowley, D. Pollard, *Mar. Micropaleontol.* **27**, 51 (1996).
28. K. B. Rodgers *et al.*, *Geophys. Res. Lett.* **30**, 16003 (2003); 10.1029/2002GL016003.
29. K. B. Rodgers, M. Latif, S. Legutke, *Geophys. Res. Lett.* **27**, 2941 (2000).
30. K. Billups, A. C. Ravelo, J. C. Zachos, *Paleoceanography* **13**, 84 (1998).
31. A. H. Oort, J. J. Yienger, *J. Clim.* **9**, 2751 (1996).
32. G. Boccaletti, R. C. Pacanowski, S. G. H. Philander, A. V. Federov, *J. Phys. Oceangr.* **34**, 888 (2004).
33. M. Huber, R. Caballero, *Science* **299**, 877 (2003).
34. M. A. Cane, *Earth Planet. Sci. Lett.* **164**, 1 (2004).
35. E. Maier-Reimer, U. Mikalojewicz, T. J. Crowley, *Paleoceanography* **5**, 349 (1990).
36. A. V. Federov, G. Philander, *Science* **288**, 1997 (2000).
37. W. Hazeleger, R. Seager, M. A. Cane, N. H. Naik, *J. Phys. Oceanogr.* **34**, 320 (2004).
38. S. Brown, H. Elderfield, *Paleoceanography* **11**, 543 (1996).
39. C. H. Lear, H. Elderfield, P. A. Wilson, *Earth Planet. Sci. Lett.* **208**, 69 (2003).
40. P. Anand, H. Elderfield, M. H. Conte, *Paleoceanography* **18**, 846 (2003); 10.1029/2002PA000846.
41. S. Levitus, T. Boyer, *World Ocean Atlas 1994*, *Vol. 4*, NOAA National Environmental and Satellite Data and Information Service, U.S. Department of Commerce, Washington, DC (1994).
42. D. W. Lea, D. K. Pak, H. J. Spero, *Science* **289**, 1719 (2000).
43. E. C. Farmer, Thesis, Columbia University (2000).

44. We thank M. Evans and M. Cane for invaluable exchange of ideas, two anonymous reviewers who greatly improved this manuscript, J. Arden for technical support, and D. Sansom for art support. Further thanks to the Ocean Drilling Program for providing samples and to the Natural Environment Research Council for providing financial support.

Supporting Online Material

www.sciencemag.org/cgi/content/full/307/5717/1948/DC1
Materials and Methods
References

30 August 2004; accepted 24 January 2005
10.1126/science.1104666

Soft-Tissue Vessels and Cellular Preservation in *Tyrannosaurus rex*

Mary H. Schweitzer,[1,2,3]* Jennifer L. Wittmeyer,[1] John R. Horner,[3] Jan K. Toporski[4]†

Soft tissues are preserved within hindlimb elements of *Tyrannosaurus rex* (Museum of the Rockies specimen 1125). Removal of the mineral phase reveals transparent, flexible, hollow blood vessels containing small round microstructures that can be expressed from the vessels into solution. Some regions of the demineralized bone matrix are highly fibrous, and the matrix possesses elasticity and resilience. Three populations of microstructures have cell-like morphology. Thus, some dinosaurian soft tissues may retain some of their original flexibility, elasticity, and resilience.

A newly discovered specimen of *Tyrannosaurus rex* [Museum of the Rockies (MOR) specimen 1125] was found at the base of the Hell Creek Formation, 8 m above the Fox Hills Sandstone, as an association of disarticulated elements. The specimen was incorpo-

rated within a soft, well-sorted sandstone that was interpreted as estuarine in origin. Although some bones are slightly deformed or crushed, preservation is excellent. MOR 1125 represents a relatively small individual of *T. rex,* with a femoral length of 107 cm, as compared to the Field Museum (Chicago) specimen (FMNH PR2081) that has a femoral length of approximately 131 cm. On the basis of calculated lines of arrested growth (LAG), we estimated that this animal was 18 ± 2 years old at death (*1*).

No preservatives were applied to interior fragments of the femur of MOR 1125 during preparation, and these fragments were reserved for chemical analyses. In addition to the dense compact bone typical of theropods, this specimen contained regions of unusual bone tissue on the endosteal surface (*2*). Cortical and endosteal bone tissues were demineralized (*3*), and

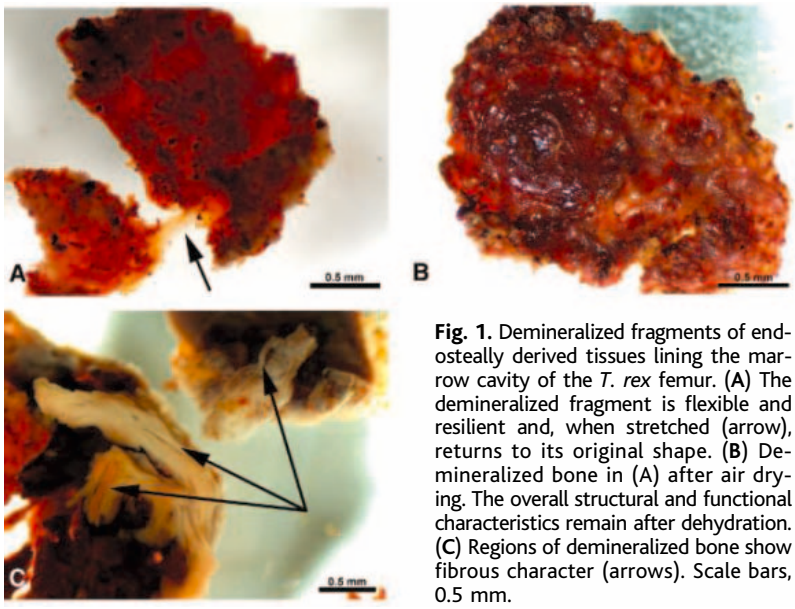

Fig. 1. Demineralized fragments of endosteally derived tissues lining the marrow cavity of the *T. rex* femur. (**A**) The demineralized fragment is flexible and resilient and, when stretched (arrow), returns to its original shape. (**B**) Demineralized bone in (A) after air drying. The overall structural and functional characteristics remain after dehydration. (**C**) Regions of demineralized bone show fibrous character (arrows). Scale bars, 0.5 mm.

[1]Department of Marine, Earth, Atmospheric Sciences, North Carolina State University, Raleigh, NC 27695, USA. [2]North Carolina State Museum of Natural Sciences, Raleigh, NC 27601, USA. [3]Museum of the Rockies, Montana State University, Bozeman, MT 59717, USA. [4]Carnegie Institution of Washington, Geophysical Laboratory, 5251 Broad Branch Road N.W., Washington, DC 20018, USA.

*To whom correspondence should be addressed. E-mail: schweitzer@ncsu.edu

†Present address: Department of Geosciences, Christian-Albrechts University Kiel, Olshausenstrasse 40, 24098 Kiel, Germany.

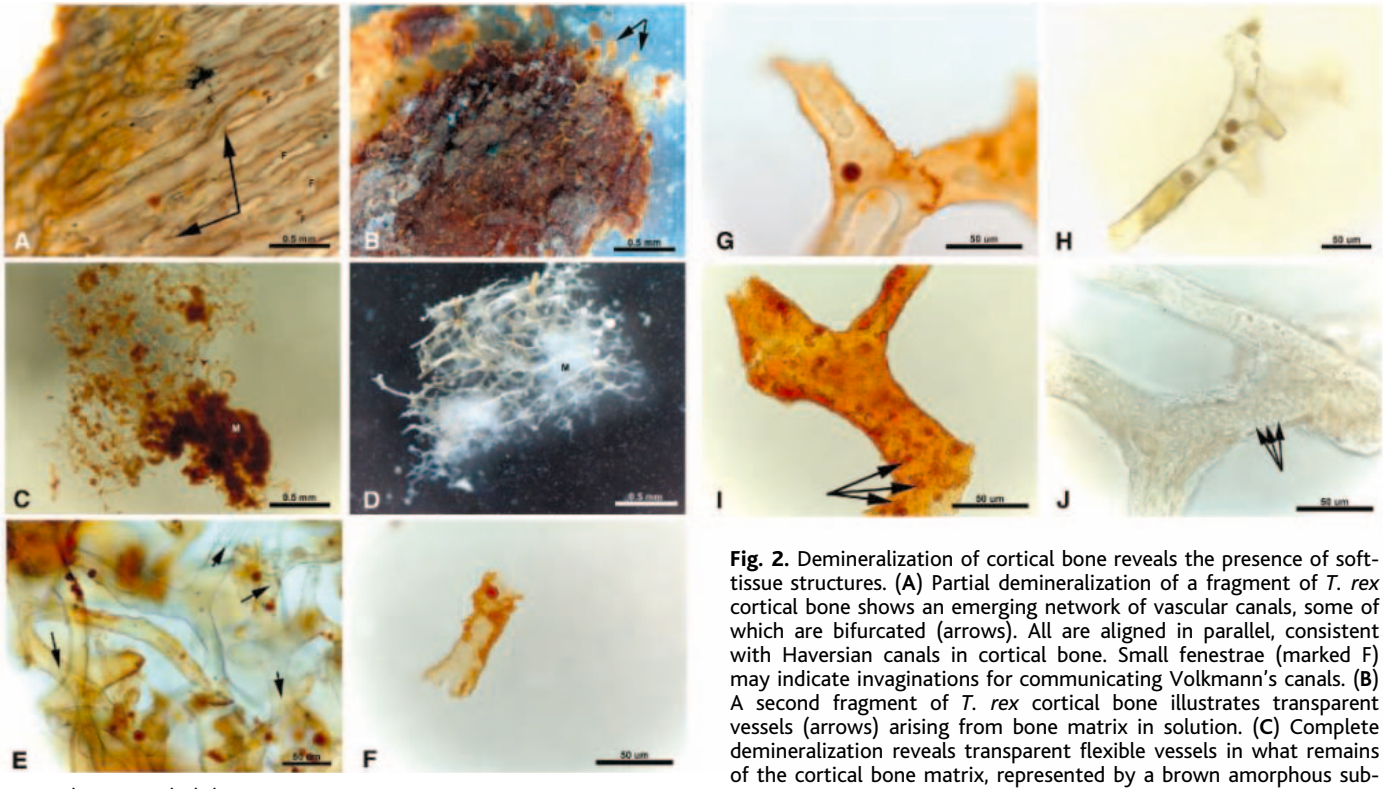

Fig. 2. Demineralization of cortical bone reveals the presence of soft-tissue structures. (**A**) Partial demineralization of a fragment of *T. rex* cortical bone shows an emerging network of vascular canals, some of which are bifurcated (arrows). All are aligned in parallel, consistent with Haversian canals in cortical bone. Small fenestrae (marked F) may indicate invaginations for communicating Volkmann's canals. (**B**) A second fragment of *T. rex* cortical bone illustrates transparent vessels (arrows) arising from bone matrix in solution. (**C**) Complete demineralization reveals transparent flexible vessels in what remains of the cortical bone matrix, represented by a brown amorphous substance (marked M). (**D**) Ostrich vessel after demineralization of cortical bone and subsequent digestion of fibrous collagenous matrix. Transparent vessels branch and remain associated with small regions of undigested bone matrix, seen here as amorphous, white fibrous material (marked M). Scale bars in (A) to (D), 0.5 mm. (**E**) Higher magnification of dinosaur vessels shows branching pattern (arrows) and internal contents. Vascular structure is not consistent with fungal hyphae (no septae, and branching pattern is not consistent with fungal morphology) or plant (no cell walls visible, and again branching pattern is not consistent). Round red microstructures within the vessels are clearly visible. (**F**) *T. rex* vessel fragment, containing microstructures consistent in size and shape with those seen in the ostrich vessel in (H). (**G**) Second fragment of dinosaur vessel. Air/fluid interfaces, represented by dark menisci, illustrate the hollow nature of vessels. Microstructure is visible within the vessel. (**H**) Ostrich vessel digested from demineralized cortical bone. Red blood cells can be seen inside the branching vessel. (**I**) *T. rex* vessel fragment showing detail of branching pattern and structures morphologically consistent with endothelial cell nuclei (arrows) in vessel wall. (**J**) Ostrich blood vessel liberated from demineralized bone after treatment with collagenase shows branching pattern and clearly visible endothelial nuclei. Scale bars in (E) to (J), 50 μm. (F), (I), and (J) were subjected to aldehyde fixation (*3*). The remaining vessels are unfixed.

after 7 days, several fragments of the lining tissue exhibited unusual characteristics not normally observed in fossil bone. Removal of the mineral phase left a flexible vascular tissue that demonstrated great elasticity and resilience upon manipulation. In some cases, repeated stretching was possible (Fig. 1A, arrow), and small pieces of this demineralized bone tissue could undergo repeated dehydration-rehydration cycles (Fig. 1B) and still retain this elastic character. Demineralization also revealed that some regions of the bone were highly fibrous (Fig. 1C, arrows).

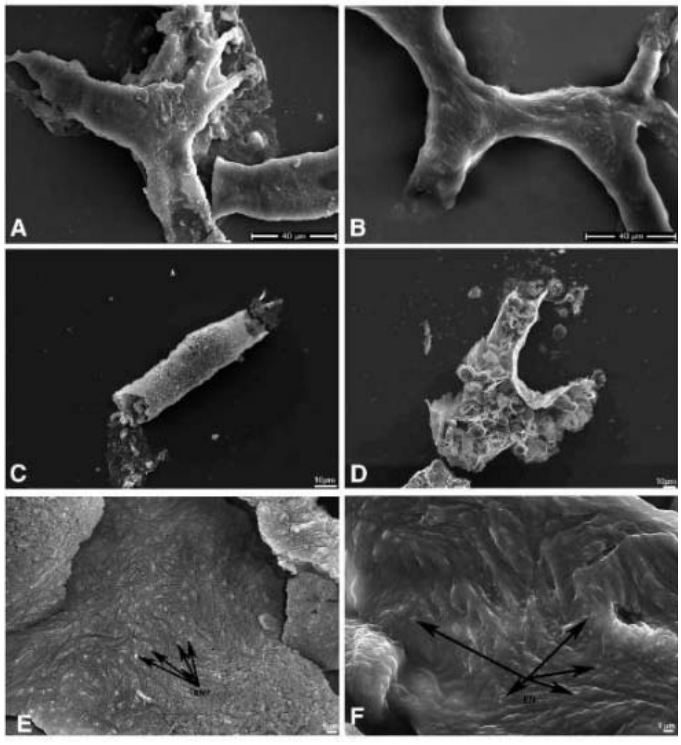

Fig. 3. SEM images of aldehyde-fixed vessels. (**A**) Isolated vessel from *T. rex*. (**B**) Vessel isolated from extant ostrich after demineralization and collagenase digestion (*3*). (**C**) Vessel from *T. rex*, showing internal contents and hollow character. (**D**) Exploded *T. rex* vessel showing small round microstructures partially embedded in internal vessel walls. (**E**) Higher magnification of a portion of *T. rex* vessel wall, showing hypothesized endothelial nuclei (EN). (**F**) Similar structures visible on fixed ostrich vessel. Striations are seen in both (E) and (F) that may represent endothelial cell junctions or alternatively may be artifacts of the fixation/dehydration process. Scale bars in (A) and (B), 40 μm; in (C) and (D), 10 μm; in (E) and (F), 1 μm.

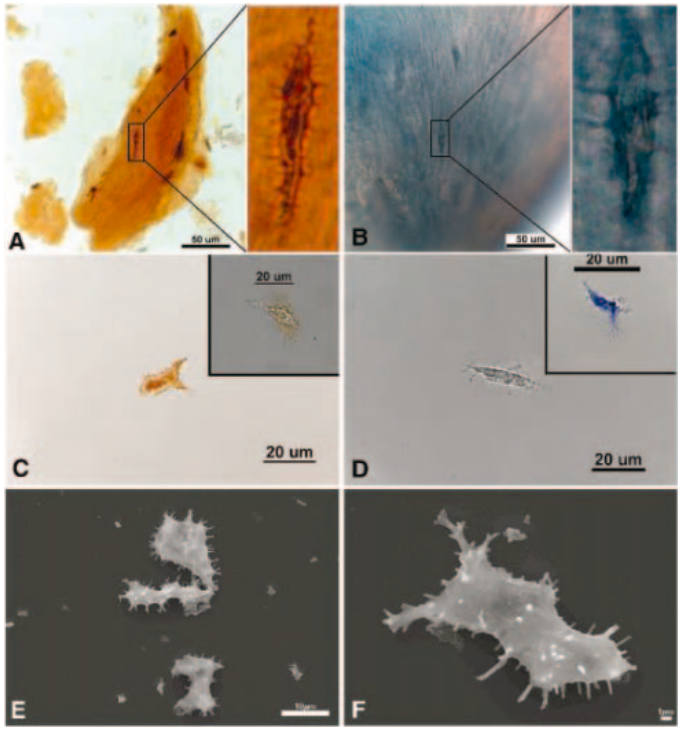

Fig. 4. Cellular features associated with *T. rex* and ostrich tissues. (**A**) Fragment of demineralized cortical bone from *T. rex*, showing parallel-oriented fibers and cell-like microstructures among the fibers. The inset is a higher magnification of one of the microstructures seen embedded in the fibrous material. (**B**) Demineralized and stained (*3*) ostrich cortical bone, showing fibrillar, parallel-oriented collagen matrix with osteocytes embedded among the fibers. The inset shows a higher magnification of one of the osteocytes. Both inset views show elongate bodies with multiple projections arising from the external surface consistent with filipodia. (**C**) Isolated microstructure from *T. rex* after fixation. In addition to the multiple filipodial-like projections, internal contents can be seen. The inset shows a second structure with long filipodia and an internal transparent nucleus-like structure. (**D**) Fixed ostrich osteocyte; inset, ostrich osteocyte fixed and stained for better visualization. Internal contents are discernible, and filipodia can be seen extending in multiple planes from the cell surface. (**E** and **F**) SEM images of aldehyde-fixed (*3*) microstructures isolated from *T. rex* cortical bone tissues. Scale bars in (A) and (B), 50 μm; in (C) and (D), 20 μm; in (E), 10 μm; in (F), 1 μm.

Partial demineralization of the cortical bone revealed parallel-oriented vascular canals that were seen to bifurcate in some areas (Fig. 2A, arrows). Occasional fenestrae (marked F) were observed on the surface of the vascular canals, possibly correlating with communicating Volkmann's canals. Complete demineralization of the cortical bone released thin and transparent soft-tissue vessels from some regions of the matrix (Fig. 2, B and C), which floated freely in the demineralizing solution. Vessels similar in diameter and texture were recovered from extant ostrich bone, when demineralization was followed by digestion with collagenase enzyme (*3*) to remove densely fibrous collagen matrix (Fig. 2D). In both dinosaur (Fig. 2C) and ostrich (Fig. 2D), remnants of the original organic matrix in which the vessels were embedded can still be visualized under transmitted light microscopy. These vessels are flexible, pliable, and translucent (Fig. 2E). The vessels branch in a pattern consistent with extant vessels, and many bifurcation points are visible (Fig. 2E, arrows). Many of the dinosaur vessels contain small round microstructures that vary from deep red to dark brown (Fig. 2, F and G). The vessels and contents are similar in all respects to blood vessels recovered from extant ostrich bone (Fig. 2H). Aldehyde-fixed (*3*) dinosaur vessels (Fig. 2I) are virtually identical in overall morphology to similarly prepared ostrich vessels (Fig. 2J), and structures consistent with remnants of nuclei from the original endothelial cells are visible on the exterior of both dinosaur and ostrich specimens (Fig. 2, I and J, arrows).

Under scanning electron microscopy (SEM) (Fig. 3), features seen on the external surface of dinosaurian vessels are virtually indistinguishable from those seen in similarly prepared extant ostrich vessels (Fig. 3, B and F), suggesting a common origin. These features include surface striations that may be consistent with endothelial cell junctions, or alternatively may be artifacts of fixation and/or dehydration. In addition, small round to oval features dot the surface of both dinosaur and ostrich vessels, which may be consistent with endothelial cell nuclei (Fig. 3, E and F, arrows).

Finally, in those regions of the bone where fibrillar matrix predominated in the demineralized tissues, elongate microstructures could be visualized among the fibers (Fig. 4A, inset). These microstructures contain multiple projections on the external surface and are virtually identical in size, location, and overall morphology to osteocytes seen among colla-

gen fibers of demineralized ostrich bone (Fig. 4B, inset). These cell-like microstructures could be isolated and, when subjected to aldehyde fixation (*3*), appeared to possess internal contents (Fig. 4C), including possible nuclei (Fig. 4C, inset). These microstructures are similar in morphology to fixed ostrich osteocytes, both unstained (Fig. 4D) and stained (*3*) for better visualization (Fig. 4D, inset). SEM verifies the presence of the features seen in transmitted light microscopy, and again, projections extending from the surface of the microstructures are clearly visible (Fig. 4, E and F).

The fossil record is capable of exceptional preservation, including feathers (*4*–*6*), hair (*7*), color or color patterns (*7*, *8*), embryonic soft tissues (*9*), muscle tissue and/or internal organs (*10*–*13*), and cellular structure (*7*, *14*–*16*). These soft tissues are preserved as carbon films (*4*, *5*, *10*) or as permineralized three-dimensional replications (*9*, *11*, *13*), but in none of these cases are they described as still-soft, pliable tissues.

Mesozoic fossils, particularly dinosaur fossils, are known to be extremely well preserved histologically and occasionally retain molecular information (*6*, *17*, *18*), the presence of which is closely linked to morphological preservation (*19*). Vascular microstructures that may be derived from original blood materials of Cretaceous organisms have also been reported (*14*–*16*).

Pawlicki was able to demonstrate osteocytes and vessels obtained from dinosaur bone using an etching and replication technique (*14*, *15*). However, we demonstrate the retention of pliable soft-tissue blood vessels with contents that are capable of being liberated from the bone matrix, while still retaining their flexibility, resilience, original hollow nature, and three-dimensionality. Additionally, we can isolate three-dimensional osteocytes with internal cellular contents and intact, supple filipodia that float freely in solution. This *T. rex* also contains flexible and fibrillar bone matrices that retain elasticity. The unusual preservation of the originally organic matrix may be due in part to the dense mineralization of dinosaur bone, because a certain portion of the organic matrix within extant bone is intracrystalline and therefore extremely resistant to degradation (*20*, *21*). These factors, combined with as yet undetermined geochemical and environmental factors, presumably also contribute to the preservation of soft-tissue vessels. Because they have not been embedded or subjected to other chemical treatments, the cells and vessels are capable of being analyzed further for the persistence of molecular or other chemical information (*3*).

Using the methodologies described here, we isolated translucent vessels from two other exceptionally well-preserved tyrannosaurs (figs. S1 and S2) (*3*), and we isolated microstructures consistent with osteocytes in at least three other dinosaurs: two tyrannosaurs and one hadrosaur (fig. S3). Vessels in these specimens exhibit highly variable preservation, from crystalline morphs to transparent and pliable soft tissues.

The elucidation and modeling of processes resulting in soft-tissue preservation may form the basis for an avenue of research into the recovery and characterization of similar structures in other specimens, paving the way for micro- and molecular taphonomic investigations. Whether preservation is strictly morphological and the result of some kind of unknown geochemical replacement process or whether it extends to the subcellular and molecular levels is uncertain. However, we have identified protein fragments in extracted bone samples, some of which retain slight antigenicity (*3*). These data indicate that exceptional morphological preservation in some dinosaurian specimens may extend to the cellular level or beyond. If so, in addition to providing independent means of testing phylogenetic hypotheses about dinosaurs, applying molecular and analytical methods to well-preserved dinosaur specimens has important implications for elucidating preservational microenvironments and will contribute to our understanding of biogeochemical interactions at the microscopic and molecular levels that lead to fossilization.

References and Notes

1. J. R. Horner, K. Padian, *Proc. R. Soc. London Ser. B* **271**, 1875 (2004).
2. M. Schweitzer, J. L. Wittmeyer, J. R. Horner, in preparation.
3. Materials and methods are available as supporting material on *Science* Online.
4. X. Xu, X. L. Wang, X. C. Wu, *Nature* **401**, 262 (1999).
5. Q. Ji *et al.*, *Nature* **393**, 753 (1998).
6. M. H. Schweitzer *et al.*, *J. Exp. Zool.* **285**, 146 (1999).
7. M. Wuttke, in *Messel–Ein Schaufenster in die Geschichte der Erde und des Lebens*, S. Schaal, W. Ziegler, Eds. (Verlag Waldemar Kramer, Frankfurt am Main, Germany, 1988), pp. 265–274.
8. D. M. Martill, E. Frey, *N. Jb. Geol. Paläont. Mh.* **2**, 118 (1995).
9. L. M. Chiappe *et al.*, *Nature* **396**, 258 (1998).
10. C. Dal Sasso, M. Signore, *Nature* **392**, 383 (1998).
11. A. W. A. Kellner, *Nature* **379**, 32 (1996).
12. N. L. Murphy, D. Trexler, M. Thompson, *J. Vertebr. Paleontol.* **33**, 91A (2002).
13. D. E. G. Briggs, P. R. Wilby, B. P. Perez-Moreno, J. L. Sanz, M. Fregenal-Martinez, *J. Geol. Soc. (London)* **154**, 587 (1997).
14. R. Pawlicki, A. Korbel, H. Kubiak, *Nature* **211**, 656 (1966).
15. R. Pawliki, M. Nowogrodzka-Zagorska, *Ann. Anat.* **180**, 73 (1998).
16. M. H. Schweitzer, J. R. Horner, *Ann. Paleontol.* **85**, 179 (1999).
17. G. Muyzer *et al.*, *Geology* **20**, 871 (1992).
18. M. H. Schweitzer *et al.*, *Proc. Natl. Acad. Sci. U.S.A.* **94**, 6291 (1997).
19. R. E. M. Hedges, *Archaeometry* **44**, 319 (2002).
20. S. Weiner, W. Traub, H. Elster, M. J. DeNiro, *Appl. Geochem.* **4**, 231 (1989).
21. G. A. Sykes, M. J. Collins, D. I. Walton, *Org. Geochem.* **23**, 1059 (1995).

22. We thank C. Ancell, J. Barnes, D. Enlow, J. Flight, B. Harmon, E. Lamm, N. Myrhvold, A. de Ricqles, and A. Steele for funding, preparation, insight, consultation, and valued feedback; and J. Fountain and K. Padian for editorial advice. Research was funded by North Carolina State University as well as by grants from N. Myhrvold (J.R.H.) and NSF (M.H.S.).

Supporting Online Material

www.sciencemag.org/cgi/content/full/307/5717/1952/DC1
Materials and Methods
Figs. S1 to S5
References

7 December 2004; accepted 26 January 2005
10.1126/science.1108397

Glycan Foraging in Vivo by an Intestine-Adapted Bacterial Symbiont

Justin L. Sonnenburg,[1,2] Jian Xu,[1,2] Douglas D. Leip,[1,2] Chien-Huan Chen,[1,2] Benjamin P. Westover,[1,3] Jeremy Weatherford,[3] Jeremy D. Buhler,[1,3] Jeffrey I. Gordon[1,2]*

Germ-free mice were maintained on polysaccharide-rich or simple-sugar diets and colonized for 10 days with an organism also found in human guts, *Bacteroides thetaiotaomicron*, followed by whole-genome transcriptional profiling of bacteria and mass spectrometry of cecal glycans. We found that these bacteria assembled on food particles and mucus, selectively induced outer-membrane polysaccharide-binding proteins and glycoside hydrolases, prioritized the consumption of liberated hexose sugars, and revealed a capacity to turn to host mucus glycans when polysaccharides were absent from the diet. This flexible foraging behavior should contribute to ecosystem stability and functional diversity.

The adult human body is a composite of many species. Each of us harbors ~10 times as many microbial cells as human cells (*1*). Our resident microbial communities provide us with a variety of metabolic capabilities not encoded in our genome, including the ability to harvest otherwise inaccessible nutrients from our diet (*2*). The intestine contains an estimated 10 trillion to 100 trillion microorganisms that are largely members of Bacteria but include representatives from

Archaea and Eukarya (*1*, *3*). Changes in diet appear to produce only modest effects on the species composition of the adult human colonic microbiota, although its metabolic activity may change considerably (*4*). The genomic foundations of these metabolic adjustments have yet to be defined in vivo.

Fermentable carbohydrates are the principal energy source for human colonic anaerobes (*4*). Recent studies of *Escherichia coli*, a facultative anaerobe with relatively minor representation in the microbiota, revealed that genetic restriction of its ability to metabolize various monosaccharides differentially compromised its ability to colonize the intestines of mice that had undergone antibiotic "knockdown" of their microbiota (*5*). The stability of an ecosystem apparently correlates with the ability of its members to mount diverse responses to environmental fluctuations; a corollary is that adaptive foraging behavior stabilizes ecosystems (*6*). Here, we use a simplified gnotobiotic mouse model of the human intestinal ecosystem to show that *Bacteroides thetaiotaomicron*, a highly abundant obligate anaerobe found in the colonic microbiota of most normal adult humans (*7*, *8*), redirects its carbohydrate-harvesting activities from dietary to host polysaccharides according to nutrient availability.

B. thetaiotaomicron is a glycophile that can break down a broad array of dietary polysaccharides in vitro [reviewed in (*3*)]. This capacity is reflected in its genome (*9*), which has the largest repertoire of genes involved in acquisition and metabolism of polysaccharides among sequenced microbes, including 163 paralogs of two outer-membrane proteins that bind and import starch, 226 predicted glycoside hydrolases, and 15 polysaccharide lyases (*10*). In contrast, the human genome contains 98 known or putative glycoside hydrolases (*10*). More than half of the carbohydrate-degrading enzymes produced by *B. thetaiotaomicron* are predicted to be secreted into the periplasmic or extracellular space and thus, in principle, are capable of liberating oligo- and monosaccharides from undigested dietary polysaccharides and host mucus for consumption by *B. thetaiotaomicron*, other members of the microbiota, or the host.

Adult germ-free male mice were maintained on a standard autoclaved chow diet rich in plant polysaccharides. Gas chromatography–mass spectrometry (GC-MS) (*11*) established that glucose, arabinose, xylose, and galactose were the predominant neutral sugars present in this chow (mole ratio = 10:8:5:1). Seven-week-old mice were colonized with a single inoculum of *B. thetaiotaomicron* and killed 10 days later (a period that spans two to three cycles of turnover of the intestinal epithelium and its overlying mucus layer). Colonization density, in terms of colony-forming units per milliliter, ranged from 10^7 to 10^9 in the distal small intestine (ileum) to 10^{10} to 10^{11} in the cecum and proximal colon. Scanning electron microscopy revealed that *B. thetaiotaomicron* was attached to small food particles and embedded in mucus (Fig. 1).

The cecum is an anatomically distinct structure, located between the distal small intestine and proximal colon, that is a site of great microbial density and diversity in conventionally raised mice (*12*). Nutrient use by *B. thetaiotaomicron* in the cecum was defined initially by whole-genome transcriptional profiling. Cecal contents, including the mucus layer, were removed immediately after killing of nonfasted mice ($n = 6$), and RNA was extracted (*11*). The *B. thetaiotaomicron* transcriptome was characterized with the use of custom GeneChips containing probe pairs derived from 4719 of the organism's 4779 predicted genes (table S1) (*11*). The results were compared to transcriptional profiles obtained from *B. thetaiotaomicron* grown from early log phase to stationary phase in a chemostat containing minimal medium plus glucose (MM-G) as the sole fermentable carbohydrate source (fig. S1).

Unsupervised hierarchical clustering of the GeneChip data sets disclosed remarkable uniformity in the in vivo transcriptional profiles of *B. thetaiotaomicron* harvested from individual gnotobiotic mice (fig. S2A). A total of 1237 genes were defined as significantly up-regulated (*11*) in vivo relative to their expression in MM-G. The functions of these up-regulated genes were classified by clusters of orthologous groups (COG) analysis. The largest up-regulated group belonged to the "carbohydrate transport and metabolism" COG, whereas the largest group of genes down-regulated in vivo belonged to the "amino acid transport and metabolism" COG (fig. S3A).

The starch utilization system (Sus) proteins SusC and SusD are components of a *B. thetaiotaomicron* outer-membrane complex involved in binding of starch and malto-oligosaccharides for subsequent digestion by outer-membrane and periplasmic glycoside hydrolases (*13*). Thirty-seven SusC and 16 SusD paralogs were up-regulated in vivo by a factor of ≥10 relative to bacteria growing in MM-G (fig. S4A).

The indigestibility of xylan-, pectin-, and arabinose-containing polysaccharides in dietary fiber reflects the paucity of host enzymes required for their degradation. The human genome contains only one putative glycoside hydrolase represented in the nine families of enzymes known in nature with xylanase, arabinosidase, pectinase, or pectate lyase activities, whereas the mouse genome has none (*10*). In contrast, *B. thetaiotaomicron* has 64 such enzymes (table S2) (*10*), many of which were selectively up-regulated in vivo by factors of 10 to 823. These included five secreted xylanases, five secreted arabinosidases, and a secreted pectate lyase (Fig. 2, A to C) (fig. S4B).

GC-MS analysis of total cecal contents harvested from fed germ-free mice (*11*) revealed that xylose, galactose, arabinose, and glucose were the most abundant monosaccharide components (Fig. 2D). After 10 days of colonization by *B. thetaiotaomicron*, significant reductions in cecal concentrations of three prominent hexoses (glu-

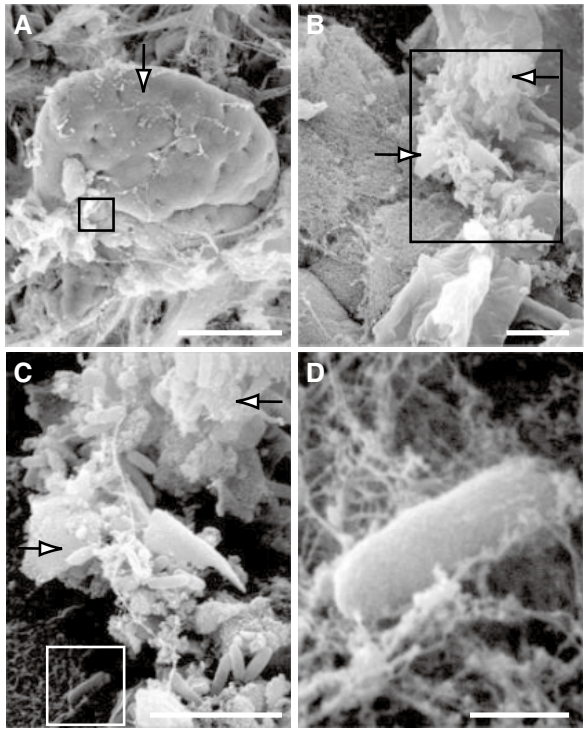

Fig. 1. Scanning electron microscope images showing distribution of *B. thetaiotaomicron* within its intestinal habitat. (**A**) Low-power view of the distal small intestine of *B. thetaiotaomicron*–monoassociated gnotobiotic mice, showing a villus (arrow) viewed from above. (**B** to **D**) Progressively higher power views showing *B. thetaiotaomicron* associated with luminal contents (food particles, shed mucus) [arrows in (B) and (C)] and embedded in the mucus layer overlying the epithelium [boxed region in (C), larger image in (D)]. Scale bars, 50 μm (A), 5 μm [(B) and (C)], 0.5 μm (D).

[1]Center for Genome Sciences, [2]Department of Molecular Biology and Pharmacology, [3]Department of Computer Science and Engineering, Washington University, St. Louis, MO 63108, USA.

*To whom correspondence should be addressed. E-mail: jgordon@molecool.wustl.edu

cose, galactose, and mannose) were observed. There were no significant decreases in pentoses or amino-sugars (Fig. 2D). The selective depletion of hexoses likely reflects the combined effects of microbial and host utilization. *B. thetaiotaomicron* colonization increased expression of the principal sodium/glucose transporter Sglt1 in the intestinal epithelium, reflecting an enhancement of host utilization of liberated monosaccharides (*14*). Moreover, of the 1237 bacterial genes up-regulated in vivo, 310 were assignable (*11*) to Enzyme Commission (EC) numbers in metabolic maps in the Kyoto Encyclopedia of Genes and Genomes (KEGG) (*15*). The results of this metabolic reconstruction were consistent with active delivery of mannose, galactose, and glucose to the glycolytic pathway, and arabinose and xylose to the pentose phosphate pathway [fig. S5; see (*16*) for maps of all *B. thetaiotaomicron* genes with EC assignments that exhibited changed expression in vivo versus MM-G].

Host mucus provides a "consistent" endogenous source of glycans in the cecal habitat that could offer alternative nutrients to the microbiota

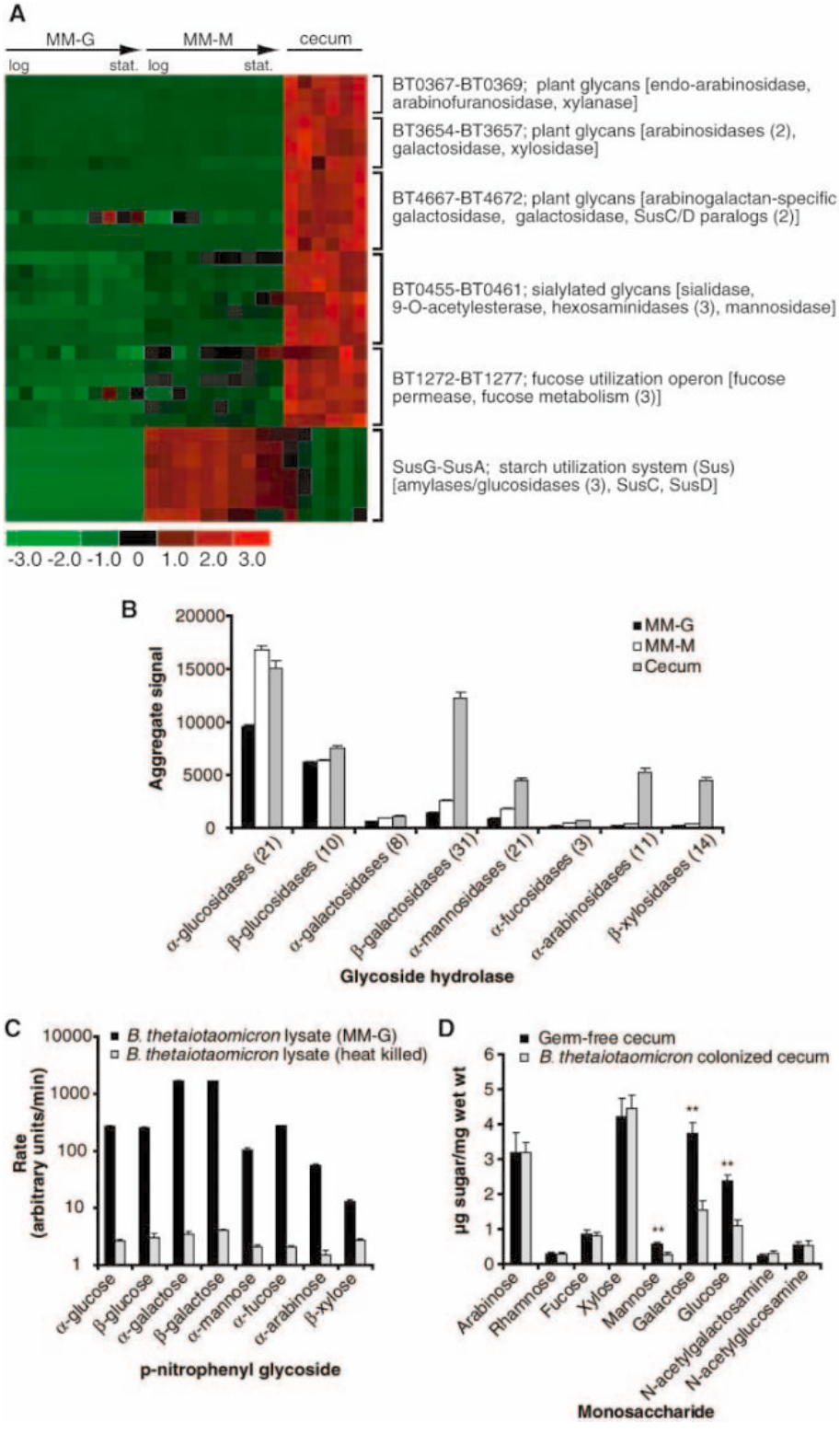

Fig. 2. Carbohydrate foraging by *B. thetaiotaomicron*. (**A**) *B. thetaiotaomicron* gene expression during growth from log phase to stationary phase in minimal medium containing 0.5% glucose (MM-G) or 0.5% maltotriose (a simplified starch composed of three α1-4–linked glucose residues; MM-M) versus the ceca of monoassociated gnotobiotic mice fed a polysaccharide-rich diet. Predicted operons (*21*) are shown together with their component gene products. All genes listed were significantly up-regulated in vivo relative to MM-G according to criteria defined in (*11*). Note that during growth in MM-G versus MM-M, only 13 of the 4719 genes queried exhibit a factor of ≥10 difference in their expression. Eight of these genes constitute a Sus operon (*22*): Its three Sus α-amylases are the only ones among 241 *B. thetaiotaomicron* glycoside hydrolases and polysaccharide lyases whose expression changes by a factor of ≥10 as a result of exposure to maltotriose, underscoring the specificity of the organism's induced responses to the glycosidic linkages that it must process [e.g., compare α- and β-glucosidases in (B) and data in (C)]. (**B** and **C**) Selective induction of glycoside hydrolases in vivo. (B) Induction of expression of groups of glycoside hydrolases in the cecum relative to MM-G and MM-M (see table S4 for a list of genes; the number of genes in each group is indicated in parentheses; summed GeneChip signals for *B. thetaiotaomicron* transcripts called "present" for individual samples within an experimental group were averaged to calculate the aggregate mean signal ± SEM). (C) Biochemical evidence of *B. thetaiotaomicron*'s "preparedness" for degrading glycans. Lysates were generated from bacteria during late log-phase growth in MM-G. The organism produces a portfolio of hydrolases capable of processing a wide variety of glycosides, even when exposed to a single fermentable monosaccharide. Mean values ± SD of triplicate assays are shown. (**D**) GC-MS of neutral and amino-sugars in cecal contents from germ-free versus *B. thetaiotaomicron*–colonized mice [n = 4 animals per group; mean values ± SEM are shown; asterisks indicate a statistically significant difference compared to germ-free (P < 0.01, Student's t test)].

during periods of change in the host's diet. *B. thetaiotaomicron* embeds itself in this mucus layer (Fig. 1D). GeneChip analysis provided evidence that the bacterium harvests glycans from mucus. For example, in vivo, *B. thetaiotaomicron* exhibited significant up-regulation (by factors of 2 to 10; $P < 0.05$) of (i) an operon (BT0455-BT0461) that encodes a sialidase, sialic acid–specific 9-*O*-acetylesterase, mannosidase, and three β-hexosaminidases (Fig. 2A); (ii) a mucin-desulfating sulfatase (BT3051); and (iii) a chondroitin lyase (BT3350). Fucose in host glycans is an attractive source of food: It typically occupies a terminal α-linked position and is constitutively produced in the cecal mucosa (*17*). We found that two secreted α-fucosidases (BT1842, BT3665) and a five-component fucose utilization operon (BT1272-BT1277) were induced (Fig. 2A). Operon induction, which occurs through the interaction of L-fucose with a repressor encoded by its first open reading frame (ORF) (*18*), is indicative of bacterial import and utilization of this hexose.

To determine whether the absence of fermentable polysaccharides in the diet increases foraging on mucus glycans, we compared *B. thetaiotaomicron* gene expression in the ceca of two groups of age- and gender-matched adult gnotobiotic mice. One group received the standard polysaccharide-rich chow diet from weaning to killing. The other group was switched to a diet devoid of fermentable polysaccharides but rich in simple sugars (35% glucose, 35% sucrose) 14 days before colonization. All mice were colonized with *B. thetaiotaomicron* for 10 days, and bacterial gene expression was defined in each of their ceca at the time of killing.

The presence or absence of polysaccharides in the diet did not produce a significant effect on the density of cecal colonization (*19*). Using the transcriptional profiles of 98 *B. thetaiotaomicron* genes from the "replication, recombination, and repair" COG as biomarkers, we found that the cecal bacterial populations clustered most closely to cells undergoing log-phase growth in vitro, irrespective of the diet (fig. S2B and table S3).

The simple-sugar diet evoked a *B. thetaiotaomicron* transcriptional response predominated by genes in the "carbohydrate transport and metabolism" COG (fig. S3B). Glycoside hydrolase and polysaccharide lyase genes that were up-regulated in vivo by a factor of ≥2.5 relative to MM-G cultures segregated into distinct groups after unsupervised hierarchical clustering (Fig. 3) (fig. S6). The group of 24 genes most highly expressed on the simple-sugar diet encoded enzymes required for degradation of host glycans (e.g., eight hexosaminidases, two α-fucosidases, a sialidase) and did not include any plant polysaccharide–directed arabinosidases or pectin lyases. In addition, all components of the fucose utilization operon (BT1272-BT1277) were expressed at higher levels in mice fed the simple-sugar diet (average induction greater than MM-G by a factor of 12) than in mice fed the polysaccharide-rich diet (average induction greater than MM-G by a factor of 6). The sialylated glycan degradation operon (BT0455-BT0461) exhibited a comparable augmentation of expression on the simple-sugar diet.

A similar cluster analysis revealed two distinct groups of genes encoding carbohydrate binding/importing SusC/SusD paralogs: a group of 61 expressed at highest levels in *B. thetaiotaomicron* from the ceca of mice fed a polysaccharide-rich diet, and a group of 21 expressed at highest levels with a simple-sugar diet (fig. S7). Thirteen of the SusC/SusD paralogs expressed at highest levels on a polysaccharide-rich diet are components of predicted operons that also contain ORFs specifying glycoside hydrolases and polysaccharide lyases. Five pairs of the SusC/SusD paralogs expressed at highest levels on a simple-sugar diet are part of predicted operons. No SusC/SusD paralogs from one diet group are found in operons containing up-regulated glycoside hydrolase genes from the other diet group (fig. S8). Together, the data indicate that subsets of *B. thetaiotaomicron*'s genome are dedicated to retrieving either host or dietary polysaccharides (depending on their availability), although it appears that when both sources are available, harvesting energy from the diet is preferred.

Diet-associated changes in glycan-foraging behavior were accompanied by changes in the expression of *B. thetaiotaomicron*'s capsular polysaccharide synthesis (CPS) loci (fig. S9). Relative to growth in MM-G, *CPS3* was down-regulated in vivo irrespective of host diet, *CPS4* was up-regulated in the ceca of mice fed a polysaccharide-rich diet, and *CPS5* was up-regulated with a high-sugar diet (fig. S9). The

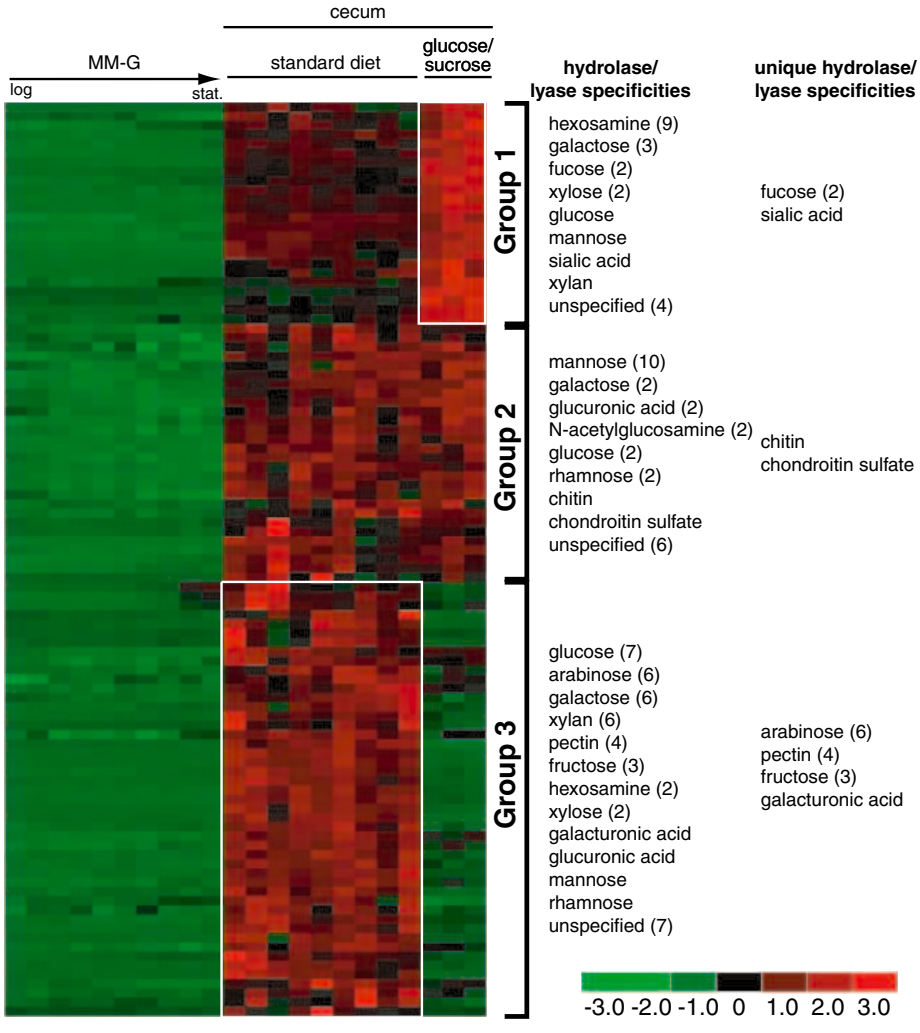

Fig. 3. Diet-associated changes in the in vivo expression of *B. thetaiotaomicron* glycoside hydrolases and polysaccharide lyases. Unsupervised hierarchical clustering yields the following groups of genes up-regulated in vivo by a factor of ≥2.5 on average, relative to their average level of expression at all growth phases in MM-G: group 1, highest expression on a simple-sugar diet, includes activities required for degradation of host glycans; group 2, equivalent expression on both diets; group 3, highest on a polysaccharide-rich standard chow diet; includes enzymes that degrade plant glycans. Average relative differences in expression in vivo versus in vitro (MM-G) are shown in fig. S6. Predicted enzyme substrate specificities unique to the group are listed at the right.

other five CPS loci did not manifest significant differences in their expression during growth in vitro versus in vivo, nor with diet manipulation. These findings suggest that *B. thetaiotaomicron* is able to change its surface carbohydrates in response to the nutrient glycan environment that it is accessing and perhaps also for evading a host immune response (*17*).

A schematic overview of how *B. thetaiotaomicron* might scavenge for carbohydrates in the distal intestine is shown in fig. S10. Bacterial attachment to food particles, shed mucus, and exfoliated epithelial cells is directed by glycan-specific outer-membrane binding proteins (exemplified by SusC/SusD paralogs) (*20*). *B. thetaiotaomicron* contributes to diversity and stability within the gut by adaptively directing its glycan-foraging behavior to the mucus when polysaccharide availability from the diet is reduced. Hence, host genotype and diet intersect to regulate the stability of the microbiota. Coevolution of glycan structural diversity in the host, together with an elaborate repertoire of nutrient-regulated glycoside hydrolase genes in gut symbionts, endows the system with flexibility in adapting to changes in diet. Although our study has focused on the glycan-foraging behavior of *B. thetaiotaomicron* in monoassociated germ-free mice, similar analyses can now be used to assess the impact of other members of the gut microbiota on *B. thetaiotaomicron* and on one another. The results should help to define the molecular correlates of behaviors that underlie the assembly and maintenance of microbial communities in dynamic nutrient environments. They should also provide a framework for developing effective ways to manipulate these communities to promote health or treat various diseases.

References and Notes

1. D. C. Savage, *Annu. Rev. Microbiol.* **31**, 107 (1977).
2. L. V. Hooper, T. Midtvedt, J. I. Gordon, *Annu. Rev. Nutr.* **22**, 283 (2002).
3. J. Xu, J. I. Gordon, *Proc. Natl. Acad. Sci. U.S.A.* **100**, 10452 (2003).
4. A. A. Salyers, *Am. J. Clin. Nutr.* **32**, 158 (1979).
5. D.-E. Chang *et al.*, *Proc. Natl. Acad. Sci. U.S.A.* **101**, 7427 (2004).
6. S. Yachi, M. Loreau, *Proc. Natl. Acad. Sci. U.S.A.* **96**, 1463 (1999).
7. W. E. Moore, L. V. Holdeman, *Appl. Microbiol.* **27**, 961 (1974).
8. To date, *B. thetaiotaomicron* has only been documented in the gastrointestinal tracts of rodents and humans, as judged by analysis of the 1594 rRNA entries in GenBank (22 November 2004 release) that are ≥650 base pairs and assignable to the Cytophaga-Flavobacterium-Bacteroides division.
9. J. Xu *et al.*, *Science* **299**, 2074 (2003).
10. CAZy Database (http://afmb.cnrs-mrs.fr/CAZY).
11. See supporting data on *Science* Online.
12. F. Backhed *et al.*, *Proc. Natl. Acad. Sci. U.S.A.* **101**, 15718 (2004).
13. J. A. Shipman, J. E. Berleman, A. A. Salyers, *J. Bacteriol.* **182**, 5365 (2000).
14. L. V. Hooper *et al.*, *Science* **291**, 881 (2001).
15. GenomeNet, Kyoto University (www.genome.ad.jp).
16. See further data at http://gordonlab.wustl.edu/metaview/bt.
17. L. Bry, P. G. Falk, T. Midtvedt, J. I. Gordon, *Science* **273**, 1380 (1996).
18. L. V. Hooper, J. Xu, P. G. Falk, T. Midtvedt, J. I. Gordon, *Proc. Natl. Acad. Sci. U.S.A.* **96**, 9833 (1999).
19. J. L. Sonnenburg *et al.*, data not shown.
20. J. Sonnenburg, L. T. Angenent, J. I. Gordon, *Nature Immunol.* **5**, 569 (2004).
21. B. P. Westover, J. D. Buhler, J. L. Sonnenburg, J. I. Gordon, *Bioinformatics*, published online 11 November 2004 (10.1093/bioinformatics/bti123).
22. K. H. Cho, D. Cho, G.-R. Wang, A. A. Salyers, *J. Bacteriol.* **183**, 7198 (2001).

23. We thank D. O'Donnell, M. Karlsson, S. Wagoner, L. Gaynon, J. Dant, and the University of California, San Diego, Glycotechnology Core Facility for invaluable assistance, and our colleagues R. Ley, F. Backhed, and E. Sonnenburg for many helpful comments. Supported by NIH grants DK30292 and DK052574. All GeneChip data sets have been deposited in Gene Expression Omnibus under accession number GSE2231 (www.ncbi.nlm.nih.gov/geo).

Supporting Online Material

www.sciencemag.org/cgi/content/full/307/5717/1955/DC1
Materials and Methods
Figs. S1 to S10
Tables S1 to S4
References

22 December 2004; accepted 3 February 2005
10.1126/science.1109051

Introduced Predators Transform Subarctic Islands from Grassland to Tundra

D. A. Croll,[1]* J. L. Maron,[2] J. A. Estes,[1,3] E. M. Danner,[1] G. V. Byrd[4]

Top predators often have powerful direct effects on prey populations, but whether these direct effects propagate to the base of terrestrial food webs is debated. There are few examples of trophic cascades strong enough to alter the abundance and composition of entire plant communities. We show that the introduction of arctic foxes (*Alopex lagopus*) to the Aleutian archipelago induced strong shifts in plant productivity and community structure via a previously unknown pathway. By preying on seabirds, foxes reduced nutrient transport from ocean to land, affecting soil fertility and transforming grasslands to dwarf shrub/forb-dominated ecosystems.

Nearly half a century ago, Hairston *et al.* (*1*) proposed that plant productivity and composition were influenced by apex predators through cascading trophic interactions. According to their "Green World" view, the direct effects of predators on herbivore populations transcend multiple trophic levels indirectly to enhance plant community productivity and biomass. Despite great progress in food web ecology, the indirect effects of top predators on vegetation dynamics in terrestrial systems remain unresolved and actively debated (*2–6*). Compelling demonstrations of multitrophic predator impacts on entire plant communities are scarce, in part because the spatial and temporal scales necessary to perform the appropriate community-wide experiments are daunting.

The introduction of predators to islands provides an opportunity to explore the indirect effects of predators on vegetation. Introduced predators commonly have devastating direct effects on their prey (*7*). The histories of these introductions are often well known, and the relative simplicity and isolation of insular systems facilitate the study of whole-community responses. Here we investigate how the introduction of arctic foxes (*Alopex lagopus*) to the Aleutian archipelago affected terrestrial ecosystems across this 1900-km island chain.

The Aleutian archipelago is a remote series of physically similar volcanic islands extending westward from the Alaska Peninsula (Fig. 1). The archipelago currently supports 29 species of breeding seabirds, together numbering >10 million individuals (*8*). Seabirds deliver nutrient-rich guano from productive ocean waters (*9*) to the nutrient-limited plant communities (*10*, *11*). Historically, seabirds inhabited most islands along the Aleutian chain. Following the collapse of the maritime fur trade in the late 19th and early 20th centuries, foxes were introduced to >400 Alaskan islands as an additional fur source (*12*). The introduced foxes severely reduced local avifaunas, especially seabirds (*13*). However, several islands remained fox free, either because introductions failed or were not undertaken (*12–14*). Hence, a large-scale natural experiment to evaluate the effects of exotic predators on insular ecosystems was unwittingly initiated more than a century ago. We use this experiment to show how differing seabird densities on islands with and without foxes affect soil and plant nutrients; plant abundance, composition, and productivity; and nutrient flow to higher trophic levels. These determinations

[1]Department of Ecology and Evolutionary Biology, Island Conservation, University of California–Santa Cruz, Santa Cruz, CA 95060, USA. [2]Division of Biological Sciences, University of Montana, Missoula, MT 59812, USA. [3]U.S. Geological Survey, Western Ecological Research Center, Santa Cruz, CA 95060, USA. [4]U.S. Fish and Wildlife Service, 95 Sterling Highway, Homer, AK 99603, USA.

*To whom correspondence should be addressed. E-mail: croll@biology.ucsc.edu

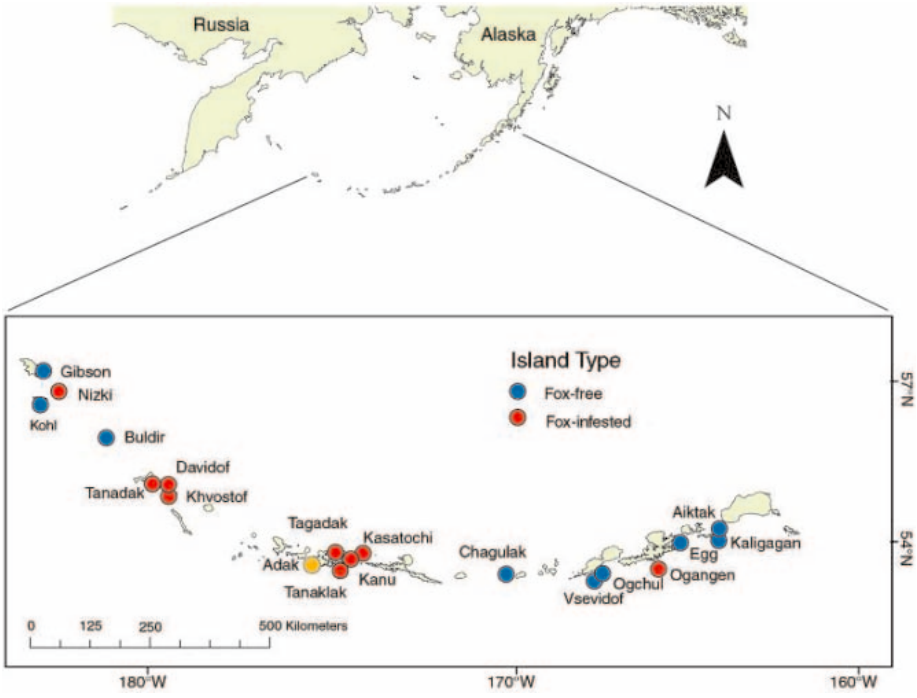

Fig. 1. The Aleutian archipelago with sample islands indicated in red (fox-infested) and blue (fox-free). Adak Island, the location of fertilization experiments, is indicated with a yellow dot.

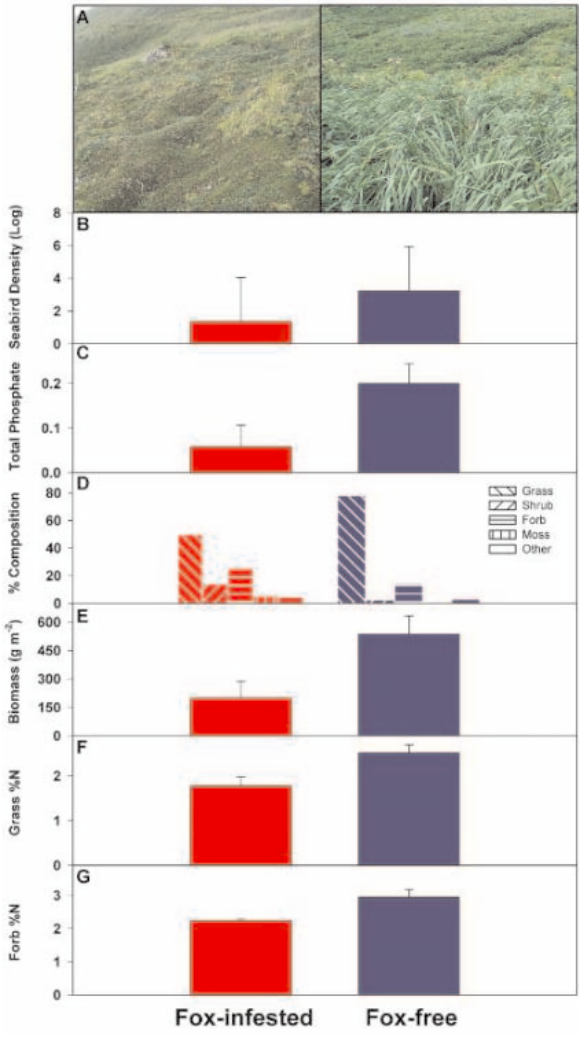

Fig. 2. Mean (±SE) values for parameters sampled on fox-infested (red) and fox-free (blue) islands in the Aleutian archipelago. (**A**) Photographs of typical plant communities on fox-infested (Ogangan Island) versus fox-free (Buldir Island) islands. (**B**) Logarithm of the density (birds m^{-2}) of breeding seabirds estimated from population counts made by the U.S. Fish and Wildlife Service (*26*). (**C**) Soil Bray phosphorous (%). (**D**) Composition of island plant community from point contact counts of 1-m^2 photo quadrats. (**E**) Grass biomass (g dry weight m^{-2}). (**F**) Percent nitrogen composition of the dominant grasses (*Leymus molis* or *Calamagrostis nutkanensis*). (**G**) Percent nitrogen composition of a common forb (*Achillea borealis*).

were based on contrasts among 18 islands (9 with foxes and 9 fox free) (Fig. 1) that were matched as carefully as possible for size and location in the archipelago (*12*).

A geographical information system (GIS) was used to superimpose spatially explicit grids over maps of each island. All islands were sampled at the completion of the growing season (August) between 2001 and 2003. We established a 30 m by 30 m plot at each of the grid crosspoints (12 to 32 per island, depending on island size) (*12*), within which we sampled plant species presence and cover; aboveground plant biomass; total soil N, P, and $\delta^{15}N$; and %N and $\delta^{15}N$ from a common grass (in most cases *Leymus mollis* but in some instances *Calamagrostis nutkanensis*) and forb (*Achillea borealis*) (*12*). At each island, we also haphazardly sampled $\delta^{15}N$ in at least five individuals from a diverse group of terrestrial consumers, including a mollusk (*Deroceras laeve*), arachnid (*Cybaeus reticulates*), dipteran (*Scathophaga impudicum*), and passerine bird (Lapland longspurs, *Calcarius lapponicus*, and song sparrows, *Melospiza melodia*). $\delta^{15}N$ was measured to determine the degree to which nitrogen-based nutrients were marine derived. Soils and organisms that obtain their N from locally fixed sources have lower $\delta^{15}N$ values than those that obtain their N from higher trophic levels, such as marine fish and zooplankton (*15*, *16*).

Breeding seabird densities were almost two orders of magnitude higher on fox-free than on fox-infested islands (Fig. 2B) (Mann-Whitney rank sum, $T = 36$, $P < 0.001$) (*12*). We estimate that this reduction in seabird abundance translates to a decline in annual guano input from 361.9 to 5.7 g m^{-2} (median values; $T = 42$, $P = 0.005$) (*12*). The resulting difference in marine nutrient input is reflected in soil fertility. Total soil phosphorus on fox-free islands was more than three times that on fox-infested islands (Fig. 2C) ($F_{1,16} = 8.01$, $P = 0.012$) (*12*). Although seabird colonies are often concentrated on the perimeter of islands, guano-derived nutrients can be broadly redistributed across islands and not solely concentrated within the colonies (*17*).

The different soil fertilities between fox-free and fox-infested islands corresponded with strong shifts among island types in the biomass and nutrient status of terrestrial plants, as well as overall composition of the plant community (Figs. 2, A to D, and 3A). Grass biomass was almost a factor of 3 higher (Fig. 2E) ($F_{1,15} = 10.58$, $P = 0.005$), shrub biomass was a factor of 10 lower (0.48 ± 0.31 versus 4.95 ± 0.84 g m^{-2}; $F_{1,15} = 19.97$, $P < 0.001$), and the nitrogen content in grasses and forbs was significantly greater on fox-free versus fox-infested islands (Fig. 2, F and G) ($F_{1,16} = 8.28$, $P = 0.01$ and $F_{1,13} = 12.51$, $P = 0.004$ for grasses and forbs, respectively). Plant communities on fox-free islands were graminoid dominated, whereas those on fox-infested islands had a

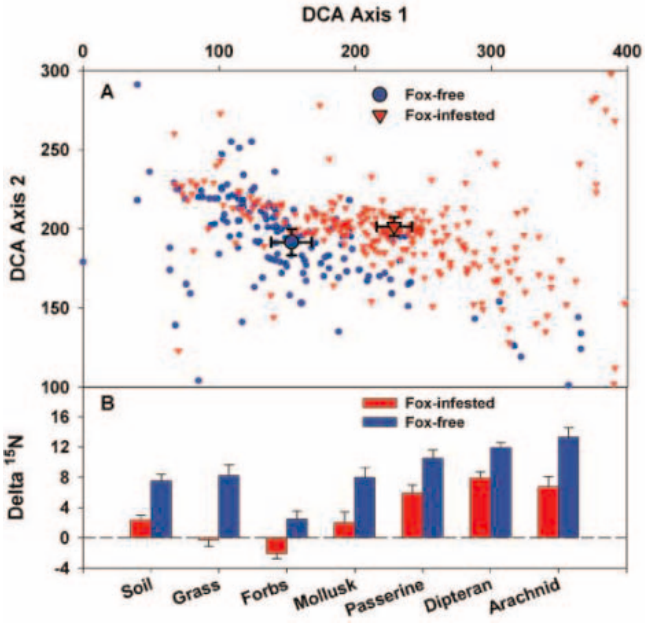

Fig. 3. (**A**) Detrended correspondence analysis (DCA) comparing plant assemblages (based on the presence or absence of species) on fox-infested (red triangles) and fox-free (blue circles) islands. Analysis was conducted on species presence data from one of the three 1-m^2 quadrats within 30 m by 30 m plots on the two island types. Each small point represents a census of plant species occurrence within a 1-m^2 quadrat. Large points represent the mean ± 99% confidence interval axis scores from all samples taken across each island type. (**B**) Stable nitrogen isotope ($\delta^{15}N$ mean ± SE) analyses of soils and a suite of common species across trophic levels on fox-infested (red) and fox-free (blue) islands.

more equitable distribution of graminoids, shrubs, and forbs (Fig. 2D).

$\delta^{15}N$ measures from soils, plants, and consumers all indicate that fox introductions reduced nitrogen input from sea to land. $\delta^{15}N$ was significantly greater in soils from fox-free islands compared with fox-infested islands (Fig. 3B) ($F_{1,16} = 14.07$, $P = 0.002$). Similar patterns in $\delta^{15}N$ between fox-free and fox-infested islands were evident in grasses, forbs, mollusks, passerines, dipterans, and arachnids (Fig. 3B). These findings demonstrate that fox-free islands are strongly subsidized by marine-derived nutrients, which in turn assist in fueling the ecosystem at higher trophic levels.

To test whether differences in the magnitude of nutrient subsidies transported by seabirds onto fox-free versus fox-infested islands could have produced the observed differences in plant communities, we conducted a fertilization experiment on a large fox-infested island. Experimental nutrient additions to a community representative of fox-infested islands over 3 years caused a 24-fold increase in grass biomass (24.33 ± 6.05 g m^{-2}) compared with control plots (0.51 ± 0.38 g m^{-2} increase; two-factor analysis of variance, $F_{1,20} = 23.96$, $P < 0.001$) and a rapid shift in the plant community to a grass-dominated state. In fertilized plots, grass increased from 22 (±2.7%) to 96 (±17.3%) of total plant biomass, whereas grass biomass in control plots was relatively unchanged (11.4 ± 3.0% and 12.1 ± 1.2% of total biomass at the start and end of the experiment, respectively) (*12*). In a parallel experiment (*18*), we disturbed and fertilized plots to mimic the effects of both seabird burrowing and guano addition. Here we found that disturbance negatively rather than positively affected grass biomass; the effects of fertilization alone were far greater than the joint effects of disturbance and fertilization. These results confirm the importance of nutrient limitation in these ecosystems and establish that nutrient delivery in the form of seabird guano is sufficient to explain observed differences in terrestrial plant communities between islands with and without foxes.

In total, our results show that the introduction of foxes to the Aleutian archipelago transformed the islands from grasslands to maritime tundra. Fox predation reduced seabird abundance and distribution, in turn reducing nutrient transport from sea to land. The more nutrient-impoverished ecosystem that resulted favored less productive forbs and shrubs over more productive grasses and sedges.

These findings have several broad implications. First, they show that strong direct effects of introduced predators on their naïve prey can ultimately have dramatic indirect effects on entire ecosystems and that these effects may occur over large areas—in this case across an entire archipelago. Second, they bolster growing evidence that the flow of nutrients, energy, and material from one ecosystem to another can subsidize populations and, importantly, influence the structure of food webs (*19*–*21*). Finally, they show that the mechanisms by which predators exert ecosystem-level effects extend beyond both the original conceptual model provided by Hairston *et al.* and its more recent elaborations (*22*). Trophic cascades (*23*, *24*) have traditionally been thought to involve a series of strictly top-down interactions, where predators, by affecting herbivore populations and altering the intensity of herbivory, ultimately influence plant production at the base of food webs (*25*). Our work illustrates that predators, by thwarting the transport of nutrients between systems, can have powerful indirect effects on systems via a route different from that of classic trophic cascades. The impact of highly mobile predators and their prey on the transport of materials between ecosystems remains poorly understood. Because few ecosystems support food webs that are undisturbed either through introductions or extirpations, it may be that the all-too-common addition or deletion of predators from systems have had substantial but largely unexplored effects.

References and Notes

1. N. G. Hairston Jr., F. E. Smith, L. B. Slobodkin, *Am. Nat.* **94**, 421 (1960).
2. J. Halaj, D. H. Wise, *Ecology* **83**, 3141 (2002).
3. R. T. Paine, *J. Mammal.* **81**, 637 (2000).
4. G. A. Polis, A. L. W. Sears, G. R. Huxel, D. R. Strong, J. Maron, *Trends Ecol. Evol.* **15**, 473 (2000).
5. M. L. Pace, J. J. Cole, S. R. Carpenter, J. F. Kitchell, *Trends Ecol. Evol.* **14**, 483 (1999).
6. O. J. Schmitz, P. A. Hamback, A. P. Beckerman, *Am. Nat.* **155**, 141 (2000).
7. M. Williamson, *Island Populations* (Oxford Univ. Press, Oxford, 1981).
8. There are several reasons why the Aleutian archipelago provides an ideal large-scale experimental system to study the effects of introduced predators: (i) Most islands are small; (ii) high-latitude floral diversity is relatively low; (iii) there are no native vertebrate herbivores; (iv) the islands are geologically and climatologically homogeneous with similar overall soil properties; (v) the large number of islands in the archipelago provides the opportunity for meaningful replication; (vi) the islands are isolated from anthropogenic nutrient inputs; and (vii) fox introductions were not targeted for particular island types, and the history of introductions is reasonably well known.
9. N. R. Council, *The Bering Sea Ecosystem* (National Academy Press, Washington, DC, 1996).
10. F. S. Chapin III, G. R. Shaver, A. E. Giblin, *Ecology* **76**, 694 (1995).
11. G. R. Shaver, F. S. Chapin III, *Arct. Alp. Res.* **18**, 261 (1986).
12. Materials and methods are available as supporting material on *Science* Online.
13. E. P. Bailey, *U.S. Fish Wildl. Serv. Resour. Publ.* **193**, 1 (1993).
14. G. V. Byrd, J. L. Trapp, C. F. Zeillemaker, *Trans. 59th N. Am. Wildl. Nat. Resour. Conf.*, 317 (1994).
15. T. E. Dawson, S. Mambelli, A. H. Plamboeck, P. H. Templer, K. P. Tu, *Annu. Rev. Ecol. Syst.* **33**, 507 (2002).
16. D. E. Schneider, S. C. Lubetkin, in *Food Webs at the Landscape Level*, G. A. Polis, M. E. Power, G. R. Huxel, Eds. (Univ. Chicago Press, Chicago, 2004), pp. 12–24.
17. P. D. Erskine *et al.*, *Oecologia* **117**, 187 (1998).
18. J. L. Maron *et al.*, data not shown.
19. G. A. Polis, S. D. Hurd, *Am. Nat.* **147**, 396 (1996).
20. G. A. Polis, M. E. Power, G. R. Huxel, *Food Webs at the Landscape Level* (Univ. of Chicago Press, Chicago, 2004).
21. J. F. Kitchell *et al.*, *Limnol. Oceanogr.* **44**, 828 (1999).
22. S. D. Fretwell, *Oikos* **50**, 291 (1987).
23. S. R. Carpenter, J. F. Kitchell, *Bull. Ecol. Soc. Am.* **74**, 186 (1993).
24. R. T. Paine, *J. Anim. Ecol.* **49**, 667 (1980).
25. J. Terborgh *et al.*, *Science* **294**, 1923 (2001).
26. U.S. Fish and Wildlife Service, "Beringian Seabird Colony Catalog Computer Database" (U.S. Fish and Wildlife Service, Homer, AK, 2004).

27. We thank S. Buckelew, S. Elmendorf, and the Fox/Seabird field teams for field assistance; K. Bell and crew of the M/V Tiglax for ship support; and S. Talbot, J. Williams, and the Alaska Maritime National Wildlife Refuge for advice and logistical assistance. R. Ostfelt, J. Kitchell, T. Martin, D. Pearson, R. Callaway, and R. Holt provided important comments on the manuscript. Supported by NSF OPP-9985814 (J.A.E. and D.A.C.) and NSF OPP-0296208 (J.L.M.).

Supporting Online Material

www.sciencemag.org/cgi/content/full/307/5717/1959/DC1
SOM Text
References and Notes

8 December 2004; accepted 26 January 2005
10.1126/science.1108485

Gene Regulation at the Single-Cell Level

Nitzan Rosenfeld,[1]* Jonathan W. Young,[3] Uri Alon,[1]
Peter S. Swain,[2]* Michael B. Elowitz[3]†

The quantitative relation between transcription factor concentrations and the rate of protein production from downstream genes is central to the function of genetic networks. Here we show that this relation, which we call the gene regulation function (GRF), fluctuates dynamically in individual living cells, thereby limiting the accuracy with which transcriptional genetic circuits can transfer signals. Using fluorescent reporter genes and fusion proteins, we characterized the bacteriophage lambda promoter P_R in *Escherichia coli*. A novel technique based on binomial errors in protein partitioning enabled calibration of in vivo biochemical parameters in molecular units. We found that protein production rates fluctuate over a time scale of about one cell cycle, while intrinsic noise decays rapidly. Thus, biochemical parameters, noise, and slowly varying cellular states together determine the effective single-cell GRF. These results can form a basis for quantitative modeling of natural gene circuits and for design of synthetic ones.

The operation of transcriptional genetic circuits (*1*–*5*) is based on the control of promoters by transcription factors. The GRF is the relation between the concentration of active transcription factors in a cell and the rate at which their downstream gene products are produced (expressed) through transcription and translation. The GRF is typically represented as a continuous graph, with the active transcription factor concentration on the *x* axis and the rate of production of its target gene on the *y* axis (Fig. 1A). The shape of this function, e.g., the characteristic level of repressor that induces a given response, and the sharpness, or nonlinearity, of this response (*1*) determine key features of cellular behavior such as lysogeny switching (*2*), developmental cell-fate decisions (*6*), and oscillation (*7*). Its properties are also crucial for the design of synthetic genetic networks (*7*–*11*). Current models estimate GRFs from in vitro data (*12*, *13*). However, biochemical parameters are generally unknown in vivo and could depend on the environment (*12*) or cell history (*14*, *15*). Moreover, gene regulation may vary from cell to cell or over time. Three fundamental aspects of the GRF specify the behavior of transcriptional circuits at the single-cell level: its mean shape (averaged over many cells), the typical deviation from this mean, and the time scale over which such fluctuations persist. Although fast fluctuations should average out quickly, slow ones may introduce errors in the operation of genetic circuits and may pose a fundamental limit on their accuracy. In order to address all three aspects, it is necessary to observe gene regulation in individual cells over time.

Therefore, we built "λ-cascade" strains of *Escherichia coli*, containing the λ repressor and a downstream gene, such that both the amount of the repressor protein and the rate of expression of its target gene could be monitored simultaneously in individual cells (Fig. 1B). These strains incorporate a yellow fluorescent repressor fusion protein (*cI-yfp*) and a chromosomally integrated target promoter (P_R) controlling cyan fluorescent protein (*cfp*). In order to systematically vary repressor concentration over its functional range (in logarithmic steps), we devised a "regulator dilution" method. Repressor production is switched off in a growing cell, so that its concentration subsequently decreases by dilution as the cell divides and grows into a microcolony (Fig. 1C). We used fluorescence time-lapse microscopy (Fig. 1D; fig. S1 and movies S1 and S2) and computational image analysis to reconstruct the lineage tree (family tree) of descent and sibling relations among the cells in each microcolony (fig.

[1]Departments of Molecular Cell Biology and Physics of Complex Systems, Weizmann Institute of Science, Rehovot, 76100, Israel. [2]Centre for Non-linear Dynamics, Department of Physiology, McGill University, 3655 Promenade Sir William Osler, Montréal, Québec, Canada, H3G 1Y6. [3]Division of Biology and Department of Applied Physics, Caltech, Pasadena, CA 91125, USA.

*These authors contributed equally to this work
†To whom correspondence should be addressed. E-mail: melowitz@caltech.edu

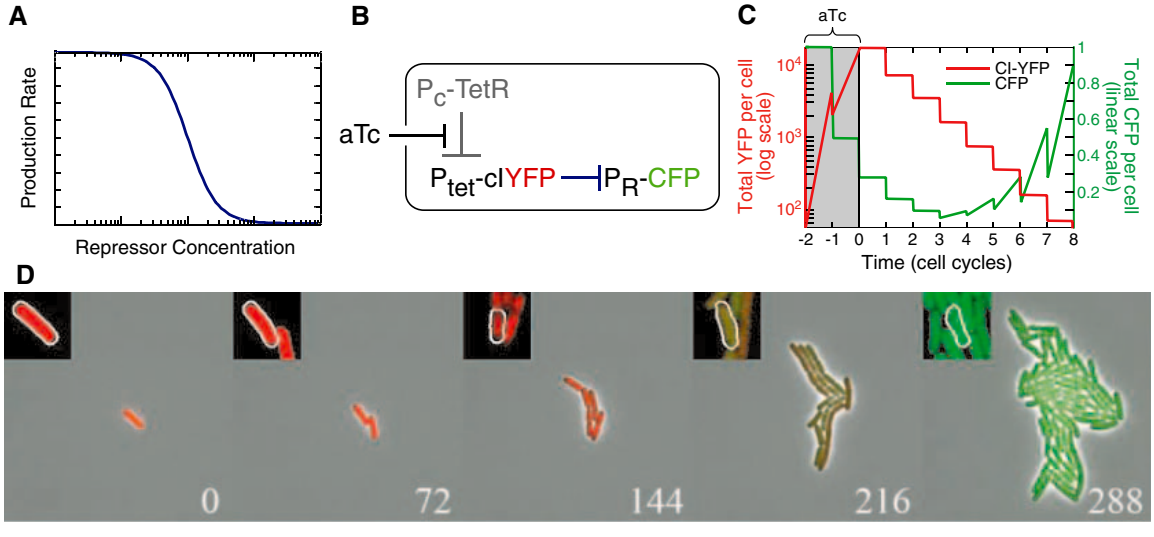

Fig. 1. Measuring a gene regulation function (GRF) in individual *E. coli* cell lineages. (**A**) The GRF is the dependence of the production rate of a target promoter (*y* axis) on the concentration of one (or more) transcription factors (*x* axis). (**B**) In the λ-cascade strains (*16*) of *E. coli*, CI-YFP is expressed from a tetracycline promoter in a TetR+ background and can be induced by anhydrotetracycline (aTc). CI-YFP represses production of CFP from the P_R promoter. (**C**) The regulator dilution experiment (schematic): Cells are transiently induced to express CI-YFP and then observed in time-lapse microscopy as repressor dilutes out during cell growth (red line). When CI-YFP levels decrease sufficiently, expression of the *cfp* target gene begins (green line). (**D**) Snapshots of a typical regulator dilution experiment using the O_R2*–λ-cascade strain (see fig. S3) (*16*). CI-YFP protein is shown in red and CFP is shown in green. Times, in minutes, are indicated on snapshots. (Insets) Selected cell lineage (outlined in white). Greater time resolution is provided in fig. S1.

S2). For each cell lineage, we quantified over time the level of repressor (x axis of the GRF) and the total amount of CFP protein (Fig. 2A). From the change in CFP over time, we calculated its rate of production (y axis of the GRF) (*16*).

Regulator dilution also provides a natural in vivo calibration of individual protein fluorescence. Using the lineage tree and fluorescence data, we analyzed sister cell pairs just after division (Fig. 2B). The partitioning of CI-YFP fluorescence to daughter cells obeyed a binomial distribution, consistent with an equal probability of having each fluorescent protein molecule go to either daughter (*16*). Consequently, the root-mean-square error in CI-YFP partitioning between daughters increases as the square root of their total CI-YFP fluorescence. Using a one-parameter fit, we estimated the fluorescence signal of individual CI-YFP molecules (Fig. 2B and supporting online material). Thus, despite cellular autofluorescence that prohibits detection of individual CI-YFP molecules, observation of partitioning errors still permits calibration in terms of apparent numbers of molecules per cell.

The mean GRFs obtained by these techniques are shown in Fig. 3A for the P_R promoter and a point mutant variant (fig. S3). These are the mean functions, obtained by averaging individual data points (Fig. 3B) in bins of similar repressor concentration, indicating the average protein production rate at a given repressor concentration. Their cooperative nature would have been "smeared out" by population averages (*6*, *17*, *18*).

These mean GRF data provide in vivo values of the biochemical parameters underlying transcriptional regulation. Hill functions of the form $f(R) = \beta/[1 + (R/k_d)^n]$ are often used to represent unknown regulation functions (*1*, *6–10*). Here, k_d is the concentration of repressor yielding half-maximal expression, n indicates the degree of effective cooperativity in repression, and β is the maximal production rate. Hill functions indeed fit the data well (Fig. 3A and Table 1). The measured in vivo k_d is comparable to previous estimates (*2*, *12*, *13*, *19*) (see supporting online text). The significant cooperativity observed ($n > 1$) may result from dimerization of repressor molecules and cooperative interactions between repressors bound at neighboring sites (*2*, *12*, *13*, *19*, *20*). A point mutation in the O_R2 operator, O_R2^* (*20*) (fig. S3), significantly reduced n and increased k_d (Fig. 3A and Table 1). Note that with similar methods it is even possible to measure effective cooperativity (n) for native repressors without fluorescent protein fusions (*16*).

We next addressed deviations from the mean GRF. At a given repressor concentration, the standard deviation of production rates is ~55% of the mean GRF value. Such variation may arise from microenvironmental differences (*21*), cell cycle–dependent changes in gene copy number, and various sources of noise in gene expression and other cellular processes (*22*). We compared microcolonies in which induction occurs at different cell densities (*16*). The results suggested that the measured GRF is robust to possible differences among the growth environments in our experiments (fig. S6). We analyzed the effect of gene copy number, which varies twofold over the cell cycle as DNA replicates. The CFP production rate correlated strongly with cell-cycle phase; cells about to divide produced on average twice as much protein per unit of time as newly divided cells (*16*). Thus, gene dosage is not compensated. Nevertheless, after normalizing production rates to the average cell-cycle phase (*16*), substantial variation still remains in the production rates, and their standard deviation is ~40% of the mean GRF (Fig. 3). The deviations from the mean GRF show a log-normal distribution (see supporting online text and fig. S5).

These remaining fluctuations may arise from processes intrinsic or extrinsic to gene expression. Intrinsic noise results from stochasticity in the biochemical reactions at an individual gene and would cause identical copies of a gene to express at different levels. It can be measured by comparing expression of two identically regulated fluorescent proteins (*22*). Extrinsic noise is the additional variation originating from fluctuations in cellular components such as metabolites, ribosomes, and polymerases and has a global effect (*22*, *23*). Extrinsic noise is often the dominant source of variation in *E. coli* and *Saccharomyces cerevisiae* (*22*, *24*).

To test whether fluctuations were of intrinsic or extrinsic origin, we used a "symmetric branch" strain (*16*) that produced CFP and YFP from an identical pair of P_R promoters (Fig. 4D, movie S3). The difference between CFP and YFP production rates in these cells indicates ~20% intrinsic noise in protein production [averaged over 8- to 9-min intervals (*16*)], suggesting that the extrinsic component of noise is dominant and contributes a variation in protein production rates of ~35%.

Our measurements provide more detailed analysis of extrinsic noise in two ways. First, in previous work (*22*), extrinsic noise included fluctuations in upstream cellular components, including both gene-specific and global factors. Here, we quantify the extrinsic noise at known repressor concentration, and so extrinsic noise encompasses fluctuations in global cellular components such as polymerases or

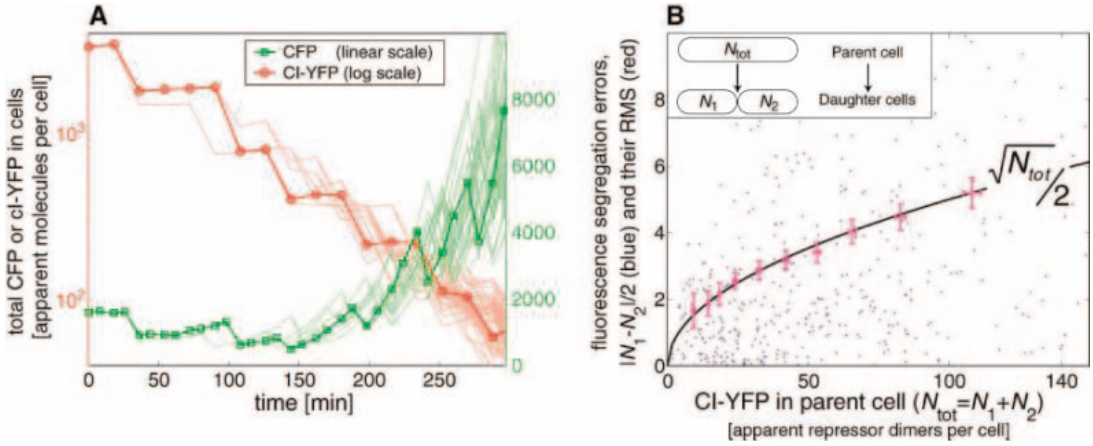

Fig. 2. Data and calibration. (**A**) Fluorescence intensities of individual cells are plotted over time for the experiment of Fig. 1D. Red indicates CI-YFP, which is plotted on a logarithmic y axis to highlight its exponential dilution: As CI-YFP is not produced, each division event causes a reduction of about twofold in total CI-YFP fluorescence. Green indicates CFP, which is plotted on a linear y axis to emphasize its increasing slope, showing that CFP production rate increases as the CI-YFP levels decrease. A selected cell lineage is highlighted (also outlined in Fig. 1D). (**B**) Analysis of binomial errors in protein partitioning to find v_y, the apparent fluorescence intensity of one independently segregating fluorescent particle (*16*). Cells containing N_{tot} copies of a fluorescent particle (total fluorescence $Y_{tot} = v_y \cdot N_{tot}$) undergo division (inset). If each particle segregates independently, N_1 and N_2, the number of copies received by the two daughter cells, are distributed binomially, and satisfy $\sqrt{\left\langle \left(\frac{N_1 - N_2}{2}\right)^2 \right\rangle} = \sqrt{N_{tot}}/2$. A single-parameter fit thus determines the value of v_y. Here we plot $|N_1 - N_2|/2$ (in numbers of apparent molecule dimers) versus $N_{tot} = N_1 + N_2$. Blue dots show the scatter of individual division events. Crosses (red) show the root-mean-square (RMS) error in protein partitioning and its standard error. The expected binomial standard deviation is shown in black.

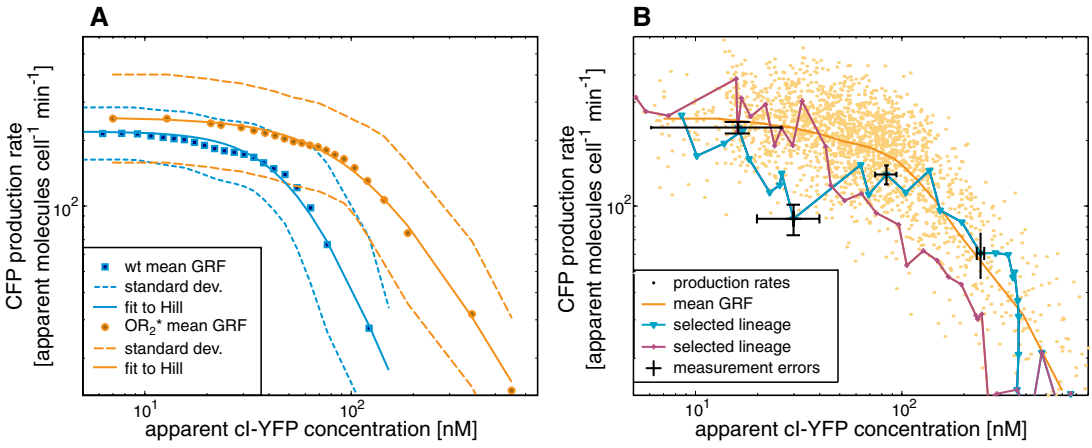

Fig. 3. The GRF and its fluctuations. (**A**) The mean regulation function of the wild-type λ-phage P_R promoter (blue squares) and its O_R2-mutated variant (O_R2*, orange circles) are plotted with their respective standard deviations (dashed/dotted lines). Hill function approximations (using parameters from Table 1) are shown (solid lines). (**B**) Variation in the O_R2* GRF. Individual points indicate the instantaneous production rate of CFP, as a function of the amount of CI-YFP in the same cell, for all cells in a microcolony of the O_R2*–λ-cascade strain. The time courses of selected lineages in this microcolony are drawn on top of the data, showing slow fluctuations around the mean GRF. CI-YFP concentration decreases with time, and consecutive data points along a trajectory are at 9-min intervals. Typical measurement errors (black crosses) are shown for a few points. Data are compensated for cell cycle–related effects (*16*).

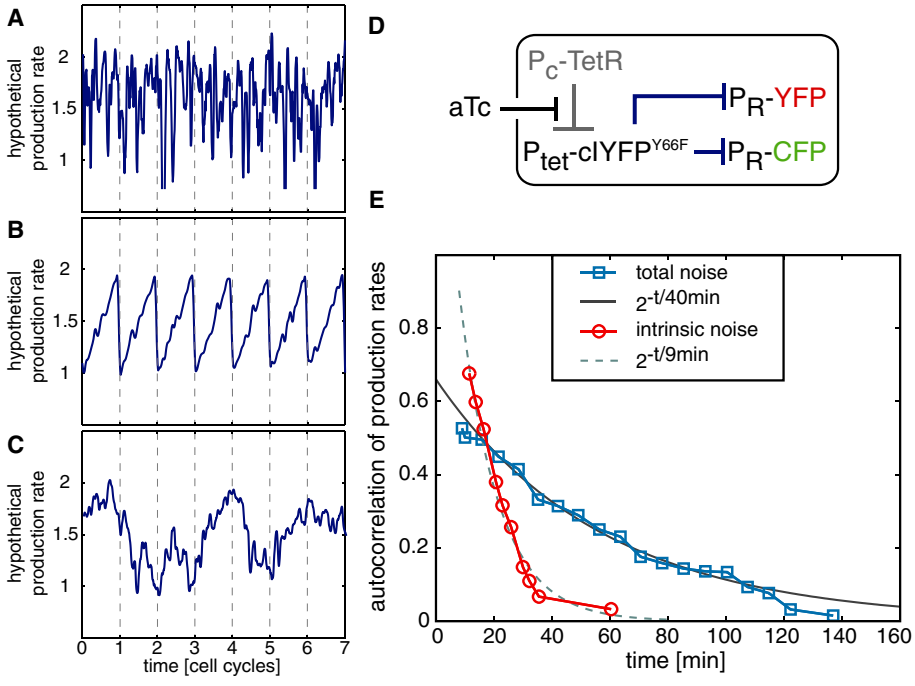

Fig. 4. Fluctuations in gene regulation. (Left) Three types of variability observed here. (**A**) Fast fluctuations in CFP production, similar to those produced by intrinsic noise. (**B**) Periodic, cell cycle–dependent oscillations in CFP production, which can result from DNA replication. (**C**) Slow aperiodic fluctuations, such as extrinsic fluctuations in gene expression. (**D**) Intrinsic and extrinsic noise can be discriminated using a symmetric-branch strain (*16*) of *E. coli*, containing identical, chromosomally integrated λ-phage P_R promoters controlling *cfp* and *yfp* genes. The strain also expresses nonfluorescent CI-YFP from a Tet-regulated promoter. (**E**) The autocorrelation function of the relative production rates in the λ-cascade strains (blue squares) shows that the time scale for fluctuations in protein production is $\tau_{corr} \sim 40$ min (blue). The difference between production rates of YFP and CFP in the symmetric branch strain has a correlation time of $\tau_{intrinsic} < 10$ min (red). The data and correlations presented are corrected for cell cycle–related effects (*16*).

Table 1. In vivo values of effective biochemical parameters. Molecular units are estimated using binomial errors in protein partitioning (*16*) (Fig. 2B), which may have systematic errors up to a factor ~2. Concentrations are calculated from apparent molecule numbers divided by cell volumes estimated from cell images (*16*), with an average volume of 1.5 ± 0.5 μm³ (for which 1 nM = 0.9 molecule/cell).

Parameter	P_R	P_R (O_R2*)
n (degree of cooperativity in repression)	2.4 ± 0.3	1.7 ± 0.3
k_d [concentration of repressor yielding half-maximal expression (nM)]	55 ± 10	120 ± 25
β [unrepressed production rate (molecules · cell^{-1} · min^{-1})]	220 ± 15	255 ± 40

ribosomes but not in the concentration of the repressor, CI. Second, dynamic observations permit us to measure extrinsic noise in the rate of protein expression rather than in the amount of accumulated protein. The present breakdown should be more useful for modeling and design of genetic networks.

In cells, fast and slow fluctuations can affect the operation of genetic networks in different ways. Previous experiments (*22*, *24*–*26*) used static "snapshots" to quantify noise at steady state and were thus unable to access the temporal dynamics of gene expression. However, a similar steady-state distribution of expression levels can be reached by fluctuations on very different time scales (Fig. 4). Fluctuations can be characterized by their autocorrelation time, τ_{corr} (*16*). The magnitude of τ_{corr} compared with the cell-cycle period is crucial: Fluctuations longer than the cell cycle accumulate to produce significant effects, whereas more rapid fluctuations may "average out" as cellular circuits operate (*27*, *28*). In these data, three types of dynamics are observed (Fig. 4, A to C): Fast fluctuations, periodic cell-cycle oscillations due to DNA replication, and aperiodic fluctuations with a time scale of about one cell cycle.

We found that the trajectories of single-cell lineages departed substantially from the mean GRF over relatively long periods (Fig. 3B), with $\tau_{corr} = 40 \pm 10$ min (Fig. 4E). This value is close to the cell cycle period, $\tau_{cc} = 45 \pm 10$ min, indicating that, overall, fluctuations typically persist for one cell cycle. Therefore, if a cell produces CFP at a faster rate than the mean GRF, this overexpression will likely continue for roughly one cell cycle, and CFP levels will accumulate to higher concentrations than the mean GRF would predict.

In contrast, the autocorrelation of the intrinsic noise (*16*) decays rapidly: $\tau_{intrinsic} < 10$ min $\ll \tau_{corr}$ (Fig. 4E). Thus, the observed slow fluctuations do not result from intrinsic noise; they represent noise extrinsic to CFP expression (see supporting online text). The concentration of a stable cellular factor would be expected to fluctuate with a time scale of the cell cycle period (*7*, *10*). For instance, even though intrinsic fluctuations in production rates are fast, the difference between the total amounts of YFP and CFP in the symmetric branch experiments has an autocorrelation time of $\tau_{total} = 45 \pm 5$ min (*16*). A similar time scale may well apply to other stable cellular components such as ribosomes, metabolic apparatus, and sigma factors. As such components affect their own expression as well as that of our test genes, extrinsic noise may be self-perpetuating.

These data indicate that the single-cell GRF cannot be represented by a single-valued function. Slow extrinsic fluctuations give the cell and the genetic circuits it comprises a memory, or individuality (*29*), lasting roughly one cell cycle. These fluctuations are substantial in amplitude and slow in time scale. They present difficulty for modeling genetic circuits and, potentially, for the cell itself: In order to accurately process an intracellular signal, a cell would have to average its response for well over a cell cycle—a long time in many biological situations. This problem is not due to intrinsic noise in the output, noise that fluctuates rapidly, but rather to the aggregate effect of fluctuations in other cellular components. There is thus a fundamental tradeoff between accuracy and speed in purely transcriptional responses. Accurate cellular responses on faster time scales are likely to require feedback from their output (*1*, *4*, *6*, *10*, *30*). These data provide an integrated, quantitative characterization of a genetic element at the single-cell level: its biochemical parameters, together with the amplitude and time scale of its fluctuations. Such systems-level specifications are necessary both for modeling natural genetic circuits and for building synthetic ones. The methods introduced here can be generalized to more complex genetic networks, as well as to eukaryotic organisms (*18*).

References and Notes

1. M. A. Savageau, *Biochemical Systems Analysis* (Addison-Wesley, Reading, MA, 1976).
2. M. Ptashne, *A Genetic Switch: Phage Lambda and Higher Organisms* (Cell Press and Blackwell Science, Cambridge, MA, ed. 2, 1992).
3. H. H. McAdams, L. Shapiro, *Science* **269**, 650 (1995).
4. E. H. Davidson *et al.*, *Science* **295**, 1669 (2002).
5. S. S. Shen-Orr, R. Milo, S. Mangan, U. Alon, *Nature Genet.* **31**, 64 (2002).
6. J. E. Ferrell Jr., E. M. Machleder, *Science* **280**, 895 (1998).
7. M. B. Elowitz, S. Leibler, *Nature* **403**, 335 (2000).
8. T. S. Gardner, C. R. Cantor, J. J. Collins, *Nature* **403**, 339 (2000).
9. A. Becskei, B. Seraphin, L. Serrano, *EMBO J.* **20**, 2528 (2001).
10. N. Rosenfeld, M. B. Elowitz, U. Alon, *J. Mol. Biol.* **323**, 785 (2002).
11. F. J. Isaacs, J. Hasty, C. R. Cantor, J. J. Collins, *Proc. Natl. Acad. Sci. U.S.A.* **100**, 7714 (2003).
12. K. S. Koblan, G. K. Ackers, *Biochemistry* **31**, 57 (1992).
13. P. J. Darling, J. M. Holt, G. K. Ackers, *J. Mol. Biol.* **302**, 625 (2000).
14. R. J. Ellis, *Trends Biochem. Sci.* **26**, 597 (2001).
15. M. Mirasoli, J. Feliciano, E. Michelini, S. Daunert, A. Roda, *Anal. Chem.* **74**, 5948 (2002).
16. Materials and methods are available as supporting material on *Science* Online.
17. P. Cluzel, M. Surette, S. Leibler, *Science* **287**, 1652 (2000).
18. G. Lahav *et al.*, *Nature Genet.* **36**, 147 (2004).
19. I. B. Dodd *et al.*, *Genes Dev.* **18**, 344 (2004).
20. B. J. Meyer, R. Maurer, M. Ptashne, *J. Mol. Biol.* **139**, 163 (1980).
21. J. A. Shapiro, *Annu. Rev. Microbiol.* **52**, 81 (1998).
22. M. B. Elowitz, A. J. Levine, E. D. Siggia, P. S. Swain, *Science* **297**, 1183 (2002).
23. P. S. Swain, M. B. Elowitz, E. D. Siggia, *Proc. Natl. Acad. Sci. U.S.A.* **99**, 12795 (2002).
24. J. M. Raser, E. K. O'Shea, *Science* **304**, 1811 (2004).
25. E. M. Ozbudak, M. Thattai, I. Kurtser, A. D. Grossman, A. van Oudenaarden, *Nature Genet.* **31**, 69 (2002).
26. W. J. Blake, M. Kærn, C. R. Cantor, J. J. Collins, *Nature* **422**, 633 (2003).
27. H. H. McAdams, A. Arkin, *Proc. Natl. Acad. Sci. U.S.A.* **94**, 814 (1997).
28. J. Paulsson, *Nature* **427**, 415 (2004).
29. J. L. Spudich, D. E. Koshland Jr., *Nature* **262**, 467 (1976).
30. P. S. Swain, *J. Mol. Bio.* **344**, 965 (2004).

31. We thank Z. Ben-Haim, R. Clifford, S. Itzkovitz, Z. Kam, R. Kishony, A. J. Levine, A. Mayo, R. Milo, R. Phillips, M. Ptashne, J. Shapiro, B. Shraiman, E. Siggia, and M. G. Surette for helpful discussions. M.B.E. is supported by a CASI award from the Burroughs Wellcome Fund, the Searle Scholars Program, and the Seaver Institute. U.A. and M.B.E. are supported by the Human Frontiers Science Program. P.S.S. acknowledges support from a Tier II Canada Research Chair and the Natural Sciences and Engineering Research Council of Canada. N.R. dedicates this work to the memory of his father, Yasha (Yaakov) Rosenfeld.

Supporting Online Material

www.sciencemag.org/cgi/content/full/307/5717/1962/DC1
Materials and Methods
SOM Text
Figs. S1 to S6
References and Notes
Movies S1 to S3

29 October 2004; accepted 4 February 2005
10.1126/science.1106914

Noise Propagation in Gene Networks

Juan M. Pedraza and Alexander van Oudenaarden*

Accurately predicting noise propagation in gene networks is crucial for understanding signal fidelity in natural networks and designing noise-tolerant gene circuits. To quantify how noise propagates through gene networks, we measured expression correlations between genes in single cells. We found that noise in a gene was determined by its intrinsic fluctuations, transmitted noise from upstream genes, and global noise affecting all genes. A model was developed that explains the complex behavior exhibited by the correlations and reveals the dominant noise sources. The model successfully predicts the correlations as the network is systematically perturbed. This approach provides a step toward understanding and manipulating noise propagation in more complex gene networks.

The genetic program of a living cell is determined by a complex web of gene networks. The proper execution of this program relies on faithful signal propagation from one gene to the next. This process may be hindered by stochastic fluctuations arising from gene expression, because some of the components in these circuits are present at low numbers, which makes fluctuations in concentrations unavoidable (*1*). Additionally, reaction rates can fluctuate because of stochastic variation in the global pool of housekeeping genes or because of fluctuations in environmental conditions that affect all genes. For example, fluctuations in the number of available polymerases or in any factor that alters the cell growth rate will change the reaction rates for all genes. Recent experimental studies (*2*–*5*) have made substantial progress identifying the factors that determine the fluctuations in the expression of a single gene. However, how expression fluctuations propagate from one gene to the next is largely unknown. To address this issue, we designed a gene network (Fig. 1A) in which the interactions between adjacent genes could be externally controlled and quantified at the single-cell level.

This synthetic network (*6*) consisted of four genes, of which three were monitored in single *Escherichia coli* cells by cyan, yellow, and red fluorescent proteins (CFP, YFP, and RFP). The first gene, *lacI*, is constitutively transcribed and codes for the lactose repressor, which down-regulates the transcription of the second gene, *tetR*, that is bicistronically transcribed with *cfp*. The gene product of *tetR*, the tetracycline repressor, in turn down-regulates the transcription of the third gene, reported by YFP. The fourth gene, *rfp,* is under

Department of Physics, Massachusetts Institute of Technology, Cambridge, MA 02139, USA.

*To whom correspondence should be addressed: E-mail: avano@mit.edu

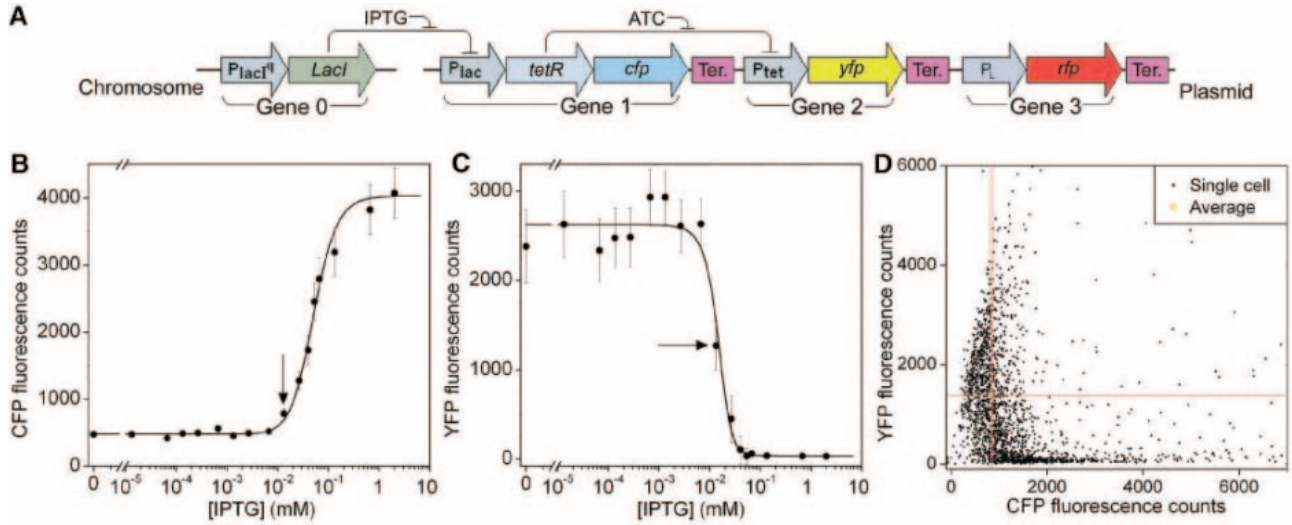

Fig. 1. (**A**) A schematic design of the network. (**B** and **C**) Average CFP and YFP expression as a function of IPTG concentration in the steady state. Each experimental data point was obtained from ~2000 single-cell measurements. The solid lines are fits obtained from the Langevin model (*23*). (**D**) Scatter plot of the fluorescence levels for the entire population at [IPTG] = 13 μM. This corresponds to the points marked by the arrows in (B) and (C). The red lines indicate the average CFP and YFP expression.

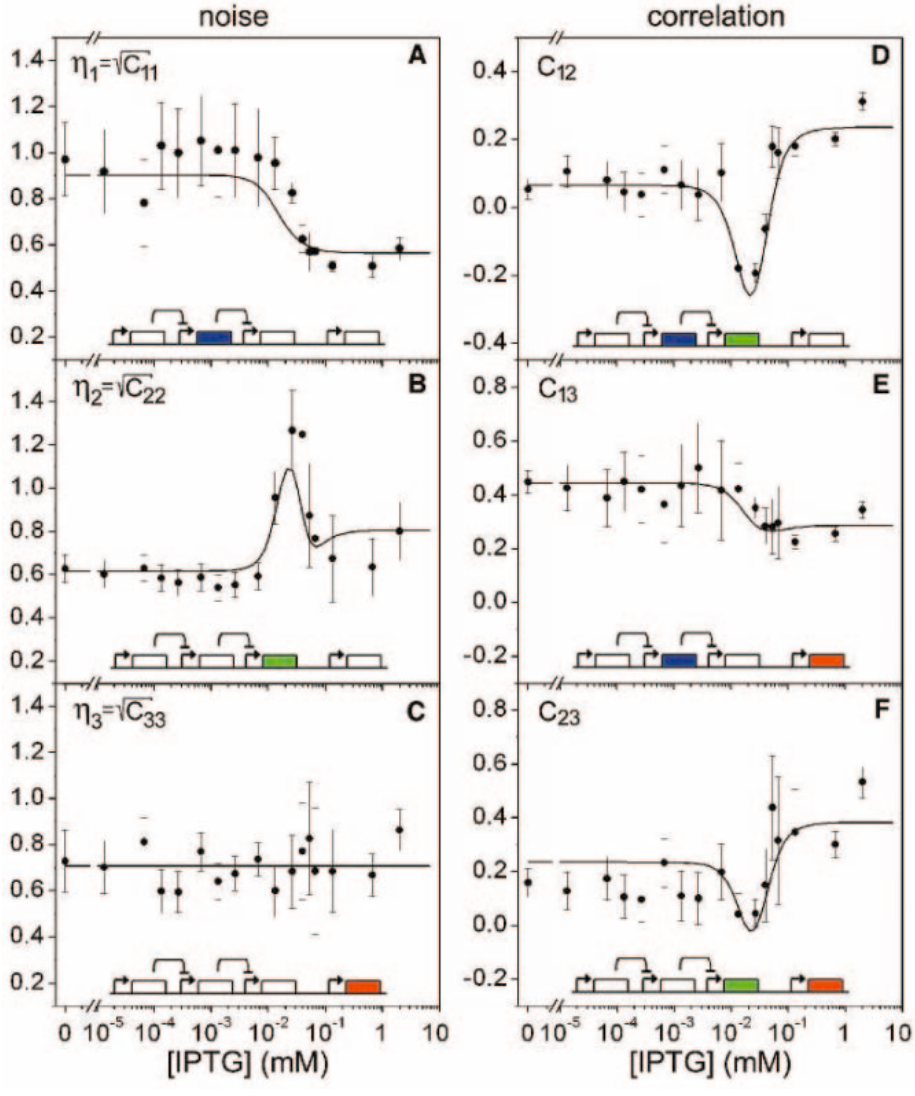

Fig. 2. (**A** to **C**) Coefficient of variation $\eta_i = \sqrt{C_{ii}}$ of the expression in genes 1 to 3 as a function of IPTG concentration in the steady state. (**D** to **F**) Correlation between the expression levels of genes 1 and 2, 1 and 3, and 2 and 3, respectively. The solid lines are predictions from the Langevin model (*23*).

the control of the lambda repressor promoter P_L, which is a strong constitutive promoter. Because this gene is not part of the cascade, this reporter was used to evaluate the effect of global fluctuations. This cascade was used to measure how fluctuations in an upstream gene (*tetR*, reported by CFP) transmit downstream (and are reported by YFP). The inducers isopropyl-β-D-thiogalactopyranoside (IPTG) and anhydrotetracycline (ATC) bind to and inhibit the repression of the lactose and tetracycline repressors, respectively, and were used to tune, respectively, the expression of the upstream gene and the coupling between the two genes.

We assayed the response of single cells to various amounts of inducers by using automated fluorescence microscopy. In each experimental run, the level of the three fluorescent reporters was quantified for ~2000 individual cells. Figure 1B shows that the average signal of the upstream gene displayed a sigmoidal response to changes in the concentration of IPTG in the growth media. In response, the average signal of the downstream gene (Fig. 1C) behaved inversely and decreased sharply at larger IPTG concentrations. The enhanced sensitivity of the YFP response, compared to the CFP response, when IPTG is varied demonstrates the utility of cascades for generating steep switches (*7*–*10*). However, the average expression alone does not capture the population behavior, because the expression of most cells is quite different from the average (Fig. 1D). Even for a fixed IPTG concentration, the fluctuations in gene expression resulted in a broad distribution that reflects the interaction between the upstream and downstream genes.

To quantify the expression fluctuations and the degree of correlation between different genes, we computed the correlation

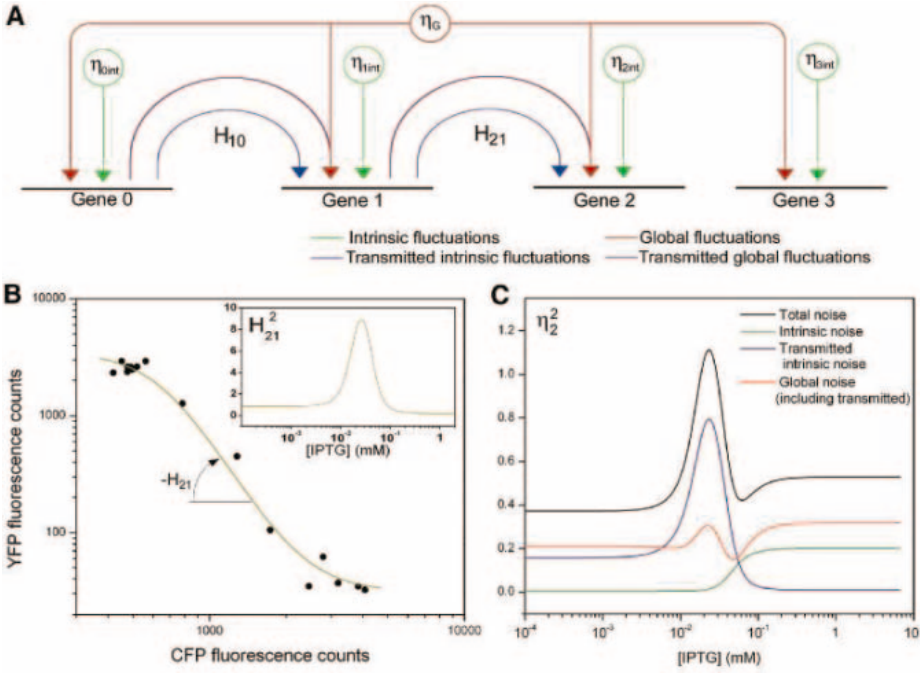

Fig. 3. (**A**) A sketch of the propagation of the fluctuations, showing how the two sources of noise, intrinsic and global, can result in many components. (**B**) The logarithmic gain H_{21} is obtained as the negative of the slope in log-log space of the mean expression of YFP as a function of mean CFP expression. (Inset) The square of H_{21} as a function of IPTG. (**C**) Noise in the downstream gene (Fig. 2B) decomposed into the different sources of noise. The total noise (black) is the result of the intrinsic noise in this gene (green), the transmitted noise from the intrinsic fluctuations in upstream genes (blue), and the global noise (red).

$C_{ij} = \frac{\langle F_i F_j \rangle - \langle F_i \rangle \langle F_j \rangle}{\langle F_i \rangle \langle F_j \rangle}$ from the fluorescence levels F_i in individual cells. The brackets $\langle \ldots \rangle$ denote averaging over all cells in the population, and the indices i and j refer to the gene number as defined in Fig. 1A. Because each cell is characterized by three different expression values (F_1, F_2, and F_3), the statistical properties of this network are summarized by the three self-correlations, C_{11}, C_{22}, and C_{33}, and the three cross-correlations, C_{12}, C_{13}, and C_{23}. The self-correlation is identical to the square of the coefficient of variation, η_i, which is defined as the standard deviation of the expression distribution normalized to the mean expression. These six correlations were plotted as a function of the IPTG concentration (Fig. 2). The correlations behave in a nonintuitive manner. For example, the noise properties of the upstream gene, reflected in η_1 (Fig. 2A), are very different from those of the downstream gene, reflected in η_2 (Fig. 2B), even though both genes are repressed by a single upstream repressor (Fig. 1A). The correlations C_{13} and C_{23} are also dependent on IPTG concentration (Fig. 2, E and F). Because RFP is not part of the cascade, one might expect a correlation that is independent of IPTG.

To clarify these issues, we developed a stochastic model that allows for a systematic interpretation of the data in terms of the different components of the noise. The coefficients of variations and correlations can be derived from the model analytically, enabling a direct fit to the entire experimental data set (*11*). Our model is based on the Langevin approach (*7*, *12*, *13*), in which the deterministic differential equations describing the dynamics of the system are modified by adding stochastic terms (*6*, *14*) that reflect the two sources of noise: intrinsic fluctuations due to low numbers of molecules and global fluctuations in cellular components that change the reaction rates for all genes.

Using the resulting expressions (*15*) for the correlations, we can decompose the noise in each gene into three components: intrinsic noise in that specific gene, transmitted intrinsic noise from the upstream genes, and global noise modulated by the network (Fig. 3A). The intrinsic noise (Fig. 3A, green arrows) arises mostly from low copy numbers of mRNAs (*2*, *3*, *16*). The second noise component, the transmitted intrinsic noise (Fig. 3A, blue arrows), includes the transmitted fluctuations of each of the upstream genes in the network and depends on three factors: the intrinsic noise for that upstream gene; the effect of temporal averaging (*6*, *16*), which depends on the lifetimes of the proteins; and the susceptibility of the downstream gene to the upstream one. We characterize this susceptibility through the logarithmic gain H_{ji} (*16*, *17*) (Fig. 3B). The logarithmic gain reflects how the average expression of the downstream gene j changes as the expression of the upstream gene i is varied. For example, the main term in the transmitted intrinsic noise from gene 1 to gene 2 (Fig. 1A) is proportional to the squared logarithmic gain H_{21}^2 (Fig. 3B, inset). The pronounced peak in H_{21}^2 occurs at an IPTG concentration for which the response of the downstream gene is most sensitive to changes in the upstream signal. Consistently, the downstream fluctuations reach a maximum at this concentration (Fig. 2B) (*6*). The last component of the noise reflects the effect of the global fluctuations. It includes the direct effect on the gene, the transmitted effect from the upstream genes (Fig. 3A), and the effect of the correlated transmission, which depends on the interactions. The latter illustrates the main difference between transmitted intrinsic and transmitted global noise. The different intrinsic noise sources are uncorrelated, whereas the global fluctuations arise from the same sources (Fig. 3A). This means that the transmitted global noise (Fig. 3A, purple arrows) does not simply add to the direct global noise (Fig. 3A, red arrows). Because both fluctuations came from the same sources, correction terms arise that depend on the strength (and sign) of the interaction (*15*).

In Fig. 3C, these different noise components are shown for gene 2. The intrinsic component (Fig. 3C, green line) varies as the inverse of the square root of the mean, resulting in increased noise at higher IPTG concentrations. The transmitted intrinsic component (Fig. 3C, blue line) corresponds roughly to the square of the logarithmic gain (Fig. 3B, inset) times the noise in the upstream gene (Fig. 2A) (*18*). The global noise component (Fig. 3C, red line) is not constant but rather shows the modulation as explained above. Thus, the main features of the noise in this gene are determined by the network interactions, rather than by its own intrinsic noise characteristics.

The effect of modulating the global noise is also demonstrated by the behavior of the correlations between noninteracting genes (Fig. 2, E and F). A global fluctuation that raises the expression of RFP will also raise the expression of YFP and CFP. An increased CFP expression will result in a decreased YFP expression by an amount that depends on the interaction between gene 1 and gene 2 and hence will vary with IPTG (*19*). This can be seen in the expression for the correlations (*15*). A consequence of this modulation is that the correlations C_{12} and C_{23} display qualitatively similar behavior as IPTG is varied (Fig. 2, D and F). This indicates that C_{23} is dominated by the global noise that is transmitted from gene 1 to gene 2. Similarly, the correlation C_{13} is dominated by the global noise transmitted from gene 0 to gene 1 and therefore displays a different behavior compared to C_{12} and C_{23} (*6*).

We directly quantified the intrinsic and extrinsic noise for genes 1 to 3 as a function

of the IPTG concentration (Fig. 4, A and B) by measuring the correlation between CFP and YFP in constructs in which both reporters were driven by the same promoter (*3*, *5*, *6*). The total noise was generally dominated by extrinsic fluctuations. The experimentally obtained intrinsic and extrinsic noise of genes 1 and 2 was consistent with the predictions of the model.

To probe the predictive power of the stochastic model, we used it to predict the noise and correlations as the coupling between genes 1 and 2 was altered by adding ATC to the growth media (*6*). We compared these predictions to experimental results. As an example, η_2 and C_{12} are shown in Fig. 4, C and D. Both η_2 and C_{12} display rich behavior as a function of both the IPTG and ATC concentrations. As is seen in Fig. 4C, a small perturbation to the network can transform a maximum in the η_2-IPTG curve (Fig. 4C, black) into a step (red) or even a minimum (green). These features were faithfully predicted by the model (Fig. 4D). Similarly, the model correctly predicts correlation C_{12} (Fig. 4, E and F) and the other correlations (*6*). These experiments demonstrate that the stochastic model is not only descriptive but also has predictive power and can therefore be used as a design tool for synthetic circuits.

Our results show that the noise in a gene affects expression fluctuations of its downstream genes. This transmitted noise can be calculated from the interactions between upstream and downstream genes as quantified by the logarithmic gains. Thus, it is not necessary to have low numbers of molecules to have large fluctuations, because noise could be transmitted from upstream genes. We show that the noise has a correlated global component that is modulated by the network. Thus, even in a network where all components have low intrinsic noise, fluctuations can be substantial and the distributions of expression levels depend on the interactions between genes. Measuring the correlation between a constitutive gene and a gene embedded in a network provides a sensitive probe for correlated sources of noise. This would have been difficult to reveal by monitoring single genes (*2*, *4*) or two copies of the same gene (*3*, *5*). Our results highlight the importance of including stochastic effects in the study of regulatory networks. This will be necessary for understanding faithful signal propagation in natural networks (*20*) as well as for designing noise-tolerant synthetic circuits (*21*).

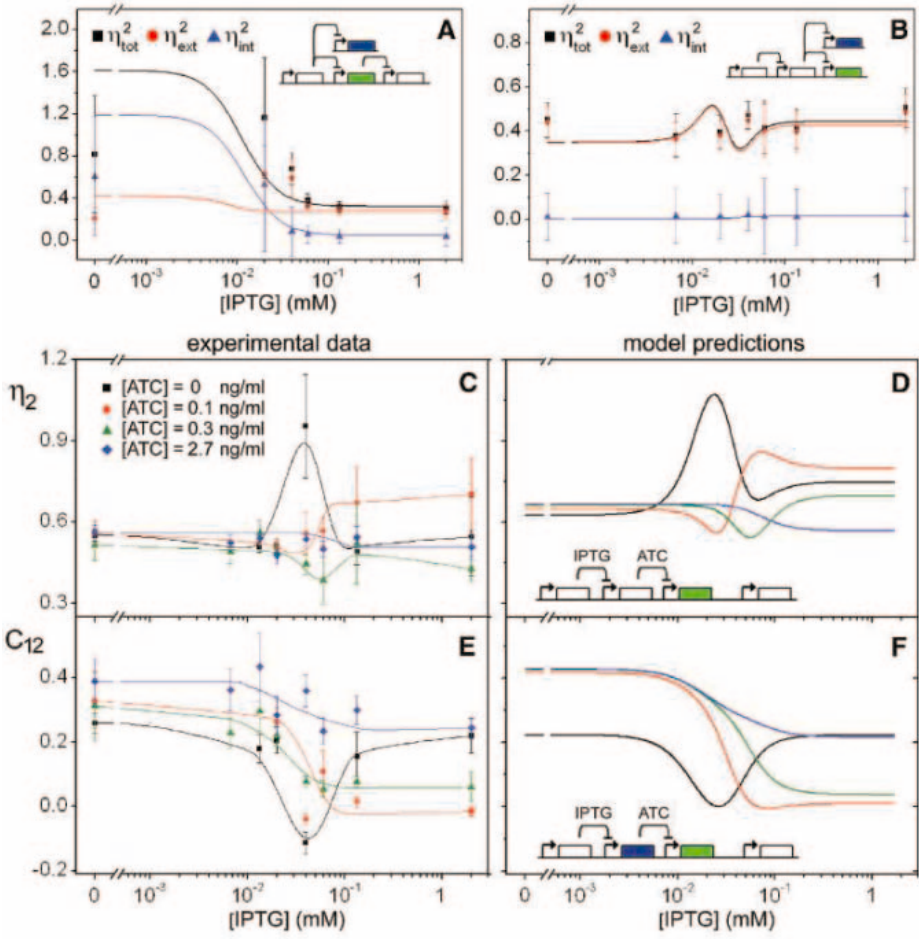

Fig. 4. (**A** and **B**) Experimentally determined intrinsic and extrinsic noise as a function of IPTG (*3*, *6*). The solid lines represent predictions by the stochastic model. (A) Two copies of the *lac* promoter are driving CFP and YFP. (B) Two copies of the *tet* promoter are driving CFP and YFP. The model parameters used are those in table S1, except for the basal transcription, which was adjusted to the measured value (*6*). (**C** and **E**) Coefficient of variation η_2 and correlation C_{12} as a function of IPTG concentration in the steady state for different levels of ATC. The solid lines are guides to the eye. Each experimental data point was obtained from ~1000 single-cell measurements (*23*). (**D** and **F**) Predictions for η_2 and C_{12} from the Langevin model, given the parameters obtained previously (*6*).

References and Notes

1. C. V. Rao, D. M. Wolf, A. P. Arkin, *Nature* **420**, 231 (2002).
2. E. M. Ozbudak *et al.*, *Nature Genet.* **31**, 69 (2002).
3. M. B. Elowitz, A. J. Levine, E. D. Siggia, P. S. Swain, *Science* **297**, 1183 (2002).
4. W. J. Blake, M. Kaern, C. R. Cantor, J. J. Collins, *Nature* **422**, 633 (2003).
5. J. M. Raser, E. K. O'Shea, *Science* **304**, 1811 (2004).
6. Materials and methods are available as supporting material on *Science* Online.
7. M. Thattai, A. van Oudenaarden, *Biophys. J.* **82**, 2943 (2002).
8. P. B. Chock, E. R. Stadtman, *Proc. Natl. Acad. Sci. U.S.A.* **74**, 2766 (1977).
9. A. Goldbeter, D. E. Koshland Jr., *Proc. Natl. Acad. Sci. U.S.A.* **78**, 6840 (1981).
10. J. E. Ferrell Jr., E. M. Machleder, *Science* **280**, 895 (1998).
11. We fitted the analytical results to all means, noises, and correlations simultaneously. To test the resulting parameters (table S1), we conducted Monte Carlo simulations of the network using Gillespie's stochastic simulation algorithm (*22*). The results from the Langevin model are consistent with these simulations.
12. T. B. Kepler, T. C. Elston, *Biophys. J.* **81**, 3116 (2001).
13. J. Hasty *et al.*, *Proc. Natl. Acad. Sci. U.S.A.* **97**, 2075 (2000).
14. N. G. van Kampen, *Stochastic Processes in Physics and Chemistry* (North-Holland, Amsterdam, 1981).
15. The interaction between two genes is determined by the rate of synthesis from the downstream gene as a function of the concentration of upstream proteins (y_i); this will be called the transfer function. Assuming that the interactions are Hill-type repressions, the parameters for the transfer function $f_2(y_1)$ for the repression between genes 1 and 2 can be obtained from the two means, up to the conversion constants from fluorescence counts to protein numbers. To match the notation in previous studies (*16*), we define the logarithmic gain corresponding to genes i and j as $H_{ji} = -\frac{\bar{y}_j}{\bar{y}_i}\frac{1}{\gamma_j}\frac{\partial f_j(y_i)}{\partial y_i}\Big|_{\bar{y}_i}$, where γ_j is the decay rate of gene j and the overbar denotes the steady state average. The global and plasmid noise are characterized by the parameters η_G and η_N, respectively (*6*). Subscripts 0 to 3 correspond to genes *lacI*, *cfp*, *yfp*, and *rfp* (Fig. 1A). $\eta_{i\,\mathrm{int}}$ denotes the intrinsic noise in gene i. In this notation, the total noise in genes 0 to 3 is given by

$$\eta_0^2 = \eta_{0\,\mathrm{int}}^2 + \eta_G^2$$

$$\eta_1^2 = \eta_{1\,\mathrm{int}}^2 + \frac{1}{2}H_{10}^2\eta_{0\,\mathrm{int}}^2 + \eta_G^2\left(1 + \frac{1}{2}H_{10}^2 - H_{10}\right) + \frac{1}{2}\eta_N^2$$

$$\eta_2^2 = \eta_{2\,\mathrm{int}}^2 + \frac{1}{2}H_{21}^2\eta_{1\,\mathrm{int}}^2 + \frac{3}{8}H_{21}^2H_{10}^2\eta_{0\,\mathrm{int}}^2 + \eta_G^2\left(1 + \frac{1}{2}H_{21}^2 + \frac{3}{8}H_{21}^2H_{10}^2 - H_{21} - \frac{3}{4}H_{21}^2H_{10} + \frac{1}{2}H_{21}H_{10}\right) + \eta_N^2\left(\frac{1}{2} + \frac{3}{8}H_{21}^2 - \frac{3}{4}H_{21}\right)$$

$$\eta_3^2 = \eta_{3\,\mathrm{int}}^2 + \eta_G^2 + \frac{1}{2}\eta_N^2$$

The expressions for the correlations are

$$C_{12} = -\frac{1}{2}H_{21}\eta^2_{1\,\mathrm{int}} - \frac{3}{8}H_{21}H^2_{10}\eta^2_{0\,\mathrm{int}} + \eta^2_G\left(1 - \frac{1}{2}H_{21} - \frac{1}{2}H_{10} - \frac{3}{8}H_{21}H^2_{10} + \frac{3}{4}H_{21}H_{10}\right) + \eta^2_N\left(\frac{1}{2} - \frac{3}{8}H_{21}\right)$$

$$C_{13} = \eta^2_G\left(1 - \frac{1}{2}H_{10}\right) + \frac{1}{2}\eta^2_N$$

$$C_{23} = \eta^2_G\left(1 - \frac{1}{2}H_{21} + \frac{1}{4}H_{21}H_{10}\right) + \eta^2_N\left(\frac{1}{2} - \frac{3}{8}H_{21}\right)$$

16. J. Paulsson, *Nature* **427**, 415 (2004).
17. M. A. Savageau, *Biochemical Systems Analysis* (Addison-Wesley, Reading, MA, 1976).
18. The expression for the transmitted noise in η_2 cannot be rewritten as the transmission of the total steady-state noise in gene 1 only (*6*, *15*).
19. J. Paulsson, M. Ehrenberg, *Q. Rev. Biophys.* **34**, 1 (2001).
20. L. H. Hartwell *et al.*, *Nature* **402** (suppl.), C47 (1999).
21. J. Hasty, D. McMillen, J. J. Collins, *Nature* **420**, 224 (2002).
22. D. T. Gillespie, *J. Phys. Chem.* **81**, 2340 (1977).
23. Duplicated measurements are averaged. The error bars reflect the standard deviation of run-to-run differences and the error within each measurement as determined by bootstrapping.

24. We thank T. S. Gardner, J. J. Collins, R. Lutz, and H. Bujard for their kind gift of plasmids; M. Thattai, A. Becskei, and H. Lim for helpful discussions and suggestions; and B. Kaufmann for his help with the initial constructs. Supported by NSF CAREER grant no. PHY-0094181 and NIH grant no. R01-GM068957.

Supporting Online Material

www.sciencemag.org/cgi/content/full/307/5717/1965/DC1
Materials and Methods
Figs. S1 to S3
Tables S1 and S2
References and Notes

23 December 2004; accepted 18 February 2005
10.1126/science.1109090

RNA-Dependent Cysteine Biosynthesis in Archaea

Anselm Sauerwald,[1] Wenhong Zhu,[3] Tiffany A. Major,[4] Hervé Roy,[5] Sotiria Palioura,[1] Dieter Jahn,[6] William B. Whitman,[4] John R. Yates 3rd,[3] Michael Ibba,[5] Dieter Söll[1,2]*

Several methanogenic archaea lack cysteinyl–transfer RNA (tRNA) synthetase (CysRS), the essential enzyme that provides Cys-tRNA^{Cys} for translation in most organisms. Partial purification of the corresponding activity from *Methanocaldococcus jannaschii* indicated that tRNA^{Cys} becomes acylated with *O*-phosphoserine (Sep) but not with cysteine. Further analyses identified a class II–type *O*-phosphoseryl-tRNA synthetase (SepRS) and Sep-tRNA:Cys-tRNA synthase (SepCysS). SepRS specifically forms Sep-tRNA^{Cys}, which is then converted to Cys-tRNA^{Cys} by SepCysS. Comparative genomic analyses suggest that this pathway, encoded in all organisms lacking CysRS, can also act as the sole route for cysteine biosynthesis. This was proven for *Methanococcus maripaludis*, where deletion of the SepRS-encoding gene resulted in cysteine auxotrophy. As the conversions of Sep-tRNA to Cys-tRNA or to selenocysteinyl-tRNA are chemically analogous, the catalytic activity of SepCysS provides a means by which both cysteine and selenocysteine may have originally been added to the genetic code.

The translation of cysteine codons in mRNA during protein synthesis requires cysteinyl-tRNA (Cys-tRNA^{Cys}). Cys-tRNA^{Cys} is normally synthesized from the amino acid cysteine and the corresponding tRNA isoacceptors (tRNA^{Cys}) in an adenosine triphosphate (ATP)–dependent reaction catalyzed by cysteinyl-tRNA synthetase (CysRS). Genes encoding CysRS, *cysS*, have been detected in hundreds of organisms encompassing all three living domains (*1*). The only exceptions are certain methanogenic archaea, the completed genome sequences of which encode no open reading frames (ORFs) with obvious homology to known *cysS* sequences (*1*). Because of the discovery that the genomes of a number of methanogenic archaea either lack *cysS* (*Methanocaldococcus jannaschii*, *Methanothermobacter thermautotrophicus*, and *Methanopyrus kandleri*) or can dispense with it (*Methanococcus maripaludis*), the formation of Cys-tRNA^{Cys} in these organisms has been a much studied and increasingly contentious topic (*2*, *3*). A noncognate aminoacyl-tRNA synthetase [aaRS (*4*–*6*)] and a previously unassigned ORF (*7*) were variously implicated in Cys-tRNA^{Cys} formation. Recent studies failed to provide conclusive support for either of these routes, leaving the mechanism of Cys-tRNA^{Cys} formation still in doubt (*2*).

Previous investigations of archaeal Cys-tRNA^{Cys} biosynthesis have been hampered by the significant levels of noncognate tRNA routinely cysteinylated and detected by conventional filter binding assays. This problem was circumvented with a more stringent assay of Cys-tRNA^{Cys} formation: gel-electrophoretic separation of uncharged tRNA from aminoacyl-tRNA (aa-tRNA) and subsequent detection of the tRNA moieties by sequence-specific probing (*8*). Given that *M. jannaschii* is a strict anaerobe, and considering that earlier aerobic purification erroneously identified prolyl-tRNA synthetase (*4*, *5*), we used anaerobic conditions for all procedures unless otherwise indicated. When these procedures were used to monitor acylation of total *M. maripaludis* tRNA by an undialyzed *M. jannaschii* cell-free extract (S-100), tRNA^{Cys} was charged with an amino acid that gave rise to the same mobility shift (*9*) exhibited by standard *M. maripaludis* Cys-tRNA^{Cys} generated by *M. maripaludis* CysRS (*1*) (Fig. 1A, lanes 7 and 8). Further optimization of the reaction at this stage showed that Zn^{2+} and ATP were also required for the successful formation of charged tRNA^{Cys}. When the S-

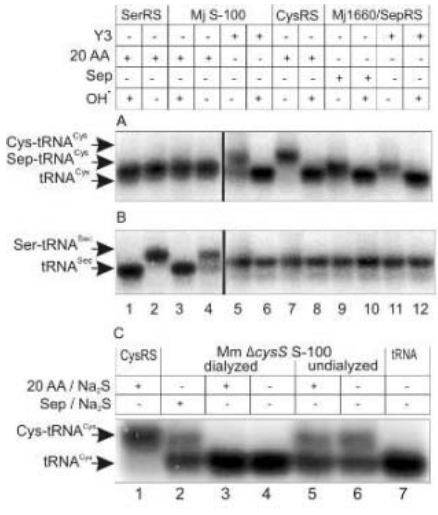

Fig. 1. Acid urea gel electrophoresis and Northern blot analysis of total *M. maripaludis* tRNA charged with *M. maripaludis* SerRS, dialyzed *M. jannaschii* S-100, *M. maripaludis* CysRS, and *M. jannaschii* SepRS in the presence of 20 amino acids (20 AA), phosphoserine, or a *M. jannaschii* S-100 cell-free extract filtrate (Y3). Half of each tRNA sample was deacylated by mild alkaline hydrolysis ($^-$OH). The blots were probed with ^{32}P-labeled oligonucleotides complementary to *M. maripaludis* tRNA^{Cys} (**A**) and *M. maripaludis* tRNA^{Sec} (**B**). Total *M. maripaludis* tRNA charged with dialyzed or undialyzed *M. maripaludis* Δ*cysS* S-100 cell-free extract (*20*) in the presence of 20 amino acids and Na_2S, or Sep and Na_2S (**C**). The blot was analyzed with ^{32}P-labeled oligonucleotides complementary to *M. maripaludis* tRNA^{Cys}.

[1]Department of Molecular Biophysics and Biochemistry, and [2]Department of Chemistry, Yale University, New Haven, CT 06520–8114, USA. [3]Department of Cell Biology, The Scripps Research Institute, La Jolla, CA 92037, USA. [4]Department of Microbiology, University of Georgia, Athens, GA 30602–2605, USA. [5]Department of Microbiology, The Ohio State University, Columbus, OH 43210–1292, USA. [6]Department of Microbiology, Technische Universität Braunschweig, D-38106 Braunschweig, Germany.

*To whom correspondence should be addressed. E-mail: soll@trna.chem.yale.edu

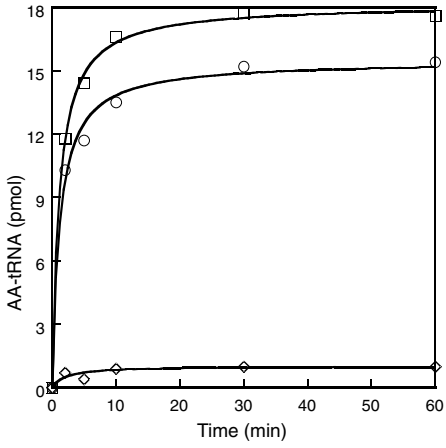

Fig. 2. Amino acid specificity of *M. jannaschii* SepRS. Aminoacylation by the recombinant *M. jannaschii* SepRS was tested with the filter binding assay (as described in SOM). *M. jannaschii* unfractionated tRNA charged with Sep (squares), total *M. maripaludis* tRNA and *M. jannaschii* SepRS incubated with Sep (circles), or with a 20–amino acid mixture (diamonds).

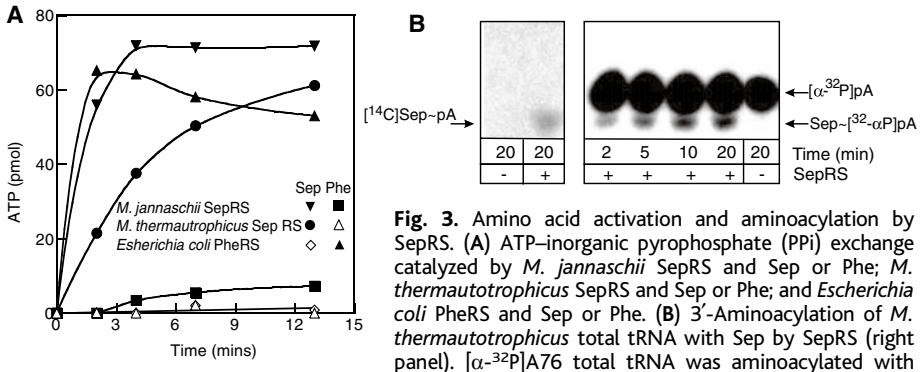

Fig. 3. Amino acid activation and aminoacylation by SepRS. (**A**) ATP–inorganic pyrophosphate (PPi) exchange catalyzed by *M. jannaschii* SepRS and Sep or Phe; *M. thermautotrophicus* SepRS and Sep or Phe; and *Escherichia coli* PheRS and Sep or Phe. (**B**) 3′-Aminoacylation of *M. thermautotrophicus* total tRNA with Sep by SepRS (right panel). [α-^{32}P]A76 total tRNA was aminoacylated with Sep by using SepRS (0.1 μM) and was subjected to RNase P1 digestion; the products were separated by thin-layer chromatography (TLC) and then visualized by phosphor imaging. Quantification of Sep~[α-^{32}P] indicated that about 3% of the total tRNA can be aminoacylated with Sep. The position of migration of Sep~pA was independently confirmed using [^{14}C]Sep (left).

100 fraction was dialyzed, all enzyme activity was lost and could not be recovered by addition of a mixture of the 20 canonical amino acids (Fig. 1A, lanes 3 and 4). These data established that tRNA^{Cys} charging took place in the S-100 extract but not as a result of direct acylation of cysteine to tRNA^{Cys} and not by a Ser-tRNA^{Cys}–dependent conversion mechanism (*10*). In contrast, the dialyzed S-100 extract supplemented with 20 amino acids formed Ser-tRNA^{Sec} (Fig. 1B, lanes 3 and 4), as did *M. maripaludis* seryl-tRNA synthetase (Fig. 1B, lanes 1 and 2). This result is consistent with a tRNA-dependent transformation of serine to selenocysteine (Sec) as seen in bacteria (*11*). On the basis of these results, we reasoned that the Cys-tRNA^{Cys}–forming activity consisted of one or more enzymes and some low-molecular-weight substrates that together participated in a tRNA-dependent amino acid biosynthesis pathway.

To identify the components of the Cys-tRNA^{Cys} biosynthetic pathway, the *M. jannaschii* S-100 extract was separated into two fractions: a low-molecular-mass "filtrate" (Y3) derived by a membrane filtration step (cutoff at 3 kD) and a protein fraction. Addition of Y3 to the dialyzed *M. jannaschii* S-100 restored activity (Fig. 1A, lanes 5 and 6). Both the protein and the filtrate fractions were purified individually by various chromatographic procedures; the activity was assayed by reconstitution of purified fractions from both sources [see supporting online material (SOM)]. Chromatographic analysis of the filtrate initially implicated *O*-phosphoserine (Sep) as one of the components in Y3 necessary for formation of Cys-tRNA^{Cys}. This was subsequently verified using the L-enantiomer of this amino acid (see SOM for details). Significant advancement in the protein purification strategy was derived from a proteomic analysis of various partially purified column chromatographic fractions (*12*). Repeated liquid chromatography (LC)–mass spectrometry (MS) analysis in the pattern LC-LC-MS-MS identified 20 proteins in the most active fractions, of which 13 were excluded because of their predicted functions or inconsistent phylogenetic distribution. Of the remaining seven proteins, two of the most abundant (Mj1660 and Mj1678) were consistently observed in genomes lacking *cysS*. Although Mj1660 is a paralog of the α subunit of phenylalanyl-tRNA synthetase (PheRS), it is inactive in Phe-tRNA formation (*13*). Mj1678 has been annotated as a putative pyridoxal phosphate–dependent enzyme. On the basis of its high homology to known class II aaRSs, we speculated that Cys-tRNA^{Cys} biosynthesis could be initiated by Mj1660 with Sep as one of the substrates. His$_6$-Mj1660, produced and purified heterologously from *Escherichia coli*, was found to stably attach Sep to tRNA^{Cys} in an efficient aerobic ATP-dependent reaction, which suggested that it could function as an aaRS (Fig. 1A, compare lanes 9 and 10 with lanes 11 and 12, and Fig. 2). However, tRNA^{Sec} was not a substrate for Mj1660 (Fig. 1B, lanes 9 to 12). Specificity for Sep was further supported by the observation that His$_6$-Mj1660 and its *M. thermautotrophicus* counterpart His$_6$-Mth1501 both catalyzed Sep-dependent and tRNA-independent ATP-[^{32}P]pyrophosphate exchange, a reaction characteristic of aaRSs (Fig. 3A) (*14*). No pyrophosphate exchange activity was detected with either His$_6$-Mj1660 or His$_6$-Mth1501 when Sep was replaced by phenylalanine. Sep was unable to stimulate ATP-[^{32}P]pyrophosphate exchange by *E. coli* PheRS, which indicated that it is a specific substrate for Mj1660-type proteins. Analysis of the position of aminoacylation by using *M. thermautotrophicus* total tRNA labeled with [^{32}P] in the terminal pA residue showed that Sep was attached to the 3′ terminus, the normal site for aminoacylation by aaRSs (Fig. 3B). A similar conclusion came from the protection against periodate oxidation of charged tRNA^{Cys} (*9*). In light of these various enzymatic activities and their specificities, we propose that Mj1660-type proteins are classified as aaRSs and are consequently renamed *O*-phosphoseryl-tRNA synthetase (SepRS, encoded by *sepS*). Like pyrrolysyl-tRNA synthetase (PylRS), which acylates a suppressor tRNA with pyrrolysine, SepRS belongs to an emerging set of synthetases that use modified amino acids but not their canonical counterparts (*15*, *16*). Amino acid sequence similarities indicate that both PylRS and SepRS are subclass IIc aaRSs most closely related to the canonical PheRS. The relative scarcity and narrow phylogenetic distributions of both PylRS and SepRS make it unclear whether these enzymes recently diverged from PheRS or, instead, coevolved with PheRS from a common ancestor.

Attachment of Sep to tRNA^{Cys} by SepRS is a chemically plausible first step in Cys-tRNA^{Cys} synthesis, as Sep-tRNA could feasibly be converted to Cys-tRNA in the presence of a synthase and the appropriate sulfur donor. Analogous pretranslational amino acid modifications have been described for the synthesis of asparaginyl-, formylmethionyl-, glutaminyl-, and selenocysteinyl-tRNAs (*17*). To investigate whether such a transformation accounts for Cys-tRNA^{Cys} formation, preformed Sep-tRNA^{Cys} was incubated with a dialyzed *M. jannaschii* S-100 extract in the presence of Na_2S. Electrophoretic analysis of the resulting aa-tRNA indicated formation of a product whose mobility was consistent with Cys-tRNA^{Cys} (Fig. 4A). On the basis of the above proteomic analysis, we postulated that Mj1678 encoded the enzymatic component responsible for converting Sep-tRNA^{Cys} to Cys-tRNA^{Cys}. His$_6$-Mj1678, produced heterologously in *E. coli*, was found to efficiently convert preformed Sep-tRNA^{Cys} into Cys-tRNA^{Cys} in an anaerobic reaction in the presence of pyridoxal phosphate (PLP) and Na_2S (Fig. 4B,

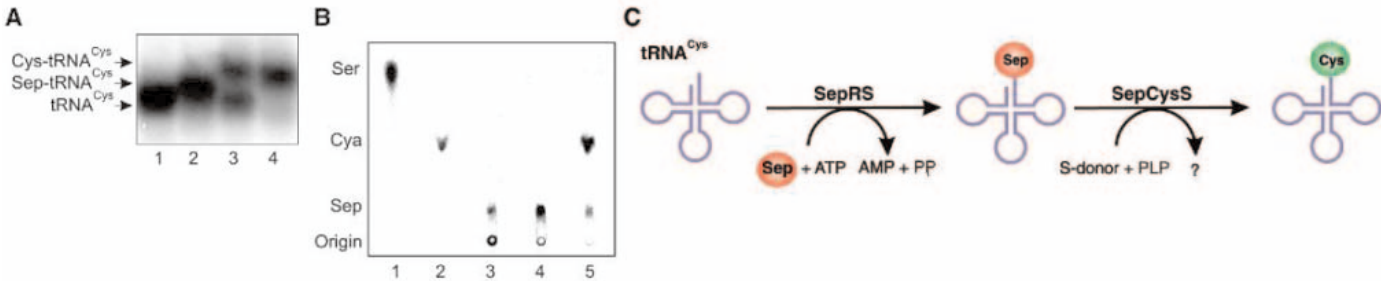

Fig. 4. Conversion of in vitro synthesized Sep-tRNA^{Cys} to Cys-tRNA^{Cys}. (**A**) Aminoacylation of tRNA^{Cys} monitored by acid urea gel electrophoresis and Northern blotting. Lane 1, total *M. maripaludis* tRNA; lane 2, tRNA^{Cys} charged with Sep by recombinant *M. jannaschii* SepRS; lane 3, Sep-tRNA^{Cys} incubated with dialyzed *M. jannaschii* cell-free S-100 extract in the presence of dithiothreitol (DTT) and Na_2S; lane 4, tRNA^{Cys} charged with cysteine by *M. maripaludis* CysRS. (**B**) Phosphorimages of TLC separation of [^{14}C]Sep and [^{14}C]Cys recovered from the aa-tRNAs of the SepCysS activity assay (see SOM). Cysteine was analyzed in its oxidized form as cysteic acid (Cya). Lane 1, Ser marker; lane 2, cysteine from Cys-tRNA^{Cys} generated with *M. maripaludis* CysRS; lane 3, Sep from Sep-tRNA^{Cys} made with *M. jannaschii* SepRS; lane 4, Sep-tRNA^{Cys} incubated with *E. coli* S-100 cell-free extract in the presence of DTT and Na_2S (see SepCysS assay in SOM); lane 5, Sep-tRNA^{Cys} converted to Cys-tRNA^{Cys} with recombinant MJ1678 protein in the presence of DTT and Na_2S (see SepCysS assay in SOM). (**C**) Scheme of Cys-tRNA^{Cys} formation in methanogenic archaea.

lane 5). The natural sulfur donor of the reaction remains uncharacterized. On the basis of the conversion activity, we suggest that Mj1678 is a Sep-tRNA:Cys-tRNA synthase (SepCysS; encoded by *pscS*). SepRS and SepCysS, both of which are encoded in all archaea lacking *cysS*, together provide a facile two-step pathway for the synthesis of Cys-tRNA^{Cys} by means of Sep-tRNA^{Cys} (Fig. 4C). This route is consistent with the earlier observation that Sep is a precursor of cysteine in *M. jannaschii* (*18*). As in other organisms (*19*), the proposed route of Sep formation involves D-3-phosphoglycerate dehydrogenase (MJ1018) and an as yet unidentified phosphoserine aminotransferase.

From available genome sequences, the organismal distributions of SepRS and SepCysS are apparently coupled. To date, *sepS* and *pscS* have only been detected in the genomes of the methanogenic archaea *M. jannaschii*, *M. maripaludis*, *M. thermautotrophicus*, *M. kandleri*, *Methanococcoides burtonii*, the *Methanosarcinaceae*, and in *Archaeoglobus fulgidus*. Although some of these organisms lack *cysS*, others, such as *M. maripaludis*, also encode a canonical CysRS and thus contain two potentially functional pathways for Cys-tRNA^{Cys} synthesis (*20*). Comparable redundancy is seen for Asn-tRNA^{Asn} synthesis in many bacteria, where the tRNA-dependent route is the sole pathway for asparagine biosynthesis (*21*). Present knowledge of the genes required for archaeal amino acid biosynthesis suggests that the SepRS/SepCysS pathway may provide the only means for de novo production of cysteine in a number of organisms (e.g., *M. jannaschii, M. maripaludis*), whereas other organisms (e.g., *Methanosarcinaceae*) have both tRNA-dependent and tRNA-independent routes to cysteine. In contrast, most nonmethanogenic archaea with known genomes (e.g., *Aeropyrum, Sulfolobus, Pyrococcus, Pyrobaculum, Thermoplasma, Picrophilus*, *Halobacteria*) encode *O*-acetylserine sulfhydrylase (*22*) or cysteine synthase, which suggests that cysteine biosynthesis is tRNA-independent in these organisms.

To investigate whether the SepRS/SepCysS pathway can act as the sole route for cysteine biosynthesis we used *M. maripaludis*, which has a facile genetic system. This organism has both a dispensable CysRS (*20*) and the *sepS* and *pscS* genes but no known pathway for de novo biosynthesis of free cysteine. Biochemical evidence of a functional SepRS/SepCysS pathway in *M. maripaludis* extracts is presented in Fig. 1C. In dialyzed extracts of a *cysS* deletion mutant, Cys-tRNA^{Cys} biosynthesis is dependent on the addition of Sep and Na_2S (Fig. 1C, lane 2). To test if the SepRS/SepCysS pathway is necessary for cysteine biosynthesis, the *sepS* gene was deleted from the chromosome of the wild type of *M. maripaludis*. The resulting *ΔsepS* strain was a cysteine auxotroph (Fig. 5). Although it grew at a rate comparable to that of wild type on complete medium, it was unable to grow in the absence of exogenous cysteine. These findings indicate that under certain conditions the SepRS/SepCysS pathway can provide the sole source of cysteine for the cell via Cys-tRNA^{Cys}. Reliance on such a route clearly satisfies the requirements for cysteine during protein synthesis, but how cysteine is made available for other metabolic processes is less clear. One possibility is that hydrolysis of Cys-tRNA^{Cys} directly provides free cysteine, as previously proposed for free Asn synthesis via Asn-tRNA^{Asn} in certain bacteria (*21*). In addition, protein turnover in the cell would be expected to contribute more significantly to the cellular cysteine pool when CysRS is absent, as the free amino acid is not itself a substrate for protein synthesis in such cases. Finally, most of the organisms harboring the SepRS/SepCysS pathway are methanogens, which, even in the absence of glutathione, may not require a large pool of free cysteine for redox buffering in the cytoplasm. Methanogens contain high levels of the essential coenzyme 2-mercaptoethanesulfonate (*23*), which may

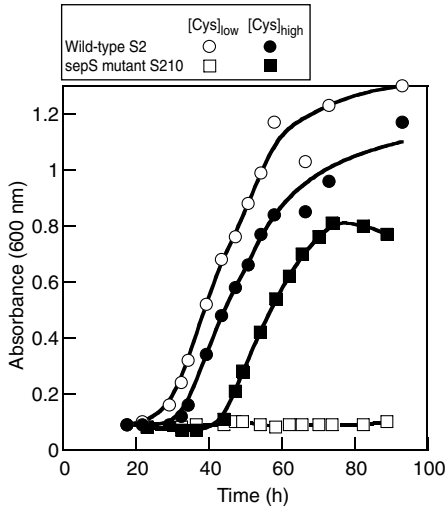

Fig. 5. Growth response of the *ΔsepS* mutant and wild-type *M. maripaludis* strain S2 to the presence and absence of cysteine in mineral media containing acetate. About 2 × 10^3 cells were inoculated into prewarmed McAV medium containing 3 mM coenzyme M for a final cysteine concentration of <0.16 μM ([Cys]$_{low}$) or into the same medium with 3 mM cysteine ([Cys]$_{high}$). Wild-type S2 (circles), and *sepS* mutant S210 (squares).

fulfill the redox buffering function of free cysteine. For thermophilic organisms, replacement of the heat-labile cysteine with the thermostable 2-mercaptoethanesulfonate may be an additional benefit.

The discovery of the SepRS/SepCysS pathway raises the question as to whether this mechanism predates direct charging by CysRS and tRNA-independent cysteine biosynthesis. Similar scenarios have been suggested for Asn-tRNA and Gln-tRNA biosynthesis, where the tRNA-dependent pathways have been proposed as the original routes for synthesis of both the aa-tRNAs and the corresponding amino acids (*24–26*). If SepRS/SepCysS was indeed the ancestral pathway for cysteine synthesis via Cys-tRNA, a lack of alternative cysteine bio-

synthetic capacity may explain why certain organisms have retained this route. This would be consistent with earlier proposals that CysRS (*27*, *28*) and cysteine itself (*22*, *29*, *30*) were the last—or very late—canonical additions to the genetic code. The recent demonstration in mammalian cells (*31*) of the Ser-tRNA^{Sec} to Sep-tRNA^{Sec} conversion by a special kinase [present also in archaea (*31*)] implicates the Sep moiety as an intermediate in Sec synthesis. As the conversions of Sep-tRNA to Cys-tRNA or Sec-tRNA are chemically analogous (using suitable sulfur or selenium donors, respectively), the addition of selenocysteine to the genetic code may have been patterned on an accepted route for cysteine formation, the SepRS/SepCysS pathway.

Note added in proof: A recently published bioinformatics analysis has suggested that Mj1660 is a class II CysRS (*32*).

References and Notes

1. T. Li *et al.*, *FEBS Lett.* **462**, 302 (1999).
2. B. Ruan *et al.*, *J. Bacteriol.* **186**, 8 (2004).
3. A. Ambrogelly *et al.*, *Cell. Mol. Life Sci.* **61**, 2437 (2004).
4. C. Stathopoulos *et al.*, *Science* **287**, 479 (2000).
5. R. S. Lipman, K. R. Sowers, Y. M. Hou, *Biochemistry* **39**, 7792 (2000).
6. C. M. Zhang, Y. M. Hou, *RNA Biol.* **1**, 35 (2004).
7. C. Fabrega *et al.*, *Nature* **411**, 110 (2001).
8. U. Varshney, C. P. Lee, U. L. RajBhandary, *J. Biol. Chem.* **266**, 24712 (1991).
9. A. Sauerwald, unpublished observations.
10. H. S. Kim, U. C. Vothknecht, R. Hedderich, I. Celic, D. Söll, *J. Bacteriol.* **180**, 6446 (1998).
11. A. Böck, M. Thanbichler, M. Rother, A. Resch, in *Aminoacyl-tRNA Synthetases*, M. Ibba, C. S. Francklyn, S. Cusack, Eds. (Landes Bioscience, 2004), pp. 320–327.
12. C. S. Giometti *et al.*, *J. Chromatogr. B Anal. Technol. Biomed. Life Sci.* **782**, 227 (2002).
13. R. Das, U. C. Vothknecht, *Biochimie* **81**, 1037 (1999).
14. R. Calendar, P. Berg, *Prog. Nucl. Acid Res. Mol. Biol.* **1**, 375 (1966).
15. C. Polycarpo *et al.*, *Proc. Natl. Acad. Sci. U.S.A.* **101**, 12450 (2004).
16. S. K. Blight *et al.*, *Nature* **431**, 333 (2004).
17. M. Ibba, H. D. Becker, C. Stathopoulos, D. L. Tumbula, D. Söll, *Trends Biochem. Sci.* **25**, 311 (2000).
18. R. H. White, *Biochim. Biophys. Acta* **1624**, 46 (2003).
19. M.-J. Basurko *et al.*, *IUBMB Life* **48**, 525 (1999).
20. C. Stathopoulos *et al.*, *Proc. Natl. Acad. Sci. U.S.A.* **98**, 14292 (2001).
21. B. Min, J. T. Pelaschier, D. E. Graham, D. Tumbula-Hansen, D. Söll, *Proc. Natl. Acad. Sci. U.S.A.* **99**, 2678 (2002).
22. K. Mino, K. Ishikawa, *FEBS Lett.* **551**, 133 (2003).
23. W. E. Balch, R. S. Wolfe, *J. Bacteriol.* **137**, 264 (1979).
24. J. T. Wong, *Proc. Natl. Acad. Sci. U.S.A.* **72**, 1909 (1975).
25. D. C. Jeffares, A. M. Poole, D. Penny, *J. Mol. Evol.* **46**, 18 (1998).
26. M. Di Giulio, *J. Mol. Evol.* **55**, 616 (2002).
27. J. Avalos, L. M. Corrochano, S. Brenner, *FEBS Lett.* **286**, 176 (1991).
28. K. Farahi, G. D. Pusch, R. Overbeek, W. B. Whitman, *J. Mol. Evol.* **58**, 615 (2004).
29. M. Di Giulio, M. Medugno, *J. Mol. Evol.* **49**, 1 (1999).
30. D. J. Brooks, J. R. Fresco, *Mol. Cell. Proteomics* **1**, 125 (2002).
31. B. A. Carlson *et al.*, *Proc. Natl. Acad. Sci. U.S.A.* **101**, 12848 (2004).
32. A. Sethi, P. O'Donoghue, Z. Luthey-Schulten, *Proc. Natl. Acad. Sci. U.S.A.* **102**, 4045 (2005).

33. We thank D. Graham, M. Hohn, D. Huynh, S. Kochhar, L. Regan, J. Rinehart, J. Sabina, J. Salazar, S. Schauer, K. O. Stetter, and M. Thomm for providing advice, materials, and access to resources. This work was supported by grants from the National Institute of General Medical Sciences (M.I., D.S., and J.R.Y.), the Department of Energy (D.S. and W.B.W.), the Deutsche Forschungsgemeinschaft (D.J.), and the Fonds der Chemischen Industrie (D.J.).

Supporting Online Material

www.sciencemag.org/cgi/content/full/307/5717/1969/DC1
Materials and Methods
Figs. S1
References and Notes

6 December 2004; accepted 25 January 2005
10.1126/science.1108329

Structural Insights into the Activity of Enhancer-Binding Proteins

Mathieu Rappas,[1,2] Jorg Schumacher,[1] Fabienne Beuron,[1,2] Hajime Niwa,[1,2] Patricia Bordes,[1] Sivaramesh Wigneshweraraj,[1] Catherine A. Keetch,[3] Carol V. Robinson,[3] Martin Buck,[1] Xiaodong Zhang[1,2]*

Activators of bacterial σ^{54}–RNA polymerase holoenzyme are mechanochemical proteins that use adenosine triphosphate (ATP) hydrolysis to activate transcription. We have determined by cryogenic electron microscopy (cryo-EM) a 20 angstrom resolution structure of an activator, phage shock protein F [$PspF_{(1-275)}$], which is bound to an ATP transition state analog in complex with its basal factor, σ^{54}. By fitting the crystal structure of $PspF_{(1-275)}$ at 1.75 angstroms into the EM map, we identified two loops involved in binding σ^{54}. Comparing enhancer-binding structures in different nucleotide states and mutational analysis led us to propose nucleotide-dependent conformational changes that free the loops for association with σ^{54}.

Gene expression is regulated at the level of RNA polymerase (RNAP) activity. Bacterial RNAP containing the σ^{54} factor requires specialized activator proteins, referred to as bacterial enhancer-binding proteins (EBPs), that interact with the basal transcription complex from remote DNA sites by DNA looping (*1*–*4*). EBPs bind upstream activating sequences via their C-terminal DNA binding domains and form higher order oligomers that use adenosine triphosphate (ATP) hydrolysis to activate transcription (*5*, *6*). The central σ^{54}-RNAP–interacting domain of EBPs is responsible for adenosine triphosphatase (ATPase) activity and transcription activation (*7*–*9*) and belongs to the larger AAA+ (ATPase associated with various cellular activities) family of proteins (*10*–*12*). Well-studied EBPs include phage shock protein F (PspF), nitrogen-fixation protein A (NifA), nitrogen-regulation protein C (NtrC), and C_4-dicarboxylic acid transport protein D (DctD) (*1*–*3*, *7*, *13*).

PspF from *Escherichia coli* forms a stable oligomeric complex with σ^{54} at the point of ATP hydrolysis (*14*). PspF-ADP.AlF$_x$ (a complex of adenosine diphosphate and aluminum fluoride, where x is the number of fluorine atoms equal to 3 or 4) alters the interaction between σ^{54} and promoter DNA similarly to PspF hydrolyzing ATP (*15*) and was thus deemed a functional hydrolysis intermediate. Activator nucleotide hydrolysis–dependent events couple the chemical energy of hydrolysis to transcriptional activation. The highly conserved and EBP-specific GAFTGA amino acid motif (fig. S1) (*16*) is a crucial mechanical determinant for the successful transfer of energy from ATP hydrolysis in EBPs to the RNAP holoenzyme via the small N-terminal EBP-interacting domain of σ^{54} (called region I, ~56 residues and sufficient for PspF interaction) (*1*, *14*, *17*–*19*).

The lack of structural information has hindered progress toward understanding the basis of this energy transfer process required for transcriptional activation. We now present a structure-function analysis of one such system using the following: (i) a cryo-EM reconstruction of PspF's AAA+ domain [residues 1 to 275, $PspF_{(1-275)}$] in complex with σ^{54} at the point of ATP hydrolysis (mimicked by in situ–formed ADP.AlF$_x$), (ii) the crystal structure of nucleotide-free (apo) $PspF_{(1-275)}$ at 1.75 Å resolution, and (iii) mutational analysis.

Nanoelectrospray mass spectroscopy of a $PspF_{(1-275)}$–σ^{54} complex with ADP.AlF$_x$ established that six monomers of $PspF_{(1-275)}$ are in complex with a monomeric σ^{54}, consistent with AAA+ proteins functioning as hexamers (*10*, *12*). The three-dimensional (3D) recon-

[1]Department of Biological Sciences, [2]Centre for Structural Biology, Imperial College London, London, SW7 2AZ, UK. [3]Department of Chemistry, Cambridge University, Lensfield Road, Cambridge, CB2 1EW, UK.

*To whom correspondence should be addressed. E-mail: xiaodong.zhang@imperial.ac.uk

struction of the $PspF_{(1-275)}$–ADP.AlF_x–σ^{54} complex (~240 kD) obtained by cryo-EM of native samples (figs. S3 and S4) shows a $PspF_{(1-275)}$ hexamer interacting with one σ^{54}. Class averages show well-defined ringlike structures displaying six subunits of $PspF_{(1-275)}$ within a simple ring and clear extra density for σ^{54} located ~15 Å above the ring (Fig. 1, A to C). The clear hexagonal ring structure has a diameter of ~125 Å and a central pore of ~20 Å; from the side, the ring is ~40 Å in height (Fig. 1C and fig. S5B). These dimensions are consistent with other hexameric AAA+ proteins (*20*, *21*).

Viewed from the side, the hexamer appears concave, with a central depression that readily accommodates the σ^{54} density. A 90° rotation along the sixfold axis reveals that the σ^{54} density, which runs along the ring, is elongated, bent, and thicker in the middle (fig. S5A). This "horseshoe"-shaped extra density resembles the envelope model of σ^{54} (*22*). The estimated mass of σ^{54} is ~30 kD, which is much higher than the 6-kD region I and less than the 54-kD σ^{54}. Therefore, we postulate that although we see more than just region I, which is sufficient for PspF binding, there are parts of σ^{54} that are not visualized in our reconstruction because they are mobile (*23*).

To confirm the presence and integrity of σ^{54} in the particles, we marked N- and C-termini of σ^{54} using nanogold beads. Single-cysteine σ^{54} constructs [$^{46C}\sigma^{54}$ and $^{474C}\sigma^{54}$ (*24*)] were covalently linked to nanogold beads before forming the $PspF_{(1-275)}$–ADP.AlF_x–σ^{54} complex. The negative stained samples were then analyzed with EM. Detection of nanogold beads in both experiments confirmed the presence and the integrity of σ^{54} in the complex (Fig. 1D).

When displayed at lower contour levels, the 3D electron density map shows weak densities connecting the $PspF_{(1-275)}$ ring to σ^{54} (Fig. 1C, arrow). Based on earlier biochemical results (*14*, *18*), we postulate that the connecting densities, found almost at right angles to the $PspF_{(1-275)}$ ring (Fig. 1C), mark the location of certain GAFTGA motifs within the $PspF_{(1-275)}$ hexamer in stable association with region I of σ^{54}.

To facilitate localizing PspF, we determined the crystal structure of apo $PspF_{(1-275)}$ in space group $P6_5$ at 1.75 Å resolution using multiwavelength anomalous dispersion (MAD) phasing (table S1) (*25*). The structure displays a typical AAA+ protein organization, consisting of an α/β Rossmann fold followed by an α-helical domain (Fig. 2). The GAFTGA motif forms the tip of a loop (L1) inserted into helix 3 of the α/β domain. Another loop (L2), consisting of residues 130 to 139, is inserted between helix 4 and strand 4 (Fig. 2). The extremities of both loops (L1 and L2) show high degrees of flexibility, with the tip of L1 being the most flexible, and no electron

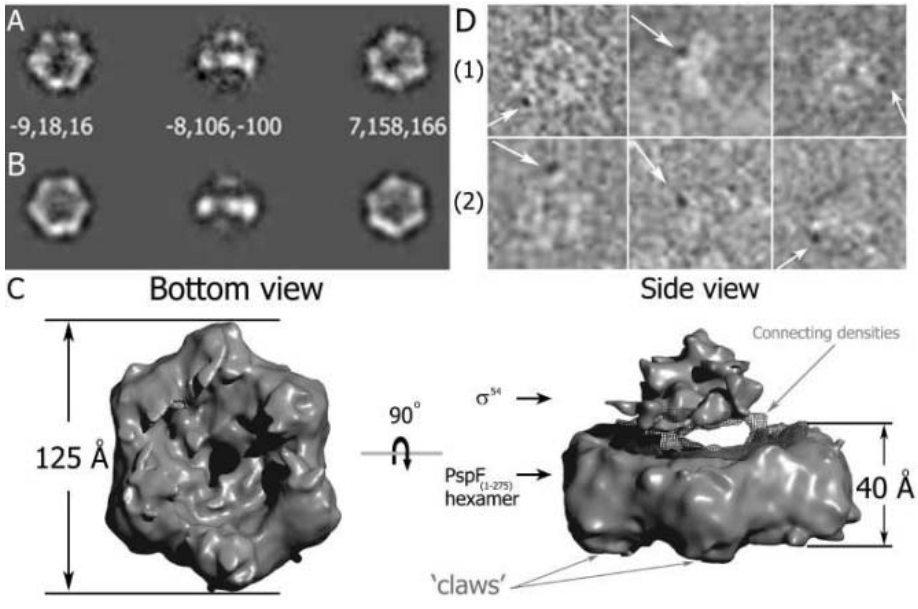

Fig. 1. EM analysis of the $PspF_{(1-275)}$–ADP.AlF_x–σ^{54} complex. (**A**) Three of the 123 final class averages used to generate the 3D cryo-EM reconstruction, together with their assigned Euler angles (in white, Euler angles α, β, and γ). (**B**) Respective reprojections of the 3D model. (**C**) Surface renderings of the final 3D cryo-EM map of the complex; bottom and side views of the complex are displayed. Also shown as mesh is the EM map displayed at a lower threshold to highlight the ring to σ^{54} connecting densities. (**D**) Part 1 shows the negative stain of the $PspF_{(1-275)}$–ADP.AlF_x–$^{46C}\sigma^{54}$ nanogold-labeled complex; arrows indicate the nanogold bead. Part 2 shows the negative stain of the $PspF_{(1-275)}$–ADP.AlF_x–$^{474C}\sigma^{54}$ nanogold-labeled complex.

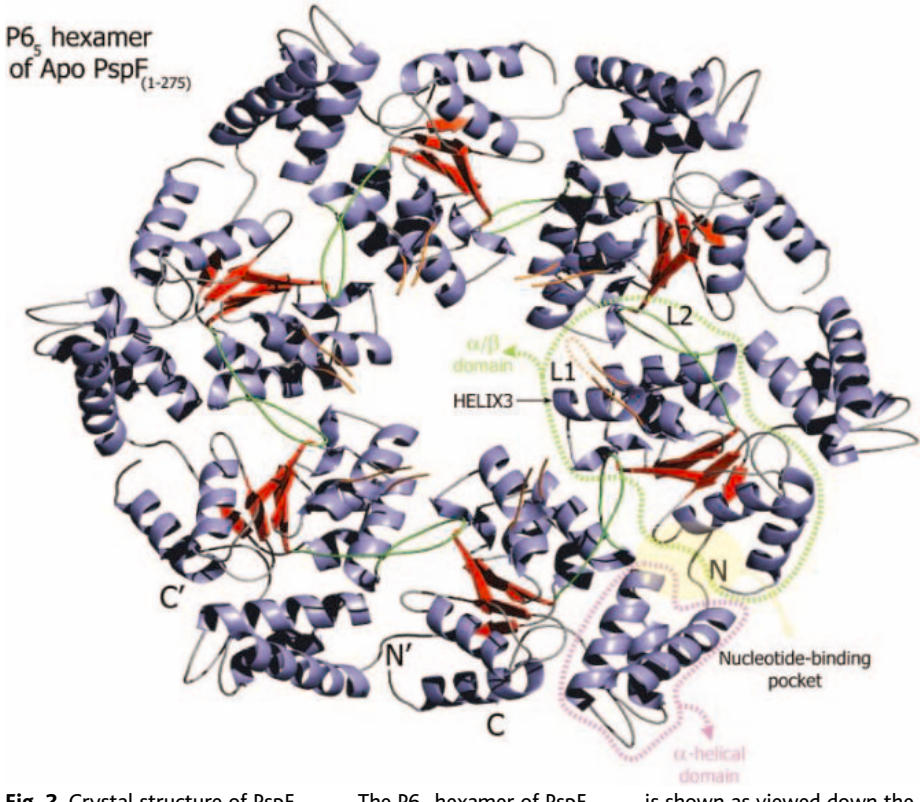

Fig. 2. Crystal structure of $PspF_{(1-275)}$. The $P6_5$ hexamer of $PspF_{(1-275)}$ is shown as viewed down the sixfold axis. Both α/β (green) and α-helical domains (pink) of one monomer are contoured with dashed lines. The nucleotide-binding pocket is highlighted in yellow and is located in the cleft between the α/β and α-helical domain at the interface with the adjacent monomer. N- and C-termini of two adjacent monomers are also shown. Color coding is as follows: blue, helices; red, central β sheet; orange, L1; and green, L2. The tip of the highlighted L1 is shown as a dotted line because residues 82 to 89 were not resolved in our crystal structure.

density was observed for this region (residues 82 to 89).

Initially, a monomer of $PspF_{(1-275)}$ was visually fitted into the EM map as a rigid body, so that the α-helical domain sat in a "claw" of the ring (Fig. 3A). This fitting positioned the L1 and L2 loops in close proximity to one of the weak connecting densities contacting σ^{54} (Fig. 3, A and B). From the fitted model, we generated a hexamer and then visually readjusted individual subunits to better fit the EM map. L1 and L2 loops were either adjusted to fit the connecting densities or removed when no EM density was observed to account for them (fig. S6, A and B) (*25*). It appears that at least two adjacent $PspF_{(1-275)}$ monomers contact one σ^{54} at the point of ATP hydrolysis. We infer that at the point of ATP hydrolysis, certain L1 and L2 loops extend upward to maintain a stable interaction of PspF with σ^{54}. When successfully engaged with σ^{54}, L1 and L2 are more structured.

To investigate the link between the nucleotide-bound state and the location of the GAFTGA-containing L1, we compared the apo PspF structure with the structures of different forms of *Aquifex aeolicus* NtrC1 (Protein Data Bank codes 1NY5 and 1NY6), which has 47% sequence similarity to PspF in its AAA+ domain, including an ADP-bound state thought to be incompetent for stable σ^{54} interaction (*3*). Our apo $PspF_{(1-275)}$ crystal structure and that of ATP-soaked crystals (data not shown) are similar, suggesting that the apostructure presented here is close to the ATP bound form, which is σ^{54}-interaction competent (*15*). Aligning on the conserved P loops resulted in overall good alignment (Fig. 4A), with differences in the relative orientation of the α-helical domain to the α/β domain as well as the position of helices 3 and 4, suggesting a nucleotide-dependent change in domain relationships (*12*, *26*).

Closer examination reveals important differences in the properties and positions of L1 and L2 (Fig. 4, A to C). In NtrC1 (1NY6), the branch part of L1 is at a right angle to the stem part and points into the central pore of the ring, with a twisted L2 lying in close proximity (Fig. 4B) (*13*). Discrete interactions stabilize the branch part of L1 in NtrC1, notably the interactions between E212 in L1 (equivalent to E81 in PspF) and R262 (R131) and K267 (Q136) in L2 (*16*). Also, L263 (V132) of the tip of L2, F216 (F85) of the L1 tip, and A206 [the β carbon atom (C_β) of S75] of helix 3 form a hydrophobic cluster that locks the GAFTGA motif in a buried and unfavorable conformation for stable σ^{54} interaction (Fig. 4B and fig. S1). Based on our EM map, in this conformation the GAFTGA motif cannot stably contact σ^{54}.

In $PspF_{(1-275)}$, the relative rotation of helices 3 and 4 disrupts the hydrophobic interactions between F85 of L1, V132 of L2, and C_β of S75 of helix 3, whereas interactions between the stem part of L1 and helix 3 (i.e., between H80 and S75, and H92 and E76) are strengthened (Fig. 4C). We hypothesize that these changes in interactions are nucleotide dependent. Indeed, these interactions form part of a larger network that involves residues R95 and R98 of helix 3, and S62 of the central β sheet, which includes the Walker B motif (D107 and E108) and is responsible for nucleotide hydrolysis (Fig. 4C). This interaction network is well suited to relay nucleotide-dependent movements of the central β sheet, which originate in the Walker B motif, to helix 3 and more importantly to L1, with its GAFTGA motif. A similar network in NtrC1 appears to be based mostly on hydrophobic interactions

To investigate the functionality of the interaction network believed to ultimately control the GAFTGA-containing L1, we conducted structure-based single amino acid mutational analyses. Disruption of the proposed network linking the ATP active site to the GAFTGA loop is predicted to cause a decrease in nucleotide-dependent activities of $PspF_{(1-275)}$. To examine this hypothesis, we mutated H92, which interacts with E76 of

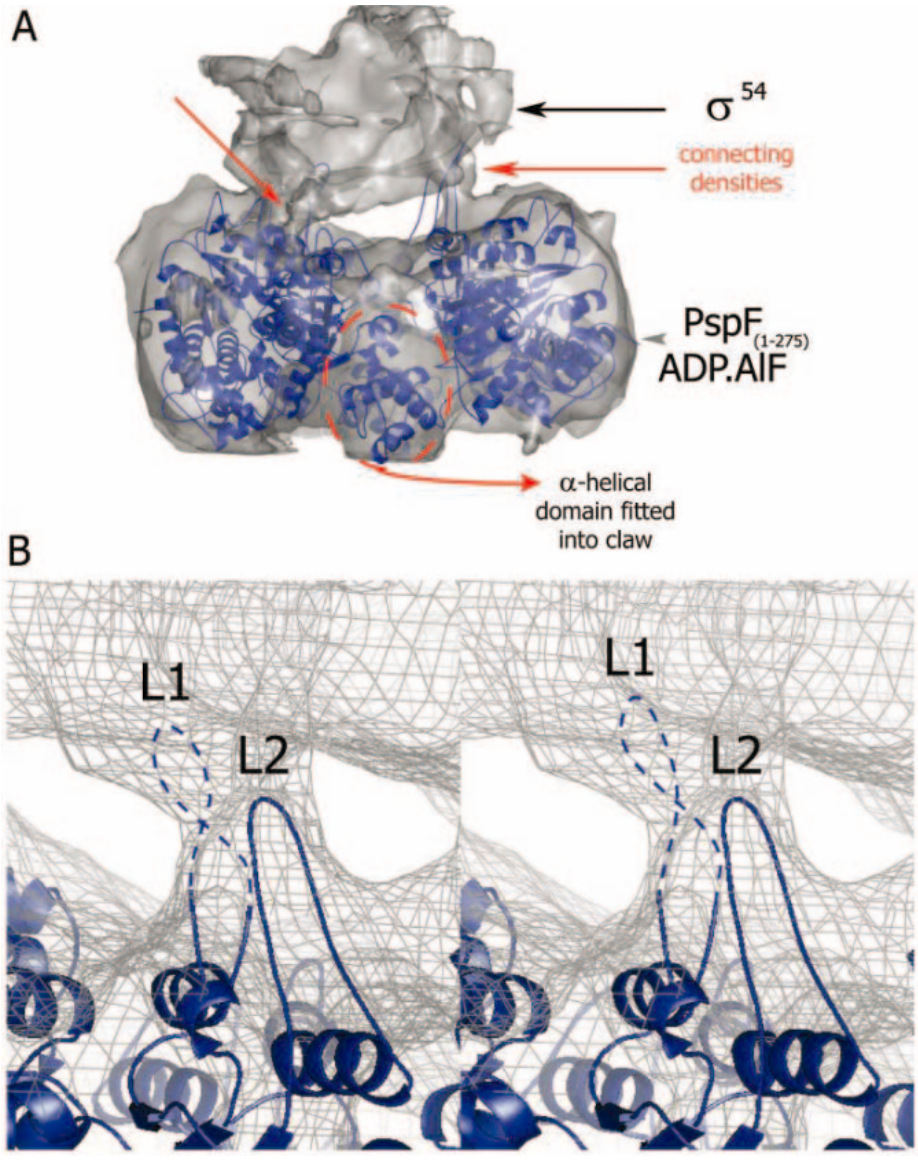

Fig. 3. Fitting of the $PspF_{(1-275)}$ crystal structure into the EM electron density map of the $PspF_{(1-275)}$–$ADP.AlF_x$–σ^{54} complex. (**A**) The front view of the EM density is colored transparent gray and the $PspF_{(1-275)}$ crystal structure has a blue ribbon representation. The fitting of the α-helical domain into one "claw" of the hexameric ring is highlighted; the densities connecting $PspF_{(1-275)}$ to σ^{54} are indicated by red arrows. (**B**) Cross-eye stereo view of the fitting of one pair of L1 and L2 loops into the connecting densities; the tip of L1 is shown as a dotted line because residues 82 to 89 are not resolved. When positioned in the densities, the loops extend upward almost at a right angle to the plane of the hexamer.

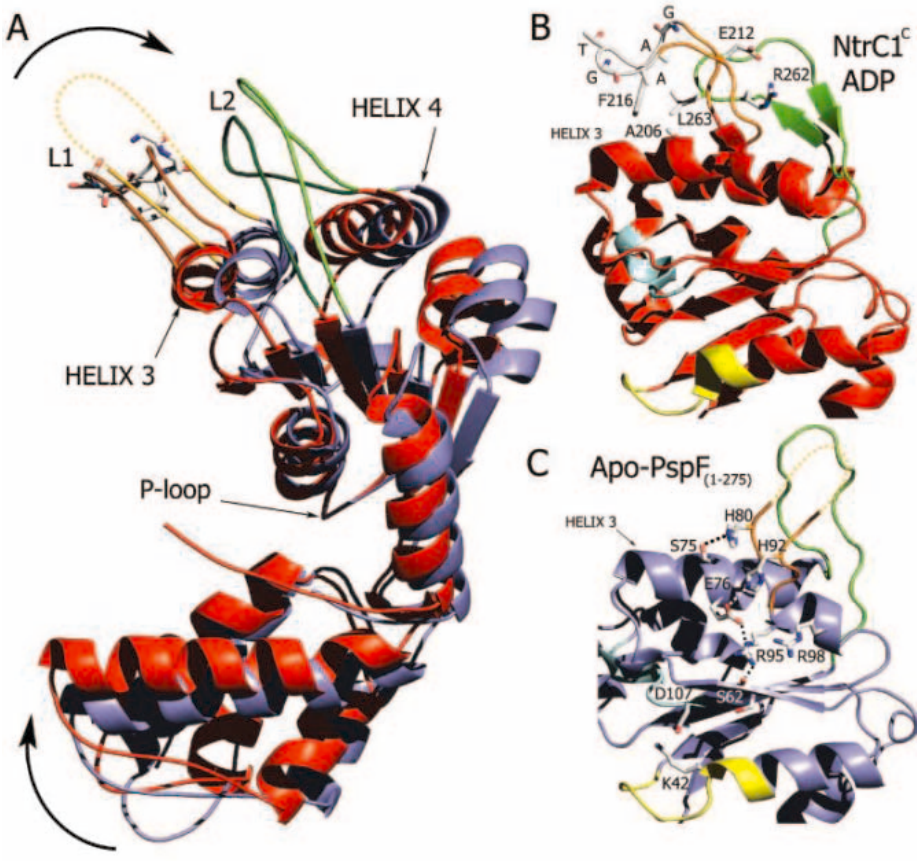

Fig. 4. Nucleotide-dependent relocation of L1 and L2 loops. (**A**) Ribbon representation of the P loop–superimposed AAA+ structures of NtrC1 (red) and $PspF_{(1-275)}$ (blue). L1 loop structures are in orange, with a darker shade for NtrC1 L1 and the tip of $PspF_{(1-275)}$'s L1 as a dotted line. L2 loop structures are in green, with a darker shade for NtrC1. The NtrC1 L1-GAFTGA motif is shown as sticks. Apparent relocations of the α-helical domain and helices 3 and 4 are highlighted by arrows. (**B**) Close-up of the α/β domain of NtrC1. Color coding is as follows: yellow, Walker A; cyan, Walker B; orange, L1; and green, L2. The L1-GAFTGA motif, A206, and L263 are shown as sticks. Also shown as sticks are E212 and R262 to highlight their role in coordinating L1 and L2. (**C**) Close-up of the α/β domain of $PspF_{(1-275)}$ using the same color coding as in (B). Residues shown as sticks are part of the Walker B motif–to–L1 network. Also shown as sticks is the catalytic K42 residue of the Walker A motif. The L1-GAFTGA motif is shown as a dotted line.

helix 3 (Fig. 4C), either into F, to mimic the overall geometry while eliminating the charge effects, or into R, to maintain the overall charge (R is also the most frequent residue in this position in EBPs) (fig. S1). R95, on the other hand, which interacts with both E76 and S62 of the central β sheet, was mutated into either A or the more related K. $PspF_{(1-275)}^{R95A}$ and $PspF_{(1-275)}^{H92F}$ each fail in all measurable post–ATP binding activities (fig. S1 and table S2) (*27*). In both cases, the mutations severely disrupt the network of interactions and thus block any communication of the conformational signal beyond the mutated residues. In contrast, $PspF_{(1-275)}^{R95K}$ and $PspF_{(1-275)}^{H92R}$ retained most of the in vitro activities measured, including transcriptional activation (table S2). The Walker B–to–L1 network is consistent with properties of many mutant forms of DctD and NtrC (*28*, *29*), supporting the existence of a common EBP nucleotide-dependent communication pathway.

To determine the functionality of the hydrophobic interactions that lock the tip of L1 in the NtrC1 structure, we mutated F85 and V132. $PspF_{(1-275)}^{V132A}$ retained its nucleotide-binding activity but lacked ATPase activity. $PspF_{(1-275)}^{F85A}$ likewise lacked ATPase activity, but $PspF_{(1-275)}^{F85L}$ and $PspF_{(1-275)}^{F85W}$ showed ATP binding and some ATPase activity, with mutation to W leading to an increase in ATPase activity (table S2). These results suggest that the stability of the L1-L2 hydrophobic interaction has direct effects on the ATP hydrolysis cycle. $PspF_{(1-275)}^{V132A}$ can engage σ^{54} in an ADP.AlF_x-dependent manner, suggesting an effect on the release of γ-phosphate (table S2). Disrupting this interaction would impair this stage of the ATPase cycle, whereas strengthening it [e.g., $PspF_{(1-275)}^{F85W}$] would increase ATPase activity. $PspF_{(1-275)}^{F85W}$ fails to stably bind σ^{54}, demonstrating that the integrity of the GAFTGA motif is crucial for σ^{54} interaction (*15*, *18*). The proposed communication pathway in PspF links changes in the ATP hydrolysis site to conformational changes in the GAFTGA-containing L1 loop that remodel the σ^{54}-RNAP holoenzyme to activate transcription.

References and Notes

1. I. Rombel, A. North, I. Hwang, C. Wyman, S. Kustu, *Cold Spring Harbor Symp. Quant. Biol.* **63**, 157 (1998).
2. M. Buck, M. T. Gallegos, D. J. Studholme, Y. Guo, J. D. Gralla, *J. Bacteriol.* **182**, 4129 (2000).
3. X. Zhang *et al.*, *Mol. Microbiol.* **45**, 895 (2002).
4. A. Wedel, S. Kustu, *Genes Dev.* **9**, 2042 (1995).
5. D. L. Popham, D. Szeto, J. Keener, S. Kustu, *Science* **243**, 629 (1989).
6. W. V. Cannon, M. T. Gallegos, M. Buck, *Nat. Struct. Biol.* **7**, 594 (2000).
7. H. Xu, T. R. Hoover, *Curr. Opin. Microbiol.* **4**, 138 (2001).
8. E. Morett, L. Segovia, *J. Bacteriol.* **175**, 6067 (1993).
9. D. J. Studholme, R. Dixon, *J. Bacteriol.* **185**, 1757 (2003).
10. A. N. Lupas, J. Martin, *Curr. Opin. Struct. Biol.* **12**, 746 (2002).
11. A. F. Neuwald, L. Aravind, J. L. Spouge, E. V. Koonin, *Genome Res.* **9**, 27 (1999).
12. T. Ogura, A. J. Wilkinson, *Genes Cells* **6**, 575 (2001).
13. S. Y. Lee *et al.*, *Genes Dev.* **17**, 2552 (2003).
14. M. Chaney *et al.*, *Genes Dev.* **15**, 2282 (2001).
15. W. Cannon, P. Bordes, S. R. Wigneshweraraj, M. Buck, *J. Biol. Chem.* **278**, 19815 (2003).
16. Single-letter abbreviations for the amino acid residues are as follows: A, Ala; C, Cys; D, Asp; E, Glu; F, Phe; G, Gly; H, His; K, Lys; L, Leu; Q, Gln; R, Arg; S, Ser; T, Thr; V, Val; and W, Trp.
17. Y. K. Wang, J. H. Lee, J. M. Brewer, T. R. Hoover, *Mol. Microbiol.* **26**, 373 (1997).
18. P. Bordes *et al.*, *Proc. Natl. Acad. Sci. U.S.A.* **100**, 2278 (2003).
19. V. Gonzalez, L. Olvera, X. Soberon, E. Morett, *Mol. Microbiol.* **28**, 55 (1998).
20. F. Beuron *et al.*, *J. Mol. Biol.* **327**, 619 (2003).
21. J. Furst, R. B. Sutton, J. Chen, A. T. Brunger, N. Grigorieff, *EMBO J.* **22**, 4365 (2003).
22. D. I. Svergun, M. Malfois, M. H. Koch, S. R. Wigneshweraraj, M. Buck, *J. Biol. Chem.* **275**, 4210 (2000).
23. K. S. Murakami, S. Masuda, S. A. Darst, *Science* **296**, 1280 (2002).
24. P. C. Burrows, K. Severinov, A. Ishihama, M. Buck, S. R. Wigneshweraraj, *J. Biol. Chem.* **278**, 29728 (2003).
25. Materials and methods are available as supporting material on *Science* Online.
26. J. Wang *et al.*, *Structure* (*Cambridge*) **9**, 1107 (2001).
27. P. Bordes, S. R. Wigneshweraraj, X. Zhang, M. Buck, *Biochem. J.* **378**, 735 (2004).
28. Y. K. Wang, T. R. Hoover, *J. Bacteriol.* **179**, 5812 (1997).
29. J. Li, L. Passaglia, I. Rombel, D. Yan, S. Kustu, *J. Bacteriol.* **181**, 5443 (1999).

30. We thank the members of M.B. and X.Z.'s laboratories for their help and useful discussions throughout this work; I. Leiros at The European Synchrotron Radiation Facility and beamline scientists at Daresbury for their help in data collection; and Imperial College Centre for Biomolecular Electron Microscopy for support. This work is supported by Biotechnology and Biological Sciences Research Council funding to X.Z. and M.B. Coordinates for the reported structures have been deposited in the Protein Data Bank with accession codes 2BJW and 2BJV. The EM map has been deposited in the electron microscopy database (EMDB) with accession code EMD-1109.

Supporting Online Material

www.sciencemag.org/cgi/content/full/307/5717/1972/DC1
Materials and Methods
Figs. S1 to S6
Tables S1 and S2
References

1 October 2004; accepted 11 February 2005
10.1126/science.1105932

Loss of Imprinting of *Igf2* Alters Intestinal Maturation and Tumorigenesis in Mice

Takashi Sakatani,[1]* Atsushi Kaneda,[1]* Christine A. Iacobuzio-Donahue,[2,3]* Mark G. Carter,[5] Sten de Boom Witzel,[2] Hideyuki Okano,[6] Minoru S. H. Ko,[5] Rolf Ohlsson,[7] Dan L. Longo,[5] Andrew P. Feinberg[1,3,4]†

Loss of imprinting (LOI) of the insulin-like growth factor II gene (*IGF2*) is an epigenetic alteration that results in a modest increase in IGF2 expression, and it is present in the normal colonic mucosa of about 30% of patients with colorectal cancer. To investigate its role in intestinal tumorigenesis, we created a mouse model of *Igf2* LOI by crossing female $H19^{+/-}$ mice with male $Apc^{+/Min}$ mice. Mice with LOI developed twice as many intestinal tumors as did control littermates. Notably, these mice also showed a shift toward a less differentiated normal intestinal epithelium, reflected by an increase in crypt length and increased staining with progenitor cell markers. A similar shift in differentiation was seen in the normal colonic mucosa of humans with LOI. Thus, altered maturation of nonneoplastic tissue may be one mechanism by which epigenetic changes affect cancer risk.

Genomic imprinting is a parent-of-origin gene-silencing mechanism thought to be important in growth regulation. Loss of imprinting (LOI) of the human insulin-like growth factor II gene (*IGF2*), or activation of the normally silent maternally inherited allele, occurs in many common cancers (*1*). About 10% of the population shows LOI of *IGF2*, and this molecular trait is associated with a personal and/or family history of colorectal neoplasia (*2*, *3*).

To investigate the mechanism by which LOI of *IGF2* contributes to intestinal tumorigenesis, we created a mouse model. Previous analyses of mouse models by other groups have shown that *Igf2* is activated more than 25-fold in pancreatic tumors induced by the SV40 large T antigen (*4*) and that forced overexpression of *Igf2* causes intestinal tumor formation and hyperproliferation of crypt epithelium (*5*, *6*). Our model was designed to more closely mimic the human situation, where LOI causes only a modest increase in *IGF2* expression. We took advantage of the fact that imprinting of *Igf2* is regulated by a differentially methylated region (DMR) upstream of the nearby untranslated *H19* gene. Deletion of the DMR leads to biallelic expression (LOI) of *Igf2* in the offspring when the deletion is maternally inherited (*7*–*9*) (fig. S1). To model intestinal neoplasia, we used *Min* mice with an *Apc* mutation (*10*). We crossed female $H19^{+/-}$ with male $Apc^{+/Min}$, comparing littermates harboring *Apc* mutations with or without a maternally inherited *H19* deletion, and thus with or without LOI. In comparison with $H19^{+/+}$ [hereafter referred to as LOI(−) mice], the $H19^{-/+}$ mutant mice [hereafter referred to as LOI(+) mice] showed an approximate doubling in *Igf2* mRNA levels that did not vary with age or *Min* status (fig. S2). This is consistent with the two- to threefold increase in *Igf2* mRNA levels in normal human colonic mucosa or Wilms tumors that are LOI(+) (*3*, *11*). The amount of Igf2 protein was also doubled in the intestine of LOI(+) mice (fig. S2). The LOI(+) mice developed about twice as many adenomas in both small intestine and colon as did the LOI(−) mice, and this difference was statistically significant (Table 1). Mice with LOI also had longer intestinal crypts, the site of epithelial stem cell renewal (*12*, *13*) (fig. S3). This increase in length was specific to the crypts, progressed over time [1.2-fold increase ($P < 0.01$) in mice at 42 days of age and 1.5-fold increase ($P < 0.0001$) in mice at 120 days], and was independent of *Apc* status. The increase in crypt length was not due to differences in cell proliferation, because there was no statistically significant difference in proliferating cell nuclear antigen labeling index between LOI(+) and LOI(−) Min mice (3.8 ± 0.9 versus 3.1 ± 1.5, respectively), nor was there a difference in the distribution (*14*) of proliferative cells within the crypt (0.39 ± 0.04 versus 0.38 ± 0.03, respectively; P = not significant). The LOI(+) and LOI(−) mice showed no difference in crypt apoptotic rates, as assessed histomorphologically and by in situ terminal deoxynucleotidyl transferase–mediated dUTP nick-end labeling (TUNEL); both genotypes had an average of 1 apoptotic cell per 20 crypts. There was also no difference in the rate of branching of intestinal crypts; both LOI(+) and LOI(−) mice had one or two total branched crypts below the intestinal surface.

We hypothesized that the increase in crypt length of the small intestine was due to a shift in the ratio of undifferentiated to differentiated epithelial cells in the mucosa. To test this, we immunostained for four antigens that mark undifferentiated versus differentiated epithelial cell development: villin, a structural component of the brush border cytoskeleton in gastrointestinal tract epithelia (*15*); ephrin-B1, the ligand of the EphB2/EphB3 receptors that play a role in allocating epithelial cells within the crypt-villus axis in intestinal epithelium (*16*); musashi1, an RNA-binding protein selectively expressed in neural and intestinal progenitor cells and key to

Table 1. Increased adenoma number and surface area in LOI(+) Min mice. Displayed are the adenoma counts, as well as counts corrected for intestinal surface area alone or for both intestinal and adenoma surface area. Values are given as the mean ± SE; P value was calculated by Student's t test.

Genotype	N	Small intestine	Fold increase; P value	Colon	Fold increase; P value
		Number of adenomas			
LOI(−) Min	81	27.7 ± 1.3	2.2;	1.3 ± 0.1	2.2;
LOI(+) Min	59	60.4 ± 3.7	<0.00001	2.9 ± 0.3	<0.0001
		Surface area of adenomas (% of intestine occupied by adenomas)			
LOI(−) Min	81	2.2 ± 0.1	2.4;	2.3 ± 0.3	2.5;
LOI(+) Min	59	5.5 ± 0.4	<0.00001	5.8 ± 0.9	<0.001
		Number of adenomas/10 cm² of intestine			
LOI(−) Min	81	10.8 ± 0.5	1.8;	3.7 ± 0.5	1.9;
LOI(+) Min	59	19.2 ± 1.1	<0.00001	7.0 ± 0.8	<0.0001

[1]Department of Medicine, [2]Department of Pathology, [3]Oncology Center, [4]Department of Molecular Biology and Genetics, Johns Hopkins University School of Medicine, Baltimore, MD 21205, USA. [5]Laboratory of Genetics, National Institute on Aging, National Institutes of Health, Baltimore, MD 21224, USA. [6]Department of Physiology, Keio University School of Medicine, Tokyo 160-8582, Japan. [7]Department of Development and Genetics, Uppsala University, S-752 36 Uppsala, Sweden.

*These authors contributed equally to this work.
†To whom correspondence should be addressed. E-mail: afeinberg@jhu.edu

maintaining the stem cell state (*17*, *18*); and twist, a transcriptional factor of the basic helix-loop-helix family originally identified as a mesodermal progenitor cell marker (*19*) that is also involved in loss of differentiation of epithelial cells (*20*, *21*).

Consistent with their biological roles in differentiated enterocytes, immunostaining for both villin and ephrin-B1 was detected within the cytoplasm of enterocytes lining the villi of the small intestine and within the villus-crypt interface in LOI(−) mice (Fig. 1A, fig. S4). The LOI(+) mice, in contrast, showed lower levels of villin and ephrin-B1 and a contraction of the differentiated epithelial cell compartment (Fig. 1B, fig. S4).

Expression of the progenitor cell marker musashi1 was observed in scattered cells within the lower half of intestinal crypts in LOI(−) mice (Fig. 1C), whereas numerous musashi1-positive cells were identified within the intestinal crypts of LOI(+) mice (Fig. 1D). The LOI(+) mice also showed intense staining within enterocytes lining the intestinal villi compared with LOI(−) mice (Fig. 1, E and F). A semiquantitative analysis confirmed increased musashi1 staining in the LOI(+) mice, independent of *Apc* status (table S1). Immunostaining for twist also revealed a marked increase in the number and intensity of positively staining cells in the crypts of LOI(+) mice (fig. S5). These changes were progressive over time (Fig. 1, figs. S4 and S5).

Because this shift affects normal mucosa, one prediction of this dedifferentiation model is that the increased number of adenomas is due to an increase in tumor initiation rather than an increase in tumor progression. Supporting this idea, there was no difference in the ratio of microadenomas [<5 crypts each (*22*)] to macroadenomas (≥5 crypts each) between LOI(+) Min mice (36 micro-/27 macroadenomas) and LOI(−) Min mice (16 micro-/14 macroadenomas) at 120 days. An independent mouse model of LOI, in which point mutations had been introduced in three of the four CCCTC-binding factor (CTCF) target sites within the *H19* DMR (*23*) (figs. S1 and S6), was also examined by immunostaining. Another advantage of this model is that, unlike the deletion model, *H19* expression is intact in the DMR mutation model (fig. S7). Loss of *H19* might have independent effects given its known role in mRNA translation in trans (*24*). Nevertheless, a shift in the ratio of differentiated to undifferentiated cells was also seen in the normal epithelium of these LOI(+) mice (Fig. 2, A to D, shows immunohistochemical staining for musashi1 and villin in colon epithelium).

Finally, we compared the normal mucosa of patients requiring biopsy during colonoscopic screening, whose LOI status was previously determined (*2*). No morphological differences were noted by conventional microscopy. However, 10 of 11 patients with LOI in the colon showed increased musashi1 staining extending to the upper half of colonic crypts and/or surface epithelium, compared with 5 of 15 patients without LOI (P = 0.004, Fisher's exact test) (Fig. 2, E and F; fig. S8). Altered colon epithelial maturation was also found in all four patients with LOI restricted to the colon (P = 0.03) and in six of seven patients with LOI in both peripheral blood lymphocytes and colon (P = 0.03), compared with patients without LOI.

The sensitivity was reduced but the specificity increased when musashi1 staining was combined with a second marker, twist; increased staining was seen in 6 of 11 patients with LOI, compared with 1 of 14 patients without LOI (P = 0.02, Fisher's exact test) (Fig. 2, G and H). Although twist staining alone did not attain statistical significance (P = 0.07), the two markers were nonoverlapping, suggesting heterogeneity in the downstream effects of LOI.

In summary, this study suggests a cellular mechanism by which epigenetic alterations in normal cells may affect cancer risk, namely, by altering the balance of differentiated and undifferentiated cells. The epigenetically mediated shift in normal tissue to a more undifferentiated state, as described here, might increase the target cell population for subsequent genetic alterations or might act alone in tumor initiation. In LOI-mediated Wilms tumor in the rare disorder Beckwith-Wiedemann syndrome (BWS), tumors arise because of an expanded population of nephrogenic precursor cells (*25*). We observed pancreatic islet cell hyperplasia, a feature of BWS, in LOI(+) Min mice (*26*), suggesting that LOI may also predispose to the development of other tumor types. Genetic mechanisms that alter cell differentiation and/or disrupt crypt architecture have been described (*27*–*30*), although these mechanisms are not common in normal human tissue. Whether the shift in epithelial maturation is a more specific predictor of cancer risk than LOI itself is an important question that will require studies of large numbers of patients using more molecular markers.

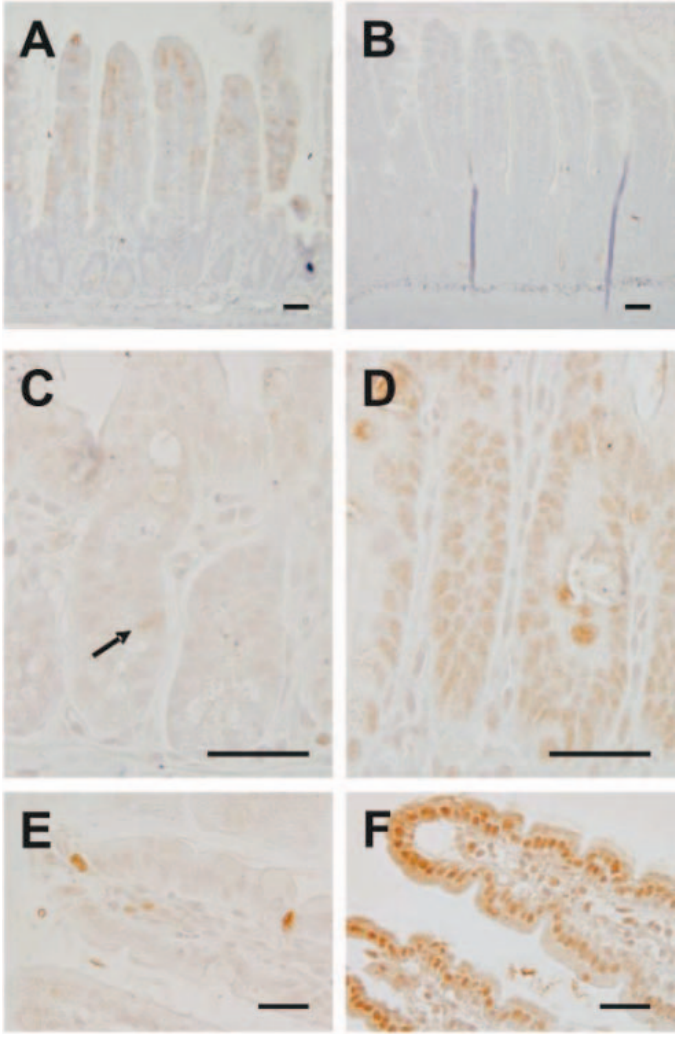

Fig. 1. Immunohistochemical analysis of villin and musashi1 in 120-day-old LOI(−) and LOI(+) mice. **(A)** In LOI(−) mice, villin protein expression is noted in a cytoplasmic distribution throughout differentiated enterocytes lining intestinal villi and within the crypt-villus interface. **(B)** In LOI(+) mice, villin expression is markedly decreased. **(C)** In LOI(−) mice, musashi1 expression is detected within the cytoplasm and nuclei in rare cells within intestinal crypts (arrow), the location of intestinal stem cells and the undifferentiated epithelial cell compartment. **(D)** In marked contrast, musashi1 cytoplasmic and nuclear labeling is detected throughout the intestinal crypts of LOI(+) mice. **(E)** In LOI(−) mice, rare musashi1-positive cells are detected within the overlying intestinal villi representing the differentiated epithelial compartment. **(F)** In LOI(+) mice, intense cytoplasmic and nuclear expression of musashi1 is detected within enterocytes lining intestinal villi. Bars, 10 μm.

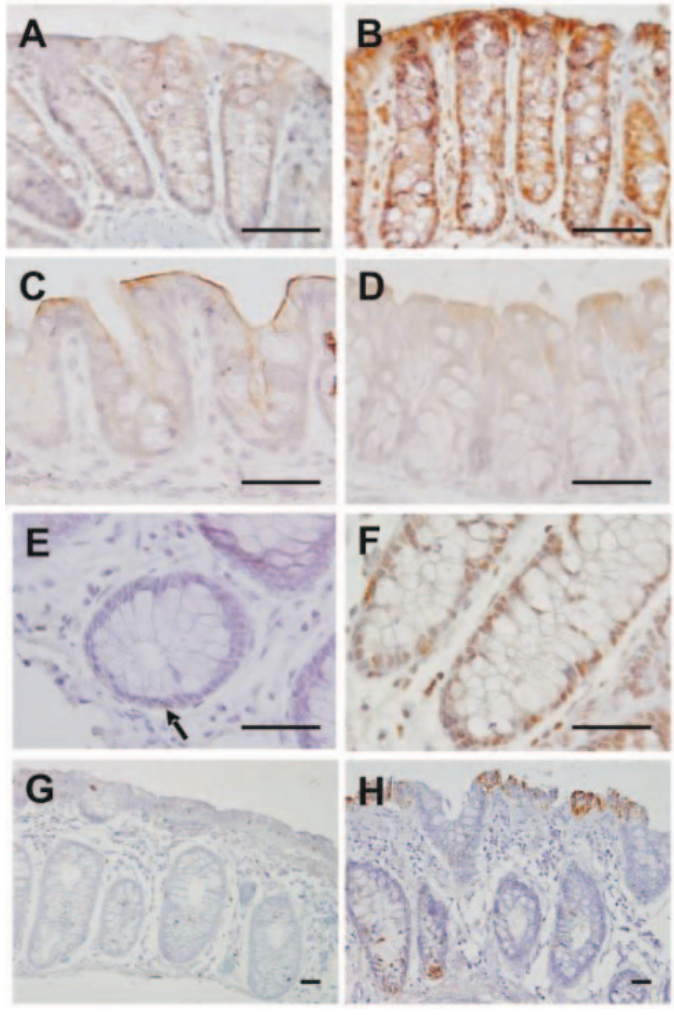

Fig. 2. A shift to less differentiated colon epithelium in a mouse *H19* DMR mutation model and in colonoscopy patients with LOI. (**A**) Musashi1 immunostaining in LOI(−) mice shows rare crypt epithelial cells with cytoplasmic labeling. (**B**) In contrast, LOI(+) mice show aberrant musashi1 staining in both a cytoplasmic and nuclear pattern throughout the colonic epithelium. (**C**) Villin immunostaining in LOI(−) mice shows cytoplasmic labeling that includes the brush border. (**D**) In contrast, in LOI(+) mice, villin staining of the brush border on the surface epithelial cells is absent. (**E**) In colonoscopy patients without LOI, rare musashi1-positive cells are detected in crypt epithelial cells (arrow). Low-power view is available in fig. S8. (**F**) In contrast, in colonoscopy patients with LOI, musashi1 labeling is present throughout colonic crypts and extends to the surface epithelium (see also fig. S8). (**G**) In colonoscopy patients without LOI, only weak labeling for twist is detected. (**H**) In colonoscopy patients with LOI, patchy but strong twist labeling is present in the crypt and surface epithelium. Bars, 10 μm.

References and Notes

1. A. P. Feinberg, *Semin. Cancer Biol.* **14**, 427 (2004).
2. H. Cui *et al.*, *Science* **299**, 1753 (2003).
3. K. Woodson *et al.*, *J. Natl. Cancer Inst.* **96**, 407 (2004).
4. G. Christofori, P. Naik, D. Hanahan, *Nat. Genet.* **10**, 196 (1995).
5. A. B. Hassan, J. A. Howell, *Cancer Res.* **60**, 1070 (2000).
6. W. R. Bennett, T. E. Crew, J. M. Slack, A. Ward, *Development* **130**, 1079 (2003).
7. P. A. Leighton, R. S. Ingram, J. Eggenschwiler, A. Efstratiadis, S. M. Tilghman, *Nature* **375**, 34 (1995).
8. M. A. Ripoche, C. Kress, F. Poirier, L. Dandolo, *Genes Dev.* **11**, 1596 (1997).
9. Materials and methods are available as supporting material on *Science* Online.
10. L. K. Su *et al.*, *Science* **256**, 668 (1992).
11. J. D. Ravenel *et al.*, *J. Natl. Cancer Inst.* **93**, 1698 (2001).
12. S. Sell, G. B. Pierce, *Lab. Invest.* **70**, 6 (1994).
13. G. H. Segal, R. E. Petras, in *Histology for Pathologists*, S. S. Sternberg, Ed. (Lippincott-Raven, Philadelphia, 1997), pp. 495–518.
14. M. Lipkin, E. Deschner, *Cancer Res.* **36**, 2665 (1976).
15. A. B. West *et al.*, *Gastroenterology* **94**, 343 (1988).
16. E. Batlle *et al.*, *Cell* **111**, 251 (2002).
17. Y. Kaneko *et al.*, *Dev. Neurosci.* **22**, 139 (2000).
18. C. S. Potten *et al.*, *Differentiation* **71**, 28 (2003).
19. O. M. Borkowski, N. H. Brown, M. Bate, *Development* **121**, 4183 (1995).
20. L. R. Howe, O. Watanabe, J. Leonard, A. M. Brown, *Cancer Res.* **63**, 1906 (2003).
21. J. P. Thiery, M. Morgan, *Nat. Med.* **10**, 777 (2004).
22. C. J. Torrance *et al.*, *Nat. Med.* **6**, 1024 (2000).
23. V. Pant *et al.*, *Genes Dev.* **17**, 586 (2003).
24. Y. M. Li *et al.*, *J. Biol. Chem.* **273**, 28247 (1998).
25. J. B. Beckwith, N. B. Kiviat, J. F. Bonadio, *Pediatr. Pathol.* **10**, 1 (1990).
26. T. Sakatani *et al.*, data not shown.
27. A. P. Haramis *et al.*, *Science* **303**, 1684 (2004).
28. M. van de Wetering *et al.*, *Cell* **111**, 241 (2002).
29. W. Yang, L. Bancroft, C. Nicholas, I. Lozonschi, L. H. Augenlicht, *Cancer Res.* **63**, 4990 (2003).
30. A. Velcich *et al.*, *Science* **295**, 1726 (2002).

31. We thank S. Tilghman for the H19 deletion mouse strain, A. Hershfeld for technical assistance, and B. Vogelstein, E. Fearon, B. Beckwith, R. Hruban, and A. Sawa for helpful discussions. Supported by NIH grants R01CA65145 (A.P.F.), K08CA106610 (C.A.I.-D.), a Uehara Memorial Foundation grant (A.K.), and the Swedish Cancer Research Foundation (R.O.). The Johns Hopkins University and the NIH have filed a provisional patent application on the LOI mouse cancer model and immunohistochemical marker use. A.P.F. is a paid consultant to Epigenomics AG.

Supporting Online Material

www.sciencemag.org/cgi/content/full/1108080/DC1
Material and Methods
Figs. S1 to S8
Table S1
References

30 November 2004; accepted 13 January 2005
Published online 24 February 2005;
10.1126/science.1108080
Include this information when citing this paper.

Protein Fractionation Kits

The Qproteome kits, based on spin or gravity-flow columns, enable fast, standardized fractionation of complex protein matrices for initial purification or preprocessing for polyacrylamide gel electrophoresis or mass spectroscopic analysis. These kits can also be used to localize or characterize biomarkers in cells grown under different conditions or isolated from different tissues. Kits are available that separate proteins on the basis of glycosylation patterns, their subcellular localization, their affinity to nucleic acids, and their overall solubility.

Qiagen For information 800-426-8157 www.qiagen.com

Seqware Data Center

Seqware Data Center is a sequence data management and personal BLAST software system that enables scientists to easily maintain and search annotated sequence collections. Seqware comes with GenBank pre-loaded. Seqware Data Center includes a powerful database and a fast, fully functional BLAST server. It is a scalable solution that helps individual scientists, workgroups, and core facilities manage their proprietary DNA sequences along with public sequence collections on a local personal computer or a network. The amount of sequence data efficiently stored by Seqware is limited only by disk space. Seqware automatically updates GenBank from the NCBI data repository, and makes it easy to create, manage, update, and annotate sequence sets; edit and annotate records in the database; run flexible context searches; and store, automatically update, and reuse BLAST results.

Ariadne Genomics For information 847-644-1557 www.ariadnegenomics.com

Digital Imaging System

The Kodak Image Station 4000 features high-resolution, cooled, charge-coupled device (CCD) camera technology for comprehensive fluorescence, luminescence, radiographic, and chromogenic imaging capability. The system's 4-million-pixel CCD and 10× optical zoom lens provide spatial resolution of up to 10 μm per pixel. True 16-bit imaging provides highly accurate grayscale resolution and a broad linear dynamic range for quantitative imaging of membranes, electrophoresis gels, plates, tissues, and in vivo assays. It is available in two configurations. The IS4000MM features multiwavelength illumination to improve the detection sensitivity and reduce background for most fluorescence labels. It allows imaging of multi-fluorescence assays. In addition, the ability to select and apply longer excitation wavelengths improves the penetration of light into tissue, enabling whole body in vivo molecular imaging research via the detection of fluorescently tagged biomolecules in living animals and plants. The IS4000R contains broadband ultraviolet illumination capability to image ultraviolet fluorescent dyes as well as chemiluminescent and colorimetric labels. An optional x-ray imaging module is available.

Eastman Kodak For information 877-SIS-HELP www.kodak.com/go/imagestation

Ion Channel Screening

The Flyscreen 8500 is an ion channel screening system. It offers true whole-cell recordings in mammalian cells without a micromanipulator or microscope and extremely low and stable access resistance. It features fully automated whole cell patch clamp screening, two to six parallel independent electrode positions, asynchronous whole-cell recordings in mammalian cells, and individual disposable recording tips. Applications include assay development, secondary screening, lead optimization, and expression cloning.

flyion GmbH For information +49 7071 68 88 3-0 www.flyion.com

Microplate Automation

The versatile QuickStack conveyor and gripper-based microplate automation system features a modular approach that enables it to adapt to a wide range of applications. It can bring microplates to and from dispensers, readers, washers, and more. New versions have been adapted to vials and other labware. Conveyor-based versions are economical for simple tasks and long travel. Gripper-based versions provide enhanced capabilities, such as recessed nest access, stacking of multiple instruments, and dynamic scheduling.

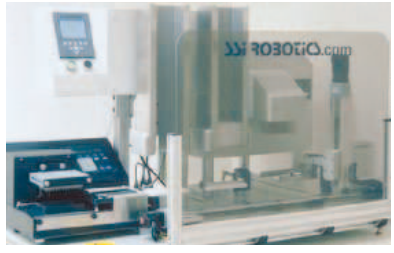

SSI Robotics For information 949-481-5874 www.ssirobotics.com

Refrigerated Microcentrifuge

The Z233 MK-2 refrigerated microcentrifuge provides high-speed capabilities, intelligent control, and a wide variety of rotor options, including a new 6 x 30-ml angle rotor. It features a brushless induction motor capable of attaining speeds of up to 15,000 rpm/21,380 × g. A microprocessor controls all run parameters, including rate of acceleration and brake intensity. The user-friendly control panel includes easy-to-turn knobs for setting parameters and large digital displays for viewing values. A g-force conversion program permits speed to be set in either rpm or rcf and allows both to be displayed during a run. Ten rotors are available, including the high-capacity 44 × 1.5-ml micro rotor.

Labnet For information 888-LABNET1 www.labnetlink.com

Literature

Cambrex Bioproducts Catalog 2005 features products for molecular biology, bioassays, cell biology, cell culture, and endotoxin detection. The catalog includes more than 40 new products, including cell-based assay systems, fluorescent cell stains, visceral preadipocyte cells, rat and mouse neuronal cells, serum-free media systems, classical media, and endotoxin monitoring systems.

Cambrex For information 207-594-3400 www.cambrex.com

Newly offered instrumentation, apparatus, and laboratory materials of interest to researchers in all disciplines in academic, industrial, and government organizations are featured in this space. Emphasis is given to purpose, chief characteristics, and availability of products and materials. Endorsement by *Science* or AAAS of any products or materials mentioned is not implied. Additional information may be obtained from the manufacturer or supplier by visiting www.science.labvelocity.com on the Web, where you can request that the information be sent to you by e-mail, fax, mail, or telephone.

» advances in:

Proteomics

Preparing Proteins

Advances in understanding the nature and function of proteins demand effective means of isolating the entities. Several new technologies complement the tried and true methods in facilitating that work. BY PETER GWYNNE AND GARY HEEBNER

In this issue:

- Protein isolation
- Affinity chromatography
- 2-D gel electrophoresis
- High performance liquid chromatography
- Automation for proteomics
- Microfluidics

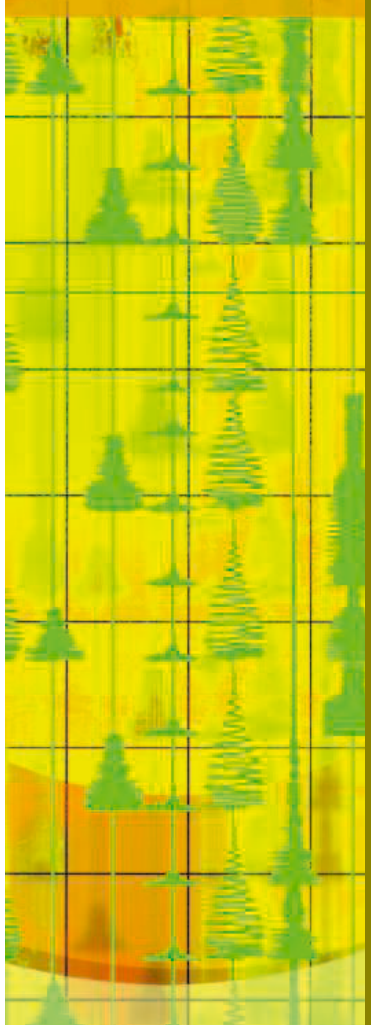

The emergence of genomics has opened the way to the next stage of research on the nature of life: proteomics. But for scientists trained to solve genomic problems, proteins mean trouble. Not only do they exist in huge numbers. Individually, proteins are more sophisticated than other biomolecules. Unlike DNA, which exists as linear strands, proteins take on three-dimensional shapes. An individual protein starts out as a peptide chain made up of 20 or so amino acids, and is then folded into a complex and fairly fragile three-dimensional structure. That physical structure ultimately determines any protein's activity.

Those complex and changeable structures make it difficult for researchers to track down proteins' activities. The difficulty applies particularly to low abundance proteins, which often get lost in clusters of more abundant proteins. "Low abundance proteins are often the most interesting, and they remain a problem," says Darwin Asa, drug discovery development manager at **ESA**.

MULTIPLE TECHNOLOGIES

Researchers who investigate all types of proteins must deal with another factor that differentiates proteomics from genomics. While structural genomics in the area of sequencing the human genome was generally approached with a single technology," explains Achim Wehren, global marketing manager for biopharma at **Tecan**, "several technologies and methodologies are available for proteomics."

Emerging tools and technologies have become key factors in facilitating several advances in proteomics. "One of the biggest achievements is the increased resolution of mass spectrometry," says Donald Finley, product manager for recombinant protein expression at **Sigma-Aldrich**. "It enables us to see things we haven't seen before." Mark McDowall, strategic development manager for MS at **Waters Corporation**, extends that thought. "Prefractionation of proteins by multidimensional chromatography before mass spectrometry and multiplexing mass spectrometry analyses allow scientists to extract more information from a minimal amount of sample," he says. Those approaches, adds Tom Wheat, principal scientist and manager in Waters's life science application laboratory, "help to enrich the low abundance proteins so that we can use elegant software to extract information about these important proteins. There have been some very exciting things happening with the software for interpreting these analyses."

Improved forms of liquid chromatography have also become significant tools in isolating and identifying proteins. "Methods such as multi- MORE ›››

This is the first of four special supplements this year on Advances in Proteomics. The next will appear in the 29 April issue of Science.

Inclusion of companies in this article does not indicate endorsement by either AAAS or Science, *nor is it meant to imply that their products or services are superior to those of other companies.*

» advances in: Proteomics

plexed liquid chromatography and nano-high performance liquid chromatography coupled to electrospray or matrix-assisted laser desorption/ionization mass spectrometry [MALDI-MS] will definitely have an impact on proteomics research," says Carsten Buhlmann, product manager for laboratory-on-a-chip assays at **Agilent Technologies**. **Nanostream** offers what it calls micro parallel liquid chromatography through its Veloce system, a microfluidic method that provides high throughput chromatographic separations.

Studies of proteomics don't always demand new technology. "We often have to go back to the old methods, like 2-D gels and sometimes 1-D gel electrophoresis followed by mass spectrometry," says Deb Chakravarti, director of proteomics and Beckman professor at the **Keck Graduate Institute** and editor-in-chief of *Current Proteomics*, published by **Bentham Science Publishers**. "We have to know the whole bag of tricks." Wehren explains the outcome of such knowledge on proteomics. "Technology," he says, "is driving the field."

UNFAMILIAR PRINCIPLES AND APPROACHES

Emerging technologies often involve principles and approaches unfamiliar to scientists untrained in proteomics. "With the drive to come up with biological issues, people are less interested in studying the nuances of the chemistry," explains George Lipscomb, product manager for protein expression and purification at Sigma-Aldrich. To ease those individuals into the protein world, suppliers increasingly emphasize user-friendliness. "The power of studying proteomics is bringing in a lot of people with diverse training and experience," Finley says. "They need the absolute, simplest, most robust protocols available." Why? "Nonproteomics people have to have an understanding of the results," adds Chakravarti. "There's a push for guidelines for experiments and interpretation of protein identification results."

That puts the pressure on suppliers. "If your kit is not user-friendly," says Shou Wong, manager of global R&D and business development at Merck KGaA which owns **EMD Biosciences**, "people won't want to use it." At the same time, vendors cannot afford to sell equipment that lacks appeal to proteomic specialists. "The trick here is to maximize ease of use but also to allow advanced users to have access to the advanced options," Buhlmann explains.

Tecan sets out to create user friendliness by the breadth of its instruments' appeal. "Once you have bought our liquid handling systems you usually have multiple applications," Wehren says. "When your application repertoire changes, you can easily reconfigure your instrument."

Two approaches help to familiarize newcomers to proteomics with the tools and technologies that facilitate research in the field. "Technical support is important," Wong says. "Users can follow the instructions but still make simple mistakes; that's where support comes in." Wehren echoes that point. "We have been in the instrument market for 25 years," he points out. "We have a very strong service organization." In addition, Chakravarti says, "We're finding more and more need for training workshops for proteomics. Many current curricula are predominantly oriented to recombinant DNA."

ONE KEY FACTOR

Newcomers to proteomics need to understand one key factor. "You can break proteomics into two types," Wong explains. "You have the native proteins, from natural samples such as tissues, and recombinant proteins that scientists try to overexpress by biotechnological methods."

To understand proteins' makeup, scientists must first isolate and separate intact proteins from cells or tissue. The processes involve several steps, each of which can cause the degradation or loss of the proteins of interest if carried out incorrectly. Avoiding such problems is particularly critical in the case of low abundance proteins. So is choosing the right approach. "There are perhaps up to a dozen principles of protein separation available," says Wheat of Waters.

As the first step in isolating a protein, scientists must disrupt the cells or tissue and extract the protein fraction of interest. Disruption generally requires a strong denaturing solution. Often based on detergents such as CHAPS, such solutions also include urea for rapid inactivation of any enzymes that might degrade the target proteins. Researchers often add protease inhibitor cocktails that prevent the proteins from degrading in crude cellular extracts that contain many active proteases. Several suppliers that specialize in protein chemistry, including **BD Biosciences Clontech**, EMD Biosciences, and **Pierce Biotechnology**, provide chemicals and reagents of this type.

Many of these companies have also developed kits that provide researchers with relatively simple tools for isolating proteins without developing their own protocols from scratch. "For recombinant proteins, EMD Biosciences offers everything for protein expression and purification," Wong says. "EMD Biosciences has ligation independent cloning which allows you to clone genes in an orientation dependent fashion such that the insert can go into your vector in only one orientation. Since this process doesn't use ligase, its efficiency is very high; the whole process takes less than five minutes at room temperature with an efficiency of 99 percent or better." For native proteins from tissues and cell cultures, EMD Biosciences has developed efficient user-friendly extraction kits to purify nuclear proteins (the NucBuster Protein Extraction Kit), total proteins from bacteria, yeast and mammalian cells and tissues (ProteoExtract Complete Proteome Extraction Kits), and partial and subcellular proteins from mammalian cells (the ProteoExtract Partial Proteome Extraction and ProteoExtract Subcellular Proteome Extraction Kit).

PHYSICAL AND CHEMICAL PROPERTIES

Once they have isolated a mixture of proteins from a cell, researchers can separate the individual proteins according to physical properties such as their size, shape, and charge, or such chemical characteristics as hydrophobicity and affinity for other molecules. Affinity chromatography is a popular method of separating a specific protein or family of proteins. This method takes advantage of the fact that some proteins bind to specific substrates or to antibodies generated specifically for that purpose. MORE ›››

» advances in: Proteomics

When available, antibodies raised against a protein offer highly specific tools for separating or purifying one protein from a mixture for further analysis.

Antibodies generated to a specific protein can be used to "fish" for a unique protein in a cellular extract. Chromatography media packed in columns secure the antibodies to a solid support. This allows protein-containing samples, buffers, and other solutions to be run through a column, capturing the protein of interest, followed by elution of the protein-antibody complexes. This elution is accomplished by changing solvent conditions in the column, which diminishes the strength of the protein-ligand interaction.

Several companies, including **IBA GmbH**, EMD Biosciences, **Promega**, and Sigma-Aldrich, have developed novel protein purification systems based on the insertion of small peptide sequences into a specific protein that can enable isolation of the protein using a molecule with a strong affinity to the peptide sequence. Many researchers use a HIS type of tag for inexpensive purification of recombinant proteins. EMD Biosciences offers a line of His-tag affinity products from vectors that contain a wide range of tags to purification resins and kits. Sigma-Aldrich's HIS-Select family of products purifies histidine-containing fusion proteins with high selectivity. The company also offers its FLAG system, designed for highly sensitive detection of recombinant protein. "It adds a small octopeptide tag to a protein," Finley explains. "The tag tends to end up on the outside of a protein instead of being folded in. It's one of our most popular products in the recombinant protein arena."

Purification and detection tools for many other fusion proteins are also available. For example, Sigma-Aldrich offers agarose-based affinity resins for purification of c-Myc, HA, and Maltose Binding Protein fusion proteins.

TWO TYPES OF GEL

Scientists developed two-dimensional (2-D) gel electrophoresis specifically to separate mixtures of proteins. The systems consist of two types of gel electrophoresis; the first dimension is based on isoelectric focusing (IEF), while the second uses a denaturing polyacrylamide gel matrix.

The first gel (or dimension) traditionally incorporates ampholytes that form a pH gradient in the gel. This gradient helps to separate the proteins based on the isoelectric point of each protein. Having separated a mixture of proteins in this first dimension, the scientist places the separated proteins on a vertical gel electrophoresis unit. This second dimension is usually a denaturing sodium dodecyl sulfate polyacrylamide gel (SDS-PAGE) – a relatively routine tool found in most laboratories.

Companies such as **Bio-Rad Laboratories**, **GE Healthcare,** and **Invitrogen** offer complete systems with the units, power supplies, and accessories required to perform protein separations. These and other companies also produce precast polyacrylamide gels and/or IEF strips that provide highly consistent results and allow scientists to use the systems without having to master the casting of polyacrylamide gels, which can be technically difficult.

To identify the proteins separated by 2-D gel electrophoresis, scientists typically use mass spectrometry (MS). "We recently introduced the MALDI micro MX system to identify proteins excised from 2-D gels," reports McDowall of Waters. "The novel thing is that it's multiplexed. It performs MS-MS on all the peptide components at the same time in parallel. You "burn" less sample and you no longer need to serially select each peptide precursor ion for fragmentation, so that it's very easy to use compared with traditional PSD."

Another separation approach, high performance liquid chromatography (HPLC), refers to the separation of molecules under high pressure in a stainless steel column filled with a solid matrix. Companies that specialize in HPLC include Agilent Technologies, **Grace Vydac, Phenomenex**, and Waters.

ATTRACTIVE FORCES

HPLC vendors use the attractive forces between molecules that carry oppositely charged groups in two different ways. Ion pairing primarily concerns rather small molecules, while ion exchange chromatography (IEC) can separate almost any type of charged molecule, from large proteins to small nucleotides and amino acids. In IEC, charged particles in the form of a solid matrix bind reversibly to proteins or other molecules. The bound molecules are then detached by increasing the salt concentration or by altering the pH of the mobile phase. Researchers frequently use ion exchangers that contain diethyl aminoethyl or carboxymethyl groups to study proteins and peptides under widely varying conditions.

Waters has taken the process a stage further with its nanoACQUITY Ultra Performance Liquid Chromatography System. "It's a new workhorse for proteomics to prepare and introduce samples for mass spectrometry," Wheat explains. "We've developed new packing materials based on much smaller particles that provide greater chromatographic resolution, peak capacity, MS sensitivity, and speed."

Agilent Technologies, meanwhile, plans to launch a new HPLC chip later this year. "It will offer maximum sensitivity and MORE ›››

Running with the Tides

Individuals who work in oligonucleotide- and peptide-based therapeutics, diagnostics, and vaccines will have the opportunity to bring themselves fully up-to-date on their field at the TIDES 2005 Oligonucleotide and Peptide Technology and Product Development Conference in Boston. The only industry event for manufacturing and development of oligonucleotide and peptide products, the event will run from May 1 to May 5 at the Boston Convention and Exhibition Center, and will focus on present progress and the future potential of both fields.

The conference, hosted by **IBC USA**, will outline novel technologies and commercialization strategies for therapeutics, diagnostics, and research. It will also detail methods of minimizing risk and improving the economics of the supply chain, and will provide progress reports on leading clinical and preclinical candidates from the two fields. Highlights include an update from the U.S. Food and Drug Administration, keynotes from Robert Langer of MIT and Homer Pearce of Eli Lilly, a tutorial session on how to avoid pitfalls, an analysis of best practices for validating process and analytical methods, details of the latest technology advances, and a small interactive group discussion on how to define starting materials. Individuals can register to attend through the website or by phone at 508-616-5550.

» www.ibclifesciences.com/Tides

» advances in: Proteomics

minimum sample size," Buhlmann says. "It will integrate sample handling, sample separation, and sample spraying into the mass spectrometer on a chip device that is reusable and very easy to run."

Having separated proteins in an HPLC column, scientists must then detect them. While mass spectrometry remains the most popular approach, electrochemical detectors also provide highly sensitive and selective detection in HPLC, capable of quantifying picogram to femtogram levels of proteins in a sample. "When an electrochemical detector operates, it oxidizes a compound," ESA's Asa says. "Our electrochemical detectors are 100 percent efficient in their oxidation of compounds going through the cell. That makes the analysis much easier at the other end."

ESA also offers what it calls the Corona CCA detector. "It's probably one of the easiest HPLC detectors in existence," Asa claims. "You just have to hook it up to a nitrogen source, plug it into your HPLC, and turn it on. And it delivers in gaps left by other HPLC detectors."

AUTOMATION AND MICROFLUIDICS

Like practitioners in other fields of life science, proteomics scientists increasingly rely on automation and robotics to pursue their research. Tecan's Cellerity system, designed for use in protein production among other applications, illustrates the value of automation. "It's a self-contained system for automated cell culturing that handles all the tasks necessary to grow, maintain, harvest, seed, and plate cell lines without user intervention for several days," Wehren says. "We see increasing demands for this system."

Several companies are now developing microfluidic devices and systems that can help to automate the handling processes involved in protein isolation and purification. "Microfluidics can integrate multiple manual steps in the workflow into integrated chip devices like the HPLC chip systems, giving high ease of use and good standardization," explains Buhlmann. "If you're looking for compliance, it's important to have validated analytic methods."

Last November, Agilent launched an automated lab-on-a-chip platform that permits automatic sizing and quantitation of thousands of protein samples from microtiter plates running overnight. "You can analyze up to 4,480 samples in an unattended way," Buhlmann explains. "You feed the machine with all the chips and samples, and in the morning you can see the results in your database."

Agilent has also developed the 2100 Bioanalyzer System that uses **Caliper**'s LabChip devices to analyze proteins and other molecules. "The system gives high resolution and high reproducibility," Buhlmann says. "And it's much faster than the traditional SDS-PAGE approach. You can get digital data for 10 samples in half an hour rather than four hours."

Successfully unraveling the function and structure of proteins clearly begins with obtaining a target protein with its native characteristics still intact. Manufacturers who specialize in protein chemistry and proteomics research continue to improve the tools used in this field. Those tools have already led to significant advances. "In proteomics research, I see a lot of progress in the area of biomarkers," Chakravarti of the Keck Graduate Institute says. "There's a special focus on early diagnosis. There's also interest in the localization of proteins within the cell." Adds Sigma-Aldrich's Lipscomb: "Proteomics has much more to do with human disease than genomics, in terms of biomarkers for cancer, for example."

Chakravarti cites *Current Proteomics* to illustrate the promise enabled by new tools for proteomics. "We've completed our first year and have published 26 review articles in four issues," he says. "The wide areas covered by these articles give you an idea of how diverse the field is."

Peter Gwynne (pgwynne767@aol.com) is a freelance science writer based on Cape Cod, Massachusetts, U.S.A. Gary Heebner (gheebner@cell-associates.com) is a marketing consultant with Cell Associates in St. Louis, Missouri, U.S.A.